VOLCANIC GEOLOGY OF GALUNGGUNG, WEST JAVA, INDONESIA

A thesis

submitted in partial fulfilment

of the requirements for the Degree

of

Doctor of Philosophy in Geology

in the

University of Canterbury

by

Sutikno Bronto

University of Canterbury

1989

ABSTRACT

Galunggung volcano is located in West Java, Indonesia and covers an area about 275 km^2. The volcano is very active and the slopes are highly populated (over 1.5 million people). There is therefore always the threat of volcanic disaster. This study investigates the character of past Galunggung volcanic activity and assesses likely future activity in order to advise on volcanic hazard and risk. The approach involves a study of stratigraphy, mineralogy and petrology of the Galunggung rocks, and the presentation of volcanic hazard zonation maps.

Galunggung volcanic rocks are included within the Galunggung Group and can be divided into Old Galunggung Formation, Tasikmalaya Formation and Cibanjaran Formation. The first formation represents rocks of Old Galunggung stratovolcano (50,000 - 10,000 yrs. BP ?), the second formation covers rocks erupted during caldera formation (4200 ± 150 yrs. BP) and the third one comprises rocks erupted in 1822, 1894, 1918 and 1982-83.

The Old Galunggung Formation consists mainly of pyroclastic flow, pyroclastic fall and lahar deposits and lava flows which have a total rock volume of about 56.5 km^3. This activity ended with the intrusion of a cryptodome under the crater. The cryptodome blocked the existing vent and subsequent activity moved to the weakest part of the old cone to the ESE, resulting in the caldera forming-event. This destructive eruption formed a horseshoe-shaped caldera and ejected more than 20 km^3 of material comprising debris avalanche, pyroclastic flow, pyroclastic fall, pyroclastic surge and lahar deposits. Historic eruptions separated by relatively long dormant periods produced less voluminous (< 0.4 km^3) volcanic deposits.

Galunggung volcanic rocks are basalt (49 - 53 % SiO_2) to basaltic andesite (53 - 57 % SiO_2) having porphyritic textures with medium-sized phenocrysts (15 - 40 %), mainly plagioclase (av. 18 %) and clinopyroxene (1.6 %). Olivine is observed in basic rocks, whereas orthopyroxene and magnetite are present in the most evolved rocks. Amphibole is common in pyroclastic deposits and gabbro clasts ejected during caldera formation.

On the basis of Mg contents, Galunggung rocks are divided into : 1. high-Mg basalt (12.5 - 10 % MgO), 2. "Transitional" high-Mg basalt (9 - 6.5 % MgO), 3. low-Mg basalt (< 6 % MgO), 4. high-Mg basaltic andesite (7 - 6 % MgO) and 5. low-Mg basaltic andesite (< 5 % MgO). The high-Mg basalts are subdivided into low-K high-Mg basalt (<

0.4 % K_2O) and medium-K high-Mg basalt (0.6 % K_2O).

Alkali and incompatible elements increase whereas Mg, Fe, Ca and compatible trace elements decrease with increasing SiO_2. The high-Mg basalts are the most primitive Galunggung rocks with highest Mg# = 75 - 69, Ni (up to 193 ppm), and Cr (711 ppm) but lowest incompatible elements. The "primitiveness" of the basalts is also reflected by their $^{230}Th/^{232}Th$ ratio (= 0.68) which is one of the lowest ratios yet found.

The Galunggung high-Mg basalts are considered to represent liquid compositions which have been derived from upper mantle peridotites. The low-K high-Mg basalt originate from spinel-peridotite by 15 % melting at about 50 km depth, and the medium-K high-Mg basalt from plagioclase-peridotite by 25 - 40 % melting at about 30 km depth. These primitive magmas probably rose rapidly to the surface as mantle "diapirs".

During Old Galunggung volcanic activity, low-K high-Mg basalt magma moved upward diapirically and formed a magma chamber in the crust at a depth of about 10 km. Fractionation of this magma formed low-Mg basalts and basaltic andesites. This activity ended when a medium-K high-Mg basalt intruded as a cryptodome. Another low-K high-Mg basalt magma migrated into the crust and fractionated to produce low-Mg basalt - basaltic andesite. Gas was trapped and high water pressure was attained; and amphibole gabbro solidified in the roof of the magma body. These rocks were erupted during the Galunggung caldera forming-event.

In 1982-83, a new generation of low-K high-Mg basalt magma was erupted. Fractionation in a conduit system changed compositions at the top part but not significantly in the lower part of the magma body. During the eruptive sequence firstly low-Mg basaltic andesite, then high-Mg basaltic andesite, "transitional" high-Mg basalt, and finally the low-K high-Mg basalt were erupted. Rhyolite pumice erupted in September 1982 is considered to be a product of melting of Miocene dacite by the high temperature (1300^{o}C) Galunggung high-Mg basalt magma.

Galunggung eruptions vary from non-violent effusive to destructive explosive events. These create hazards which are divided into four levels. First degree hazards are long-term and require further study. In this thesis hazard maps are presented for second, third and fourth degree hazards. Evacuation routes are suggested away from the volcano as all arrangements must be planned well in advance of an actual event.

CONTENTS

LIST OF FIGURES

LIST OF TABLES

APPENDICES

MAPS IN THE BACK COVER

1. Geologic Map of Galunggung, scale 1 : 50,000
2. Geologic Map of Galunggung caldera, scale 1 : 10,000
3. Location Map, scale 1 : 50,000

I INTRODUCTION

I.1 Background

Indonesia is located in a very active volcanic area. There are 128 active volcanoes (Neumann van Padang, 1951; Kusumadinata, 1979; Tjia et al., 1980; Sudradjat, 1984), and every year, since 1980, at least two of these have erupted. The country has a population of over 170 million. Consequently, volcanic disasters affecting large areas and numbers of people are very common. The Volcanological Survey of Indonesia is charged with reducing volcanic hazard by undertaking research and monitoring the active volcanoes.

Galunggung is one of Indonesia's most active volcanoes and hence merits serious attention. Although the volcano is characterised by intermittent eruptions separated by long dormant periods, it has erupted very destructively over both short and long periods. This means that volcanic disasters constantly threaten people living in the surrounding area. No detailed study of Galunggung volcano has previously been done. The present thesis aims to fill this gap in our knowledge.

I.2 Purpose and Scope

The purpose of this study is to understand the character of past Galunggung volcanic activity in order to provide a guideline for future activity and hence minimise volcanic hazard. The approach

involves a study of the stratigraphy and petrology of the Galunggung primary volcanic rocks (lavas and pyroclastics), most of which are well exposed following the 1982-1983 eruption.

Through petrological study of rocks from each of Galunggung's periods of activity it is hoped that an evolutionary model of Galunggung volcanic activity can be established. Furthermore, it may be possible to use these data for prediction and monitoring of the behaviour of future eruptions, thus reducing volcanic hazard.

I.3 Field Location and Physiography

Galunggung volcano is located in the district of Tasikmalaya, West Java, Indonesia, about 100 km southeast of Bandung (Fig.I.1). Tasikmalaya, the nearest city, is situated 17 km southeast of the volcano.

Galunggung volcanic area covers approximately 275 km^2, and is elliptical in outline with a major diameter (northwest - southeast) of 27 km and a minor diameter of 13 km. The area is bordered by Karacak volcano in the west, Telagabodas volcano in the north, Sawal volcano in the east-northeast, and Tertiary rocks of Southern Mountain in the south (Fig.I.2).

The physiography of Galunggung volcano may be divided into the volcanic cone, the caldera and the "hilly area". The volcanic cone is preserved in the western and southern parts, reaching altitudes up to 2168 m, and has an inactive crater known as Guntur crater or "Kawah Saat " (Dry Crater) at the summit. This crater has a circular form, 500 m across and 100 - 150 m deep, and is surrounded by a rim that is

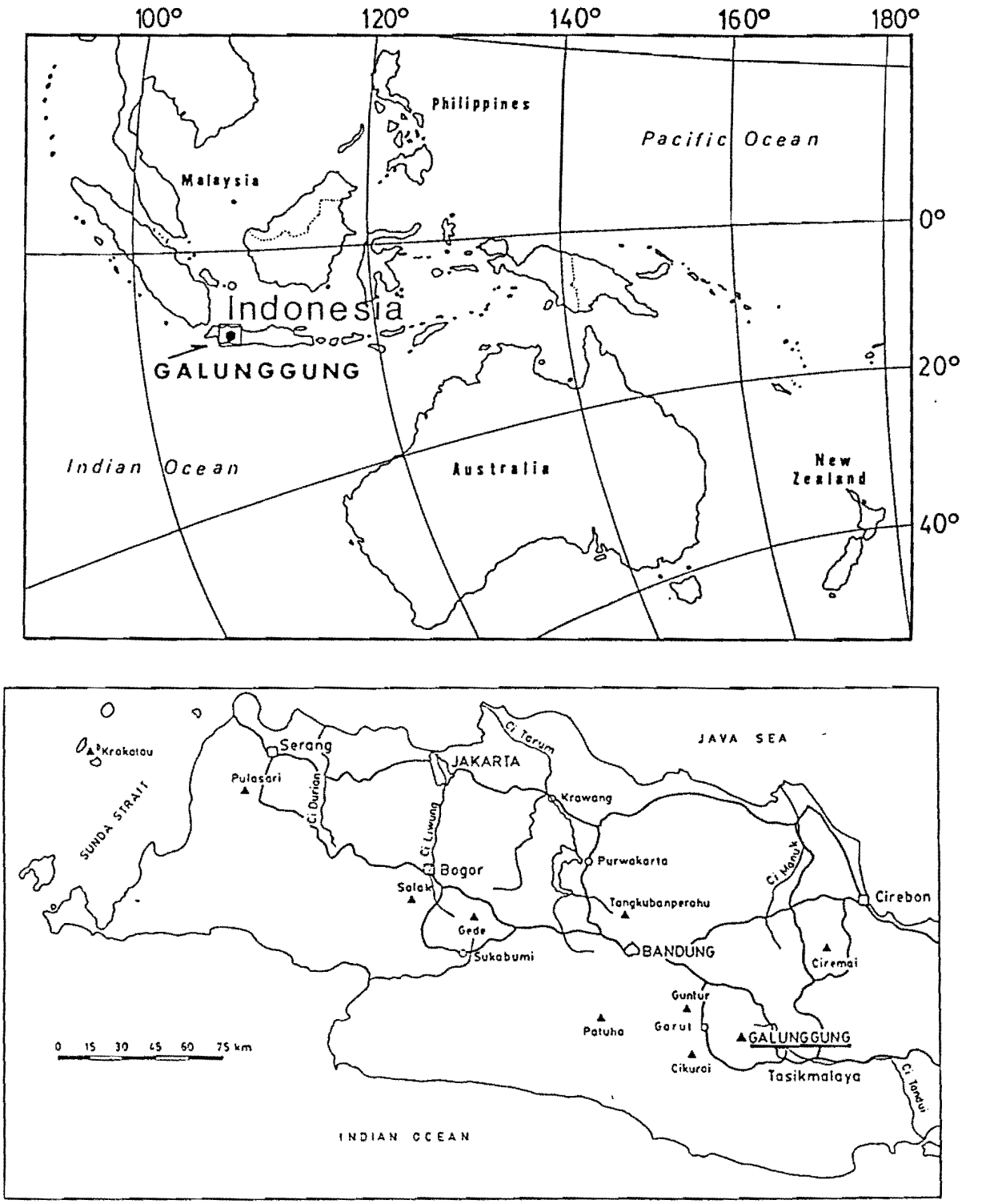

Figure I.1 Index map showing the location of Galunggung volcano in West Java, Indonesia.

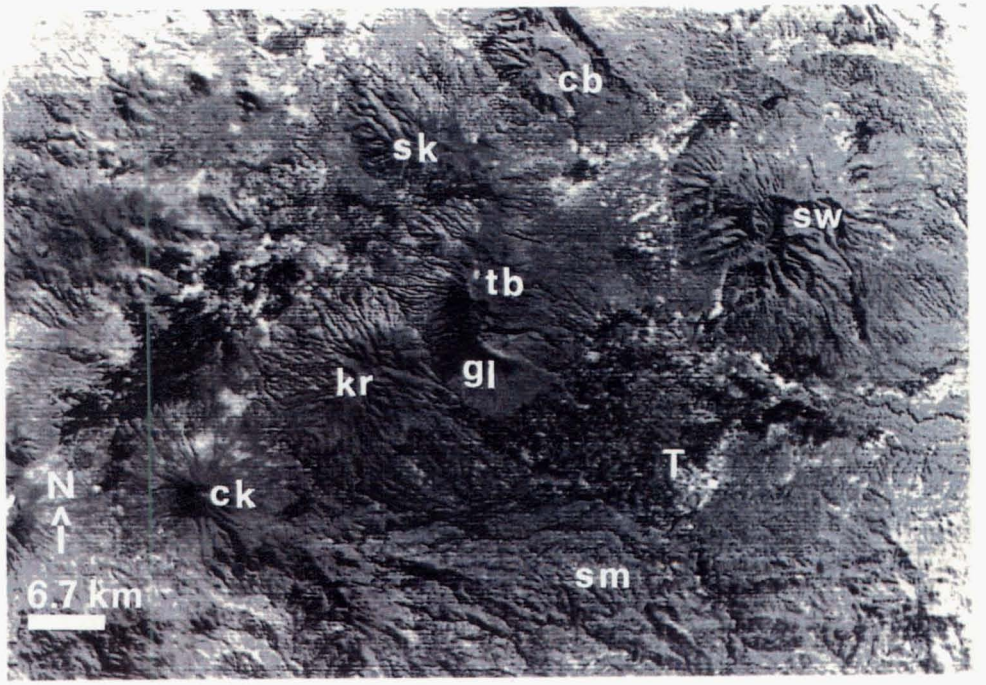

Figure I.2 Physiography of Galunggung volcano (gl) and surrounding areas (ck = Cikurai, kr = Karacak, tb = Telagabodas, sk = Sedakeling, cb = Cakrabuwana, sw = Sawal, T = Tasikmalaya city, sm = Southern Mountain).

Figure I.3 Galunggung caldera seen from Sinagar village (in the southeast). A depression at the top right is an old inactive crater. The active crater is behind Mount Welirang that is occupied by dark pyroclastic fall deposits erupted in 1982-83. The light coloured deposit is a pyroclastic flow deposit erupted in 1982 and deposited in Ci Banjaran valley, (28 August 1985, 08.00 h).

in places only 0.5 - 1.0 m wide. The southeast part of the old Galunggung crater is cut by the Galunggung caldera rim (Fig. I.3). The slope of the cone decreases from 30^{o} near the summit to 5^{o} on the lower slopes.

The caldera is horseshoe-shaped, opening to the east - southeast (Fig.I.3), and is 9 km long and 2 - 7 km wide. The height of the caldera wall decreases from about 1000 m in the west-northwest to 10 m in the east-southeast. The active crater is situated inside the caldera, and has a circular form approximately 1000 m across and 150 m deep. A cinder cone 250 m by 165 m across, and rising to 30 m above the crater floor was formed during the final stages of the 1982-83 eruption. As there are many waterfalls carrying debris into the active crater but no drainage out from it, a lake has formed around the cinder cone. In December 1986 the cinder cone was completely covered by water.

A "hilly area" is located east-southeast of Galunggung volcano, directly opposite of the open horseshoe-shaped caldera. The area is characterised by numerous hills on Tasikmalaya plain (351 m), and is known as "The Thousand Hills of Tasikmalaya". The hills are 5 - 50 m high, conical in form, and have slopes of 5 - 15^{o}.

Three main drainage patterns occur in Galunggung and surrounding areas : Ci Manuk to the north, Ci Tandui to the east and Ci Wulan to the south.

I.4 Previous Study

Since the eruption of October 1822, numerous papers have

described Galunggung activity. A list of the pre-1975 papers has been compiled by Kusumadinata (1979). The first historic activity at Galunggung (1822) was described by van den Elysinga (1822), van der Capellen (1823), Müller (1839), Junghuhn (1850) and Lyell (1872).

The next eruption (October 1894) was reported by de Kock (1895), Fennema (1896), Figee and Onnen (1897) and Veth (1903). An eruption of July 1918 was described by Escher (1919 & 1920), Visser (1919 & 1921), Kemmerling (1921), Taverne (1922) and Stehn (1923). Van Es (1924) described all of the above historic eruptions and gave a detailed account of the 1822 eruption.

Galunggung volcano has been observed intermittently since 1925 (e.g. Petroeschevsky, 1925; Stehn, 1935; Geological Survey of Indonesia, 1942; Adiwinata, 1950; Somantri, 1955; Adnawidjaja & Rothpletz, 1958; Hadikusumo, 1959; Kusumadinata, 1959; Suryo, 1959 a, b; Djajawinangun, 1963; Alzwar, 1969; and Partosentiko, 1972). Tulus et al. (1979) inspected the effects of the 1979 tectonic earthquake on the southern part of West Java including the Galunggung volcano.

A study of "The Thousand Hills of Tasikmalaya" was made by Escher (1925 & 1930), and Gorshkov (1959) compared the hills in Galunggung with the 1956 gigantic "directed blast" of Bezymianny. Geochemical data were first presented by Neumann van Padang (1951), and these, together with isotopic data, were reported by Whitford & Nicholls (1973, 1976), Whitford (1975a, b), Nicholls & Whitford (1976, 1978), Nicholls et al. (1980), and Whitford et al. (1979, 1981). Kusumadinata (1967 & 1979), and Hadian et al. (1974) prepared a volcanic hazards zonation map of Galunggung, based on topography and the distribution of volcanic products of recorded eruptions. Regional geologic mapping was done by Budhitrisna (1982).

Shortly before the eruption of 1982-1983, the Volcanological Survey of Indonesia carried out a series of investigations on Galunggung, including seismic monitoring (Rasjid, 1982) and geologic mapping (Juwarna et al., 1986; Miller, 1982; Wirakusumah, et al., 1981). Katili & Sudradjat (1984) compiled a list of data relating to the 1982-83 Galunggung eruption. Finally, volcanic hazard assessment was discussed by Sudradjat & Tilling (1984), and Suryo & Clarke (1985).

I.5 Accessibility

Tasikmalaya and another small city, Singaparna, can be reached by public transportation from Bandung where the main office of the Volcanological Survey of Indonesia is located. Galunggung volcano observatory is situated at Sayuran village, 6 km north of Singaparna. It can be reached by jeep or motorcycle. However, access to Galunggung caldera and surrounding areas is only by foot. Geological access to the caldera walls requires a rope (Fig. I.4). Galunggung crater is now filled by a lake, so the collection of data on the cinder cone and the crater wall can only be achieved by swimming or by means of a rubber boat (Fig. I.5-6).

The summit of Old Galunggung crater can only be reached from Parentas village on the northwest slope of Galunggung. A rope is needed to go up to the crater rim and down to the crater floor. During fieldwork, a base camp was established in Sayuran observatory. In addition, to the collection of rock samples in the Old Galunggung crater and the Galunggung caldera, two camps were established for 4 and 5 days.

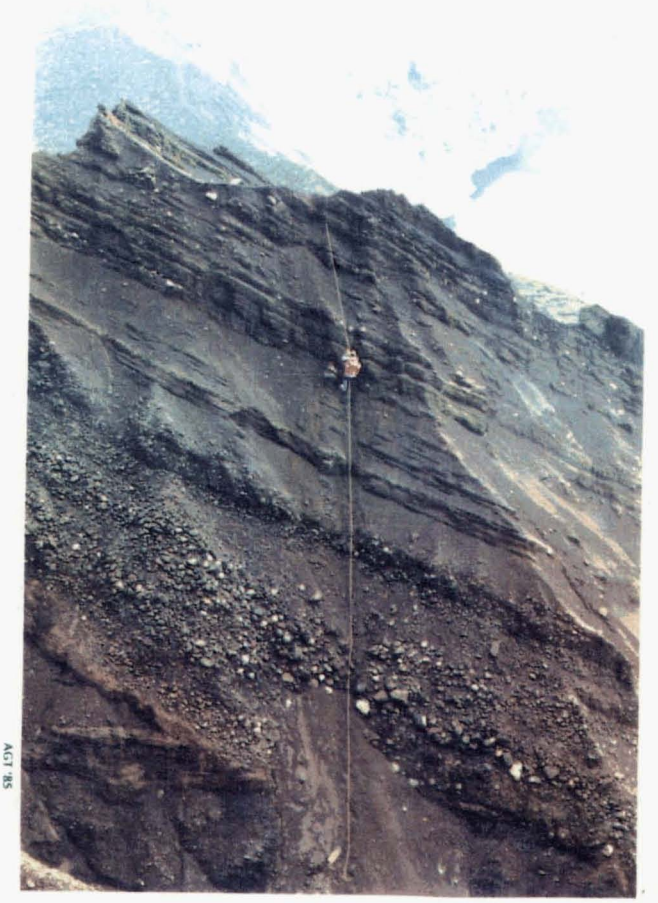

Figure I.4 Collecting rock samples from the wall of 1982-83 pyroclastic deposits. In the background is the Galunggung active crater lake, (28 July 1985, 11.00 h).

Figure I.5 Swimming across the lake to collect rock samples from the 1982-83 cinder cone, (30 July 1985, 10.30 h).

Figure I.6 Collecting rock samples from the crater wall using a rubber boat, (6 September 1985).

The fieldwork was completed between early July and early October 1985. Theoretically, that was a dry season in the area. However, it rained frequently and the higher parts of Galunggung, above 1000 m, were nearly always cloudy. A second period of fieldwork and data compilation in Indonesia was done between October and December 1986.

Sampling lava flows and volcanic bombs in the Galunggung caldera wall could not always be done systematically because the wall in places is almost vertical and reaches up to 1000 m in height.

II GEOLOGICAL SETTING

II.1 Introduction

The geology of West Java was first described by van Bemmelen (1949) and the Geological Survey of Indonesia (GSI, 1977). The area was then systematically remapped at a scale of 1 : 100,000 (e.g. Budhitrisna, 1982; Djuri, 1973; Kastowo, 1975) by the Geological Research and Development Centre (GRDC; before 1979 known as GSI).

Recent studies (e.g. Martodjojo, 1984) have revised and added some new names based on formal lithostratigraphic practice. In addition, deep oil drilling exploration (> 3000 m) in the northern part of West Java and in the Java Sea has provided new information particularly on basement metamorphic rocks (e.g. Padmosukismo & Yahya, 1974).

In this discussion, a local geologic map of Tasikmalaya (Budhitrisna, 1982) is presented, together with the stratigraphic interpretation of Martodjojo (1984).

In general, the oldest rocks exposed on West Java are Late Cretaceous - Eocene in age. Sedimentary and volcanic rocks interdigitated until the Pliocene when the whole area was uplifted, and some areas were covered by Quaternary volcanics. Intrusive activity also occurred during the period of uplift.

II.2 Physiography of West Java

West Java can be divided into five physiographic regions (Fig. II.1). The **Plain of Jakarta** is a low plain, about 40 km wide, extending from Serang to Cirebon in the northern part of West Java. The low plain consists mainly of alluvial and lahar deposits from volcanoes in the hinterland, with occasional exposures of slightly folded older sediments.

The **Bogor Zone** is an area of hills and mountains, about 40 km across, to the south of the Plain of Jakarta. Hills are composed of strongly folded strata whereas the mountains consist of intrusions such as the Sanggabuwana Complex, West of Purwakarta.

The **Bandung Zone** is a series of longitudinal ridges and intermontane depressions, situated in the central part of West Java, and 40 km wide. The ridges comprise old sediments, whereas the depressions are filled with young volcanics and alluvial deposits derived from the surrounding areas. The depressions form the high plains of Sukabumi (600 m), Cianjur (459 m), Bandung (715 m), Garut (711 m) and Tasikmalaya (351 m).

In the southern part of West Java, the **Southern Mountain Zone** has an average width of 50 km and a gentle slope southward to the Indian Ocean. The central part of this zone (Pengalengan section) is a high mountainland with several peaks over 2000 m, whereas the western (The Jampangs) and eastern parts (Karangnunggal section) are lower, reaching altitudes of about 1000 m.

In general, **Quaternary Volcanoes** occur in the central part of West Java. They are interjacent to the high plains or at the border between Bandung Zone and Bogor Zone or between Bandung Zone and South-

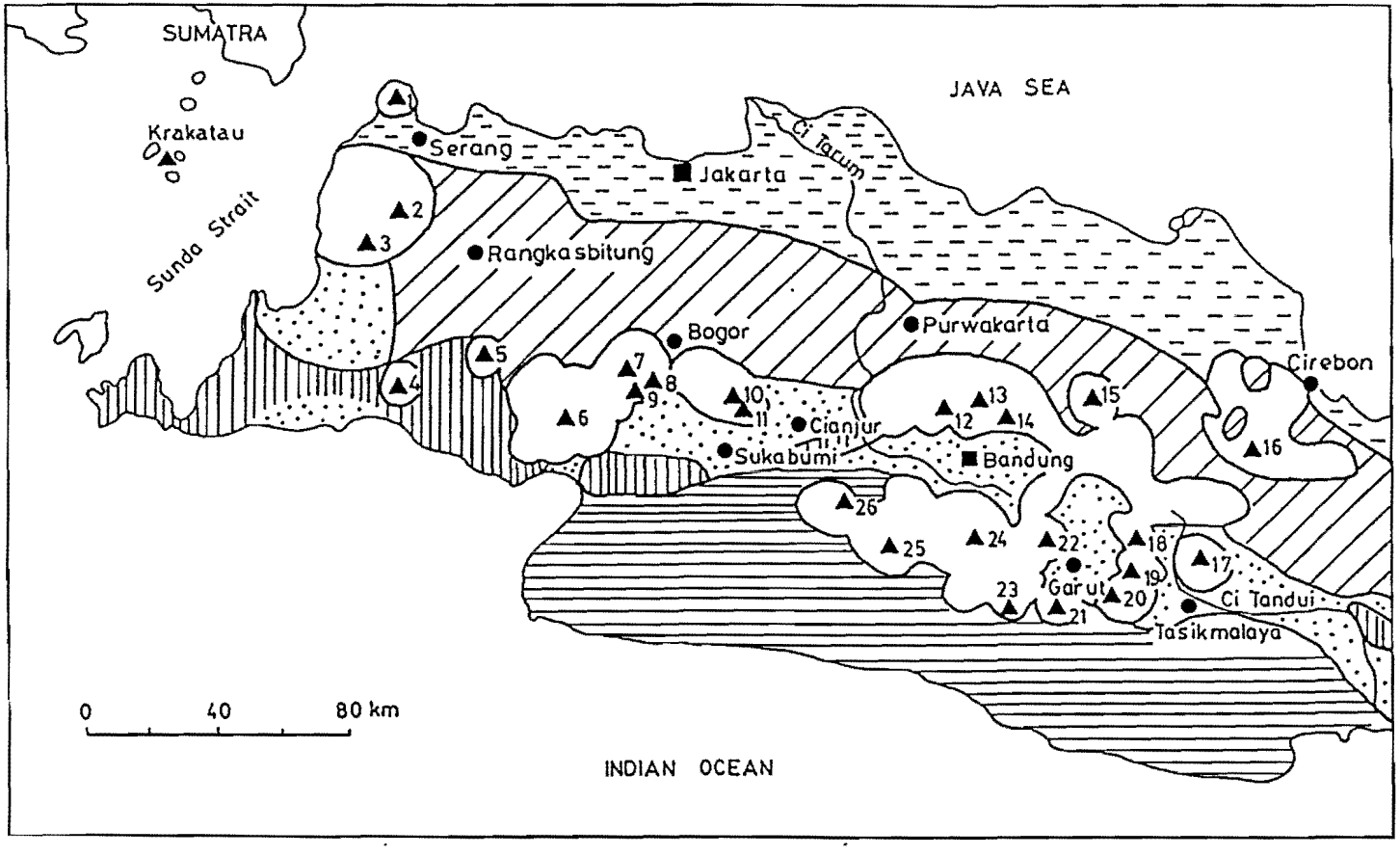

Figure II.1 Physiographic sketch map of West Java simplified after van Bemmelen (1949).

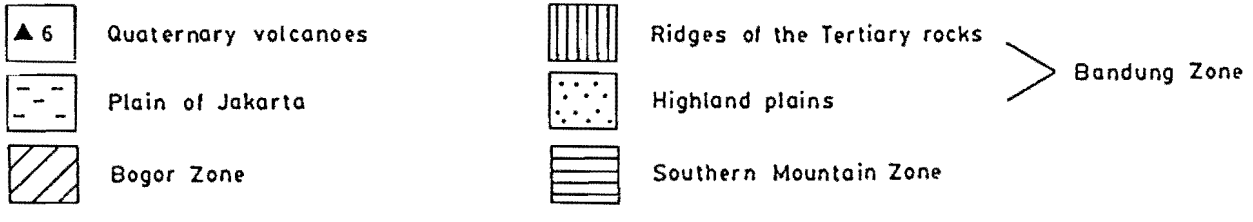

ern Mountain Zone. Galunggung, together with Karacak and Telagabodas volcanoes, separates Garut from Tasikmalaya high plains.

II.3 Stratigraphy

On the basis of sedimentary characteristics of Tertiary rocks, Martodjojo (1984) has divided West Java into three regional areas (Fig. II.2). The **Continental Platform** is in the northern part of West Java, and corresponds closely to the physiographic region of the Plain of Jakarta. This area is characterised by shallow marine sedimentary rocks up to 5000 m thick, and a simple geological structure.

The **Bogor Basin** includes Bogor, Bandung and Southern Mountains Zones of van Bemmelen (1949). The sediments in this area are mostly derived from igneous and sedimentary rocks (e.g. andesite, basalt, tuff and limestone) and are estimated to be more than 7000 m thick. These rocks are interpreted as gravity flow deposits (Martodjojo, 1984) deposited in an intra-arc basin overlying Paleogene rocks of fore-arc basin (Syahbuddin et al., 1986).

The **Banten Area** (Rangkasbitung Basin, Syahbuddin et al., 1986) is located in the western part of West Java. According to Syahbuddin et al. (1986) this basin has changed from fore-arc (Cretaceous - Early Tertiary) to intra-arc (Late Eocene - Oligocene) through back-arc basins during Early Miocene. The Rangkasbitung Basin is probably separated from the Bogor Basin by a major fault.

Most Quaternary volcanoes, including Galunggung, are situated in the Bogor Basin. So, in the following section, discussion of the stratigraphy will concentrate on the area, and in particular the

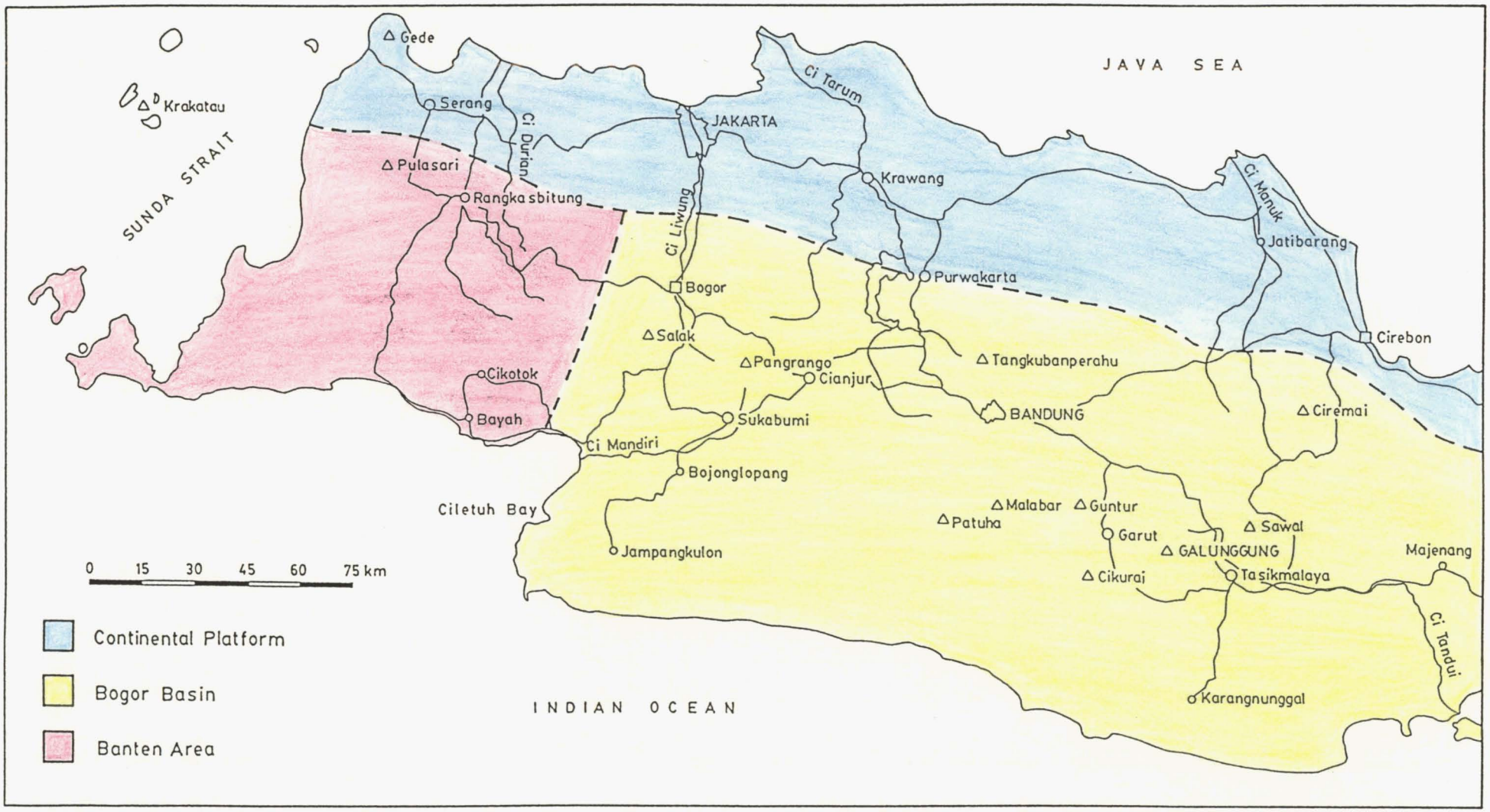

Figure II.2 Sedimentation areas in West Java modified after Martodjojo (1984) and Syahbuddin et al. (1986).

Tasikmalaya region.

II.3.1 Cretaceous - Eocene

The general stratigraphy of the Bogor Basin is shown in Table II.1. The oldest rocks (Cretaceous - Eocene age) in West Java are a melange complex (Thayib et al., 1977) comprising metamorphosed basic and ultrabasic rocks (peridotites, gabbros and pillow lavas) and sedimentary rocks (serpentinite, chloritic schists, phyllites and quartzites) together with chert, black shale, greywacke and limestone (Martodjojo et al., 1978). These rocks are exposed in the southwestern part of West Java (Ciletuh area). Elsewhere on Java, the melange complex is only found in Luk Ulo and Jiwo Hills, Central Java, but basic and ultrabasic rocks are absent.

The basic and ultrabasic rocks of the melange complex in the Ciletuh area have a similar age to granite intrusions in the Java Sea, the andesitic to basaltic volcanic rocks exposed at Cikotok (South Banten area), and the subsurface Jatibarang Formation found in the northern part of West Java (Arpandi and Padmosukismo, 1975; Martodjojo, 1984; Padmosukismo and Yahya, 1974; Samsu, 1975). The Jatibarang Formation unconformably overlies Triassic metamorphic basement rocks and rocks of the formation are dated at 215 Ma (Martodjojo, 1984).

The intrusive and volcanic rocks may represent Cretaceous - Eocene volcanism in West Java. The Ciletuh melange appears to represent the old subduction zone, whereas eruptive centres in the Java Sea and an area between Cikotok and Jatibarang may represent a magmatic arc (Fig. II.3).

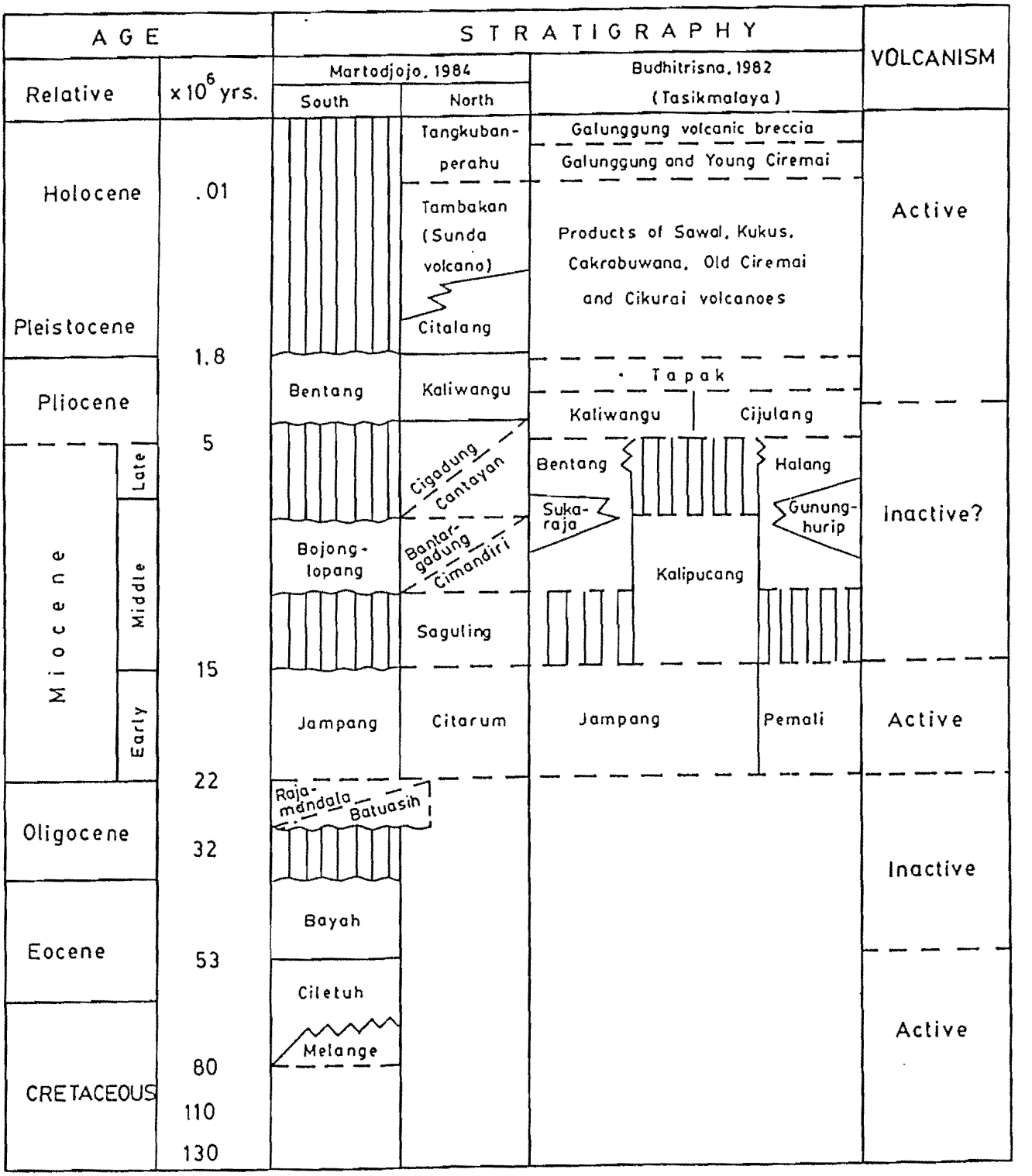

Table II.1 History of the Bogor Basin simplified after Budhitrisna (1982) and Martodjojo (1984).

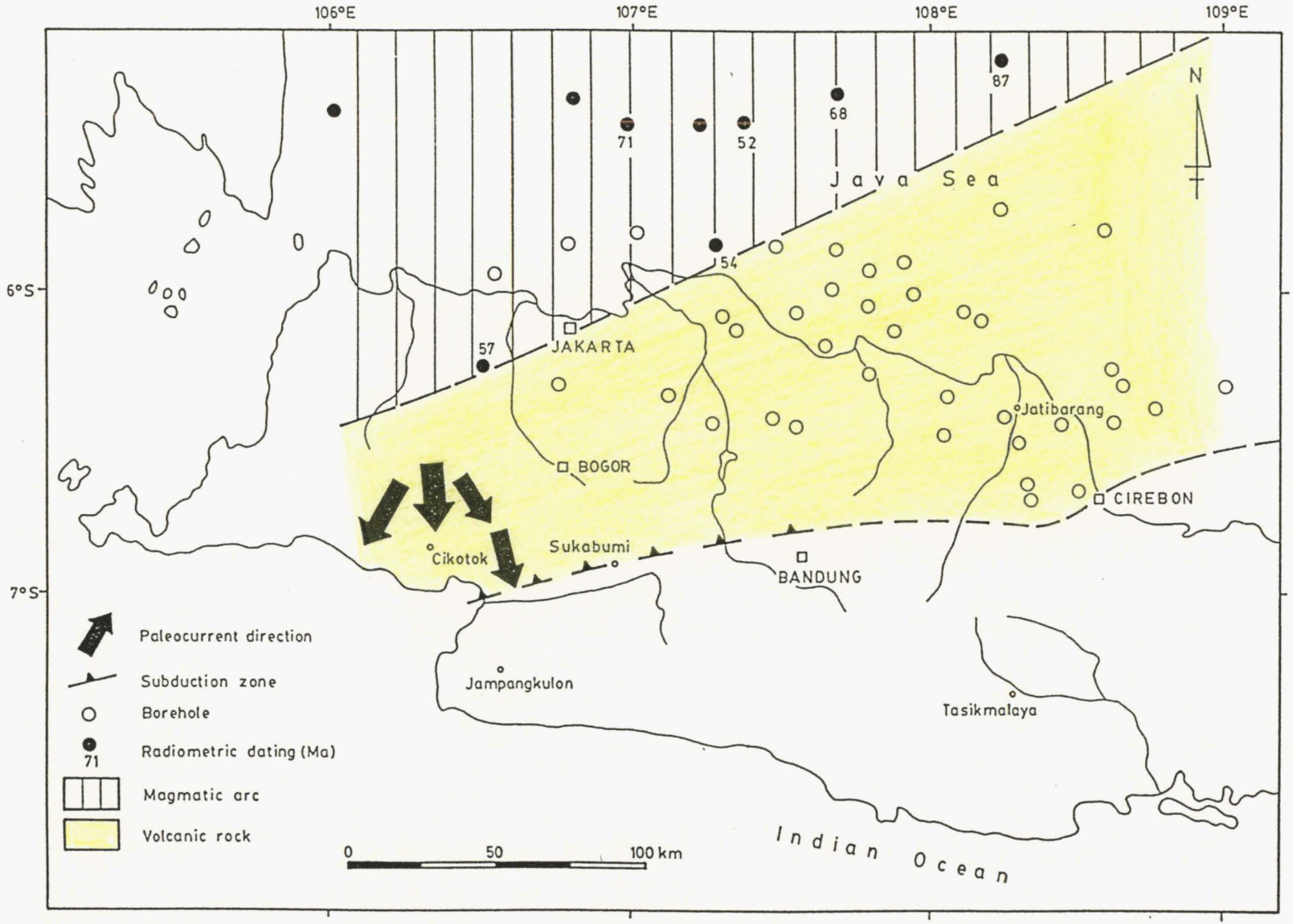

Figure II.3 Cretaceous volcanism in West Java modified after Martodjojo (1984).

The melange complex is overlain by the Ciletuh Formation, comprising sedimentary rocks which are also well exposed in the Ciletuh area. This formation consists of claystones and shales, alternating with sandstones in the lower part, whereas the upper part is composed of quartz sandstones and breccias. The total thickness of the Ciletuh Formation is about 1400 m. The contact between the melange complex and the Ciletuh Formation is always faulted. Previous studies (e.g. van Bemmelen, 1949; Soekamto, 1975; Thayib et al., 1977) assumed that the melange complex was unconformably overlain by the Ciletuh Formation. However, Martodjojo et al. (1978) and Martodjojo (1984) interpreted that the contact between the two units is "conformable". On the basis of the accretionary prism model (Karig, 1975; Karig et al., 1979, 1980; Karig & Sharman, 1975; Moore & Karig, 1980), the Ciletuh Formation is considered to be "pond" deposits on the inner slope of the subduction trench and the original contact with the underlying melange complex was depositional. "Pond" deposits in North Island of New Zealand (Johnstone, 1975; van der Lingen & Pettinga, 1980) are also reported to overlie unconformably the melange deposits.

The Bayah Formation conformably overlies the Ciletuh Formation. The lower part of this unit is dominated by quartz sandstones, gradually changing upwards to interbedded sandstones, claystones and coals. The thickness of this formation varies from 200 m to 1500 m.

II.3.2 Oligocene

Oligocene sedimentary rocks are divided into Batuasih and Rajamandala Formations. The Batuasih Formation consists of calcareous

claystones with intercalations of thin sandy siltstone. Pyrite is common. This formation has a thickness of 110 m to 570 m. The Rajamandala Formation is mainly limestones, up to 100 m thick. The two formations are likely to represent a facies change from anaerobic marginal marine (the Batuasih Formation) to shallow marine (the Rajamandala Formation) environments.

II.3.3 Miocene

Miocene rocks are volcanic or sedimentary. The volcanic rocks, previously named "Old Andesite Formation" (Verbeek and Fennema, 1896; van Bemmelen, 1949), are now grouped into the Jampang Formation in the south and Citarum Formation in the north (Martodjojo, 1984). In the lower part, the Jampang Formation is dacitic to andesitic composition, and comprises mostly fine-grained volcaniclastics up to lapilli size. The upper part is dominated by basaltic breccias and lavas with occasional clasts of limestone. The thickness of the formation is at least 2000 m. Small intrusions of diorite and dacite (Fig. II.4) are found in the south and southeast of Galunggung (Budhitrisna, 1982). The Citarum Formation mainly consists of tuffaceous sandstones, siltstones and claystones, with intercalations of marl, and has a total thickness of more than 1250 m.

In the Jampang Formation, lava flows only occur around Jampang-kulon where there is a large positive gravity anomaly (more than 200 mgals; Untung, 1974; LEMIGAS, 1975). In addition, paleocurrent directions in the breccias suggest a derivation to the south or southwest (Fig.II.5). These probably represent exposed vent areas.

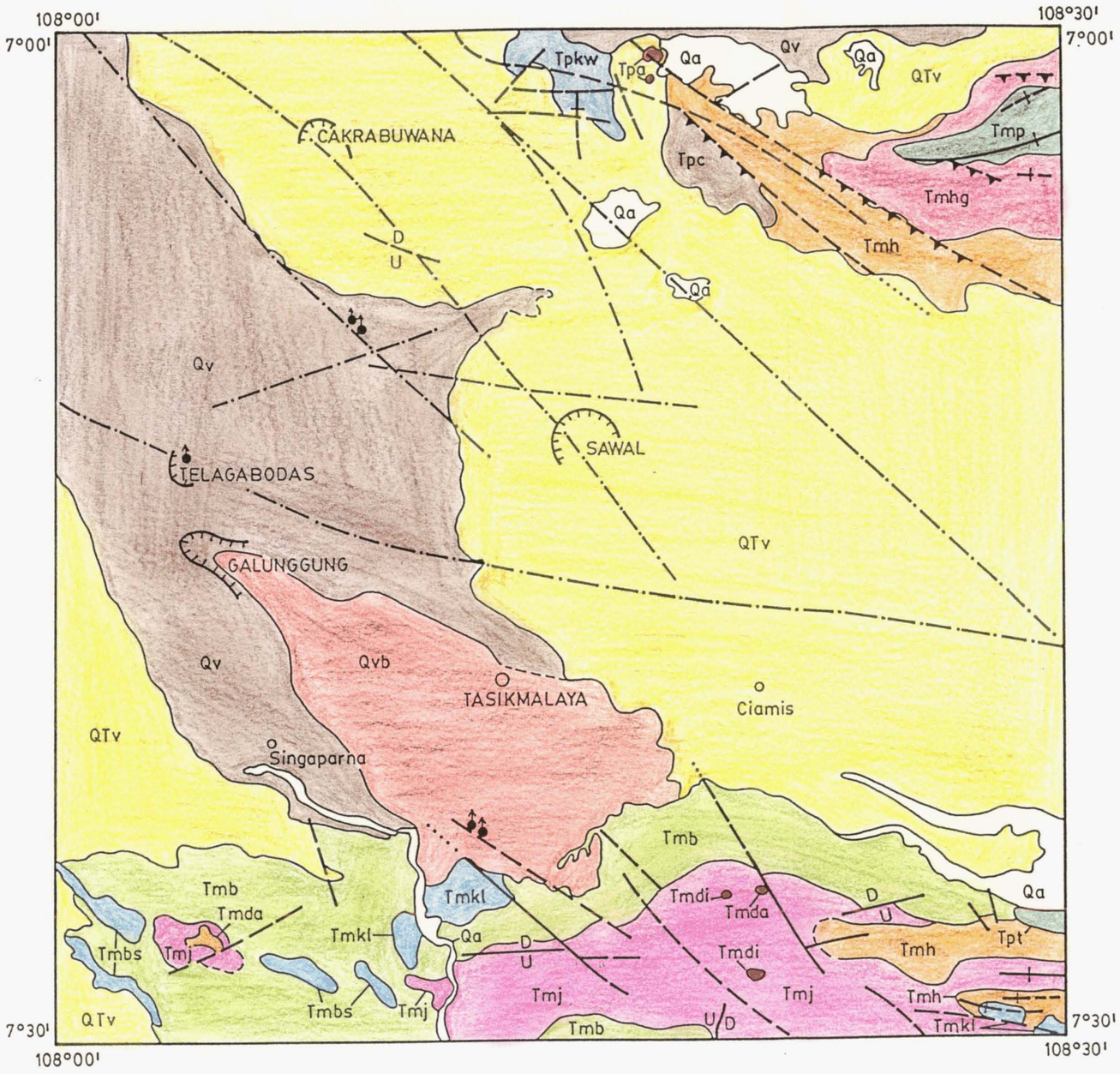

EXPLANATION

- Qa — Alluvium
- Qvb — Galunggung volcanic breccias
- Qv — Young volcanic products
- QTv — Old volcanic products
- Tpt — Tapak Formation: sandstones and sandy marls
- Tpkw — Kaliwangu Formation: claystones, sandstones, conglomerates and limestones
- Tpc — Cijulang Formation: andesitic volcanic breccias, lavas, dikes and tuffs
- Tmh — Halang Formation: sandstones, siltstones and claystones
- Tmhg — Gununghurip Member of Halang Formation: volcanic breccias and conglomerates
- Tmb — Bentang Formation: tuffaceous- and calcareous sandstones, conglomerates and breccias
- Tmbs — Sukaraja Member of Bentang Formation: sandy- and reef limestones
- Tmkl — Kalipucang limestone : coral limestones
- Tmp — Pemali Formation: globigerina marls
- Tmj — Jampang Formation : andesitic to basaltic volcanic breccias, lavas and tuffs

- Tpa — Andesite, hornblende andesite
- Tmda — Dacite
- Tmdi — Diorite
- Caldera or crater rim
- Hot spring

0 5 10 15 20km

- Thrust fault
- Normal fault (U/D)
- Fault
- Lineament
- Fold

Figure II.4 Geologic map of Tasikmalaya quadrangle, West Java (Budhitrisna, 1982).

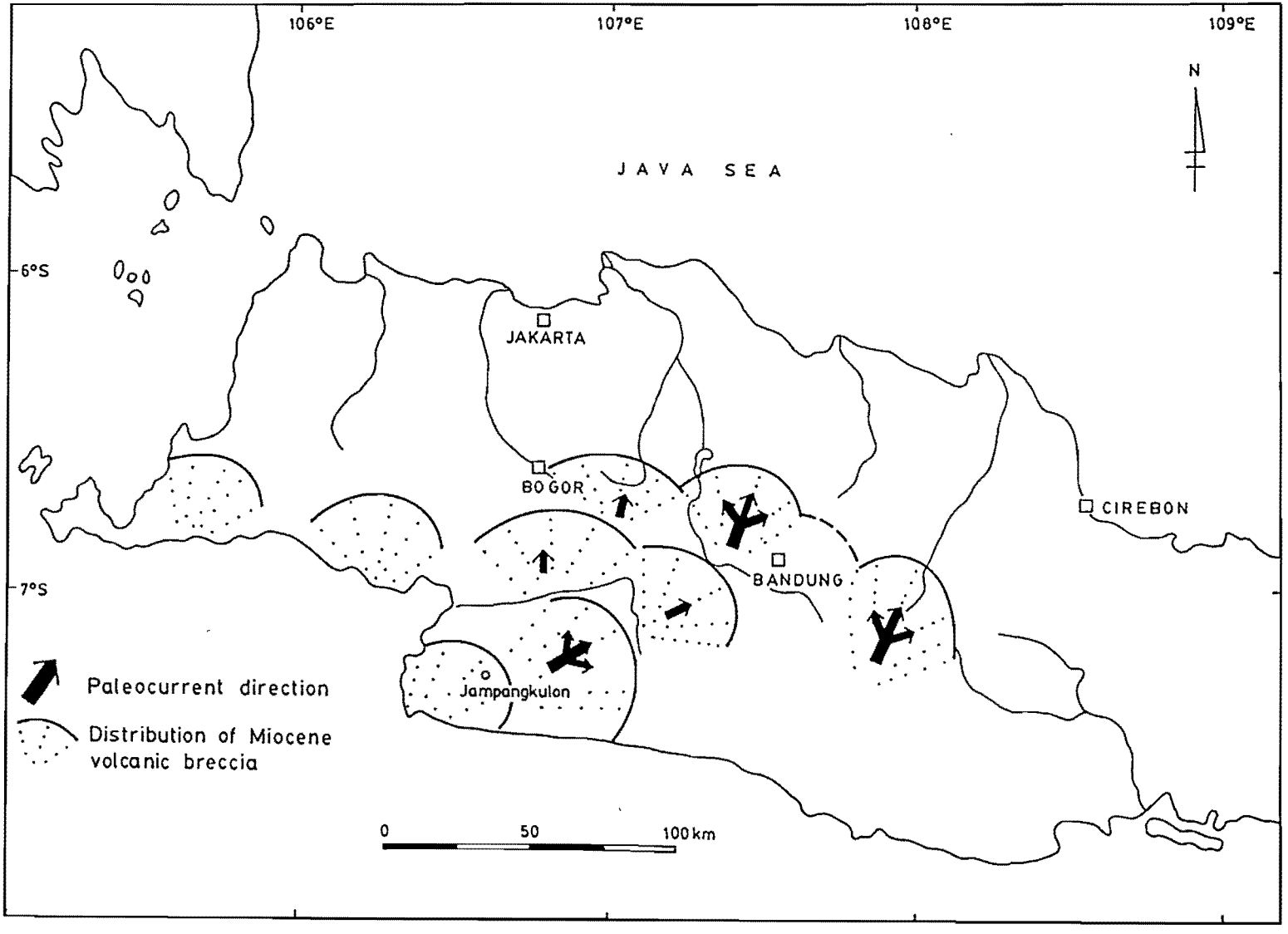

Figure II.5 Distribution of Miocene volcanic breccias and their paleocurrent directions (Martodjojo, 1984).

Early Miocene sedimentary rocks are named the Pemali Formation and comprise Globigerina marls with intercalated sandy limestones. These rocks are exposed in the northeastern part of Tasikmalaya quadrangle and have a maximum thickness of about 500 m. In the north of the area (Arjawinangun quadrangle) the rocks form the Cinambo Formation (Djuri, 1973; Martodjojo, 1984).

Sedimentary rocks deposited during Middle Miocene are grouped into four formations (Table II.1). In the northern part of the Bogor Basin, the Saguling Formation consists of sedimentary breccias, thinning upwards, whereas greywacke sandstones thicken, and has a total thickness of about 1750 m. The Bantargadung Formation consists of alternating tuffaceous sandstones and claystones, up to 640 m thick, and the Cimandiri Formation of claystones with intercalated conglomerates, sandstones and limestones containing abundant mollusca fossils. The Bantargadung and the Cimandiri Formations have similar ages and are considered to be facies equivalents, conformably overlying the Saguling Formation. Although limestones are intercalated with clastic sediments, they are also given formation status, e.g. the Bojonglopang Formation in the southern part of the Bogor Basin.

Late Miocene sedimentary rocks occur also in four formations. The Cigadung Formation is located in the west (Ci Mandiri valley), the Cantayan Formation in the north (southwest Purwakarta), the Halang Formation in the east (Tasikmalaya) and the Bentang Formation in the south. These formations consist of breccias alternating with conglomerates, tuffaceous sandstones, siltstones, claystones and rarely limestone. The total thickness of these rocks approaches up to 700 m. According to Martodjojo (1984) these rocks are the youngest marine sediments in the Bogor Basin.

II.3.4 Pliocene

Pliocene volcanic and sedimentary rocks both occur in West Java. The volcanic rocks comprise andesitic breccias, lavas, dikes and tuffs which are locally distributed in the eastern part of West Java. The volcanic rocks form the Cijulang Formation in the Tasikmalaya quadrangle (Budhitrisna, 1982) and the Kumbang Formation to the east (Majenang quadrangle; Kastowo, 1975). The maximum thicknesses of the Cijulang Formation and the Kumbang Formation are approximately 1000 m and 2000 m respectively. Many small intrusions of andesite and dacite, e.g. Sanggabuwana Complex in southwest Purwakarta, around Ciremai volcano and in Majenang area are considered to be associated with the Pliocene volcanic rocks.

Pliocene sedimentary rocks occur in the north (the Kaliwangu Formation), whereas in the south and east they occur in the Tapak and Bentang Formations. The Kaliwangu Formation is widely distributed from south of Krawang to Cirebon, and is composed of tuffaceous sandstones and claystones with intercalated lignites and conglomerates. It is also characterised by abundant mollusca. The maximum thickness is approximately 1000 m. The Kaliwangu Formation is the only formation which extends across two physiographic regions, the Bogor Basin in the south (intra-arc basin) and the Plain of Jakarta (back-arc basin) in the north (Martodjojo, 1984). The Tapak-Bentang Formations comprise mainly sandstones and marls with intercalated breccias and limestones, and up to 500 m thick.

II.3.5 Pleistocene - Recent

From Pleistocene to Holocene, West Java was dominated by volcanism. "Reworked" Pleistocene volcanic rocks in the northern part of West Java are grouped into the Citalang and the Tambakan Formations (Martodjojo, 1984), whereas there are many extinct volcanoes (e.g. Sunda), and active volcanoes, such as Tangkubanperahu.

In the Tasikmalaya region, Quaternary extinct volcanoes include Cakrabuwana, Cikurai, Karacak, Kukus, Old Ciremai and Sawal, while active volcanoes include Galunggung, Telagabodas and (Young) Ciremai. Volcanic deposits from Galunggung caldera are termed "Galunggung volcanic breccias" (Budhitrisna, 1982).

The Citalang Formation consists of interbedded conglomerates and tuffaceous sandstones with intercalated breccias, siltstones and claystones. These are up to 1000 m thick, contain vertebrate fossils (van Bemmelen, 1949), and were deposited on alluvial plain or braided stream (Martodjojo, 1984). The Tambakan Formation is mainly composed of laharic breccias with intercalated sandy tuffs, claystones and lignites, having a maximum thickness of approximately 470 m.

II.4 Geological Structure

A study of Landsat images on West Java (Fig.II.6) reveals that there are four major lineaments : N45^{o}E, N10^{o}W, N30^{o}W and N55^{o}W. A high density of lineaments is found in the vicinity of Bogor and southwest Cirebon, with a concentration of shallow and intermediate earthquake foci around the Bogor lineaments.

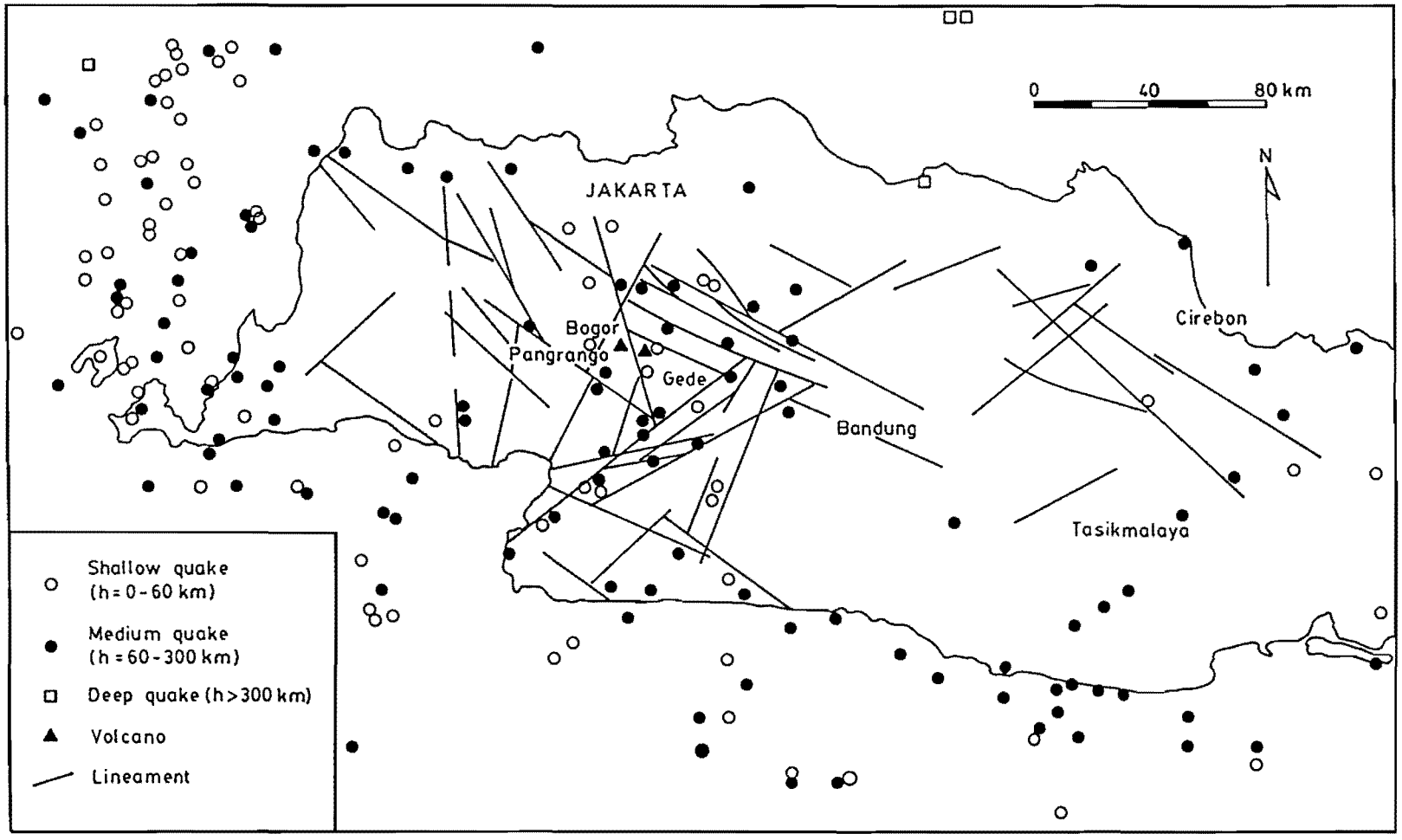

Figure II.6 Lineament patterns from landsat images and distribution of earthquake epicentres (Suwijanto, 1978).

Some of the lineaments are related to the fault patterns in West Java which have three main directions (Fig.II.7) : southwest - northeast faults (e.g. Cimandiri Fault), northwest - southeast (e.g. Baribis Fault), and north - south (e.g. Cidurian Fault). The first two groups are dominantly strike-slip faults (Katili & Sudradjat, 1984), whereas the north-south faults are dominantly normal (Padmosukismo & Yahya, 1974). The three fault systems all affect the Triassic - Jurassic basement metamorphic rocks (Koesoemadinata & Pulunggono, 1975).

The three fault orientations are also dominant in the wider region of Kalimantan, Java and Sumatra (Fig.II.8). In the west, a northwest direction ("Sumatra Fault System") predominates, whereas in the western and eastern parts of the Java Sea, the faults are north and northeast striking ("Meratus Trend"), respectively.

The northwest trending fault system in Sumatra is represented by the Sumatra Fault (Katili & Hehuwat, 1967; Katili, 1970), extending the whole length of Sumatra (1650 km long). This is an active dextral strike-slip fault with a lateral displacement of 20-25 km and a horizontal slip-rate of about 6 cm/yr. Considerable differential vertical movements must also have taken place, producing basins and intervening highs (Koesoemadinata & Pulunggono, 1975). The basins are elongate in shape parallel to the Sumatra Fault; several may be of caldera origin.

The northeast striking faults are found mostly from geophysical and oil drilling exploration programmes. The north trending faults are normal and represent extension related to the other systems developed when the Indian Ocean - Australian plate moved to the north in Cretaceous - Early Paleogene.

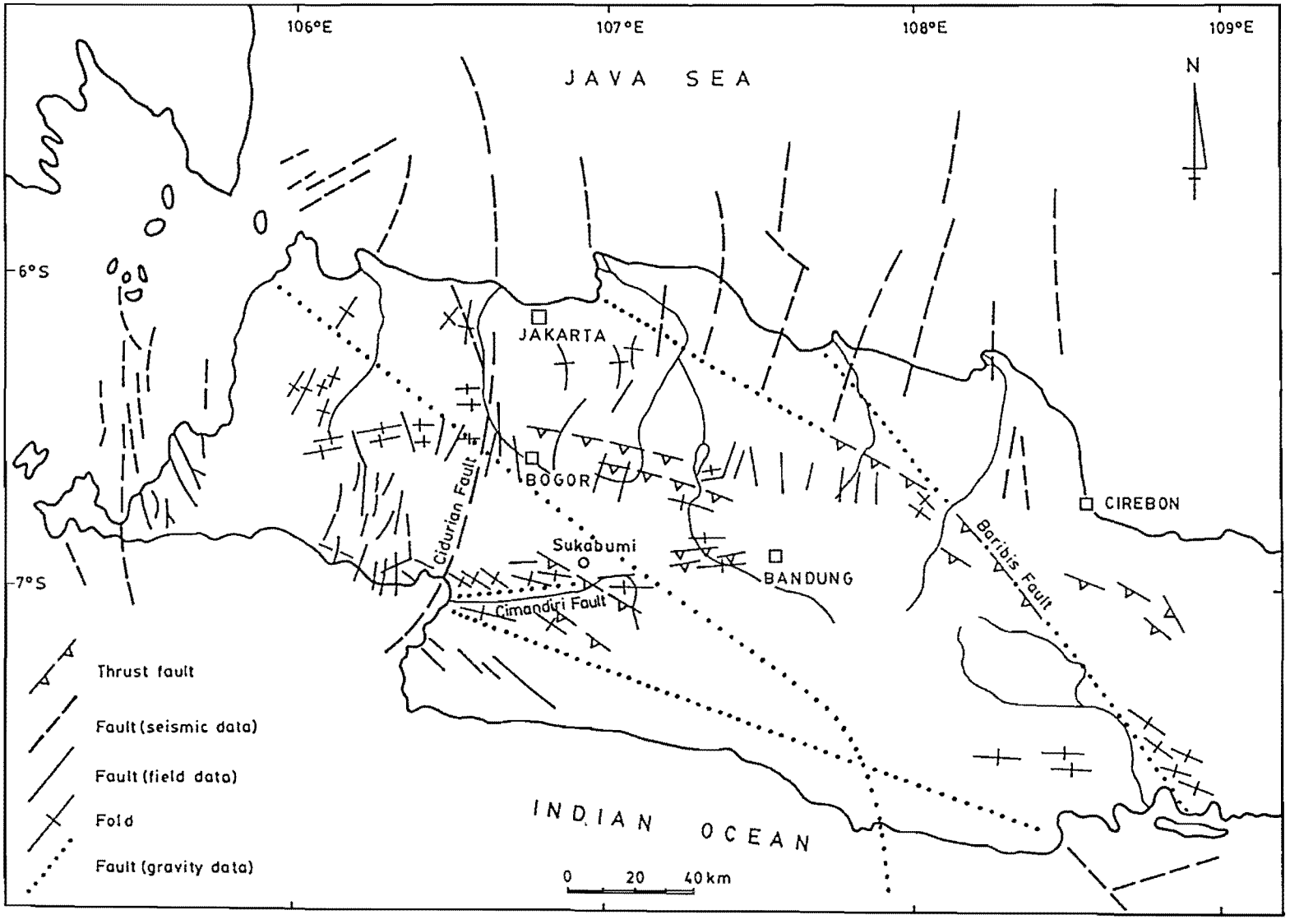

Figure II.7 General geological structure of West Java (Martodjojo, 1984).

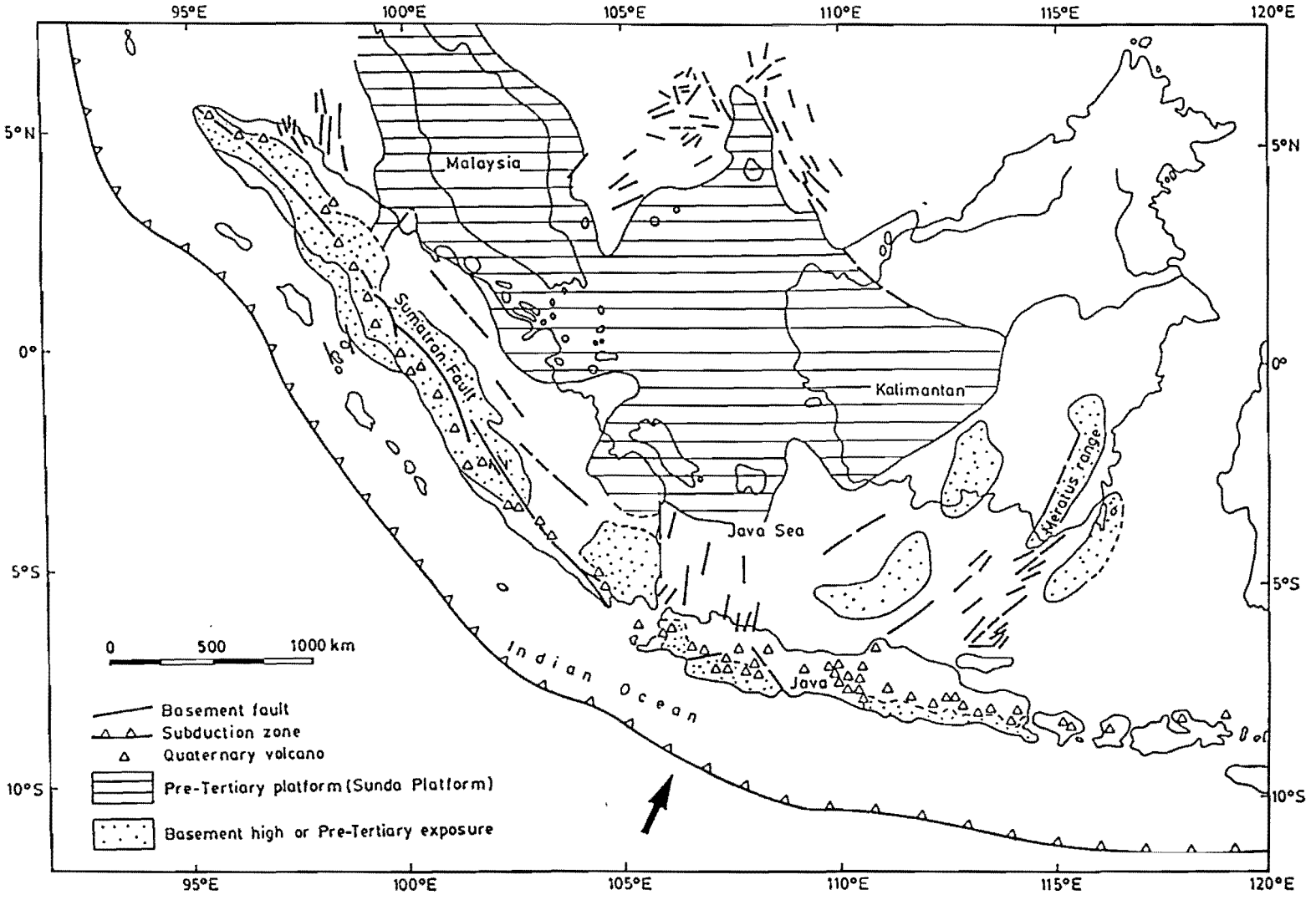

Figure II.8 Major tectonic framework of the Western Indonesia simplified after Koesoemadinata & Pulunggono, 1975 and Moore et al., 1980.

II.5 Tectonic Evolution

Tectonically, Indonesia is very complex as it lies at the junction between three lithospheric plates, namely the Indian - Australian, the Pacific and the Eurasian plates (Katili, 1975). The boundaries of these plates are either represented by trenches or strike-slip faults.

Western Indonesia is tectonically related to the plate movements associated with the opening of the Indian Ocean (Fig.II.9). In the Early Cretaceous (130 - 80 Ma), India drifted away to the northwest from Antarctica-Australia along a transform fault known as the Wallaby Fracture Zone. The transform fault is parallel to the Sumatra Fault which possibly dates from this period.

In the Cretaceous - Early Paleogene (80 - 50 Ma), the Indian Ocean plate moved rapidly (15.0 - 17.5 cm/yr) to the north with the respect to Antarctica. Consequently, the plate was obliquely subducted along a transform fault in the west of Sumatra but nearly perpendicular to Java. This produced volcanism in Western Indonesia (Fig.II.10) which forms a terrestrial volcanic arc separated from the Sunda Platform by back arc basins (Koesoemadinata & Pulunggono, 1975). The Jatibarang Formation and volcanic rocks at Cikotok were formed in the intra-arc basin. Volcanism ceased from 50 - 30 Ma probably due to the slow rate of movement (3 - 7 cm/yr) of the Indian Ocean plate. The area submerged, and deposition in the Bogor Basin formed the Ciletuh, Bayah, Batuasih and Rajamandala Formations.

The Indian Ocean and Australian plates united 32 Ma ago as a single plate moving to the north northeast ($N30^{o}E$?) at a rate of 5.0 - 6.5 cm/yr (Martodjojo, 1984), and causing the Miocene volcanism

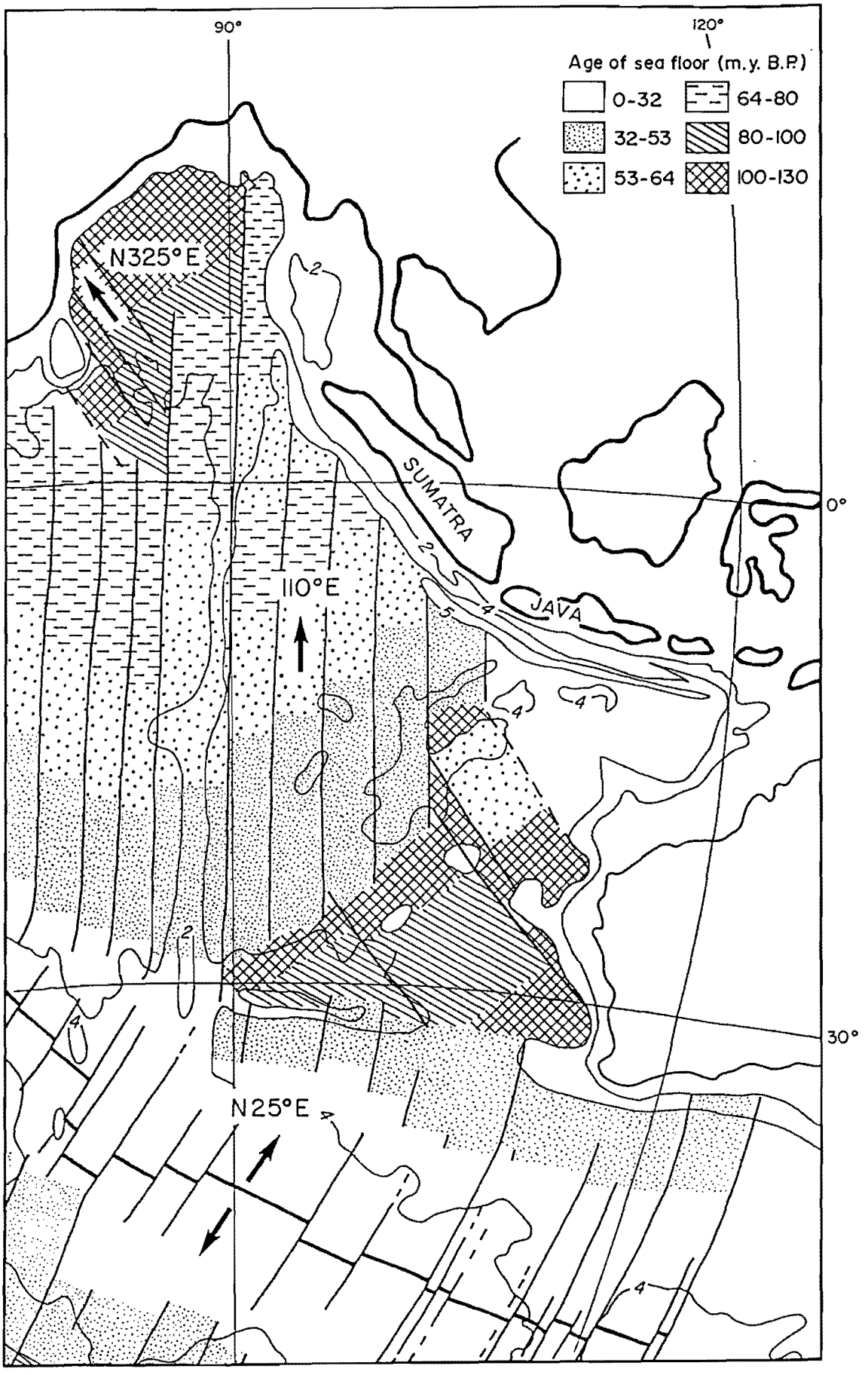

Figure II.9 Age of sea-floor basement in Indian Ocean (modified after Johnson et. al, 1976).

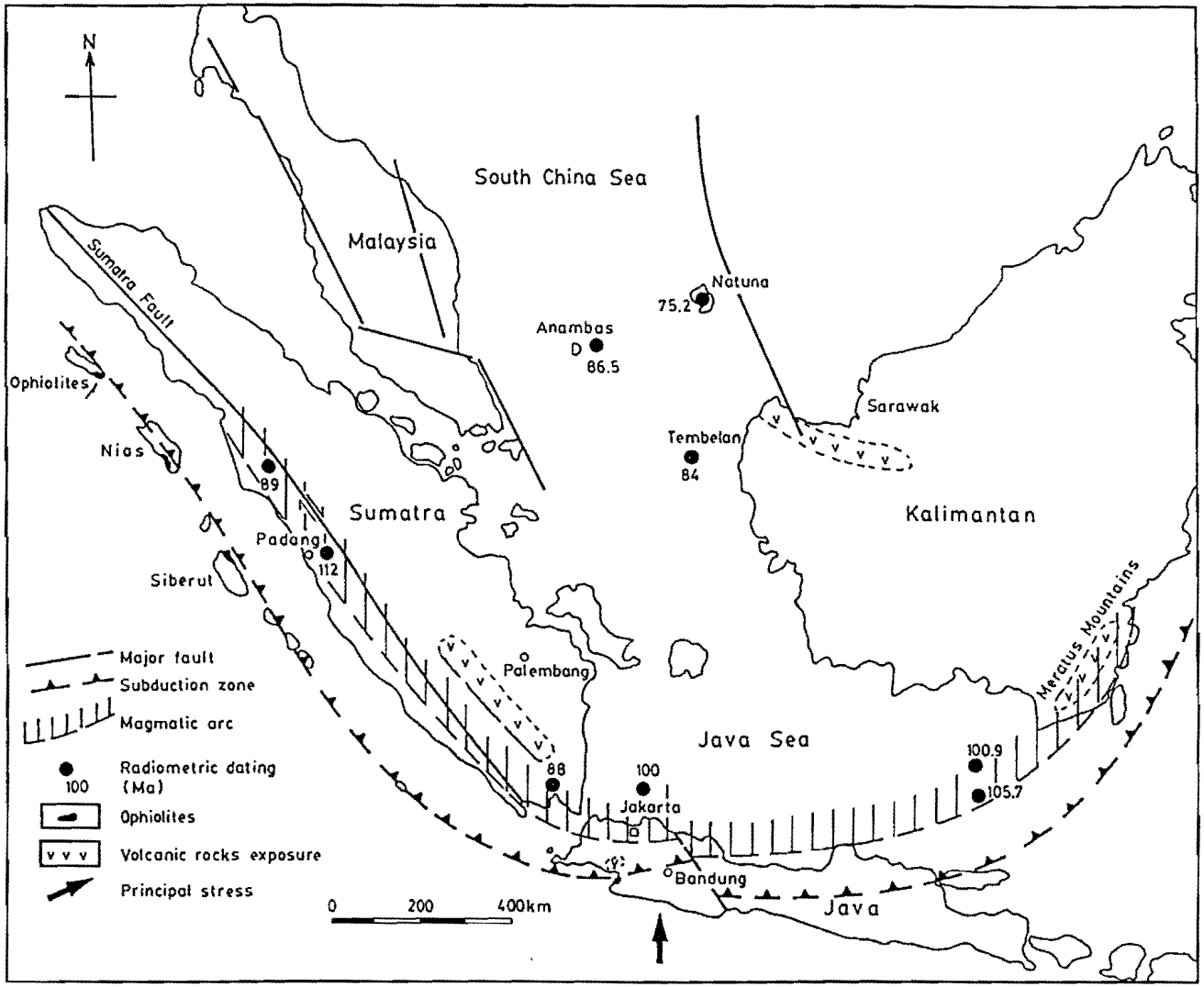

Figure II.10 Cretaceous volcanism in Western Indonesia (modified after Hutchison, 1973; Katili, 1973b, 1975; Sano et al., 1978).

(Fig.II.11) in Western Indonesia. In the western part of the area, the subduction zone maintained its orientation with the trench aligned E-W, parallel to and south of the Small Sunda Islands. This produced the Miocene volcanic arc which extends eastward to the Small Sunda Islands. In West Java, the Miocene volcanic deposits were deposited in the Bogor Basin forming the Jampang and the Citarum Formations. This volcanism terminated at the end of the Early Miocene and sedimentation (e.g. from the Saguling to the Kaliwangu Formations) occurred until the Pliocene.

Many authors (e.g. Bolliger & de Ruiter, 1975; Katili, 1975) consider that in the Late Pliocene a major uplift of Java began. This was accompanied by a new period of volcanism, producing the Cijulang Formation and continuing until the Present time as Quaternary volcanism (Fig.II.12).

On the basis of the Indian - Eurasia pole of Minster & Jordan (1978), Chase (1978) and Moore et al. (1980) reported that the Indian Ocean - Australian plate has moved to the N25^{o}E at a rate of 7.5 cm/yr in south of Java since 3 Ma. This has caused Quaternary volcanism in the Western Indonesia.

II.6 Quaternary Volcanism and Tectonics

In Western Indonesia, Quaternary volcanism is related to the subduction zone in the Indian Ocean that extends and bends from west of North Sumatra to south of Java. The position of Sumatra and Java with respect to the direction of the Indian Ocean - Australian plate movement (N25^{o}E) causes differences in tectonics and volcanism in the

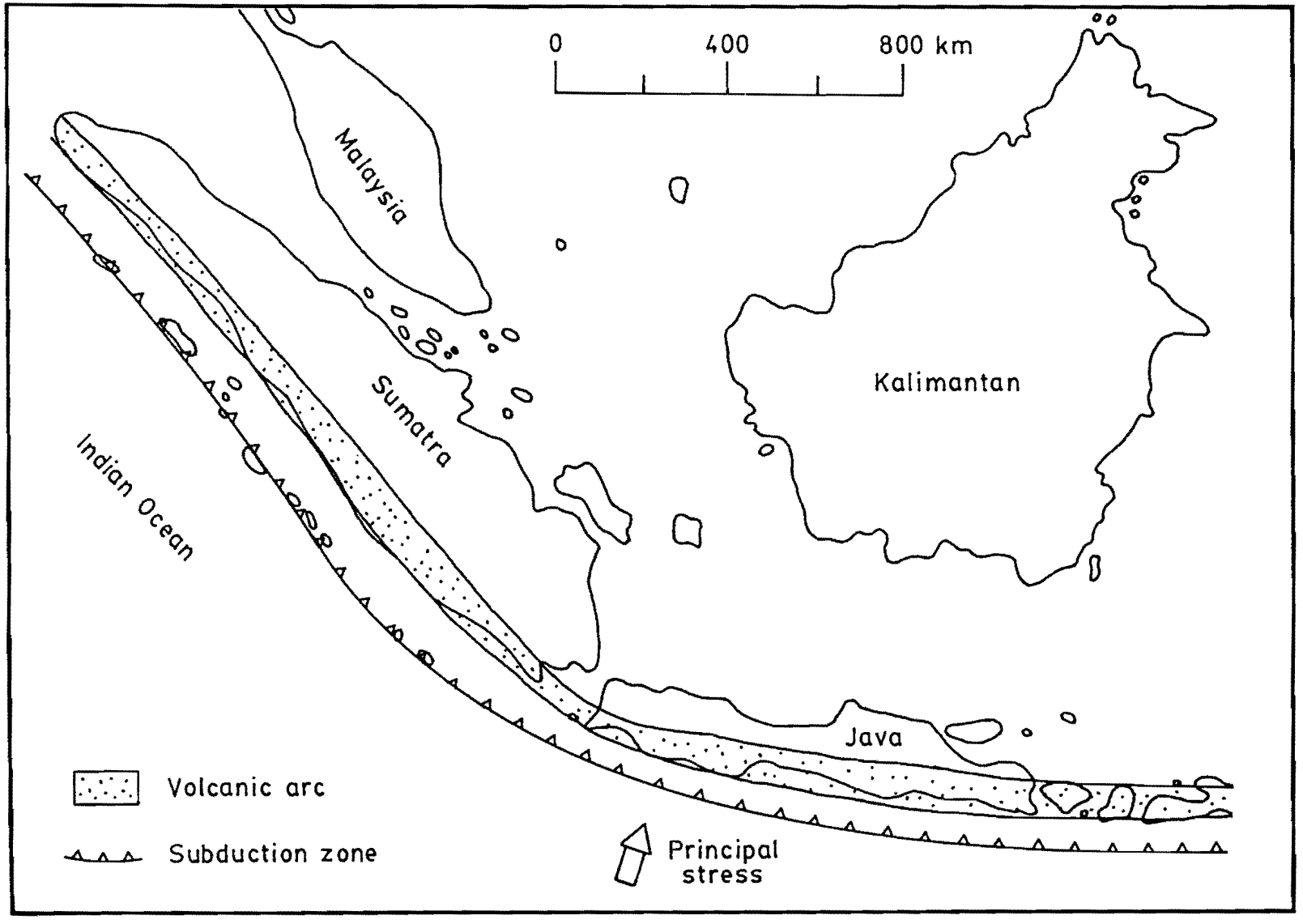

Figure II.11 Miocene volcanism in Western Indonesia (Katili, 1975).

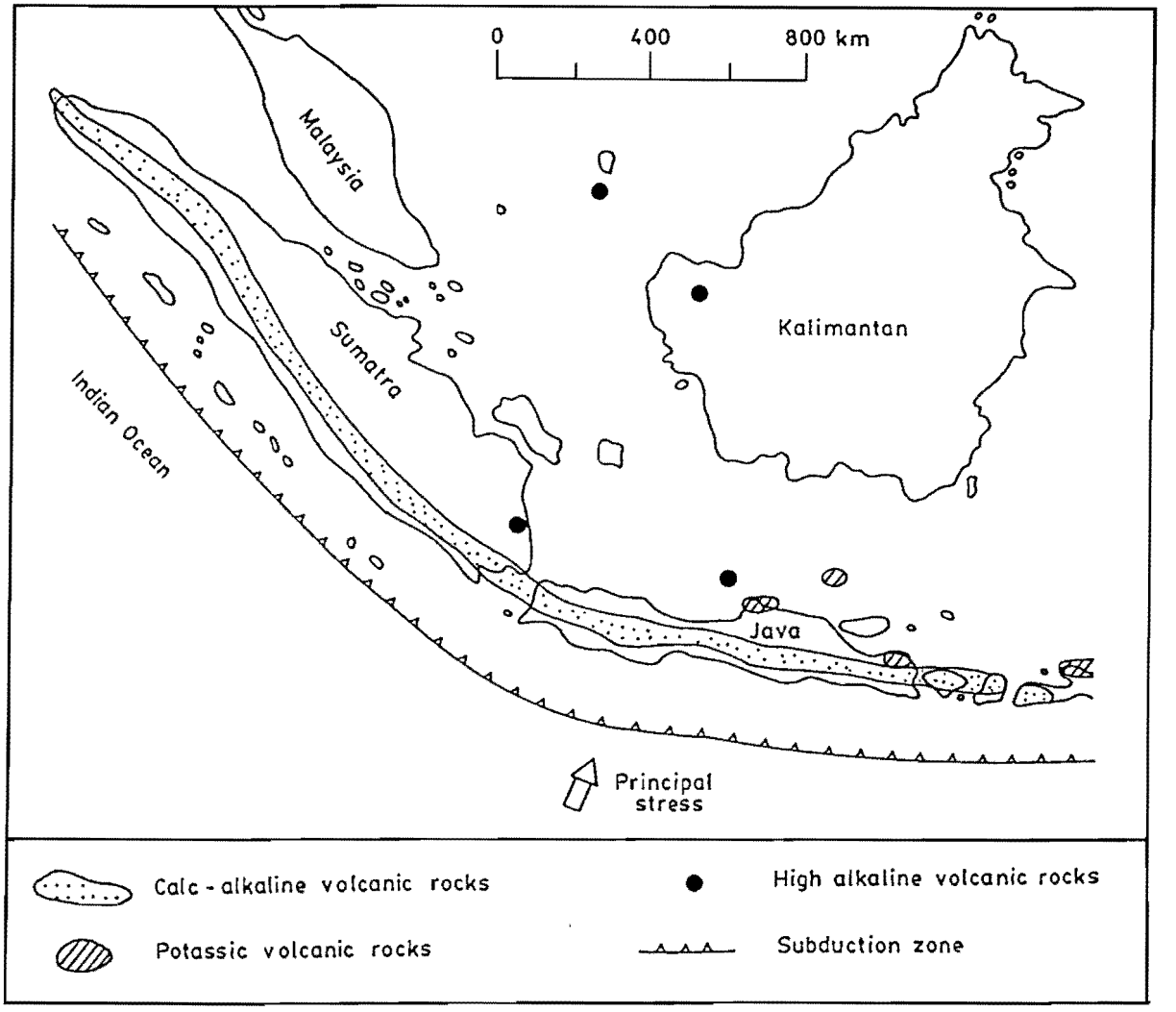

Figure II.12 Late Cenozoic to Present volcanism in Western Indonesia (Katili, 1975).

two areas.

Subduction direction is nearly perpendicular to Java but is highly oblique to North Sumatra. Similarly, the depth of the trench decreases from 7000 m to 3500 m, slab inclination changes from 65^{o} to 40^{o}, and perpendicular subduction rate decreases from 7.5 cm/yr to 4.2 cm/yr, (Moore et al., 1980; Newcomb & McCann, 1987; Sano et al., 1978). The oblique convergence in Sumatra has produced dextral strike-slip faults of the Sumatra Fault System. Although the island is characterised as relatively aseismic from the lack of large magnitude earthquakes, it has the high potential to produce thrust earthquakes (Newcomb & McCann, 1987). Also, this island has a low frequency of volcanic activity but eruptions have been explosive ones producing voluminous welded ignimbrites. Elongated calderas which are parallel to the Sumatra Fault suggest that volcanism is strongly controlled by structure. Java, on the other hand, typically has deep earthquakes, from 150 km to 360 km to the north of the island, and few non welded ignimbrites were produced from circular-shaped calderas. A summary of the tectonics of West Java is illustrated in Figure II.13.

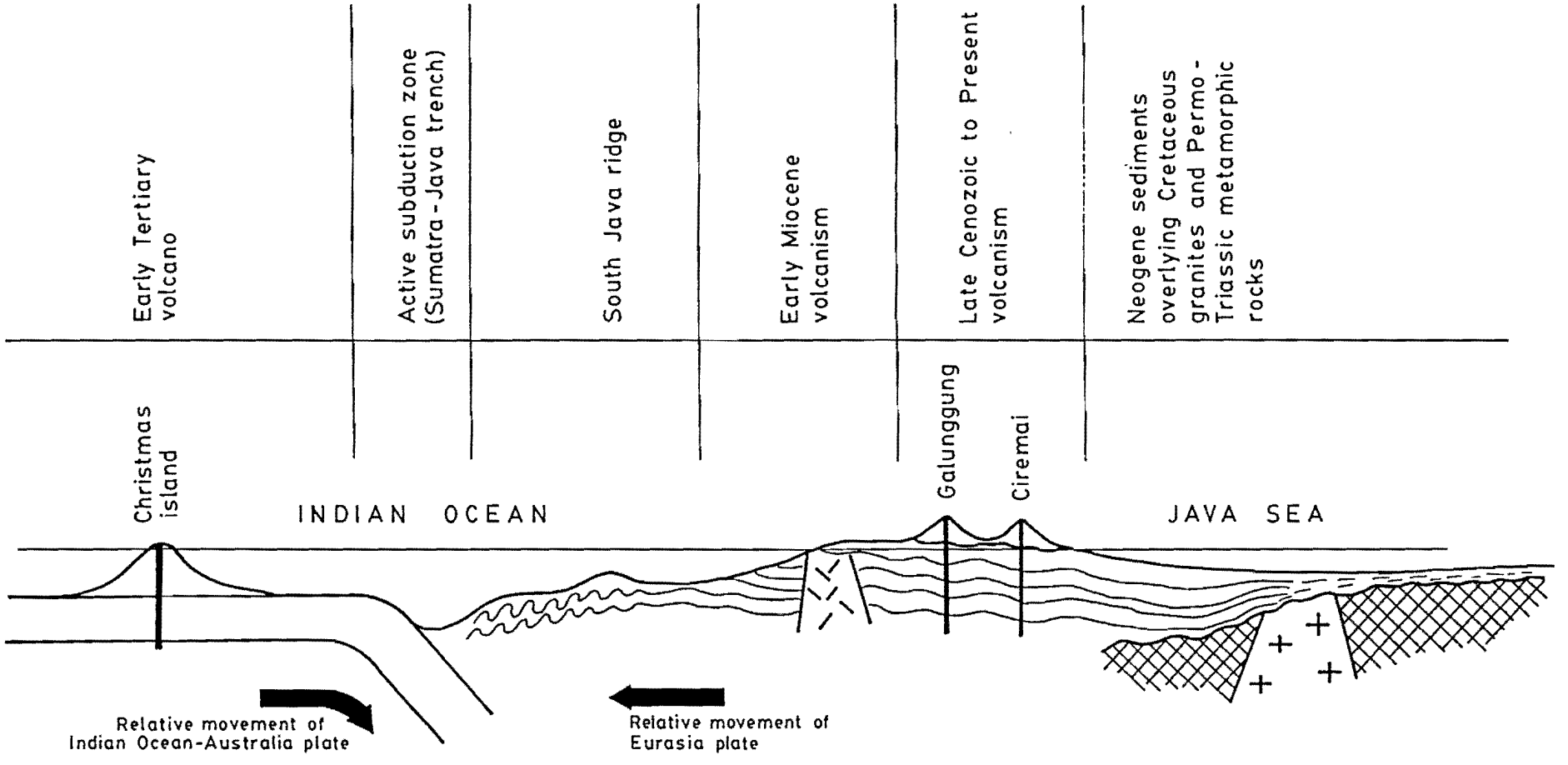

Figure II.13 Plate tectonic schematic section (SSW-NNE) across West Java.

III GEOLOGY OF GALUNGGUNG VOLCANO

III.1 Introduction

Since 1980, there have been many stratigraphic and geological mapping studies of Quaternary active volcanoes in Indonesia. The main purposes have been to understand the eruptive characters of each volcano to assess volcanic hazards. Volcanoes which have abundant lava flows are considered less explosive thus less dangerous than those dominated by pyroclastic flows and lahars. However, such studies are difficult in tropical countries such as Indonesia because : 1. Erosion is very fast in the high level areas which usually have steep slopes. Only resistant rocks such as lava flows, dikes and domes remain. The lowland areas are cultivated and highly populated. 2. Many years after an eruption has terminated the uncultivated areas become covered by dense tropical forest. 3. So far, little absolute dating has been done. Thus, the best time to study the stratigraphy of an active volcano is during and shortly after an eruption.

At Galunggung, stratigraphy of volcanic rocks can be observed clearly following the 1982-83 eruption. However, the thickest strata is exposed in the caldera wall which is inaccessible, and these rocks are usually hydrothermally altered.

In the following sections, the nomenclature and terminology applied to Galunggung volcanic deposits are presented. The stratigraphy of prehistoric volcanic products is described in section III.4 together with the nature of volcanic deposits erupted in historic times and an outline of the eruptive history. This is followed briefly

by descriptions of solfatara and fumarole fields and a discussion of the tectonic setting of the Galunggung volcano. This chapter concludes with a summary of Galunggung geologic history.

III.2 Nomenclature

The formal terminology applied to lithostratigraphic units follows usage of the 1982 edition of AGI Dictionary Geological Terms and International Stratigraphic Guide (ISSC; Hedberg, 1976) :

Formation is the primary unit in lithostratigraphy consisting of a succession of strata useful for mapping or description. Most formations possess distinctive lithologic features that may indicate genetic relationships. Ordinarily, the upper and lower boundaries of a formation are determined lithologically, but they may be unconformities. The age or time span of a formation is not necessarily the same wherever it is recognized.

Member is the formal lithostratigraphic unit next in rank below a formation. A member is recognized within the formation and named specifically if possesses lithologic characters distinguishing it from adjacent parts of the same formation.

Group is the formal lithostratigraphic unit next in rank above a formation. The term applies most commonly to a sequence of two or more contiguous associated formations with significant unifying lithologic features in common.

III.3 Terminology

Two kinds of classification of volcanic rock may be used; a lithological descriptive classification and a genetic classification. The first, used mainly in fragmental volcanic deposits, is primarily descriptive, defining major lithological characteristics of a volcanic deposit such as grain size. A genetic classification is also necessary to interpret relationship between deposits in terms of eruptive mechanism and geochemical evolution.

In this thesis genetic terms are used only for volcanic deposits for which the origins can be clearly established from their lithology, overall geometry and field relations. Terms used are defined below :

III.3.1 Volcanic Debris Avalanche

Large horseshoe-shaped craters, open at one end, with hummocky deposits of volcanic debris at their base, have long been noted in many volcanic regions. Nakamura (1978) and Ui (1983) termed the hummocky volcanic debris as a "volcanic dry avalanche deposit". It is defined as " a volcaniclastic deposit formed as a result of large-scale sector collapse of a volcanic cone associated with some form of volcanic activity". The term is similar to "dry mud-flow" (Murai, 1961), "debris flow" (Mizuno, 1975; Cattermole, 1982; Sigurdsson, 1982), "rock slide avalanche" (Voight et al., 1981; Glicken, 1983). The latter two terms accurately describe the emplacement processes, and "debris avalanche" has increasingly been used for the resulting

deposits (Soya & Katsui, 1981; Mimura et al., 1982; Newhall, 1982; Crandell et al., 1984). Finally, Siebert (1984) named it as "volcanic debris avalanche deposit".

The volcanic debris avalanche deposits are characterised by :

1. Hummocky surfaces with non-integrated drainage.
2. The hummocks vary widely in morphology. They may be conical, elliptical or oval in shape with the long axis in many cases pointing radially away from the volcano, parallel to the flow direction (Glicken, 1982).
3. The largest hummocks tend to be concentrated near the axis of the deposits, with size decreasing toward the margins.
4. Source regions, if not filled by younger material, are usually horseshoe-shaped in plan.
5. Good exposures often show intact strata of the original stratovolcano mostly dipping less then 35 degrees (Mimura et al., 1982). The strata are alternating layers of lava and pyroclastic material with abundant fractures, and minor faults.
6. Deposits may be locally intimately associated with pyroclastic flows (Glicken, 1982).
7. Inter-hummock areas often consist of secondary lahars and reworked material (Ui, 1983).
8. The hummocky, horst and graben morphology of the deposits most likely represents lateral spreading of a body that was deformed by faulting during transport rather than by uniform flow (Glicken et al., 1981).

III.3.2 Pyroclastic Deposits

Pyroclastic deposits are those formed by fragmentation of magma and rock by explosive volcanic activity (Wright, et al., 1980; Cas & Wright, 1987). Sparks & Walker (1973) identified three basic types of pyroclastic deposit : 1. Pyroclastic fall, 2. Pyroclastic flow, and 3. Pyroclastic surge.

III.3.2.1 Pyroclastic Fall

This is produced when material is explosively ejected from a vent into the atmosphere producing an eruption column in the form of a convective plume. The plume expands and pyroclasts fall back under the influence of gravity at varying distances from the source. The geometry and size of the deposits reflects the eruption column height, wind velocity and direction (Wilson et al., 1978). Pyroclastic fall deposits are characterised by :

1. Mantle wedging, maintaining a uniform thickness over restricted areas covering all but the steeper topography.
2. They are generally well sorted and sometimes show internal stratification due to variations in eruptive column conditions.
3. Graded bedding structures, usually normally graded, are common.
4. Carbonised wood is generally lacking in these pyroclastic materials, but when it does occur it is invariably restricted to near vent deposits.

III.3.2.2 Pyroclastic Flow

Pyroclastic flows involve the lateral movement of pyroclasts as a gravity controlled, hot, high concentration gas/solid dispersion, which may in some instances be partly fluidized (Sparks, 1976). Their deposits are characterised by :

1. Topographic control, filling valleys and depressions.
2. Poor sorting. They sometimes show coarse-tail grading (Smith, 1960a; Sparks, 1976). In proximal parts, the deposits contain coarse grain materials consisting of juvenile, accessory and accidental materials.
3. Individual deposits generally do not have internal structure. They are massive although the superposition of a number of flow units can give the appearance of stratification. Each flow unit is regarded as the deposit of a single pyroclastic flow. However, sometimes roughly normal graded bedding can be seen in proximal and distal areas, whereas bomb-rich material is concentrated along the central part the deposit.
4. Non-welded pyroclastic flow deposits are still loose, may easily collapse and form vertical cliffs.
5. Fumarole pipes may occur in which the fine ash fraction has been lost enriching the pipes in crystals, lithics or vesicular fragments (Roobol & Smith, 1976). These fumarole pipes are caused by secondary explosions when cold water flows through the very hot deposit.

6. Carbonised wood or charcoal may be present.
7. Poor sorting in pyroclastic flows is attributed to high particle concentrations and not turbulence, with the dominant flow mechanisms probably being laminar (Wright & Walker, 1981; Wilson, 1980).

III.3.2.3 Pyroclastic Surge

Surges involve the lateral movement of pyroclasts as expanded, turbulent, and low concentration gas/solid dispersions (Wright et al., 1980). "Pyroclastic surge" is a general name for surge deposits which may be of three types (Fisher & Schmincke, 1984) :

1. Ground surge; which underlies the deposits of many small to intermediate - volume pyroclastic flow deposits. This type of surge appears to develop largely from eruption column collapse.
2. Ash cloud; that overlies and extends beyond the margins of pyroclastic flows.
3. Base surge; that forms from hydroclastic eruptions.

Pyroclastic surges are characterised by :

1. Showing unidirectional sedimentary bedforms (cross-stratification, dunes, antidunes, planar laminations, pinch and swell structures, chute and pool structures) and individual laminae are generally well sorted (Wohletz & Sheridan, 1979).
2. They may contain carbonised wood.

3. The distribution of a pyroclastic surge does not depend on the topography because of its low concentration and low density. The deposits do mantle topography but tend to accumulate thickest in depressions.

III.3.3 Lahar

The term lahar was introduced by van Bemmelen (1949) for a mudflow containing debris and angular blocks of volcanic origin. Neall (1976) defines a lahar as a large mudflow or debris flow mostly composed of volcaniclastic detritus, often including large blocks, on or surrounding the flanks of a volcano. This lahar is originally mobilized by addition of water and gravity alone becomes the motivating force. Two types of lahar are distinguished in Indonesia (Suryo & Clarke, 1985); crater lake-generated lahars and rain-generated lahars. The first kind of lahar is caused either by eruption through a crater lake (primary lahar) or by collapse of a crater lake wall (breakthrough lahar).

Rain-generated lahars occur when rain mixes with unconsolidated pyroclastic materials turning into a saturated mass with high density flow. If the material is still hot, such as with pyroclastic flows, a hot lahar will be formed. When the deposit is already cold, the result is a cold lahar. Minor lahars which occur on Galunggung have been generated by pyroclastic flows moving down river valleys. The hot flows contact with water presenting "secondary explosions" which flow down as hot lahar accompanied by white steam. Minor cold lahars occur after river water is dammed by unconsolidated collapsed materials which is

then breached suddenly. In general, lahar deposits are characterised by :

1. Association with stratovolcanoes. They may comprise significant volumes of the volcanoes' bulk.
2. Lahars follow pre-existing valleys and the deposits may be interstratified with lava flows, pyroclastic deposits derived from the same area and with alluvial material.
3. They leave thin layers on steep slopes and in the head waters of valleys, but become thicker in valley bottoms and form fans that coalesce, or else form broad individual lobes in lowland areas. On very low slopes they have somewhat similar distribution to pyroclastic flow deposits.
4. Lahars may be mono- or heterolithologic. Monolithologic lahars can also be distinguished by their colour during flow, such as grey to dark grey, depending on the original colour of primary deposits. Heterolithologic lahars are usually brown to reddish brown, they entrain older and more weathered materials.
5. Surfaces of lahar deposits tend to be remarkably flat over wide areas, with very abundant sand size matrix and boulders "floating" in the matrix.
6. Particles carried in lahars vary from clay to boulder size. The percentages of each size fraction vary enormously from deposit to deposit and also within a single deposit from proximal to distal locations. However, coarse fractions usually decrease in both size and angularity (angular to subrounded) with distance.
7. Lahar deposits are poorly sorted and structureless, although

the long axes of large boulders may parallel flow direction.

8. Lahar deposits commonly contain wood fragments; some of which may be partly or wholly carbonised and derived from pyroclastic deposits.
9. Compared with pyroclastic flow deposits, lahar deposits are usually denser, muddy and wet. They may contain volcanic bombs whose surfaces have been smoothed during transport or which may have fractured into smaller and sharp fragments.

III.3.4 Lava, Dome and Dike

Lava is a general term for molten effusive and also for the rock that is solidified from it (Bates & Jackson, 1980). A single lava flow is a lateral, surficial outpouring from a vent or a fissure and the solidified body of rock that is so formed. Lava flows tend to flow along pre-existing drainage channels on the slopes of the edifice. Where exposures are extensive, individual flows can often be traced subaerially or in the subsurface for distances of several kilometres.

A volcanic dome is a mass of solid rock that forms when pasty lava is extruded from a vent and is too viscous to flow laterally more than a few tens or hundreds of metres. A cryptodome (meaning hidden dome) is the result of intrusion of magma at shallow depth beneath a crater.

A dike is a tabular igneous intrusion that cuts across the bedding or foliation of the country rocks (Bates & Jackson, 1980). Some dikes tend to be either parallel or radial in pattern.

III.4 Stratigraphy and Historic Records

All Galunggung volcanic rocks are included within the **Galunggung Group**. This is divided into : **Old Galunggung Formation**, **Tasikmalaya Formation**, and **Cibanjaran Formation**. The names are already well established and very good exposures are available. Old Galunggung Formation covers rocks erupted during Old Galunggung volcanic activity whereas Tasikmalaya Formation is a rock unit produced during Galunggung caldera formation. Rocks in Cibanjaran Formation are products of historic eruptions in 1822, 1894, 1918 and 1982-83. In this description, historic records collected from the literature are included. Subaerial distribution of these formations is given in geologic maps at 1 : 50,000 and 1 : 10,000 scales presented inside the back cover of this volume together with 1 : 50,000 location map. Stratigraphy of the Galunggung volcanic rocks is also shown in Table III.1.

III.4.1 Old Galunggung Formation

Galunggung was originally a stratovolcano known as Guntur volcano (+2168 m). Unfortunately there is another Guntur volcano in Indonesia (Neumann van Padang, 1951, number 13) and hence some confusion. To avoid this "Old Galunggung" is used in this thesis for volcanic activity before the caldera forming event.

Although the crater is still present the details of Old Galunggung activity are largely unknown. Carbon dating of charcoal collected from a layer of debris avalanche material gives an age of

Table III.1 Stratigraphy of the Galunggung Group.

AGE	FORMATION	Explanation
	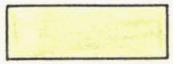 Alluvial	Reworked, unconsolidated material: clay - boulder
1983 1982 1918 1894 1822	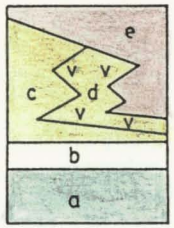 CIBANJARAN a. Products of 1822 & 1894 eruptions b. 1918 Lava dome c. 1982-83 Pyroclastic fall deposit d. 1982 Pyroclastic flow deposit e. 1982-83 Lahar deposit	The 1822 eruption occurred from 13.00 to 17.00 h. on 8 October, produced mainly debris avalanche, pyroclastic flow and surge deposits, and killed 4011 people. The 1894 eruption was on 17-19 October, only ejected pyroclastic fall deposit. The 1918 lava dome extruded on 16-19 July was completely destroyed by eruptions in 1982. The 1982-83 eruption occurred on 5 April - January, mainly produced pyroclastic flow and fall deposits; some of them were reworked to become lahar deposits. There were no deaths, but 35,000 people were evacuated and total damage was approximately $US 100 million.
4200 ± 150 yrs. BP	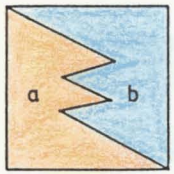 TASIKMALAYA a. Debris avalanche deposit b. Pyroclastic flow and lahar deposits	Formation of the horseshoe-shaped Galunggung caldera.
10,000 - 50,000 yrs. BP	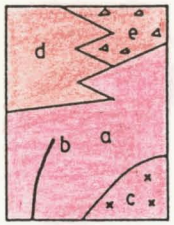 OLD GALUNGGUNG a. Lavas and intercalated pyroclastic deposits. b. Dikes c. Cryptodome d. Pyroclastic fall and flow deposits e. Lahar deposit	Constructive period of Old Galunggung stratovolcano that ended with an intrusion of a cryptodome beneath the crater.

20,000 - 25,000 years BP (Kartakusumah, 1984). It is suggested that activity occurred during the period 50,000 - 10,000 years BP, and produced approximately 56.5 km^3 volcanic rocks.

Old Galunggung volcanic rocks consist of lava flows, pyroclastic deposits, dikes, a cryptodome and lahar deposits. Mappable pyroclastic and lahar deposits can be considered as members of the Old Galunggung Formation. Stratigraphy of the Old Galunggung volcanic rocks can be observed clearly in the walls of Old Galunggung crater and Galunggung caldera (Fig. III.1) after the 1982-83 eruption.

The oldest lava flow is exposed in the deepest southwest caldera wall (Fig.III.2A, sample number 20271, location 22). A lava flow in the summit crater rim (sample L35, location 35) is considered the youngest lava extruded by Old Galunggung volcano. Collected samples in the northeast caldera wall also show their stratigraphic position (Fig. III.2B). Correlation between the lava flows in the both side of caldera walls is difficult. This is due to the channelised nature of many lava flows. Thus, precise correlation is only possible using radiometric dating techniques

In addition, volcanic deposits in the crater and caldera walls, particularly in the lower parts, are hydrothermally altered. Fresh rock samples may be obtained on outer slopes but outcrops are very rare and their stratigraphic positions are unknown.

III.4.1.1 Lava flows

Lava flows are rarely exposed in deep river valleys on the outer slopes of the volcano, mostly above 900 m, but they are numer-

Figure III.1 Stratification of lava flows intruded by a dike in the NE wall of Galunggung caldera, (28 July, 1985).

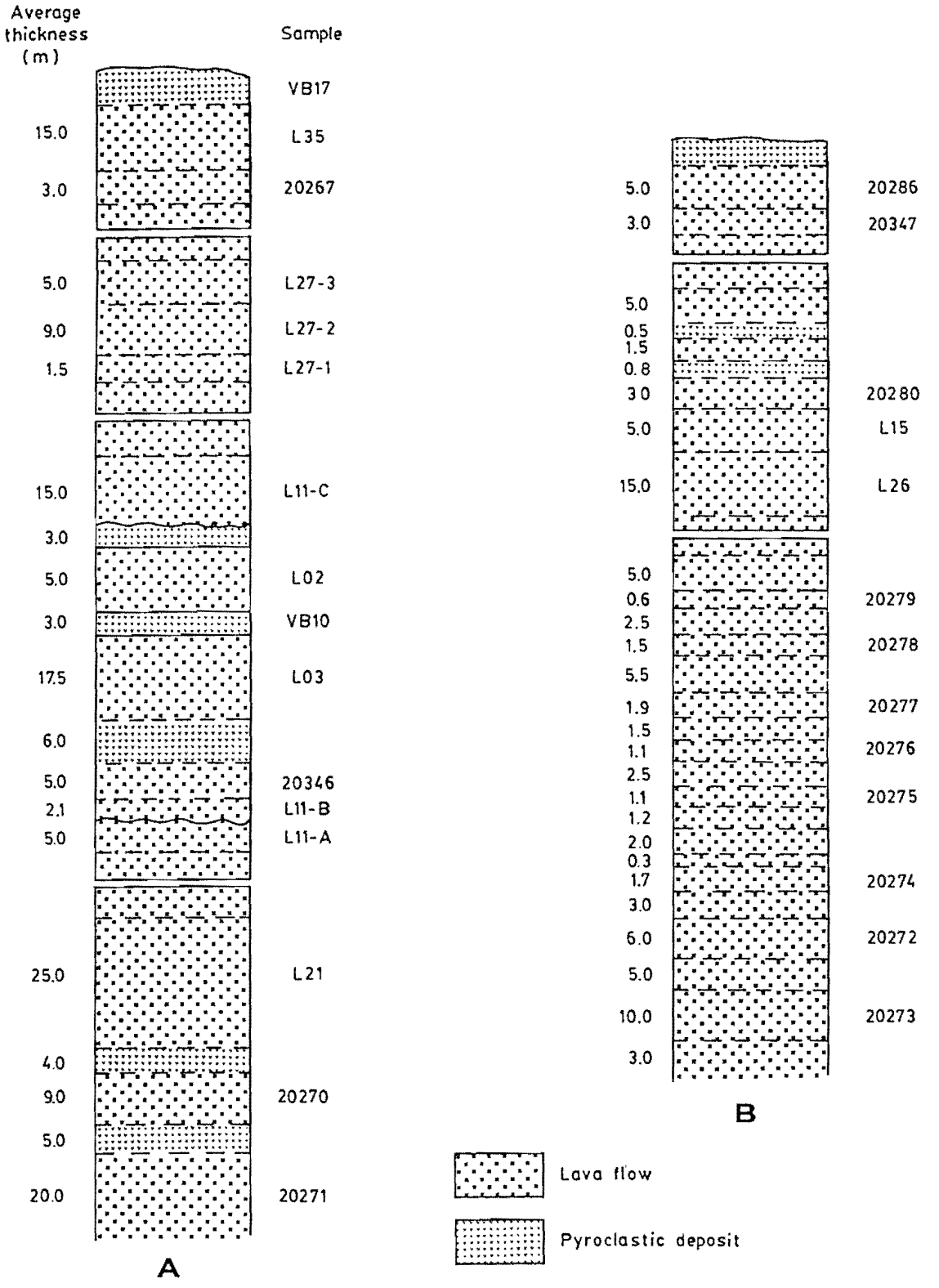

Figure III.2 Sample collections representing stratigraphic position of Old Galunggung lavas in the SW (A) and NE (B) caldera walls.

ous in the walls of Galunggung caldera (+ 600 m up to summit). The flows are well stratified (Fig.III.2) with an apparent dip increasing from 3^{o} on the dip slope to 15^{o} around the summit crater. Unfortunately, only parts of the wall can be reached for sampling.

Lava flows with weathered soil in the upper part (L11-A) and erosional surface (L-02) are found in the southwest wall of the Galunggung caldera. These suggest that Old Galunggung was not continuously active but some dormant periods occurred.

The inner parts of lava flows are massive. Outward, the lavas are brecciated to blocky as loose materials (Fig. III.3); the contact between individual lava flows is therefore often obscured. Inner parts of flows are usually light to dark grey whereas the outer parts are oxidised and hence brick red to reddish brown. This implies that the temperature of the flows was high (above $500^{o}C$) and oxygen circulated freely, accounting for the absence of charcoal (Lockwood & Lipman, 1980). The brecciated and blocky lavas in the upper part of the flows are usually thicker than those in the lower parts and the massive ones. The massive lavas vary between 1 and 15 m in thickness and show lensoid or wedged forms in the caldera wall. Occasionally, platy joints occur between blocky and massive portions. Columnar joints are found only in very thick massive lavas. These reflect cooling and solidification under stagnant conditions.

III.4.1.2 Pyroclastic Deposits

Old Galunggung pyroclastic deposits are observed in Galunggung caldera walls and on the outer slope of the volcano, but they are usu-

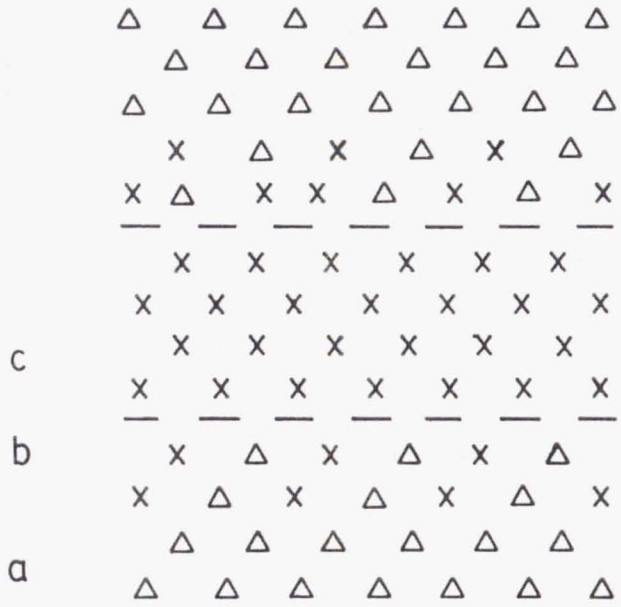

Figure III.3 A gradual change in the lower part of a lava flow from loose blocky (a), through brecciated (b), to massive (c) in the middle part of the flow.

ally poorly exposed. Two kinds, pyroclastic flow deposits and pyroclastic fall deposits, are recognised.

Pyroclastic flow deposits are well exposed in the upper sections of the southwest caldera wall (Fig.III.4). Lithologic sections of each location are given in Appendix 1.5 - 10. The deposits are thick (3.5 - 25.0 m), but are not widely distributed. This suggests the pyroclastic flows are valley filling deposits. The pyroclastic flow deposits are poorly sorted, structureless, and loose to slightly indurated. The materials are predominantly ash to lapilli in size.

Although pyroclastic fall deposits are generally much thinner than pyroclastic flows, they are widely distributed around Galunggung volcano mainly on the south and east slopes. On the west slope, Old Galunggung pyroclastic fall deposits are covered by younger pyroclastic falls particularly those which were erupted in 1982. In the lower parts of the Galunggung caldera wall, pyroclastic fall deposits (Fig. III.5) are more abundant. This implies that in the initial stages Old Galunggung volcanic activity often produced pyroclastic debris rather than lava flows.

The pyroclastic fall deposits are typically stratified, well sorted, and normally graded. Grain size of the materials decreases with distance from the vent but most is lapilli to ash grade; while bombs and blocks are restricted to an area immediately around the crater.

III.4.1.3 Dikes

In the southwest and northeast walls of the Galunggung caldera,

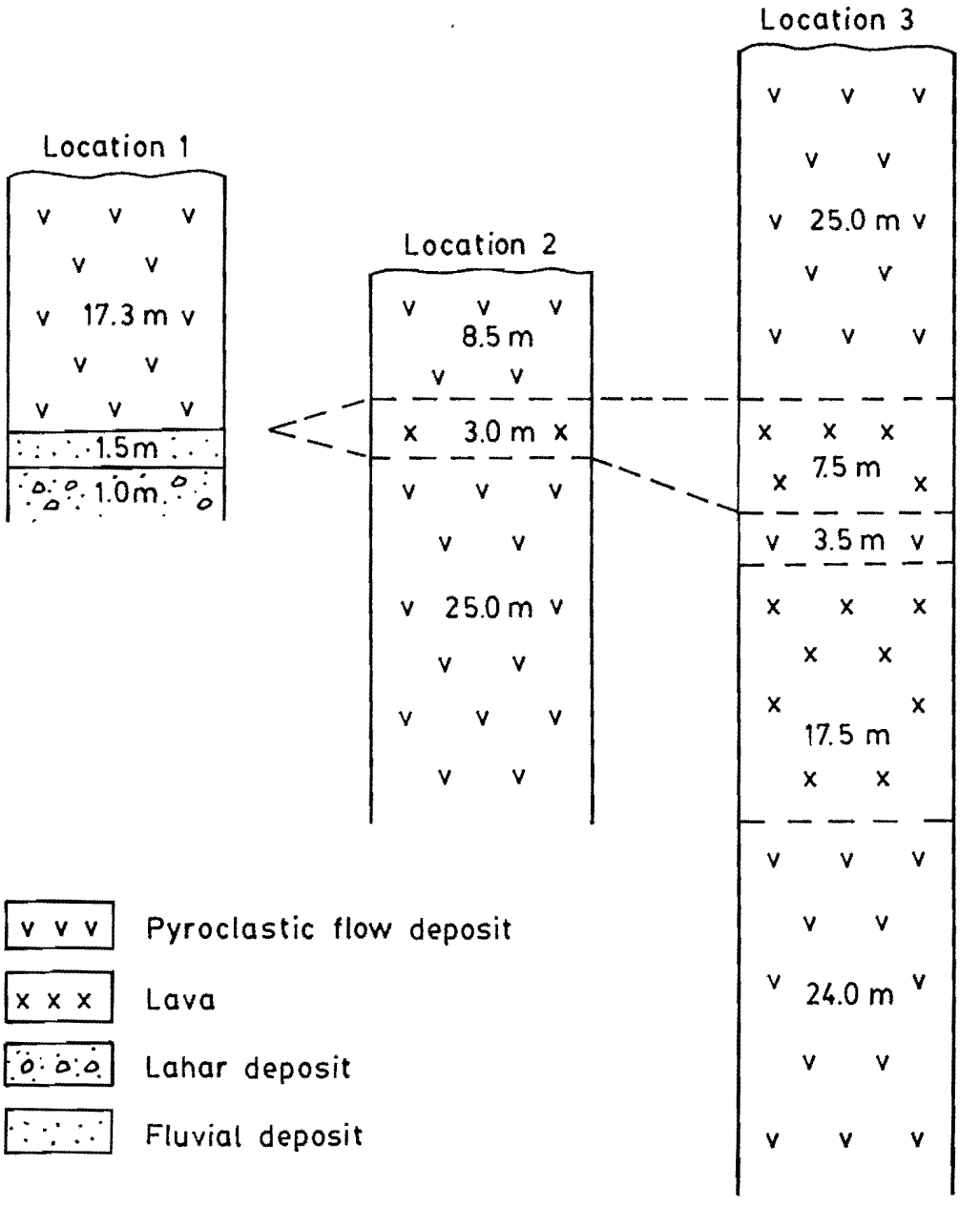

Figure III.4 Pyroclastic flow deposits with intercalated lavas, lahar and fluvial deposits in the SW wall of the Galunggung caldera.

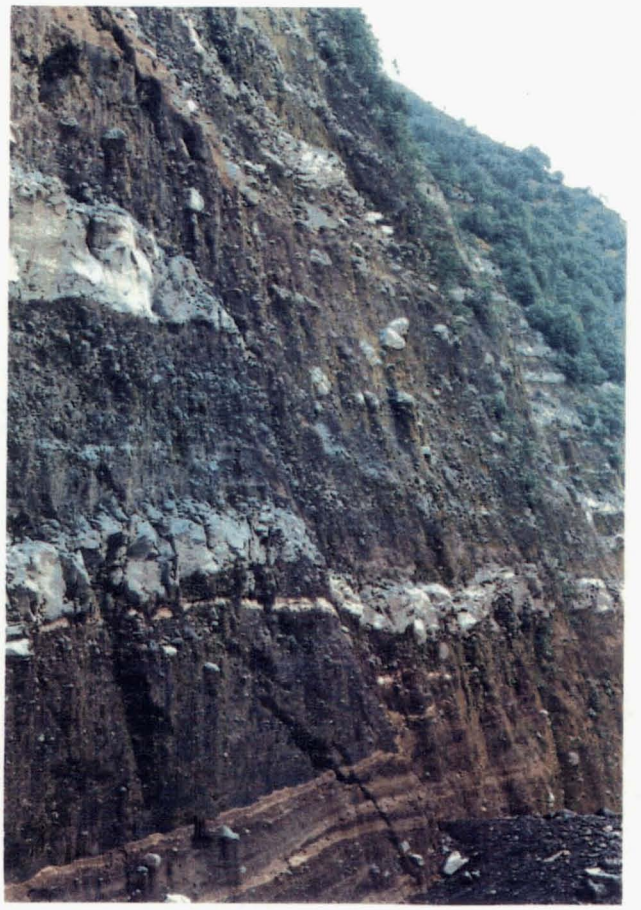

Figure III.5 Stratification of pyroclastic fall deposits overlain by lava flows in the SW wall of the Galunggung caldera (location 20).

dikes are well exposed (Fig.III.6). There are four dikes in the southwest wall and two dikes in the northeast wall, each 2 - 5 m thick. Another dike is found in the Welirang active crater wall. The dikes cut sequences of lava flows and pyroclastic deposits in the lower and middle parts of the caldera walls but probably did not reach the surface of the volcano. In the volcanic slope area, outside of the caldera, dikes are not found.

III.4.1.4 Cryptodome

A cryptodome is located in the north wall of the Galunggung caldera under Old Galunggung crater (Fig.III.7). The cryptodome is approximately 250 m across, and about 500 m high. The age of the cryptodome is not yet known but could date from the end of the Old Galunggung activity as it was already present in the vent of Old Galunggung crater prior to caldera formation. After emplacement of the cryptodome, volcanic activity moved from the summit crater to the southeast flank, firstly to form Galunggung caldera then the present active crater.

III.4.1.5 Lahar Deposits

On the peneplain area and lower volcano slope, lahar deposits are very dominant. However these areas are already cultivated, so good exposures are limited in deep river valleys. Reworked lahar deposits commonly interdigitate with pyroclastic flow deposits. The lahar depo-

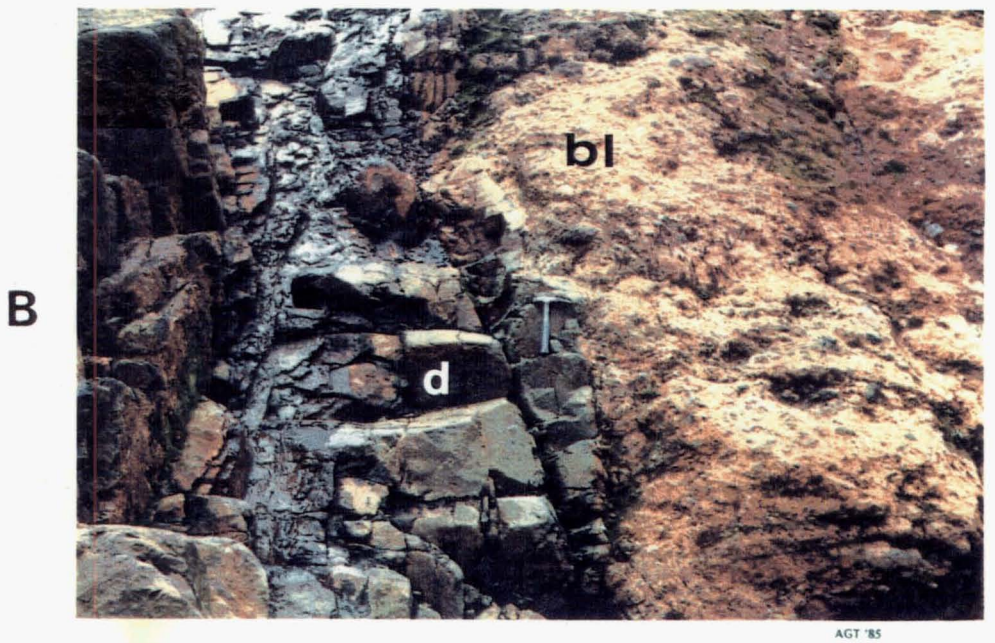

Figure III.6 A. Dike (d) intruding a pyroclastic unit (p) and a lava flow (l). B. Dike (d) intruding a brecciated lava flow (bl) in the SW wall of the Galunggung caldera (location 20 and 25, respectively), (30 July and 2 August 1985).

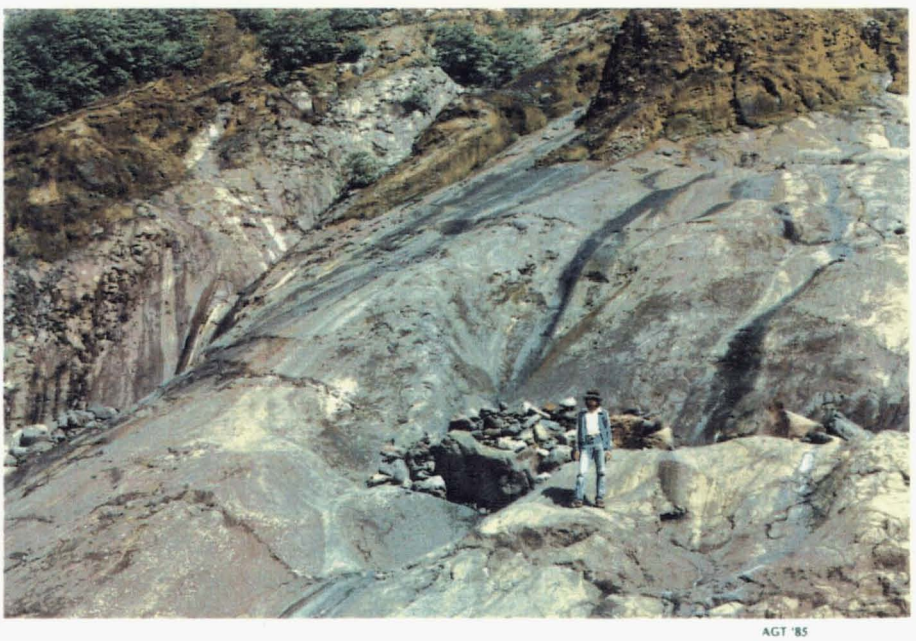

Figure III. 7 Lava cryptodome in north wall of the Galunggung caldera, beneath Old Galunggung crater (1 August 1985).

sits are commonly indurated, poorly sorted with boulders floating in abundant silt-sand size matrix. The thickness varies from 1.0 - 2.5 m. Occasionally, they contain wood fragments. Boulders are usually subangular to subrounded, whereas smaller clasts are relatively more angular.

III.4.2 Tasikmalaya Formation

Around 4200 ± 150 years BP a gigantic eruption occurred. The southeastern part of Old Galunggung (approximately 16 km^3) collapsed and slid down to form a debris avalanche deposit which now forms more than 3,600 hills (Escher, 1925). Junghuhn (1853) named the hills " The Thousand Hills of Tasikmalaya". This eruption also produced pyroclastic flow deposits some of which were "reworked" to form lahar deposits. All these volcanic rocks are included in the Tasikmalaya Formation. Tasikmalaya is a city at the base of the southeastern slope, where the debris avalanche deposits are situated. The Tasikmalaya Formation consists of: 1. Volcanic debris avalanche, 2. Pyroclastic flow and 3. lahar deposits.

III.4.2.1 Volcanic Debris Avalanche Deposit

Old Galunggung volcanic debris forms numerous hills on the Tasikmalaya plain. Such material is also found inside the Galunggung caldera where it forms several hills such as Pasir Linggajati, Pasir Malang, Gunung Welirang and Gunung Bunder (Fig.III.8).

Figure III.8 Several features of volcanic debris avalanche deposits from Galunggung volcano.

A Fractured lava in the west wall of Gunung Bunder (inside the caldera)

B Alternating lava and pyroclastic materials at Gunung Goong (12 km SE active crater)

C Fractured lava at Gunung Bango (12 km SE active crater)

D Mixed materials from ash to block in size, located at south of Tasikmalaya city (20 km SE active crater)

Figure III.8A

Figure III.8B

Figure III.8C

Figure III.8D

Volcanic debris avalanche deposit is distributed laterally as fan-shaped deposit southeastward from the Galunggung caldera, covering approximately 170 km^2, and extending to 23 km from the active crater. This area is typical hummocky. The largest hummocks, up to 50 m in height and 500 m in diameter and conical in shape, are concentrated around the axis of the deposits. Inter-hummock areas often consist of lahar and fluvial deposits. An isolated depression forming a lake (Situ Gede) is also present.

Most outcrops of the volcanic debris avalanche show intact stratifications of lava flows and pyroclastic deposits (Fig.III.8B-C) which are similar to those in the Galunggung caldera walls. The strata are only slightly disrupted but lava flows are always fractured. A mixture of volcanic debris avalanche consisting of unoriented lava blocks and rock fragments in matrix of ash to lapilli in size is usually found in the marginal and distal parts of the deposits (Fig.III.8D).

Close to the northeast Galunggung caldera wall, between Sinagar village and Pasir Ngemplong, lava flows are massive. Nevertheless, toward the active crater those lavas become gradually fractured. These features can be traced from Sinagar to the head of Ci Banjaran in which the Galunggung caldera wall becomes higher. The massive lavas probably collapsed shorter vertical distances compared with the fractured ones.

Gunung Welirang, with its crescentic form, was interpreted as a part of volcanic cone or lava dome erupted after caldera formation. However, a topographic map made before 1822 eruption (van Es, 1924; Map 2) shows that Gunung Welirang was not crescentic but longitudinal in shape and Ci Kunir drained the active crater at that time. Gunung

Welirang is composed of alternating lava flows and a small proportion of pyroclastic debris. These lavas are fractured in a similar way to those of the volcanic debris avalanches further downslope. The strata in the Welirang wall have been tilted southwestward. This suggests that Gunung Welirang is a debris avalanche which remained in the caldera. The crescentic shape of Gunung Welirang at the present time was caused by deposition around the crater rim during eruptions in 1822, 1894 and 1982-83.

III.4.2.2 Pyroclastic flow Deposits

Pyroclastic flow deposits are distributed within Galunggung caldera between Ci Kunir and Ci Banjaran. In the west wall of Gunung Bunder (location 9), pyroclastic flows overlie the volcanic debris avalanche. The best outcrop is found in Ci Kunir valley (Fig.III.9-10) near Kedung village (location 6). Three layers of pyroclastic flow deposit alternating with pyroclastic surge and lahar deposits are observed in this location. The upper pyroclastic flow deposit wedges downstream whereas the lahar wedges upstream.

The pyroclastic flows are dark grey to brownish grey, structureless and unconsolidated although they become denser on the surface where water has flowed through them. The material is dominated by ash although volcanic bombs and blocks are present. Radiocarbon dating of charcoal collected from the upper pyroclastic flow gives an age 4200 ± 150 yrs. BP.

Pyroclastic surges are much thinner than pyroclastic flows and only locally distributed but typically have internal structures, such

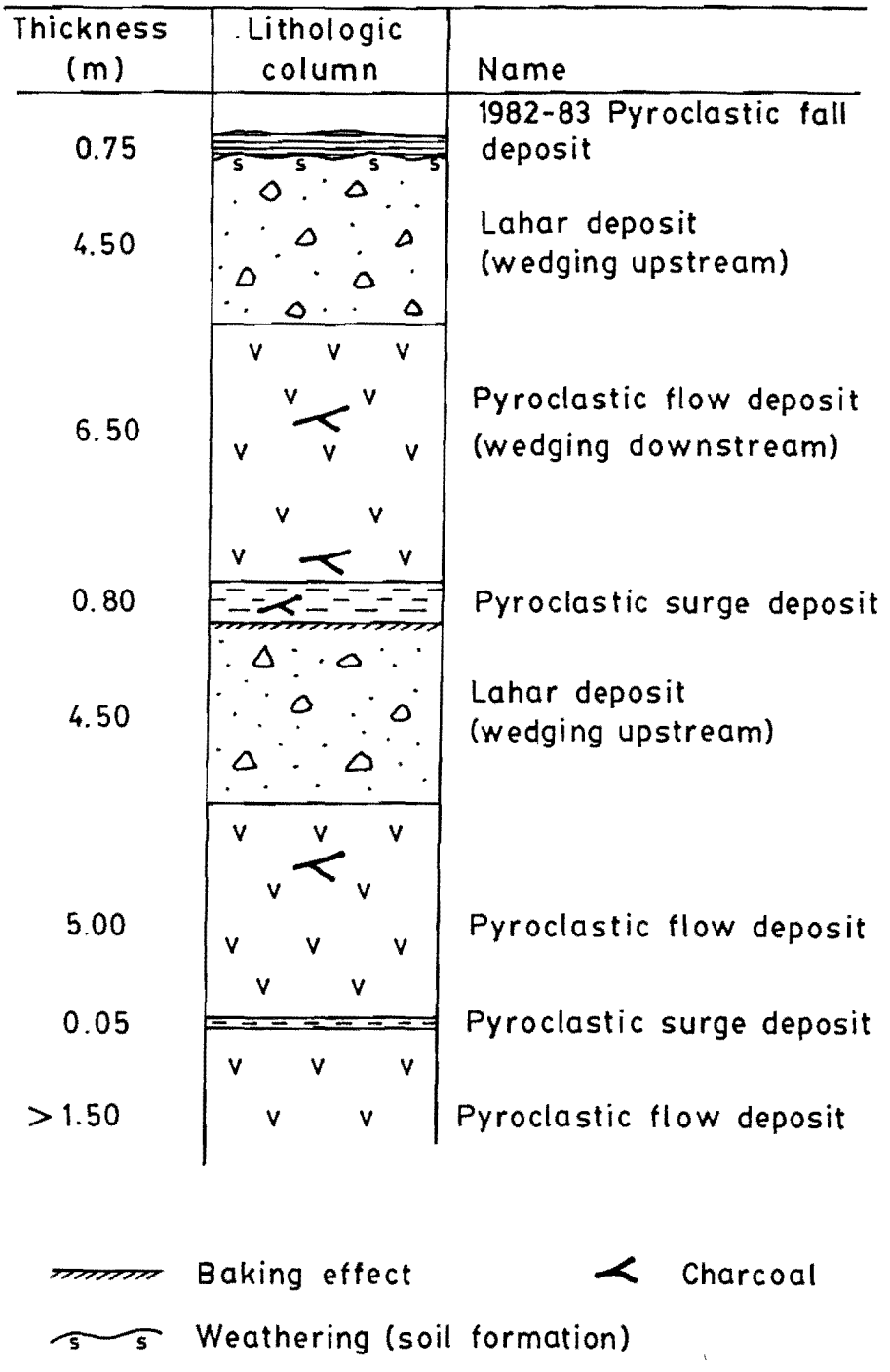

Figure III.9 Pyroclastic and lahar deposits generated during Galunggung caldera formation (the Tasikmalaya Formation) exposed in Ci Kunir valley (location 6).

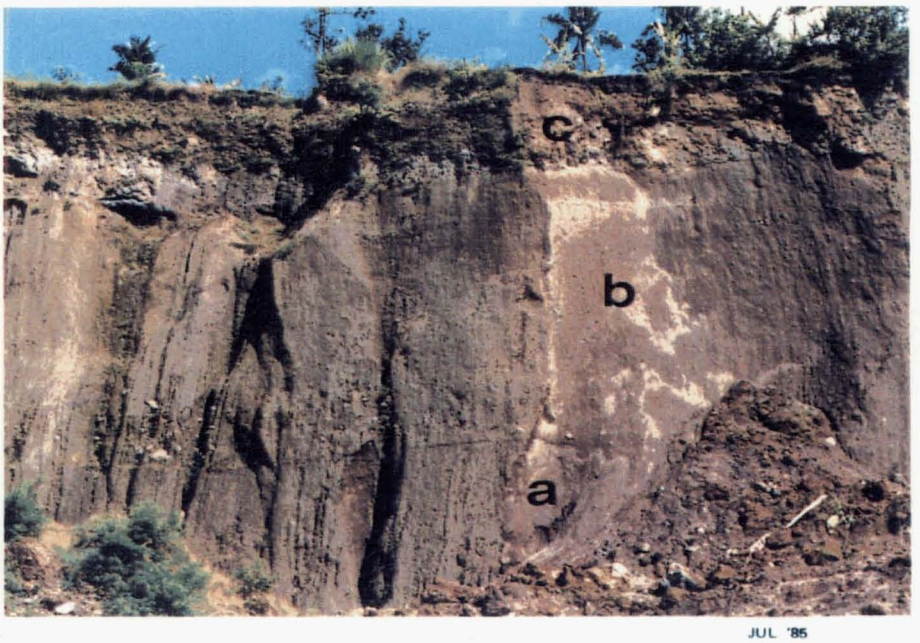

Figure III.10 Pyroclastic flow deposits (a & b) and a lahar deposit (c) generated during Galunggung caldera formation. Dark layers in the most upper part are pyroclastic fall deposits erupted in 1982. Location 6.

as planar, crossbedding and antidunes composed of fine ash (silt - sand size). Baking effects (reddish brown) are occasionally observed on the underlying rocks.

III.4.2.3 Lahar Deposits

Lahar deposits of caldera formation are well exposed along Ci Kunir valley. They are widely distributed around the hills of volcanic debris avalanche deposits. However, contact between the two deposits is rarely seen because the area is highly cultivated. Lahars are brown, consolidated and poorly sorted with intercalations of fluvial deposits. These consist of subangular to subrounded pebbles to boulders in a silt to sand size matrix.

III.4.3 Cibanjaran Formation

The Cibanjaran Formation comprises pyroclastic flow deposits, pyroclastic fall deposits and lahar deposits formed during historic eruptions in 1822, 1894, 1918 and 1982-83. In 1918 a lava dome was formed but this was completely destroyed by the 1982-83 eruption. A small volume of a lava flow was also extruded at the end of the 1982-83 eruption.

III.4.3.1 Eruption in 1822

Before the eruption of 8 October 1822, the upstream part of Ci Kunir was in the active crater (Figure III.11). Three waterfalls coming from the inactive summit crater entered the active crater. These are still present and likely always supplied water to form a crater lake. A precursor to the 1822 eruption occurred in July 1822 when Ci Kunir water was muddy (Lyell, 1872; van Es, 1924). Inspection of the crater reported that muddy water was hot, and occasionally, a vertical column of steam was seen to rise from the crater.

Junghuhn (1853) and Verbeek & Fennema (1885) reported that the volcanic disaster in 1822 was caused by "hot mud flow". Original reports based on information from local people were reinvestigated by van Es (1924) and he doubts the interpretation of Junghuhn (1853) and Verbeek & Fennema (1885).

The eruption occurred on 8 October 1822, and its sequence can be explained as follows :

Between 13.00 - 14.00 h., blasts were heard and a large vertical column of steam moved rapidly upward from the crater. The volcano was then covered (by a pyroclastic eruption ?) and the surrounding areas became completely dark. The volcano erupted "glowing mud" together with "burned sulphur" which were ejected eastward to Ci Tandui, up to 18 km from the volcano.

The paroxysmal event occurred at 15.00 h. Reddish (hot ?) sandy ash fell down close to the crater, while cold ash fell on the west and south flanks of the volcano up to 40 km away, and destroyed vegetation. At 16.00 h. the blasts declined, indicating decreasing of eruption intensity. This was followed by a menacingly quiet period at

Figure III.11 Topographic maps of Galunggung crater (simplified after van Es, 1924 and Rochanan et. al, 1984).

A Situation before the 1822 eruption

B Situation in 1883

C Situation in November 1895 (after the 1894 eruption)

D Situation in 1908

E Situation in 1924 (after the 1918 eruption)

F Situation in August - December 1983 (after the 1982-83 eruption)

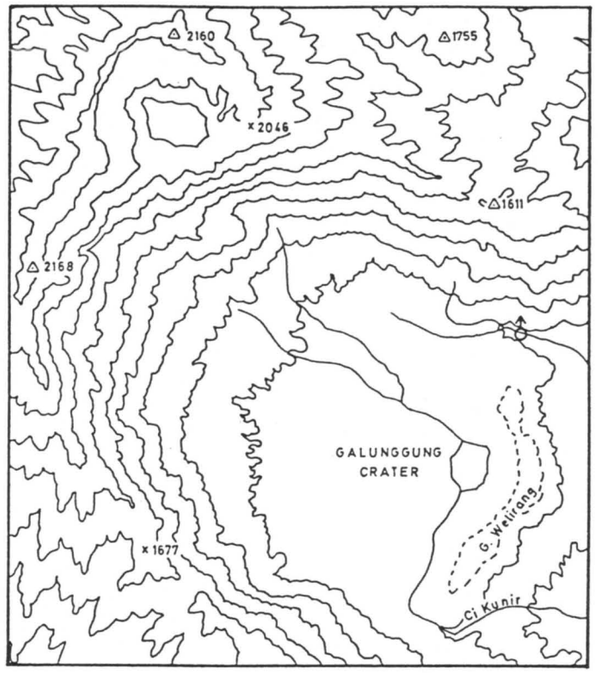

Figure III.11A (Before 1822) 0 0.5 1 KM

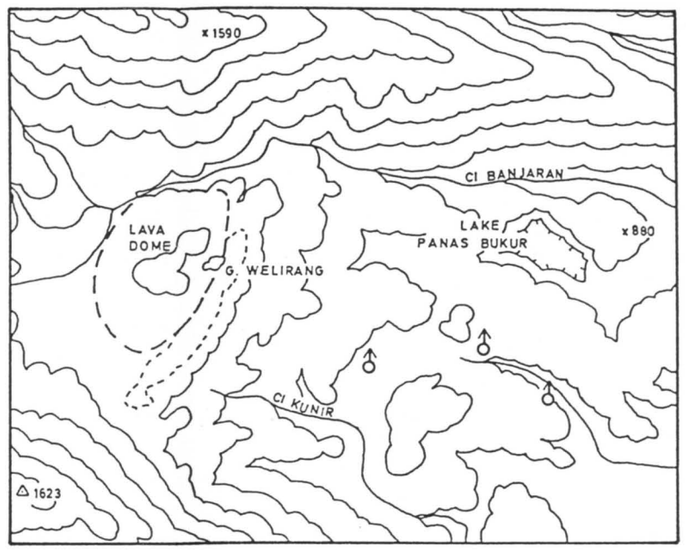

Figure III.11 B (In 1883) 0 0.5 1 KM

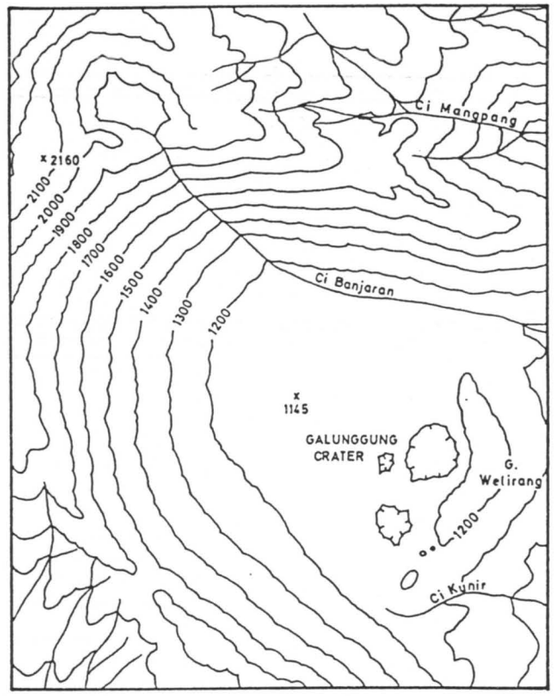

Figure III.11 C (In 1895) 0 0.5 1 KM

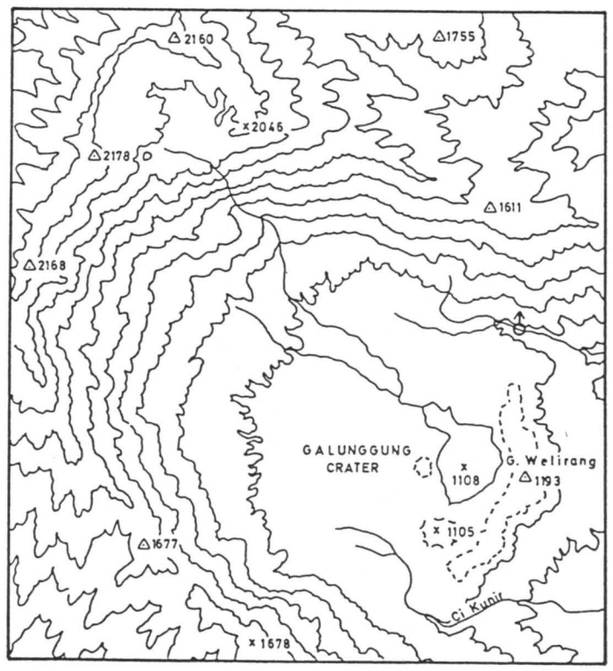

Figure III.11D (In 1908) 0 0.5 1 KM

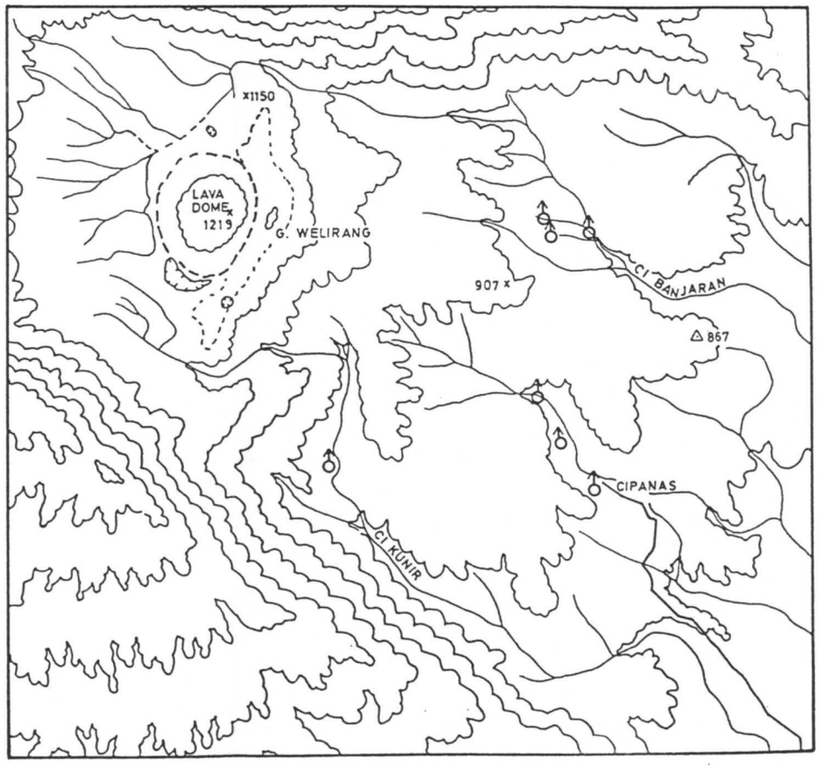

Figure III.11 E (In 1924) 0 0.5 1 KM

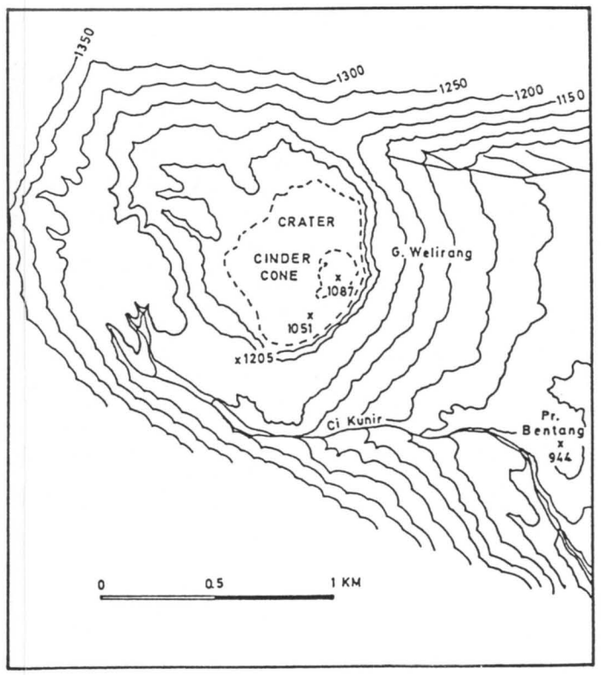

Figure III.11 F (In 1983)

about 17.00 h.

In the evening, the air became clear and Galunggung volcano could be seen with only partly burned trees left in forest. Downslope, about 10 km to the east, there were only few bald trees remained as the only indication where destroyed villages were located. Although the wind direction was to the west, eruptions were directed easterly (Fig. III.12). Ejected particles reached distant villages but those nearby (that were not affected) were generally only covered by thin ash. The original report also described a thick cloud moving down from the volcano, accompanied by hurricanes knocking down houses. Junghuhn (1853) indicated that "glowing mud" was flying above coconut trees.

Casualties were reported as follows :

" At Ciburuy and Lewibangan, death people lied down 15 feet from the villages, they likely wanted to escape but were suddenly impeded by " mud" and were killed. A woman holding her baby sat beside a tree while another one guiding her two children apparently liked to run away. At Indihiang village (14 km east of the crater), the most suffered area, a woman with her baby suckling was burned and killed. However, the baby was still alive. After the eruption she was taken by a native woman and was in a good health. In the same village, a man was also saved because of a miracle. He wanted to escape but was struck by a coconut tree and its leaves covered his body, so the "hot mud" did not burn him."

" In the margin of destroyed area, most people were alive but were burned injure. "

The term "glowing mud" and " burned sulphur" reflect high temperature and smell of sulphur. Based on these data van Es (1924)

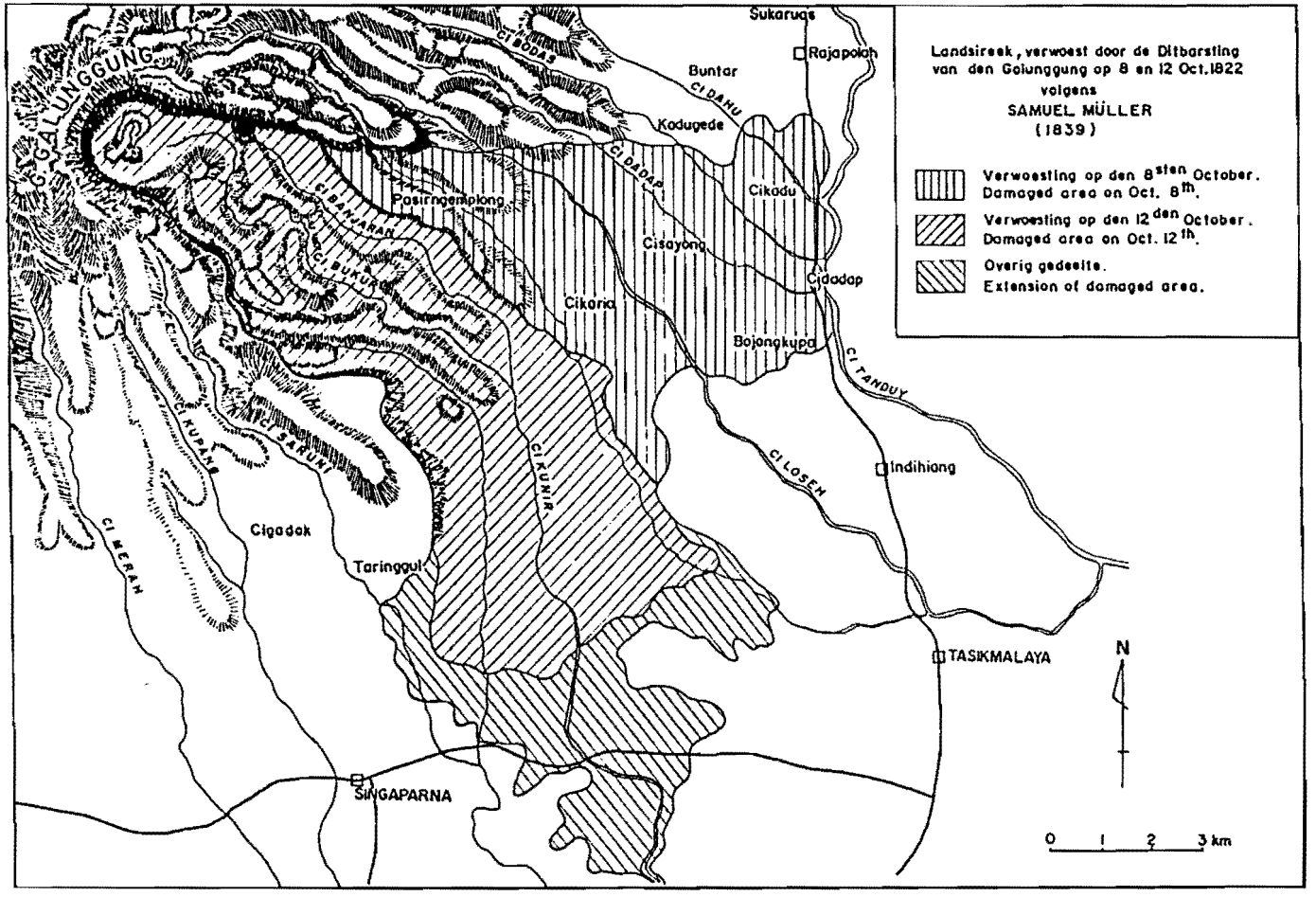

Figure III.12 Damaged areas on 8 and 12 October 1822 caused by the 1822 eruption (Müller, 1839).

argued that the volcanic disaster was caused by a "nuee ardente" that was similar to that erupted at Mount Pelée on 8 May 1902 and destroyed the city of St. Pierre (Lacroix, 1904). The information suggests that the "glowing mud" was a large ash cloud possibly a pyroclastic surge. This moved rapidly to the east, crossed ridges and depressions (Fig. III.12) while many metres of pyroclastic flow deposits were reported to be deposited in river valleys. Part of the pyroclastic flow materials mixed with river water to become hot lahars. The pyroclastic surge deposit is no longer preserved because pyroclastic surges are typically fine grained, thin layered, and easily eroded, and the affected area is intensively cultivated.

Rain continuously fell from 9 to 12 October 1822 and hot lahars flowed southeastward following the streams. People escaped from the first disaster and tried to run away by crossing the rivers, but they were killed in the hot lahars. Similarly, people from different areas which were not affected by the pyroclastic surge and flow were also killed in streams. The highest rain fell at night on 12 October 1822. This caused lahars which overflowed from the river valleys to the plains and destroyed bridges and villages. People ran to the debris avalanche hills but only a few of them who reached to the highest hills were saved, as the low hills were also covered by hot lahars.

According to Lyell (1872) another eruption occurred on the night of 12 October which was more violent than the previous one. The eruption was accompanied by a violent earthquake and the face of the volcano was utterly changed, its summit "broken down" on one side to form new hills and valleys. The occurrence of the new hills were also reported by Junghuhn (1850). The eruption during the night of 12 October was disputed by van Es (1924) because there was no forked light-

ning during the explosions. He considered that the explosions were caused by "lahar storms". In the 1982-83 eruption, lahars formed during heavy rainfalls were accompanied by secondary (steam) explosions. These happened when cold rain water suddenly came into contact with hot pyroclastic flow materials, producing high steam pressure in the deposits. So, explosions taking place through the night of 12 October 1822 were likely to have been caused by steam explosions in the pyroclastic flow deposits. The noise of the lahar was certainly heard when they flowed down and were felt like earthquakes. There is no doubt that new valleys were formed, because in the morning of 13 October, after rainfall stopped, it was observed that the Ci Banjaran had joined with Ci Kunir where previously as it had joined with Ci Juhung and Ci Loseh. However, origin of the new hill is not clear. The hills were possibly caused by a landslide that occurred together with lahars during the night of 12 October. Unfortunately, the hills formed at that time are not distinguished on the map so they cannot be distinguished from debris avalanche hills formed during the Galunggung caldera formation. Fieldwork results described below tend to suggest that the 1822 debris avalanches occurred during the eruption on 8 October.

Pyroclastic deposits and lahars devastated the area for 40 km to the east and south of the volcano. The eruption killed 4011 people, mostly overwhelmed by the pyroclastic flow and surge. Neumann van Padang (1951) estimated that more than 100 x 10^6 m^3 of lahar deposits covered the area to the southeast of the volcano.

In Figure III.11B, a lava dome was plotted, but it is not clear whether the lava dome was extruded at the end of the 1822 eruption or some time afterwards but before the 1894 eruption. In addition, the 1894 eruption described below only lasted several days as vertical

eruptions. It is unlikely that relatively short and small vertical eruptions could completely destroy the lava dome. Furthermore, in the same figure, a lake (Panas Bukur) was also present. This is not mentioned or shown on the map produced before the 1822 eruption (Fig. III.11A). Two possibilities are : 1. the lake was formed before the 1822 eruption but it was not identified because of dense forest, or 2. the lake was formed during the 1822 eruption. In Figure III.11E, a small crater that was probably formed during the 1894 eruption is shown at south flank of Gunung Welirang. These data suggest that flank eruptions occurred in the past and they may occur in the future, too.

A pyroclastic flow deposit and a volcanic debris avalanche deposit erupted in 1822 are well preserved upstream in the Ci Banjaran (Fig.III.13). Radiocarbon dating of wood fragments in fluvial material below these deposits gives an age of 590 ± 150 years BP (Fig.III.14). This indicates that Galunggung volcano had a long period of dormancy before the 1822 eruption. The pyroclastic flow formed valley filling deposit, such as at between Pasir Malang and southwest wall of Galunggung caldera (location 4), but the best outcrop is found along Ci Banjaran (location 30 - 14), where the pyroclastic flow deposit is overlain by the volcanic debris avalanche deposit.

The 1822 pyroclastic flow deposit is typically fresh and dark grey and structureless, but weathers to brown on the surface. The deposit is loose and consists of abundant ash. Occasionally, the pyroclastic flow deposit directly underlies the 1982-83 deposits when the debris avalanche deposit is absent.

Although the volcanic debris avalanche deposit is covered by pyroclastic deposits of the 1982-83 eruption, its morphology is clearly identifiable and it forms a ridge (about 2 km in length and

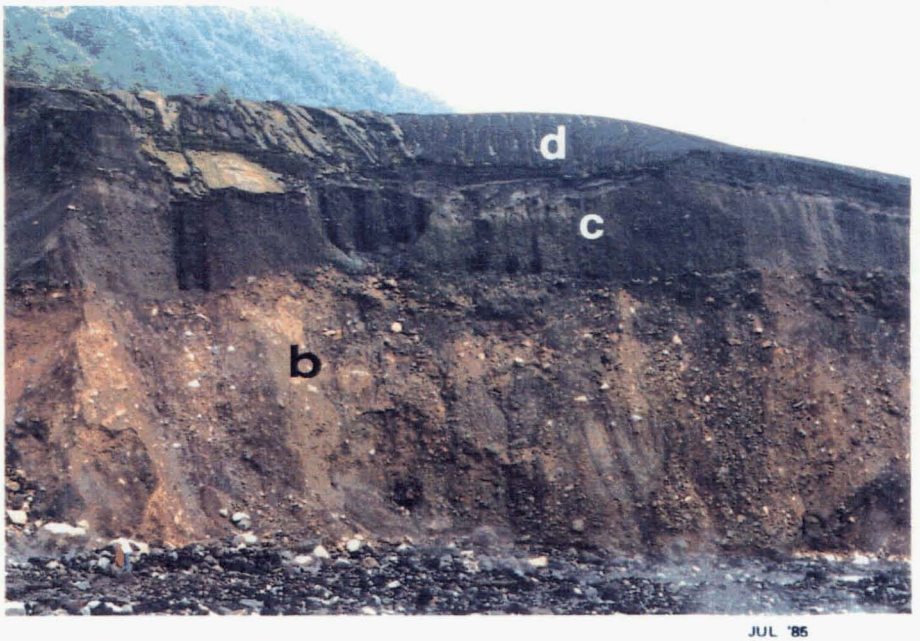

Figure III.13 Pyroclastic flow deposit (a) and volcanic debris avalanche deposit (b) erupted in 1822, overlain by pyroclastic flow and fall deposits of the 1982-83 eruption (c & d). Location 16, Ci Banjaran upstream.

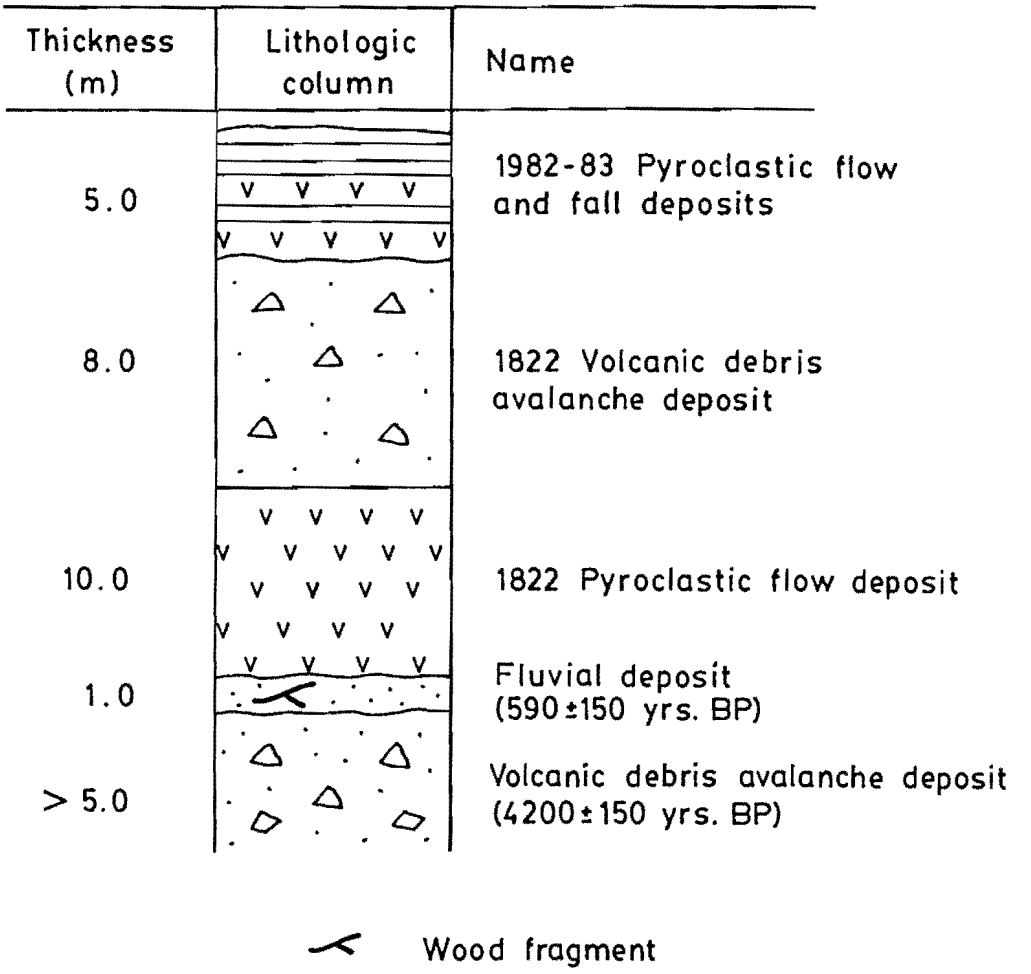

Figure III.14 Pyroclastic flow deposit and volcanic debris avalanche deposit of the 1822 eruption overlying the fluvial deposit formed in 590 ± 150 yrs. BP, and covered by the 1982-83 volcanic deposits. Location 16, Ci Banjaran upstream.

250 m width) extending from the active crater flow southeastward to the Ci Banjaran valley. The debris avalanche deposit consists of unconsolidated and unsorted material from ash to blocks which are mostly angular andesitic fragments from older rocks (Old Galunggung lavas).

III.4.3.2 Eruption in 1894

The 1894 eruption took place during the evening of 17 October, from three eruptive vents within the crater. Another eruption occurred on 18 - 19 October 1894 during which pyroclastic falls were laid down in the surrounding area and later in Bandung, Cianjur and Sukabumi (200 km WNW of Galunggung). The eruption created a new crater about 300 - 400 m across and several explosion holes. Volume of the ejected material is 22 x 10^6 m^3 of dense rock having a density of about 2.2 (Fennema, 1896). 79 Houses collapsed, mostly in the west and south of the volcano because of pyroclastic fall deposits. No casualties were reported during this eruption. Lahars on the 27 and 30 October 1894 flowed down valleys in a similar path to those of 1822. Ci Banjaran was captured, became joined to the crater region, and then filled with water to form a crater lake (e.g. van Es, 1924).

Although pyroclastic fall deposits on the crater rim were reported up to 25 m thick (van Es, 1924), most of them are now eroded. The pyroclastic fall deposits overlain by talus deposits in Ci Kunir valley are considered remnants of this deposit (Fig. III.15). Two layers of pyroclastic fall deposit occur showing normal grading from predominantly bombs at the base to ash at the top. These rocks have

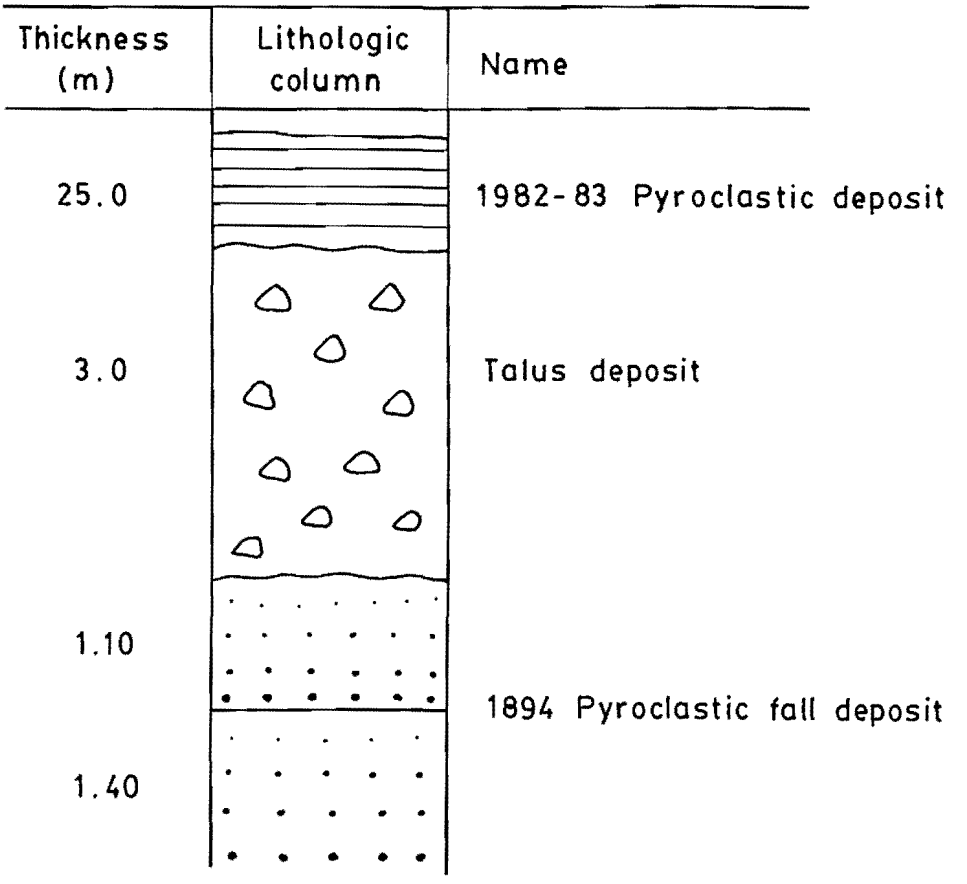

Figure III.15 Pyroclastic fall deposits of the 1894 eruption, overlain by talus deposit. Location 60, Ci Kunir upstream.

been affected by hydrothermal alteration.

Talus deposits consist of angular clasts from Old Galunggung lavas, weathered brown, with some wood and roots. In the main channel of Ci Kunir the deposit reaches up to 5 m thick. In some places, the upper part of this talus was heated (baking effect) by the 1982 pyroclastic flow and is brick red.

III.4.3.3 Eruption in 1918

This activity was preceded by earthquakes at 22.00 h on 16 July 1918. Pyroclastic falls were limited to the crater area (2 - 5 cm thick) and to the southern slope. Three days later a lava dome emerged above the crater lake surface. This dome was 85 m high and 560 m x 440 m wide (Neumann van Padang, 1951), and was known as Gunung Jadi (Fig.III.16). The 1918 lava dome was completely destroyed by eruptions in 1982-83.

III.4.3.4 Eruption in 1982-83

Observations during the six months prior to the eruption showed no significant increase in seismicity (Rasjid, 1982). Also, geological mapping carried out in the end of 1981 indicated neither surficial changes nor increasing fumarolic activity. In 1958 and 1959 (Kusumadinata, 1959), there was vigorous emission of gas, although there was no eruption. The first eruption began on 5 April 1982 accompanied by rumblings, detonations, incandescence and forked lightning, which ter-

Figure III.16 Lava dome extruded on 19 July 1918. Picture was taken from the eastern flank in December 1981.

Figure III.17 Pyroclastic flow deposit erupted on 25 April 1982 in Ci Banjaran valley, (7 May 1982).

minated in January 1983 (about 9 months later). VSI (1983) noted the total number of eruptions as 61. The chronology of the 1982-83 eruption has been described by many authors and in great detail by Katili & Sudradjat (1984). In general, the activity of the 1982-83 eruption can be summarised in terms of three phases (Table III.2).

In the initial stages, Peléean eruptions destroyed the 1918 lava dome and produced pyroclastic flow and fall deposits. Pyroclastic flows reached a maximum distance of 5.1 km from the crater down to the Ci Banjaran valley. The longest flow occurred on 8 April 1982. It was followed by another flow (4.5 km) on 25 April 1982 (Fig. III.17). Other pyroclastic flows were witnessed moving down to Ci Kunir, Cipanas and Ci Banjaran on 6 and 18 May 1982. These flows, however, were shorter than before. All were erupted at night and were identified by incandescence. Eruptions in this first phase can be considered to be the most powerful in terms of volume of ejected volcanic material (Katili & Sudradjat, 1984). On 5 June 1982 the author witnessed a small pyroclastic flow about 2 km from the crater. This was initiated by a vertical eruption, then suddenly a "cloud" fell back and flowed down along the slope of Gunung Welirang. In front of the flow, there were many bombs falling down, with a sound similar to bombs exploding. The pyroclastic flow came into Ci Kunir accompanied by secondary explosions and then flowed down to become a hot lahar. This earlier eruption lasted 6 weeks, with 9 eruptive events, ejecting material of about 270×10^6 m^3.

In the second phase, vertical (Vulcanian) eruptions producing pyroclastic fall deposit were dominant. The eruptions were accompanied by thunder and forked lightning, and eruption columns commonly reached a height of 15 to 20 km. On 24 June an eruption forced a British Air-

Table III.2 Activity of the 1982-83 eruptions.

Eruption type	Duration	Total number of eruptions	Volume ejected material
Peléean	6 weeks (5 April - May)	9	270 X 10^6 m^3 (?)
Vulcanian	3 months (June - August)	21	100 X 10^6 m^3 (?)
Strombolian	4 months (Sept.- Decemb.)	31	< 1 X 10^6 m^3
Lava extrusion	1 - 7 January		

ways 747 jet to make an emergency landing in Jakarta after all four engines cut out because of ingestion ash materials (SEAN Bull., v.7, June 1982; Tootell, 1985). A similar accident happened to another Jumbo jet when the volcano exploded again on 13 July 1982. These Vulcanian eruptions lasted for 3 months with 21 eruptive events ejecting materials approximately 100 x 10^6 m^3. Pyroclastic fall deposition depends on the wind direction, which during April to October is typically northwesterly (Fig.III.18). However, in the upper part of the troposphere and lower stratosphere (about 10 - 30 km height; Barry & Chorley, 1982), wind directions are uncertain. Occasionally, volcanic ash was distributed easterly as far as Yogyakarta city, approximately 500 km east of Galunggung and ash was also reported at Cirebon city, about 75 km northeast of Galunggung. Some eruptions clouds were observed from satellite imagery to the south [illegible] (Katili & Sudradjat, 1984, plate 15b-c).

The third eruptive phase (Strombolian eruptions) produced incandescent bombs (Fig.III.19). Ash plumes were typically very low and from November 1982 pyroclastic ejecta fell back into the crater to form a cinder cone (Fig.III.20). The cone was 250 m x 165 m across and 30 m above the crater floor. This phase was terminated by a lava extrusion in early (1 - 7) January, 1983. The lava flowed southeastward from a vent situated along the northwest striking fracture (N315^{o}E) in the cone and formed a fan-shaped flow covering an area of approximately 25 m x 30 m and about 2 - 3 m thick on the crater floor. These Strombolian eruptions lasted for 4 months with 31 eruptive events, ejecting < 1 x 10^6 m^3 of tephra. The total volume of ejected materials during the 1982-83 eruption exceeded 370 x 10^6 m^3 (Katili & Sudradjat, 1984), but more than a half of the volume has been eroded

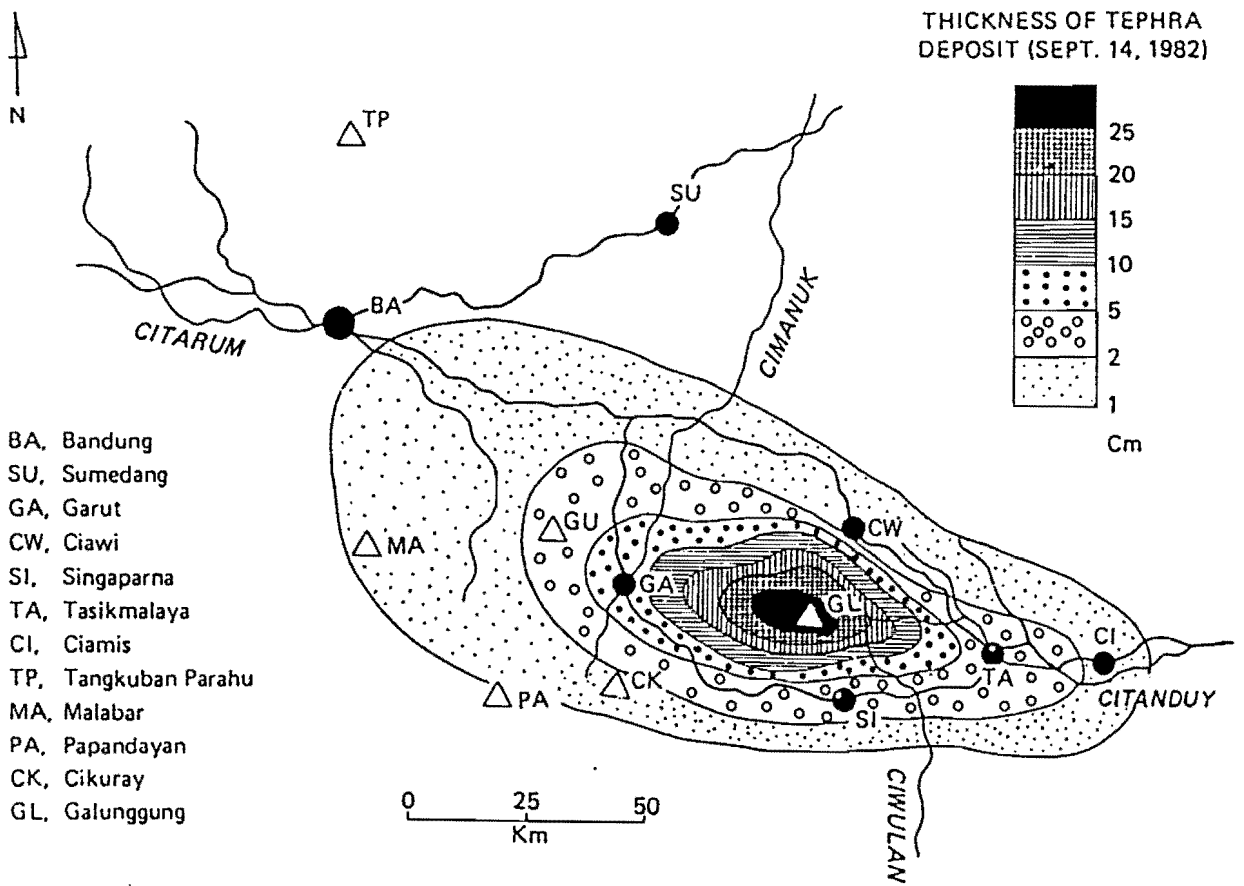

Figure III.18 Sketch map showing the distribution and thickness of pyroclastic fall deposits (up to 14 September 1982) of the 1982 Galunggung eruptions (Katili & Sudradjat, 1984).

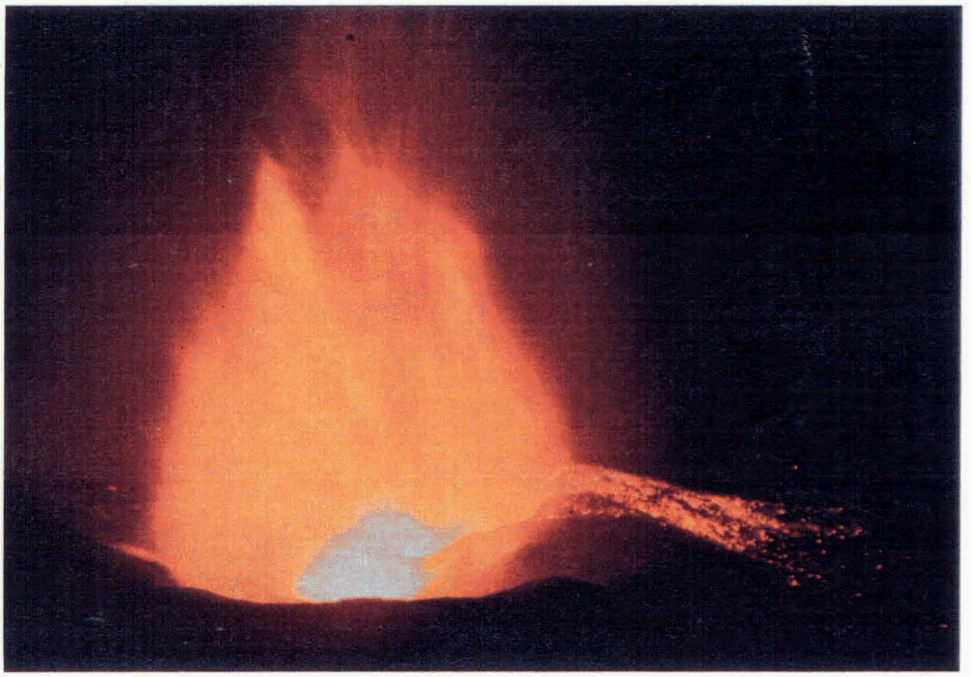

Figure III.19 Strombolian eruption in the last stage of the 1982-83 Galunggung eruption (R. Hadian, January, 1983).

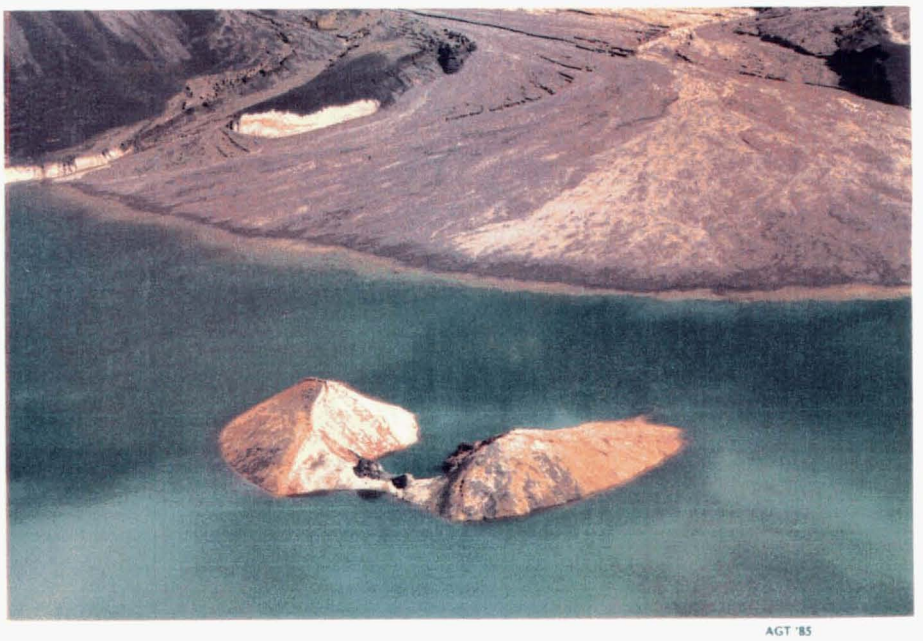

Figure III.20 Cinder cone formed in the last stage of the 1982-83 Galunggung eruption (August, 1985).

at the present time (1988).

Many waterfalls carried water and debris into the crater but there was no drainage from the crater, so a lake formed, similar to that formed at the end of the 1894 eruption. Now (1988) the cinder cone has been completely covered by lake water. During the rainy season following the eruptions, some pyroclastic deposits became "reworked" to form lahars and alluvial deposits.

The 1982-83 eruptions ultimately caused evacuation of 35,000 people and approximately 94,000 ha of cultivated land was severely affected. The total value of physical damage reported by the Governor of West Java was conservatively estimated to exceed US $ 100 million (Katili & Sudradjat, 1984), but fortunately no casualties were directly attributable to the eruptions.

III.4.3.4.1 Pyroclastic Flow Deposits

Pyroclastic flow deposits only occur inside the Galunggung caldera, particularly along the Ci Banjaran and Ci Kunir valleys (see Appendix 1.11 - 15). Figure III.21 shows four relatively thick pyroclastic flow deposits formed during the 1982-83 eruption. The stratigraphy along Ci Banjaran upstream from location 14 through 16 to 30 is complicated (see Appendix 1.11 - 13) by rapid channelised deposition and erosion of pyroclastic flow deposits and lahar deposits. However, two distinctive layers of bomb-rich pyroclastic flow deposits (Fig.III.22) are very useful in reconstructing the stratigraphy (Fig.III.23).

Along the Ci Banjaran, all 1982 pyroclastic flow deposits

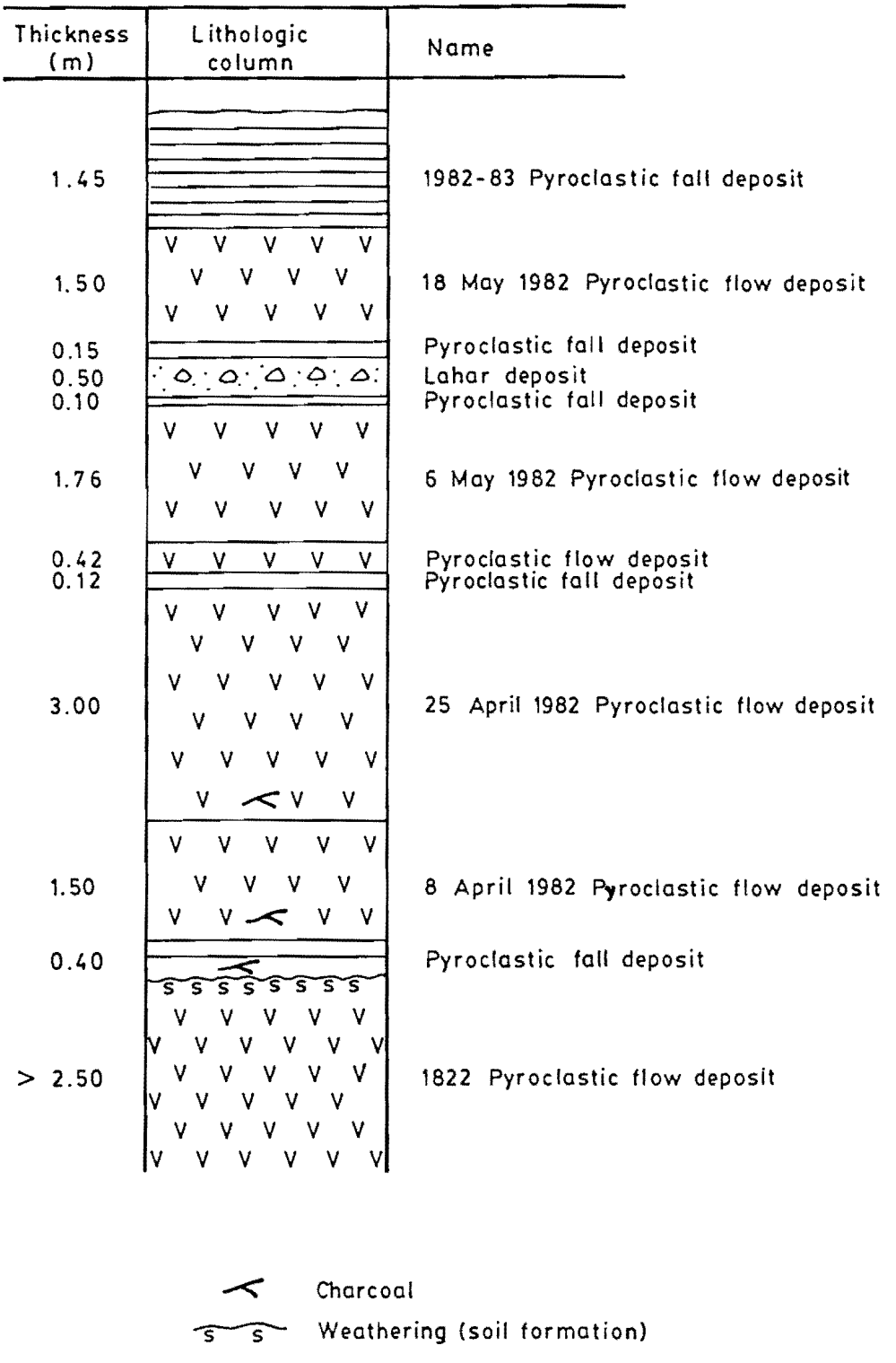

Figure III.21 Four thick pyroclastic flow deposits of the 1982-83 eruption. Location 13, 1.5 km SE the Galunggung active crater.

Figure III.22 Galunggung volcanic rocks erupted in 1982-83.

A 1. Lower dark bomb-rich pyroclastic flow deposit
2. Lahar deposit
3. Upper dark bomb-rich pyroclastic flow deposit
4. Pyroclastic flow deposit

B Middle part of the bomb-rich pyroclastic flow deposits, location 14, Ci Banjaran upstream, (17 July, 1985)

C 1. Lower dark bomb-rich pyroclastic flow deposit
2. Lahar deposit
3. Upper dark bomb-rich pyroclastic flow deposit
4. Pyroclastic flow deposit (?)
5. Alternating pyroclastic flow and fall deposits, location between 14 - 16, Ci Banjaran upstream, (25 September 1985)

D 1. Pyroclastic flow deposit erupted in 1822
2. Pyroclastic flow deposit
3. Lower bomb-rich pyroclastic flow deposit
4. Lahar deposit
5. Upper bomb-rich pyroclastic flow deposit
6. Pyroclastic flow deposit (?)
7. Alternating pyroclastic flow and fall deposits, location 16, (25 September 1982)

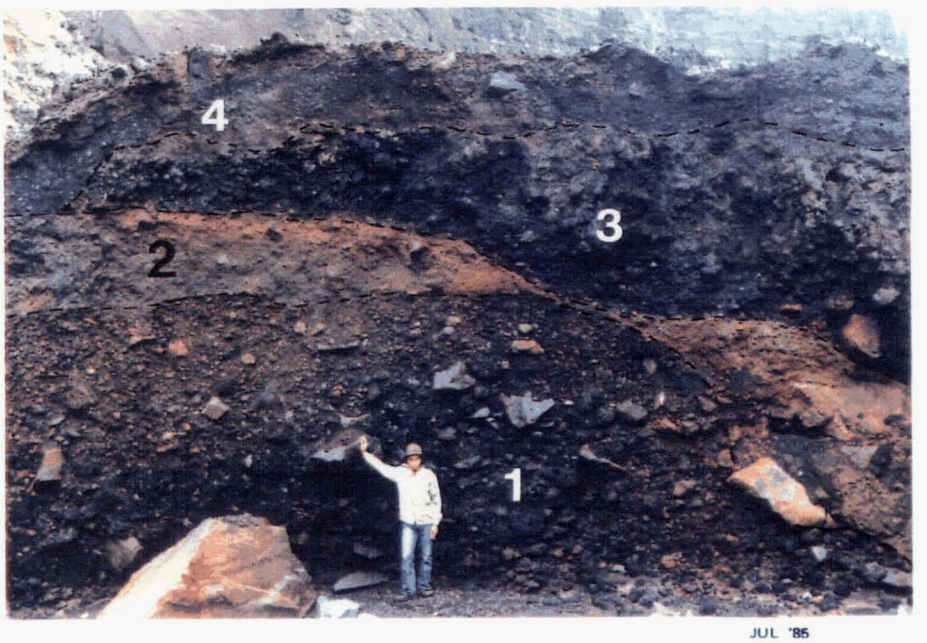

Fig. III 22A

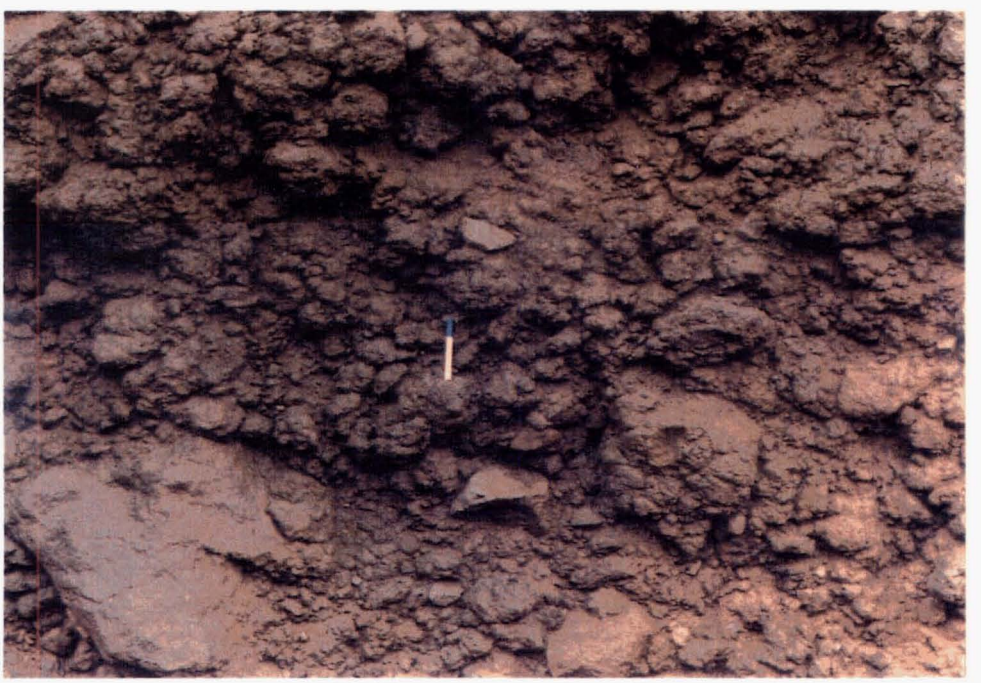

Fig. III. 22B

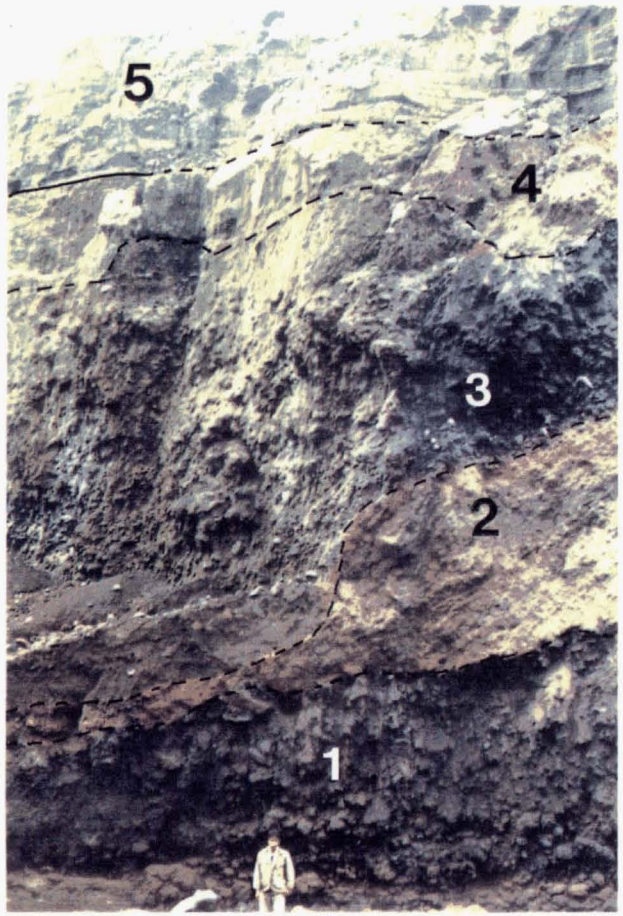

Fig. III.22C

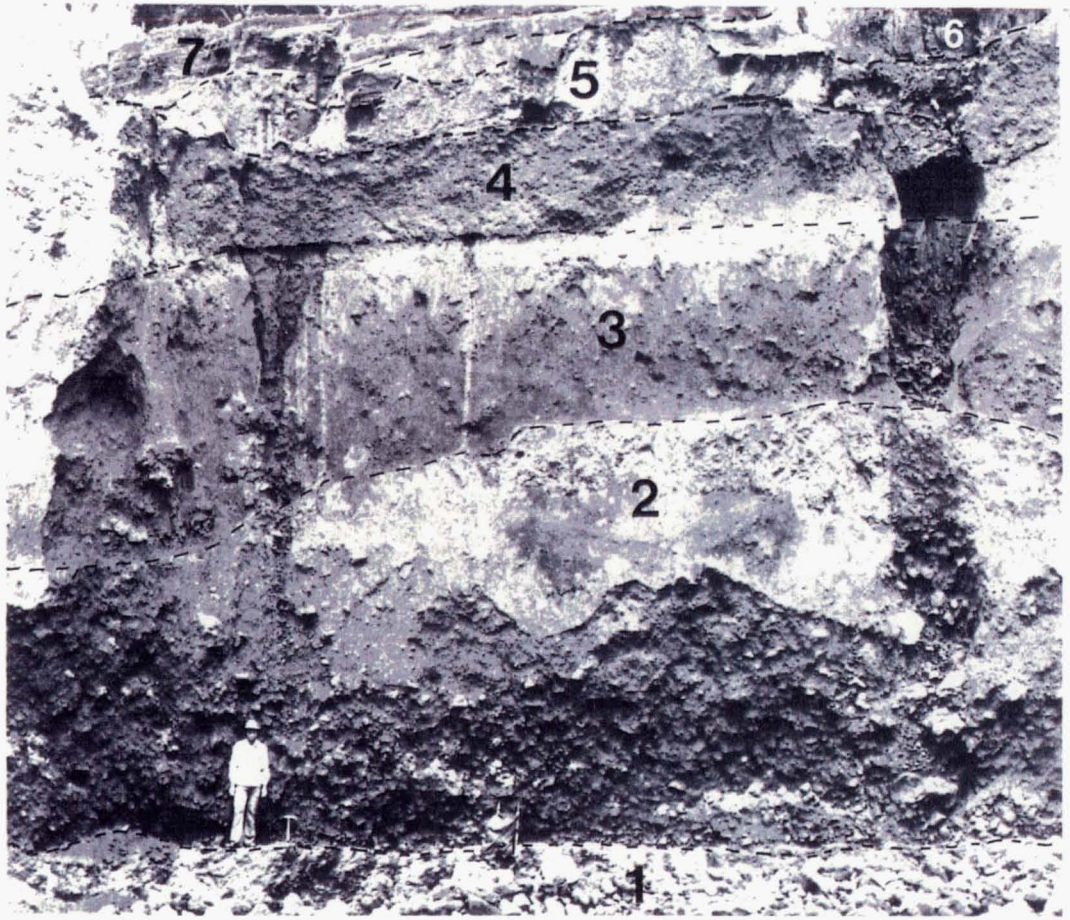

Fig. III.22D

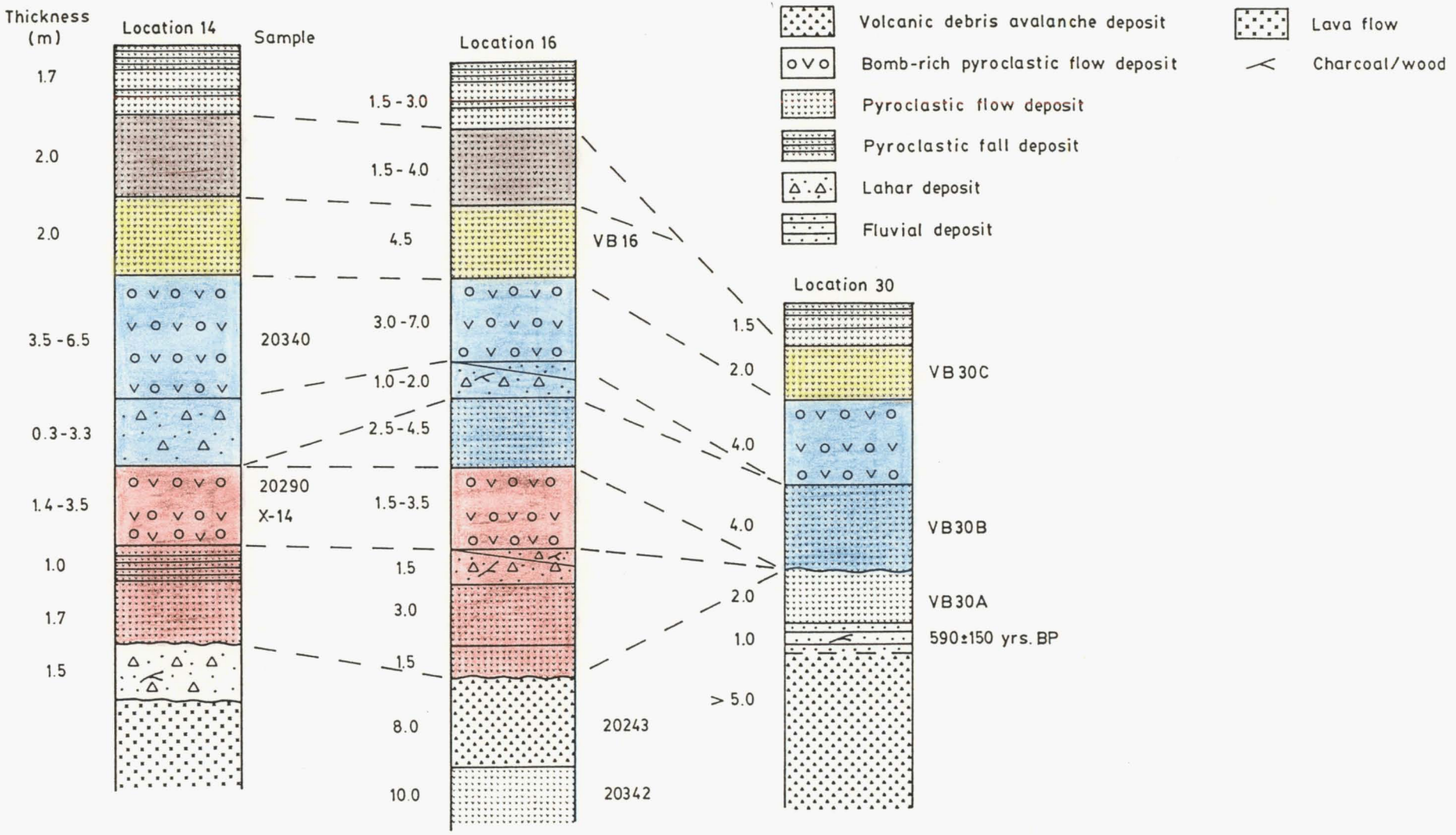

Figure III.23 Correlation of the 1982-83 volcanic deposits along Ci Banjaran upstream. Colours represent time of activity : red (8 April), blue (25 April), yellow (16 May) and brown (18 May ?).

overlie the 1822 volcanic debris avalanche and pyroclastic flow deposits. The 1982 pyroclastic flow deposits commonly alternate with lahars and are dominated upward by pyroclastic fall deposits. The bomb-rich pyroclastic flow deposits are typically darker (black), abundant bombs particularly in the middle part of the deposit and close to the source. Older andesitic blocks are up to 1.5 m in diameter, angular and massive, occur close to the crater.

Overall, the 1982 pyroclastic flow deposits are unconsolidated and contain abundant ash. Their bombs are breadcrust type. At first, pyroclastic flow deposits were dirty white to light grey when they were hot, but the top part rapidly oxidised to brick red then reddish brown. On cooling, the internal part becomes dark grey. A darker color for the bomb-rich pyroclastic flow deposits may suggest lower temperature during their formation compared with the others. Thickness of the pyroclastic flow deposits changes sharply from place to place. The irregular thickness may result from variations in the pre-existing topography and erosional processes during and after their deposition.

The total volume of the 1982 pyroclastic flow deposits was estimated 5.5 x 10^6 m^3 (Bronto et al., 1983). Nevertheless, most has been eroded (1988) and only a little of it is still present, mainly in the Ci Banjaran and Ci Kunir valleys.

III.4.3.4.2 Pyroclastic Fall Deposits

Pyroclastic fall deposits were widely distributed during the eruption but most have been eroded since then. In the Galunggung caldera , pyroclastic fall deposits vary from 1 to 10 m thick, up to a

maximum of 30 m around the active crater. A section through the deposits is given in Appendix 1.16. In the Old Galunggung crater the pyroclastic deposits are about 20 m thick, while at Parentas village, 7 km NW of Galunggung, they reach up to 60 cm thick.

The pyroclastic fall deposits are very well stratified showing normal graded bedding with the size of the material ranging from ash to bomb and block depending on the distance of deposition and the strength of the eruption.

Pyroclastic fall deposits erupted in the initial stage, from April to May 1982, are grey and composed of andesitic materials. But in the final stage, from September to December 1982, the materials become darker and basaltic in composition. Pumice was also ejected in September, which was blanketed by basaltic material.

Bombs are largely of breadcrust type in the initial stage, but changed to fusiform or well rounded and finally cow dung bombs at final stage of eruptions. These bombs are scattered around the crater. The changing bomb shape is probably controlled by viscosity of magma that becomes less viscous with time. At the end of activity, pyroclastic fall deposits resulted from Strombolian eruptions and formed cinder cone in the Galunggung crater.

III.4.3.4.3 Pyroclastic Surge Deposits

Rare pyroclastic surge deposits usually occur as thin irregular layers composed by reddish to brownish grey fine ash (silt - sand in size), with internal structures such as cross - laminations, antidunes and planar - laminations. They often occur with pyroclastic fall depo-

sits but a pyroclastic surge did occur in association with a pyroclastic flow on 8 April 1982. The surge was directed southeastward and burned houses at Pasirngemplong village, whereas the pyroclastic flow flowed downstream along Ci Banjaran valley (Fig. III.24A). This was possibly similar to the "glowing cloud" (ash cloud type of pyroclastic surge) which destroyed the city of St. Pierre (e.g. Macdonald, 1972, p. 144) when Mt. Pelée erupted on 8 May 1902 (Fig. III.24B). The straight direction of flow is also comparable to the pyroclastic surge which occurred on 9 May 1986 at Mt. St. Helens (Fig. III.24C) although this surge was generated by rock avalanche of the dome (Mellors et al., 1988). Around the burned houses, a pyroclastic surge deposit was identified as a layer showing irregular in thickness (2 - 5 cm), reddish grey fine ash and containing fine charcoal and broken roof tiles. Pyroclastic surges are also identified by trees falling in the parallel position and the charring of the surface facing towards the vent.

III.4.3.4.4 Lava Flow

A small basaltic lava flow occurred from 1 - 7 January 1983 on the south foot of cinder cone inside the Galunggung crater. The lava is however now buried by alluvium and water of the Galunggung crater lake.

III.4.3.4.5 Lahar and Alluvial Deposits

During rainy seasons unconsolidated pyroclastic deposits were

Figure III.24

A Pyroclastic surge accompanying pyroclastic flow at Galunggung erupted on 8 April 1982 and burned houses at Pasirngemplong village.

B Pyroclastic surge ("glowing cloud") accompanying pyro clastic flow ("glowing avalanche") at Mt. Pelée, erupted on 8 May 1902 and destroyed the city of St. Pierre (Macdonald, 1972).

C Pyroclastic surge and flow generated by the 9 May 1986 rock fall avalanche of Mt. St. Helens lava dome (modified after Mellors et. al, 1988).

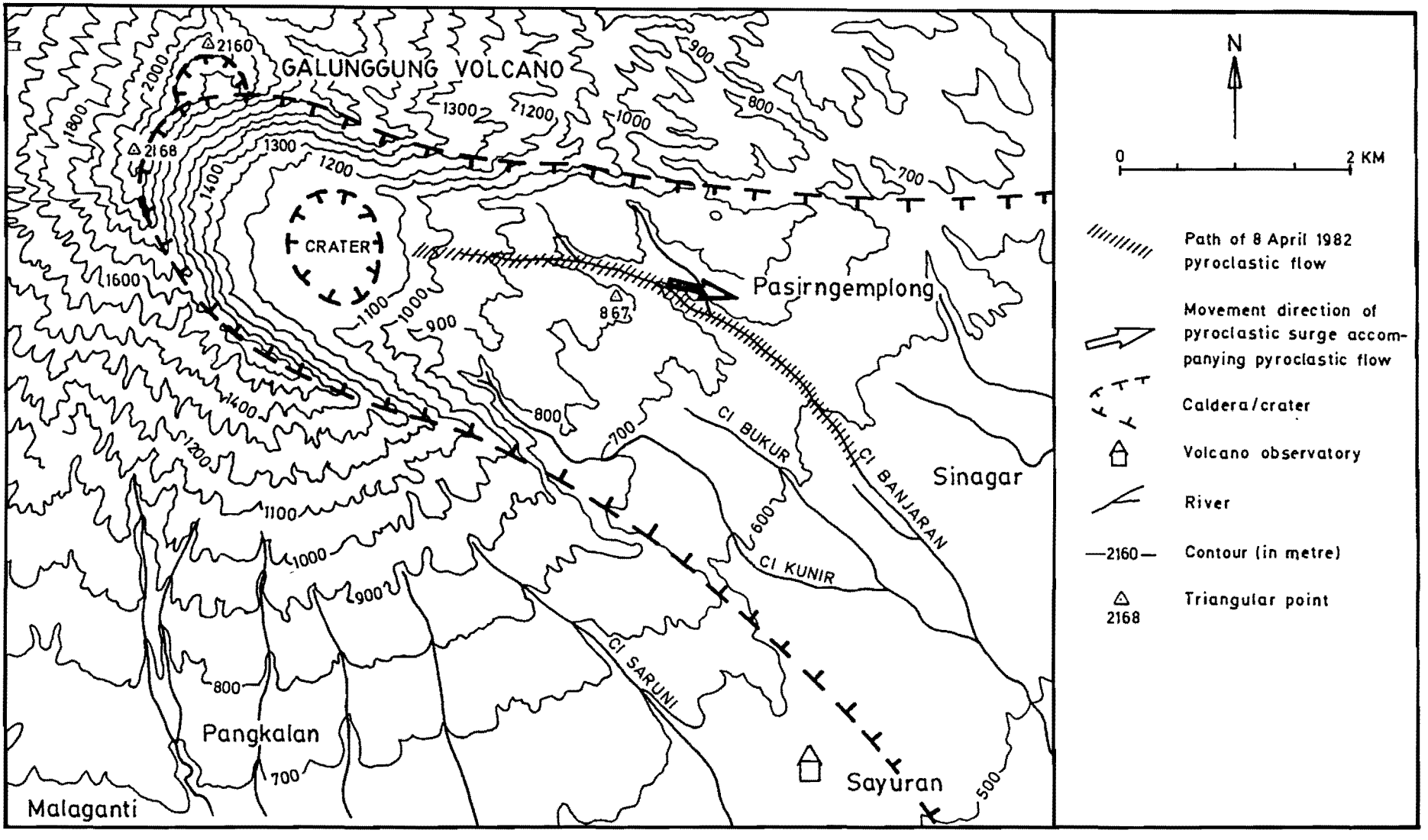

Figure III.24A

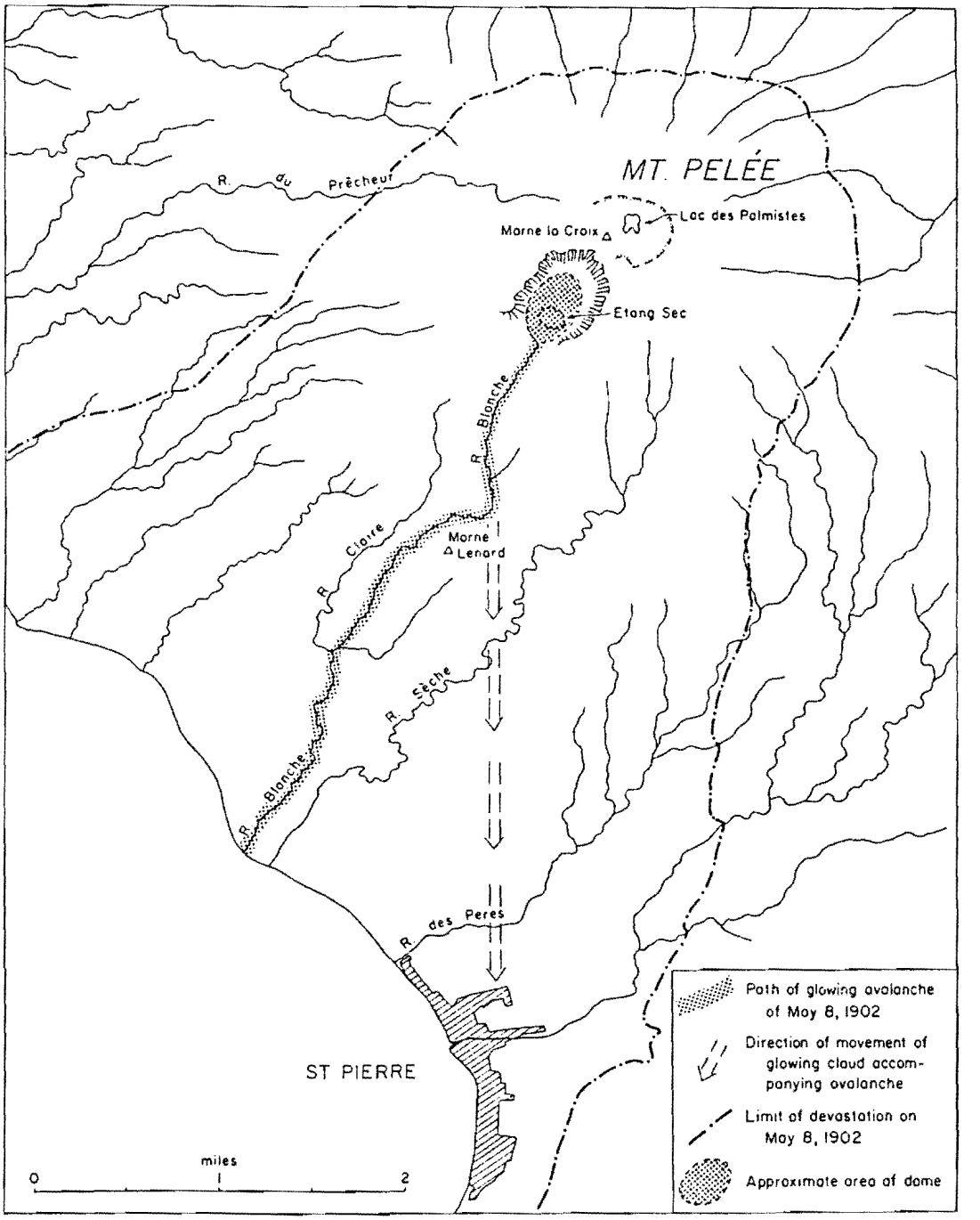

Figure III.24B

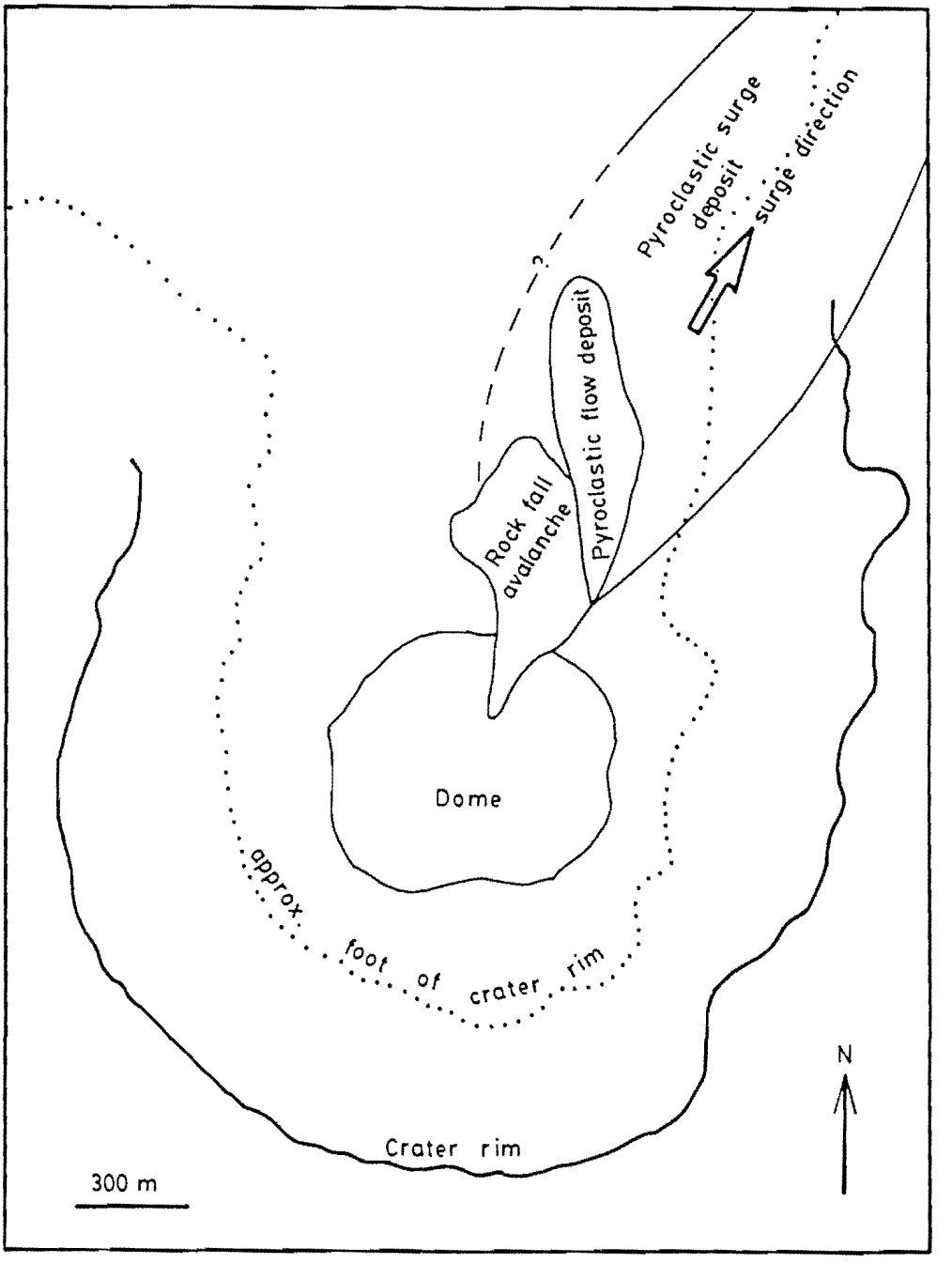

Figure III.24C

eroded and redeposited as lahar deposits. Most the deposits occur at the foot of the volcano, and the plain areas particularly in the southeast of the Galunggung volcano following the Ci Banjaran, Ci Kunir and Ci Loseh valleys. Some high places or hills composed of debris avalanche deposit are not covered by lahar deposits.

Lahar deposits are typically unsorted, structureless and commonly showing individual megablocks floating in a sandy matrix. They become indurated shortly after deposition. The diameter and angularity of the clasts decrease with distance from the source. If a water supply is added continuously, the lahars gradually change to become flood and normal river deposits with sedimentary crossbedding, graded bedding and planar bedding.

Most alluvial deposition occurred after eruption as "reworked" deposits from pyroclastics and lahars. They are distributed in the Galunggung crater and along river valleys. The material varies in size from clay to boulder and sedimentary structures.

The sequence of eruptions in 1982-83 reflects an ideal sequence of pressure reduction. The eruptions were from Peléean through Vulcanian to Strombolian types and were terminated by a lava extrusion (Table III.2). The period of each eruption types became longer in duration but the volume of ejected materials decreased with decreasing the degree of explosivity. The 1918 lava dome could be considered as a "plug" allowing volcanic energy to be accumulated and to generate explosive eruptions in the initial stage.

The total number of eruptions may relate to the rock compositions and gas content. In the earlier eruptions, ejected materials were intermediate rocks (basaltic andesites) in which gas was trapped and accumulated under a comparatively high pressure. On the other

hand, in the final stage, the rocks were basalts in which gas easily escaped causing more frequent eruptions but weaker.

III.5 Hot Springs, Solfatara and Fumarole Fields

Shortly after the 1982-83 eruption, two kind of hot springs, permanent and intermittent, formed. Permanent hot springs appeared from pre-1982-83 eruption volcanic rocks. These can be found upstream of Ci Kunir and Ci Banjaran, and in the Cipanas area. Before the 1982-83 eruption the Cipanas hot spring was used as a recreational park.

Intermittent hot springs appeared under the 1982 pyroclastic flow deposits. The hot springs resulted from cold water flowing through hot pyroclastic flow deposits. Since 1986, however, the 1982 pyroclastic flows have become cold and the hot springs disappeared.

Fumarole and solfatara fields are only found in the middle of active crater wall facing the cinder cone.

III.6 Tectonic Setting of the Galunggung Volcano

In the Tasikmalaya region, Tertiary rocks are largely disrupted by northwest-striking faults (see Fig.II.4). Lineament patterns in Quaternary volcanics of the area (Fig.III.25) display a similar orientation. These data are plotted on a rose diagram (Fig.III.26) which shows a predominance of the lineaments in N315^{o}E direction. This is similar to the fracture zone in the 1982-83 cinder cone (see

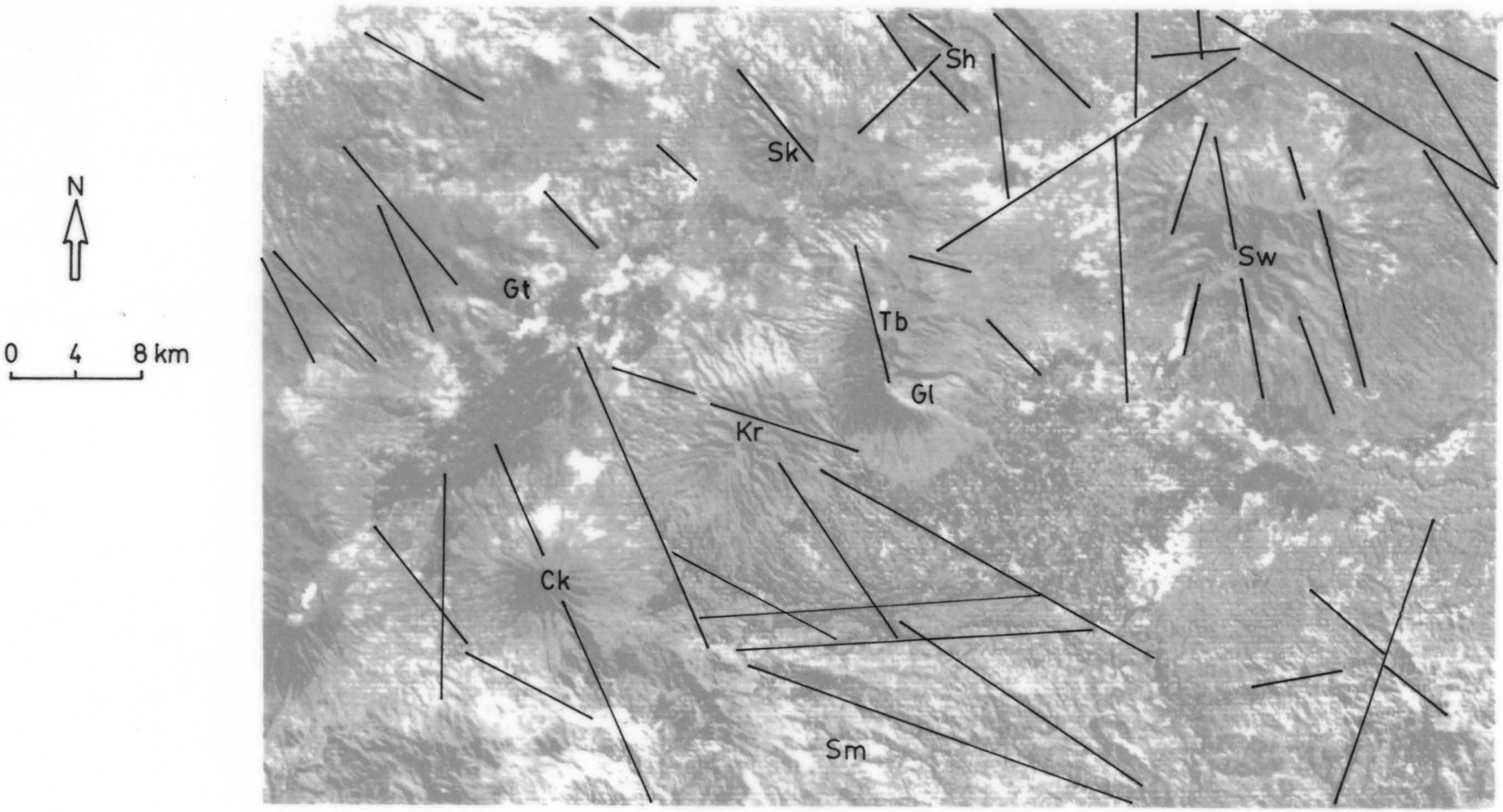

Figure III.25 Lineaments in the Quaternary volcanoes of Tasikmalaya region. Gl = Galunggung, Tb = Telagabodas, Sk = Sedakeling, Sh = Sanghiang, Sw = Sawal, Kr = Karacak, Ck = Cikurai, Gt = Guntur, Sm = Southern Mountain

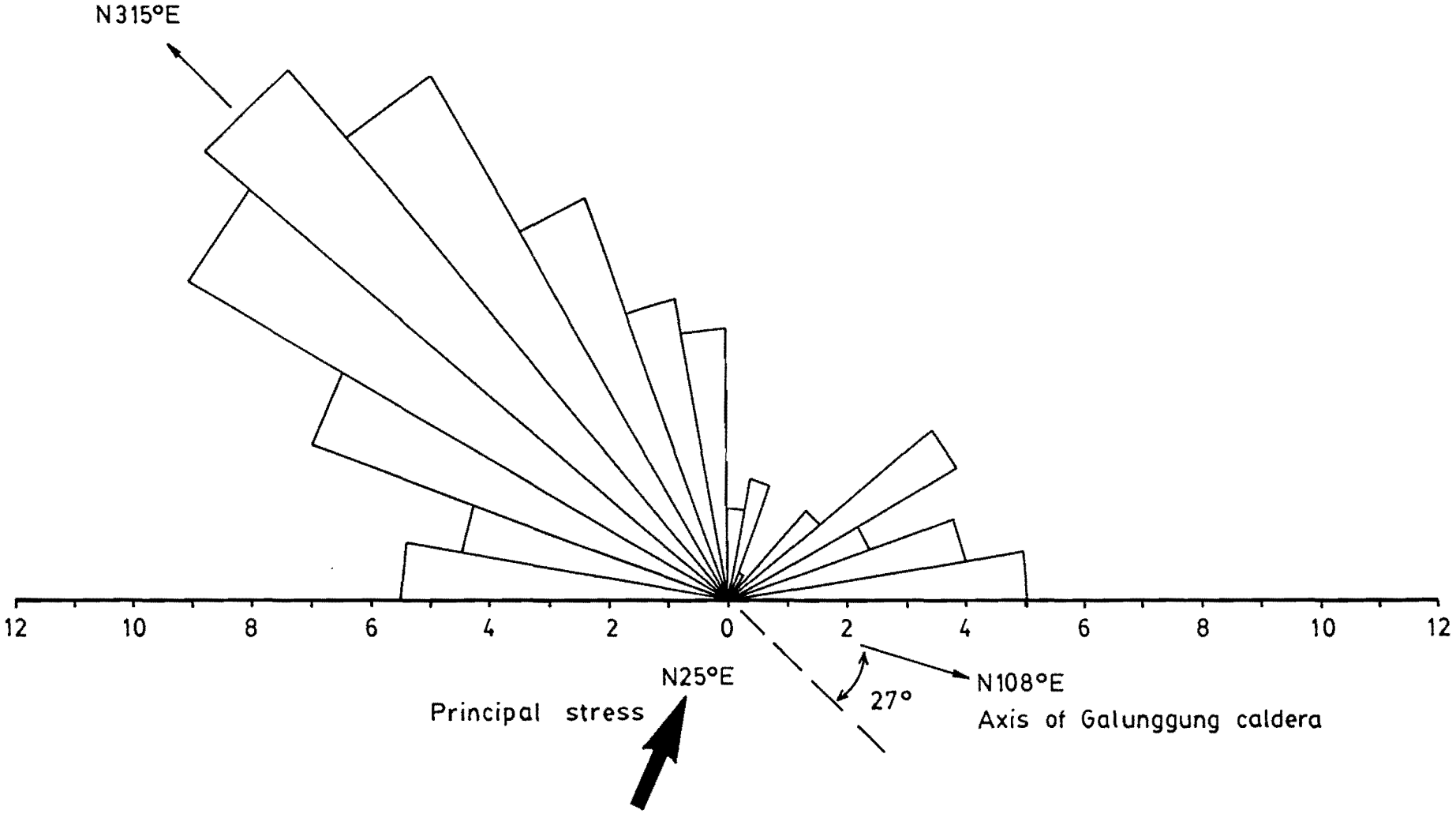

Figure III.26 Rose diagram showing a relationship between lineament patterns in Tasikmalaya region, principal stress from Indian Ocean-Australian plate movement and axis of the Galunggung caldera. Lineament data are given in Appendix I.17.

Fig.III.20), where several eruption points occurred and the January 1983 lava flow extruded (Sudradjat & Martono, 1983). Alzwar (1969) reported fumarole fields on the 1918 lava dome were situated in a north-northeast-striking fracture zone. This is parallel to the strike of dikes ($N30^{o}E$) in walls of the Galunggung caldera.

Moriya (1980) noted that at several Japanese volcanoes, the direction of axis of the avalanche caldera is at right angles to lines of fissure vents and parasitic craters. This is controlled by local and regional maximum horizontal compression (Nakamura, 1977). Siebert (1984) supported the idea by suggesting that the dilational effect of parallel dike swarms induced by the maximum horizontal compression is an important factor in major volcanic slope failures.

On this basis, structures in the Galunggung volcano can be related to the regional tectonic setting. The northwest striking lineaments and the fracture zone in the 1982-83 cinder cone are parallel to the Sumatra Fault System, while the fracture zone in the 1918 lava dome and dikes' position are similar to the principal stress derived from Indian Ocean plate movement. After emplacement of the Old Galunggung cryptodome, volcanic activity moved from the summit crater to southeast flank. This vent movement follows the Sumatra Fault System. In addition, the principal stress direction is approximately normal to the axis of Galunggung caldera. It implies that the orientation of Galunggung avalanche caldera follows a weak zone of tensional fracture.

In 1979-80, two large tectonic earthquakes (6.4 on the Richter Scale, Priyantono et al., 1980) destroyed southern part of Garut and Tasikmalaya areas. The epicentre was about 100 km south of Galunggung and the foci depth ranged from 33 km to 65 km. The energy of the

earthquakes probably triggered the Galunggung eruption in 1982-83. This is discussed in chapter VII.

III.7 Summary of Geologic History

The geologic history of Galunggung began with a constructive period of Old Galunggung stratovolcano. The earliest eruptions ejected mostly pyroclastic deposits which alternate with lava flows in the following stages. The eruptions occurred in the Old Galunggung crater. Reworked material formed lahar deposits distributed around the surrounding lower area. Dikes occupied the weak zone parallel to the principal stress derived from the Indian Ocean plate movement. This Old Galunggung volcanic activity was in pre-Historic times, probably between 50,000 and 10,000 years ago. This activity ended by intrusion of a cryptodome under the Old Galunggung crater.

The cryptodome plugged activity in the crater. Hence a new vent developed on the southeast flank of the Old Galunggung volcano. This vent migration followed the main fracture direction in the area. In 4200 ± 150 years BP an extremely large event occurred which formed the horseshoe-shaped caldera of Galunggung. The southeast part of the volcano slid onto Tasikmalaya plain as a volcanic debris avalanche deposit to form " The Thousand Hills of Tasikmalaya". But some debris avalanche material remained within the caldera to form hills such as Gunung Bunder, Gunung Welirang and Pasir Linggajati. The slope failure is oriented along a tensional fracture zone in the area. During the eruption voluminous pyroclastic flows occurred. Most of the deposits formed were eroded and redeposited to become lahars. The centre of

volcanic activity has been inside the caldera since this period.

Historic eruptions occurred in 1822, 1894, 1918 and recently 1982-83. The 1822 Peléean eruption took place for only 3 hours on 8 October, but produced volcanic debris avalanche, pyroclastic flow and lahar deposits. Casualties were more than 4000 people, mostly caused by pyroclastic surge and flow. The next eruption occurred on 17 - 19 October 1894 as Vulcanian eruptions producing pyroclastic fall deposits. Although there was some damage caused by pyroclastic falls and lahars, there were no casualties in this eruption. A non-violent eruption occurred when a lava dome was extruded on 19 July 1918. It was preceded by earthquakes on 16 July (20.00 h) followed by small explosions producing thin pyroclastic fall deposits around the crater.

Galunggung volcano had been quiet for 64 years before the eruption in 1982. The first eruption was on 5 April. The 1918 lava dome was destroyed during earlier eruptions (April - May; Peléean type) which produced pyroclastic flows as well as pyroclastic falls and some pyroclastic surges. Eruptions changed to Vulcanian type in June - August after the 1918 lava dome was completely destroyed. Towards the close of activity (September - December), Strombolian eruptions formed a cinder cone inside the crater. Finally, a lava flow flowed out in the first week of January 1983. Lahars occurred during and after eruption in rainy seasons. Inside the active crater a lake formed shortly after the eruption terminated. This also happened after the 1822 and 1894 eruptions.

IV PETROGRAPHY

IV.1 Introduction

Galunggung lava flows, lava domes, dikes and volcanic bombs, are basalt or basaltic andesite in composition and have porphyritic textures with medium-sized phenocrysts in fine-grained or glassy groundmasses. The most abundant phenocryst phase is labradorite, followed by clinopyroxene, olivine, orthopyroxene and magnetite. Amphibole occurs only in volcanic bombs erupted during the caldera forming event and at the beginning of each subsequent eruptive cycle. This mineral is also found in gabbro clasts ejected during some eruptions. Pumice clasts of rhyolite, were ejected in the 1982-83 eruption. 84 rock samples with 145 thin sections have been examined and full petrographic descriptions of each are listed in Appendix 2. Selected modal analyses are given in Table IV.1-3.

IV.2 Old Galunggung Formation

IV.2.1 Extrusive Rocks

Extrusive rocks are typically porphyritic basalt to basaltic andesite with phenocrysts of plagioclase, clinopyroxene, olivine, orthopyroxene and rarely microphenocrysts of magnetite. Percentages of the phenocrysts range from 18 - 39 % (Table IV.1). Olivine occurs in most basalts, and orthopyroxene is generally observed in basaltic

Table IV.1 Modal analyses of Old Galunggung volcanic rocks. OL = olivine, OP = orthopyroxene, CP = clinopyroxene, MA = magnetite, PL = plagioclase, and GM = groundmass.

Sample number	Mineral composition (volume %)							
	Phenocryst					GM	Explanation	
	OL	OP	CP	MA	PL			
L 35	1.1	1.0	3.8	0.2	18.8	74.9	Basalt	A sequence of
20267	1.0	0.2	4.1	0.3	20.8	73.6	Basalt	lava flows in
L27-3	0.2	0.6	1.8	-	33.6	63.8	Basaltic andesite	the SW caldera
L27-2	2.2	-	0.4	-	21.2	76.2	Basalt	wall.
L27-1	0.8	-	5.2	-	32.4	61.4	Basalt	
L11-C	0.7	-	0.8	0.1	31.4	67.0	Basalt	
VB10	2.0	-	4.8	-	17.0	76.2	Basalt	
L11-B	3.0	-	0.2	-	24.0	72.8	Basalt	
L11-A	1.8	-	-	-	24.4	73.8	Basalt	
20270	1.6	-	0.2	0.1	21.3	76.8	Basalt	
20271	-	0.4	0.6	0.4	25.8	72.8	Basalt	
20286	1.8	-	0.4	-	35.8	62.0	Basalt	A sequence of
20347	-	3.9	3.6	1.4	29.1	62.0	Basaltic andesite	lava flows in
20280	0.4	0.2	2.6	0.1	16.2	80.5	Basalt	the NE caldera
L 15	1.8	0.8	2.0	0.1	13.3	82.0	Basaltic andesite	wall.
L 26	-	3.3	0.5	0.6	30.9	64.7	Basaltic andesite	
20266	2.2	-	3.6	0.1	29.4	64.7	Basalt	Lava flows from
20285	2.5	-	6.7	0.1	22.7	68.0	Basalt	random sampling
20287	0.4	-	4.0	-	21.6	74.0	Basalt	and debris ava-
20288	-	4.1	1.9	0.5	23.4	70.1	Basaltic andesite	lanche deposit.
26 DK	0.3	-	-	0.1	25.0	74.6	Basalt	Dikes.
21 DK	-	0.5	1.1	0.2	23.8	74.4	Basaltic andesite	
20258	-	-	8.7	-	5.5	85.5	Basalt	Cryptodome

Table IV.2 Modal analyses of Galunggung volcanic rocks erupted during caldera formation, and the historic eruptions of 1822, 1894 and 1918. OL = olivine, OP = orthopyroxene, CP = clinopyroxene, MA = magnetite, AM = amphibole, PL = plagioclase, and GM = groundmass.

Sample number	Mineral composition (volume %)								
	Phenocryst						GM	Explanation	
	OL	OP	CP	MA	AM	PL			
20293	0.1	0.2	1.4	-	-	25.3	73.0	Basaltic andesite	1918
20292	0.4	0.8	3.0	0.2	-	23.3	72.3	Basaltic andesite	Lava dome.
20245	-	0.5	4.1	0.4	0.1	11.0	83.6	Basaltic andesite	1894
20246	1.4	0.4	1.8	-	-	19.0	77.4	Basaltic andesite	Eruption.
20342	0.8	0.9	4.2	0.3	0.2	16.3	77.3	Basalt	1822
20250	0.6	1.6	3.1	0.3	0.1	18.4	75.9	Basaltic andesite	Eruption.
VB30A	0.6	1.4	1.2	-	-	14.4	82.4	Basaltic andesite	
20289	0.1	0.9	3.7	1.9	5.0	17.6	70.8	Basaltic andesite	4200 ±
20254	-	-	-	-	-	27.6	72.4	Basalt	150 yr BP
20345	0.2	0.7	2.6	-	-	20.8	75.7	Basaltic andesite	

Table IV.3 Modal analyses of Galunggung volcanic rocks erupted in 1982-83. OL = olivine, OP = orthopyroxene, CP = clinopyroxene, MA = magnetite, AM = amphibole, PL = plagioclase, and GM = groundmass.

Sample number	Mineral composition (volume %)							
	Phenocryst						GM	Explanation
	OL	OP	CP	MA	AM	PL		
20300	6.7	-	5.6	-	-	7.7	80.0	Basalt; a lava flow extruded on 1 - 7 January 1983.
20335	4.7	-	5.7	-	-	5.9	83.3	Basalt; bombs erupted between
20299	3.9	-	7.0	-	-	8.1	81.0	September - December 1982.
20339	3.8	-	6.2	-	-	7.4	82.5	
20298	3.8	-	3.7	-	-	11.5	81.0	
20324	4.8	-	2.8	-	-	9.4	83.0	Basalt; bomb erupted in June.
20297	1.6	0.1	3.1	-	-	10.0	85.2	Basalt; bomb erupted on 18 May .
20296	2.4	0.3	2.8	-	-	11.9	82.6	Basaltic andesite; bombs erup-
VB30C	1.2	0.2	4.8	-	-	8.3	85.5	ted on 6 May.
VB16	1.2	-	1.4	-	0.1	12.6	84.7	
20291	1.1	0.4	2.2	0.1	-	15.0	81.0	Basaltic andesite; bombs erup-
20295	1.1	0.2	1.1	-	-	11.8	85.8	ted on 25 April.
VB30B	0.9	-	2.9	0.1	-	10.1	86.0	
20290	0.9	0.7	7.0	-	-	15.9	75.5	Basaltic andesite; bombs erup-
20294	0.5	1.0	3.0	0.1	0.1	11.2	84.1	ted on 8 April 1982.
20322	0.2	0.7	2.5	-	0.2	10.8	85.6	
20325	-	0.7	3.0	0.1	0.7	10.2	85.3	

andesites (Fig.IV.1 & IV.2). Labradorite is the most abundant phenocryst mineral of both rock types, and the only phenocryst phase in several lavas (e.g. 20346, Fig.IV.3) and sometimes forms pilotaxitic texture (e.g. L11B, L15, L28). Occasionally, phenocrysts form a glomeroporphyritic texture consisting of mainly clinopyroxene-rich crystal clots up to 6 mm but mostly less than 3 mm. Supplementary minerals in the clots are olivine, orthopyroxene, magnetite and plagioclase. All lava flows exposed in the lower part of the Galunggung caldera wall are hydrothermally altered and frequently olivine and clinopyroxene are completely replaced by secondary minerals. There is no obvious modal trend from younger to older rocks in the Old Galunggung.

The groundmasses consist of microcrystalline plagioclase (mainly labradorite), clinopyroxene, and magnetite in volcanic glass. In basalts, olivines are also commonly observed in the groundmass, whereas groundmass orthopyroxenes are occasionally found in basaltic andesite lavas (e.g. L26). Volcanic bombs usually have a glassy groundmass (e.g. VB10). In the lava flows, groundmass texture varies from glassy through pilotaxitic to microcrystalline intergranular depending upon thickness of the lava flows; a thicker lava flow having a more crystalline groundmass than the thinner one. Groundmass crystals showing trachytoid texture are typical of the most evolved basaltic andesite lavas (20288, 20347). The variation of groundmass texture may reflect differing degrees of rapid cooling (quenching) during eruption.

Hydrothermal alteration generally affects mafic minerals, particularly olivine. Clinopyroxene, volcanic glass and rarely magnetite are affected only in the more extensively altered rocks, but plagioclase is resistant. Alteration typically produces chlorite, carbonate

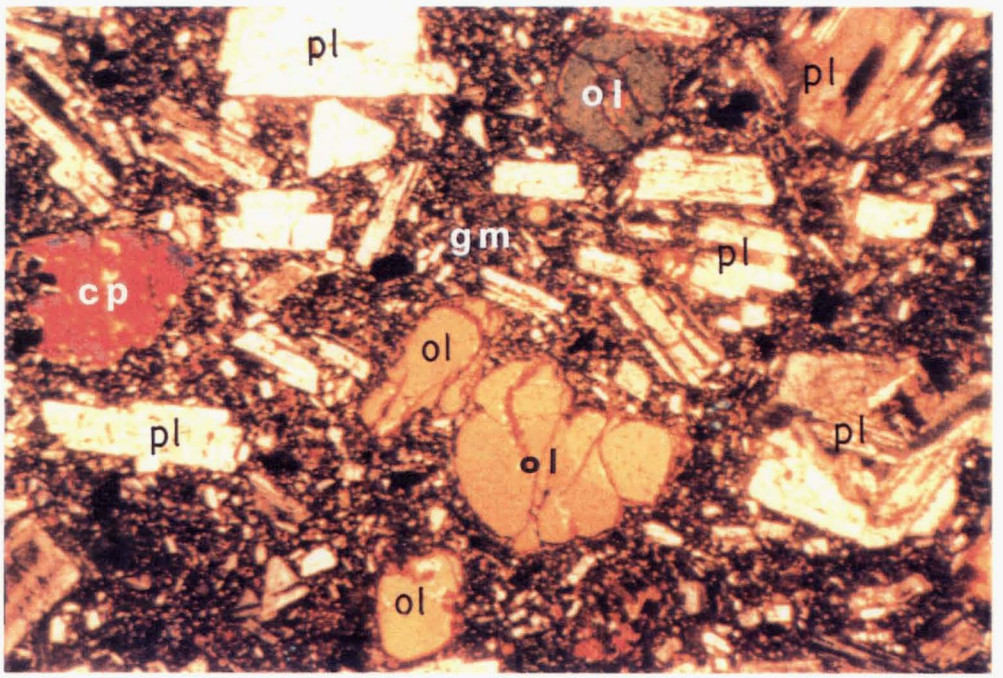

Figure IV.1 Olivine (ol) in basalt of Old Galunggung volcano, together with clinopyroxene (cp), plagioclase (pl) and magnetite (black fine grain crystals) in hypocrystalline groundmass (gm) (20266, 25 X, crossed polarized).

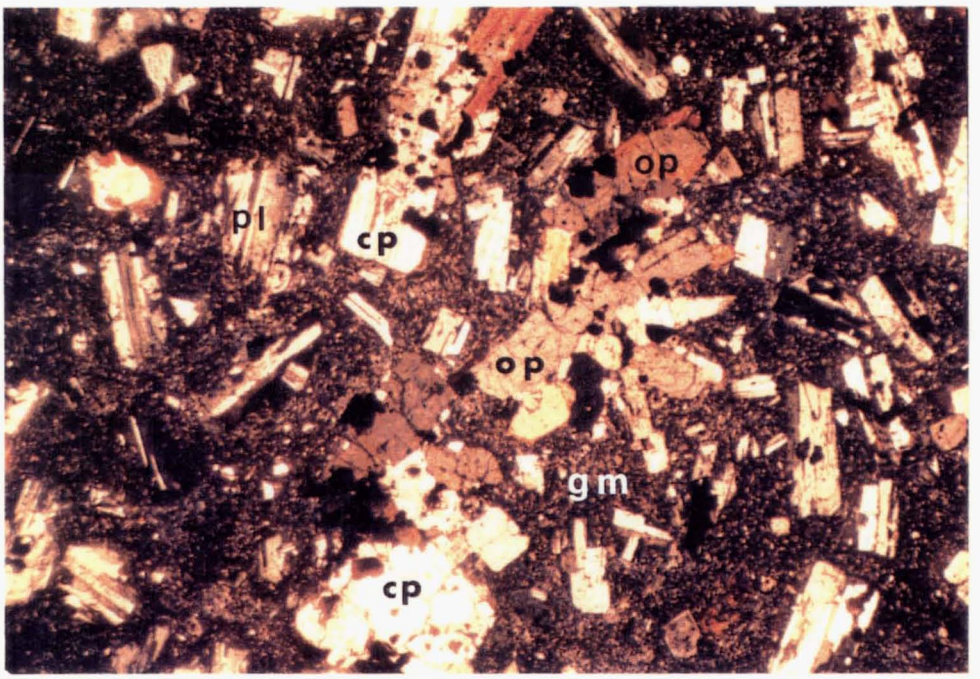

Figure IV.2 Orthopyroxene (op) in basaltic andesite of Old Galunggung volcano, together with clinopyroxene (cp), magnetite (black fine grain crystals) and plagioclase (pl) in trachytoid groundmass (gm) (20347, 25 X, crossed polarized).

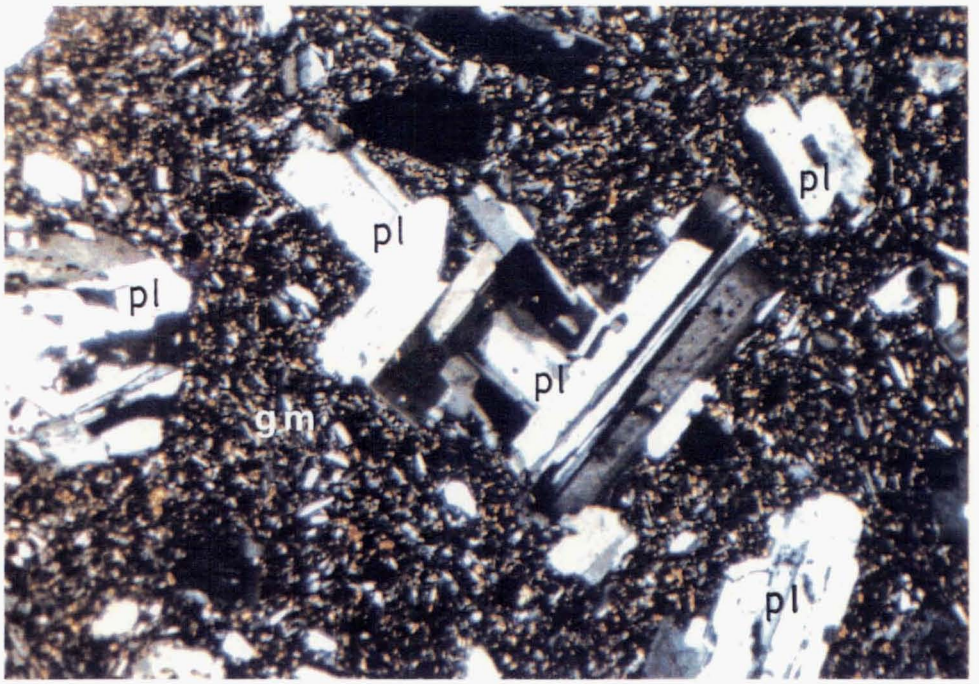

Figure IV.3 Plagioclase-rich basalt of Old Galunggung volcano. Pl = plagioclase, gm = groundmass (20270, 25 X, crossed polarized).

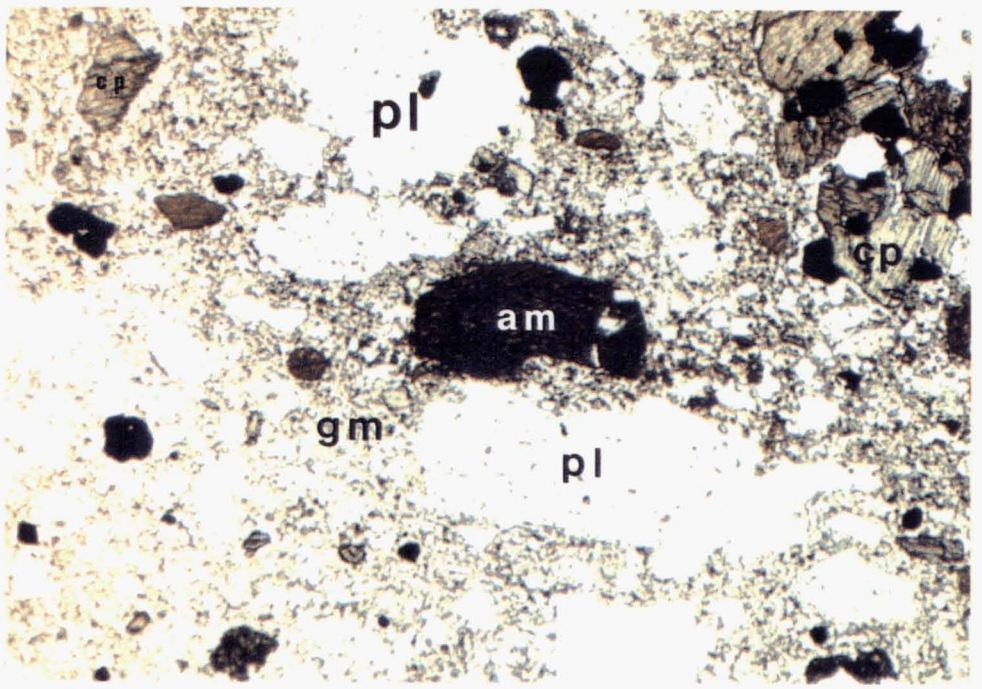

Figure IV.4 Amphibole (am) in basaltic andesite erupted during Galunggung caldera formation (4200 ± 150 yrs. BP). Cp = clinopyroxene, pl = plagioclase, gm = groundmass, and black crystals are magnetite (20289, 25 X, plane polarized).

and iron oxide.

IV.2.2 Dikes

In Galunggung volcano, most dikes are basalt, and rarely basaltic andesite. Both typically have porphyritic textures, with phenocrysts of plagioclase (dominant), olivine, orthopyroxene and clinopyroxene. These occasionally have a glomeroporphyritic texture. Modal data show that the dikes have about 25 % phenocrysts (Table IV.1).

Groundmass textures of the dikes are variable, from very fine grained pilotaxitic texture containing plagioclase laths and magnetites in abundant volcanic glass (21 DK), to intergranular texture composed of a microcrystalline groundmass of clinopyroxene, magnetite and plagioclase. This variation of groundmass texture presumably also reflects differing periods of cooling as for the extrusive rocks.

Several dikes are strongly altered such that mafic minerals have been replaced by calcite, chlorite and clay minerals.

IV.2.3 Cryptodome

The Galunggung cryptodome is a basalt which has a porphyritic texture. Most of the minerals, mainly in the groundmass, are altered to carbonate, pyrite and clay minerals (20258). Clinopyroxene and plagioclase are the only reasonably fresh minerals in the rock. Occasionally, carbonate occurs in 1 - 4 mm thick fractures.

IV.3 Tasikmalaya Formation

Bombs in pyroclastic flow deposits of the Tasikmalaya Formation range from porphyritic basalt to basaltic andesite. Based on their texture and mineralogical compositions three types of volcanic rocks are distinguished :

1. Basalt (20344) or basaltic andesite (20345) which have olivine, clinopyroxene and plagioclase phenocrysts in dark brown glassy groundmass containing acicular feldspars. In the basaltic andesite, orthopyroxene appears usually in the cores of clinopyroxenes or in crystal clots associated with clinopyroxene and magnetite. Amphibole is very rare. These rocks are situated in the lower and middle parts of three layers of pyroclastic flow deposits.

2. Basalt (20254) with plagioclase phenocrysts only in a hypocrystalline porphyritic groundmass consisting of plagioclase laths, anhedral clinopyroxenes, and magnetites in a volcanic glass. This rock is found in the middle of the pyroclastic flow deposits.

3. Basaltic andesite that is characterised by common amphibole crystals (Fig.IV.4). These occur in the upper parts of the pyroclastic flow deposits. This rock has similar phenocryst contents to the first type but its groundmass ranges from glassy to hypocrystalline porphyritic texture. In the more crystalline groundmass (20253, 20255) amphiboles are rimmed by opaque material (magnetite ?) suggesting a product of low-pressure volcanic environment (e.g. Lambert & Wyllie, 1970; Stewart, 1975). More commonly amphiboles are observed in the rocks having glassy groundmass (20289). These rocks are usually lighter in colour (light grey) than other bombs from Galunggung. Large

phenocrysts of amphibole and plagioclase (up to 40 mm and 10 mm length, respectively) occur in the bombs, together with other smaller (< 5 mm) phenocrysts. The large amphibole crystals frequently enclose small grains of clinopyroxene, magnetite and plagioclase to form a poikilitic texture. Occasionally large olivine crystals (8 mm length) are also observed (20289). Several crystal clots occur and consist of pyroxene, plagioclase and magnetite but without amphibole. The crystal clots form glomeroporphyritic texture and consist of coarse (up to 7 mm in diameter), medium and fine grain crystals (Fig.IV.5). This supports a suggestion that crystal clots represent primary igneous phase assemblages (Garcia & Jacobson, 1979; Cox et al., 1981). Modal analyses of the minerals are given in Table IV. 2.

IV.4 Cibanjaran Formation

IV.4.1 1822 Eruption Rocks

Volcanic bombs in pyroclastic flow deposits of the 1822 eruption are basalt and basaltic andesite. The rock is dark grey and has a porphyritic texture. Phenocrysts are plagioclase, clinopyroxene and orthopyroxene, with rare amphibole and microphenocrysts of olivine and magnetite (Table IV.2). Crystal clots (2 - 2.5 mm in diameter) consisting of either pyroxene or plagioclase are present, as are anhedral amphiboles (0.8 - 2. 0 mm) which are rimmed by opaque material (Fig.IV.6). Groundmass is pilotaxitic and consists of abundant plagioclase and ubiquitous magnetite and clinopyroxene in a pale brown glass.

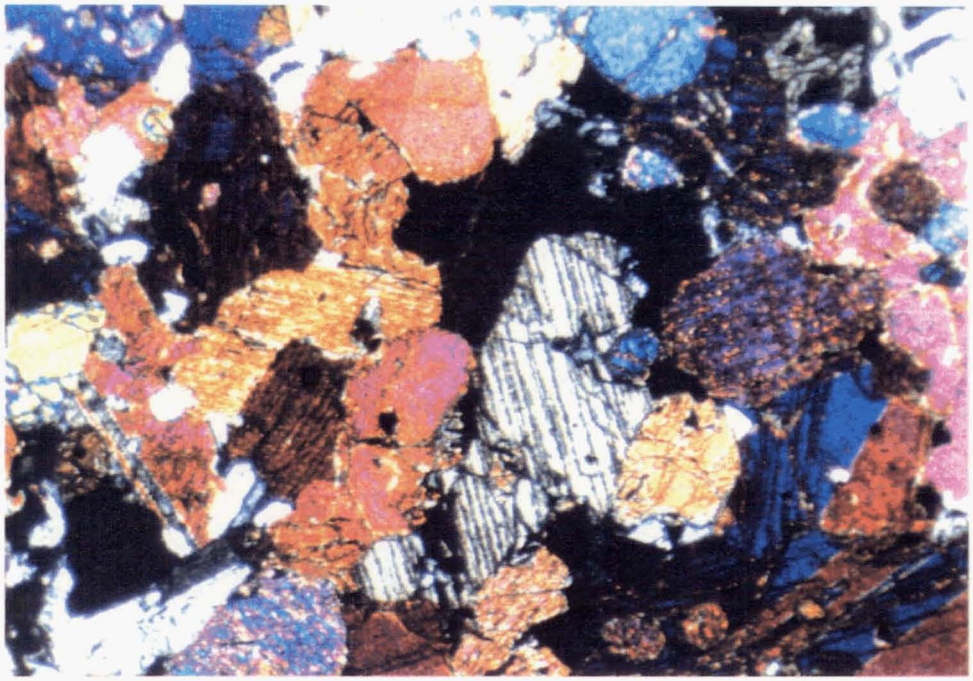

Figure IV.5A Coarse glomeroporphyritic clinopyroxene-rich crystal clots in basalt erupted during Galunggung caldera formation (20344, 25 X, crossed polarized).

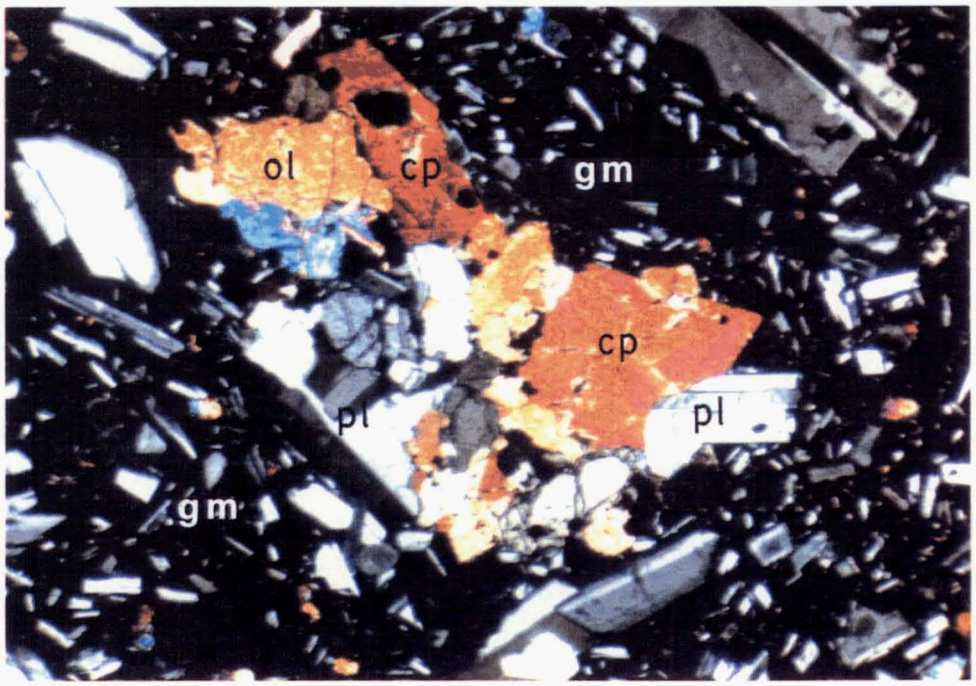

Figure IV.5B Medium glomeroporphyritic crystal clots consisting of olivine (ol), clinopyroxene (cp), plagioclase (pl), and magnetite (black fine grain crystals) in basalt erupted during Galunggung caldera formation. Gm = groundmass (20253, 25 X, crossed polarized).

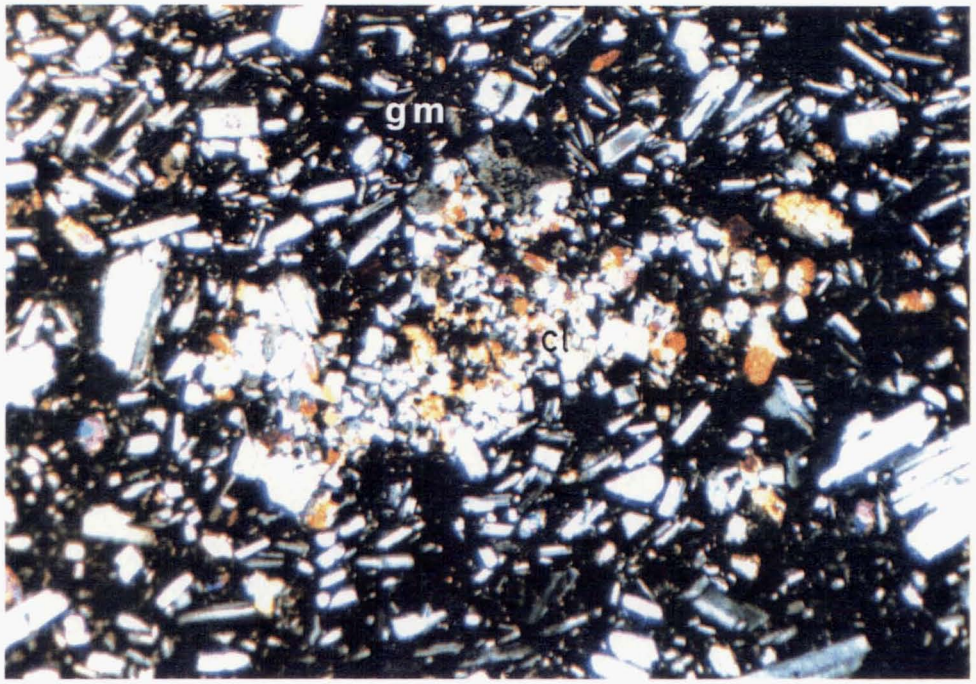

Figure IV.5C Fine glomeroporphyritic crystal clots (cl) consisting of clinopyroxene, magnetite and plagioclase in basalt erupted during Galunggung caldera formation. Gm = groundmass (20253, 25 X, crossed polarized).

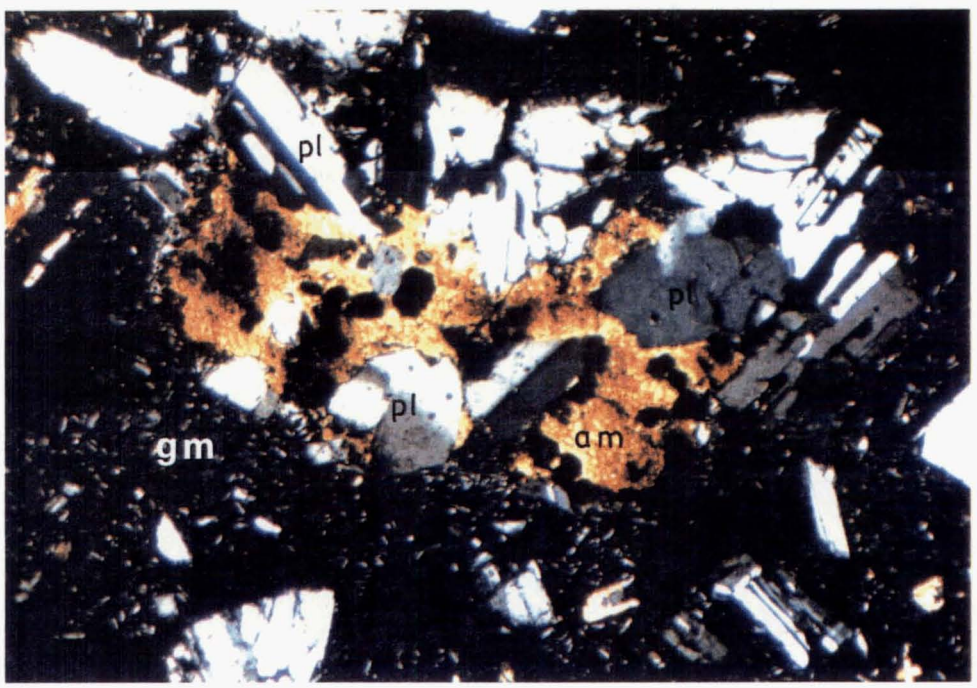

Figure IV.6 Glomeroporphyritic crystal clots consisting of amphibole (am), magnetite (black crystals) and plagioclase (pl) in basaltic andesite erupted in 1822. Gm = groundmass (VB30A, 25 X, crossed polarized).

IV.4.2 1894 Eruption Rocks

Two volcanic bombs collected are both basaltic andesite but have different petrographic features. The first sample (20246), which was gathered from the lower part of a sequence of pyroclastic fall deposits, is dark in colour and has a porphyritic texture. Phenocrysts (Table IV. 2) are olivine, clinopyroxene and plagioclase (up to 2 mm in length) in a groundmass consisting of anhedral olivine, clinopyroxene, magnetite and acicular to lath-like feldspars and glass. Orthopyroxene microphenocrysts (0.3 - 0.5 mm) are occasionally observed in aggregates with clinopyroxene and magnetite. Crystal clots (1 mm in diameter) consisting of anhedral olivine surrounded by orthopyroxenes and magnetites are observed.

Another basaltic andesite (20245) was collected from the upper part of the pyroclastic fall deposits. It has clinopyroxene, orthopyroxene and plagioclase phenocrysts in groundmass of anhedral clinopyroxene, magnetite, acicular plagioclase and glass. Some clinopyroxene and orthopyroxene phenocrysts (0.1 - 1 mm) form glomeroporphyritic crystal clots in association with magnetite microphenocrysts. Amphibole crystals (0.1 mm), rimmed by thin dusty opaques, are infrequently observed in this rock.

Plagioclase phenocrysts in the two basaltic andesites form mostly euhedral - subhedral individual crystals which are oscillatory and normally zoned. Hydrothermal activity has caused olivine to alter to greenish yellow bowlingite whereas volcanic glass alters to carbonate and chloritic materials.

IV.4.3 1918 Lava Dome

The 1918 lava dome is basaltic andesite consisting of clinopyroxene, orthopyroxene, olivine and plagioclase phenocrysts (Table IV.2). The lava dome has a variable porphyritic texture. In the central part (20292) phenocrysts are large in a fine groundmass whereas at the southeast margin (20293) there is a coarse groundmass consisting of pyroxene, magnetite, plagioclase and glass forming a pilotaxitic texture with plagioclase phenocrysts having a subparallel structure. The variation of rock texture is probably caused by mechanical segregation during extrusion. Some mafic phenocrysts, particularly olivines, are partly altered and replaced by chloritic and "dusty" opaques.

IV.4.4 1982-83 Eruption Rocks

Rocks erupted in 1982-83 are basalt to basaltic andesite, and have a porphyritic texture with phenocrysts of olivine, clinopyroxene, plagioclase and rarely orthopyroxene, and magnetite microphenocrysts. There is however a gradual change in texture and mineral abundance (Fig.IV.7) of the 1982-1983 eruption rocks from the initial (April 1982) to the final (September 1982 - January 1983) phases. Modal data of mineral phenocrysts are given in Table IV.3.

During the earlier eruptions basaltic andesites were ejected. The rocks have hypocrystalline porphyritic textures and phenocrysts of olivine, orthopyroxene, clinopyroxene, magnetite, amphibole and plagioclase. Olivines are anhedral skeletal and hollow and have coronas

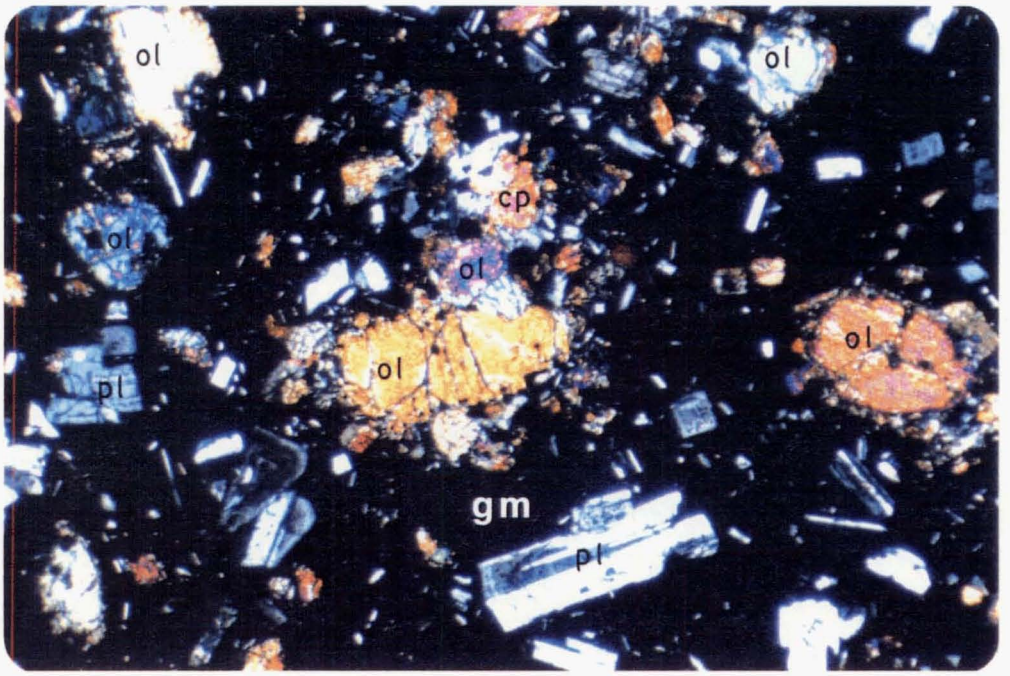

Figure IV.7A Anhedral olivine (ol) having corona of clinopyroxene, magnetite and plagioclase in basaltic andesite erupted on 18 May 1982. Cp = clinopyroxene, pl = plagioclase, gm = groundmass (20297, 25 X, crossed polarized).

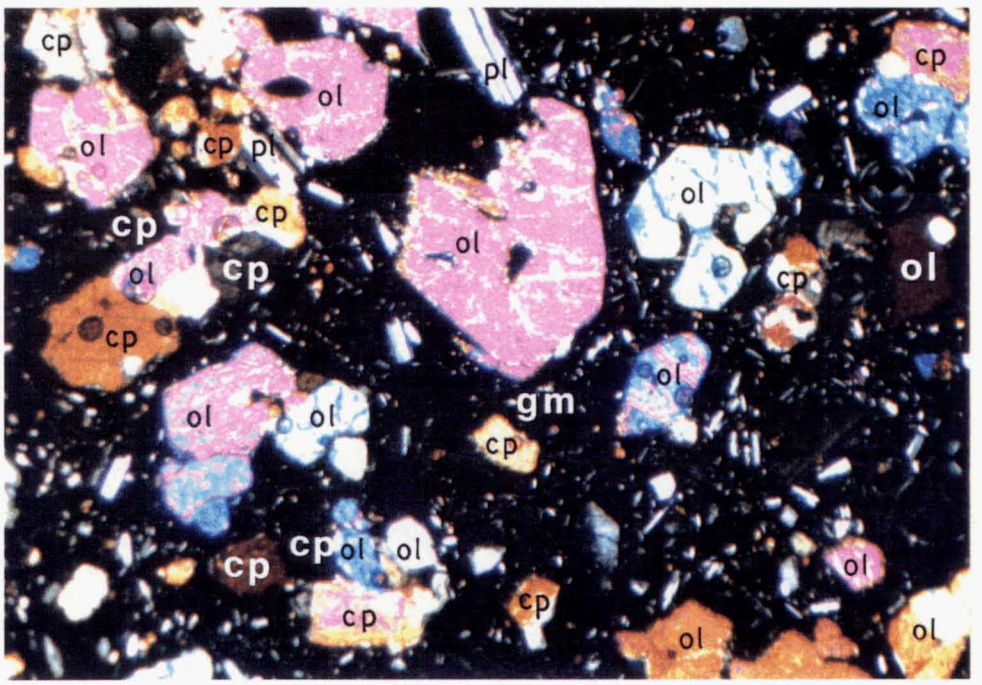

Figure IV.7B Olivine (ol) in basalt erupted on 16 September 1982. The olivine forms euhedral - subhedral, embayed and hollow crystals. Small grain crystals are enclosed by large crystals. Clinopyroxene = cp, plagioclase = pl, and gm = groundmass (20335, 25 X, crossed polarized).

of pyroxenes (Fig. IV.7A). The coronas may represent quenching texture during eruption. Some orthopyroxenes are jacketed by or in cores of clinopyroxenes associated with magnetites. Glomeroporphyritic crystal clots consisting of clinopyroxene, orthopyroxene and magnetite with anhedral olivine in the core are present. Amphibole crystals rimmed by opaques and rock fragments having granoblastic texture are infrequently observed.

In the final stage of eruption the rocks are basalt, consisting of olivine, clinopyroxene and plagioclase forming both phenocrysts and groundmass. The olivine and clinopyroxene phenocrysts become more common to form larger grains and euhedral - subhedral crystals although some of them are anhedral, skeletal, hollow, embayed forming sharp corners and edges (Fig. IV.7B) and form poikilitic texture. Consequently, their percentages increases from basaltic andesite to basalt (Tab. IV.3). On the other hand, plagioclase phenocrysts become smaller and their modal data decreases as well as groundmass proportion. Orthopyroxene and amphibole disappear whereas magnetite is present as groundmass crystals only in the basalt. Cr-spinel inclusions are however common in olivine phenocrysts and microphenocrysts in both the basaltic andesite and basalt.

IV.5 Gabbro

The only intrusive rock found in Galunggung is gabbro (Fig.IV.8). Gabbro clasts are observed in products of the caldera forming event and in the 1982-1983 eruption. The clasts were ejected as both accidental blocks and cores of volcanic bombs. They show a

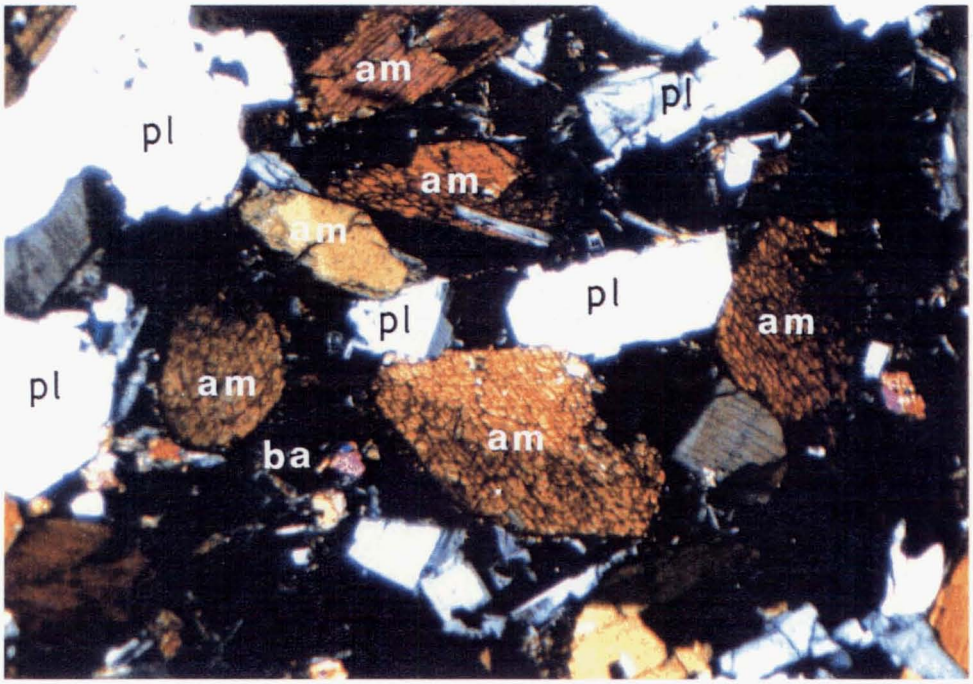

Figure IV.8A Gabbro consisting of amphibole (am) and plagioclase (pl), injected by basaltic andesite (ba) containing very fine grains of anhedral clinopyroxene and acicular plagioclase (20257, 25 X, crossed polarized).

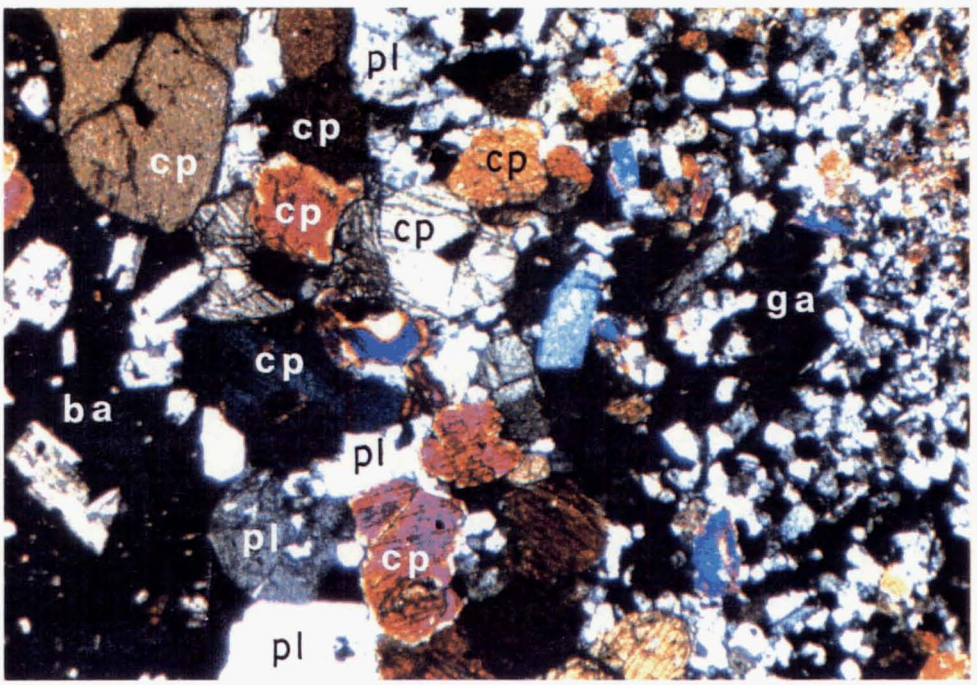

Figure IV.8B Contact between basalt (ba, left) and gabbro (ga, right, having granoblastic texture) with more crystalline clinopyroxenes (cp) and plagioclases (pl) between (20252, 25 X, crossed polarized).

holocrystalline gabbroic texture, and consist mainly of amphibole and labradorite with occasionally magnetite and clinopyroxene. The minerals vary in size, from fine-to coarse grains (up to 14 mm) and in shape (long- to short prismatic crystals) particularly for amphibole.

Three types of gabbro clasts are observed in Galunggung volcanic rocks: 1. Gabbro having highly elongated ("long") amphibole crystals (sample number 20257), 2. Gabbro having "short" amphibole crystals (sample number 20256 & 20327), and 3. gabbro affected by thermal metamorphism. These gabbros are injected by basaltic magma with a different texture in each type of gabbro clast.

The first type of gabbro has highly elongated amphibole crystals changing gradually from fine (0.5 mm) to coarse (25 mm) grains. The amphiboles are pleochroic from green to brown and some of them have thin opaque rims indicating relatively a low pressure volcanic environment (e.g. Stewart, 1975). Plagioclase forms euhedral to subhedral tabular crystals (0.5 - 5 mm length) with a wide unzoned core. Anhedral magnetites range from 0.5 to 1.5 mm and are generally broken. Injected magma is probably basaltic andesite (Fig. IV.8A) comprising very fine grain crystals (<0.1 mm) of acicular to elongated plagioclase and anhedral clinopyroxene, orthopyroxene and magnetite. Broken crystals of amphibole are occasionally observed in the injected magma. The highly elongated and acicular crystals of amphibole and plagioclase suggest rapid growth of the minerals (Eichelberger, 1978).

The second type of gabbro is characterised by short prismatic amphibole crystals (3 - 10 mm) showing poikilitic texture with enclosed minerals of plagioclase, clinopyroxene, olivine and magnetite. Amphiboles are pleochroic from green to brown and partly rimmed by thin opaque material (opacite rims). Plagioclase crystals typically

have a wide unzoned core reflecting a stable crystallisation condition. The injected magma is porphyritic basalt with predominantly phenocrysts of olivine, clinopyroxene and plagioclase in a hypocrystalline groundmass. Orthopyroxenes are occasionally observed in the cores of clinopyroxene phenocrysts. Groundmass crystals consist of anhedral olivine, clinopyroxene, magnetite and plagioclase laths in a small amount of glass. Amphiboles having poikilitic texture and lath-like plagioclase also indicate rapid growth (Eichelberger, 1978).

The third type of gabbro has a granoblastic texture affected by thermal metamorphism (Coote, 1987). Amphiboles and plagioclase are replaced by secondary minerals of clinopyroxene, magnetite and plagioclase. Injected magma is porphyritic basalt consisting of orthopyroxene, clinopyroxene, magnetite, amphibole and plagioclase in glassy groundmass. Amphiboles are pleochroic, from green to brown, and do not have opacite rims; some of them form poikilitic texture. Along the contact (1 -2 mm width) between gabbro and the injected magma, minerals form a crystalline texture (Fig. IV.8B) suggesting that the gabbro had been in equilibrium with the magma for some time before eruption.

Granoblastic textures are also observed in andesite blocks (sample number VB6-3D) ejected during Galunggung caldera formation and xenoliths in volcanic bombs (sample number 20322) erupted in early stages of the 1982 eruption. Recrystallisation mainly produces clinopyroxene, magnetite and plagioclase but brown biotite is also observed in the andesite.

IV.6 Rhyolite

Rhyolite is found only in the early phases of the 1982 Strombolian eruption (16 September). This is the first time rhyolite pumice has been found, which gives rise to a problem as to whether it is the most differentiated Galunggung magma or whether it is an accidental material.

In the Strombolian eruption, pumice is blanketed by basaltic magma. Petrographically, contact between the rhyolite pumice and basaltic material is sharp, with no reaction between the two rock types. The pumice has abundant volcanic glass, some feldspars, magnetites and few quartz minerals. Feldspars are anhedral (0.5 - 1.0 mm), mostly altered, and replaced by dusty opaques (Fig. IV.9). Euhedral quartz (0.8 - 1.0 mm) is occasionally found, whereas anhedral, very fine grain (< 0.2 mm) magnetites are scattered in the glass. Alteration also produces a brown material (limonite ?).

Figure IV.9 Altered feldspar phenocryst (FL) replaced by opaques (magnetites ?) in rhyolite pumice. GM = Groundmass (20244, 400 X, plane polarized).

V MINERALOGY

V.1 Introduction

Major-element compositions of minerals from Galunggung volcanic deposits were determined using a JXA-733 Electron Probe X-ray Microanalyser at the Department of Geology, Victoria University of Wellington, following the method of Watanabe et al. (1981). Analytical methods and a complete list of analyses are given in Appendix 3. Representative analyses of olivine, pyroxene and plagioclase from each unit are given in Table V.1 together with Ti-magnetite from Old Galunggung and amphibole from the Tasikmalaya Formation.

V.2 Olivine

V.2.1 Optical Mineralogy

In Galunggung volcanic rocks, olivines are very common, particularly in basalts, as phenocrysts (0.5 - 1.0 mm in length), microphenocrysts (0.1 - 0.4 mm) and groundmass crystals. Occasionally, olivine inclusions in clinopyroxene phenocrysts are also present. Large euhedral - subhedral olivine phenocrysts (2.5 - 8.0 mm) are found in basalt of Old Galunggung lava (L35), basaltic andesite bombs erupted during caldera formation (20289) and in the 1983 basalt lava flow (20300). Olivines are rare or absent in basaltic andesite where orthopyroxenes are present. Average modal analyses of olivine phenocrysts

Table V.1 Representative microprobe analyses of phenocryst cores of Galunggung volcanic rocks. OL = Olivine, CP = clinopyroxene, OP = orthopyroxene, PL = plagioclase, AM = amphibole, MA = magnetite.

	Cibanjaran Formation							
	1982-83 Eruption				1918 Lava dome			
	OL	CP	OP	PL	OL	CP	OP	PL
SiO_2	39.472	50.828	51.994	44.344	36.787	50.842	52.784	43.959
Al_2O_3	.036	4.200	1.118	35.846	.008	2.283	.755	35.712
TiO_2	-	.746	.221	-	-	.584	.229	.036
FeO*	11.028	5.893	21.282	.491	30.091	11.164	19.107	.393
MnO	.188	.130	.850	-	.526	.351	.511	.111
MgO	49.234	14.640	23.577	.041	32.617	14.495	24.426	.046
CaO	.212	22.939	1.393	18.971	.201	19.408	1.817	19.047
Na2O	-	.257	-	.621	-	.344	-	.782
K2O	.019	.011	-	.006	-	.045	-	.080
NiO	.233	.019	-	-	.040	-	.045	-
Cr_2O_3	-	.721	-	.055	.025	.026	-	.005
Cl	.009	.002	-	-	-	.081	-	.021
Total	100.432	100.387	100.436	100.376	100.295	99.621	99.674	100.191
Si	.973	1.874	1.831	8.176	.993	1.918	1.954	8.140
Al	.001	.182	.047	7.529	-	.102	.033	7.793
Ti	-	.021	.006	-	-	.017	.006	.005
Fe	.227	.182	.566	.011	.680	.352	.592	.061
Mn	.004	.004	.025	3.749	.012	.011	.016	.017
Mg	1.810	.804	1.238	.224	1.313	.815	1.348	.013
Ca	.006	.906	.052	-	.006	.785	.072	3.779
Na	-	.018	-	-	-	.025	-	.281
K	.001	.001	-	.011	-	.002	-	.019
Ni	.005	.001	-	-	.001	-	.001	-
Cr	-	.021	-	.011	.001	.001	-	.001
Cl	-	-	-	-	-	.005	-	.007
Total	3.027	4.014	3.765	20.038	3.006	4.033	4.023	20.115
Oxygens	4	6	6	32	4	6	6	32
Mg/(Mg+Fe)	.889	.815	.686	-	.659	.688	.695	-
Ca/(Ca+Na+K)	-	-	-	.944	-	-	-	.926

	Cibanjaran Formation				Tasikmalaya Formation				
	1822 Eruption				4200 ± 150 yrs. BP				
	OL	CP	OP	PL	OL	CP	OP	AM	PL
SiO_2	37.932	51.303	53.695	44.576	38.300	51.877	53.716	43.152	45.081
Al_2O_3	.036	2.556	1.321	35.065	.035	1.557	1.745	13.242	34.568
TiO_2	.016	.555	.205	.013	-	.332	.190	2.107	.033
FeO*	26.885	10.847	19.333	.500	18.835	9.879	15.456	11.151	.659
MnO	.565	.338	.709	.052	.342	.367	.342	.145	-
MgO	34.623	14.449	23.189	.052	42.878	15.000	26.787	14.302	.028
CaO	.155	19.449	1.505	18.721	.136	20.731	1.649	11.791	18.901
Na_2O	-	.288	.026	1.028	-	.245	.017	2.601	1.035
K_2O	-	-	.007	.028	.042	-	-	.208	-
NiO	-	.030	-	-	.037	.046	-	.073	-
Cr_2O_3	.049	-	-	.016	-	-	-	-	.067
Cl	.036	.007	.008	.012	-	-	.047	-	-
Total	100.298	99.823	99.998	100.126	100.605	100.034	99.950	98.773	100.372
Si	1.007	1.924	1.976	8.254	.977	1.940	1.944	6.242	8.327
Al	.001	.113	.057	7.652	.001	.069	.075	2.257	7.525
Ti	-	.016	.006	.002	-	.009	.004	.229	.005
Fe	.597	.340	.595	.077	.402	.309	.468	1.349	.102
Mn	.013	.011	.022	.088	.007	.012	.010	.018	-
Mg	1.369	.808	1.272	.014	1.630	.836	1.446	3.084	.008
Ca	.005	.781	.059	3.714	.004	.831	.064	1.827	3.740
Na	-	.021	.002	.369	-	.018	.001	.730	.371
K	-	-	-	.019	.001	-	-	.038	-
Ni	-	.001	-	-	.001	.001	-	.008	-
Cr	.001	-	-	.002	-	-	-	-	.010
Cl	.001	-	.001	.007	-	-	.003	-	-
Total	2.994	4.015	3.991	20.119	3.023	4.025	4.015	15.784	20.087
Oxygens	4	6	6	32	4	6	6	23	32
Mg/(Mg+Fe)	.697	.704	.681	-	.802	.730	.755	.696	-
Ca/(Ca+Na+K)	-	-	-	.905	-	-	-	-	.910

Old Galunggung Formation

50,000 - 10,000 yrs. BP (?)

	OL	CP	OP	MA	PL
SiO_2	37.843	52.019	53.259	.106	44.353
Al_2O_3	.001	2.401	1.710	3.841	35.415
TiO_2	.002	.440	-	14.606	.002
FeO*	25.168	9.391	18.549	74.992	.468
MnO	.182	-	.577	.378	.059
MgO	36.613	14.628	24.195	1.955	.079
CaO	.146	20.816	1.508	.001	18.826
Na_2O	-	.305	.105	-	.661
K_2O	-	-	.020	.009	.020
NiO	.045	-	-	-	.021
Cr_2O_3	-	-	-	.131	-
Cl	-	-	.073	.007	-
Total	100.000	100.000	99.996	96.026	99.905
Si	.998	1.936	1.956	.036	8.217
Al	-	.105	.074	1.523	7.733
Ti	-	.012	-	3.697	-
Fe	.555	.292	.570	21.107	.073
Mn	.004	-	.018	.108	.009
Mg	1.440	.812	1.325	.981	.022
Ca	.004	.830	.059	-	3.737
Na	-	.022	.007	-	.238
K	-	-	.001	.004	.005
Ni	.001	-	-	-	.003
Cr	-	-	-	.035	-
Cl	-	-	.004	.004	-
Total	3.002	4.010	4.015	27.494	20.037
Oxygens	4	6	6	32	32
Mg/(Mg+Fe)	.722	.735	.699	.044	-
Ca/(Ca+Na+K)	-	-	-	-	.939

increase from < 1.0 - 4.6 % with decreasing SiO_2 contents in rocks erupted in 1982-83 (see Table IV.3). Modal olivines are always $\leq$ 3 % in the older rocks (Table IV.1-2).

In the Old Galunggung basalts, olivine phenocrysts are commonly anhedral, although euhedral - subhedral crystals are observed. Coronas representing quench textures are common with very fine grained pyroxenes surrounding anhedral olivines, but olivines rimmed by opaque coronas are rare (L35). Probe analyses show that the pyroxene coronas consists of orthopyroxene, calcic pyroxene and pigeonite; while opaque coronas are Fe-rich olivine. Anhedral rounded olivine inclusions are commonly observed in clinopyroxene phenocrysts.

Olivines are subhedral - anhedral, rounded and elongated skeletal crystals in basalts and basaltic andesites erupted during caldera collapse and historic eruptions in 1822 and 1894. Some of them have corona of pyroxene which is occasionally in association with magnetite and plagioclase. Olivine microphenocrysts are very rare and are usually rimmed by opaque coronas in basaltic andesite of the 1918 lava dome.

Variation of olivine crystals from euhedral to anhedral (embayed, elongated skeletal, hollow, with rim reactions and occasionally poikilitic texture) occurs in basalt and basaltic andesite of the 1982-83 eruption (Fig. V.1 & IV.7). Most elongated olivine crystals having rim reactions crystallise in the earlier eruptions (April - May 1982, in basaltic andesite), but most euhedral - subhedral crystals occur in the final stage (September 1982 - January 1983, in basalt). This implies that olivines grow in the magma whose cooling rate becomes slower with time (Donaldson, 1976). Other crystal shapes appear throughout the volcanic history of Galunggung.

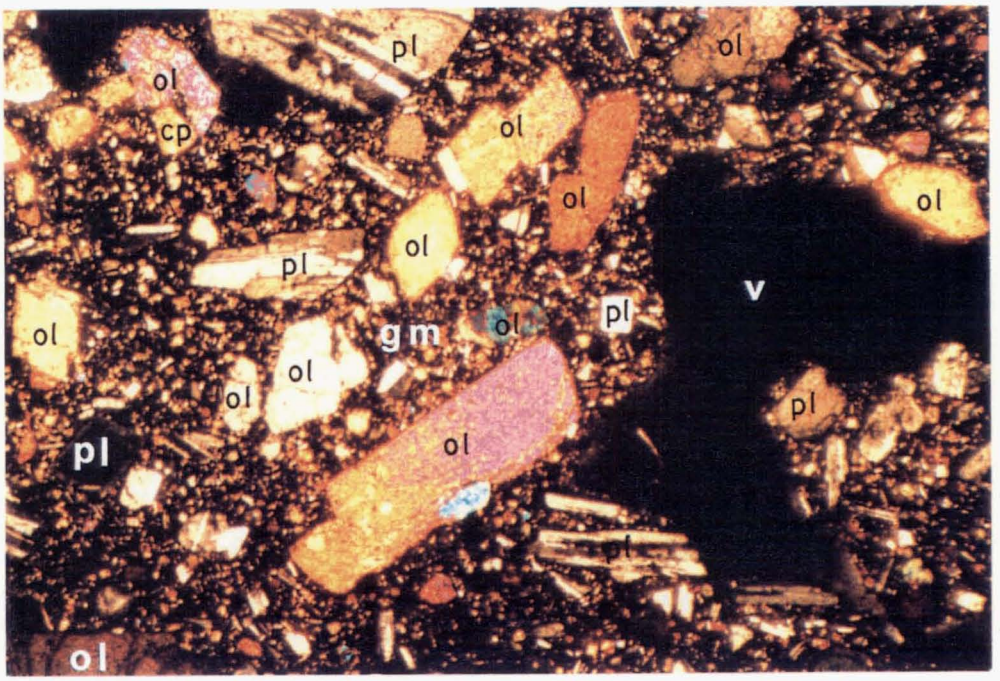

Figure V.1A Euhedral olivine crystals (ol) in basalt erupted on 1 - 7 January 1983. A large olivine crystal encloses the small one (at centre) and another olivine crystal encloses clinopyroxene (cp, above left corner). The enclosed crystals are relatively similar in size to those in the groundmass. Very fine crystals with brown birefringence in olivines are Cr-spinel. Pl = plagioclase, gm = groundmass, v = vesicle (20300, 25 X, crossed polarized).

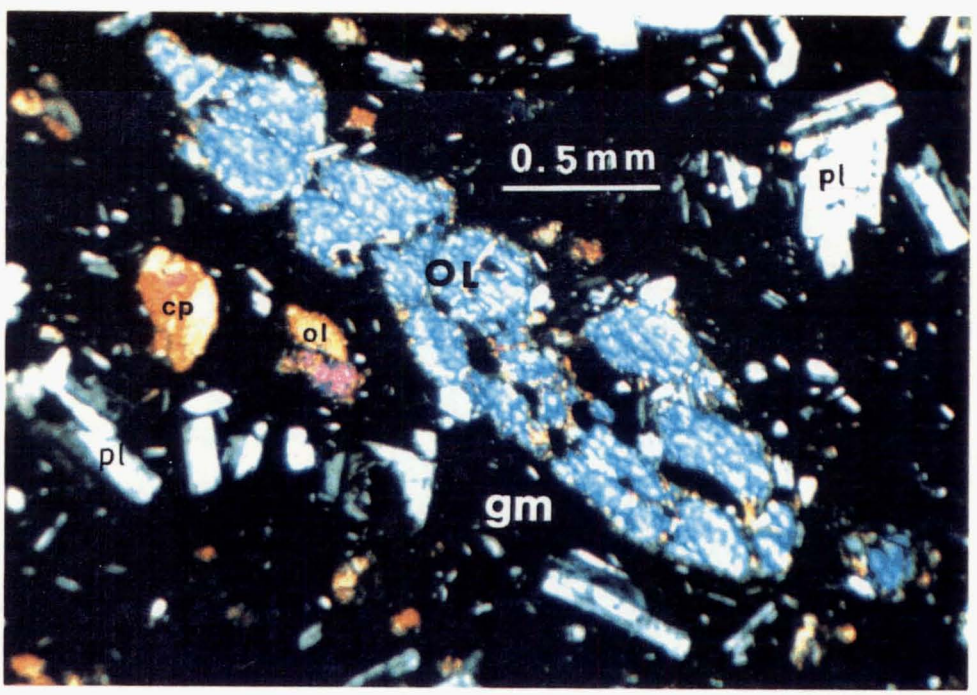

Figure V.1B Elongated, skeletal olivine crystal (ol) in basaltic andesite erupted on 25 April 1982. Cp = clinopyroxene, pl = plagioclase, gm = groundmass (20295, 25 X, crossed polarized).

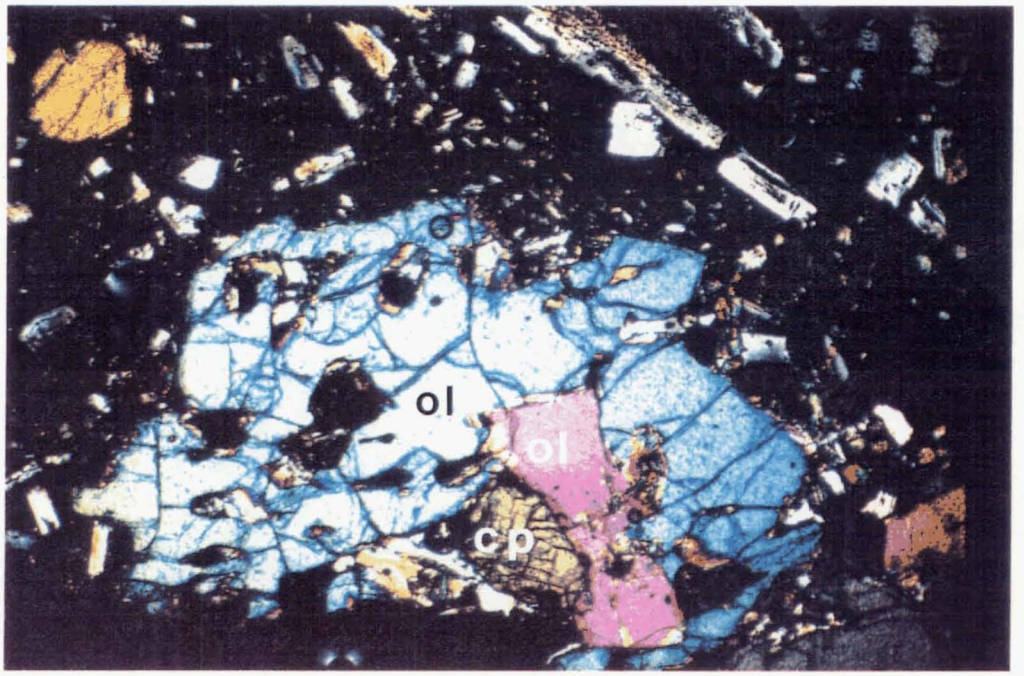

Figure V.1C Olivine (ol) showing poikilitic texture enclosing clinopyroxene (cp) and fine plagioclase crystals in basalt volcanic bomb erupted in June 1982 (20324, 25 X, crossed polarized).

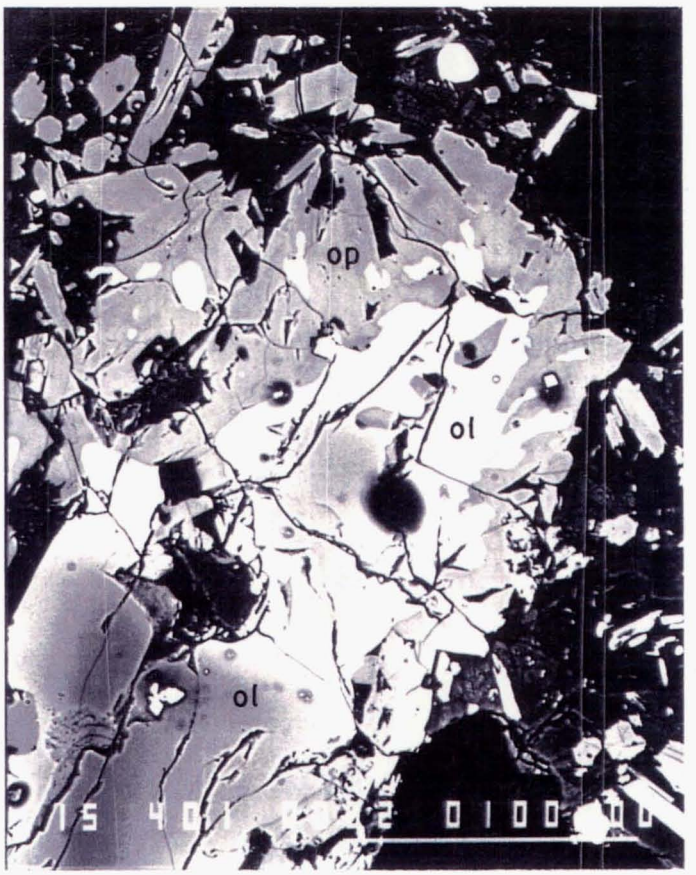

Figure V.1D Compositional variation of olivine phenocryst having corona of pyroxene in basaltic andesite volcanic bomb (VB16) erupted on 6 May 1982. Olivine core (ol, dark in centre) to rim (ol, light) to orthopyroxene (op, grey) at crystal margin. The very thin, light coloured zone at the outermost rim is clinopyroxene.

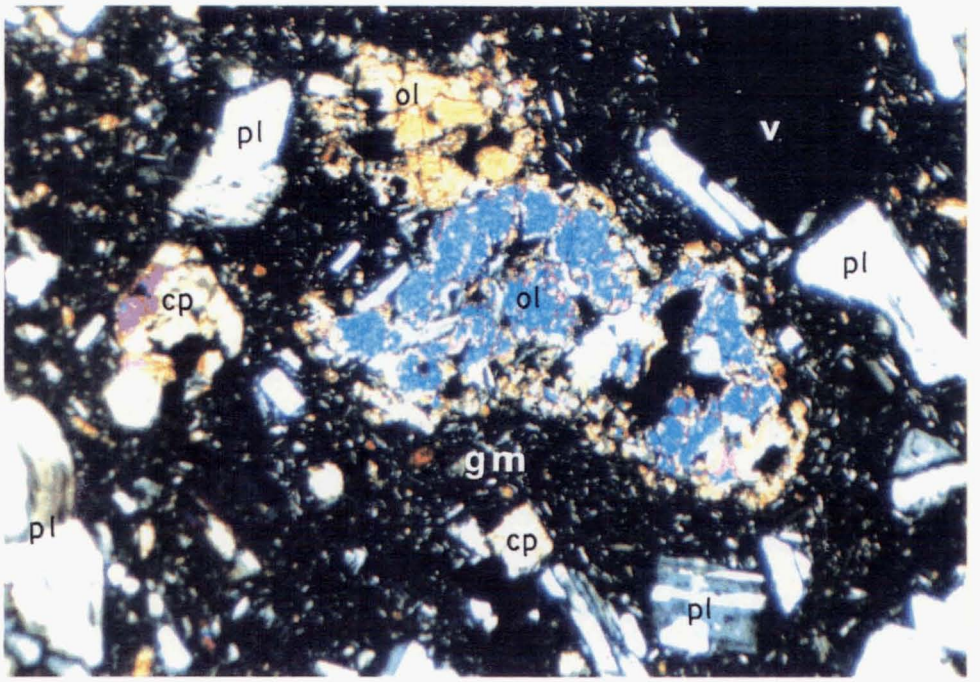

Figure V.1E Anhedral, hollow olivine crystals (ol) with corona of pyroxene in basaltic andesite erupted on 8 April 1982. Cp = clinopyroxene, pl = plagioclase, gm = groundmass, v = vesicle (20290, 25 X, crossed polarized).

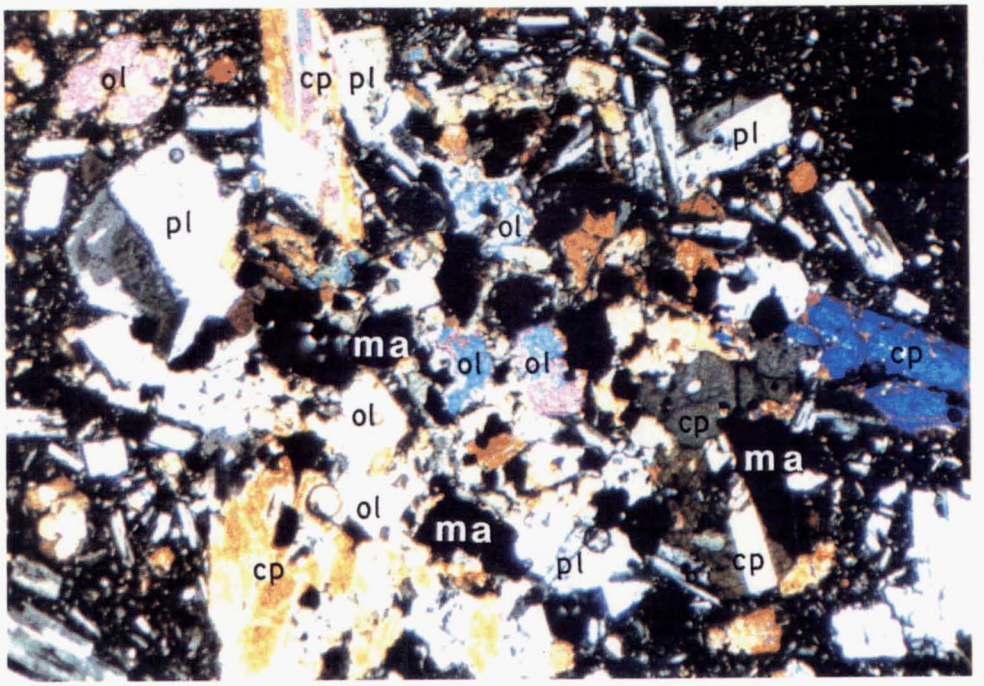

Figure V.1F Olivine (ol) surrounded by clinopyroxene (cp), magnetite (ma) and plagioclase (pl) in basalt injecting gabbro clast erupted in September - December (?) 1982 (VB19, 25 X, crossed polarized).

Rim reactions around olivines vary from very fine anhedral crystals to subhedral crystals and consist of pyroxene, magnetite and plagioclase (Fig. V.1D-F). These minerals result from reaction of olivine with the liquid (Deer et al., 1982; Flood & Vernon, 1988; Presnall, 1966) at lower temperature, probably during the quenching stage. Opaque coronas around euhedral olivine crystals, which are fairly common in basalt of the 1983 lava flow (sample number 20300), are Fe-rich olivine representing normal zoning of the mineral. Some large olivine crystals enclose smaller ones (Fig.V.1A).

The occurrence of olivines in the groundmass of Galunggung basalts, particularly those erupted in 1982-83, and as olivine microphenocrysts and phenocrysts indicate that the mineral continued to crystallise through most of the cooling history of the rocks. The euhedral - subhedral olivine phenocrysts which are normally zoned and lack pyroxene reaction rims are thought to be in equilibrium with the liquid of the host lava (Morrice and Gill, 1986).

Waxy green to greenish yellow clay material around olivine crystal rims and along the fractures is identified optically as bowlingite. This mineraloid is commonly found in lavas collected from lower parts of the Galunggung caldera and crater walls. Brownish red alteration products, normally termed iddingsite (Fig. V.2A), are only observed in weathered lava flows (e.g. L11A). Figure V.2B illustrates a transition from greenish yellow bowlingite to brown iddingsite and is taken from slightly weathered lava avalanche material (sample code LP). This suggests that hydrothermal alteration of olivine produces bowlingite which alters to iddingsite by surface weathering. Although there is a debate about the origin of iddingsite (Deer et al., 1982), Coote (1987) also stated that iddingsitization is more commonly asso-

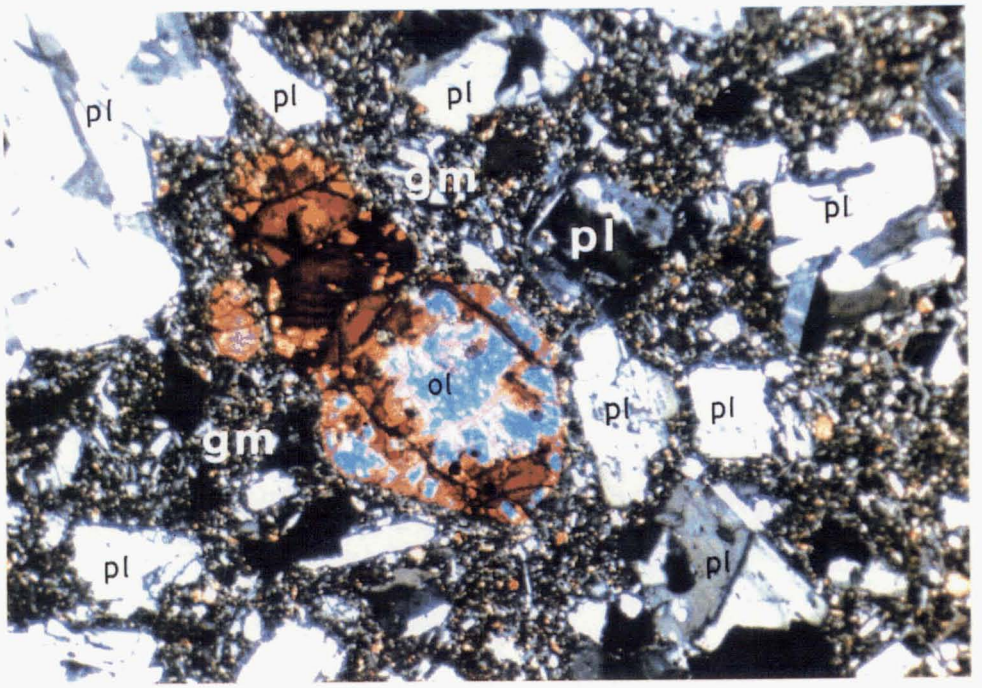

Figure V.2A Olivine (ol) altered to iddingsite (reddish brown) in basalt of Old Galunggung lava flow with top weathered soil. Pl = plagioclase, gm = groundmass (L11-A, 25 X, crossed polarized).

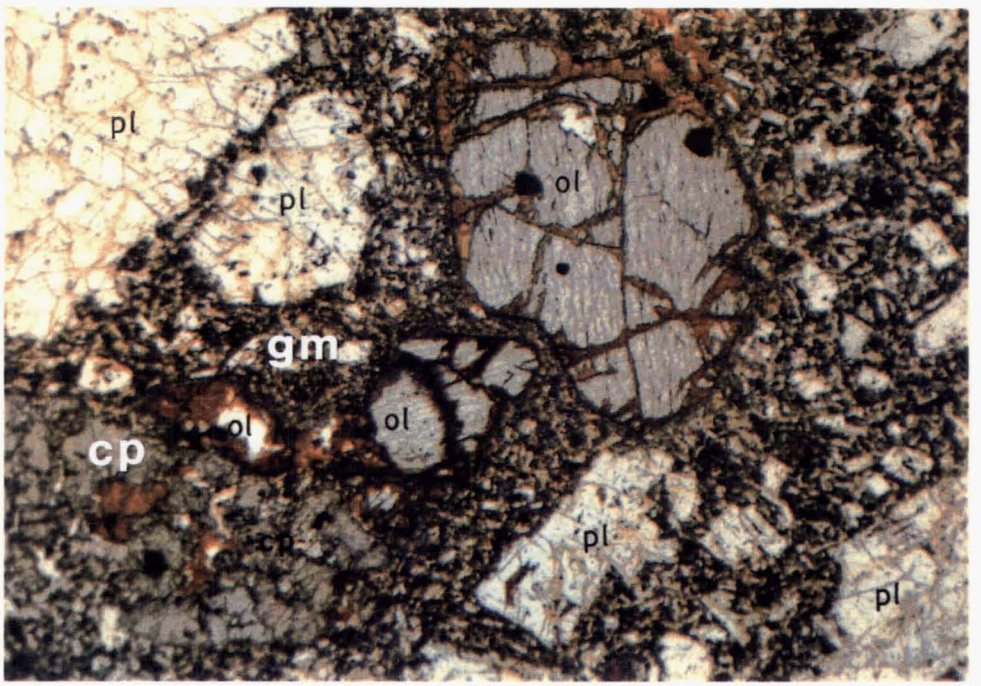

Figure V.2B Olivine (ol) altered to bowlingite (greenish yellow) that changes to iddingsite (brown) in basalt (lava flow in debris avalanche deposit). Cp = clinopyroxene, pl = plagioclase, gm = groundmass (LP, 25 X, plane polarized).

ciated with weathering than high-temperature primary magmatic processes. Carbonate is fairly common in altered olivines (e.g. 20270).

V.2.2 Mineral Chemistry

In Old Galunggung extrusive rocks (basalt - basaltic andesite), olivine compositions range from Fo_{53} to Fo_{78} (Fig. V.3A). In terms of stratigraphic position (Fig.III.2), from the lower most sample (20271), through the middle (VB10) to the upper most sample (L35) of Galunggung basalts, Fo contents decrease from Fo_{72} to Fo_{70} and Fo_{65} (Fig. V.3B). Olivines in basalt from dikes show a narrow range of composition (Fig. V.3C) from Fo_{68} in phenocryst cores to Fo_{62} in the groundmass.

In basaltic andesite produced during Galunggung caldera formation, olivines have a wide compositional range (Fig. V.3D) from Fo_{89} in phenocryst cores to Fo_{67} in phenocryst rims and groundmass crystals. Very rare anhedral olivine microphenocrysts (Fo_{88-66}) are observed in basalt erupted in 1822 (Fig. V.3E). Olivines in basaltic andesite of the 1918 lava dome are homogeneous with a composition of Fo_{66} (Fig. V.3F).

In basalt and basaltic andesite erupted in 1982-83 olivine phenocryst cores are Fo_{90-80} (maximum $Fo_{90.7}$; Nye, 1988, pers. comm.) whereas the rims and groundmasses are less than Fo_{80} (Fig. V.3G-J). In basalt the olivine phenocryst rims and groundmass crystals have a wider compositional range (Fo_{78-62}) than in basaltic andesite (Fo_{79-71}). This may relate to the optical characteristics where in basalt coronas around olivine crystals are Fe-rich olivine thus indi-

Figure V.3 Olivine compositional variation in Galunggung volcanic rocks. Circle = phenocryst core, square = phenocryst rim and groundmass crystal, filled triangle = inclusion. Filled circle and filled square are olivines in basaltic andesite and basalt from middle and upper layers of Old Galunggung lava flows, respectively.

A Olivines in basalt - basaltic andesite of Old Galunggung lava flows (random sampling).

B Olivines in basalt - basaltic andesite of Old Galunggung lava flows, from lower (circle) through middle (filled circle) to upper (filled square) layers of a sequence of lava flows in SW Galunggung caldera wall.

C Olivines in basalt of Old Galunggung dike.

D Olivines in basaltic andesite resulted during the Galunggung caldera formation.

E Olivines in basalt erupted in 1822.

F Olivines in basaltic andesite of the 1918 lava dome.

G Olivines in basaltic andesite erupted on 8 April 1982.

H Olivines in basaltic andesite erupted on 18 May 1982.

I Olivines in basalt erupted on 16 September 1982.

J Olivines in basalt erupted on 1 - 7 January 1983.

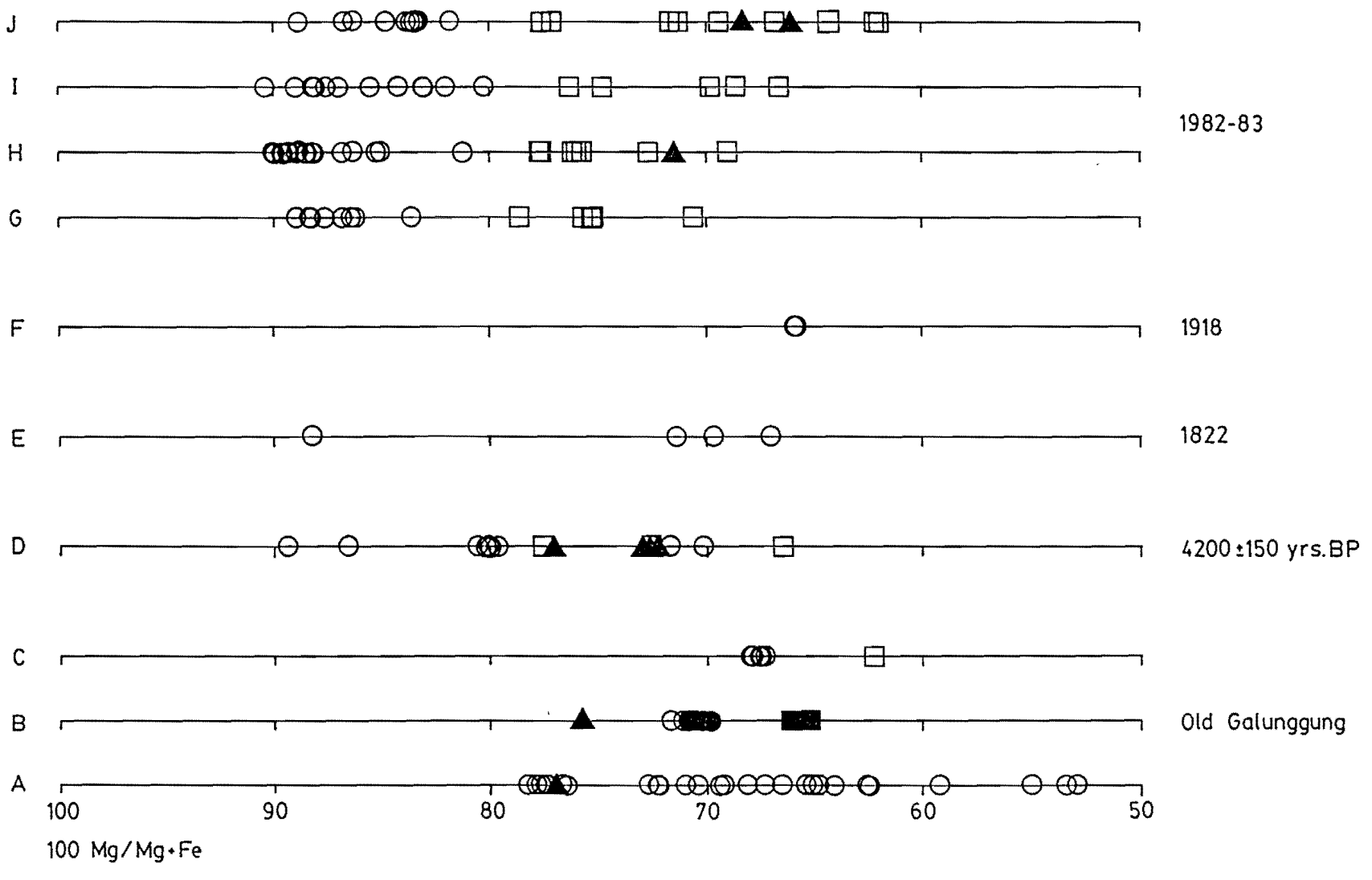
J
I
H
G
F
E
D
C
B
A
1982-83
1918
1822
4200 ±150 yrs. BP
Old Galunggung
100
90
80
70
60
50
100 Mg/Mg+Fe

cating a perfect normal zoning, whereas in basaltic andesite normal zoning in olivine is disturbed by rim reactions of pyroxene crystallisation (Fig. V.1D). The normal zoning of the olivine phenocrysts is due to fractionation and reaction with the interstitial liquid, and reflects the comparatively slower cooling path (Hermes & Schilling, 1976).

Olivine inclusions are occasionally observed in clinopyroxene and plagioclase phenocrysts. Their forsterite content is however always less than 80.

Trace elements in olivine do not show a systematic change with age of the Galunggung rocks (Table V.2). However, there is a positive correlation between NiO and MgO contents (Fig. V.4). Low Ni contents (< 0.2 % NiO) occur in olivines of basalt and basaltic andesite from Old Galunggung, 1822 and 1918 eruption rocks, and olivine phenocryst rims and groundmasses of the 1982-83 rocks. High Ni contents are observed in olivines from the caldera formation rocks (up to 0.3 %) and phenocryst cores of the 1982-83 rocks (up to 0.44 %). These olivines may be compared with olivines from upper mantle peridotite and other basic rocks (Bonatti & Michael, 1989; Deer et al., 1982; Fleet et al., 1977). The compositional overlap between phenocryst rims and olivine groundmasses suggests that the olivines crystallised under low-presure conditions (Ramsay et al., 1984).

CaO content in olivines of over 0.11 % is diagnostic of low-pressure phenocrysts (Simkin & Smith, 1970). The highest Ca content measured (0.88 % CaO) occurs in an olivine inclusion in plagioclase phenocryst (20300), but falls below the lower limit of detection in the 1918 lava dome. The Ca content of olivine in the mantle decreases as the mantle becomes more refractory (Nye & Reid, 1986). Thus the

Table V.2 Composition of trace elements in olivine crystals.

Volcanic activity	Maximum value (wt. %)					Major variation value (wt. %)					Explanation
	TiO_2	MnO	CaO	NiO	Cr_2O_3	TiO_2	MnO	CaO	NiO	Cr_2O_3	
1982-83 Eruption											
1-7 January 1983	.12	.62	.87	.44	.06	≤ .07	.02 - .5	.17 - .34	.10 - .25	≤ .05	Lava flow; high-Mg basalt
Sept. - Dec. '82	.06	.59	.24	.26	.17	≤ .04	≤ .47	.18 - .24	.10 - .16	.03 - .06	Strombolian; high-Mg basalt
25 April - May	.12	.70	.30	.35	.50	≤ .07	.10 - .50	.12 - .29	.10 - .20	≤ .10	Peléean; high-Mg basaltic andesite
8 April 1982	.05	.59	.23	.27	.09	≤ .03	.15 - .39	.15 - .23	.10 - .20	≤ .05	Peléean; low-Mg basaltic andesite
16-20 July 1918	.03	.64	.20	.04	.02	≤ .03	.53 - .64	.04 - .20	≤ .04	≤ .02	Lava dome; low-Mg basaltic andesite
8 October 1822	.03	.56	.24	.17	.16	≤ .02	.17 - .56	.12 - .17	≤ .11	≤ .07	Peléean; low-Mg basalt - basaltic andesite
4200 ± 150 yr.BP	.19	.57	.21	.30	.26	≤ .07	.15 - .47	.13 - .20	.03 - .18	≤ .10	Caldera formation; low-Mg basalt - basaltic andesite
Old Galunggung	.07	.56	.26	.13	.05	≤ .05	.45 - .54	.15 - .23	.02 - .06	≤ .05	Dike; low-Mg basalt - basaltic andesite
	.10	.63	.33	.10	.10	≤ .06	.42 - .61	.12 - .18	≤ .10	≤ .10	Lava flow; low-Mg basalt - basaltic andesite

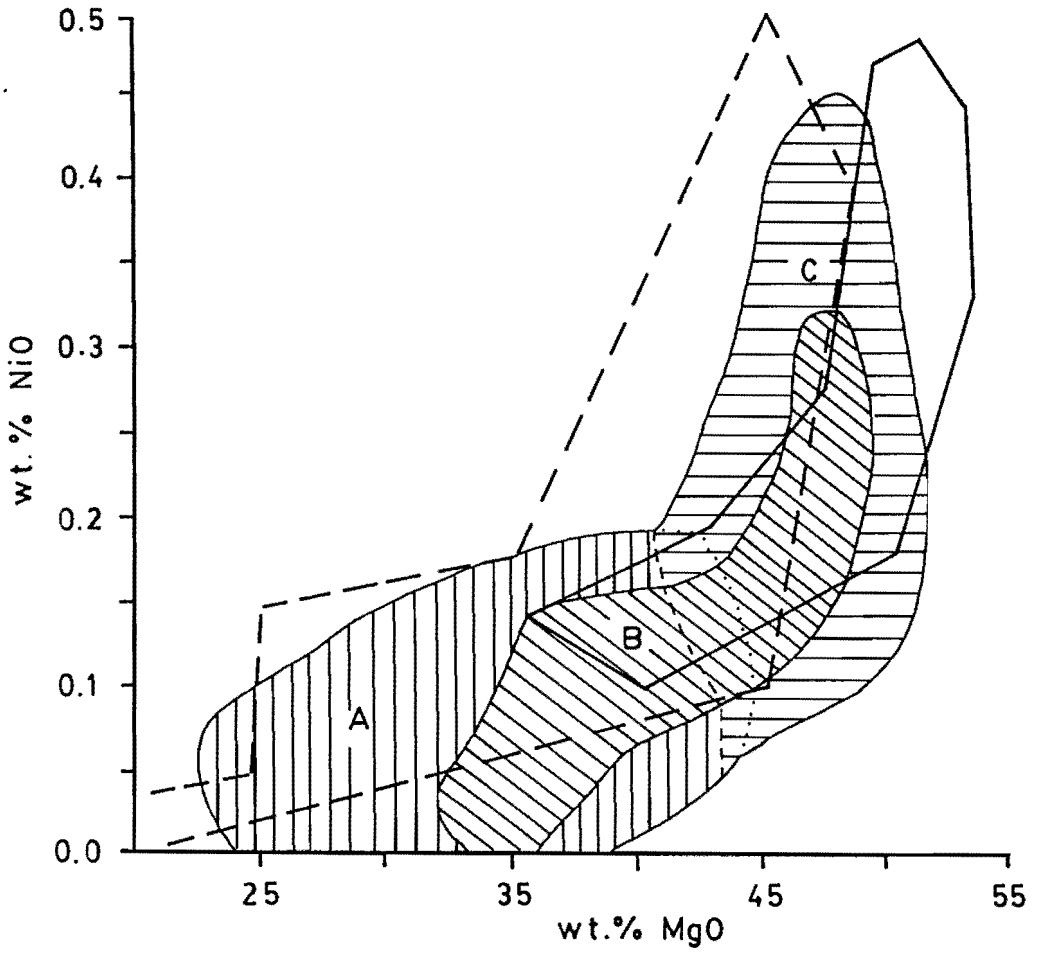

Figure V.4 Variation of MgO and NiO contents in olivines from Galunggung volcanic rocks compared with olivines of upper mantle peridotite (continuous line) and olivines of basalts, diabases and layered intrusions (broken line) (after Deer et al., 1982; Fleet et al., 1977).

A Olivines in basalt - basaltic andesite of Old Galunggung and historic eruptions in 1822 and 1918, and olivine phenocryst rims and groundmass crystals in basalt - basaltic andesite erupted in 1982 - 83

B Olivines in basaltic andesite erupted during the Galunggung caldera formation

C Olivine phenocryst cores in basalt - basaltic andesite erupted in 1982-83

high CaO content of olivines in the Galunggung rocks suggests that the olivines are magmatic. The slightly higher CaO contents of rims versus cores are obtained in the olivines of the 1983 lava flow. This may be due to decreasing pressure as melt crystallised and moved to the surface (Stormer, 1973).

Mn content rarely exceeds 0.3 % MnO in Mg-rich olivines (> Fo_{80}), but it is usually higher in olivine of Fo < 70. Ti is below detection limit in very high-Mg olivine phenocryst cores, but is concentrated in olivine phenocryst rims and groundmass crystals. Another trace element, Cr, reaches up to 0.5 % Cr_2O_3.

In short, most of the pre-1982 rocks contain anhedral crystals which have < Fo_{80}, low Mg and Ni contents. On the other hand, olivines in the 1982-83 rocks vary from euhedral-subhedral to anhedral crystals and the phenocryst cores have > Fo_{80}, high Mg and Ni contents. This implies that the 1982-83 basalt is more primitive than the earlier basalts. The compositional changes in olivines are much more influenced by petrogenetic processes than time and stratigraphic position. By having a similar composition to euhedral-subhedral olivines, the anhedral (rounded, elongated and embayed) crystals are more likely to be caused by the change of pressure and temperature conditions as a magma moves towards the surface, than by compositional disequilibrium (Cox et al., 1981). These data may also suggest that olivine crystallised in the magma and the phenocrysts are in equilibrium with their groundmass (Cox et al., 1981; Morrice and Gill, 1986; Roeder & Emslie, 1970). The highest crystallisation temperature of olivines having Fo_{90} is 1313 ^{o}C. This will be discussed in the chapter VII.

V.3 Pyroxene

Pyroxenes can be divided into two group in Galunggung volcanic rocks, namely calcic pyroxene and magnesium-iron pyroxene (Deer et al., 1978a,b). Representative analyses are given in Table V.1. The calcic pyroxenes range from diopside through salite to augite in composition, and the magnesium-iron pyroxenes consist of orthopyroxene and pigeonite.

The calcic pyroxenes appear in Galunggung rocks of different compositions from basalt to basaltic andesite, whereas orthopyroxenes are only common in basaltic andesites. Pyroxenes having a pigeonitic composition occur as very fine grain groundmass crystals or olivine coronas.

V.3.1 Calcic Pyroxene

V.3.1.1 Optical Mineralogy

Calcic pyroxenes or clinopyroxenes (e.g. Kerr, 1977; Shelley, 1981), are neutral to pale green in color; present as phenocrysts (0.3 - 4.0 mm), inclusions, groundmass crystals, orthopyroxene rims and coronas. The crystals vary from euhedral to anhedral as well as phenocryst abundance from nil up to 7 % (Table IV.1 - 3) with the average 1.6 %.

In basalts and basaltic andesites of Old Galunggung volcanic rocks, some calcic pyroxene phenocrysts contain inclusions of magnetite and plagioclase showing poikilitic texture, while inclusions of

olivine and glass are occasionally observed. Oscillatory-normal zoned clinopyroxenes are present in basaltic andesites erupted during caldera formation (20253) and in 1894 (20246).

In basalts erupted in 1982-83, calcic pyroxene phenocrysts crystallised with Mg-rich olivines and Cr-spinels, whereas in high silica basaltic andesite, the mineral coexists with orthopyroxenes and magnetites. Most calcic pyroxenes are euhedral-subhedral crystals; some of them form glomeroporphyritic crystal clots. However, anhedral crystals (e.g. embayed, hollow with poikilitic texture) are not uncommon. Figure V.5A represents euhedral, hollow and normally zoned clinopyroxene phenocryst enclosing small grains of olivine, clinopyroxene and plagioclase crystals which are comparable in size with the groundmass. Also, there is a gradual change in size of the clinopyroxene minerals from groundmass crystals through microphenocrysts to phenocrysts. Figure V.5B illustrates a large clinopyroxene crystal encloses the small ones. These data suggest that clinopyroxene phenocrysts grew in the magma.

Calcic pyroxene groundmass crystals and coronas around olivine and orthopyroxene phenocrysts are common as anhedral fine grain prismatic crystals (< 0.1 mm) showing quench texture. However, the mineral is absent in groundmass of the high silica basaltic andesite (e.g. 20288,20347). Calcic pyroxenes as orthopyroxene rims will be described in the V.3.2.1.

V.3.1.2 Mineral Chemistry

Most calcic pyroxenes in the Old Galunggung extrusive rocks,

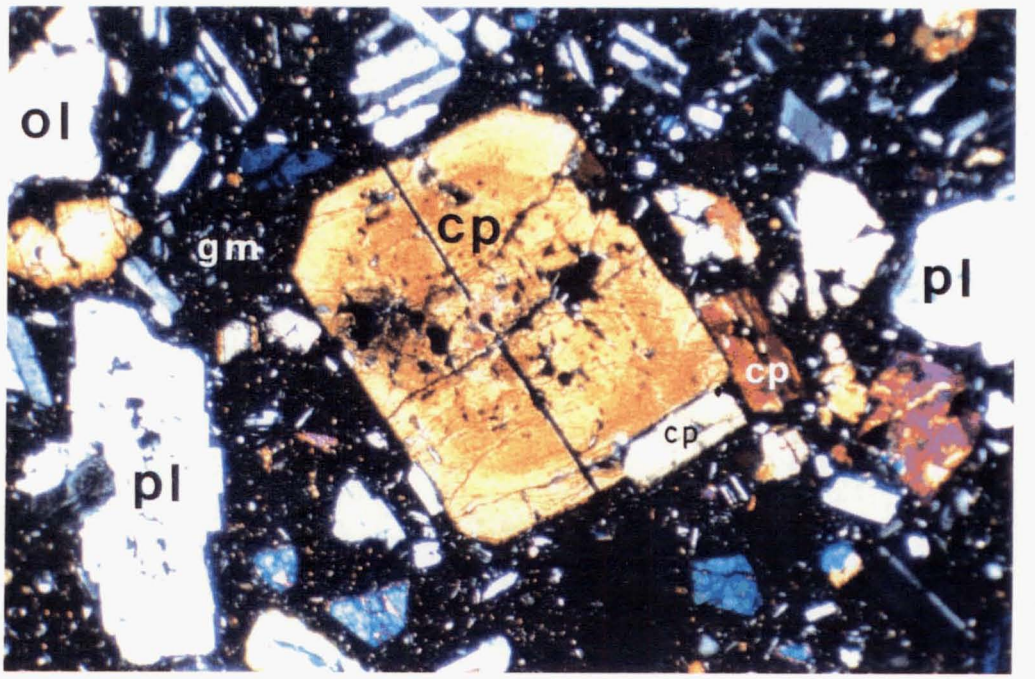

Figure V.5A Clinopyroxene (cp), euhedral normally zoned, enclosing small grains of olivine (red birefringence, at centre), clinopyroxene and plagioclase in basalt volcanic bomb erupted on 3 December 1982. Pl = plagioclase, gm = groundmass (20339, 25 X, crossed polarized).

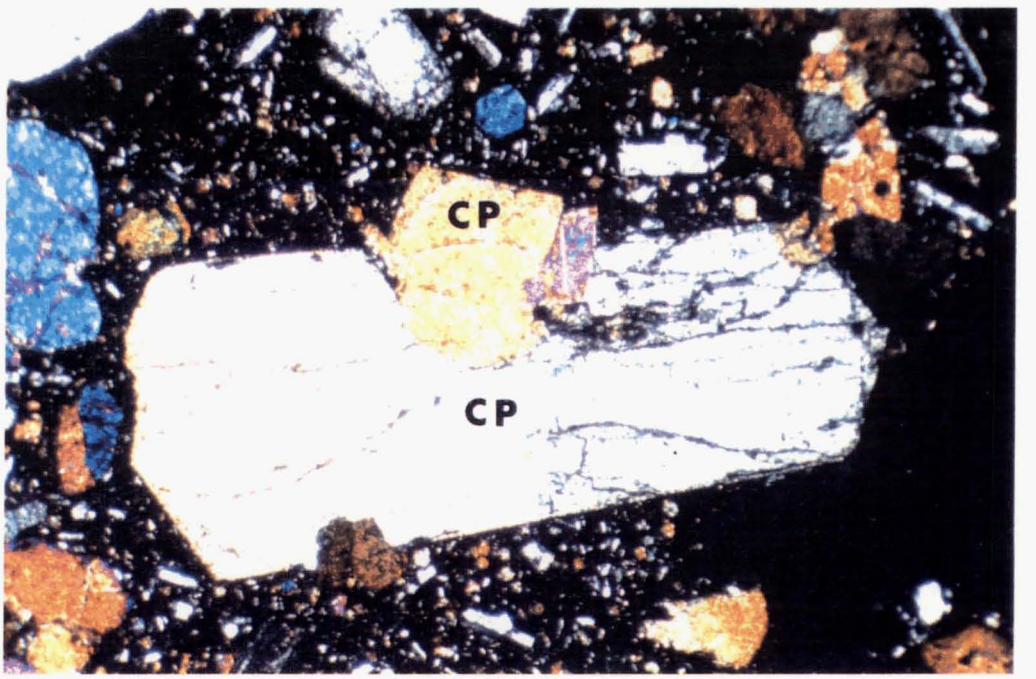

Figure V.5B Clinopyroxene (cp), large grain enclosing small grains in basalt lava flow erupted on 1 - 7 January 1983 (20300, 25 X, crossed polarized).

from basalt to basaltic andesite, are augite (Fig. V.6), ranging from $Ca_{43}Mg_{42}Fe_{15}$ in phenocryst cores to $Ca_{32}Mg_{43}Fe_{25}$ in groundmasses. Calcic pyroxene phenocryst rims, groundmasses and inclusions have relatively lower Ca but higher Fe contents compared with the phenocryst cores. Diopside ($Ca_{47}Mg_{46}Fe_7$) and salite ($Ca_{48}Mg_{40}Fe_{12}$) compositions are occasionally found in the phenocryst cores. Selected analyses based on the stratigraphic position (Fig.V.7 and Fig.III.2), and bulk rock (Fig.V.8), apparently, do not vary systematically in composition.

All calcic pyroxene phenocrysts in the Old Galunggung dikes are also augite (Fig. V.9A) with an average core composition of $Ca_{41}Mg_{42}Fe_{17}$. By contrast, all calcic pyroxene phenocrysts in the Old Galunggung cryptodome are diopside (Fig. V.9B). Their compositions range between $Ca_{47}Mg_{47}Fe_6$ and $Ca_{48}Mg_{42}Fe_{10}$. The contents of Al, Ti, Na and Cr are listed in Table V.3.

Compositions of diopside differ from augite and are shown in Figure V.10. Al and Ti contents increase with increasing Fe ratios in diopside; whereas in augites Ti contents are relatively constant and Al contents decrease with increasing Fe ratios. Although Cr contents in augites are constantly low they vary up to 0.024 atomic per cent (0.82 % Cr_2O_3) in diopside. This variation of Cr contents is likely related to the Mg contents in the mineral.

Calcic pyroxene compositional variation in rocks erupted during caldera formation is shown in Figure V.11. In basalt injecting gabbro clast some clinopyroxene compositions are diopside ($Ca_{50}Mg_{43}Fe_7$), whereas in basaltic andesite the calcic pyroxenes are augite ($Ca_{43}Mg_{41}Fe_{16}$) and salite ($Ca_{47}Mg_{40}Fe_{13}$). In the 1822 eruption rocks (Fig. V.12A) most calcic pyroxenes are augites ($Ca_{43\text{-}40}Mg_{44\text{-}40}Fe_{18\text{-}15}$) with a few diopside-salite compositions ($Ca_{46\text{-}45}Mg_{47\text{-}38}Fe_{16\text{-}9}$), and in

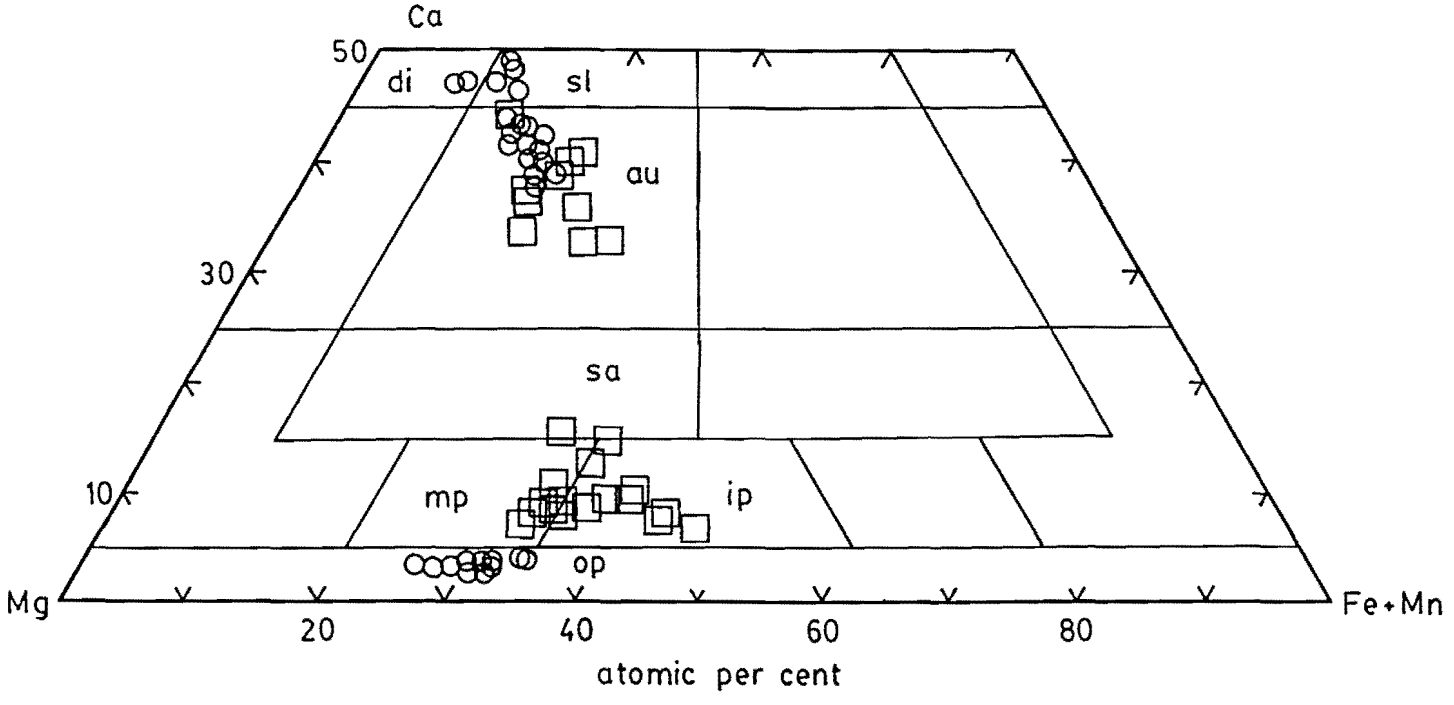

Figure V.6 Pyroxene compositional variation in Old Galunggung basalts and basaltic andesites. Au = augite, di = diopside, ip = intermediate pigeonite, mp = magnesium pigeonite, op = orthopyroxene, sa = subcalcic augite, sl = salite; circle = phenocryst core, square = phenocryst rim, groundmass crystal, inclusion and corona.

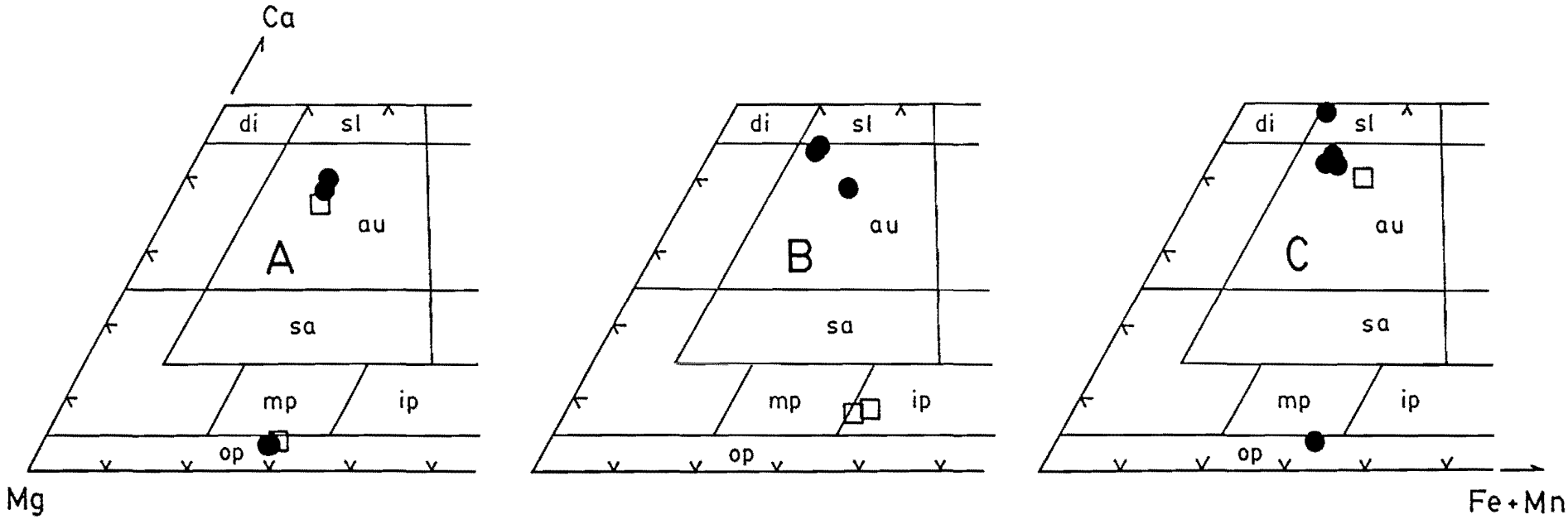

Figure V.7 Pyroxene compositional variation in Old Galunggung basalts from lower (A, 20271) to middle (B, VB 10) to upper (C, L35) layers of a sequence of lava flows in SW wall of Galunggung caldera. Filled-circle = phenocryst core, square = phenocryst rim and groundmass. Stratigraphic position refers to Fig. III.2A.

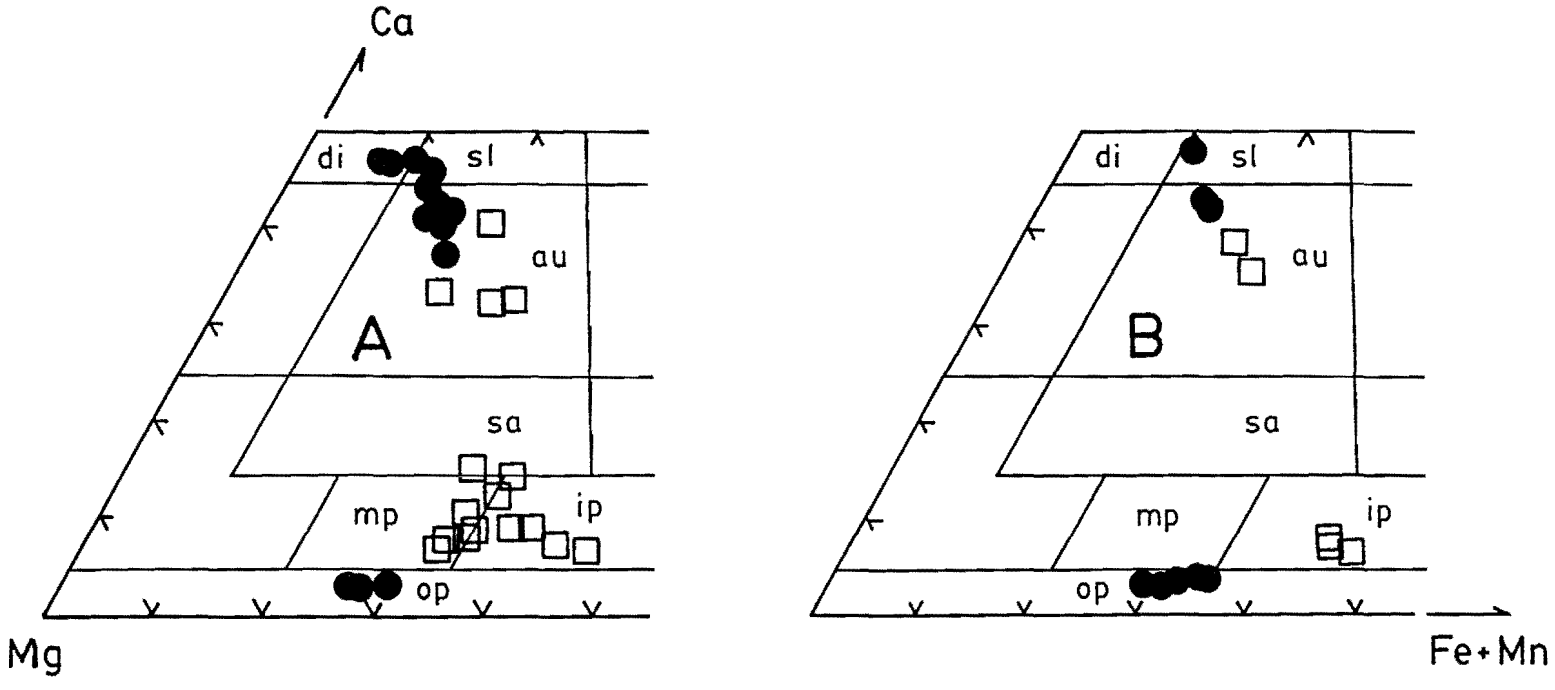

Figure V.8 Pyroxene compositional variation in basalts (A) and basaltic andesite (B) from Old Galunggung lavas. Symbols as for Fig. V.7.

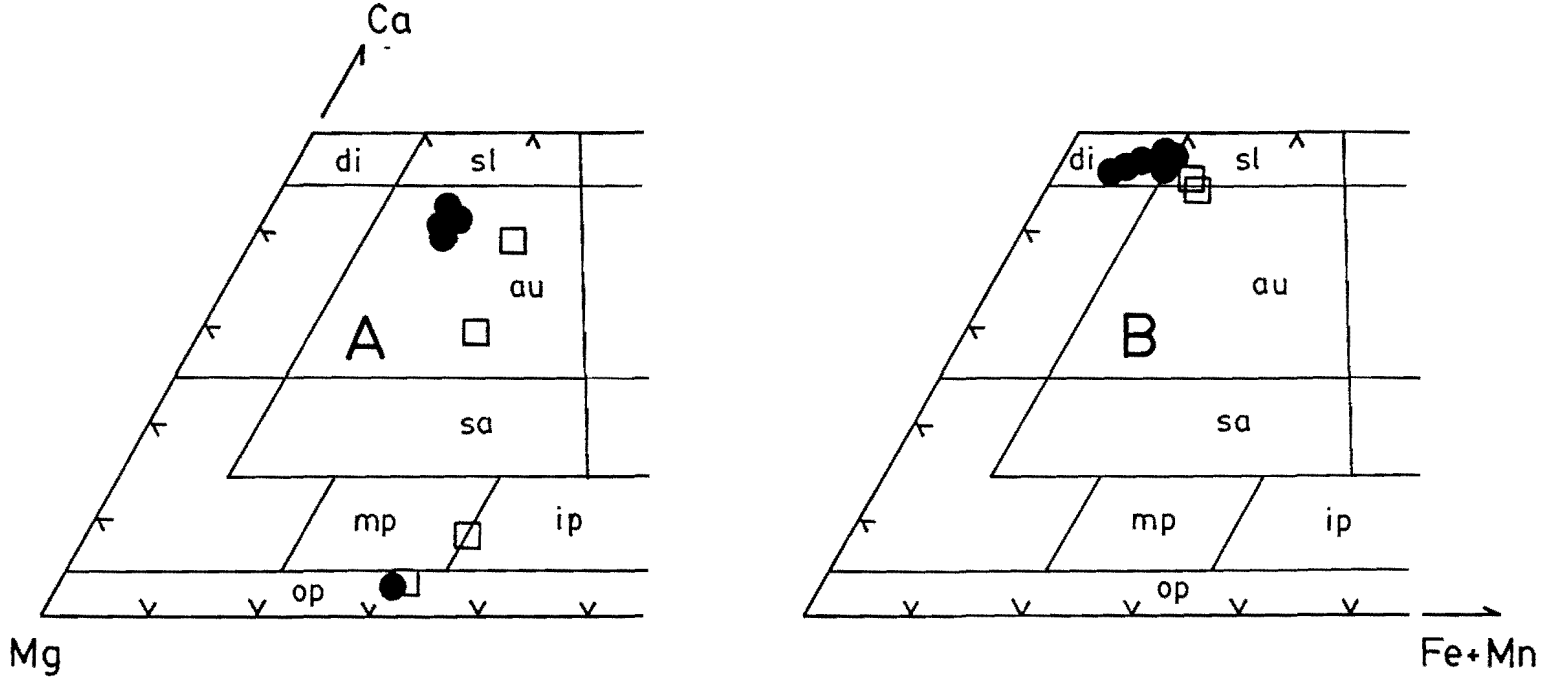

Figure V.9 Pyroxene compositional variation in Old Galunggung basalts of dike (A) and cryptodome (B). Symbols as for Fig. V.7.

Table V.3 Composition of pyroxene phenocryst cores in the Galunggung volcanic rocks. AU = augite, DI-SA = Diopside-salite, OP = orthopyroxene, R = range, and A = Average. Number of analyses for the three pyroxenes are 62, 73 and 84, respectively.

Volcanic activity	Mineral		Al_2O_3 (wt. %)	TiO_2 (wt. %)	Na_2O (wt. %)	Cr_2O_3 (wt. %)	Fe/Fe + Mg
	DI-SA	R	2.256 - 7.434	.171 - 1.163	≤ .345	.320 - 1.135	.097 - .294
		A	3.901	.521	.207	.377	.164
1982-83							
	AU	R	1.676 - 5.048	.274 - .876	.208 - .336	≤ .336	.215 - .289
Eruption		A	2.564	.498	.280	.041	.261
	OP	R	.210 - 1.774	.140 - .964	≤ .048	≤ .072	.313 - .335
		A	1.107	.261	.019	.022	.324
1918	AU	R	1.683 - 2.283	.465 - .584	.300 - .344	.026 - .029	.298 - .302
		A	1.983	.525	.322	.027	.300
Lava							
	OP	R	.755 - 1.753	.120 - .396	≤ .069	≤ .048	.299 - .322
dome		A	1.247	.305	.027	.019	.310
	DI-SA	R	3.532 - 6.479	.327 - .509	.191 - .786	.014 - .037	.182 - .294
		A	5.006	.418	.489	.026	.238
1822							
	AU	R	1.875 - 2.556	.403 - .555	.224 - .324	≤ .054	.255 - .296
Eruption		A	2.099	.464	.272	.022	.277
	OP	R	.616 - 2.098	.205 - .377	≤ .026	≤ .064	.311 - .352
		A	1.118	.297	.016	.014	.333
Caldera	DI-SA	R	2.713 - 6.529	.298 - .958	.163 - .906	≤ 1.107	.131 - .315
		A	4.464	.658	.313	.210	.215
formation							
	AU	R	1.557 - 4.059	.332 - .681	.245 - .330	≤ .073	.251 - .289
4200 ± 150		A	2.755	.514	.288	.015	.272
yrs. BP	OP	R	.850 - 2.322	.117 - .297	≤ .046	≤ .098	.215 - .336
		A	1.575	.215	.014	.021	.246
	DI-SA	R	1.877 - 6.546	.131 - 1.024	≤ .464	≤ .761	.090 - .233
Old		A	4.458	.529	.250	.369	.152
Galunggung	AU	R	1.484 - 4.771	.259 - .943	.041 - .426	≤ .224	.226 - .373
		A	2.694	.626	.332	.041	.270
	OP	R	.551 - 2.214	≤ .404	≤ 1.961	≤ .198	.267 - .354
		A	1.290	.255	.153	.024	.308
Average	DI-SA		4.457	.532	.315	.246	.192
composition	AU		2.419	.426	.299	.029	.276
	OP		1.249	.267	.046	.020	.304

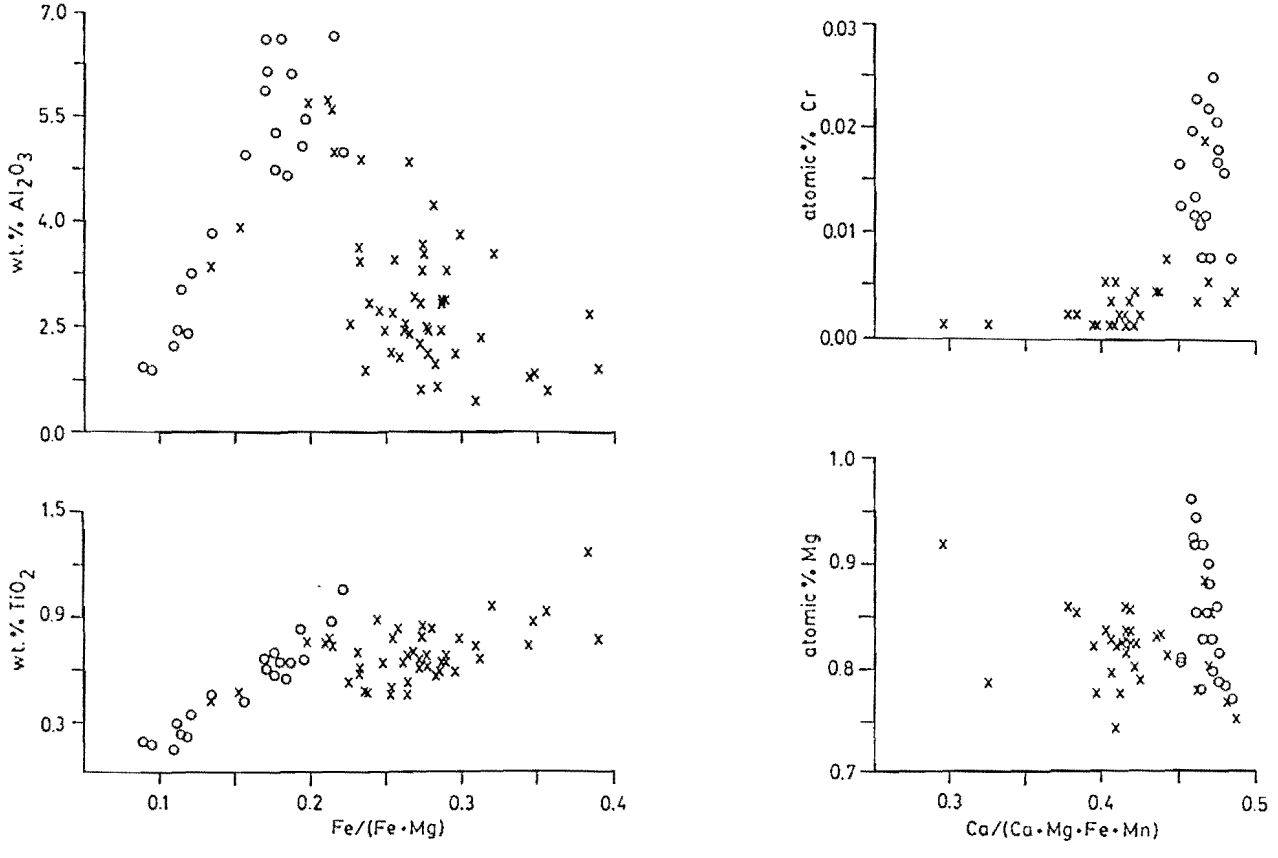

Figure V.10 Discrimination diagrams of clinopyroxenes in basalt and basaltic andesite of lava flows, bombs and dikes (cross), and a cryptodome basalt (circle) from Old Galunggung volcano. Diopside differs from augite by having (Fe/Fe + Mg) < 0.2, and (Ca/Ca + Mg + Fe + Mn) > 0.45.

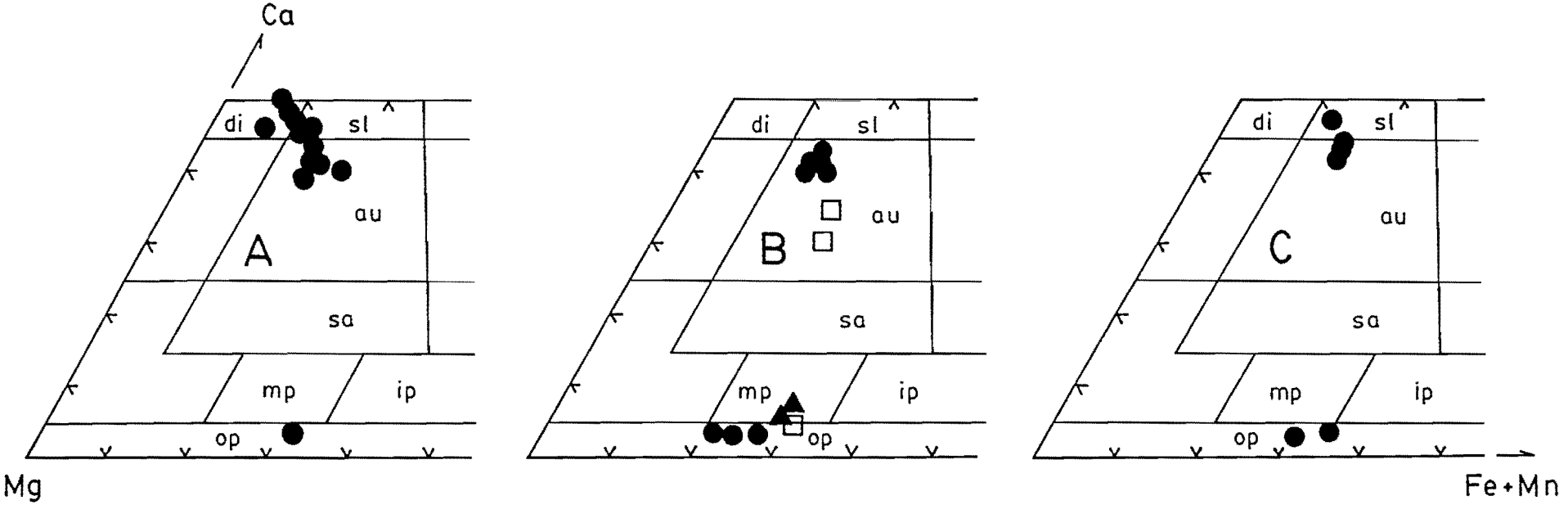

Figure V.11 Pyroxene compositional variation in basalt injecting gabbro clast with short prismatic amphibole crystals (A, 20256), in basaltic andesite injecting gabbro clast with long prismatic amphibole crystals (B, 20257), and in basaltic andesite erupted during caldera formation (C, 20289). Filled-circle = phenocryst, square = groundmass, and filled-triangle = inclusion.

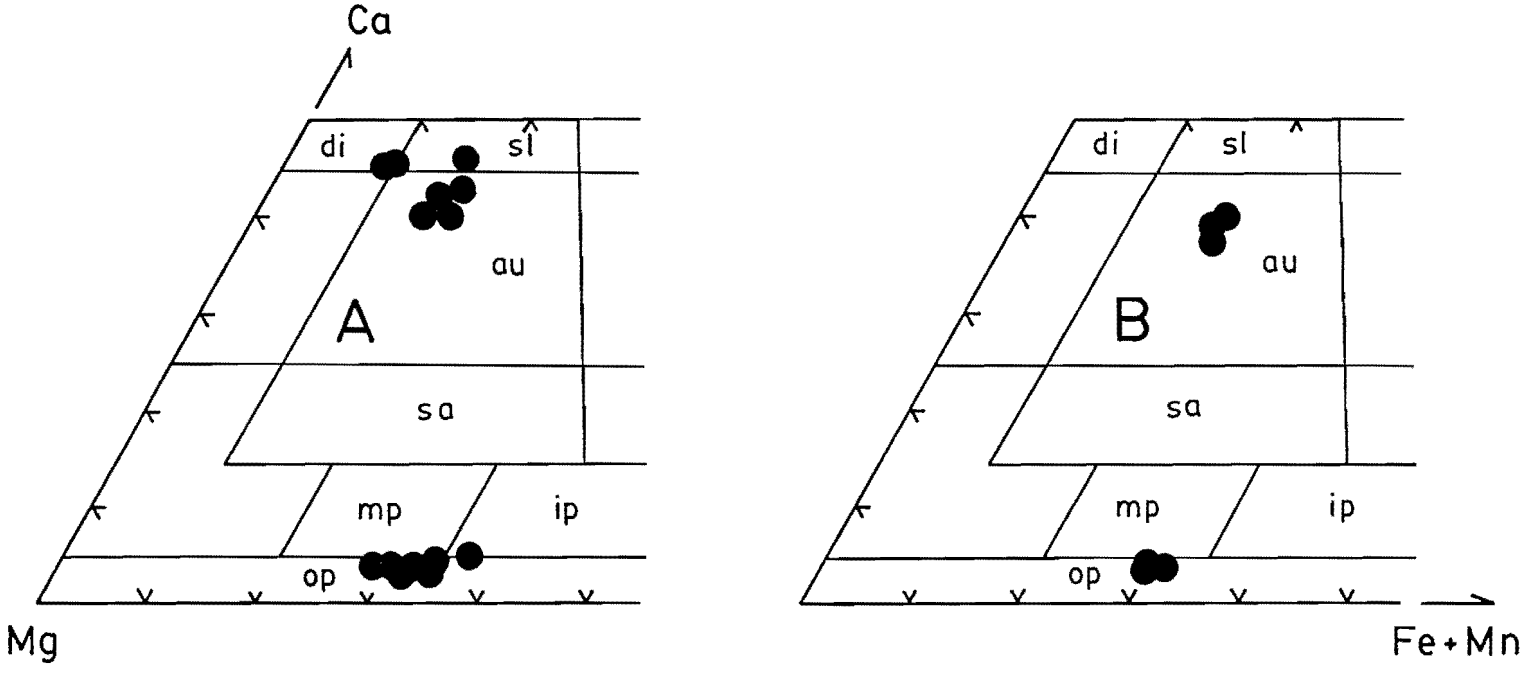

Figure V.12 Pyroxene compositional variation in basalt erupted in 1822 (A) and in basaltic andesite of the 1918 lava dome (B).

the 1918 lava dome all calcic pyroxenes (Fig. V.12B) are augite ($Ca_{40-37}Mg_{44-41}Fe_{19-18}$). There is , however, no significant compositional difference within the calcic pyroxene phenocrysts, inclusions and groundmass crystals. Variations of Al, and Ti also do not show an obvious trend. Cr contents in diopsides vary up to 0.032 atomic per cent (1.11 % Cr_2O_3) but they are not accompanied by increasing of Mg contents in the minerals (Fig.V.13).

Compositional variation of calcic pyroxenes in the 1982-1983 eruption rocks is shown in Fig.V.14. In the initial stage (April 1982), when basaltic andesites were erupted, augite compositions ($Ca_{43-32}Mg_{45-41}Fe_{23-12}$) change to diopside compositions with time and decreasing silica contents in the bulk rock. Furthermore, diopsides are the dominant compositions ($Ca_{48-45}Mg_{47-46}Fe_{9-5}$) in the final stage when basalts were erupted. Augites are observed only as narrow phenocryst rims and groundmass crystals.

Most diopsides have Fe ratios < 0.2, and show positive relationships between Al, Ti contents and Fe ratios (Fig.V.15), whereas in augites Al decreases and Ti does not give a systematic trend with increasing Fe ratios. Cr contents vary up to 0.035 atomic per cent (1.14 % Cr_2O_3) in diopsides.

The high Cr values reflect Cr values of the host rock and the fact that Cr^{3+} is preferentially partitioned into early crystallising clinopyroxene because of the high crystal field stabilisation energy of Cr^{3+} (Campbell & Borley, 1974; Wass, 1988). The increase of Cr contents is not accompanied by increasing Mg contents (Fig.V.15). This is similar to the diopsides in rocks erupted during caldera collapse and pre-1982 historic eruptions (Fig.V.13), but different to the diopsides in Old Galunggung rocks, particularly in the cryptodome

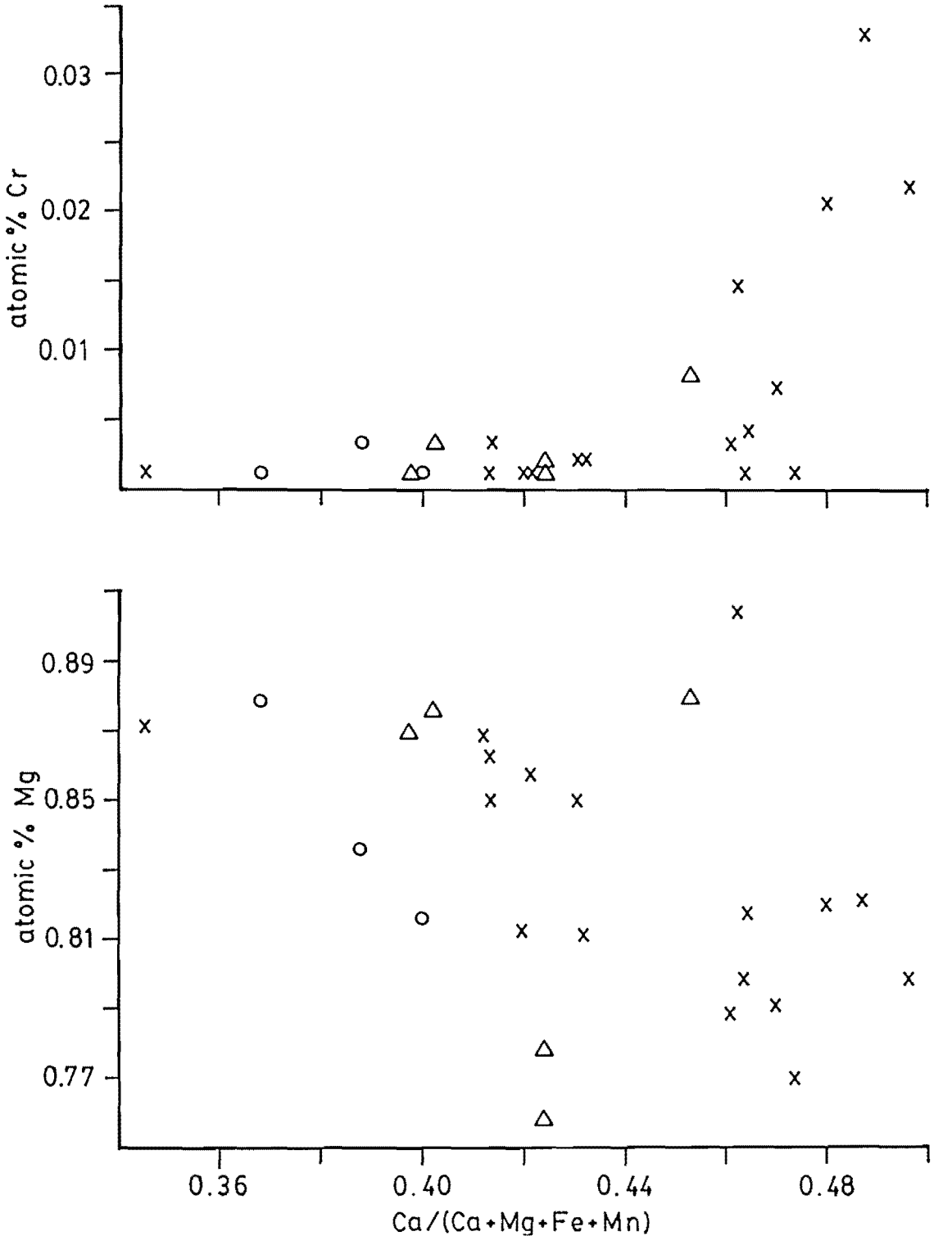

Figure V.13 Discrimination diagrams of clinopyroxene in basalt and basaltic andesite erupted during caldera formation (cross), in 1822 (triangle), and in 1918 (circle).

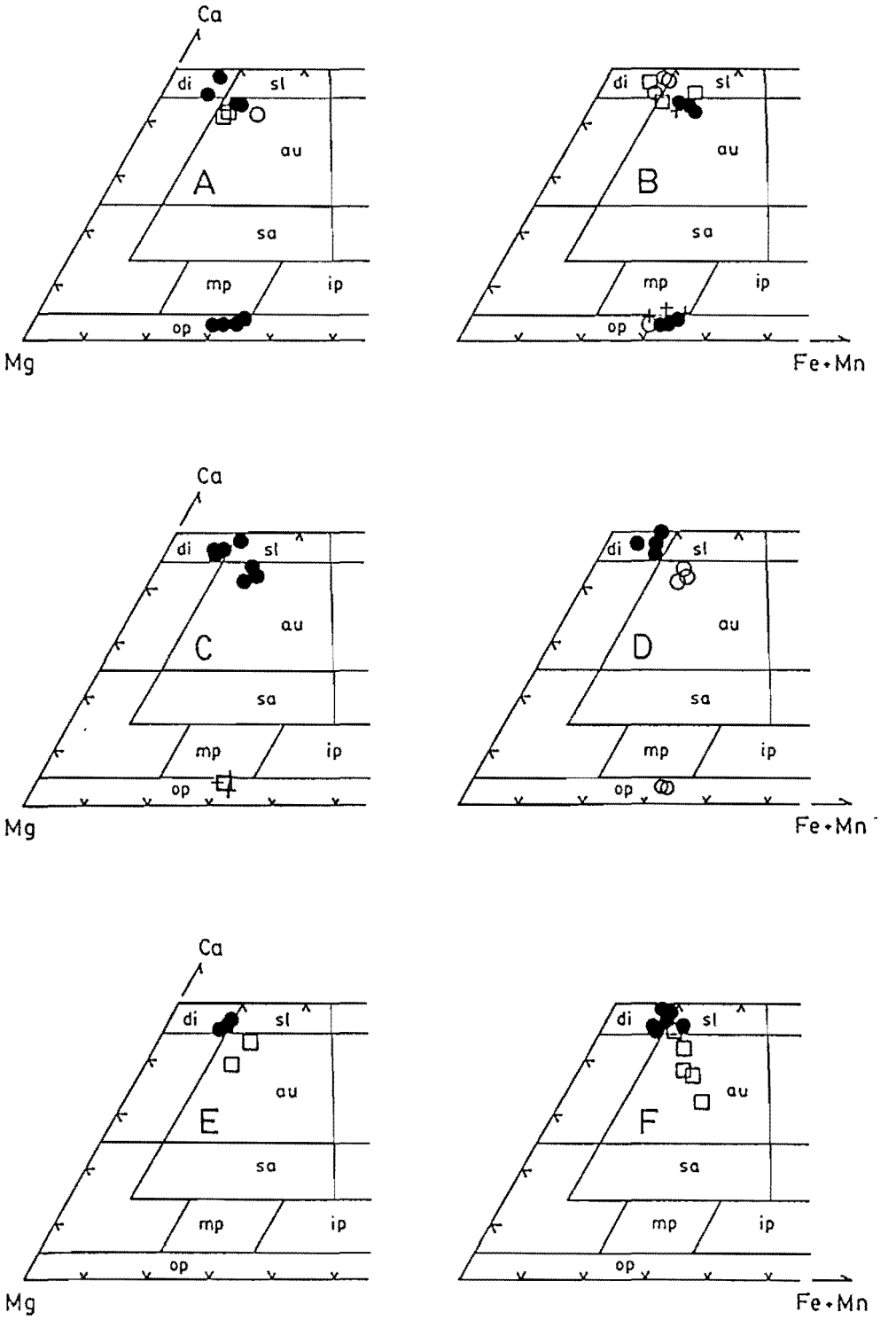

Figure V.14 Pyroxene compositional variation in basalt - basaltic andesite erupted in 1982-83. A to D are pyroxenes in basaltic andesite erupted on 8 April 1982 (20294), 25 April (20291), 6 May (VB 16), and 18 May (20297), respectively. Whereas E and F are pyroxenes in basalt erupted on 16 September 1982 and 1 - 7 January 1983, respectively. Filled-circle = phenocryst core; circle = crystal clot; square = phenocryst rim and groundmass crystal; and plus = corona around olivine crystals.

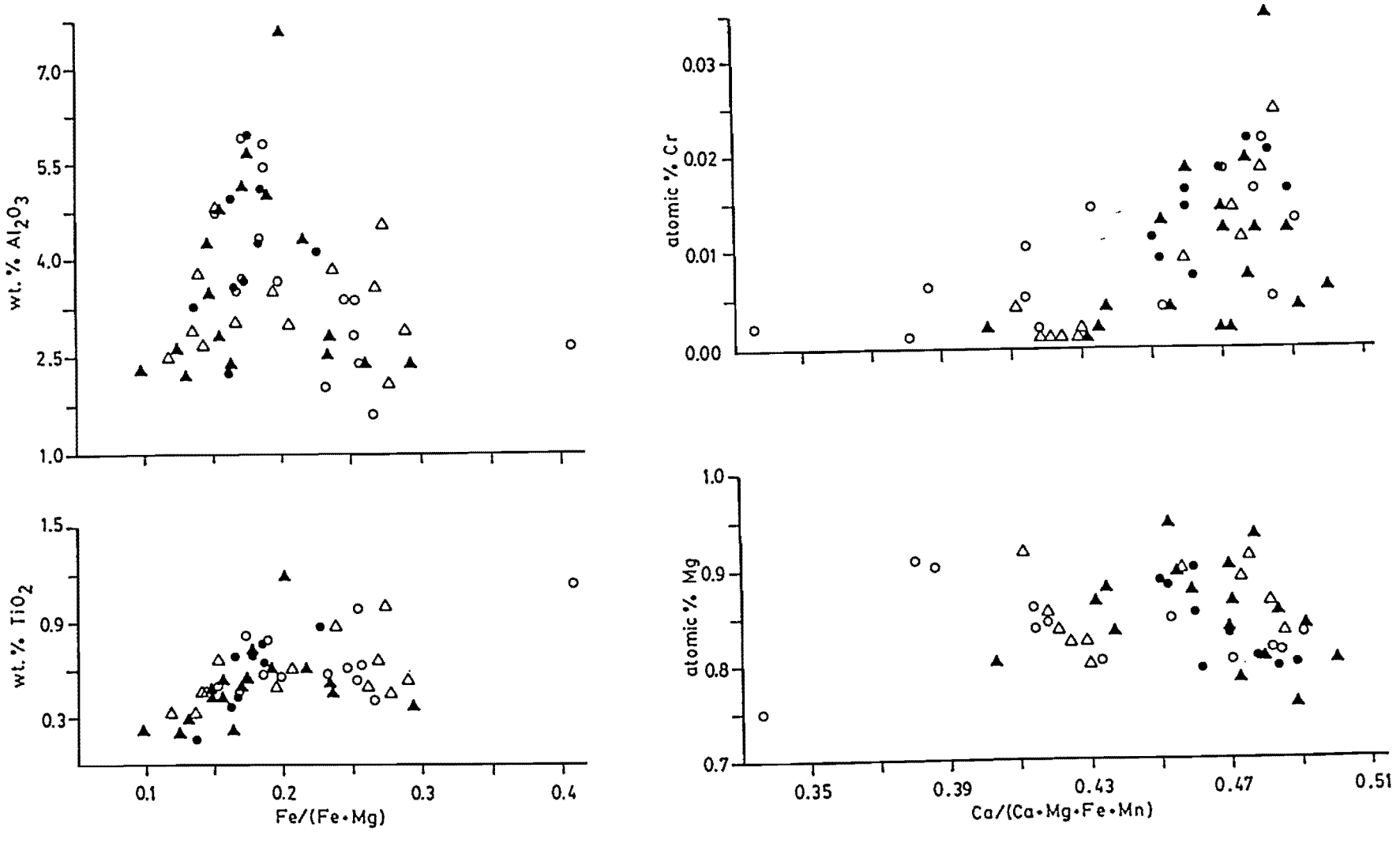

Figure V.15 Discrimination diagrams of clinopyroxenes in basaltic andesite erupted in April - May 1982 (triangle = phenocryst rim, corona and groundmass crystal; filled-triangle = phenocryst core), and in basalt erupted in September 1982 - January 1983 (circle = phenocryst rim and groundmass crystal; filled-circle = phenocryst core).

(Fig.V.10). This is due to crystallisation of high-Mg olivines which occur in rocks erupted in caldera formation and historic eruptions but are absent in the cryptodome. These clinopyroxenes, relatively high in Cr and low in Na and Ti contents, are similar to those in tholeiitic deep-sea basalts (Schweitzer et al., 1979). The presence of high-Cr calcic pyroxenes and high-Ni olivines in rocks of the 1982-83 eruption indicates a primitive magma (Kay & Kay, 1985a).

V.3.2 Orthopyroxene

V.3.2.1 Optical Mineralogy

Orthopyroxenes occur commonly in basaltic andesites particularly those having more than 55.5 % SiO_2 (Fig.V.16A) as both phenocrysts (0.5 - 2.0 mm) and in the groundmass. The minerals are weakly pleochroic from neutral to pale brown, have a parallel extinction and are commonly associated with magnetites. Glomeroporphyritic crystal clots (Coote, 1987) of orthopyroxene and clinopyroxenes are very common. In the more basic rocks, orthopyroxenes are rimmed by clinopyroxenes (Fig.V.16B) or in core of clinopyroxenes (Fig.V.16C). In the 1982-83 eruption sequence rocks, orthopyroxene phenocrysts are present in rocks of the initial stage (basaltic andesites), but abundance decreases from 1.4 % to 0.1 % (Table IV.3) as the SiO_2 content of the bulk rocks decreases. In rocks of the final eruption stage (basalts), orthopyroxenes are absent.

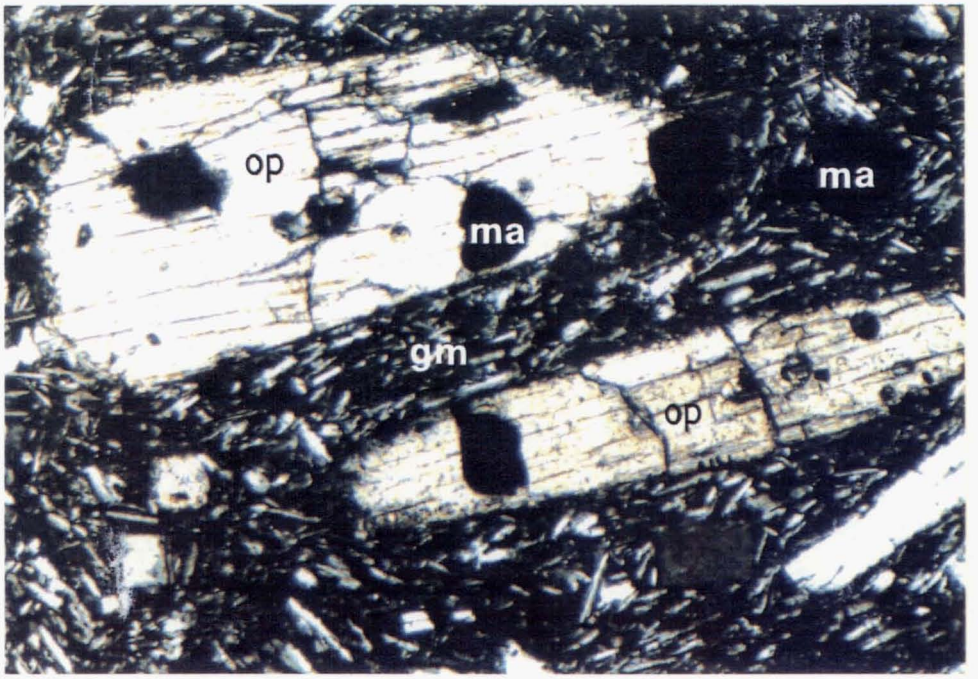

Figure V.16A Orthopyroxene phenocrysts (op) associated with magnetites (ma) in trachytoid groundmass texture (gm) in basaltic andesite of Old Galunggung lava (20347, 400 X, crossed polarized).

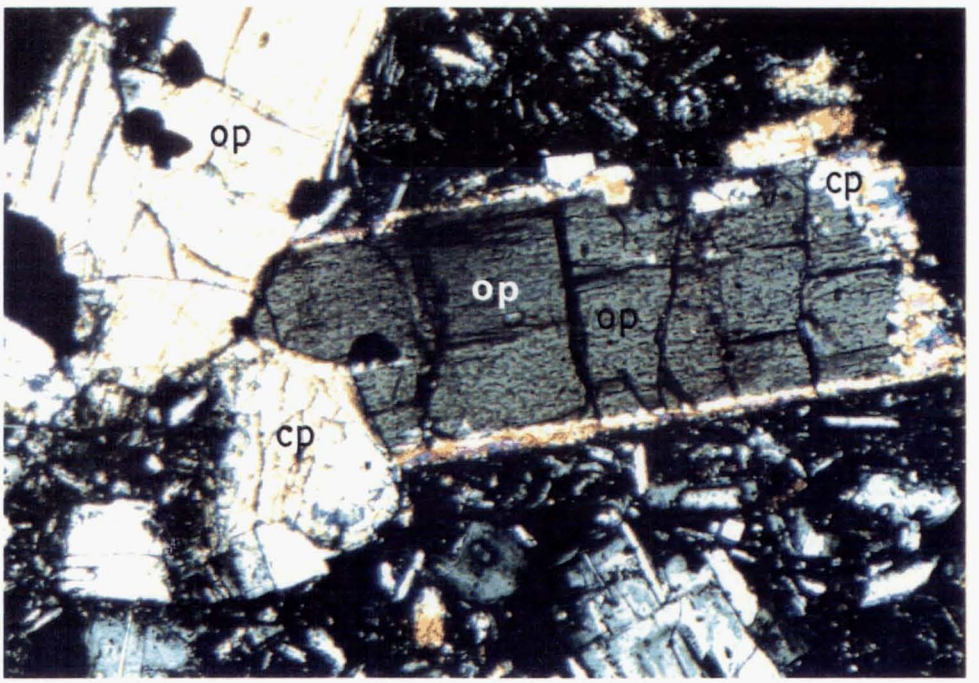

Figure V.16B Orthopyroxene (op) rimmed by clinopyroxene (cp) in basaltic andesite erupted in 1982 (20290, 400 X, crossed polarized).

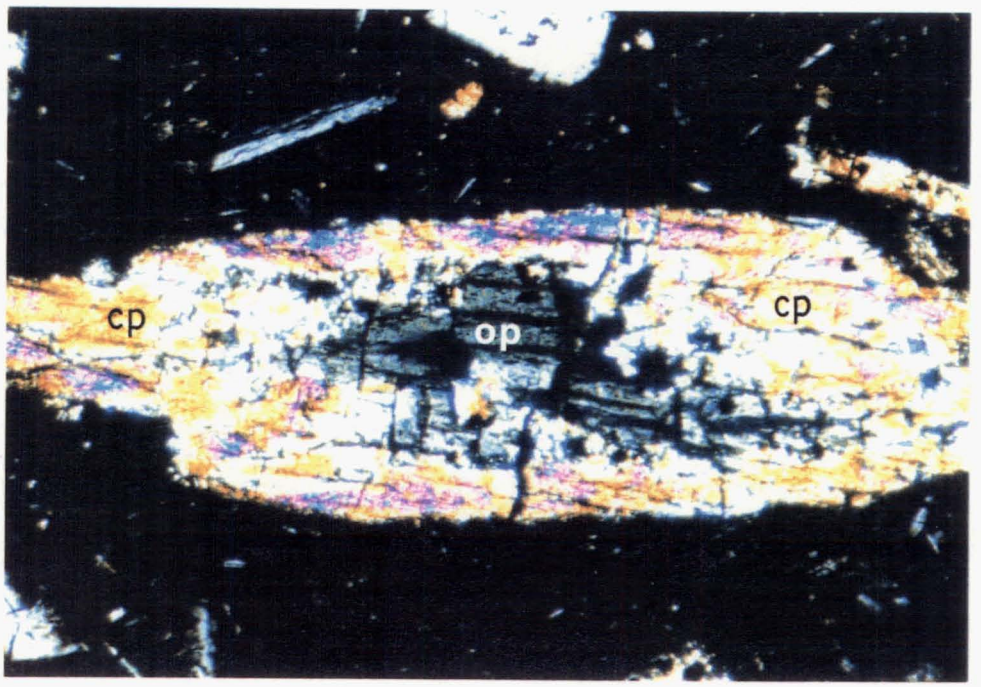

Figure V.16C Orthopyroxene (op) in core of clinopyroxene (cp) in basaltic andesite erupted in 1982 (20295, 400 X, crossed polarized).

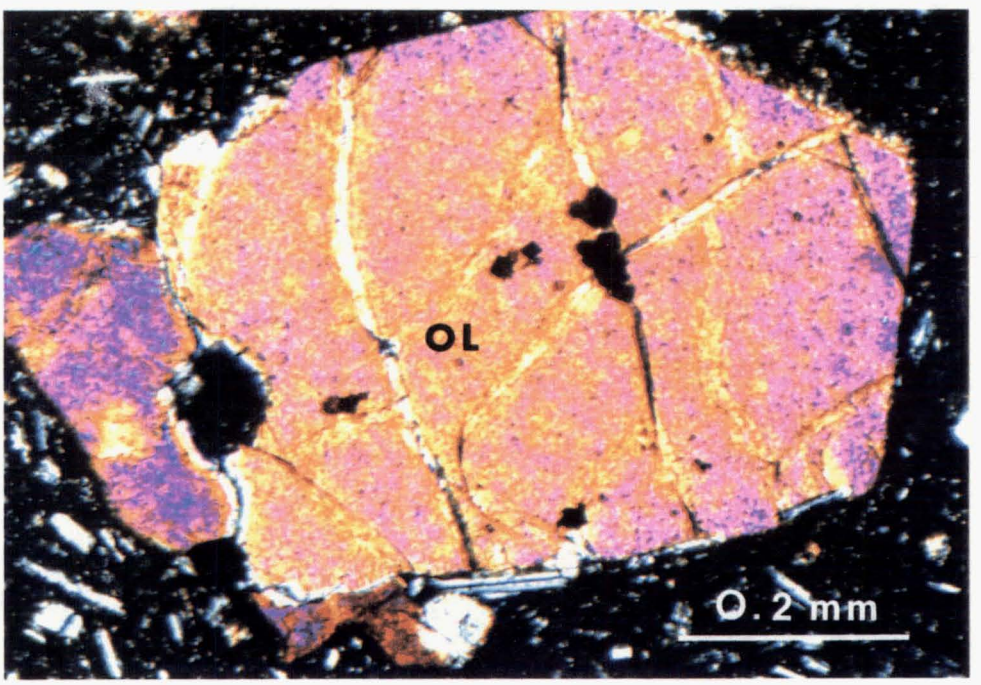

Figure V.17 Cr-spinel inclusions in olivine phenocryst (OL) in basalt erupted on 16 September 1982 (20335, 400 X, crossed polarized).

V.3.2.2 Mineral Chemistry

In Galunggung volcanic rocks orthopyroxenes are hypersthene ($Ca_{4-3}Mg_{70-61}Fe_{35-26}$; Fig.V.6-9, 11, 112 & 14), and there is no difference whether they occur as phenocrysts, in crystal clots, as core to clinopyroxene, in groundmasses or as coronas around olivines. However, in Old Galunggung basalts, orthopyroxenes have slightly lower Fe ratios (Fe/Fe+Mg= 0.27 - 0.31) than in the basaltic andesites (0.30 - 0.35). Ca concentration averages 1.75 % CaO and Al varies from 0.6 to 2.3 % Al_2O_3 with the highest concentration in basalt (20287).

More Mg-rich orthopyroxenes (Mg_{75-70}) are found as microphenocrysts and as cores to clinopyroxenes in basaltic andesite injecting gabbro clast (Fig. V.11B) erupted during caldera formation. They have lower Fe/Fe+Mg = 0.22 - 0.28 but relatively high Al (1.0 - 2.3 % Al_2O_3), whereas Ca concentrations remain constant. Orthopyroxenes in basaltic andesite bombs have Fe/Fe+Mg = 0.31 -0.34, 0.8 - 1.6 % Al_2O_3 and 1.4 - 1.9 % CaO (20289).

In the 1822 eruption rocks (basaltic andesite) orthopyroxenes (Fig.V.12A) have Mg contents ranging between Mg_{61} and Mg_{67}; and Fe ratios are 0.31 - 0.35. Al and Ca concentrations vary from 0.6 to 2.1 % Al_2O_3 and from 1.5 to 2.4 % CaO, respectively.

In the 1918 basaltic andesite lava dome, orthopyroxenes are reasonably constant in composition ($Ca_{4-3}Mg_{66-65}Fe_{31-30}$). Fe ratios are 0.3 with an average Ca content of 1.7 % CaO although Al varies from 0.8 - 2.4 % Al_2O_3.

Mg contents in orthopyroxenes become less variable converging from Mg_{68-62} to Mg_{65} from basaltic andesite to basalt erupted in 1982-83. However, Fe ratios are comparatively constant (0.3), whereas

Al (0.2 -1.77 % Al_2O_3) and Ca (1.3 - 1.7 % CaO) do not vary systematically through the 1982-83 rocks. These suggest that orthopyroxene does not have a particular compositional trend in the 1982-83 eruption rocks.

Overall, orthopyroxenes are common only in the most evolved rocks having 56 - 57 % SiO_2. The character of the mineral is similar to the orthopyroxenes in olivine andesites of the San Juan region, Colorado (Larsen et al., 1936). They reported that orthopyroxene is common in rocks with SiO_2 contents between 57 % and 59 %, but is uncommon in rocks in which the SiO_2 contents are < 54 %. Ca concentrations (> 1.5 % CaO) are relatively constant and high. This suggests that orthopyroxenes crystallised at high temperatures (1000 - 1100°C; Atlas, 1952; Deer et al., 1978a,b; Kuno, 1954), and interpretation is confirmed by crystallisation temperatures calculated using the methods of Kretz (1982) and Lindsley (1983). In addition, orthopyroxenes jacketed by or in cores of clinopyroxenes, occurring with olivine and clinopyroxene phenocrysts, and having low Al contents (<2.5% Al_2O_3) are suggestive that the mineral crystallised at low pressure shortly before solidification of the rocks (Cox & Jamieson, 1974; Deer et al., 1978b).

V.3.3 Pigeonite

Pigeonite ($Ca_{15-7}Mg_{57-49}Fe_{43-32}$) frequently occurs in the groundmasses of Old Galunggung lavas, particularly the basalts. Compositional variations of the mineral are given in Figure V.9-12. Their Fe ratios are 0.4 - 0.5; Ca contents are 3.5 - 4.5 wt.% CaO and Al_2O_3

: 0.5 -1.0 wt.%. Pigeonites also occur as coronas around olivines ($Ca_{15-9}Mg_{58-50}Fe_{40-33}$, 20285 and 20286) where they are richer in Ca content (4.2 -7.1 wt.% CaO).

In the caldera formation rocks, pigeonites are found as inclusions in plagioclase phenocrysts (e.g. sample number 20257; $Ca_{7-5}Mg_{66-63}Fe_{29-28}$) where they have a high Al (0.7 - 1.2 wt.% Al_2O_3) but low Fe/Fe+Mg = 0.3.

Pigeonitic coronas around olivine are also observed in the initial stage of the 1982-83 eruption ($Ca_{6-5}Mg_{64-63}Fe_{31}$, 20290, 20291 and VB 16). They have also Fe/Fe+Mg = 0.3 and compared with earlier pigeonites they have relatively high Al (0.9 - 1.7 wt.% Al_2O_3) but low Ca (2.6 - 3.0 wt.% CaO).

The presence of pigeonites as fine grain groundmass crystals and often as coronas around olivine is a typical feature of the volcanic phase of the tholeiitic rock series (Deer, et al., 1978a,b). The crystals probably represent rapid metastable crystallisation during quenching. Experimentally determined pyroxene relations (Kay & Kay, 1985a; Lindsley, 1983) suggest that the pigeonite in Galunggung rocks is not in equilibrium with the phenocryst pyroxenes. However, the presence of those pigeonite groundmass crystals is consistent with high crystallisation temperature.

Pyroxene crystallisation temperatures have been calculated following the methods of Kretz (1982) and Lindsley (1983). The temperatures range from 943^{o}C to 1153^{o}C; and the differences between the two methods are less than 80^{o}C. The temperatures are discussed further in Chapter VII.

V.4 Spinel

V.4.1 Optical Mineralogy

Two kinds of spinel, namely Cr-spinel and magnetite can be distinguished in Galunggung rocks. Cr-spinel is found particularly in the 1982-83 rocks, as inclusion in olivine phenocrysts, and infrequently in groundmass of the 1983 lava flow. The crystals are euhedral, very fine (< 0.01 mm), dark to brown in colour (Fig. V.17).

Magnetite is ubiquitous in nearly all Galunggung rocks where it usually occurs in the groundmass, or as inclusions in other mineral phenocrysts (< 0.1 mm). It also occurs rarely as microphenocrysts (0.2 - 0.3 mm) in basaltic andesite. The crystals are black, euhedral to anhedral, distributed either individually or in aggregates mainly with orthopyroxene. The abundance of magnetite as inclusions decreases from basaltic andesite to basalt as the percentage of orthopyroxene decreases.

V.4.2 Mineral Chemistry

Cr-spinels have < 1 % TiO_2, 12 - 20 % Al_2O_3, Fe^{3+}/Fe^{2+} ratios < 0.3, < 0.2 % MnO, 40 - 48 % Cr_2O_3, $Mg/Mg+Fe^{2+}$ ratios = 0.4 - 0.6, and ulvospinel < 3 mol.%. In groundmass, the mineral has higher MnO (0.3 %) and ulvospinel (40 %) but lower $Mg/Mg+Fe^{2+}$ ratio (0.3) than those of Cr-spinel inclusions. There is no systematic trend in Cr-spinel compositions from basaltic andesite to basalt. However, compositional changes occur probably before magnetite crystallises, in particular

decreases of Al_2O_3 (down to 3 %), MgO (3 %), Cr_2O_3 (4 %) and $Mg/Mg+Fe^{2+}$ ratios (0.1) but increases in TiO_2 (up to 12 %), Fe^{3+}/Fe^{2+} (0.4), MnO (0.4 %) and ulvospinel (36 %). The replacement of Cr-spinel by magnetite is illustrated by decreasing Cr/Cr+Al but increasing $Fe^{3+}/Cr+Al+Fe^{3+}$ ratios (Fig. V.18). These data suggest (Prevot & Mergoil, 1973) that magnetite crystals have replaced pre-existing Cr-spinel phases.

The Galunggung Cr-spinels (Fig. V.18) are typical of spinels from layered intrusions (Irvine, 1967) and are similar to spinels of Rinjani volcano (Foden, 1983). They are also similar to the Cr-spinels in Mid-Atlantic ridge basalts (Fisk & Bence, 1979; Sigurdsson & Schilling, 1976), and the associated minerals - magnesian olivine (Fo_{90}), diopsidic clinopyroxene and Cr-spinel - suggest they are peridotite derived. The low Al contents (< 40 % Al_2O_3) in Galunggung Cr-spinel indicate low pressure Cr-spinel crystallisation (Sigurdsson & Schilling, 1976; Fisk & Bence, 1980; Nye & Reid, 1986). Low Fe^{3+} contents in the mineral suggest low fO_2 in the original magma which crystallised the magnesian olivines, while high Cr/Cr+Al ratios (0.5 - 0.7) may indicate that the Cr-spinels were derived from depleted mantle sources (Bonatti & Michael, 1989; Falloon & Green, 1987).

Compositional variation of Galunggung magnetite is given in Figure V.19. Ti contents in the mineral vary from 9 to 19 % TiO_2, and the mineral can be termed titaniferous magnetite (Ti-magnetite; Deer et al., 1978a). There is no systematic compositional change with time or from basaltic andesite to basalt. However, the range of Ti contents in microphenocryst and groundmass phases of Old Galunggung rocks is wider (12 - 19 % TiO_2) than that of inclusions and the younger rocks (9 - 13 % TiO_2). This causes a wider ulvospinel mole per cent in the

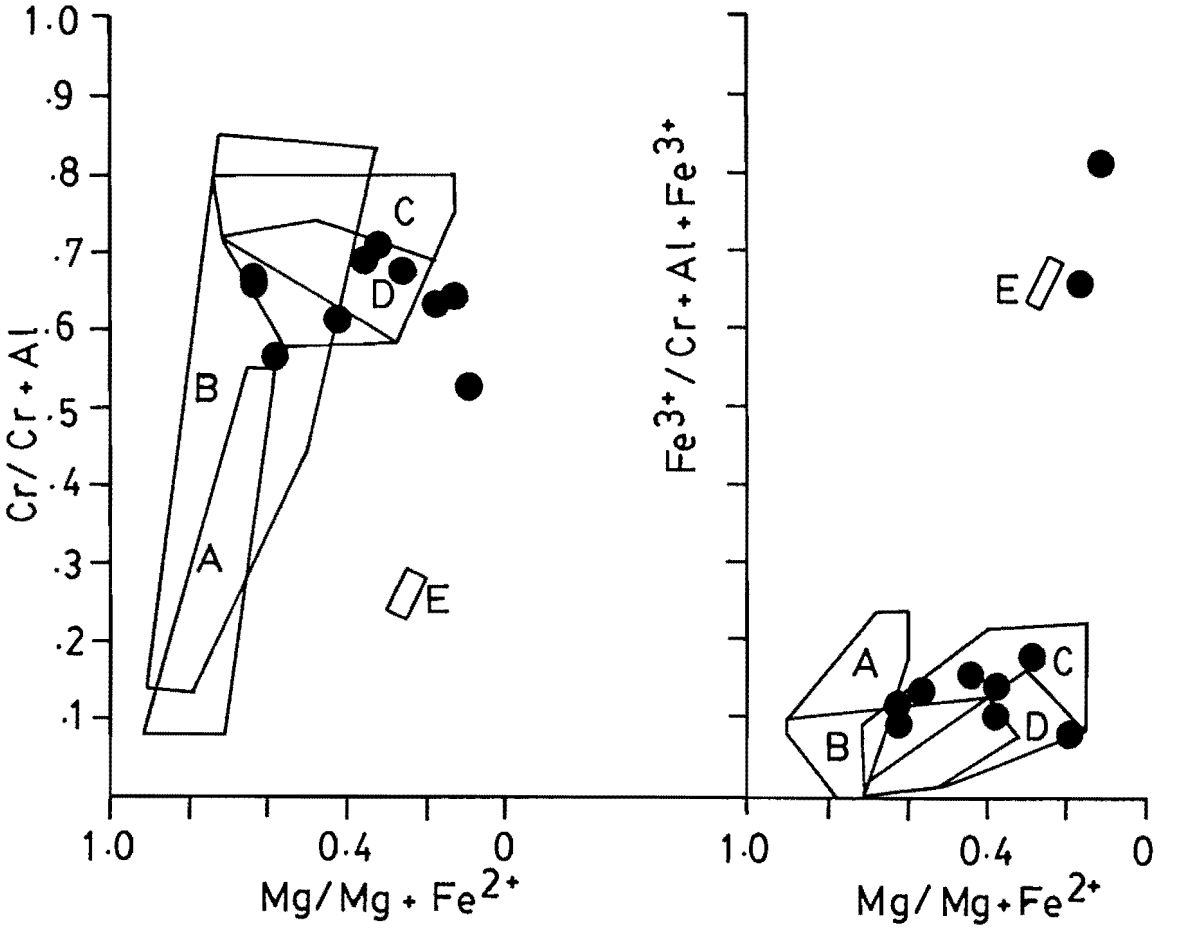

Figure V.18 Composition of Cr-spinels in the 1982-83 basalt - basaltic andesite. Fe^{3+} values are recalculated using the method of Carmichael (1967). Field indicated are those of A-spinels from ultra-mafic nodules, B- spinels from alpine peridotite, C- spinels from layered intrusions (Irvine, 1967), D- spinels from Rinjani volcano (Foden, 1983), and E-spinels from Batur volcano (Wheller, 1986).

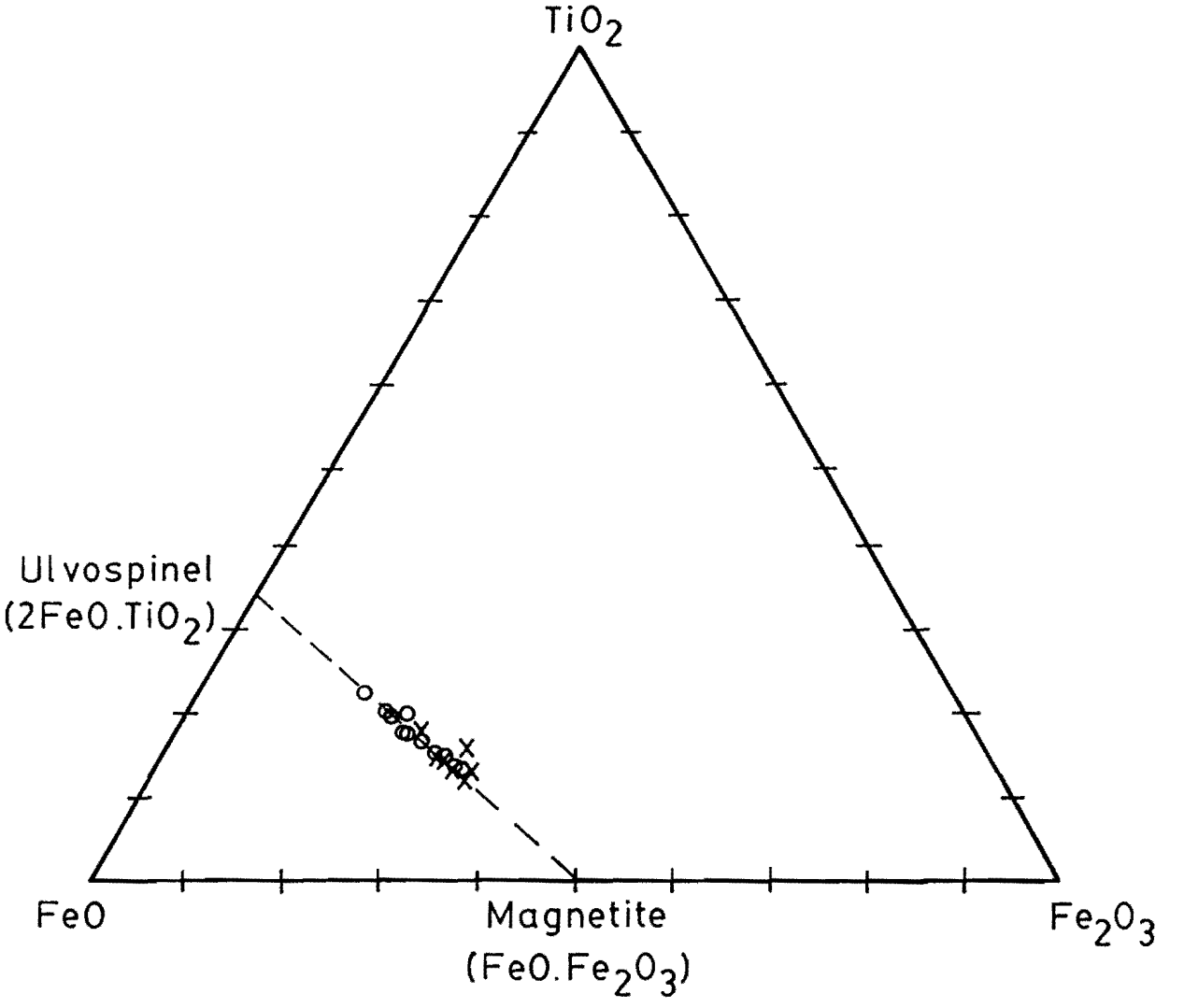

Figure V.19 Compositions of Ti-magnetite in basalt - basaltic andesite from Galunggung volcano. Phases are plotted on mol. per cent bases. Circle = microphenocryst and groundmass crystal; cross = inclusion.

first group (33 - 56 %) than in the second group (20 - 38 %). Al concentrations mostly range from 2.5 to 4.5 % Al_2O_3. They decrease down to 0.9 % in the Ti-magnetites having highest Ti (19 % TiO_2) and Fe^{2+} (47 % FeO) contents. These low Al values may be the result of low (< 10 kb) pressure crystallisation (Osborn & Watson, 1977). Deer et al. (1978a) suggested that coexisting Cr-spinel and magnetite - ulvospinel series are products at high temperature crystallisation. The absence of ilmenite in Galunggung rocks evidently reflects in part the low TiO_2 content of the magma (Ewart, 1976), or low fO_2.

V.5 Amphibole

V.5.1 Optical Mineralogy

Amphibole is common in gabbro clasts and volcanic bombs found in pyroclastic rocks erupted during caldera formation and historic eruptions in 1822, 1894 and 1982-83. The crystals vary from fine to coarse grains up to 14 mm length, and are long to short prismatic euhedral to anhedral crystals. They are strongly pleochroic from green to brown. Figure V.20 illustrates the variation of amphiboles in Galunggung rocks. Electron microprobe data show that amphibole also occurs as inclusion in plagioclase phenocrysts of the 1983 lava (20300) together with olivine and clinopyroxene (Fig. V.21).

Based on textural character and order of crystallisation (Giret et al., 1980), three types of amphibole can be distinguished in Galunggung rocks. First, euhedral-subhedral amphibole crystals, mostly green in colour (Fig. V.20A), which do not have opaque rim and are

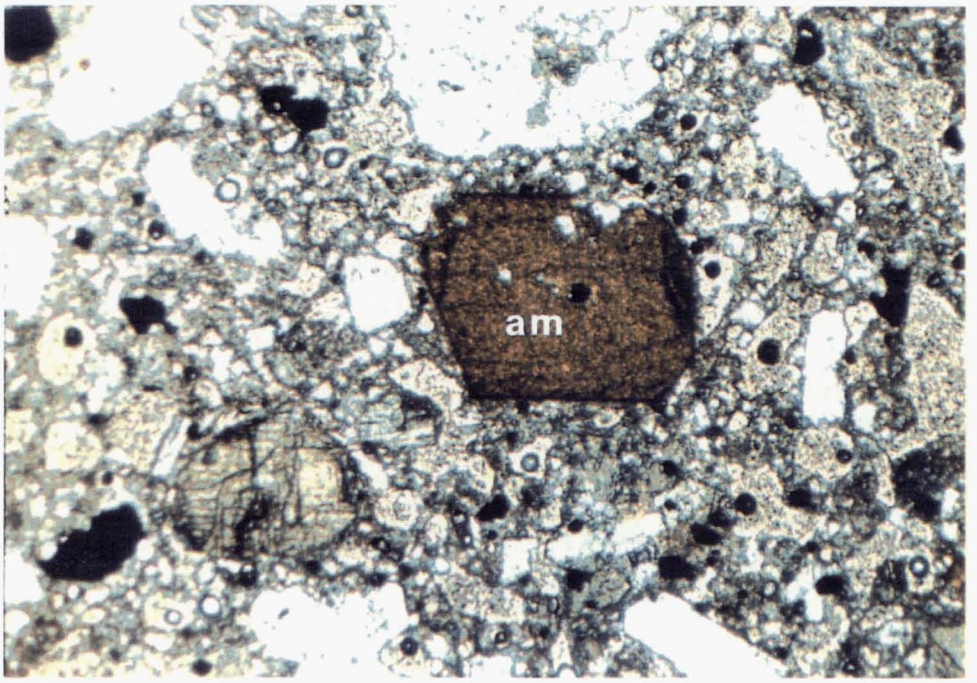

Figure V.20A Euhedral green amphibole (am) in basalt injecting gabbro clast erupted during caldera collapse (20252, 25 X, plane polarized).

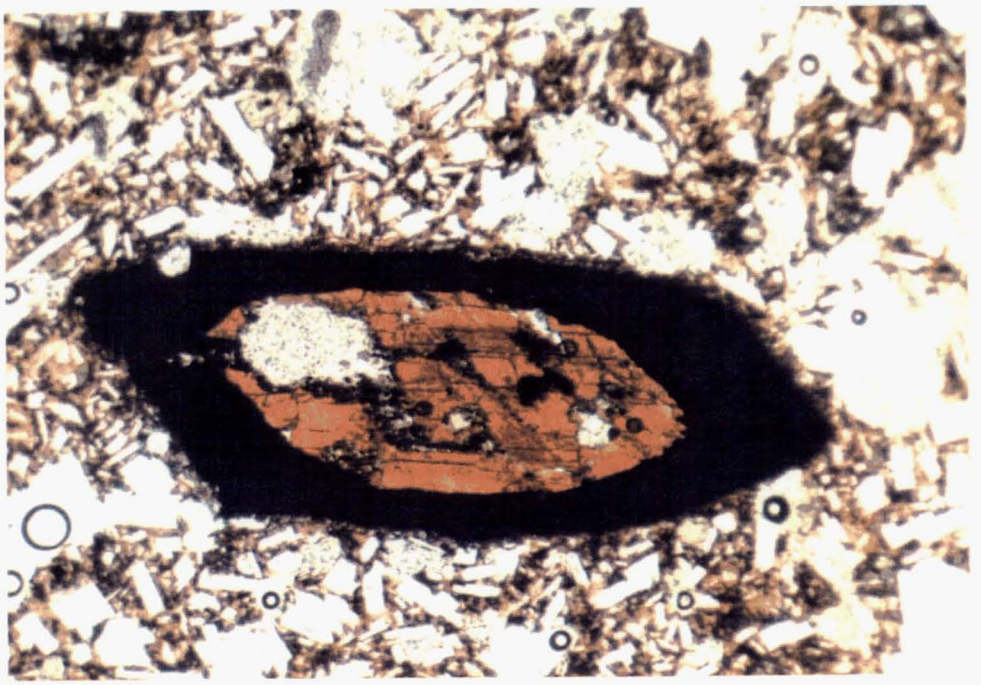

Figure V.20B Anhedral brown amphibole rimmed by opaques in basaltic andesite erupted in 1822 (VB30A, 25 X, plane polarized).

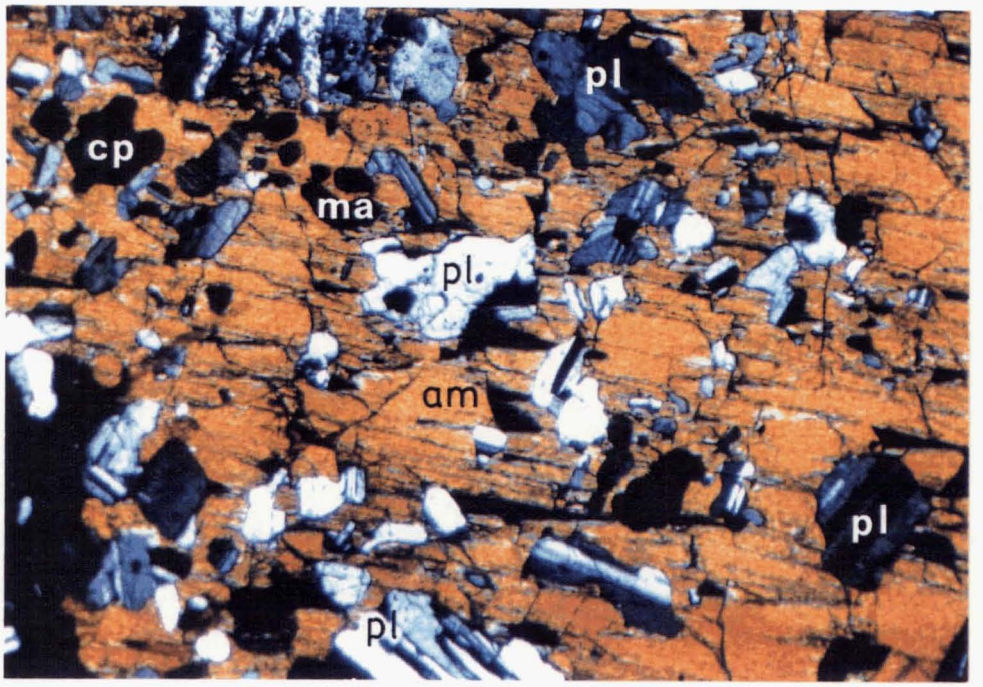

Figure V.20C Amphibole (am) encloses clinopyroxene (cp), plagioclase (pl) and magnetite (ma) to form poikilitic texture in basaltic andesite erupted during caldera collapse (20289, 25 X, crossed polarized).

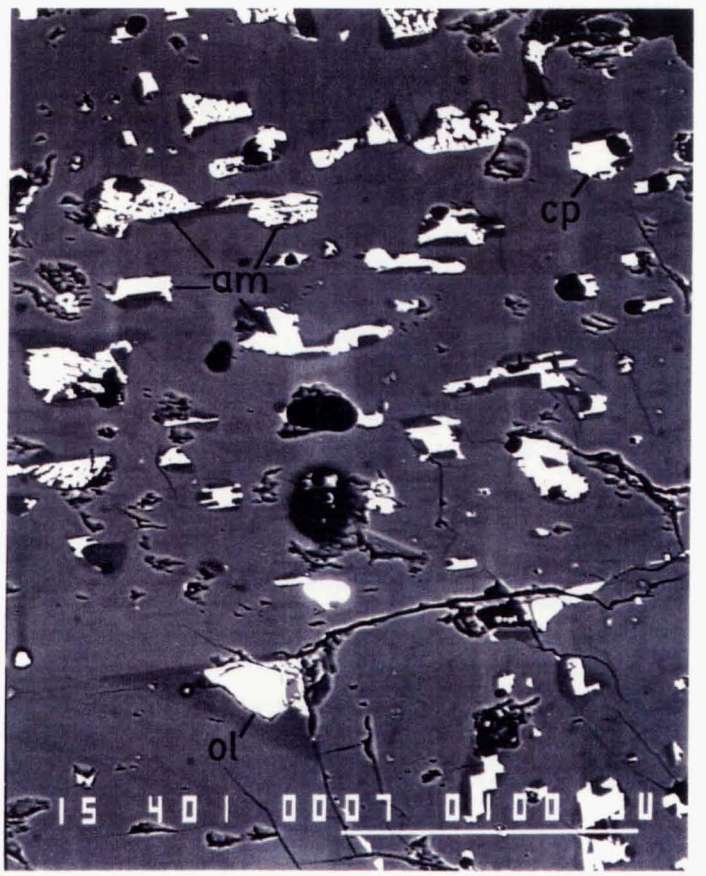

Figure V.21 Coexisting olivine (ol), clinopyroxene (cp) and amphibole (am) inclusions in plagioclase phenocryst in the 1983 basalt lava flow.

only present in rocks (20289, 20252) erupted during caldera formation. This type is considered as an early crystallisation stage of amphibole.

The second type of amphibole is mostly brown in color, rimmed by opaque materials showing relict texture (Fig. V.20B). These amphiboles, ejected in historic eruptions, usually have thicker opaque rim than in bombs and gabbro clasts erupted during caldera formation. Several are completely replaced by opaque material, which probe data indicates is Fe-rich amphibole. These oxidised amphiboles may reflect a higher temperature origin and consequently greater opportunity to react with the emplacement environment on cooling (Wones and Gilbert, 1982). Some authors (e.g. Johnson, 1977; Lambert & Wyllie, 1970; Stewart, 1975) stated that these oxidised amphiboles are the usual breakdown products of amphibole in a low-pressure volcanic environment.

The third type of amphibole has a poikilitic texture with orthopyroxenes, clinopyroxenes, magnetites and plagioclases enclosed in the amphibole crystals (Fig. V.20C). The poikilitic texture reflects a final stage of amphibole crystallisation during cooling process. This type of amphibole probably resulted from reaction between liquid and early formed pyroxene or olivine (Gill, 1981).

V.5.2 Mineral Chemistry

Amphiboles in Galunggung volcanic rocks have $(Ca + Na)_B > 1.34$ and $Na_B < 0.67$, and can be classified as calcic amphiboles (Leake, 1978). The calcic amphiboles found in bombs have a similar composition

to those in gabbro clasts. Most of them have $(Na + K)_A > 0.5$, Ti < 0.5, $Fe^{3+} < Al^{VI}$, Si = 6.0 - 6.2, and $Mg/Mg+Fe^{2+}$ = 0.7 - 0.8 (per 23 O) . These are pargasites according to the nomenclature of Leake (1978). Two analyses from the crystal rims have lower $(Na + K)_A$ (0.4), but higher Fe^{3+} (0.8 - 0.9) than the others and can be termed tschermakite (Leake, 1978). A different composition occurs in amphibole inclusions in plagioclase phenocryst of the 1983 lava flow. These amphiboles have higher SiO_2, TiO_2, FeO*, MnO and K_2O but lower Al_2O_3, MgO, CaO and Na_2O contents (Table V.4) than the earlier ones. The amphibole inclusions also have $(Na + K)_A < 0.5$, Ti < 0.5, Si = 6.8 - 7.8, but low $Mg/Mg+Fe^{2+}$ (< 0.5) and Ca (< 1.5) and can be grouped as subcalcic ferro-hornblende (Leake, 1978).

Average chemical compositions of Galunggung amphiboles compared with those from other areas are given in Table V.4. On the basis of total Al content, they can be divided into 3 groups : high (Al > 2.0), medium (2 < Al > 1.5) and low (Al < 1.5).

Galunggung amphiboles in volcanic bombs and gabbro clasts enter into high Al group that systematically decreases from 2.72 (gabbro clasts from Central Japan, Yamazaki et al., 1965) to 2.11 in medium K calc-alkaline andesites (Gill, 1981). In the latter rocks, amphiboles are comparable with those in El Chichon volcanic rocks erupted in 1982 (Luhr et al., 1984). Pargasitic amphiboles from Mt. Pelée occur in intrusive (gabbro) clasts and as xenocrysts in basaltic andesites (Bourdier et al., 1985; Dupuy et al., 1985). Their composition is close to amphibole reacted megacrysts in Rinjani andesites (Foden, 1983).

Amphiboles having medium Al content are reported in Rinjani dacites (Foden, 1983) and are comparable with those in dacite pumice

Table V.4 Chemical compositions of amphibole from Galunggung and other areas

	M-1	M-2	M-3	M-4	M-5	M-6	M-7	M-8	M-9	M-10	M-11
	(22)	(6)	(6)	(10)	(4)	(2)	(4)	(1)	(3)	(2)	(3)
SiO_2	41.51	50.94	40.56	38.92	40.47	39.85	41.02	42.40	42.34	45.39	48.01
TiO_2	2.14	2.82	2.12	3.86	2.01	2.22	2.21	2.50	3.44	1.78	.87
Al_2O_3	13.36	6.00	15.84	14.87	15.25	14.20	14.00	12.10	10.39	9.96	5.95
FeO	11.20	19.37	11.13	10.57	9.65	13.34	11.24	12.80	12.98	14.19	12.81
MnO	.18	.44	.19	.15	.12	.13	.11	.20	.26	.28	.47
MgO	14.37	7.45	13.04	13.25	15.15	13.44	14.72	13.80	13.18	13.92	14.87
CaO	11.79	8.56	12.00	12.33	12.41	12.57	11.59	11.10	10.85	10.58	10.71
Na_2O	2.52	.67	1.71	2.23	2.42	2.54	2.43	2.70	2.65	1.92	2.23
K_2O	.23	.89	.69	2.36	.47	.68	.28	.04	.91	.24	1.12
NiO	.05	.05	-	-	-	-	-	-	-	-	-
Cr_2O_3	.07	.12	-	.08	-	-	-	-	-	-	-
Cl	.02	.03	2.06	-	-	-	-	-	-	-	1.68
Total	97.37	97.34	99.33	98.55	97.94	98.87	99.45	97.64	96.99	98.26	101.13
Si	6.39	7.56	5.92	5.75	5.90	5.88	5.74	6.24	6.30	6.64	6.90
Al	2.42	1.05	2.72	2.59	2.62	2.48	2.31	2.11	1.84	1.72	1.00
Ti	.25	.31	.23	.43	.22	.25	.25	.28	.38	.20	.10
Fe	1.44	2.41	1.35	1.31	1.18	1.65	1.31	1.58	1.62	1.74	1.54
Mn	.04	.05	.02	.02	.02	.02	.01	-	.04	.04	.06
Mg	3.30	1.65	2.85	2.93	3.29	2.96	3.07	3.03	2.96	3.04	3.19
Ca	1.90	1.36	1.88	1.95	1.94	1.99	1.73	1.75	1.73	1.66	1.65
Na	.74	.19	.48	.64	.68	.44	.66	.77	.76	.54	.31
K	.04	.17	.13	.45	.08	.09	.05	.08	.14	.05	.10
Ni	.01	.01	-	-	-	-	-	-	-	-	-
Cr	.01	.03	-	-	-	-	-	-	-	-	-
Cl	.00	.01	-	-	-	-	-	-	-	-	-
Total	16.53	14.84	15.58	16.11	15.93	15.73	15.14	15.84	15.77	15.63	16.54
Fe/Fe+Mg	.30	.60	.32	.31	.26	.36	.30	.34	.35	.36	.33
Al^{IV}	1.61	.44	2.08	2.25	2.10	2.12	2.26	1.76	1.70	1.36	1.00
Al^{VI}	.80	.61	.64	.35	.52	.36	.05	.35	.14	.36	-
P Kb	8.24	1.35	9.75	9.12	9.26	8.53	7.69	6.69	5.32	4.73	1.13

M-1 : Galunggung volcanic bombs & gabbro clasts
M-2 : Inclusions in plagioclase phenocrysts of the 1983 lava
M-3 : Gabbro clasts from Central Japan (Yamazaki et al., 1965)
M-4 : Hornblendites from Westeifel FRG (Becker, 1977)
M-5 : Intrusive clasts from Mt. Pelée (Bourdier et al, 1985; Dupuy et al.,1985)
M-6 : Rinjani andesites (Foden, 1983)
M-7 : Intrusive clasts from Mt. Soufriere (Lewis, 1973)
M-8 : Medium-K calc-alkaline andesites (Gill, 1981)
M-9 : Rinjani dacites (Foden, 1983)
M-10 : Dacite pumice from Mt. Pelée (Bourdier et al, 1985)
M-11 : Rabaul pumice (andesite to rhyolite) (Heming & Charmichael, 1973)
P Kb : Pressure of crystallisation calculated following the method of Hammarstrom & Zen (1986)
Number of analyses are in bracket

clasts of St. Helens erupted in 1980 (Scarfe & Fujii, 1987) and edenitic amphiboles from Mt. Pelée (Bourdier et al., 1985).

Low Al amphiboles occur in Rabaul andesite - rhyolite pumice clasts (Heming & Carmichael, 1973) and as inclusions in plagioclase phenocrysts of the 1983 Galunggung lava flow. These amphibole inclusions are, however, considered as late stage liquid crystallisation products that are not in equilibrium with the host rock.

The Al content in amphiboles may relate to the pressure of crystallisation (Hammarstrom & Zen, 1986). This is discussed in Chapter VII.

V.6 Plagioclase

V.6.1 Optical Mineralogy

Plagioclase is the most abundant mineral (average mode 18 %) both as phenocrysts and in the groundmass of Galunggung volcanic rocks. It is typical of island arc volcanic rocks (Ewart, 1976). Phenocrysts are euhedral-subhedral crystals, generally ranging from 0.2 - 2.0 mm but may be up to 5.5 mm in size. Coarser crystals (10 mm length) are only found in bombs within pyroclastic flows produced during caldera formation and in gabbro clasts.

In some Galunggung rocks plagioclase phenocrysts may be aligned to give a trachytic texture or in glomeroporphyritic aggregates. Occasionally, hollow plagioclase-rich crystal aggregates are also found. Plagioclase phenocrysts are typically normal-oscillatory zoned, twinned (Carlsbad-Albite and Albite) and have glass inclusions. Pyrox-

ene and magnetite inclusions are fairly common whereas olivine inclusions are rare. Figure V.22A shows olivine inclusions in plagioclase megacryst in an orthopyroxene-rich basaltic andesite. The proportion of glass inclusion varies between rocks, the more glass inclusions possibly reflecting more rapid plagioclase crystallisation.

Some plagioclase phenocrysts have a wide unzoned core but no glass inclusion (Fig. V.22B). The crystals are usually euhedral-subhedral, 0.5 - 1.5 mm in length and similar to those in gabbro clasts.

Plagioclases in the groundmass are usually acicular and lath-like, form a pilotaxitic texture and have Carlsbad twinning. The acicular plagioclases, together with corroded ones, suggests rapid crystallisation. Trachytic texture apparently occurs in high silica basaltic andesite (see Fig. V.16A).

Hydrothermal alteration around the crater produces secondary minerals, i.e. chlorite, carbonate and oxide (pyrite ?). However, plagioclase is generally more resistant than mafic minerals.

V.6.2 Mineral Chemistry

Representative analyses of plagioclase phenocryst cores are shown in Table V.1, and An-Ab-Or concentration are presented in Fig. V.23-25. There is no significant difference in plagioclase compositions from Old Galunggung to the 1982-1983 eruption deposits. Plagioclase phenocryst cores have a compositional range between An_{80} and An_{95}; while their rims and groundmasses vary from An_{45} to An_{79}; most are labradorite. Plagioclase analyses are more calcic than the corre-

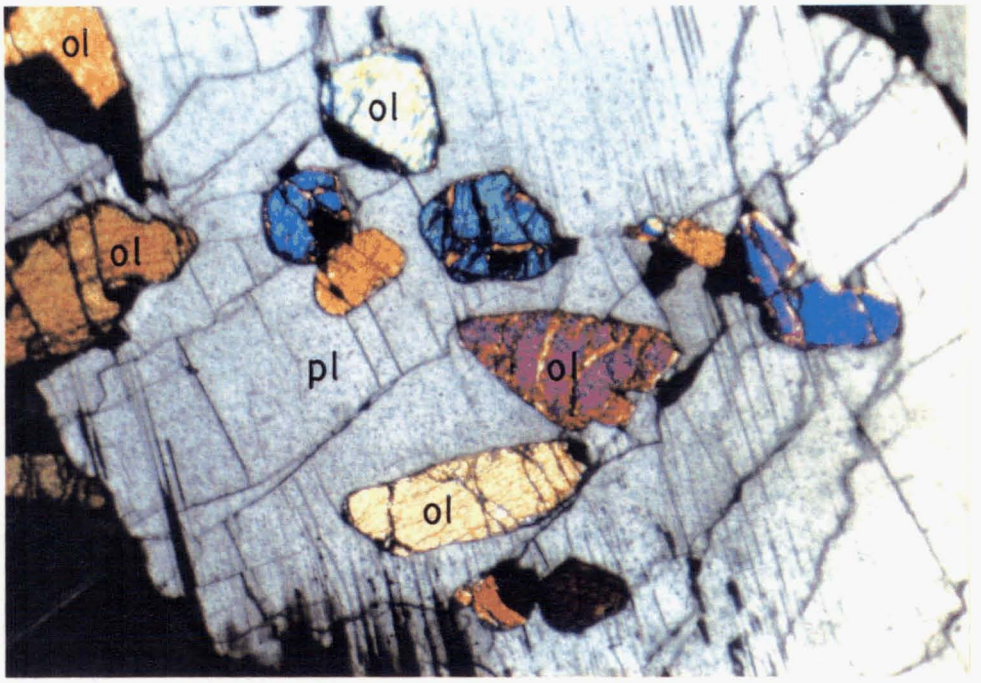

Figure V.22A Plagioclase megacryst (pl) containing olivine inclusions (ol) in orthopyroxene-rich basaltic andesite (FCB, 25 X, crossed polarized).

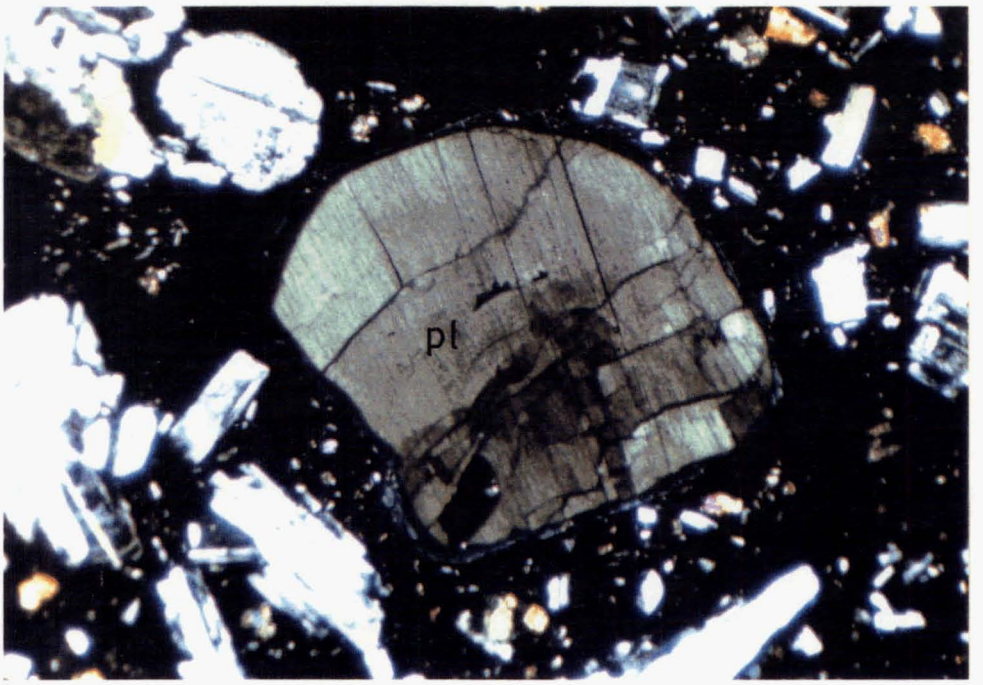

Figure V.22B Plagioclase phenocryst showing a wide unzoned core (pl) in basaltic andesite erupted in 1982 (20295, 25 X, crossed polarized).

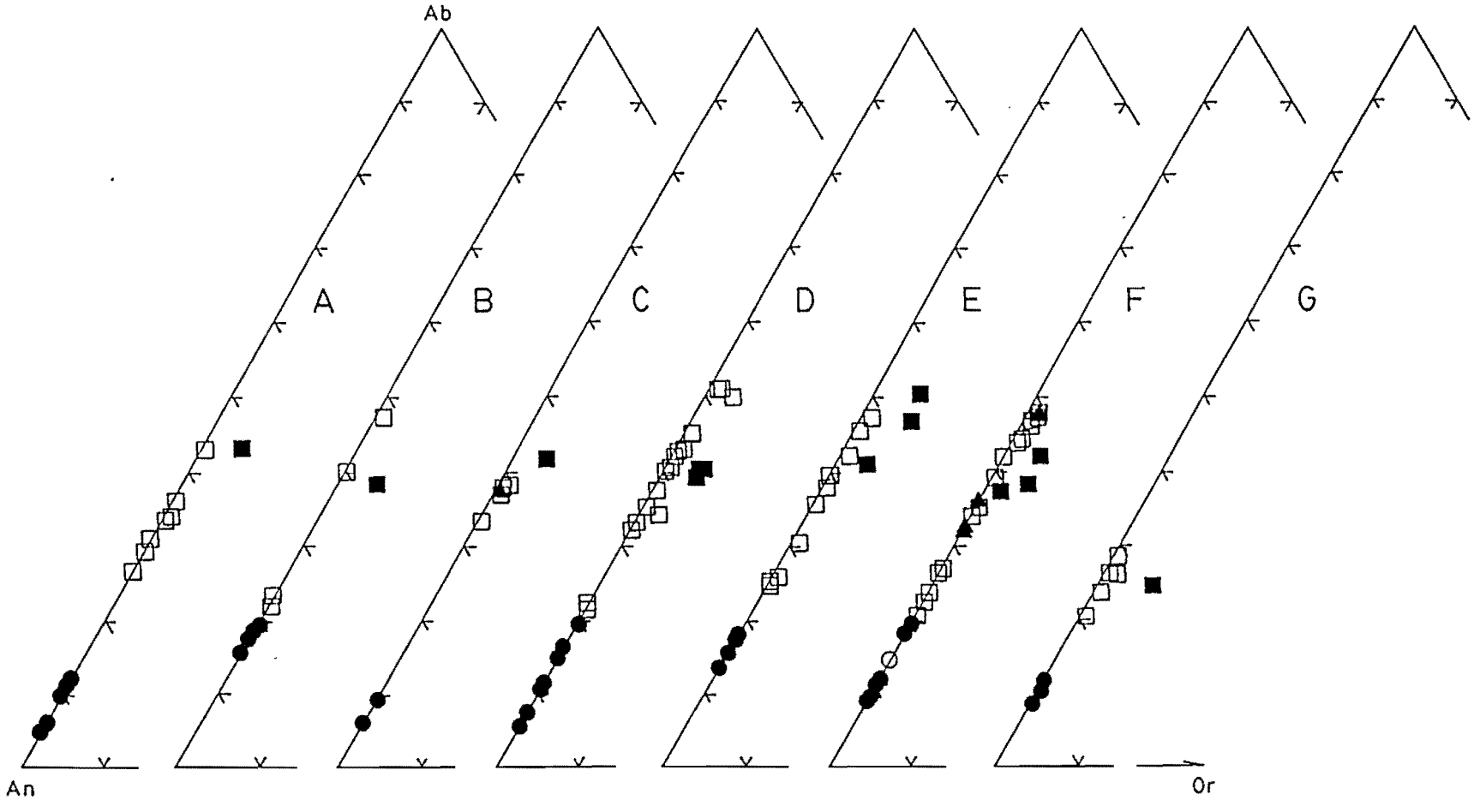

Figure V.23 Plagioclase compositional variation in Old Galunggung volcanic rocks. A, B and C are basalt lava flows in lower, middle and upper layers of a sequence of lava flows in SW wall of Galunggung caldera (see Fig. III.2A). D = basalts, E = basaltic andesite, F = basalt dikes, and G = basalt cryptodome. Filled-circle = phenocryst core; square = phenocryst rim and groundmass; filled-triangle = inclusion and filled-square = normative plagioclase.

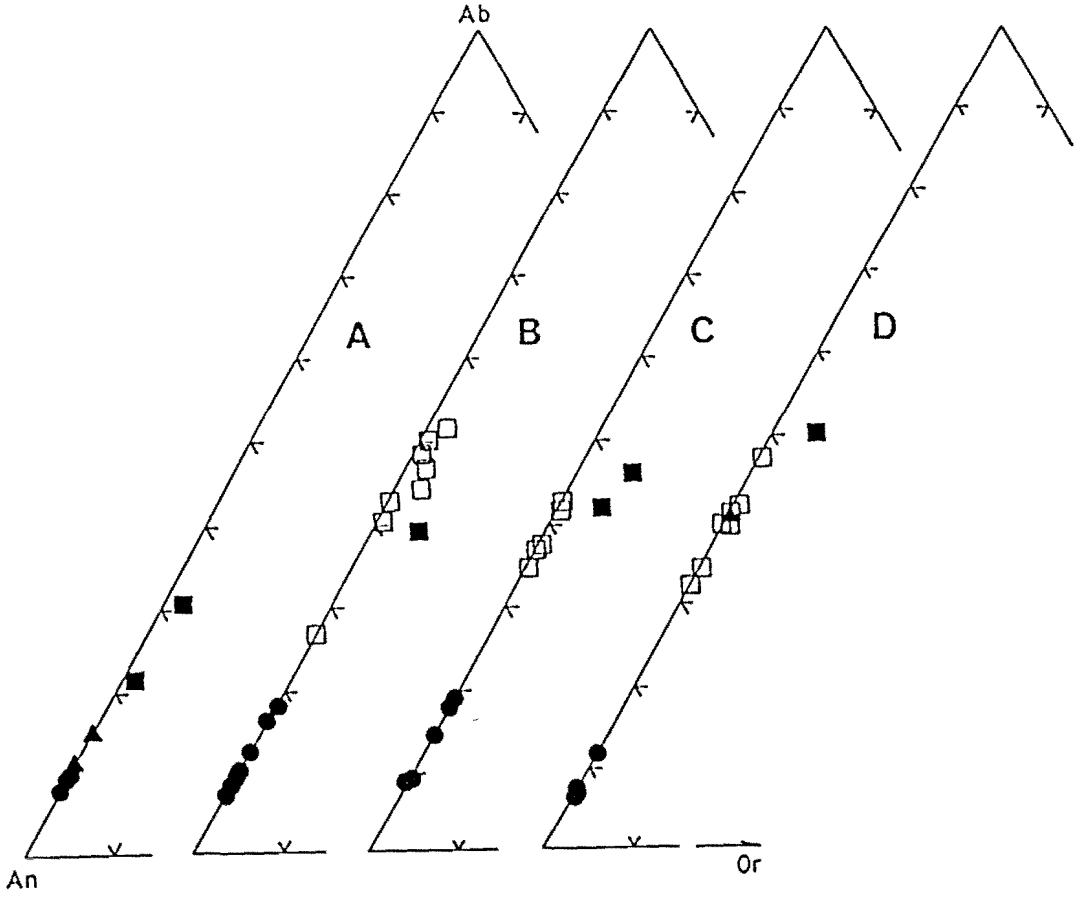

Figure V.24 Plagioclase compositional variation in rocks erupted during caldera formation (A = gabbro clasts; B = basaltic andesite bomb), in 1822 (C, basaltic andesite), and in 1918 (D, basaltic andesite). Symbols as for Fig. V.23.

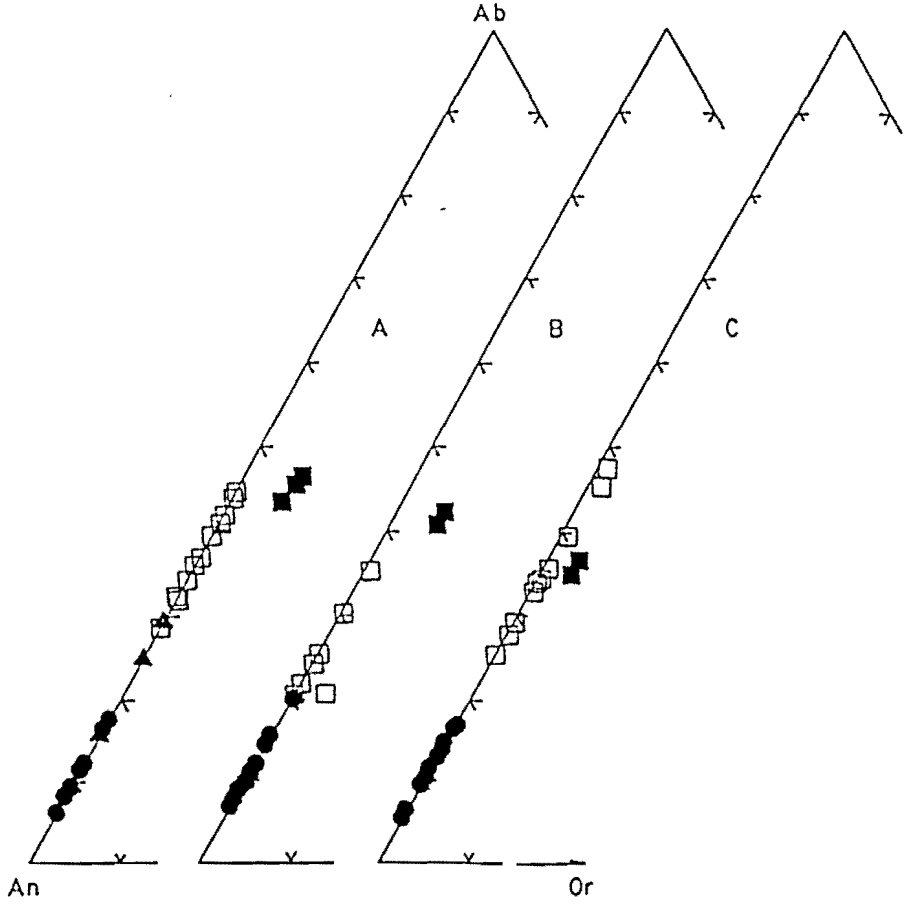

Figure V.25 Plagioclase compositional variation in basaltic andesites erupted on 8 and 25 April 1982 (A) and on 6 and 18 May 1982 (B) and in basalts erupted in September 1982 - january 1983. Symbols as for Fig. V.23.

sponding norms of bulk rocks, suggesting that potassium and to a lesser extent sodium are concentrated in the finely crystalline to glassy matrices (Hackett, 1985).

Euhedral plagioclase phenocrysts having a wide-unzoned core and no glass inclusion are optically and compositionally similar to plagioclase in the gabbro clasts. It is suggested the plagioclase originated from an intrusive gabbro. Their rims are compositionally similar to the other plagioclase phenocryst rims and groundmass crystals. Plagioclase inclusions found in clinopyroxene and amphibole crystals have a similar composition to plagioclase phenocryst cores and few of them fall into the rim-groundmass field.

VI GEOCHEMISTRY

VI.1 Introduction

Geochemistry is an important part of volcanological study in Indonesia. It is required not only to determine the origin of the volcanic rocks but also to assist in volcanic hazard assessment. In this chapter, 109 new major and trace element analyses of Galunggung volcanic rocks are related to stratigraphic position and time.

Major element data on pre-1982 volcanic rocks have been published by Neumann van Padang (1951), and Nicholls and Whitford (1976). Syarifuddin et al. (1983) reported major element analyses of the 1918 lava dome and the 1982-83 eruption volcanic rocks, and Oba et al. (1983) published analyses of volcanic bombs erupted from April to August 1982.

Most Galunggung volcanic rocks are basalt to basaltic andesite and have similar characteristics to those of other arc volcanoes (e.g. Jakes & White, 1971 & 1972). However, at the end of the Old Galunggung volcanic activity and in the 1982-83 eruption, rocks have primitive basaltic compositions which are presently uncommon in convergent plate settings (Nye & Reid, 1986). The Galunggung primitive basaltic rocks are then compared with those from other convergent plate volcanoes and mid-oceanic ridge basalts. In addition, clasts of gabbro and pumice rhyolite ejected together with Galunggung volcanic rocks are described and are compared with those from other areas.

Although the primitive basalt, gabbro and rhyolite volumetrically represent a small proportion of Galunggung, they are considered

to be important in the history and development of the volcano.

VI.2 Sample Collection and Analysis

Most samples collected were of fresh lavas and volcanic bombs. Slightly altered lavas from Old Galunggung were also analysed because of their possible significance in the stratigraphic record. The alteration, caused by hydrothermal activity, is relatively low (loss on ignition < 1.5 %) and these samples can usefully be included in any discussion (Sabine et al., 1985). Three ash samples (sand to silt size) from the 1982-83 Vulcanian eruption deposits were included because of the lack of volcanic bombs during that eruptive period.

All XRF results, together with the analytical methods are given in Appendix 4. Most XRF analyses were done in the Analytical Laboratories at University of Canterbury and Victoria University of Wellington. Three analyses were performed at the USGS XRF Laboratory at Denver (Tilling , 1987, pers. comm.) and one in the Geochemistry Laboratory, University of California, Santa Cruz (Gill, 1987, pers. comm.). There is no apparent interlaboratory variation in these XRF results.

On the basis of stratigraphic position and historic activity, analysed samples have been divided into : Old Galunggung Formation, Tasikmalaya Formation (caldera-forming event) and Cibanjaran Formation. Representative Galunggung volcanic rocks are given in Table VI.1. Although stratigraphically lavas and bombs in "megablocks" of the debris avalanche deposits belong to the Tasikmalaya Formation the rocks were erupted during Old Galunggung activities. Thus petrologically the samples are included in the Old Galunggung Formation. Rock

Table VI.1 Compositions of representative Galunggung volcanic rocks.

	Old Galunggung				Caldera formation		1822		1894	1918
	20258	20270	L27-2	20288	20344	20353	20342	VB30A	20246	4-AK
Major elements (wt %)										
SiO_2	47.06	49.67	52.33	56.88	51.25	55.02	51.08	55.50	52.61	55.11
TiO_2	.87	1.03	.94	.84	.96	.71	.90	.72	.81	.83
Al_2O_3	15.67	20.74	19.51	18.96	18.75	18.75	18.66	18.07	19.41	19.15
Fe_2O_3*	9.45	9.62	8.79	7.66	9.58	7.58	9.38	8.19	8.84	7.97
MnO	.26	.19	.17	.12	.16	.17	.19	.16	.17	.14
MgO	10.32	4.38	4.82	3.21	5.80	4.37	5.00	4.56	4.01	3.47
CaO	11.26	10.85	9.59	7.66	10.21	8.45	10.15	8.47	9.98	8.17
Na_2O	1.46	2.99	3.29	4.29	3.18	3.18	2.66	3.54	3.31	3.95
K_2O	.56	.37	.56	.71	.52	.68	.38	.70	.37	.59
P_2O_5	.11	.13	.18	.19	.14	.18	.16	.16	.15	.17
LOI	1.54	.52	-.25	-.44	-.20	.56	.74	-.10	.54	-.04
Total	98.56	100.49	99.93	100.08	100.35	99.65	99.30	99.97	100.20	99.51
Trace elements (ppm)										
Ba	44	92	121	149	70	129	77	157	148	292
Rb	18	12	13	16	10	16	7	19	16	12
Sr	188	268	310	311	283	329	293	261	282	285
Pb	8	4	4	7	6	8	6	7	6	5
Zr	43	75	76	111	65	86	69	82	69	97
Y	17	27	22	23	20	20	20	20	20	22
Sc	n.a.	n.a.	30	19	n.a.	n.a.	n.a.	20	n.a.	22
V	289	227	255	133	261	149	235	164	174	174
Cr	395	8	26	16	82	83	90	91	13	22
Ni	94	13	13	10	29	37	33	28	10	12
Ga	15	19	22	22	18	20	18	19	19	20
Mg#	71.05	50.60	55.22	48.51	55.75	56.45	54.41	55.57	50.48	49.46

Table VI.1 (Continued)

	1982-83 Eruption						
	20334	1983L	20324	VB13D	20336	WL	20294
Major elements (wt %)							
SiO_2	49.01	49.33	50.75	52.73	53.88	55.59	56.82
TiO_2	.70	.81	.80	.78	.76	.71	.70
Al_2O_3	15.09	16.29	16.21	17.64	17.97	18.08	18.34
Fe_2O_3*	9.53	9.85	9.39	8.77	8.47	7.97	7.75
MnO	.16	.17	.15	.16	.15	.16	.15
MgO	12.52	10.02	9.20	6.72	5.73	4.49	3.90
CaO	11.59	11.13	10.79	9.81	9.33	8.39	8.13
Na_2O	1.94	2.24	2.63	2.97	3.26	3.53	3.67
K_2O	.29	.35	.46	.55	.63	.71	.76
P_2O_5	.07	.10	.11	.12	.14	.15	.16
LOI	-.77	-.37	-.38	-.22	-.60	.15	-
Total	100.13	99.92	100.11	100.03	99.72	99.67	100.38
Trace elements (ppm)							
Ba	40	49	82	115	132	154	176
Rb	6	7	9	12	15	17	18
Sr	197	213	227	245	263	261	273
Pb	5	4	5	4	9	6	9
Zr	39	49	46	68	78	83	86
Y	14	18	16	20	17	20	18
Sc	n.a.	38	n.a.	29	n.a.	20	17
V	264	272	251	215	189	165	152
Cr	711	505	384	215	146	94	38
Ni	193	139	110	61	44	26	20
Ga	14	14	16	18	17	18	19
Mg#	74.70	69.57	68.77	63.25	60.32	55.66	53.09

Mg# = Molecular per cent $100Mg/Mg+Fe_{2+}$; $Fe_2O_3/FeO = 0.15$ (Brooks, 1976)
n.a.= not analysed

samples of the caldera formation are therefore volcanic bombs collected from pyroclastic flow deposits. Geochemistry of the Cibanjaran Formation is represented by volcanic bombs and lavas erupted in historic time, i.e. 1822, 1894, 1918 and 1982-83.

VI.3 Classification

There are various systems used for the classification of volcanic rocks involving modal classification (Streickeisen, 1978 & 1980), oxide weight per cent (e.g. Le Bas et al., 1986) and normative mineralogy criteria (e.g. Irvine & Baragar, 1971; Wilkinson, 1986).

In convergent plate suites a classification based on the K_2O v SiO_2 is commonly used (e.g. Peccerillo & Taylor, 1976; Ewart, 1982). Similar classifications are proposed by Johnson (1977) and the Basaltic Volcanism Study Project (BVSP, 1981), which only differ in that the boundary between basalt and basaltic andesite (= low-silica andesite of Johnson, 1977), is at 53 % SiO_2 in the Johnson and BVSP classification rather than 52 %, and that between basaltic andesite and andesite is 57 % rather than 56 %. For convenience the scheme proposed by Johnson (1977) and BVSP (1981) is used in this thesis.

Furthermore, intrusive clasts consisting dominantly of amphibole and labradorite, and having less than 53 % SiO_2 content are termed gabbro, whereas, pumice clasts having more than 68 % SiO_2 are rhyolite.

Figure VI.1 shows that Galunggung volcanic rocks are basalt and basaltic andesite. On the basis of MgO contents basalts are divided into (1) high-Mg basalt (10 - 12.5 % MgO), (2) "transitional" high-Mg

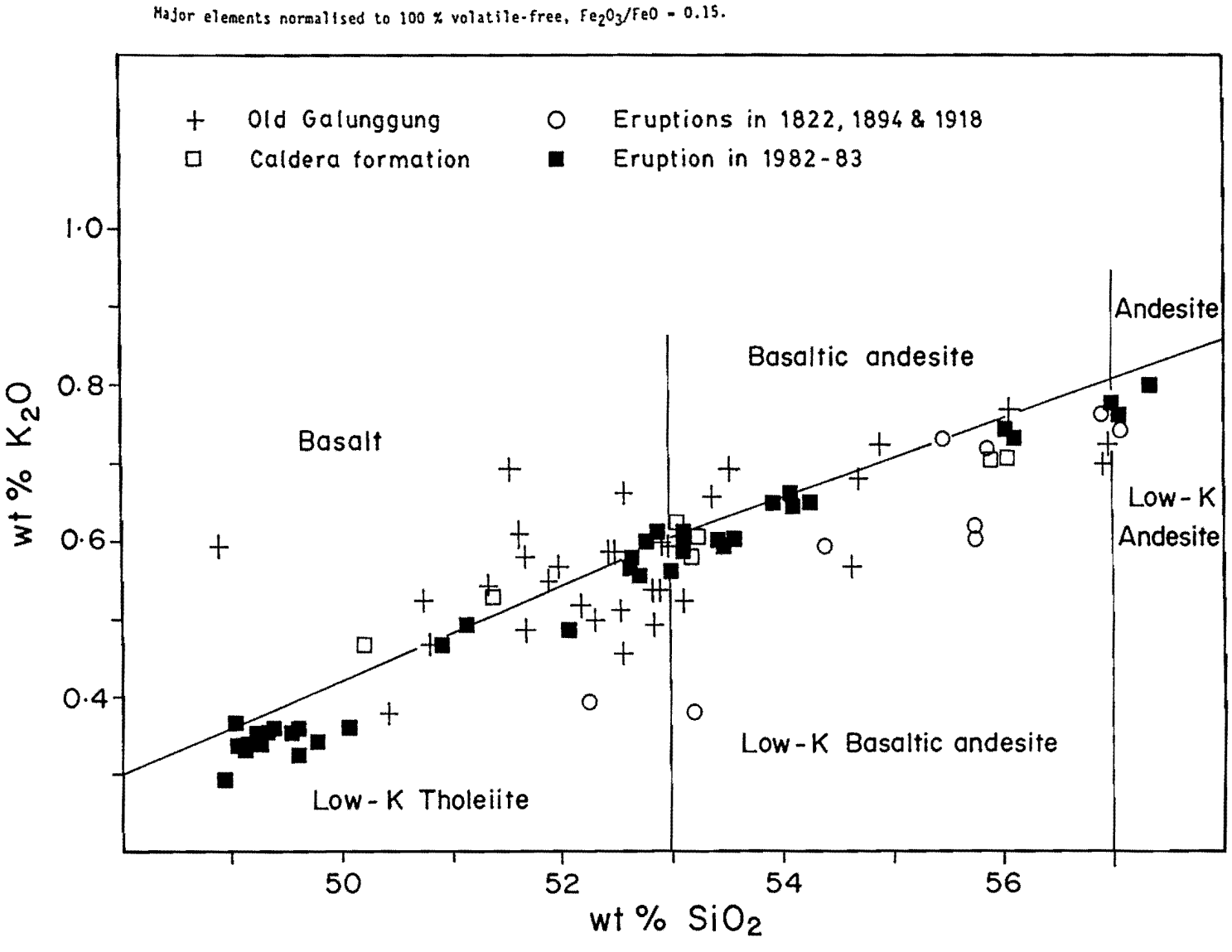

Figure VI.1 Galunggung volcanic rocks on a plot K_2O against SiO_2 diagram (BVSP, 1981).

basalt (6.5 - 9 % MgO), and (3) low-Mg basalt (< 6 % MgO). The basaltic andesite is divided into high-Mg basaltic andesite (6 - 7 % MgO) and low-Mg basaltic andesite (< 5 % MgO). The high-Mg basalt is subdivided into low-K high-Mg basalt (< 0.4 % K_2O) and medium-K high-Mg basalt (0.6 % K_2O). Table VI.2 gives the chemical characteristics of each group. The term "transitional" high-Mg basalt is used because this group (51 - 53 % SiO_2) is considered as a product of crystal fractionation from the (low-K) high-Mg basalt. In the following chapter (Chapter VII) the high-Mg basalt is considered to be a primary magma.

The sequence from low-K high-Mg basalt through "transitional" high-Mg basalt and high-Mg basaltic andesite to low-Mg basaltic andesite represents volcanic rocks erupted during 1982-83. Whereas another sequence, from low-Mg basalt to low-Mg basaltic andesite, is the product of older volcanic activity. A single medium-K high-Mg basalt forms a cryptodome of Old Galunggung.

VI.4 Galunggung Volcanic Rocks, Tholeiitic or Calc-alkaline Series ?

Many authors (e.g. Jakes & Gill, 1970 ; Miyashiro, 1974) have distinguished between tholeiitic and calc-alkaline volcanic rock series in volcanic arcs. Although some people stated that tholeiitic and calc-alkaline rocks differ in their genesis (e.g. Green & Ringwood, 1968), others (e.g. Miyashiro & Shido, 1975) believe that the two volcanic rock series came from a similar source.

Tectonically, Galunggung volcano is closer to the trench and

Table VI.2 Chemical characteristics of Galunggung volcanic rocks. Major elements are normalised to 100 % anhydrous; $Fe_2O_3/FeO = 0.15$; $Mg\# = 100\ Mg/Mg + Fe^{2+}$; $Ca^{1)} = CaO/Al_2O_3$; $Ca^{2)} = CaO/CaO + Na_2O$; na = not analysed.

	High-Mg basalt		"Transitional" high-Mg basalt	Low-Mg basalt	Basaltic andesite	
	Low-K (<0.4 % K_2O)	Medium-K (0.6 % K_2O)			High-Mg	Low-Mg
SiO_2	49 - 50	49	51 - 53	50 - 53	53 - 54	53 - 57
MgO	12.5 - 10	10.7	9 - 6.5	< 6	6 - 7	< 5
Al_2O_3	15 - 16	16	16 - 18	19 - 22	18	18 - 22
Mg#	75 - 69	71	69 - 62	58 - 43	63 - 60	57 - 41
$Ca^{1)}$	0.77 - 0.67	0.72	0.67 - 0.55	0.54 - 0.46	0.56 - 0.52	0.51 - 0.39
$Ca^{2)}$	0.86 - 0.82	0.89	0.80 - 0.75	0.79 - 0.73	0.77 - 0.73	0.76 - 0.66
Ni	193 - 119	94	110 - 55	50 - 7	61 - 44	37 - 5
Cr	711 - 418	395	384 - 177	196 - 5	198 - 148	94 - 7
Ba	37 - 63	44	82 - 116	64 - 130	77 - 134	72 - 168
Rb	6 - 8	18	9 - 14	4 - 17	12 - 16	9 - 19
Sr	197 - 222	188	227 - 256	264 - 362	245 - 263	248 - 329

has shallower earthquake foci (d = 270 km; h = 130 km; Hatherton & Dickinson, 1969) than other Java volcanoes, suggesting that it should be tholeiitic (Jakes & Gill, 1970; Morrice & Gill, 1986). Nicholls et al. (1980) reported that Galunggung is one of four tholeiitic volcanoes among dominantly CA Quaternary volcanoes on Java.

Petrographically, most Galunggung volcanic rocks do appear tholeiitic rather than calc-alkaline, as pigeonite occurs in the groundmass (Kuno, 1966; Aramaki & Ui, 1982; Kay & Kay, 1985a) and orthopyroxene occurs both as phenocrysts and groundmass (Best, 1975; Wheller, 1986). An absence of modal hornblende and low abundances of magnetite (<5.5 % volume per cent) support this observation (Morrice & Gill, 1986). Some chemical features, i.e. relatively low contents of K_2O (Fig. VI.1), Ba, Rb and Sr (Table VI.1), are also consistent (Jakes & Gill, 1970).

Miyashiro (1975) emphasised that tholeiitic rock series are characterised by a low rate of SiO_2 increase but a high rate of FeO decrease during fractional crystallisation. The Galunggung volcanic rocks cannot however be classified as tholeiitic on iron enrichment which is relatively low (7-9 % FeO*). On a plot of FeO*/MgO against SiO_2, the rocks erupted in 1982-83 (Fig. VI.2) fall within the CA series. Only the pre 1982-83 rocks appear to be part of the tholeiitic series. Nevertheless, the medium-K high-Mg basalt also falls in the CA series. This is due to higher Mg than lower Fe contents.

Detail studies on other arc volcanoes (e.g. Rabaul volcano, Heming, 1974; New Britain, Johnson, 1977; Lesser Antilles, Brown et al., 1977) also show no obvious relationship between SiO_2, FeO*, K_2O and tectonic setting. In order to follow the TH-CA classification, Kay & Kay (1985a) divided Aleutian volcanic rocks into tholeiitic, transi-

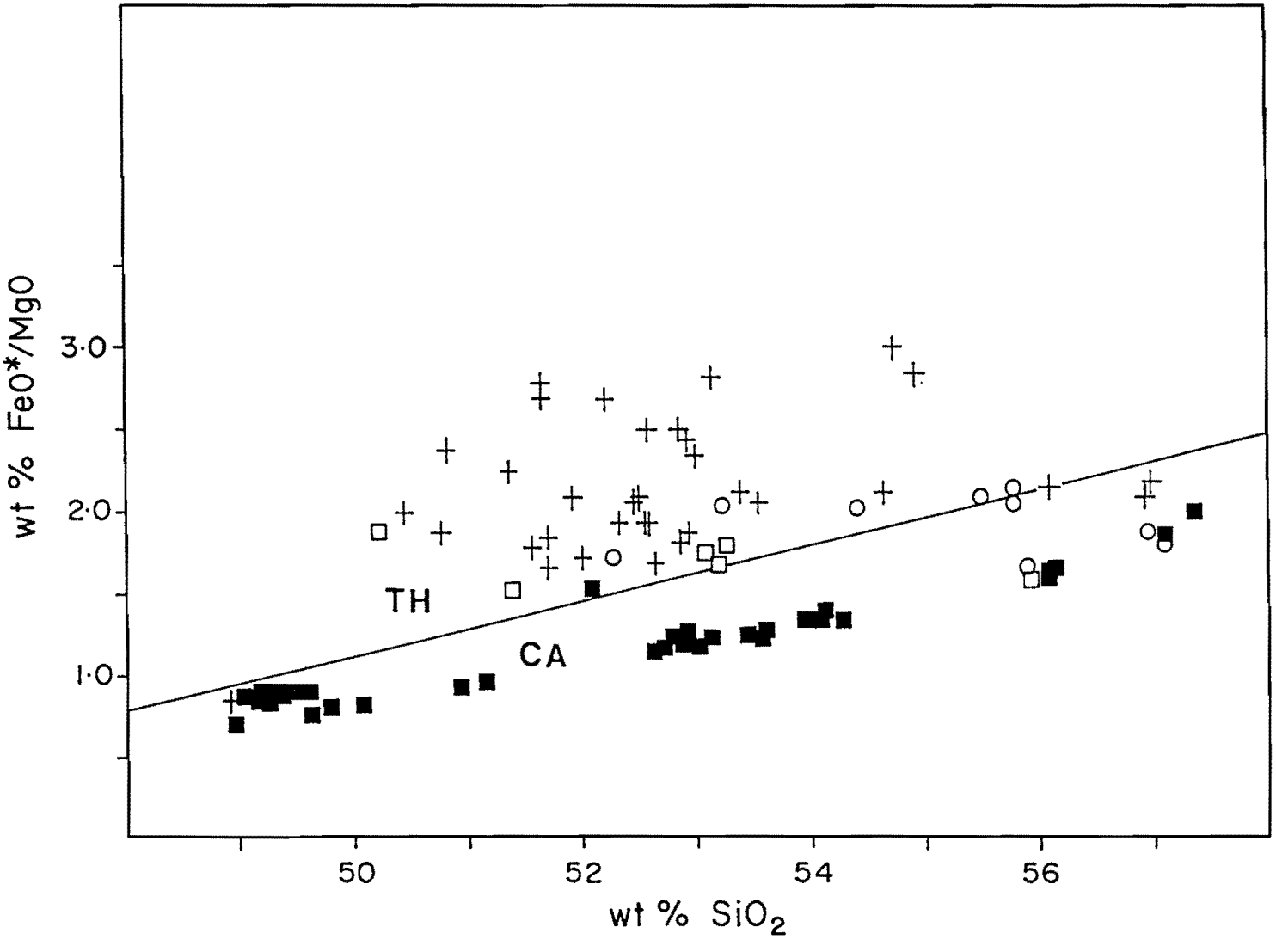

Figure VI.2 FeO*/MgO against SiO_2 in Galunggung volcanic rocks. Symbols as for Fig. VI.1. The line separating tholeiitic (TH) and calc-alkaline (CA) rock series is according to Miyashiro (1974).

tional tholeiitic, transitional calc-alkaline and calc-alkaline rocks series. Purbawinata (1988) reported that Guntur (Java) volcanic rocks although tholeiitic (Nicholls & Whitford, 1976) include both TH and CA rocks. Arculus and Johnson (1978), and Johnson et al. (1978) have stated that the concept of a world-wide standard association (e.g. island-arc tholeiitic, calc-alkalic etc.) should be discontinued. They consider it is more meaningful to recognise associations on a regional scale, and this conclusion is supported in this thesis.

VI.5 Major Element Variation

Galunggung volcanic rocks have a relatively narrow range of major element compositions, with 49 to 57 weight per cent SiO_2 (av. 52 %) and low- to medium-K (Fig. VI.1). Volcanic rocks having less than 53 % SiO_2 are normally rich in olivine; whereas rocks with 53 to 55 % SiO_2 normally have coexisting olivine and orthopyroxene, and rocks with > 55 % SiO_2 are rich in orthopyroxene and magnetite. The range of major element values is shown in Figure VI.3.

In Old Galunggung rocks TiO_2, Al_2O_3, FeO* and CaO decrease but Na_2O, K_2O and P_2O_5 increase with increasing SiO_2 content. The small decrease of TiO_2, FeO*, CaO and Al_2O_3 may reflect fractionation of Ti-magnetite, clinopyroxene and plagioclase, although there is little modal indication (see Table IV.1). MgO contents are relatively constant and low (<6 % MgO) with magnesium numbers (Mg#) less than 60. Most of the Old Galunggung rocks are Q-Hy normative (up to 7 % quartz normative) and some are Ol-Hy normative but < 5 % olivine normative. An exception is Old Galunggung cryptodome (medium-K high-Mg basalt)

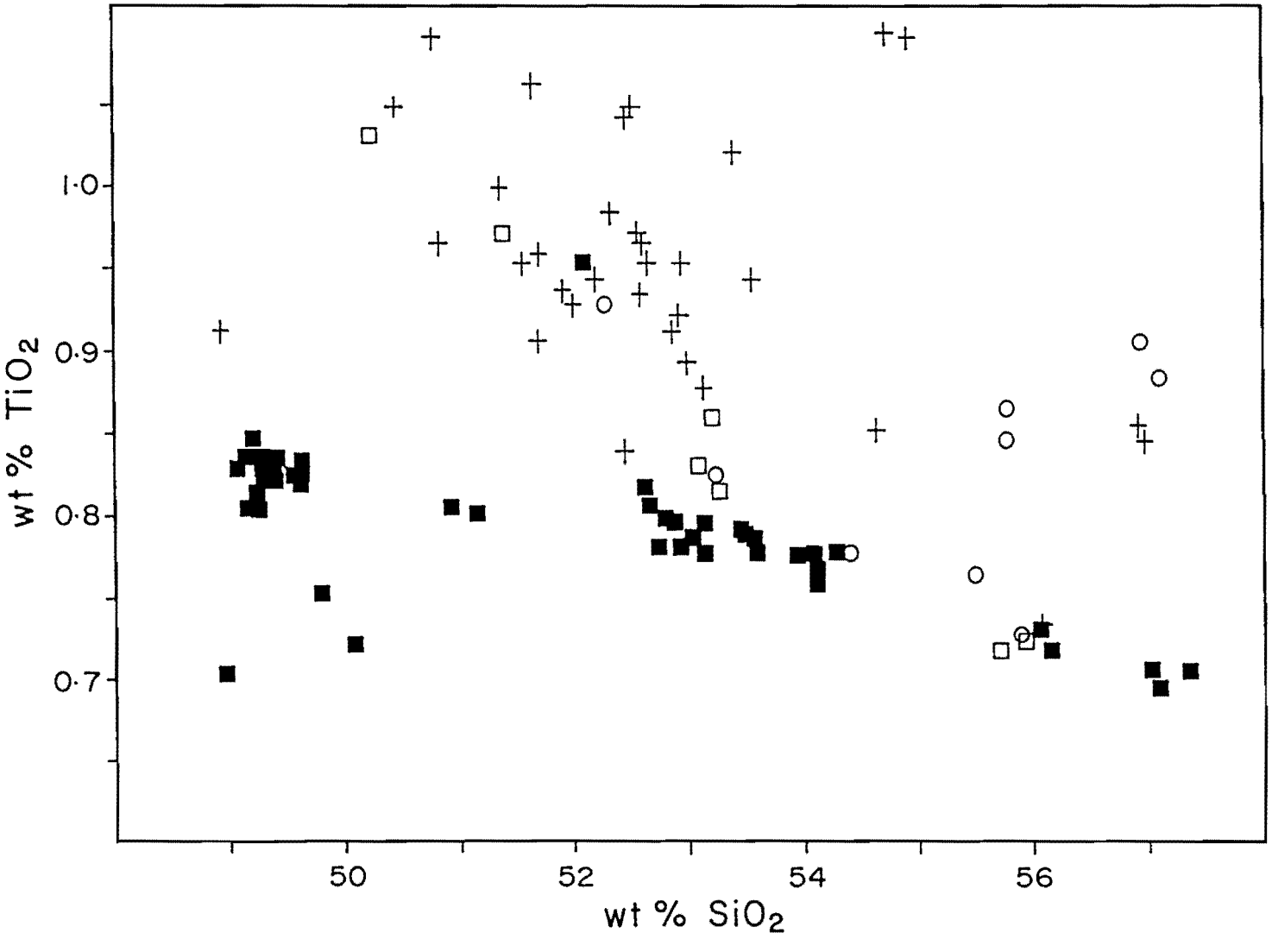

Figure VI.3 Major element Harker diagrams of Galunggung volcanic rocks. Symbols as for Fig. VI.1.

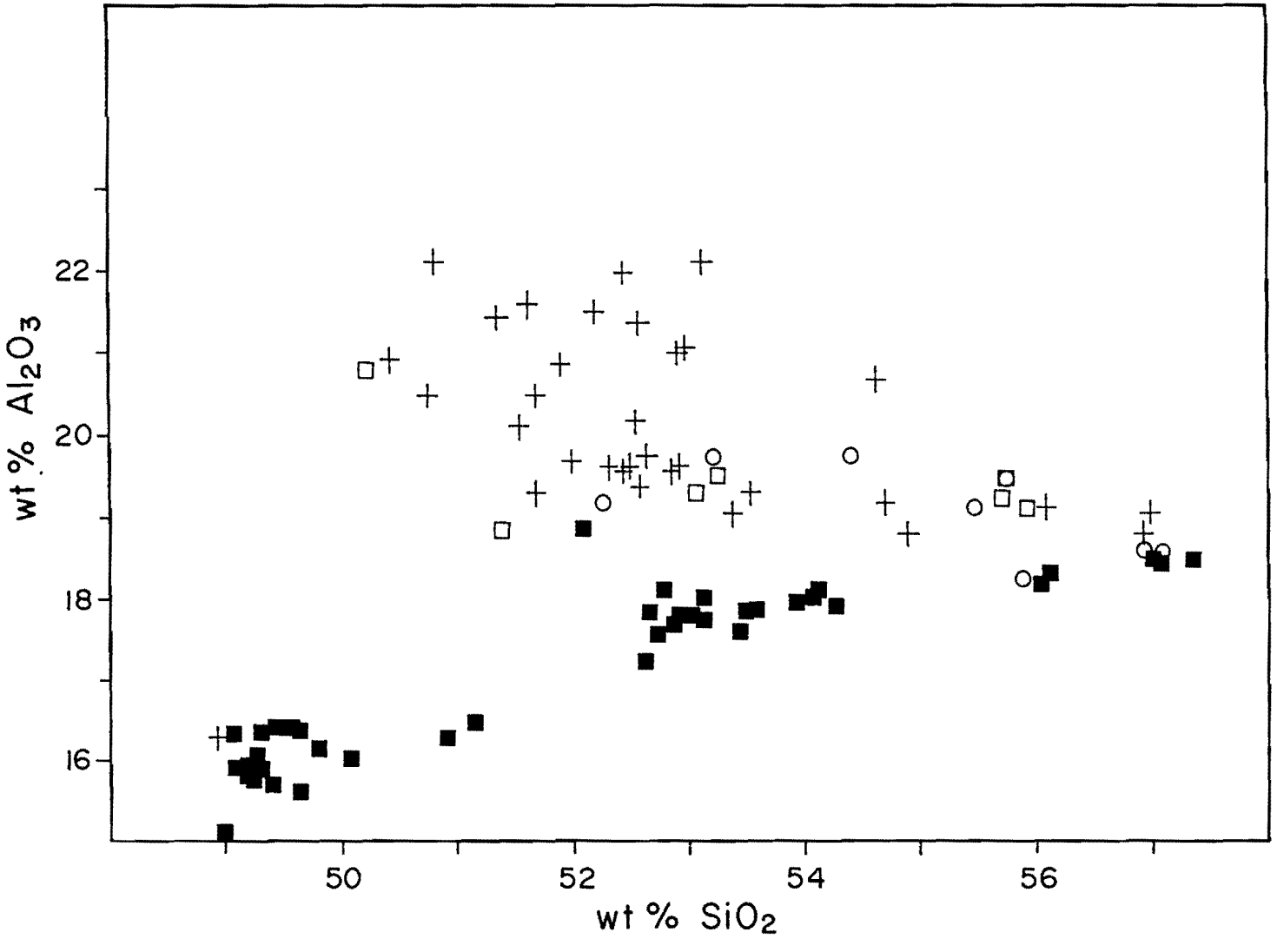
wt % Al_2O_3
22
20
18
16
50
52
54
56
wt % SiO_2

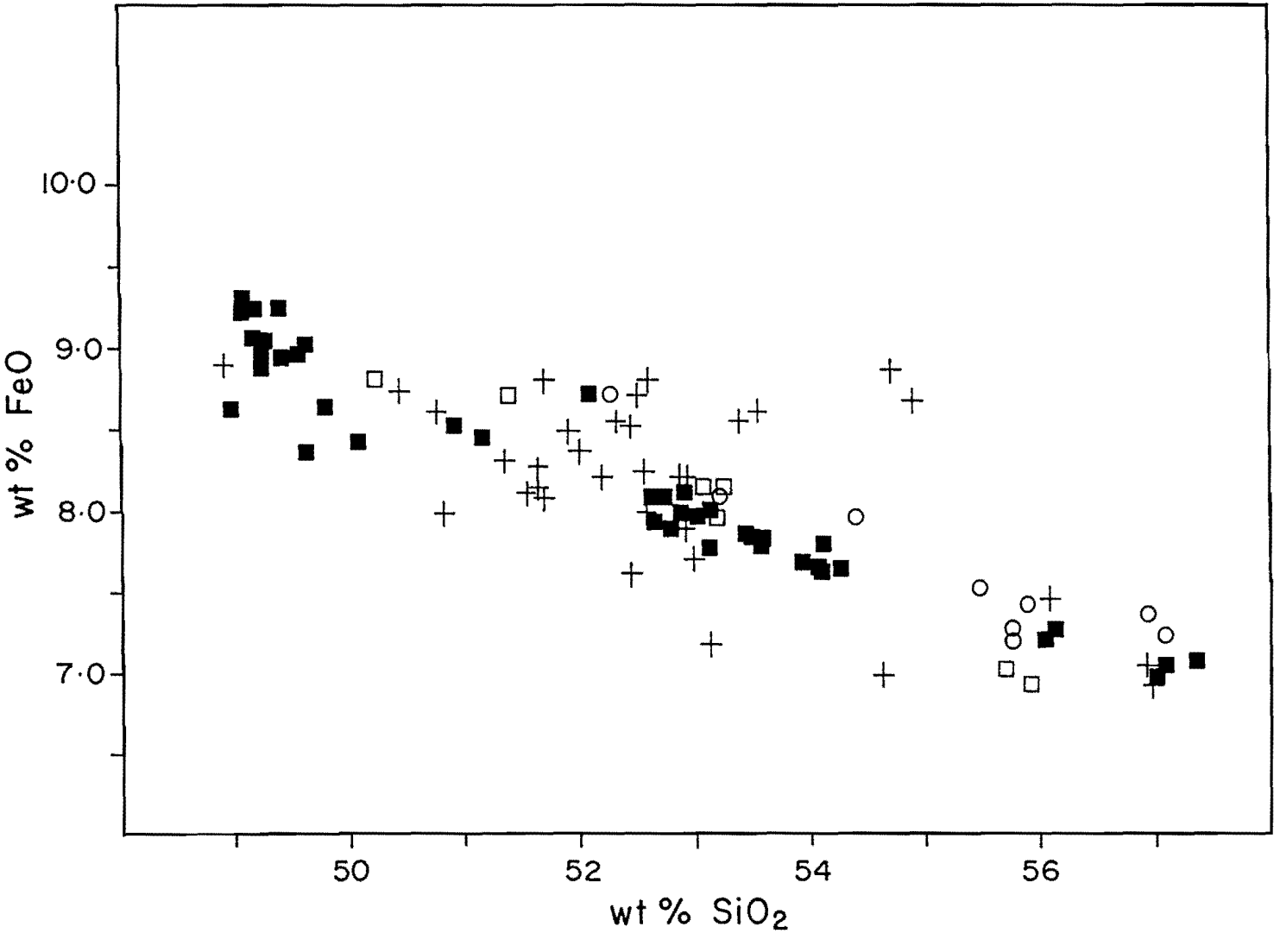
10·0
9·0
8·0
7·0
wt % FeO
50
52
54
56
wt % SiO2

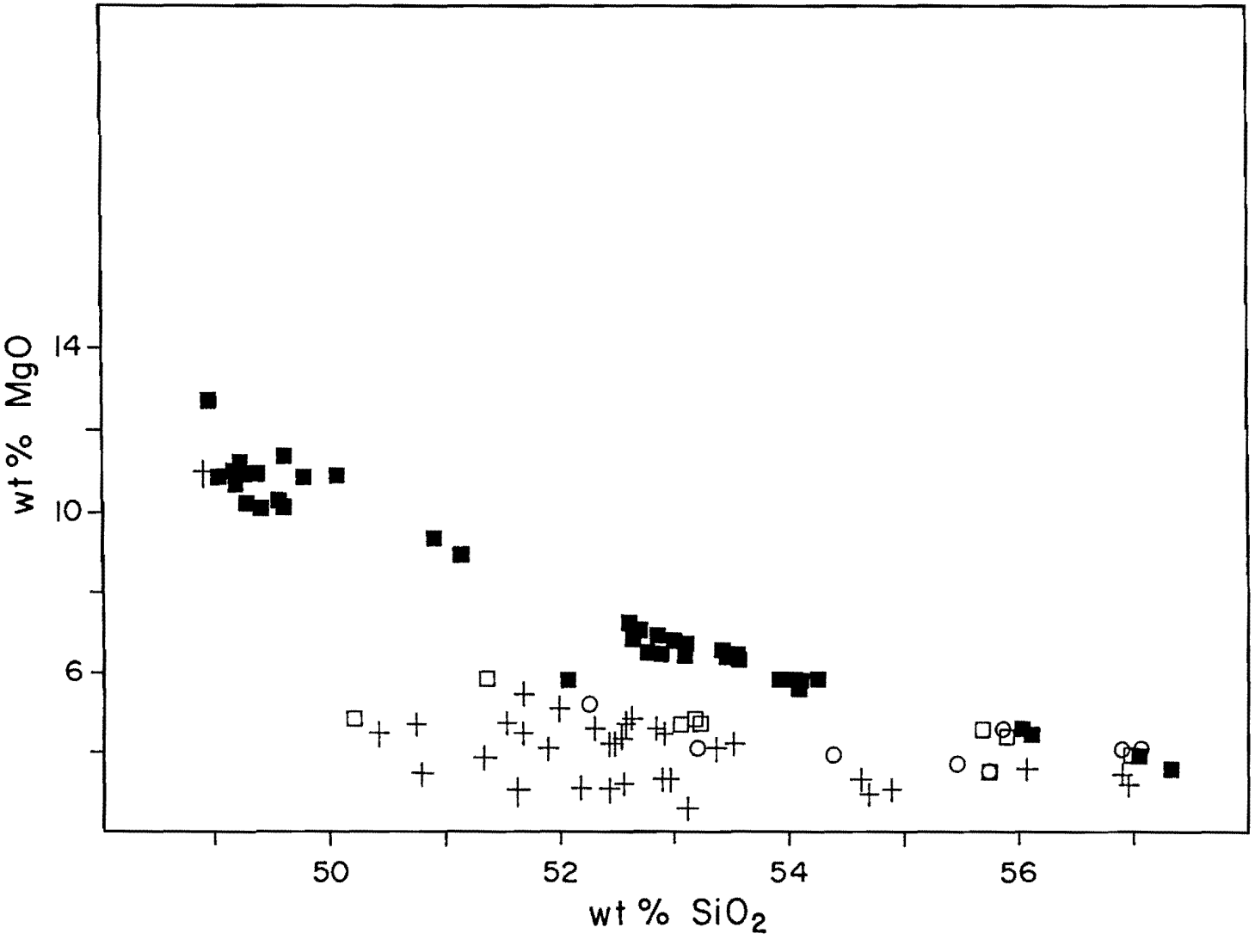
wt % MgO
14
10
6
50
52
54
56
wt % SiO2

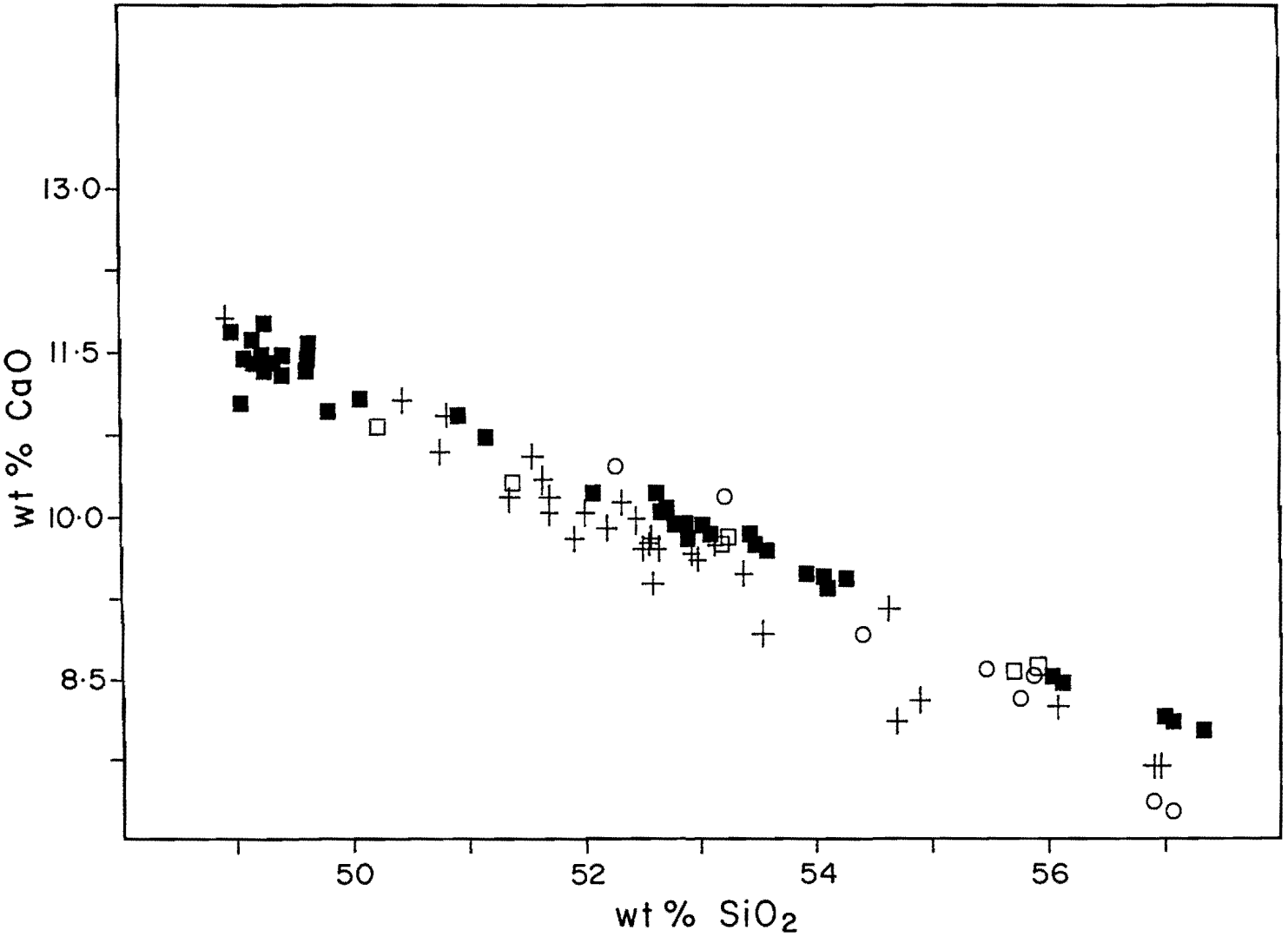
13·0
11·5
10·0
8·5
wt % CaO
50
52
54
56
wt % SiO2

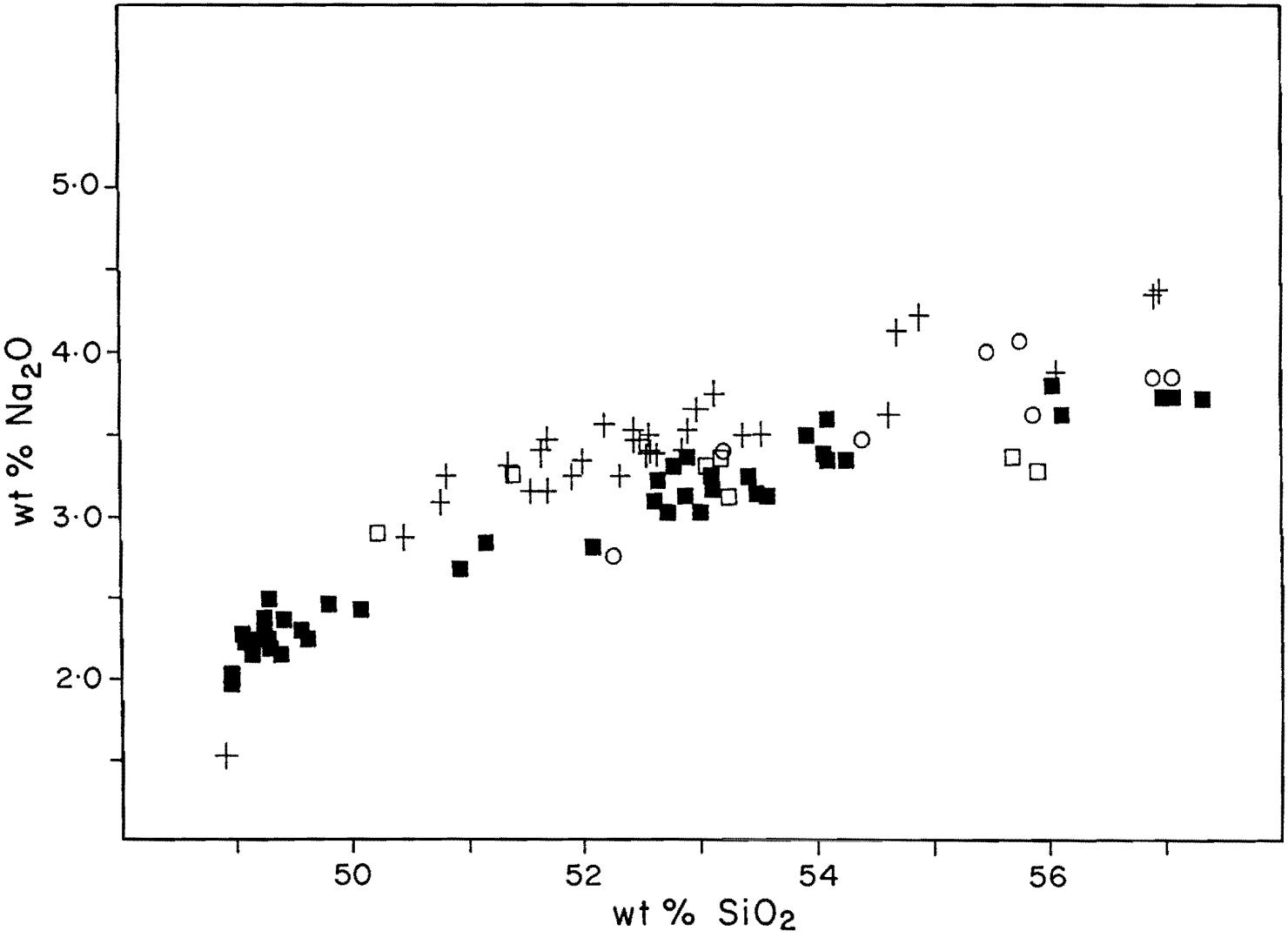
5·0
4·0
3·0
2·0
wt % Na_2O
50
52
54
56
wt % SiO_2

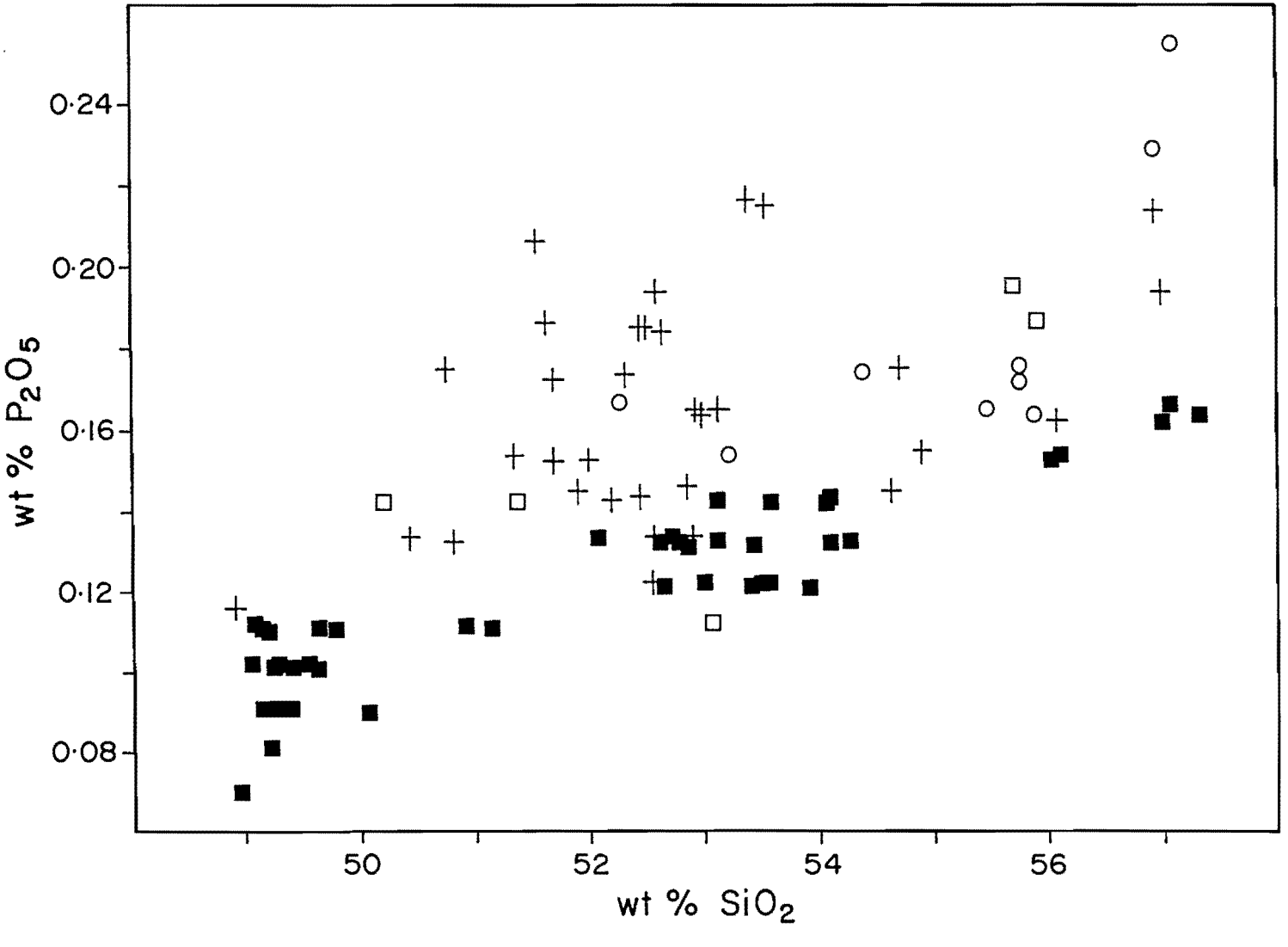
0·24
0·20
0·16
0·12
0·08
wt % P_2O_5
50
52
54
56
wt % SiO_2

which has higher MgO (10.7 %) and is Ol-Hy normative (10 % olivine normative), but has lower Al_2O_3 (16.3 %) contents than those of other Old Galunggung rocks. This may have a different petrogenetic history compared with the other Old Galunggung volcanic products.

Galunggung volcanic rocks erupted during caldera formation and in 1822, 1894 and 1918 have similar compositions (e.g. low MgO and high Al_2O_3 contents) to the major Old Galunggung rocks. The relationship between these rocks will be discussed in more detail in the following section. However, the 1982-83 eruption volcanic rocks differ markedly from the earlier rocks, and mainly primitive high-Mg basalts were erupted. The rocks are lower in TiO_2, Al_2O_3, Na_2O and P_2O_5 but are higher in MgO than those of pre-1982 rocks and are similar to the Old Galunggung cryptodome. Three sand-sized ash samples of high-Mg basalt which were erupted in July and September 1982 have slightly lower Ti (0.70 - 0.75 % TiO_2) than the others (0.80 - 0.85 % TiO_2). The low Ti content is followed by low V and Y abundances; and one of the samples (20334) is the most primitive high-Mg basalt (Mg# = 74.71, 193 ppm Ni and 711 ppm Cr) erupted during 1982-83. These data may suggest that magnetite has not yet precipitated. Furthermore, the low Ti content in the 1982-83 high-Mg basalt implies high degree of partial melting of depleted source (e.g. Fodor, 1987; Johnson et al., 1985; Pearce & Norry, 1979).

Al_2O_3 shows a steady enrichment from 16 to 19 % with increasing SiO_2 content. This is consistent with the slight increase of plagioclase modal proportions (Table IV.3) from high-Mg basalt to low-Mg basaltic andesite. The Al_2O_3 content in the 1982-83 lavas are lower than in the older rocks. This is also consistent with the modal data in which plagioclase phenocryst contents for 1982-83 average 10.5 % and older

rocks 22.5 %. A sharp increase of MgO content from 4 to 12.5 % and olivine phenocryst phase from < 1 % to 6.7 % (Table IV.3) with decreasing SiO_2 content suggests that the 1982-83 rocks are more strongly controlled by high-Mg olivine (Fo_{80-90}) fractionation than earlier rocks. A plot of Mg# against SiO_2 (Fig. VI.4) clearly shows a linear decrease of Mg# in the 1982-83 rocks, whereas older rocks show little change. One sample (silt-sized ash: 20331) has higher Al_2O_3 and TiO_2 but lower MgO contents and Mg# than other 1982-83 rocks with 52 % SiO_2. This ash may however have been secondary and derived from pre-1982 eruption rocks. In terms of high-Mg content, only the Old Galunggung cryptodome has a composition similar to the 1982-83 basalts.

VI.6 Trace Element Variation

Trace element variation is shown in Figure VI.5. In the Old Galunggung rocks incompatible elements such as Ba, Rb, Zr and Ga show a linear increase, but Sc and V decrease with increasing SiO_2 content. Sr and Y do not show an obvious trend but seem to be higher than values for 1982-83 rocks. Like Mg, Cr and Ni contents are relatively constant and low (< 100 ppm and < 40 ppm, respectively). In contrast, the cryptodome has lower Ba, Sr, Zr, Y and Ga but higher Rb, Cr and Ni contents than other Old Galunggung rocks.

Like major elements, trace elements in volcanic rocks produced during caldera formation and in historic eruptions up to 1918 also have a similar composition to Old Galunggung rocks, whereas trace elements of 1982-83 basalts have lower Sr, Y and Ga but higher Sc, Cr and

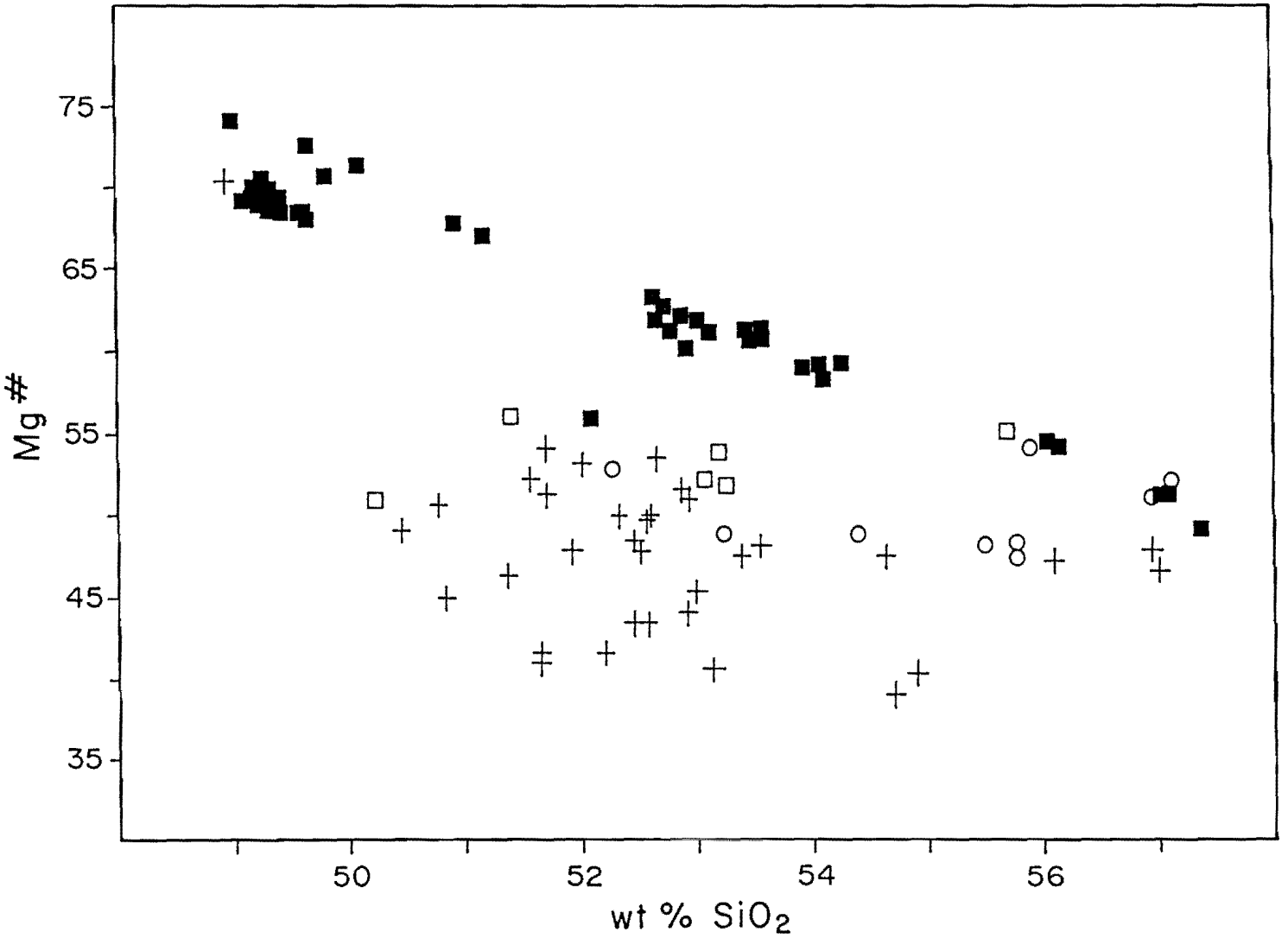

Figure VI.4 SiO_2 against magnesium number (Mg#) in Galunggung volcanic rocks. Symbols as for Fig. VI.1.

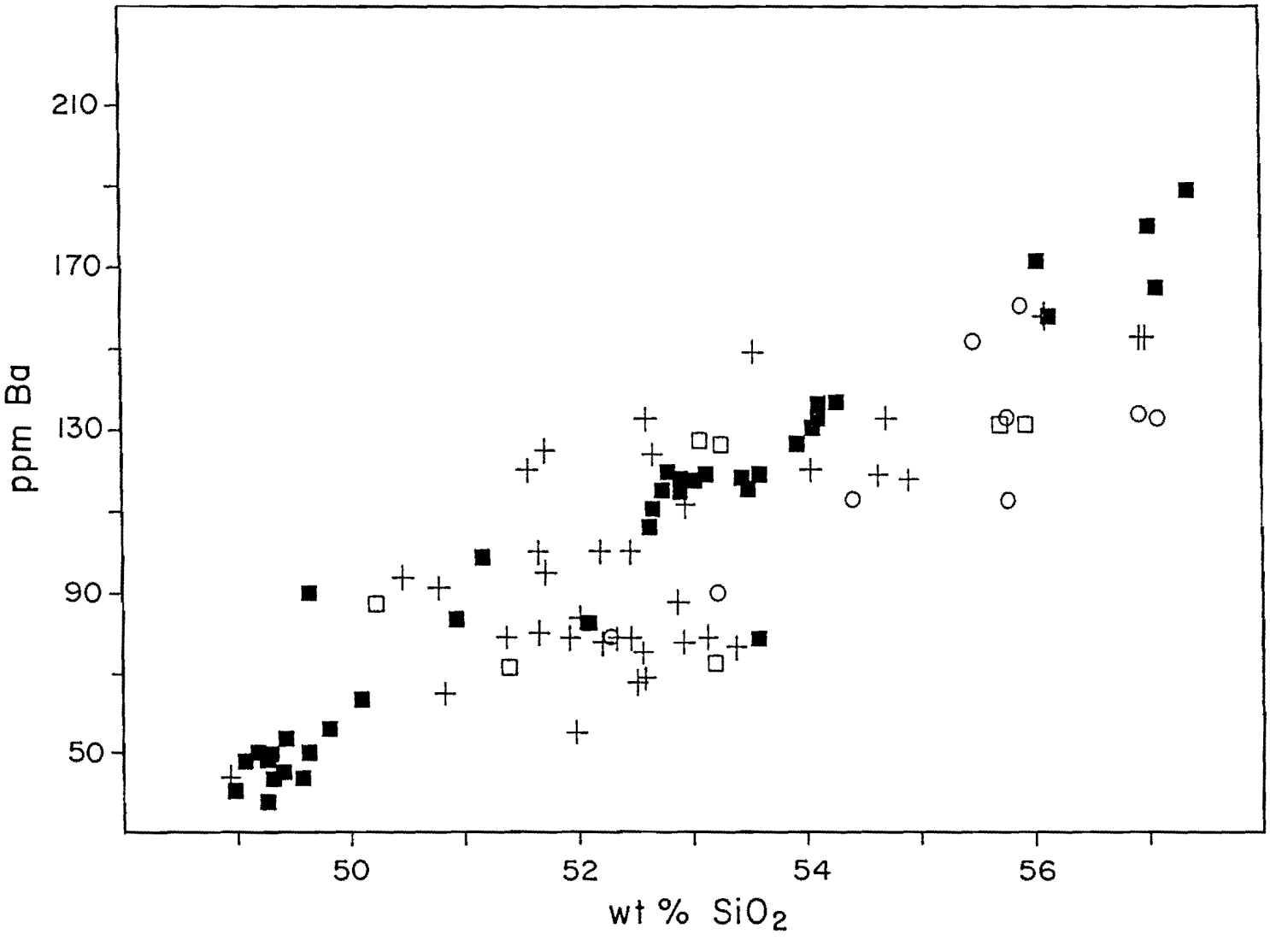

Figure VI.5 Trace element Harker diagrams of Galunggung volcanic rocks. Symbols as for Fig. VI.1.

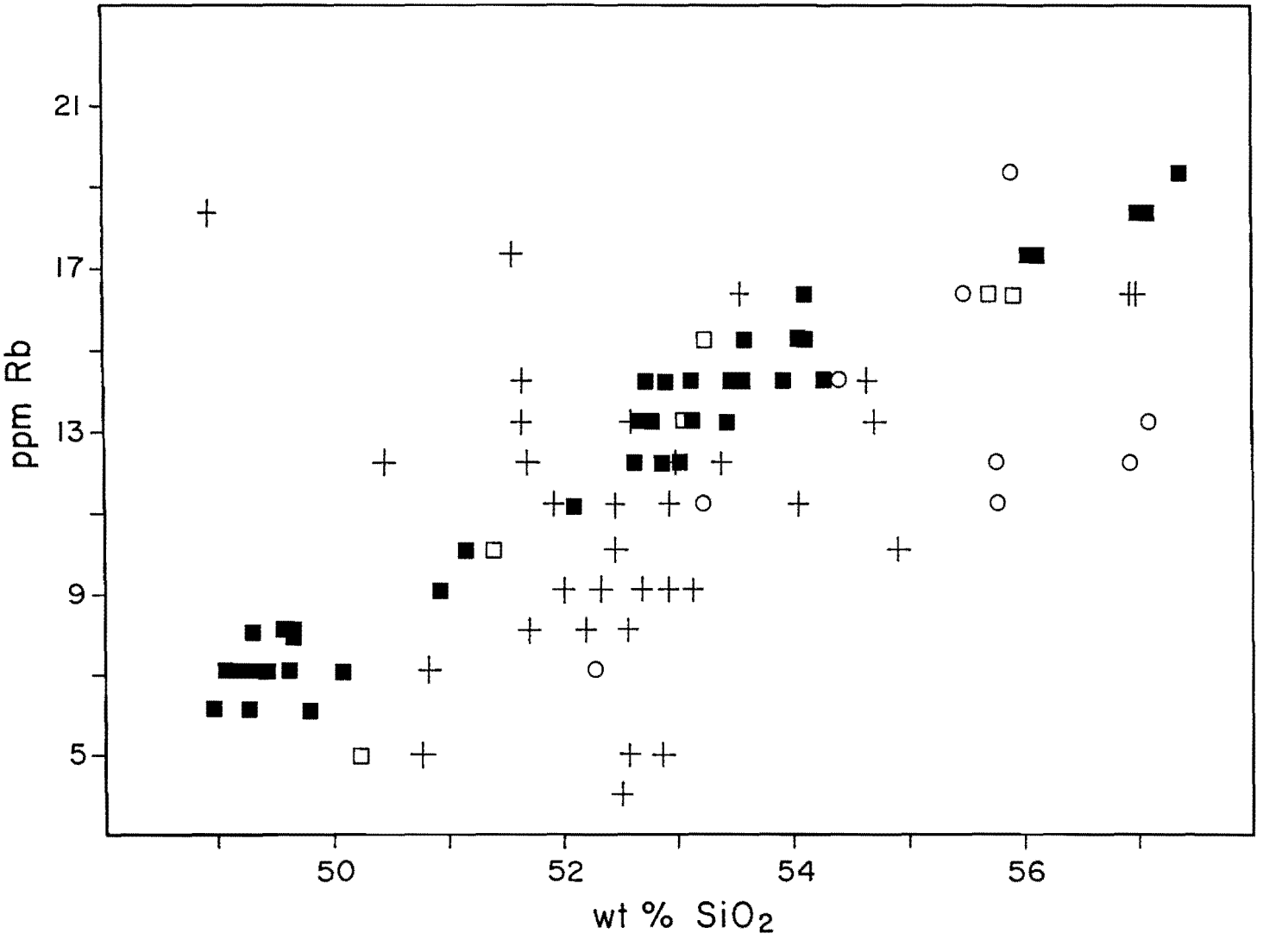
21
17
13
9
5
ppm Rb
50
52
54
56
wt % SiO2

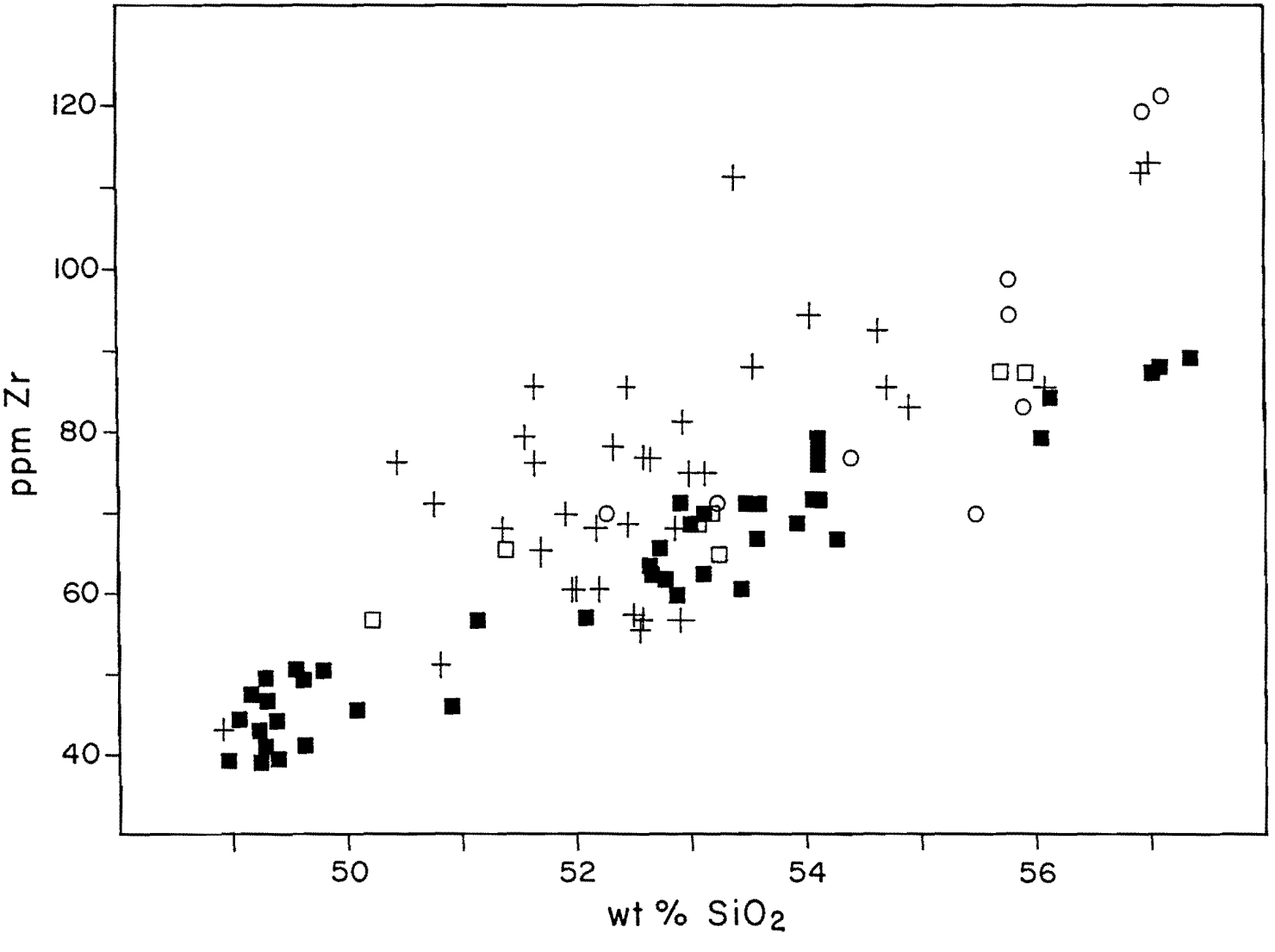
120
100
80
60
40
ppm Zr
50
52
54
56
wt % SiO2

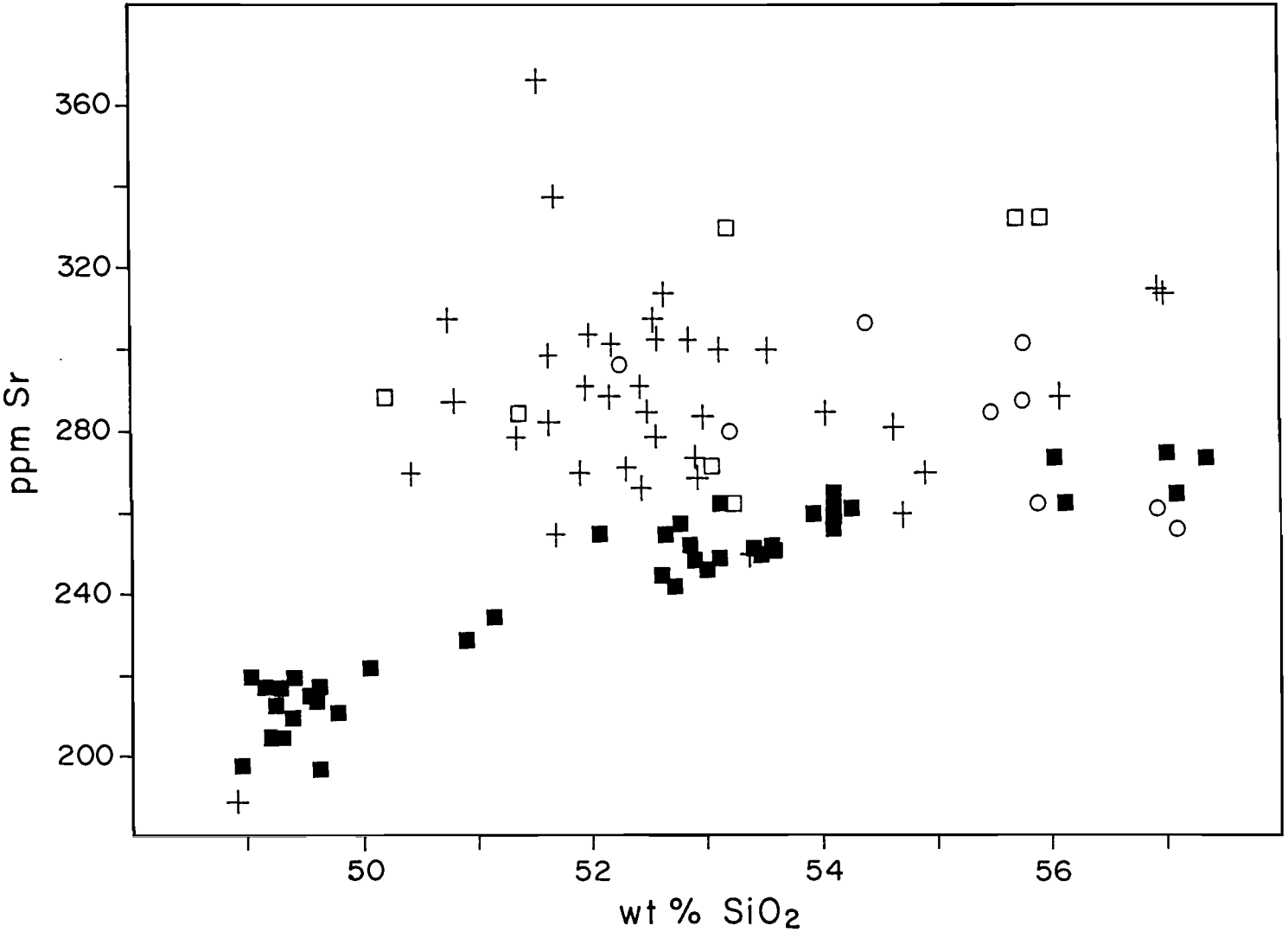
ppm Sr
360
320
280
240
200
50
52
54
56
wt % SiO2

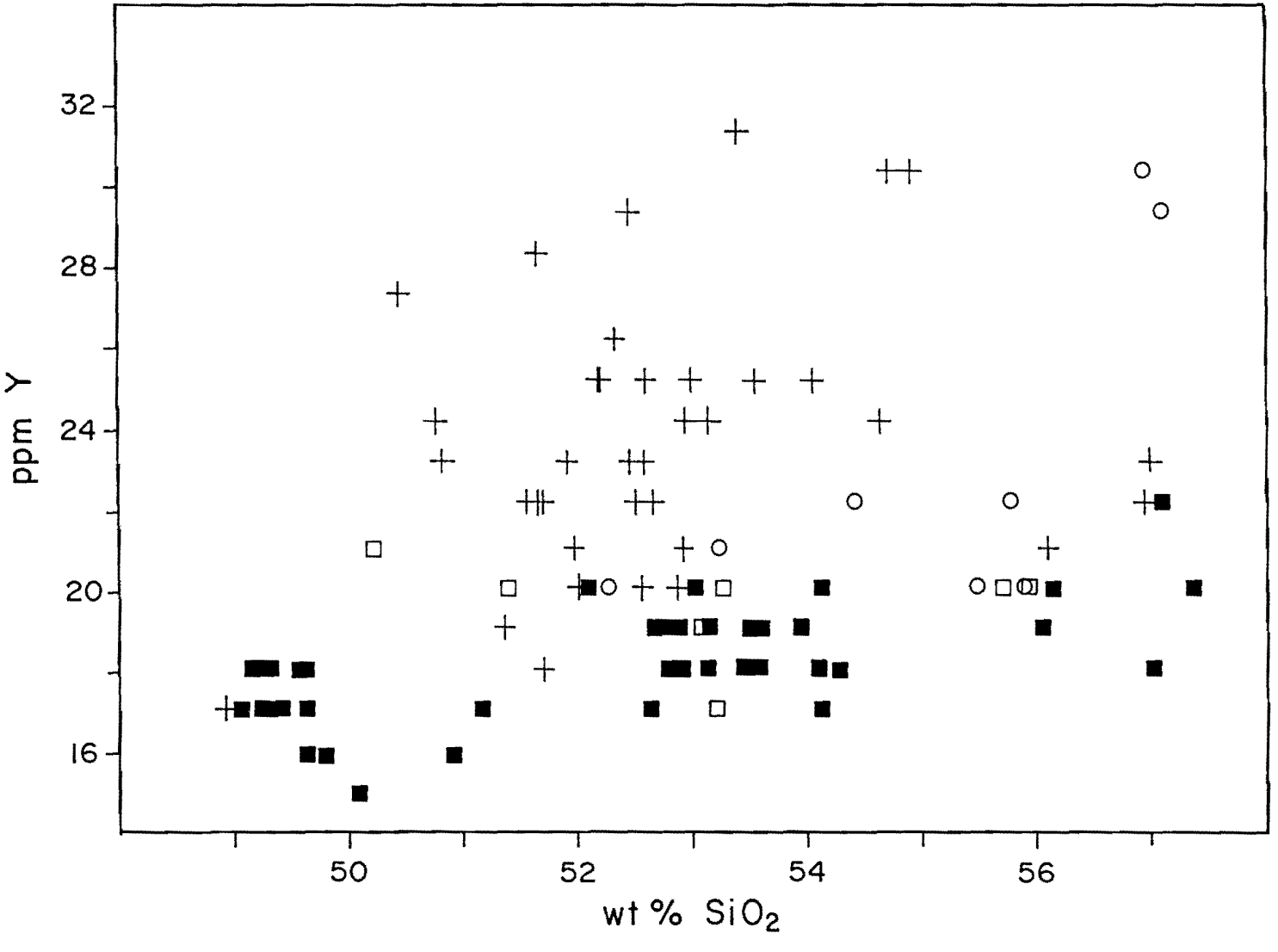
32
28
24
20
16
ppm Y
50
52
54
56
wt % SiO2

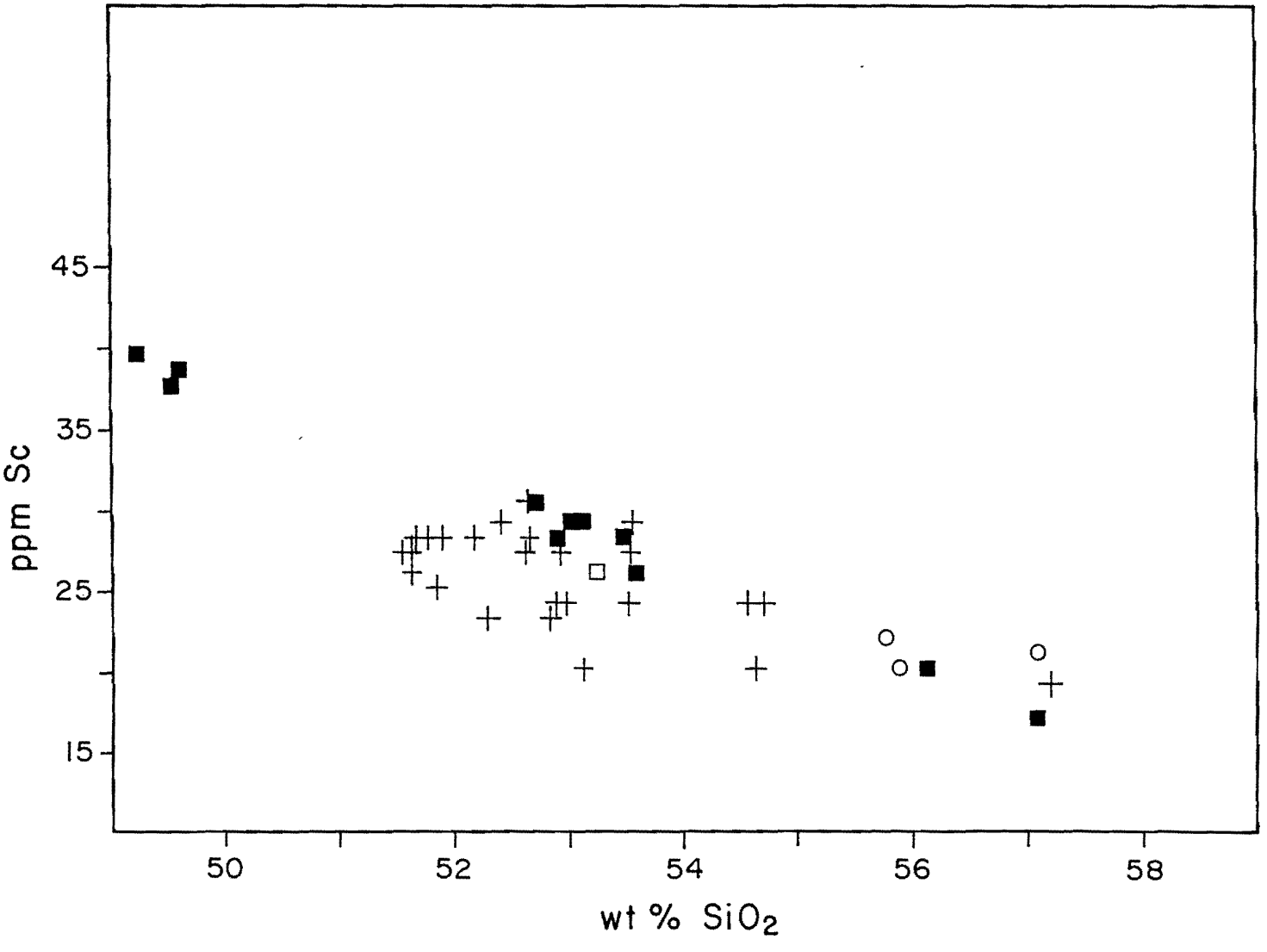
45
35
25
15
ppm Sc
50
52
54
56
58
wt % SiO2

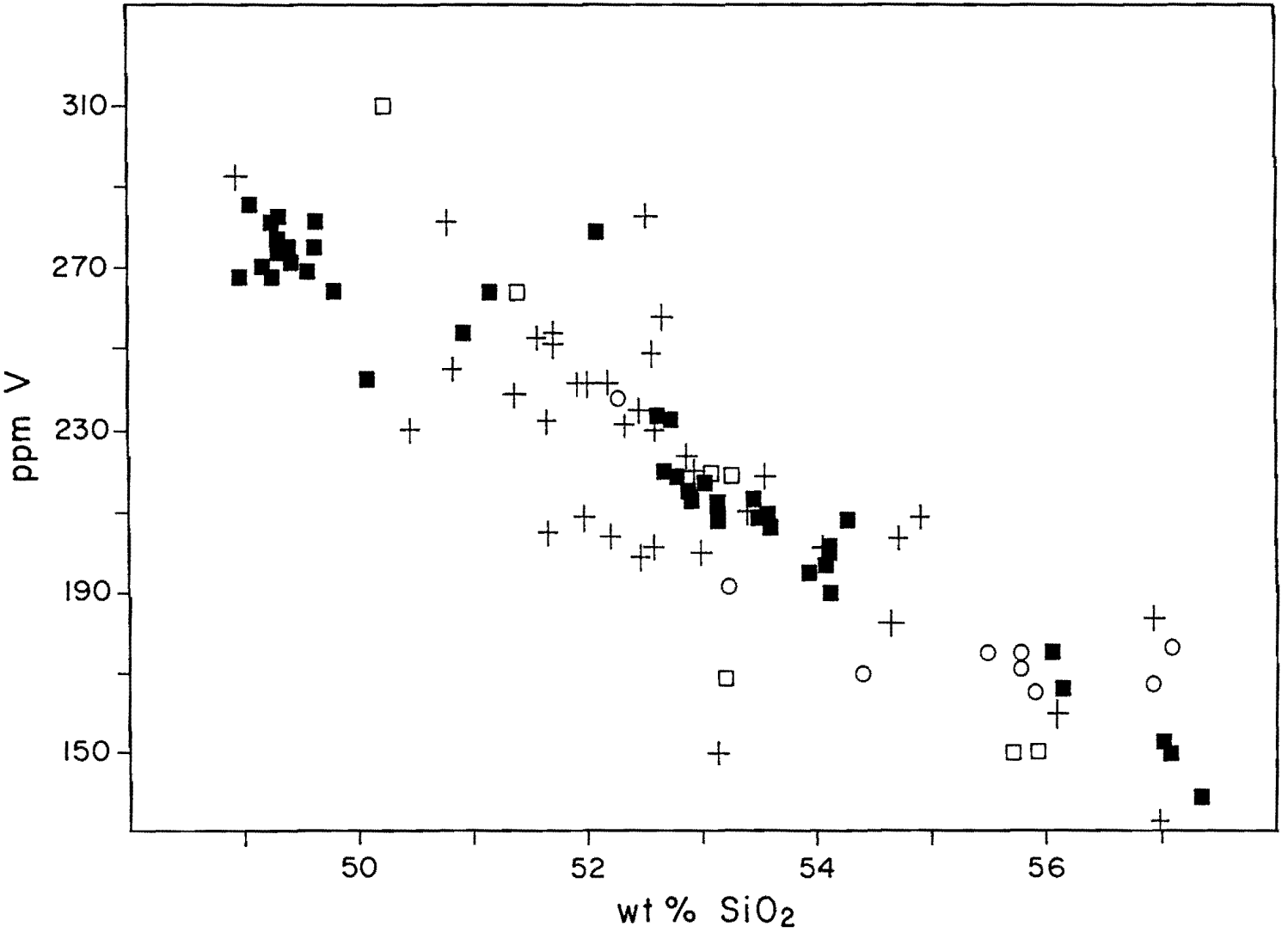
310
270
230
190
150
ppm V
50
52
54
56
wt % SiO2

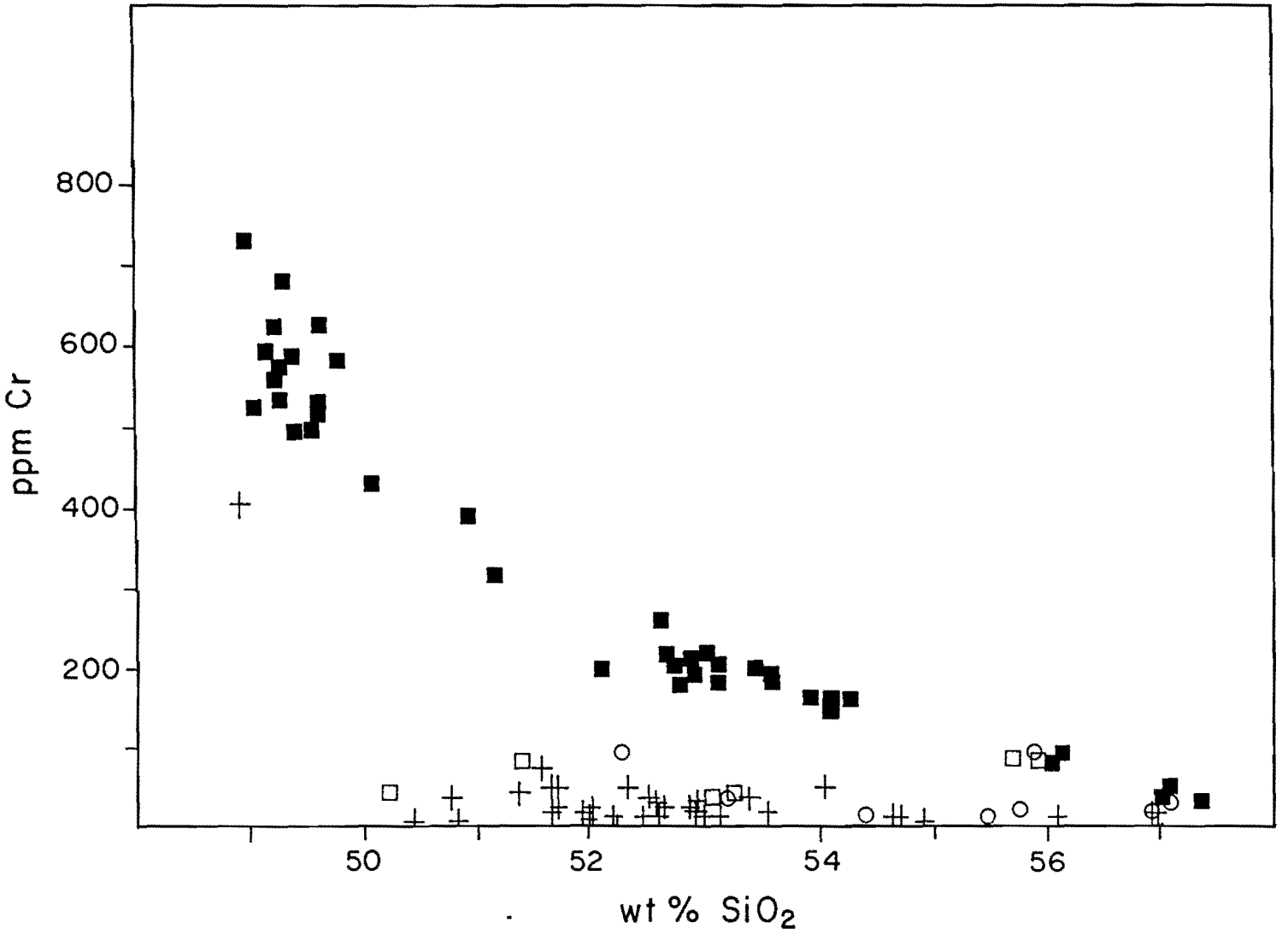
800
600
400
200
ppm Cr
50
52
54
56
wt % SiO2

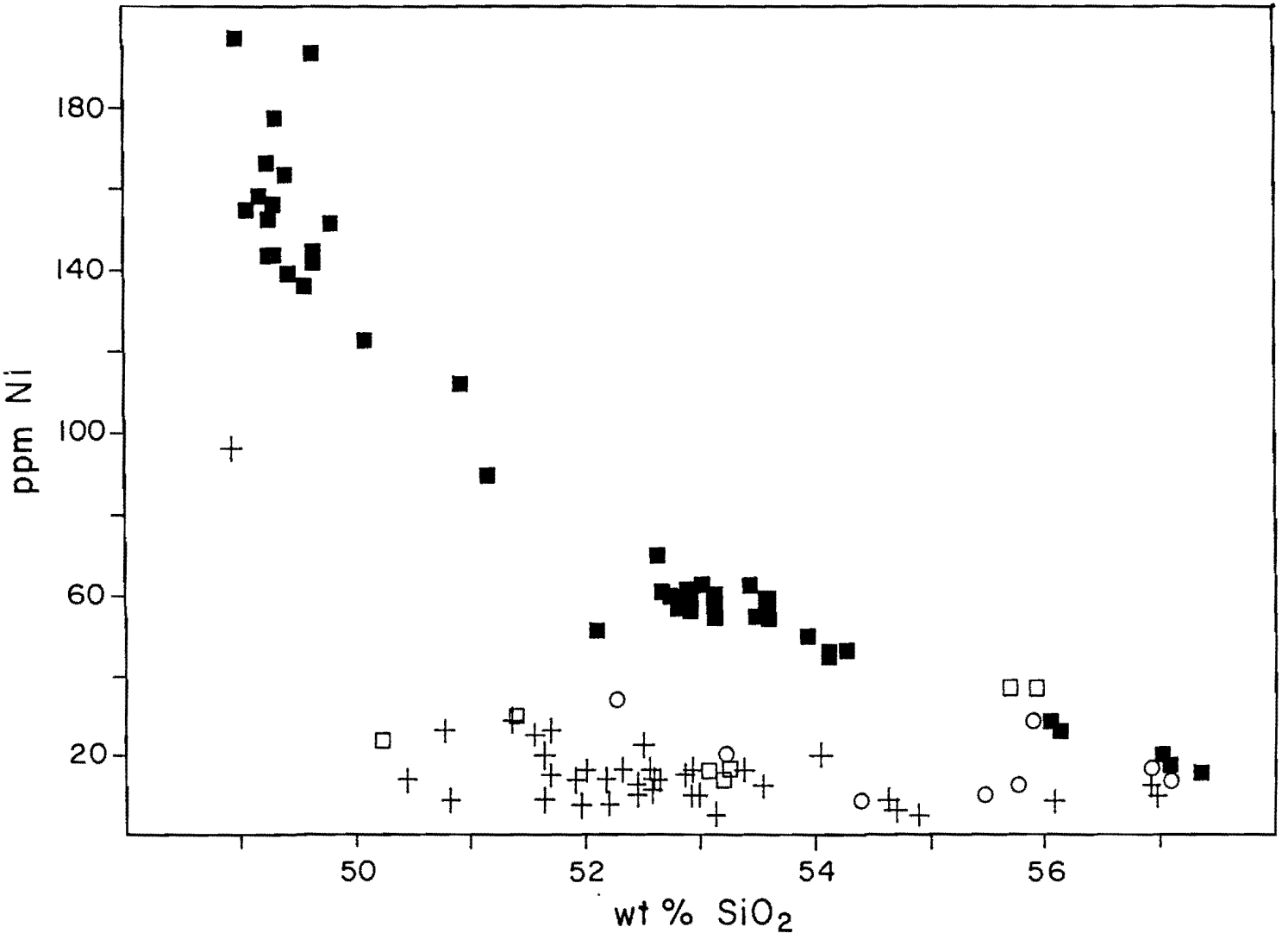
180
140
100
60
20
ppm Ni
50
52
54
56
wt % SiO2

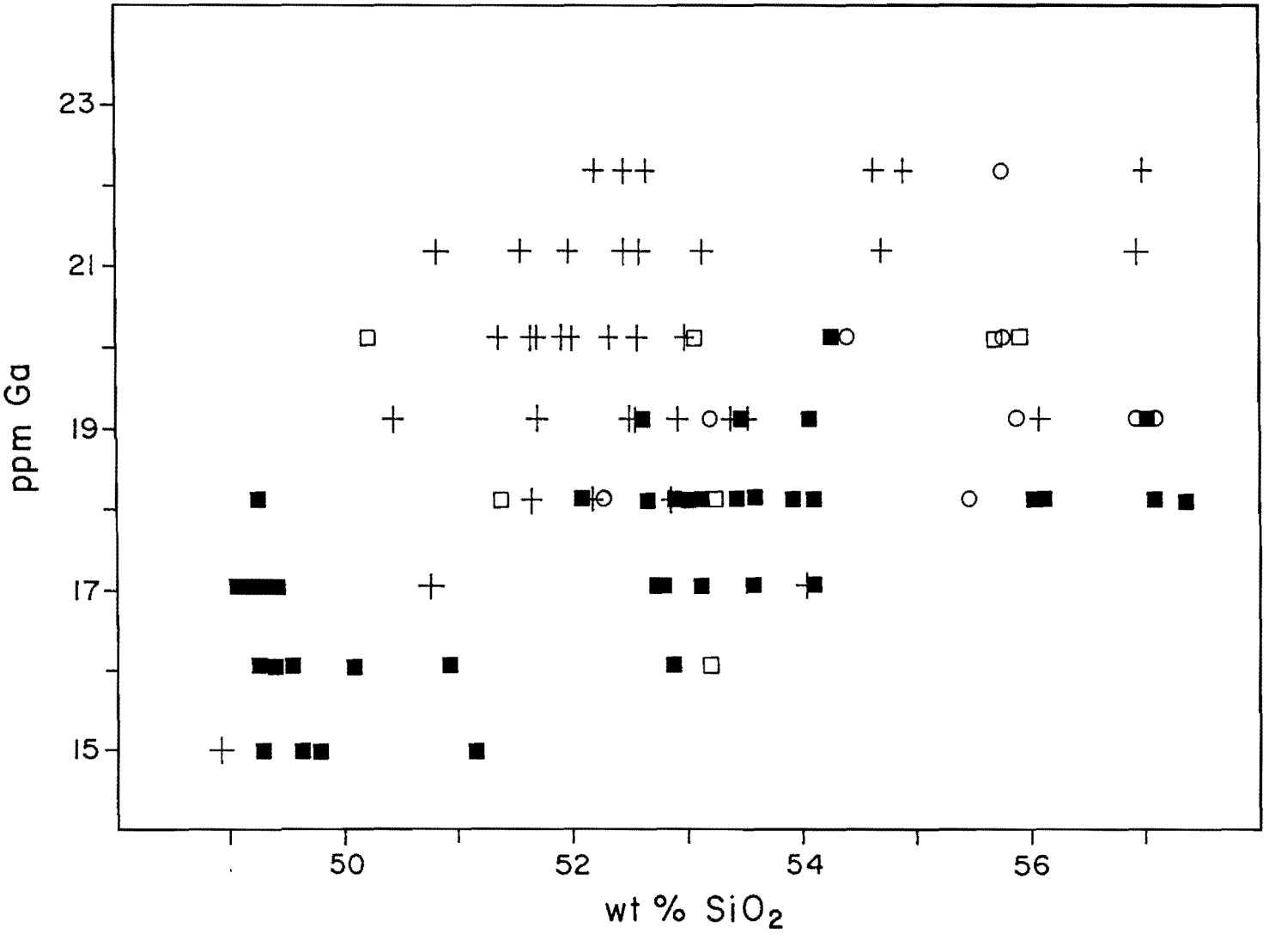
23
21
19
17
15
ppm Ga
50
52
54
56
wt % SiO2

Ni contents than those of the earlier rocks.

In the previous section (VI.3) Galunggung volcanic rocks are divided into 6 groups. Spider diagrams of each group are given in Figure VI.6-7. The pattern of Galunggung rocks, normalised to the primordial mantle composition, is flatter than those normalised to the average mid-oceanic ridge basalts (MORB). This implies that Galunggung magma source differs significantly from MORB. Although Ba and Rb are slightly enriched compared with MORB, other incompatible elements are depleted. This indicates that Galunggung rocks were derived from a depleted magma source.

Nb and Ce are scattered in Galunggung volcanic rocks, possibly due to the mobility of the elements and low precision in their determination. In addition, the incompatible elements abundance gradually increases from low-K high-Mg basalt to low-Mg basaltic andesite. This is a strong evidence of crystal fractionation.

VI.7 Compositional Variation with Stratigraphic Position and Time

In order to establish whether variation in time was occurring within the groups systematic stratigraphic sampling was undertaken. Collections were made though a sequence of Old Galunggung volcanic rocks at four locations (Fig. VI.8), but as already indicated no systematic change in composition was apparent from older to younger rocks. All of the rocks have < 6 % MgO, < 100 ppm Cr and < 35 ppm Ni although silica contents range from 50 % to 57 % SiO_2 (Table VI.3). Old Galunggung dikes have also a similar composition to the lava flows

Figure VI.6 Spidergrams of trace element concentrations in Galunggung volcanic rocks normalised to primordial mantle composition. Normalisation after Geist et al., 1985.

A Low-K high-Mg basalt

B "Transitional" high-Mg basalt — 1982-83 Eruption

C High-Mg basaltic andesite

D Medium-K high-Mg basalt — Old Galunggung cryptodome

E Low-Mg basalt

F Low-Mg basaltic andesite — Pre-1982-83 Eruptions

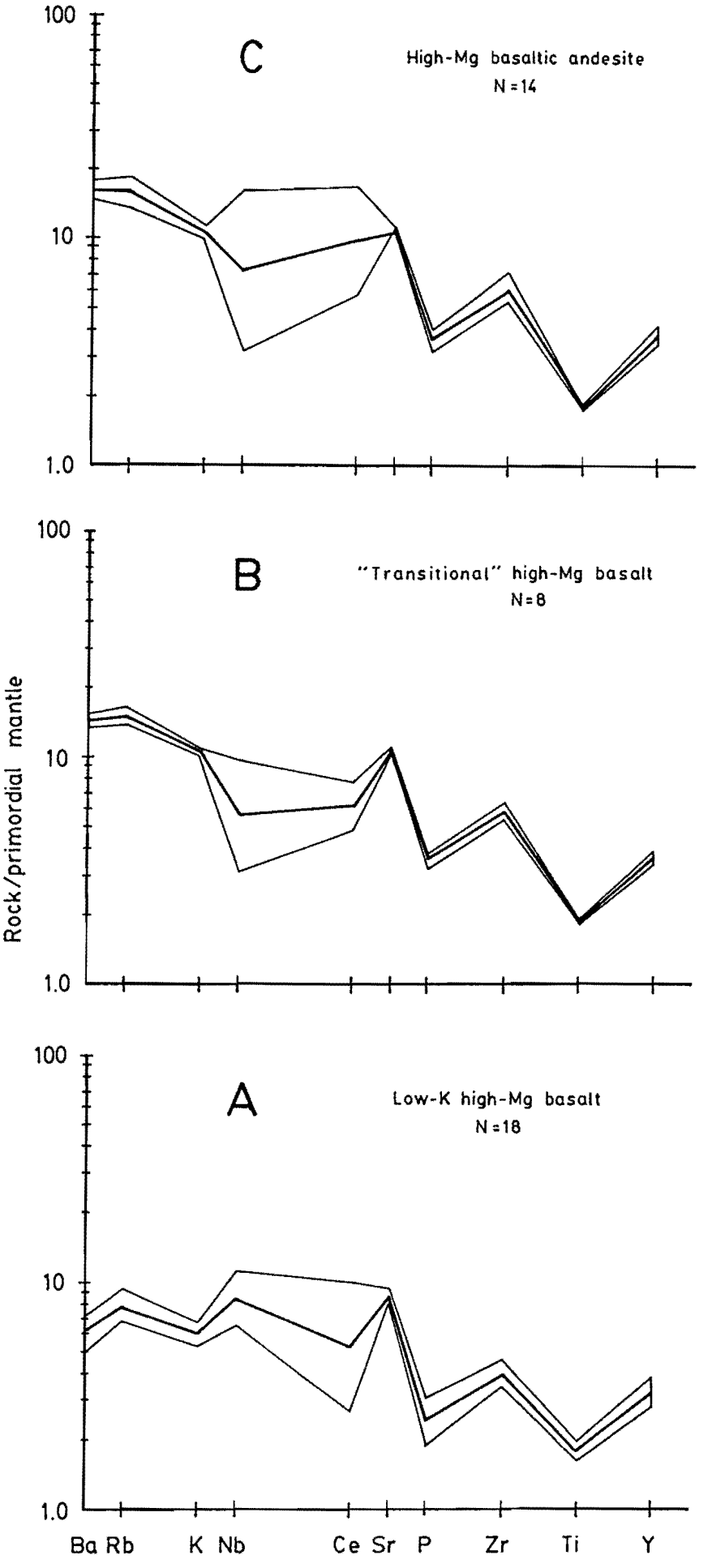
100
C
High-Mg basaltic andesite
N=14
10
1.0
100
B
"Transitional" high-Mg basalt
N=8
Rock/primordial mantle
10
1.0
100
A
Low-K high-Mg basalt
N=18
10
1.0
Ba Rb K Nb Ce Sr P Zr Ti Y

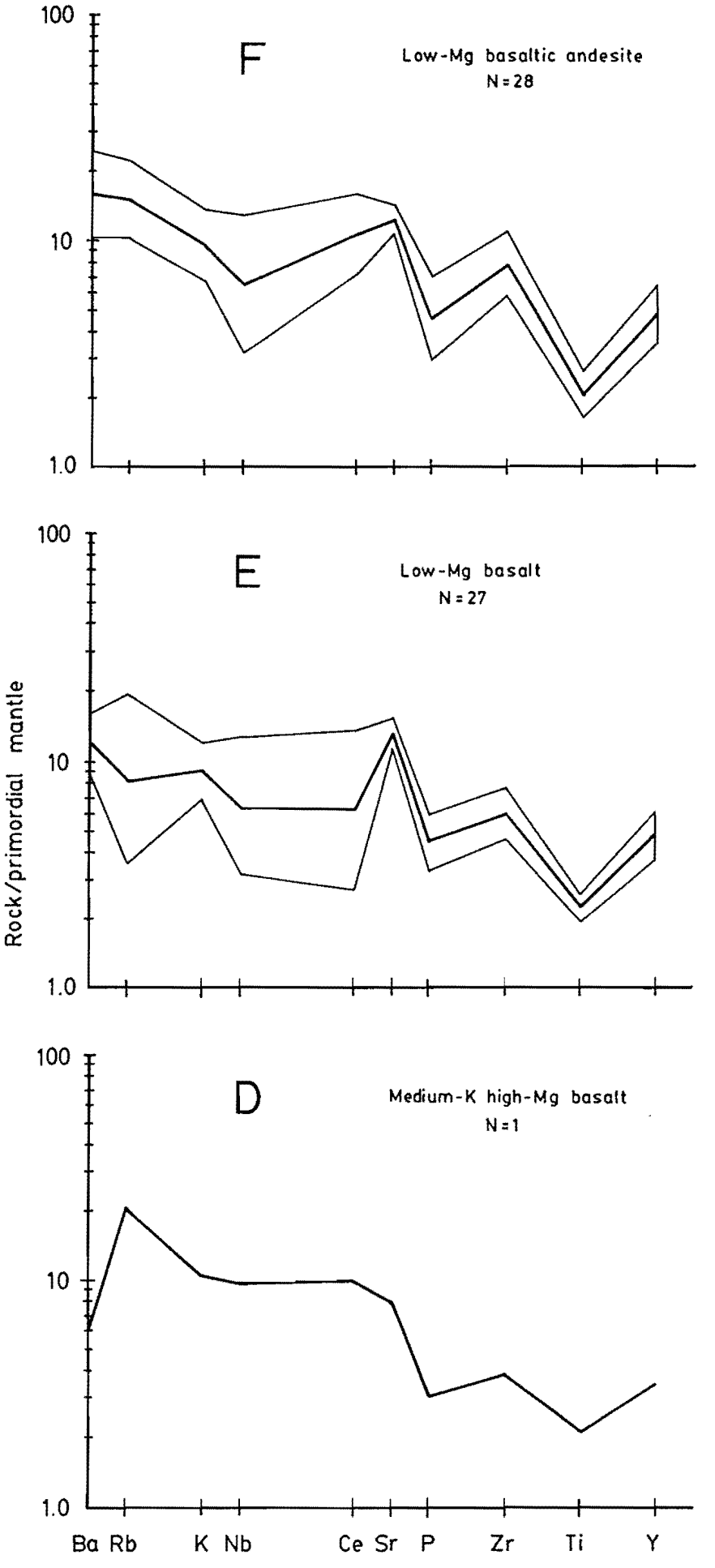
100
10
1.0
F
Low-Mg basaltic andesite
N=28
E
Low-Mg basalt
N=27
D
Medium-K high-Mg basalt
N=1
Rock/primordial mantle
Ba Rb K Nb Ce Sr P Zr Ti Y

Figure VI.7 Spidergrams of trace element concentrations in Galunggung volcanic rocks normalised to average MORB (Mid-Oceanic Ridge Basalts). Normalisation after Geist et al., 1985.

A Low-K high-Mg basalt

B "Transitional" high-Mg basalt — 1982-83 Eruption

C High-Mg basaltic andesite

D Medium-K high-Mg basalt — Old Galunggung cryptodome

E Low-Mg basalt

F Low-Mg basaltic andesite — Pre-1982-83 Eruptions

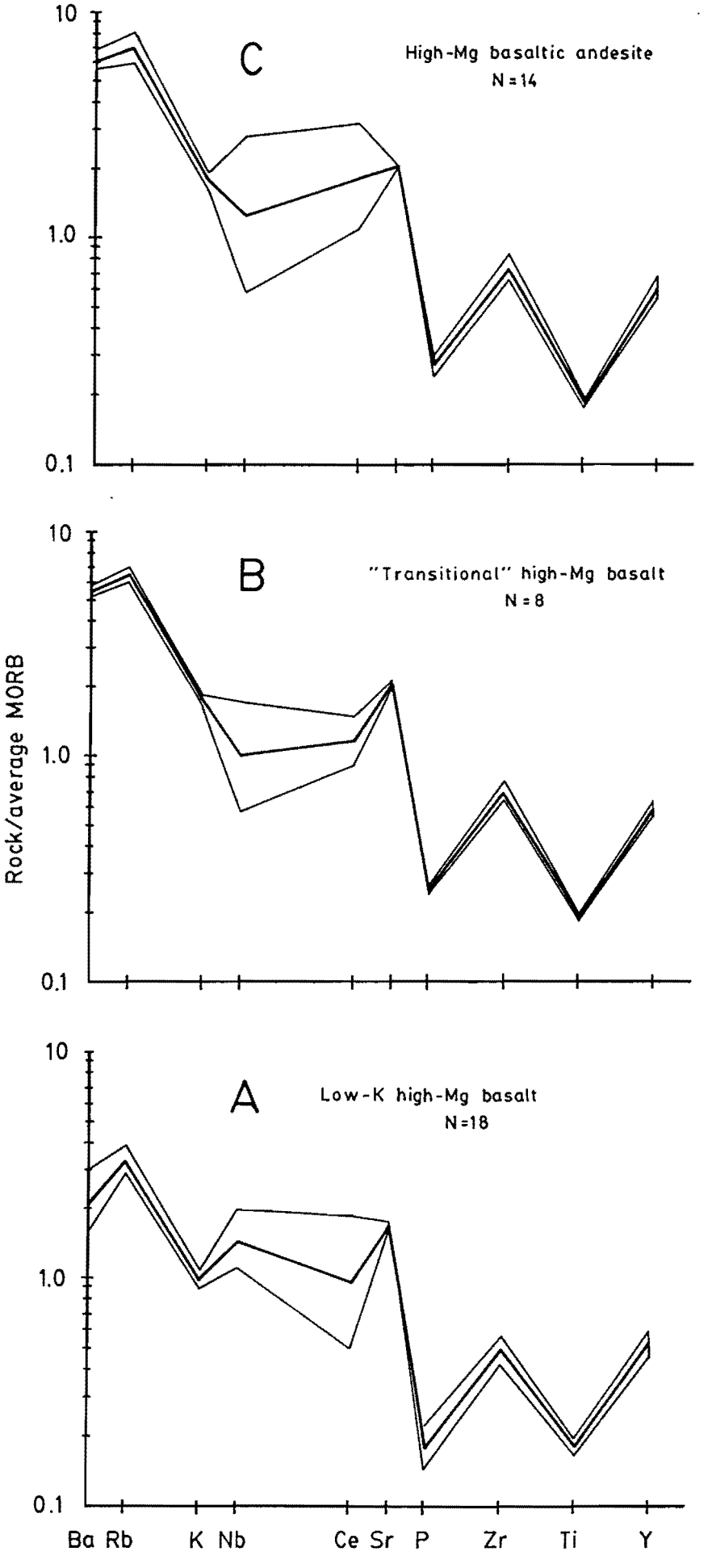
10
1.0
0.1
C
High-Mg basaltic andesite
N=14
B
"Transitional" high-Mg basalt
N=8
A
Low-K high-Mg basalt
N=18
Rock/average MORB
Ba Rb K Nb Ce Sr P Zr Ti Y

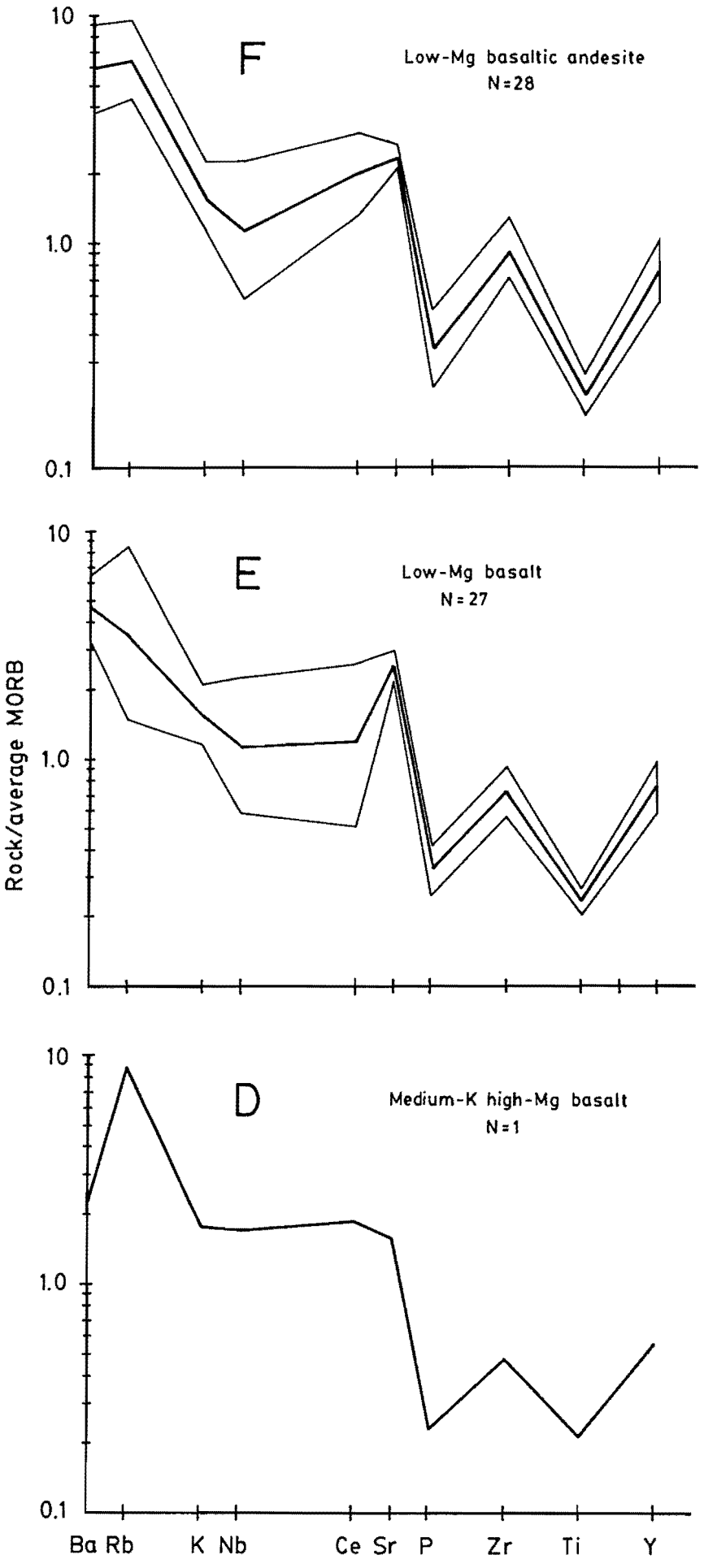
F
Low-Mg basaltic andesite
N=28
E
Low-Mg basalt
N=27
D
Medium-K high-Mg basalt
N=1
Rock/average MORB
10
1.0
0.1
Ba Rb K Nb Ce Sr P Zr Ti Y

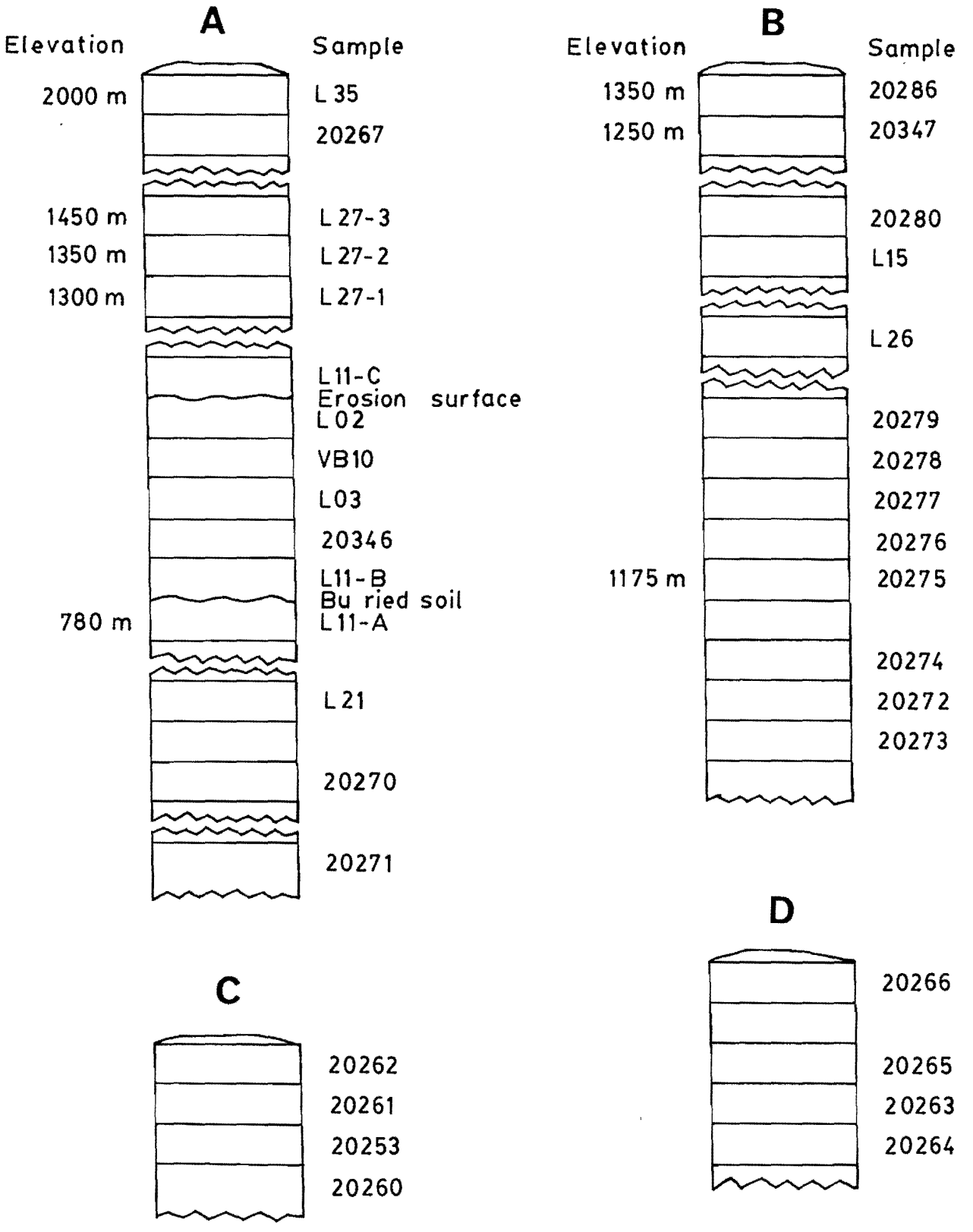

Figure VI.8 Scheme of systematic sampling on Old Galunggung volcanic rocks at SW caldera wall (A), NW caldera wall (B), Gunung Goong (C) and Welirang crater wall (D). All samples are lava flows except for sample number VB 10, 20261 and 20253 which are volcanic bombs.

Table VI.3 Variation of SiO_2, MgO, Cr and Ni contents with stratigraphic position in the Old Galunggung volcanic rocks. A is a section in the SW caldera wall, B is in the NE caldera wall, C is at Gunung Goong, and D is in the Welirang crater wall (see Fig. VI.8).

A

Sample	SiO_2	MgO	Ni	Cr
20258	48.93	10.73	94	395
L 35	52.93	4.49	16	29
20267	52.85	4.62	15	24
L27-3	53.54	4.23	12	16
L27-2	52.64	4.85	13	26
L27-1	51.55	4.66	24	72
L11-C	52.84	3.11	10	14
L 02	52.98	3.38	10	14
VB 10	51.64	3.03	20	47
L 03	54.70	3.01	6	10
20346	54.89	3.11	5	7
L 21	52.89	4.76	18	30
20270	52.90	4.21	13	8
20271	52.45	4.23	12	10

B

Sample	SiO_2	MgO	Ni	Cr
20286	51.69	4.46	15	22
20347	56.07	3.55	9	11
20280	52.10	3.58	13	15
L 15	53.56	4.15	15	34
L 26	54.55	3.66	9	20
20279	52.17	3.58	13	13
20278	52.32	3.21	11	10
20277	52.21	3.36	11	13
20276	52.16	3.40	7	12
20275	51.95	3.12	10	10
20274	52.13	3.35	12	4
20272	52.91	3.32	10	20
20273	52.57	3.27	11	10

C

Sample	SiO_2	MgO	Ni	Cr
20262	50.82	3.45	9	5
20261	53.33	4.49	16	29
20253	52.98	3.95	13	22
20260	56.92	3.41	12	17

D

Sample	SiO_2	MgO	Ni	Cr
20266	52.33	4.52	16	48
20265	52.35	4.23	22	34
20263	50.76	4.66	26	38
20264	50.31	4.60	24	37

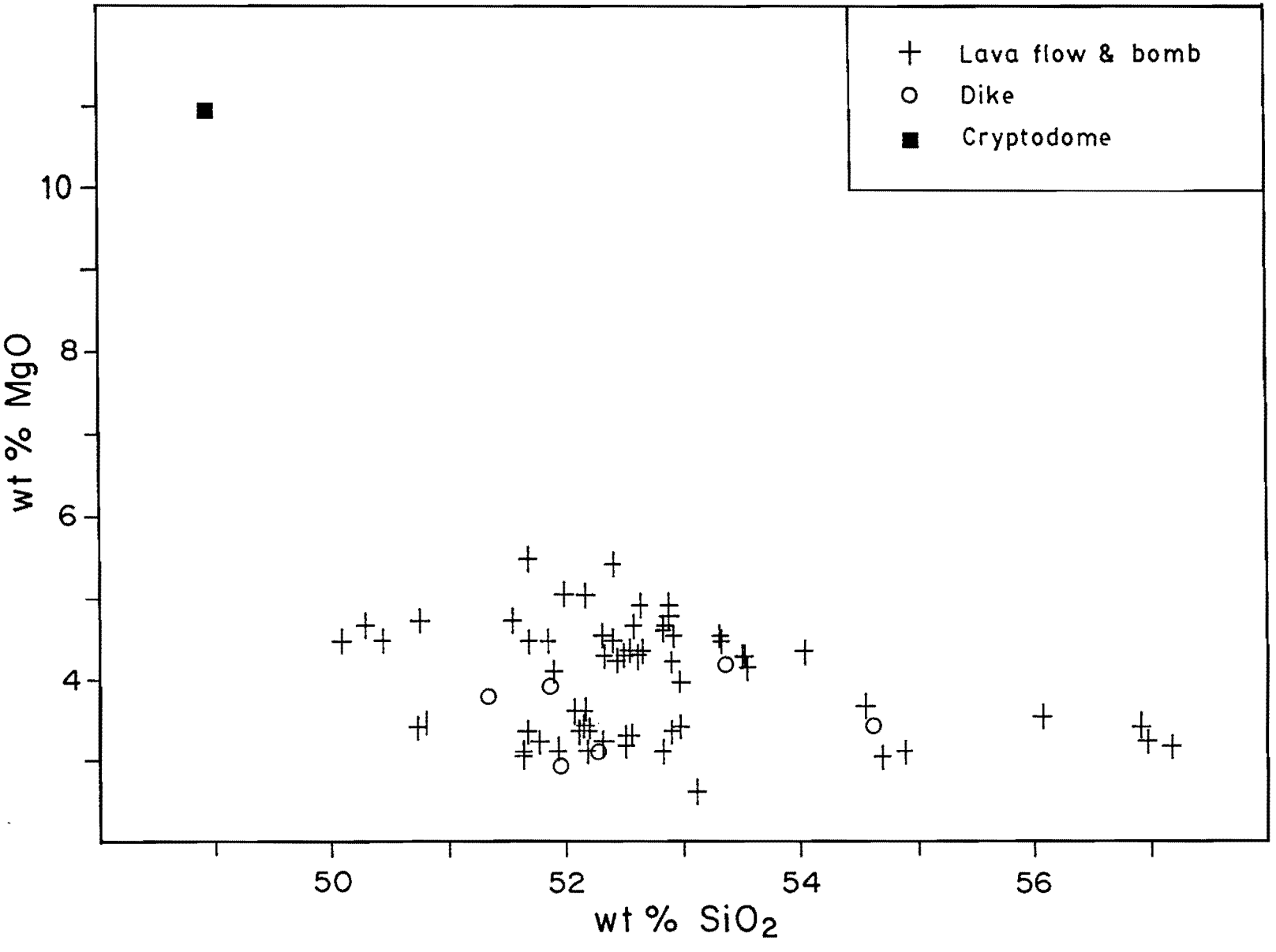

Figure VI.9 Selected variation diagrams for Old Galunggung volcanic rocks.

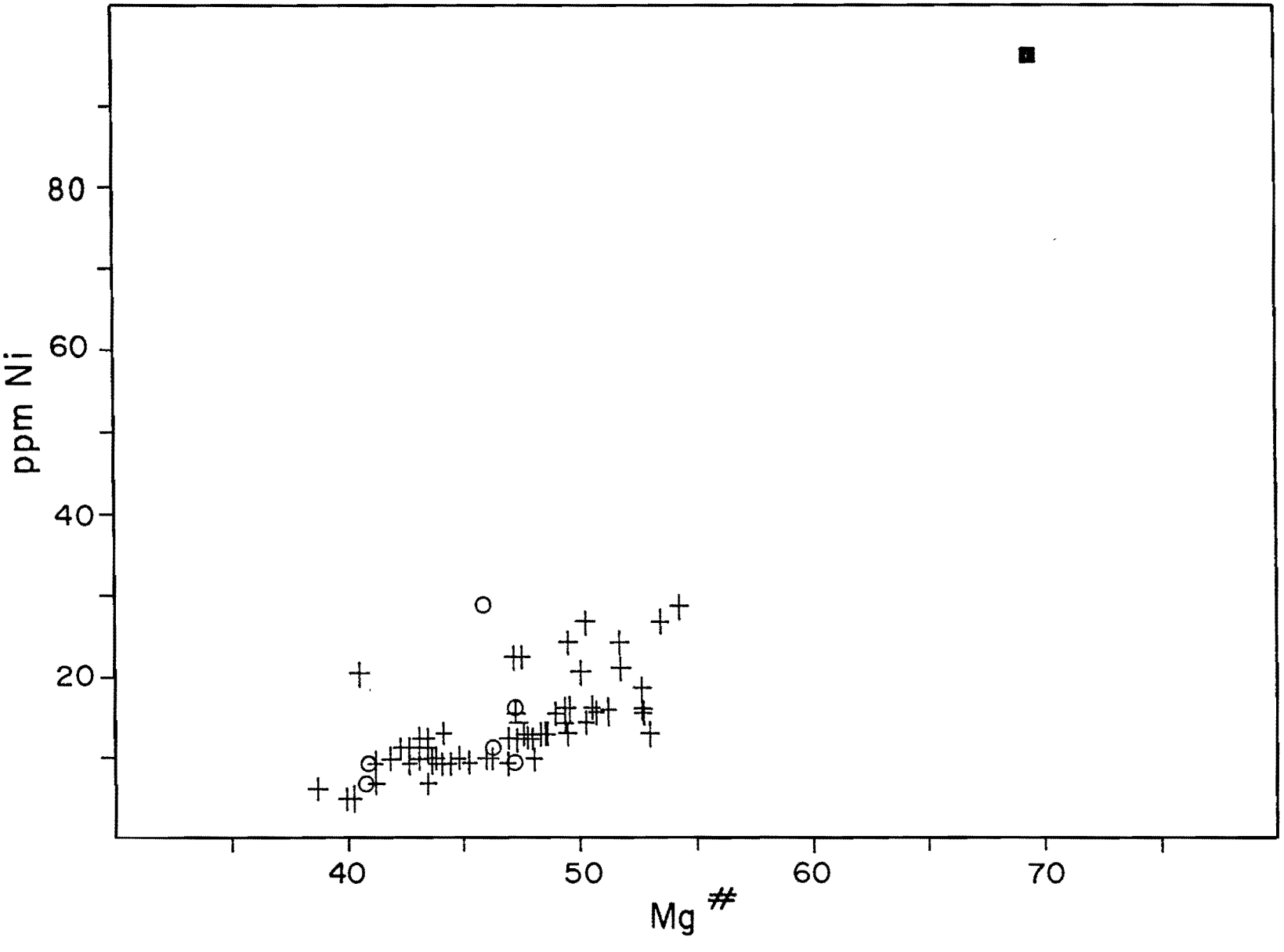
80
60
40
20
ppm Ni
40
50
60
70
Mg #

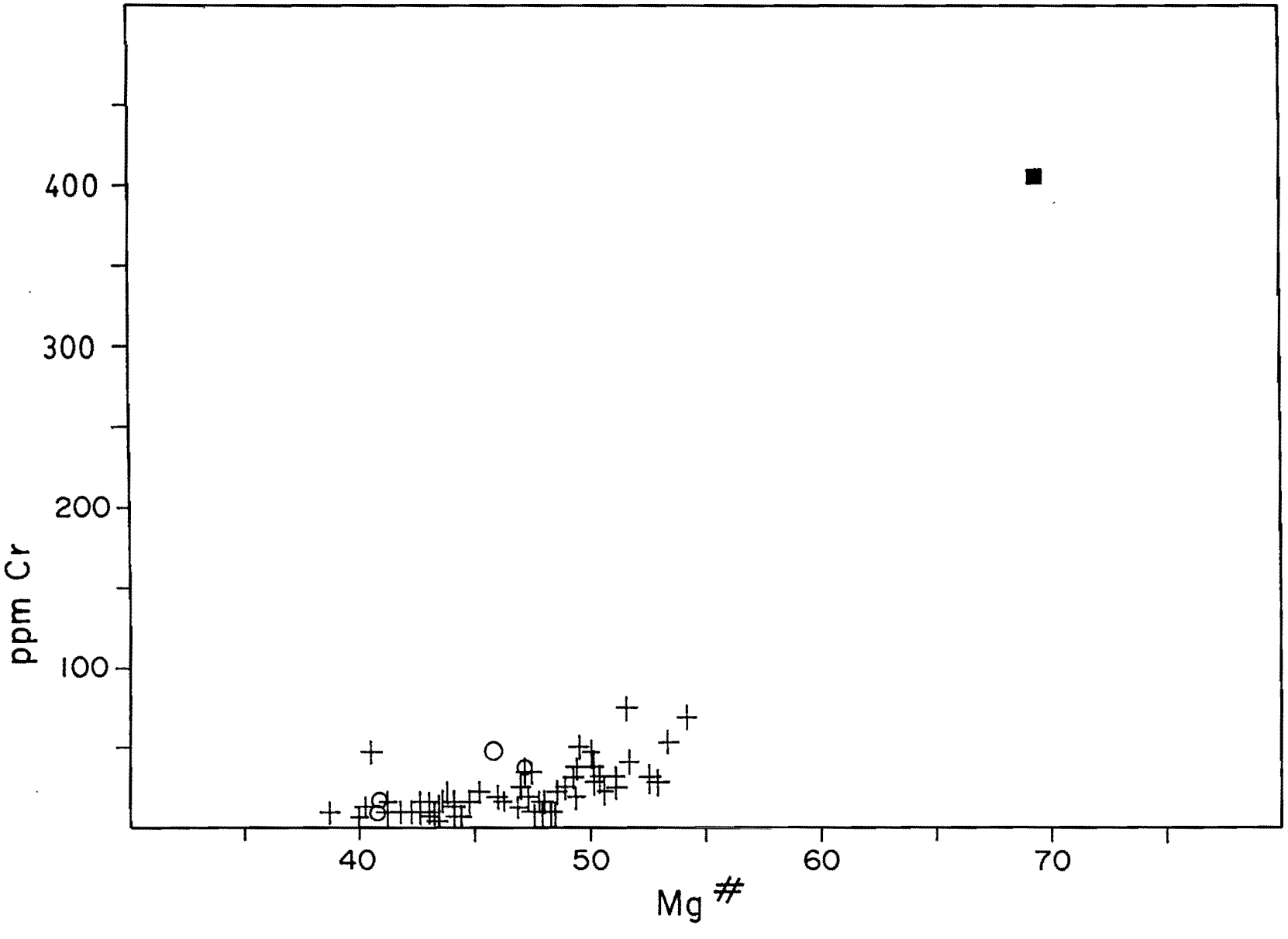
400
300
200
100
ppm Cr
40
50
60
70
Mg #

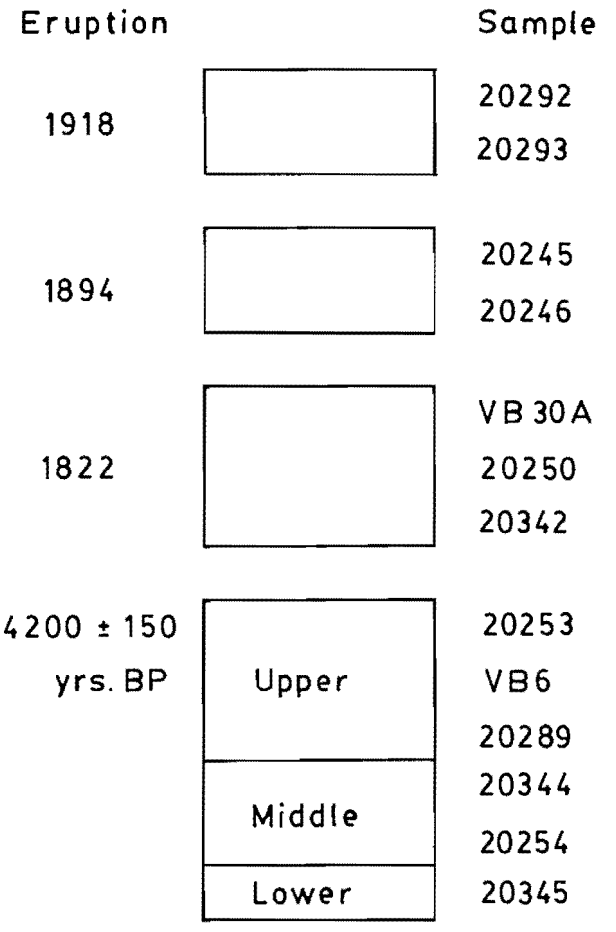

Figure VI.10 Scheme of systematic sampling from 4200 ± 150 yrs. BP (caldera formation) to 1918 eruptions. All collected samples are volcanic bombs from pyroclastic deposits except sample number 20292 and 20293 which are from the 1918 lava dome.

and volcanic bombs (Fig. VI.9). A sharp difference in composition occurs with the Old Galunggung cryptodome which has 49 % SiO_2, 10 % MgO, 395 ppm Cr and 94 ppm Ni. Although this cryptodome has slightly higher K_2O and Rb contents its K/Rb ratio is similar to other Old Galunggung rocks.

Figure VI.10 shows systematic sampling from caldera forming event up to the 1918 eruption although the number of samples collected is limited, because of sparse outcrops, oxidation and alteration of the rocks. Volcanic rocks erupted during the caldera formation do not show an obvious trend in composition from lower to upper parts (Fig. VI.11). Although SiO_2 contents vary from 50 % to 56 % SiO_2 the rocks all have < 6 % MgO, < 83 ppm Cr and < 37 ppm Ni. Volcanic rocks erupted in 1822, 1894 and 1918 have similarly low Mg, Cr and Ni contents.

The 1982-83 eruption provides an excellent opportunity to study the change in rock chemistry with time. In the initial stage (5 April 1982) the 1982-83 volcanic rocks have about 57 % SiO_2, < 5 % MgO, < 100 ppm Cr and < 30 ppm Ni (Fig. VI.12). These are similar to composition of previous rocks, mainly the 1918 lava dome with similar silica, low-Mg, Cr and Ni contents. In the final stage (September 1982 - January 1983) rocks have 49 % SiO_2, 10 - 12 % MgO, 500 - 700 ppm Cr and 130 - 190 ppm Ni. This composition is considered to be a basaltic primary magma (e.g. BVSP, 1981). Incompatible element contents in these high-Mg basalts are very low, e.g. 30 - 88 ppm Ba, 6 - 8 ppm Rb and 197 - 219 ppm Sr. Other major and trace elements also form a linear trend with time and decreasing SiO_2 content, with increasing of FeO*, CaO, TiO_2, V and Sc and decreasing Al_2O_3, Na_2O, K_2O, P_2O_5, Zr, Y and Ga. CIPW norm compositions of the rocks erupted in the initial stage

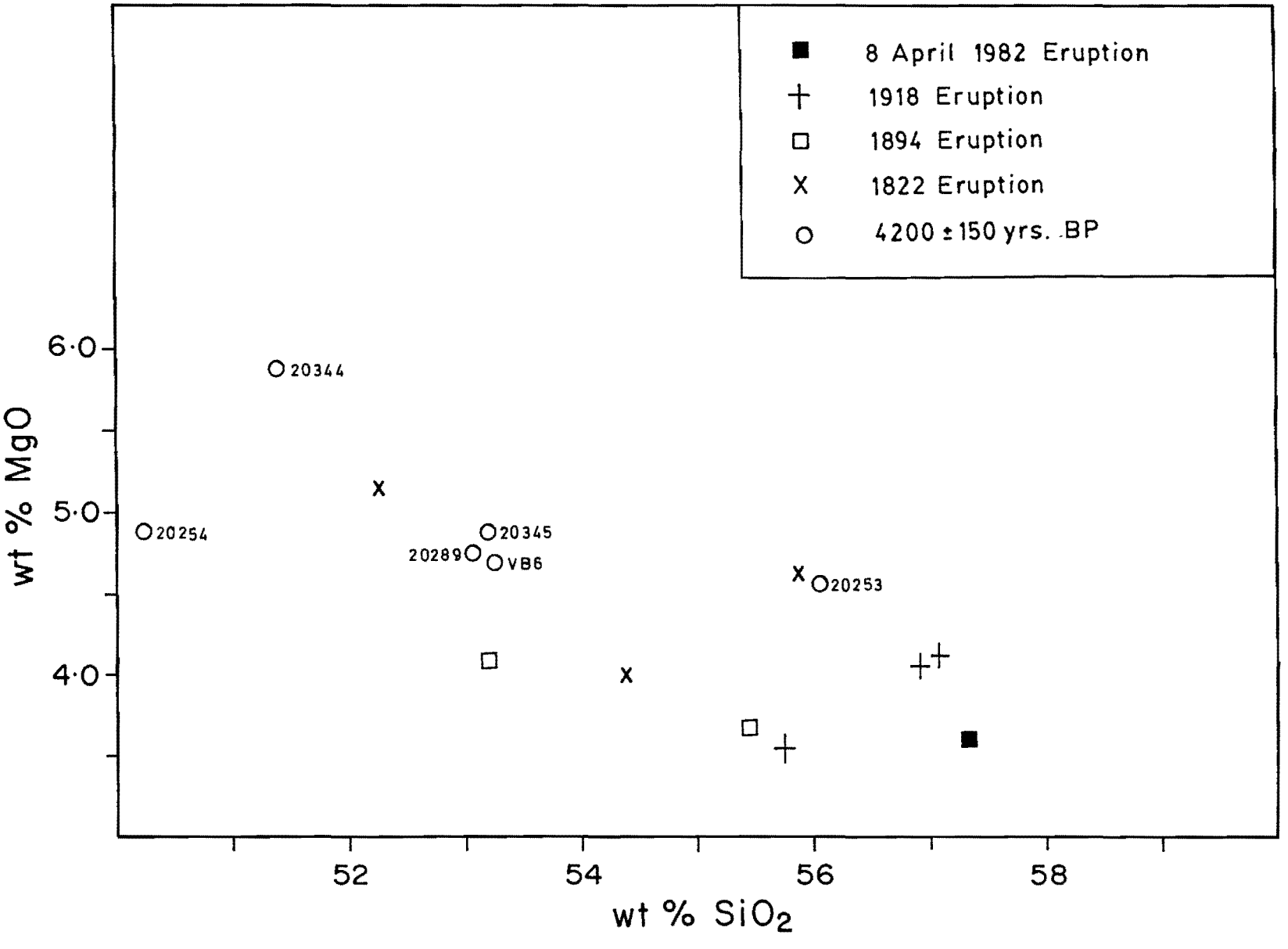

Figure VI.11 Selected variation diagrams for Galunggung volcanic rocks erupted in 4200 ± 150 yrs. BP (caldera formation) and historic times.

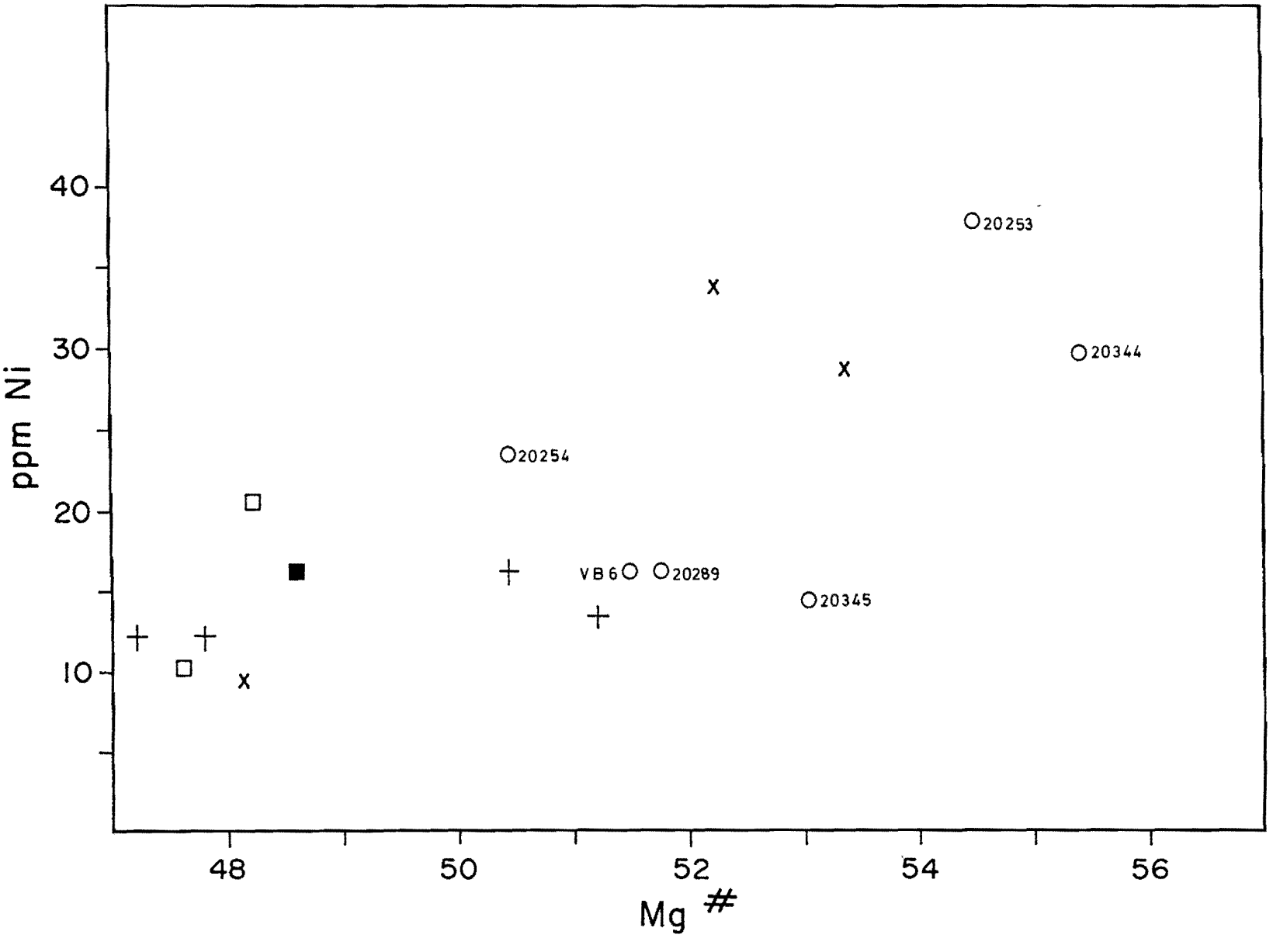
ppm Ni
40
30
20
10
48
50
52
54
56
Mg #
20253
20344
20254
VB6
20289
20345

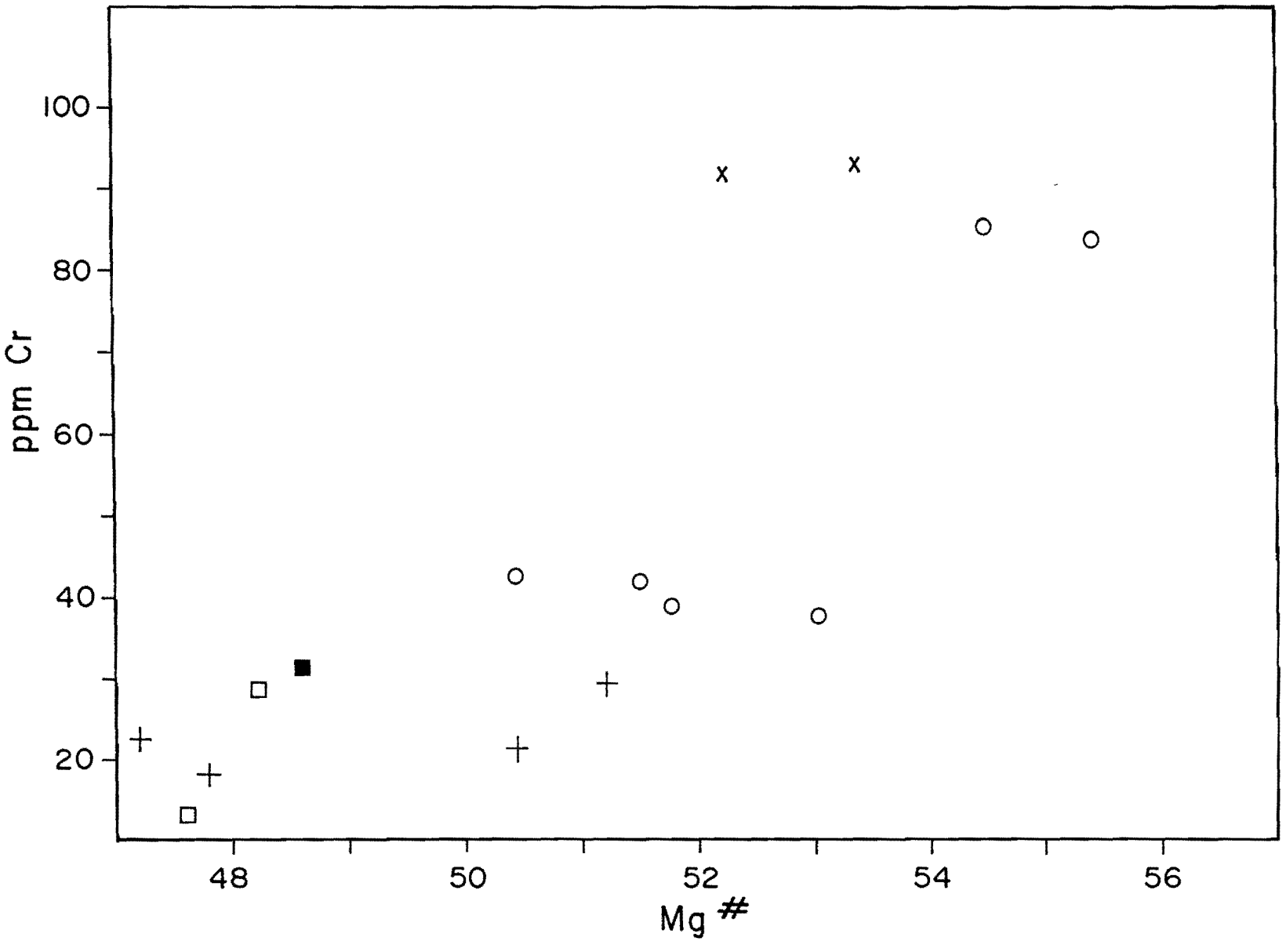
100
80
60
40
20
ppm Cr
48
50
52
54
56
Mg #

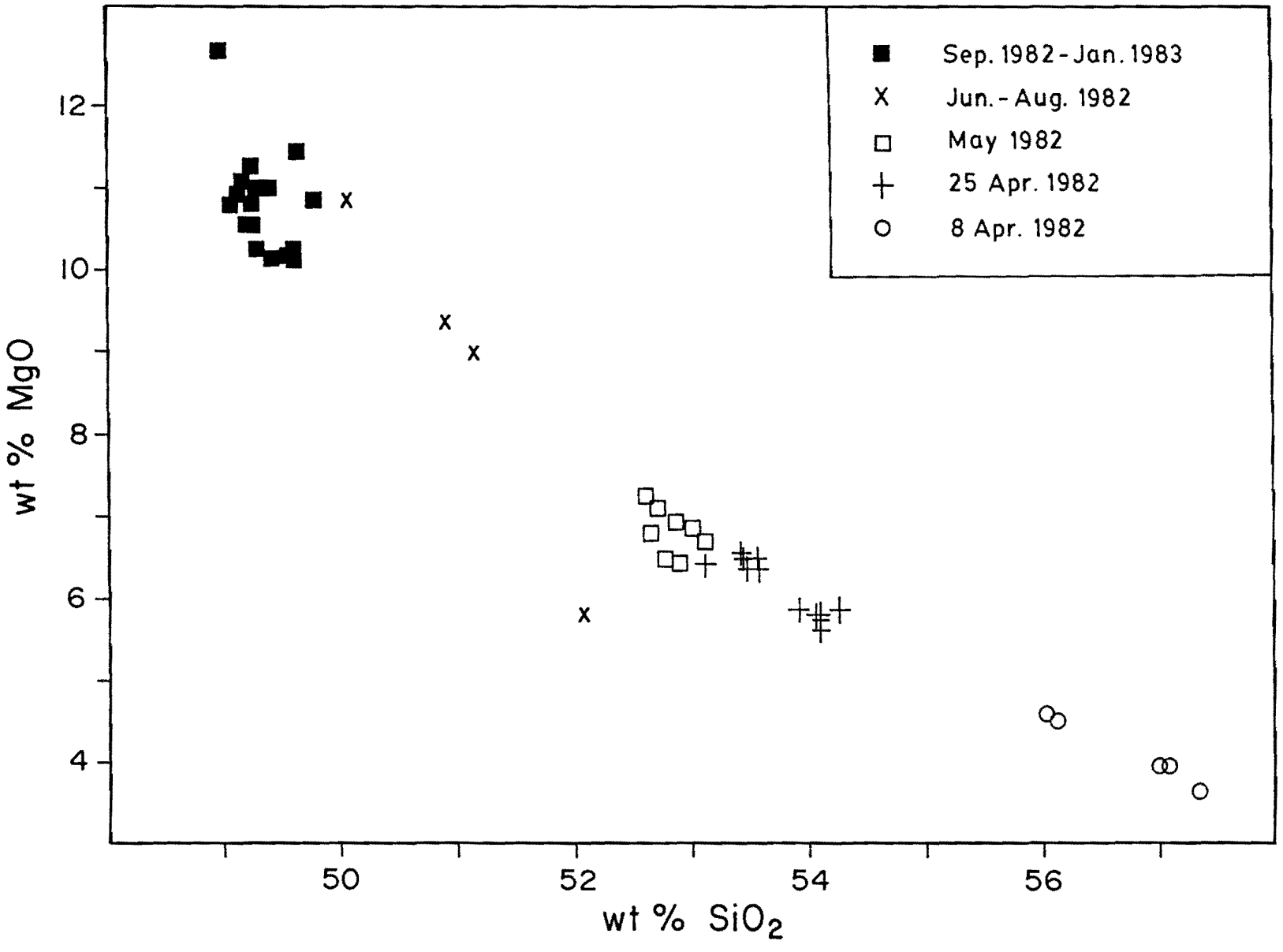

Figure VI.12 Selected variation diagrams for Galunggung volcanic rocks erupted in 1982-83.

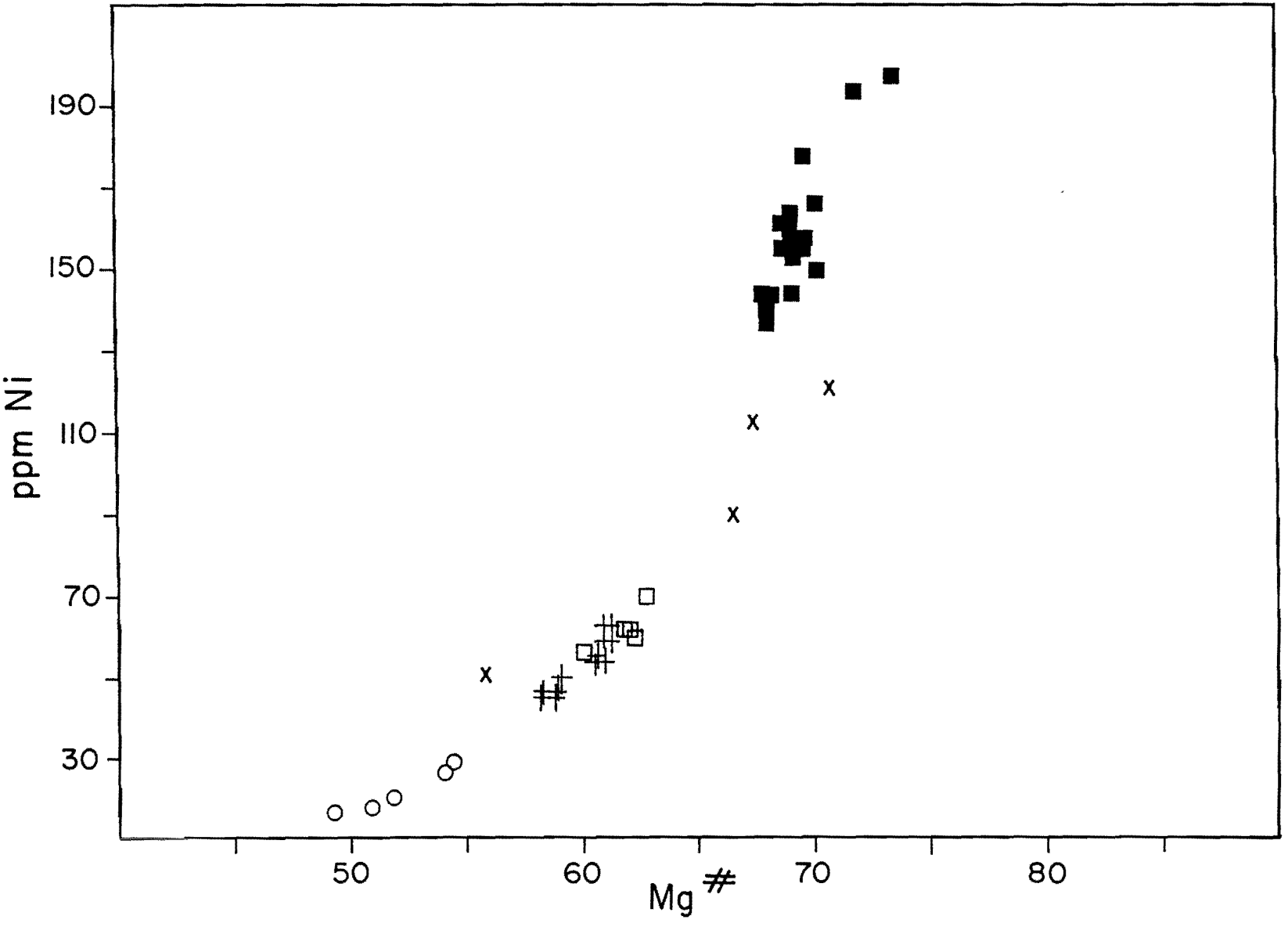
ppm Ni
190
150
110
70
30
50
60
70
80
Mg #

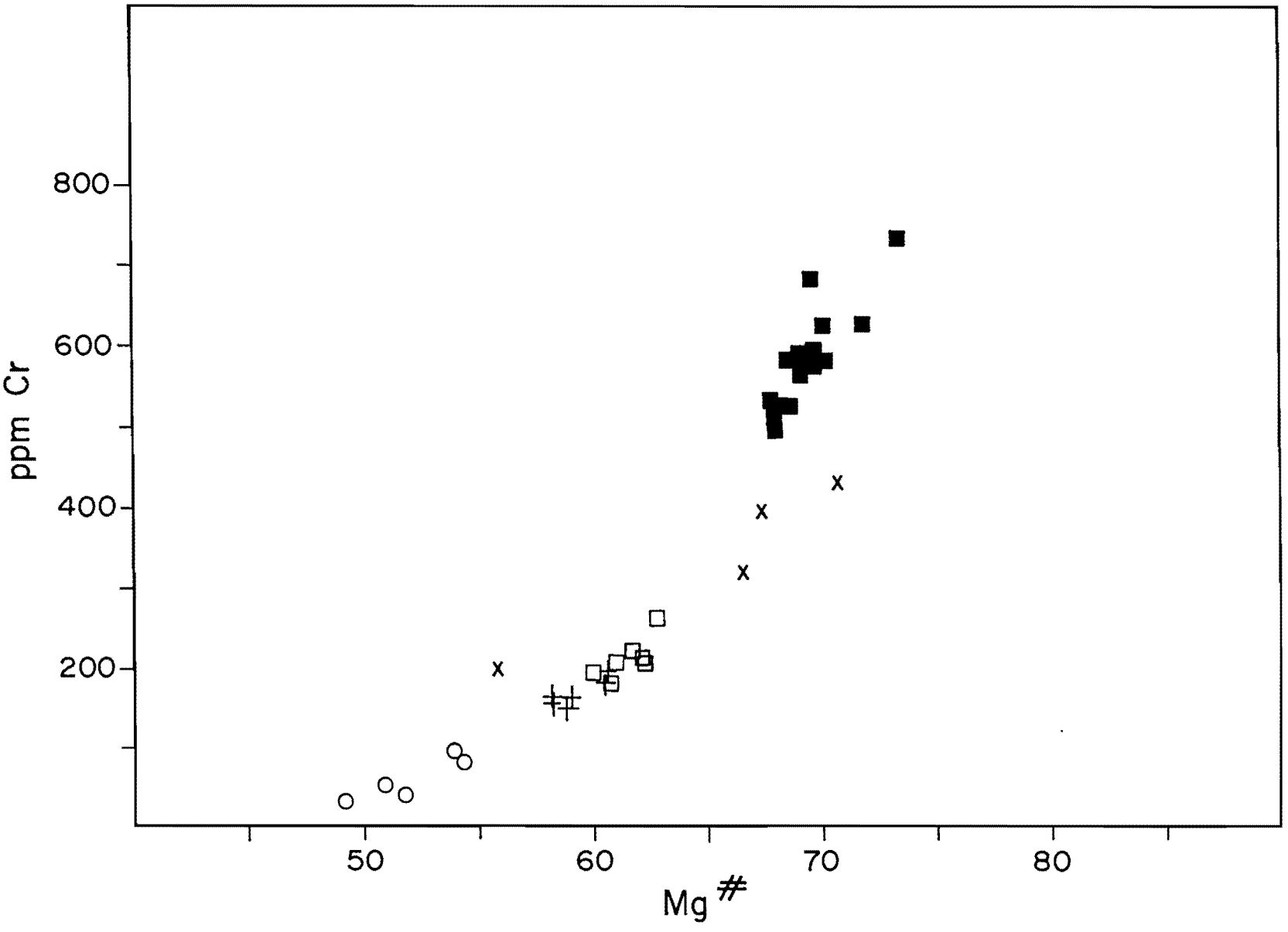
800
600
400
200
ppm Cr
50
60
70
80
Mg #

are Q-Hy normative (< 8 % quartz normative); while the products of the final stage are Ol-Hy normative (up to 17 % olivine normative). The compositional change occurred gradually during Vulcanian eruptions between June and August 1982.

VI.8 Comparison of Volcanic Rocks between Galunggung and Other Convergence Plate Volcanoes

Basaltic andesites and low-Mg basalts, which are very common at Galunggung, have similar characters to those of continental plate margin and island arc volcanoes. For example, they have low Mg, Ni and Cr contents (Ewart, 1976; Jakes & White, 1971; Perfit et al., 1980a). However, the high-Mg basalts found at Galunggung are uncommon and volumetrically less than the low-Mg basalts. Figure VI.13 presents a comparison of high-Mg basalts from Galunggung and other volcanoes in the same tectonic setting. Ni and Cr show a positive relationship to the Mg contents in the rocks. This suggests that all of the high-Mg basalts are controlled by Fo-rich olivine and Cr-spinel compositions as the earliest phases to begin crystallising (Cox et al., 1981). Slightly different trends between the arcs may imply variation in Mg and Ni content during crystal fractionation. Compared with high-Mg basalts from other island arc volcanoes, the Galunggung high-Mg basalts have relatively low contents of total Fe (8.5 - 9.0 % FeO*), Mn (0.15 % MnO), K (0.4 % K_2O), P (0.1 % P_2O_5), Ba (50 ppm), Rb (7 ppm) and Sr (200 ppm), moderate contents of Ti (0.8 % TiO_2), Ca (11.5 % CaO) and Na (2.3 % Na_2O), and slightly high contents of Al (16 % Al_2O_3).

Figure VI.13 Selected variation diagrams comparing high-Mg basalts from Galunggung and other arc volcanoes. In diagram Sr against Na_2O + K_2O, the high-Mg basalts are grouped into : high (A), medium (B) and low (C) LIL elements. References data are compiled from : Aleutian Islands (Gust & Perfit, 1987; Kienle et al., 1980; Nye & Reid, 1986; Perfit et al., 1980b), Fiji (Gill, 1970), Grenada, Lesser Antilles (Brown et al., 1977),Japan (Katsui et al., 1978; Oba, 1972; Yamamoto, 1984 & 1988), Manam volcano (Johnson et al., 1985), New Britain (Johnson, 1977; Johnson & Chappell, 1979; BVSP, 1981), New Georgia (Solomon Islands, Ramsay et al., 1985; Stanton & Bell, 1969), New Hebrides (Vanuatu Islands, Barsdell et al., 1982; Crawford et al., 1987; Gorton, 1977), New Zealand (Cole, 1973; Graham & Hackett, 1987), and Rinjani volcano (Foden, 1983). Major elements are normalised to 100 % anhydrous and Fe_2O_3/FeO = 0.15.

See p. 232 for key

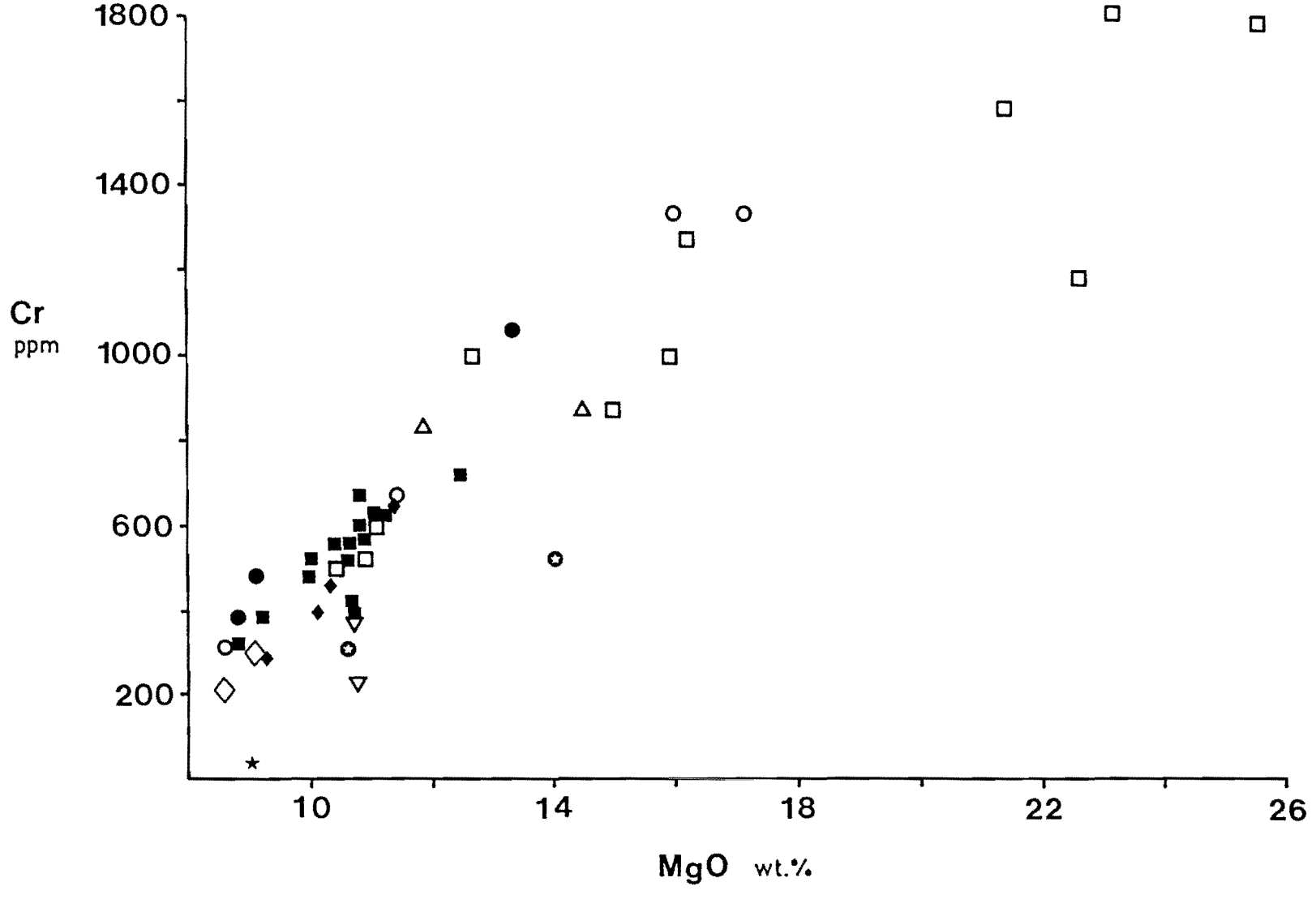

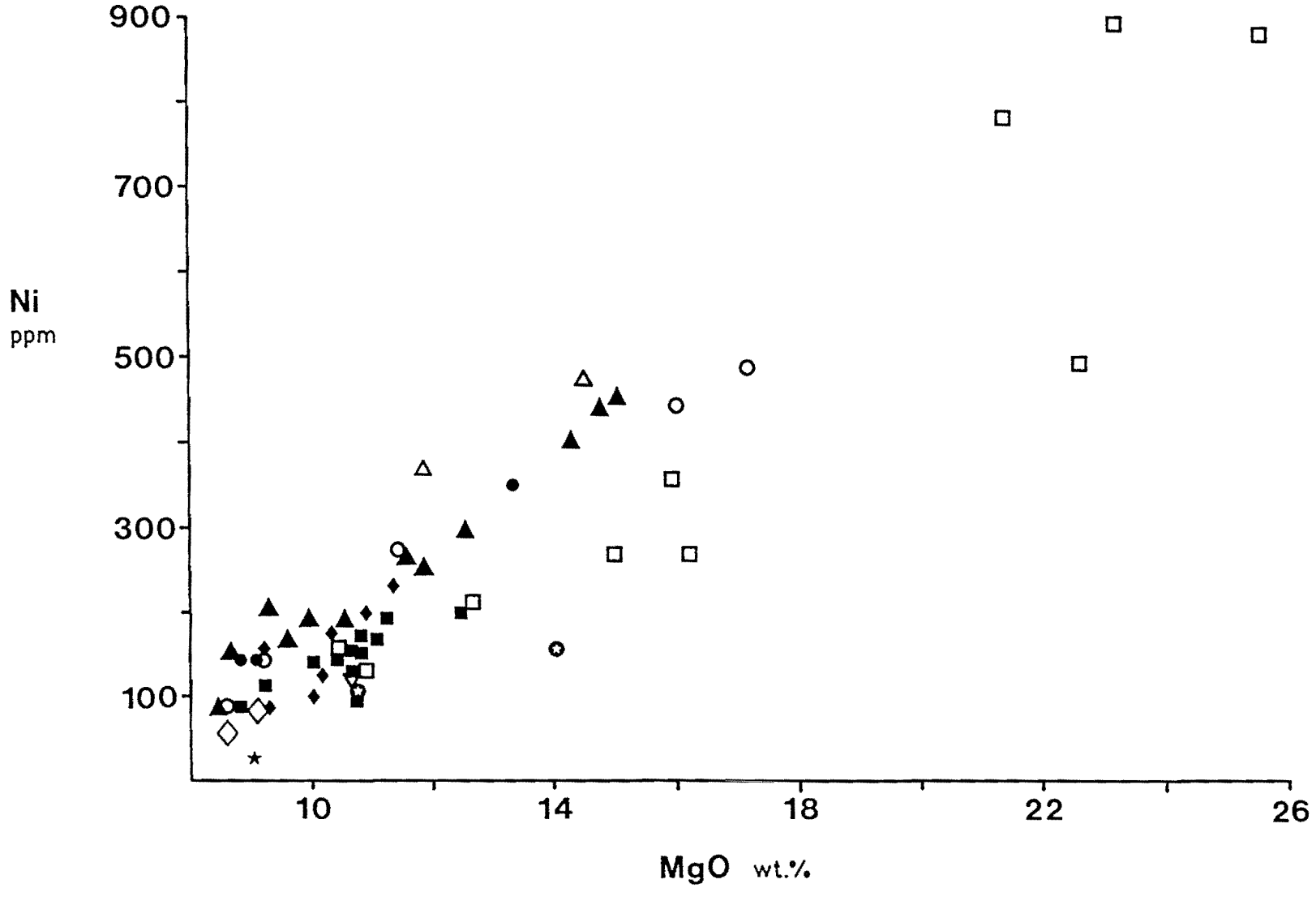
900
700
500
300
100
Ni
ppm
10
14
18
22
26
MgO wt.%

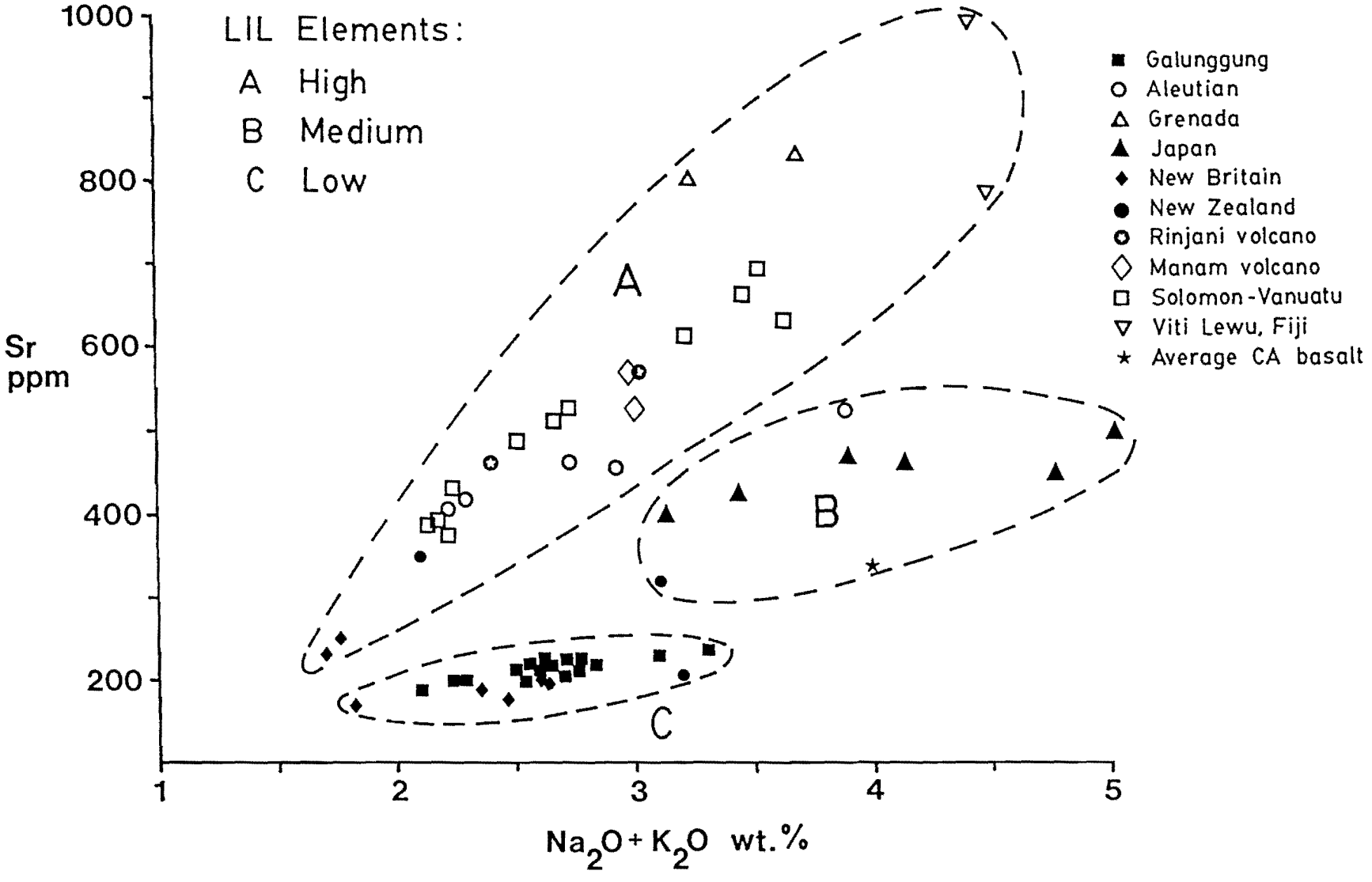
LIL Elements:
A High
B Medium
C Low
A
B
C
Galunggung
Aleutian
Grenada
Japan
New Britain
New Zealand
Rinjani volcano
Manam volcano
Solomon-Vanuatu
Viti Lewu, Fiji
Average CA basalt
Sr ppm
1000
800
600
400
200
1
2
3
4
5
$Na_2O + K_2O$ wt.%

A discrimination diagram using Sr against total alkali (Fig.VI.13C) clearly separates three groups of high-Mg basalts with high, medium and low incompatible elements (LIL elements) respectively. High-Mg basalts which consistently fall within the first group occur in Grenada (Brown et al., 1977), Manam volcano (Johnson et al., 1985), Rinjani volcano (Foden, 1983), Solomon (Ramsay et al., 1984; Stanton & Bell, 1969), Vanuatu (Barsdell et al., 1982; Crawford et al., 1987; Gorton, 1977), and Viti Lewu, Fiji (Gill, 1970). Although most high-Mg basalts from Aleutian Islands (Gust & Perfit, 1987; Nye & Reid, 1986; Perfit et al., 1980b) enter the first group, a rock sample erupted in historic time (April 1977) from Ukinrek Maars, Alaska (Kienle et al., 1980) probably can be included into the second group. The high Mg-basalts from Japan (Katsui et al., 1978; Oba, 1972; Yamamoto, 1984 & 1988) are predominant in the second group.

Two rock samples from New Britain (BVSP, 1981; Johnson, 1977; Johnson & Chappell, 1979) may be included in the first group but most fall within the third group. These are the only high-Mg basalts comparable with those of Galunggung. Data from New Zealand does not fall in a single group. This is due to crystal accumulation, as reported by Cole (1973) and Graham & Hackett (1987).

Overall, the lower content of incompatible element abundances of Galunggung high-Mg basalt is consistent with the suggestion of a depleted magma source, whereas other rocks of the first two groups were derived from enriched magma sources. However, the different Sr content could indicate they are different magma types.

VI.9 Comparison of High-Mg Basalts between Galunggung and Mid-Oceanic Ridge Basalts

Galunggung high-Mg basalts have a porphyritic texture, whereas mid-oceanic ridge basalts (MORB) display a large range in petrography from aphyric to coarsely phyric types (Wood et al., 1979). The varied textures are very dependent on cooling unit size and the nature of the liquidus phases (Bryan et al., 1976). However, mineralogical and chemical compositions of the Galunggung high-Mg basalts are similar to those of "Group I" (Bryan et al., 1976), or "normal" (N-type) (MORB's incompatible element depleted tholeiites; Shibata et al., 1979). The high-Mg basalts consist of Fo-rich olivines, diopsidic pyroxenes, Cr-spinels and calcic plagioclases. The bulk rock compositions have constant SiO_2 values, low K abundances, low K/Na ratios and low LIL elements content. This similarity supports the suggestion of Perfit et al. (1980a), and Gust & Perfit (1987) that primitive volcanic arc basalts resemble primitive MORB, and therefore could be derived from similar upper mantle sources.

Figure VI.14 illustrates a comparison between high-Mg basalts from Galunggung and Atlantic Ocean at 36°N (Wood et al., 1979; samples 411-1 and 413-1) and at 43°N (Shibata et al., 1979, samples 11-3, 11-37 and 11-90), Pacific Ocean (Kay et al., 1970; location 7°58' - 108°08'W, sample D1), Indian Ocean (Fleet et al., 1976, sample site 250 A-1 in Mozambique Basin and 257 core 11-6 in West of Australia), and Tyrrhenian Sea floor (Dietrich et al., 1977). No high-Mg basalts are found in northeastern Indian Ocean (Thompson et al., 1972) which is close to Indonesian volcanic arc. All basalts from the west flank of the East Pacific Rise (Yeats et al., 1972) are geochemically

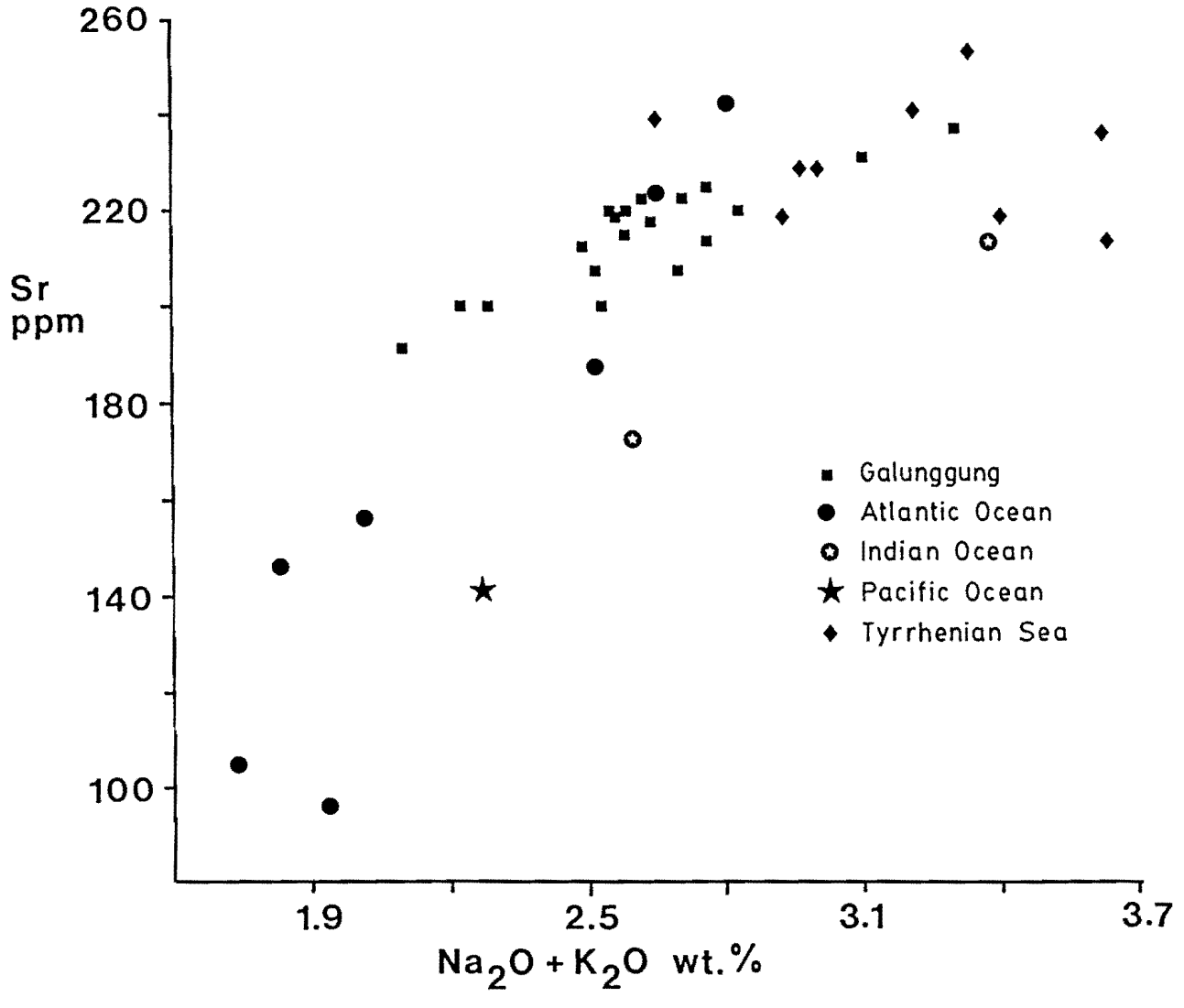

Figure VI.14 Selected diagram comparing high-Mg basalts from Galunggung, Atlantic Ocean (Shibata et al., 1979; Wood et al., 1979), Indian Ocean (Fleet et al., 1976), Pacific Ocean (Kay et al., 1970), and Tyrrhenian Sea (Dietrich et al., 1977).

homogeneous tholeiites but their Mg numbers are low (< 68). Only one sample taken from a seamount (Kay et al., 1970) is included but its petrographic view is typically plagioclase-phyric. Basalts from Tyrrhenian Sea floor (Dietrich et al., 1977) are well crystallised and have intergranular textures of plagioclase, clinopyroxene and magnetite phenocrysts in an intersertal groundmass.

The Galunggung high-Mg basalts have a more gentle slope compared with those from Atlantic Ocean, and are closer in composition to high-Mg basalts from Indian Ocean which have lower Sr contents. High-Mg basalts from Tyrrhenian Sea floor are relatively constant in composition with high total alkali (> 2.5 %) and Sr (>200 ppm). This is consistent with petrographic data. The different slope between Galunggung high-Mg basalts and MORB is also shown in spider diagrams (Fig. VI.7). These also indicate that although the Galunggung high-Mg basalts can be compared with N-type (depleted) MORB, they were derived from different magma sources.

VI.10 Gabbro

Major elements apparently show a systematic variation from gabbro affected by thermal metamorphism through gabbro having short prismatic amphiboles to gabbro having highly elongated amphiboles (Table VI.4). This trend, however, does not correlate with trace element data. Ni and Cr are very low although Mg content reaches up to 10.5 % MgO.

Compared with the Galunggung volcanic rocks, gabbro is lower in Si content. This is due to the dominant amphibole and plagioclase min-

Table VI.4 Bulk rock chemical compositions of gabbro clasts compared with hornblende gabbroic inclusions from NE Japan (Yamazaki et al., 1965), amphibolites (Heier, 1962; Evance & Leak, 1960) and appinite (Nockolds, 1940).

	20252	20256	20257	SG-1	KJ-1	AMP-1	AMP-2	APPNT	RAGF	T4	T6
SiO_2	44.21	44.10	46.84	40.22	41.56	49.45	48.13	48.68	43.13	50.03	52.19
TiO_2	1.02	0.95	1.06	1.55	1.30	0.72	1.87	1.34	2.10	0.88	0.70
Al_2O_3	16.71	22.22	21.26	21.74	22.36	17.13	17.34	17.66	17.78	18.93	20.93
FeO*	12.27	9.95	8.75	9.00	7.75	9.73	10.44	8.67	12.24	8.56	6.71
MnO	0.17	0.17	0.10	0.09	0.11	0.14	0.22	0.03	0.03	0.19	0.19
MgO	10.48	5.99	5.73	7.08	8.36	7.24	6.58	7.78	9.09	4.52	2.64
CaO	13.13	12.71	12.24	13.51	14.00	9.64	8.09	9.32	13.13	9.50	8.20
Na_2O	1.36	1.74	2.52	2.07	1.27	3.48	3.95	2.22	1.92	3.51	4.15
K_2O	0.10	0.16	0.29	0.49	0.61	0.89	0.76	1.90	0.47	3.27	3.71
P_2O_5	0.05	0.05	0.06	0.05	0.04	0.11	0.24	0.13	0.04	0.48	0.53
LOI	- 0.47	0.41	0.12	3.34	2.20	1.49	2.00	1.96	-	0.74	0.70
Total	99.03	98.45	99.37	99.14	99.56	100.02	99.62	99.69	99.93	101.00	99.69
Sr	253	350	296	326	-	-	-	-	-	-	-
Zr	9	24	33	17	-	-	-	-	-	-	-
Nb	4	5	3	5	-	-	-	-	-	-	-
Y	10	18	13	9	-	-	-	-	-	-	-
Ce	< 5	8	9	5	-	-	-	-	-	-	-
Nd	10	19	14	18	-	-	-	-	-	-	-
V	448	271	355	189	-	-	-	-	-	-	-
Cr	119	28	30	14	-	-	-	-	-	-	-
Ni	11	18	14	22	-	-	-	-	-	-	-

20252 Gabbro clast affected by thermal metamorphism
20256 Gabbro clast with short prismatic amphiboles
20257 Gabbro clast with long prismatic amphiboles
SG-1 Hornblende gabbroic inclusion, after Yamazaki et al., 1965
KJ-1 Hornblende gabbroic inclusion, after Yamazaki et al., 1965
AMP-1 Amphibolite, after Heier, 1962
AMP-2 Amphibolite, after Evance & Leak, 1960
APNT Appinite, after Nockolds, 1940
RAGF Gabbro clast from Rinjani (Foden, 1983)
T4 Nodule of alkali gabbro from Tambora (Foden, 1986)
T6 Nodule of alkali gabbro from Tambora (Foden, 1986)

eral compositions in the intrusive rock. Figure VI.15 represents incompatible element content in gabbro compared with that in Galunggung volcanic rocks and does not show a systematic relationship.

The scattered trace element content in gabbro may be a result of thermal metamorphism or due to the present of injected basaltic magma into the intrusive rock. This injection is considered as "mixing", so that bulk chemical composition cannot be used directly to evaluate trends of crystal fractionation or various melting process during magma generation (O'Hara, 1977).

However, two analyses of the Galunggung gabbro (Table VI.4, 20256 and 20257) can be compared with those from Central Japan (Yamazaki et al., 1965) in having low Si but high Al and Ca contents, and very calcic plagioclase (up to An_{95}). These are not expected in ordinary amphibolite plutons (e.g. Heier, 1962; Evance & Leak, 1960; Nockolds, 1940), but are suggested to form at the base of the crust (Yamazaki et al., 1965). Similarly, Foden (1983) has suggested that an amphibole-gabbro from Rinjani volcano (RAGF) that is comparable to the Galunggung gabbro affected by thermal metamorphism (20252) was generated in the lower crust of Sunda Arc. The low Al content in the Galunggung gabbro (and Rinjani gabbro ?) is probably due to thermal metamorphism and recrystallisation of clinopyroxene from amphibole. Another gabbro analysis (20327) that was ejected on 8 April 1982 is close to alkali gabbro of Tambora, except for K content (Foden, 1986). However, the Tambora alkali gabbro has biotite, apatite and alkali feldspar but not amphibole, and the high Si but low Ca contents in the Galunggung gabbro are probably influenced by the composition of injected magma (sample no. 20325 has 56 % SiO_2 and 8 % CaO). The origin of Galunggung gabbro is discussed together with amphibole in chap-

Figure VI.15 Sr vs SiO_2 in gabbro and volcanic rocks from Galunggung.

■ Gabbro affected by thermal metamorphism

○ Gabbro having short prismatic amphiboles

□ Gabbro having highly elongated amphiboles

+ Volcanic rocks erupted in 1982-83

X Pre-1982 volcanic rocks

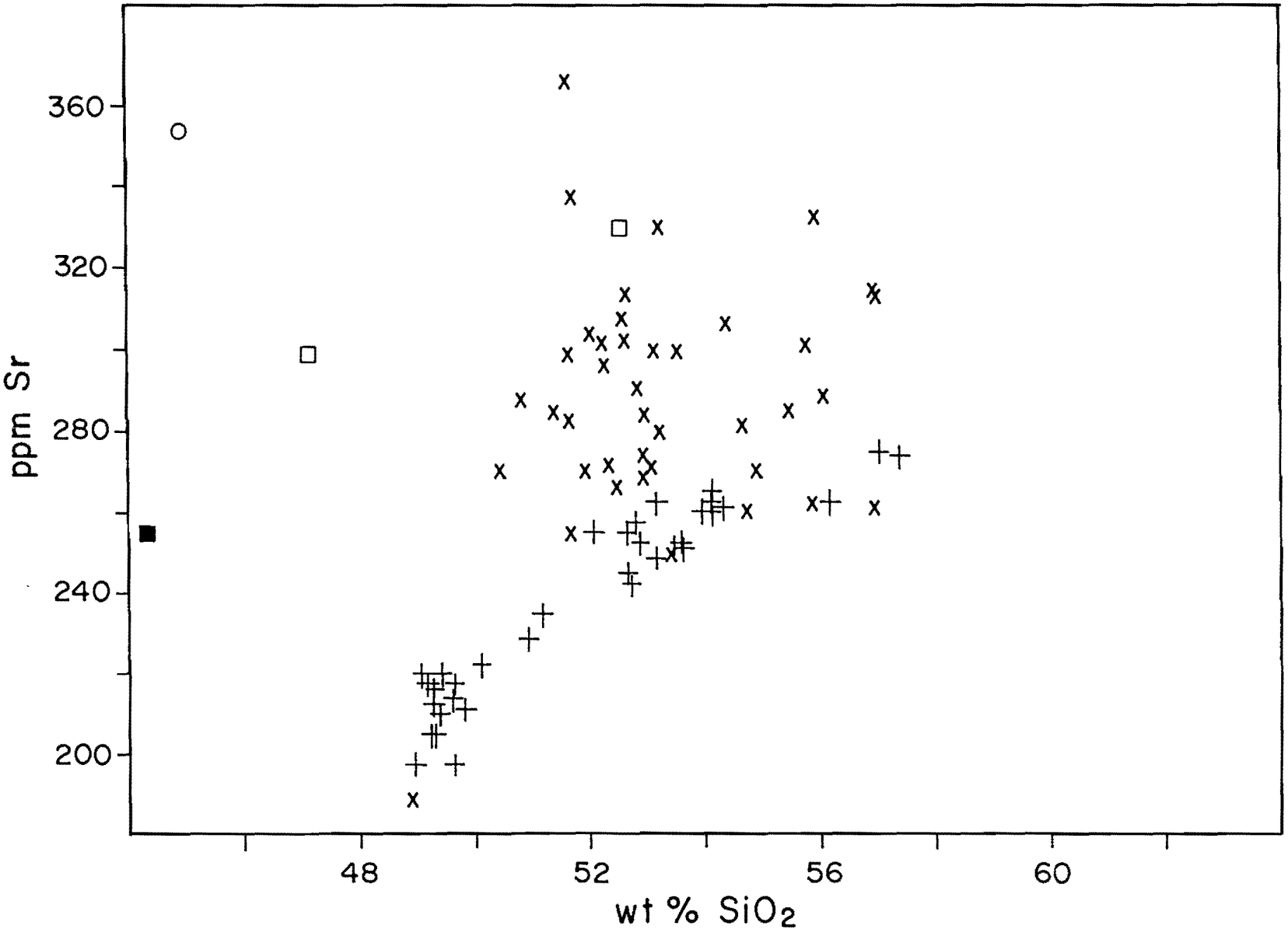
360
320
280
240
200
ppm Sr
48
52
56
60
wt % SiO2

ter VII.

VI.11 Rhyolite

There is a considerable gap in composition between Galunggung evolved rocks (basaltic andesite, up to 57 % SiO_2, Table VI.5) and the Galunggung rhyolite pumice (> 71 % SiO_2) that was only observed during the eruption of September 1982 when high-Mg basalts were erupted. Galunggung rhyolite reaches 30 % normative Qz whereas that in the Galunggung basaltic andesites it is less than 8 %. Consequently, a sharp decrease occurs in most major elements (except for Si, Na and K) and compatible trace elements from the basaltic andesite to rhyolite, probably indicating crystal fractionation of mafic minerals. Calcic plagioclase fractionation may be reflected by decreasing Al and Sr but sharply increasing K, Ba and Rb contents.

A spidergram of the Galunggung rhyolite normalised to primordial mantle composition is flatter than that normalised to average MORB (Fig. VI. 16). This pattern is similar to the spidergrams of other Galunggung volcanic rocks (see Fig. VI. 6-7). The regular increase of incompatible element abundances from the general rocks to rhyolite may indicate crystal fractionation.

Major element compositions of Galunggung rhyolite are comparable with those from Toba (Kusnaeny, 1977; Ninkovich et al., 1978; Rock et al., 1982), Krakatau (Camus et al., 1987) and Rabaul (Heming & Carmichael, 1973). Pumice from Batur (Wheller & Varne, 1986a,b), Rinjani (Foden, 1983), Mt. Pelée (Dupuy et al., 1985) and St. Helens (Scarfe & Fujii, 1987) is dacite, whereas that of Tambora (Self et al., 1984)

Table VI.5 Compositional variation of most Galunggung evolved rocks compared with those from other areas.

	20294	GLG	TOBA	KKT-1	KKT-2	KKT-3	BTR	RJN	TBR	RBL	ELCHN	PELE	STHEL
	(1)	(1)	(2)	(1)	(4)	(1)	(3)	(2)	(2)	(1)	(2)	(7)	(2)
SiO_2	57.00	71.39	72.76	66.00	69.64	77.36	65.43	65.91	57.07	76.60	57.58	63.14	62.35
TiO_2	.70	.24	.25	1.14	.85	.77	.72	.61	.61	.34	.72	.45	.73
Al_2O_3	18.40	15.36	13.61	15.23	15.14	12.26	16.18	16.76	19.85	12.76	18.39	17.38	17.83
Fe_2O_3	.92	.32	.34	.77	.47	.40	.70	.53	.67	.23	.70	.78	.66
FeO	6.16	2.18	2.26	5.10	3.14	2.68	4.64	3.04	4.43	1.58	4.70	5.22	4.41
MnO	.15	.09	.03	.16	.13	.07	.21	.12	.20	.08	.19	.17	.09
MgO	3.91	.90	.46	1.87	1.03	.26	1.07	1.13	1.57	.43	2.20	2.07	2.39
CaO	8.16	3.16	2.46	3.73	3.42	1.00	3.16	2.81	4.26	1.67	7.84	5.92	5.56
Na_2O	3.68	4.10	3.52	3.94	4.16	2.22	5.41	4.96	5.03	4.19	4.48	3.59	4.58
K_2O	.76	2.16	4.28	2.07	2.02	2.98	2.24	3.97	5.93	2.06	2.83	1.09	1.23
P2O5	.16	.09	.07	-	-	-	.25	.19	.39	.04	.38	.19	.18
Total	100.00	100.00	100.00	100.00	100.00	100.00	100.00	100.00	100.00	100.00	100.00	100.00	100.00
Ba	176	315	-	-	-	-	466	-	-	-	758	210	-
Rb	18	70	144	-	-	-	57	102	-	-	87	30.71	-
Sr	273	226	-	-	-	-	256	256	-	-	1062	279	-
Zr	86	106	-	-	-	-	176	289	-	-	140	-	-
Nb	6	8	-	-	-	-	11	9.5	-	-	19	-	-
Y	18	14	-	-	-	-	37	38.5	-	-	23	-	-
La	9	11	-	-	-	-	20	-	-	-	23	12	-
Ce	21	26	-	-	-	-	42	-	-	-	58	27	-
Nd	20	20	-	-	-	-	24	-	-	-	-	-	-
V	152	33	-	-	-	-	22	-	-	-	168	70	-
Cr	38	12	-	-	-	-	3	20.5	-	-	-	6.71	-
Ni	20	5	-	-	-	-	2	1.5	-	-	-	6	-
FeO*	6.97	2.47	2.57	5.79	3.56	3.04	5.27	3.52	5.03	1.79	5.33	5.92	5

20294 : Basaltic andesite bomb in pyroclastic flow erupted on 8 April 1982
GLG : Pumice rhyolite of Galunggung erupted in September 1982
TOBA : Pumice rhyolite of Toba (Kusnaeny, 1977; Hinkovich et al., 1978; Rock et al., 1982)
KKT-1 : Pumice dacite of pre-historic Krakatau caldera (Camus et al.,1987).
KKT-2 : Pumice rhyolite of Krakatau erupted in 1883 (Camus et al., 1987).
KKT-3 : Bomb mesostasis of Anak Krakatau erupted in 1981 (Camus et al.,1987).
BTR : Pumice of Batur caldera (Wheller & Varne, 1986a).
RJN : Pumice of Rinjani caldera (Foden, 1983).
TBR : Pumice of Tambora caldera erupted in 1815 (Self et al., 1984).
RBL : Pumice of Rabaul caldera (Heming & Carmichael, 1973).
ELCHN : Pumice of El Chichon erupted in 1982 (Luhr et al., 1984).
PELE : Mt. Pelée pumice (Dupuy et al., 1985).
STHEL : Pumice of St. Helens erupted in 1980 (Scarfe & Fujii, 1987).

Number of analyses in bracket
Major elements normalised to 100 % volatile-free, $Fe_2O_3/FeO = 0.15$.

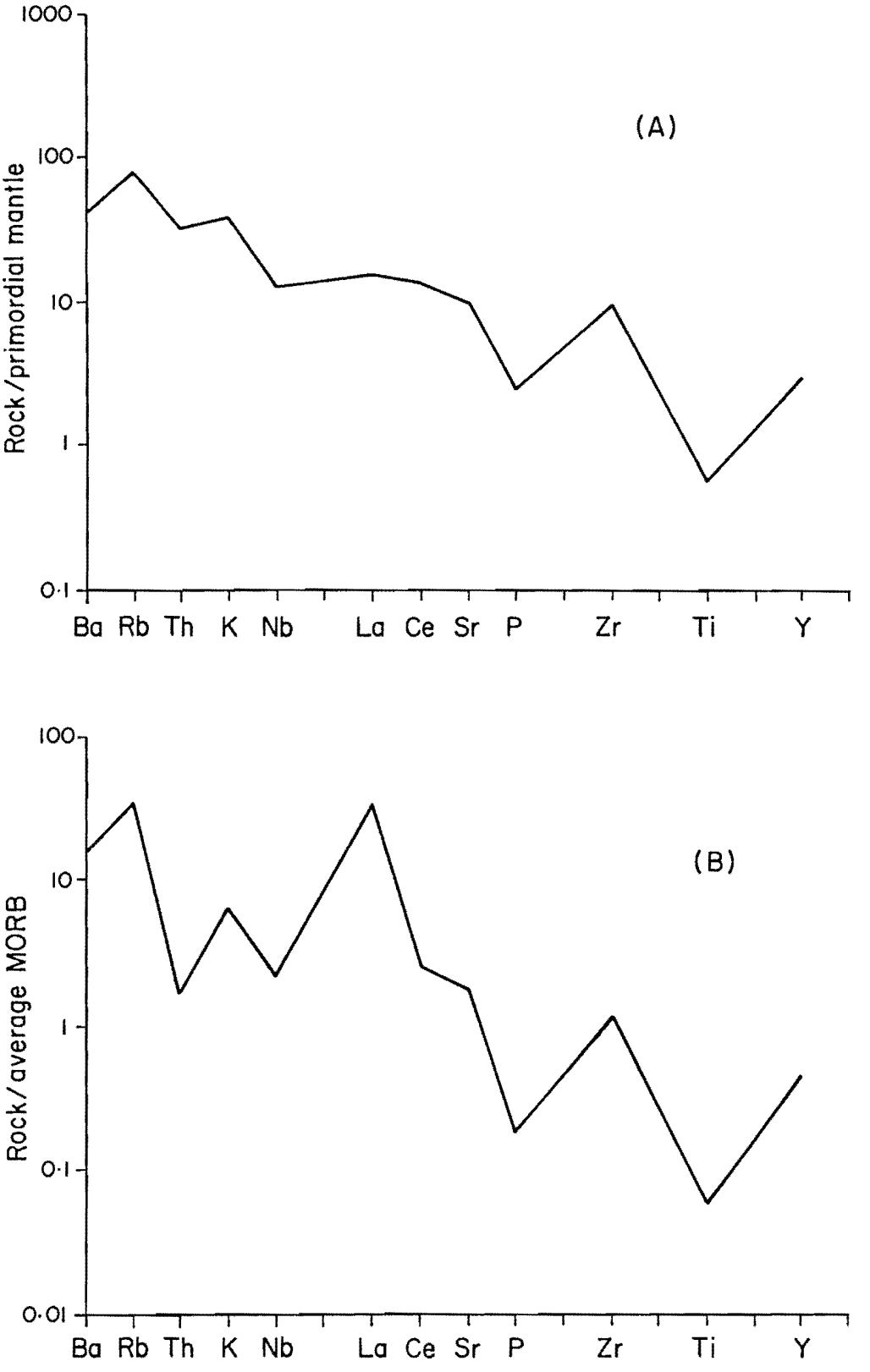

Figure VI.16 Spidergram of trace element concentrations in Galunggung rhyolite normalised to primordial mantle (A) and average MORB compositions (B). Normalisation after Geist et al., 1985.

and El Chichon (Luhr et al., 1984) is andesite. Compared with Batur dacite which is located in the same (Sunda) arc, Galunggung rhyolite has lower incompatible elements (except for Rb) but higher compatible elements. The higher Rb in Galunggung rhyolite is due to the low K and high Si contents.

VII PETROGENESIS

VII.1 Introduction

Galunggung volcanic rocks consist of both low- and high-Mg basalts and basaltic andesites. The high-Mg basalts have high Mg numbers (Mg#) and high Ni and Cr contents but low incompatible element abundances and are considered to be parental to the more evolved rocks.

There are two main questions relating to the petrogenesis of Galunggung volcanic rocks. The first is whether the high-Mg basalts at Galunggung represent primary melts and if so, the condition under which these melts formed. The second concerns the processes by which the magmas evolved.

A comparison is made between Galunggung high-Mg basalts and proposed primary melts at other volcanoes. Experimental studies concerning primary melts at oceanic spreading centres and convergent plate settings are included in this discussion.

In order to evaluate the evolution of the rocks, least squares mixing calculations are used to indicate the extent of crystal fractionation occurring in Galunggung lavas. In addition, the significance of gabbro clasts and amphibole crystals and the origin of rhyolite pumice are discussed.

VII.2 Do High-Mg Basalts at Galunggung Represent Primary Basaltic Magmas ?

VII.2.1 Primary Basaltic Magma

By definition, a primary basaltic magma is a liquid of basaltic composition that has not changed in composition since it was generated in its source region (upper mantle) by melting (BVSP, 1981). Primary magmas are parental, giving rise through differentiation processes to more evolved basalts and to other magmatic derivatives. On the other hand, parental basaltic magmas may or may not be primary. They are liquid compositions from which other associated and co-genetic magmas can be derived by processes of crystal fractionation and accumulation, contamination, liquid immiscibility and magma mixing (BVSP, 1981). In the last case, more than one parental magma may be involved. Parental magmas have higher liquidus temperatures than associated, related magmas, and crystallise phases with the highest melting points. Because in basaltic magmas those phases are Mg-rich olivine and pyroxene and Ca-rich plagioclase, parental basaltic magmas have the highest Mg/(Mg + Fe) and Ca/(Ca + Na) ratios within an association, with the exception of rocks of accumulative origin. They are also characterised by high Ni and Cr contents and low incompatible element abundances. The term primitive magma is often used synonymously with primary or parental magma to describe magmas having high Mg/(Mg + Fe) and Ca/(Ca + Na) ratios and compatible element abundances.

VII.2.2 Composition of the Upper Mantle

The upper mantle probably consists of peridotite composed chiefly of olivine (Fo_{88-92}), orthopyroxene, clinopyroxene and minor Cr-spinel (or garnet), and containing approximately 3 - 4 wt.% CaO and Al_2O_3 (e.g. Ringwood, 1975).

The most common type of peridotite occurring as nodules or xenoliths in basaltic rock is lherzolite, which Aoki and Shiba (1973) have divided into three groups : garnet lherzolite (50 - 75 km depth), spinel lherzolite (30 km depth) and plagioclase lherzolite (20 - 25 km depth). The chemical composition of each type is given in Table VII.1. Both spinel and garnet lherzolite have essentially the same mineral assemblages and textures except for the presence of garnet in the latter and it is probable that spinel lherzolite is transformed into garnet lherzolite at about 20 Kb (Kushiro & Yoder, 1966; Green & Ringwood, 1967; Ito & Kennedy, 1967; Wyllie, 1971). Spinel lherzolite nodules (and xenoliths ?) are obtained from both continental and oceanic environments (Maaløe & Aoki, 1977), and detailed investigations by White (1966), Griffin (1973) and Maaløe and Aoki (1977) indicate a representative mode of 66.7 % olivine, 23.7 % orthopyroxene, 7.8 % clinopyroxene, and 1.8 % spinel. Garnet lherzolites are only known from continental environments and have an average mode of 62.6 % olivine, 30 % orthopyroxene, 5 % garnet, 2 % clinopyroxene, and 0.4 % phlogopite (Maaløe & Aoki, 1977). Plagioclase lherzolites are uncommon among lherzolite inclusions throughout the world, but where found have mineral assemblages of olivine, pyroxene, Cr-spinel, plagioclase and pargasite (Aoki & Shiba, 1973).

Bonatti & Michael (1989) have reported that peridotites from

Table VII. 1 Estimated compositions (wt. %) of spinel lherzolite (1), garnet lherzolite (2), average for continental crust (3), and a model composition for a primitive mantle (4). Data from Maaløe & Aoki, 1977; Maaløe & Steel, 1980.

	1	2	3	4
SiO_2	44.20	44.99	60.4	44.58
TiO_2	0.13	0.06	1.0	0.15
Al_2O_3	2.05	1.40	15.7	2.43
FeO*	8.29	7.89	7.2	8.27
MnO	0.13	0.11	0.1	0.13
MgO	42.21	42.60	3.9	41.18
CaO	1.92	0.82	5.8	2.08
Na_2O	0.27	0.11	3.2	0.34
K_2O	0.06	0.04	2.5	0.11
P_2O_5	0.03	-	0.2	0.03
Cr_2O_3	0.44	0.26	-	0.41
NiO	0.28	0.32	-	0.25
Total	100.01	98.60	100.0	99.96

modern subduction zones are characterised by extremely low bulk Al_2O_3 content (< 0. 6 %) and Al_2O_3 of orthopyroxene (< 2 %) but high Fo content of olivine (> 91) and 100 Cr/(Cr + Al) spinel (> 50). According to them, these data indicate that subduction-related peridotites are the most highly depleted.

VII.2.3 Experimental Studies

VII.2.3.1 Oceanic Spreading Centre

A great deal of work has been done experimentally on the generation of mid-oceanic ridge basalts (MORB), and because of similarities between the high-Mg basalts of Galunggung and N-type MORB or olivine tholeiites (see Chapter VI.9), significant conclusions of this work are given below :

Fresh MORB generally contain very little water and other volatile constituents (Moore, 1970; Delaney et al., 1978; Takahashi & Kushiro, 1983). Most studies are therefore of anhydrous melting. Jaques & Green (1980) conclude that : 1. Olivine tholeiites are produced from moderate to large degrees of partial melting (10 - 30 %) at pressures > 7 - 8 Kb (within the spinel peridotite field). This is consistent with the study of Takahashi & Kushiro (1983) who reported that olivine tholeiites are produced at 8 - 10 Kb. 2. A similar degree of partial melting but at low pressure (< 5 Kb, within the plagioclase peridotite field, 15 - 25 km depth) produces olivine-poor tholeiites. These in turn are comparable to the medium-K high-Mg basalt of the Old Galunggung cryptodome.

High-Al olivine tholeiites (15 - 16 % Al_2O_3) form when olivine, orthopyroxene and clinopyroxene are liquidus phases (Green, 1970, 1971). They are considered as fractionated basalts coming from parental primary picritic magmas after separation of about 15 % olivine, at 60 - 70 km depth and 1400 - 1450^oC (Green et al., 1979; Stolper, 1980). This is in agreement with a study of Falloon & Green (1987b) who argue that most primitive MORB glasses are derivative compositions lying on olivine fractionation lines from picritic parents, which themselves are primary magmas at pressures greater than 10 Kb.

On the other hand, Presnall et al. (1979) and Hoover & Presnall (1982) believe that the high-Al olivine tholeiites are primary melt compositions formed at 8 Kb (< 25 km) up to 11 Kb (Presnall & Hoover, 1984, 1986). The olivine tholeiites also have high Ca (11 % CaO), Mg (9 % MgO) and Ni ($\geq$ 200 ppm) contents. It is less likely that the basalts have evolved from picritic primary magmas after extensive olivine fractionation (O'Hara, 1968, Irvine, 1979; Green et al., 1979; Elthon & Scarfe, 1980; Takahashi & Kushiro, 1983), because olivine fractionation would have eliminated Ni from the magmas (Sato, 1977, Hart & Davis, 1978), and produced low-Mg basalts.

VII.2.3.2 Convergent Plate Margins

A melting study of arc basalt magmas was done by Tatsumi et al. (1983) under both anhydrous and water-undersaturated conditions. The melt of olivine tholeiite basalt coexists with olivine and orthopyroxene at 11 Kb (35 km depth) and 1320^o C under anhydrous conditions. The high-Al basalt melt coexists with olivine, orthopyroxene and clinopy-

roxene at 15 Kb and 1340° C under anhydrous conditions and at 17 Kb (50 km depth) and 1325° C in the presence of 1.5 wt.% water.

In order to obtain the degree of partial melting, both Tatsumi et al. (1983) and Jaques & Green (1980) suggest that primary olivine tholeiite magmas are produced by a higher degree of partial melting than high-Al basalt magmas. This is supported by the fact that the former are more depleted in incompatible elements than the latter.

VII.2.4 Galunggung High-Mg Basalts

Two types of high-Mg basalts (49 - 50 % SiO_2, 10 - 12.5 % MgO, and Mg# = 69 - 75) are identified in Galunggung : (1) low-K high-Mg basalt (< 0.4 % K_2O), and (2) medium-K high-Mg basalt (0.6 % K_2O) (see Table VI.2). In the low-K high-Mg basalt, mineral phases are olivine, clinopyroxene, and plagioclase. Cr-spinels are common as inclusions in olivine phenocrysts and as microphenocrysts. The medium-K high-Mg basalt has only clinopyroxene and plagioclase phases.

Porphyritic volcanic rocks are most likely to have compositions modified by crystal accumulation or redistribution, and are therefore suspect as primary magmas (BVSP, 1981). However, Cox (1978), Cox et al. (1981) and Cox and Bell (1972) proposed that some high-Mg porphyritic lavas may not be simple cumulates, but may represent original liquid compositions. They envisage that this may be accomplished by compensated crystal settling in conduits, where crystal loss downwards is roughly balanced by crystals gained from above, so that the bulk composition of the magma is not altered substantially as solidification proceeds.

VII.2.4.1 Low-K high-Mg Basalt

VII.2.4.1.1 Identification of Liquid

The low-K high-Mg basalts erupted from Galunggung in 1982-83 have porphyritic textures and phenocryst contents ranging from 17 to 20 % (av. 17.5 %). The high-Mg basalts contain 10 - 12 % MgO. Sato (1977) concludes that most primary magmas have MgO contents in the range 10 - 12 %, and that higher MgO lavas are probably accumulative in origin. Petrography, mineral chemistry and bulk rock characteristics discussed below suggest that the basalts represent a primary melt composition.

Minerals range in size from phenocrysts (up to 2.5 mm) through microphenocrysts to groundmass crystals. This suggests that crystallisation continued throughout the cooling history of the rocks. Crystal shapes vary from anhedral to euhedral, mostly as individual grains (Fig. IV.7, Fig. V.1 & Fig. V.5). Anhedral olivine and clinopyroxene crystals are skeletal, hollow or embayed, with sharp corners and edges, and have poikilitic texture indicating rapid growth in the magma (e.g. Donaldson, 1976; Donaldson & Henderson, 1988; Lofgren, 1989). Rapid crystal growths are also indicated by a large number of glass inclusions in plagioclase phenocrysts. The rapid olivine crystallisation suggests that these rocks represent liquid compositions. Olivines form euhedral - subhedral normally zoned crystals, free of reaction rims, suggesting that crystals are not parts of a cumulate body (Nye & Reid, 1986). Large phenocrysts enclosing smaller crystals

which are comparable with groundmass are fairly common. These data suggest that the minerals crystallised in the magma and the phenocrysts are in equilibrium with their groundmasses (Morrice & Gill, 1986; Roeder & Emslie, 1970).

The mineral assemblage of forsteritic olivine, diopsidic pyroxene and calcic plagioclase, with Cr-spinel as euhedral inclusions in phenocrysts and microphenocrysts of olivine is typical of primitive basalts and is comparable to that of MORB. The high Ni content in the olivines, high Cr but low Al abundances in the Cr-spinels (Fig. V.4 & 18), and high Cr but low Na and Ti contents in the clinopyroxenes indicate that the minerals were derived from depleted mantle peridotite (e.g. Falloon & Green, 1987). This conclusion is consistent with the low alkali contents and incompatible element abundances in the bulk rock chemical composition, and a flat pattern for the ba salts when normalised to a primordial composition (Fig. VI. 6).

Crystallisation temperature calculations using olivine in the high-Mg basalts (Table VII.2) give very high values (1250 - 1313^{o}C). The highest value is consistent with the primary magmatic temperature (1320^{o}C) predicted by Tatsumi et al. (1983). This, together with the high Ni content in olivine, high-Cr content in Cr-spinel and high Ni and Cr in the bulk rocks suggest that the minerals formed on the liquidus (Cox et al., 1981).

Roeder & Emslie (1970) have shown that the equilibrium range for the partitioning of Fe/Mg between olivine and coexisting melt (Fe-Mg K_D) is 0.3 ± 0.03. This is in agreement with the average of calculated K_D values in the 1982-83 Galunggung high-Mg basalts (Table VII. 3). The calculated Fo contents are very close to the measured values and a comparison between the high-Mg basalts and porphyritic

Table VII.2 Estimates of crystallisation temperatures (°C) of Galunggung volcanic rocks, following the methods of Roeder & Emslie (1970, Kd = 0.3) (A), Glazner (1984, for 10 Kb) (B), Lindsley (1983, for 10 Kb) (C), and Kretz (1982, for 1 Atm) (D). OLV = olivine, PX = pyroxene, OPX = orthopyroxene, CPX = clinopyroxene, PLG = plagioclase, hmgb = high-Mg basalt, hmgba = high-Mg basaltic andesite, lmgb = low-Mg basalt, lmba = low-Mg basaltic andesite, C.F. = caldera formation, O.G. = Old Galunggung.

A	B		C		D	
	---		---			
OLV	OLV	PLG	OPX	CPX	PX	Explanation
1300	1313	-	-	-	-	1982 hmgb
1274	-	-	-	-	-	1982 hmgb
1270	1296	-	-	-	-	1982 hmgb
1250	1260	1199	-	1060	-	1983 hmgb
1266	1274	1192	-	1010	-	1982 hmgb
-	1179	1153	1000	1040	1040	1982 hmgba
-	1166	1145	1000	1000	940	1982 hmgba
-	1075	1147	1000	1000	1026	1982 hmgba
-	1100	1115	1000	990	1071	1982 hmgba
-	1083	1121	1000	1060	1048	1982 lmgba
-	1132	1092	1140	980	1058	1918 lmgba
-	1078	1167	1000	1040	1119	1822 lmgba
-	1125	1153	1150	1020	1088	1822 lmgba
-	1103	1174	1000	943	1064	C.F. lmgba
-	-	1001	-	1000	-	O.G. hmgb
-	1132	1162	1100	990	1084	O.G. lmgb
-	1150	1181	-	1010	-	O.G. lmgb
-	1149	1191	-	970	-	O.G. lmgb
-	1118	1202	1050	1070	1050	O.G. lmgb
-	1067	1160	1127	1100	1153	O.G. lmgba
-	-	1114	1000	1110	1054	O.G. lmgba
-	-	1073	1140	1060	1116	O.G. lmgba
-	-	1134	1040	1060	1064	O.G. lmgba

Table VII.3 Comparison between Fo calculated (Kd = 0.3) and Fo observed in cores of olivine phenocryst of the 1982-83 Galunggung high-Mg basalts.

	Calculated	Fo (100 % x Mg/Mg + Fe^{2+})		
Sample	Kd	Calculated	Observed	Explanation
JPL10	0.2744	90.08	90.72	Av. calc.
20300	0.2849	88.24	88.90	Kd = 0.3
20298	0.3480	87.07	87.50	

primary magmas from Japan (Yamamoto, 1988) is given in Figure VII. 1. These suggest that the 1982-83 Galunggung high-Mg basalts are in equilibrium with mantle olivines of composition Fo_{88-90} (BVSP, 1981). Sato (1977) argued that the equilibrium range for an equivalent Ni-Mg K_D is 2.0 - 2.6, but values obtained for the 1982-83 high-Mg basalts are higher (average = 3.9).

All data described above suggest that minerals in the 1982-83 Galunggung high-Mg basalts are magmatic, and grew shortly before eruption. The compositions of phenocryst cores are in equilibrium with the groundmass crystals, and it is concluded that the bulk rock chemical compositions represent liquid compositions.

The Galunggung low-K high-Mg basalt is one of the most primitive rocks known in a continental margin setting, having very low alkali and incompatible element abundances. The "primitiveness" of Galunggung high-Mg basalt is also reflected by its $^{230}Th/^{232}Th$ ratio (= 0.68) which is one of the lowest ratios yet found (Williams et al., 1983). These data indicate that the Galunggung high-Mg basalts are not fractionated basalts coming from a more primitive composition. Comparable primitive high-Mg basalts erupted in pre-historic times are found only in New Britain (Johnson, 1977; Johnson & Chappell, 1979; $^{87}Sr/^{86}Sr$ = 0.70319; DePaolo & Johnson, 1979). The characteristic of high-Mg basalts from both Galunggung and New Britain supports the conclusion of Bonatti & Michael (1989) that peridotites in continental margin settings are highly depleted.

Table VII. 4 compares Galunggung low-K high-Mg basalts with possible primary magmas at Galunggung calculated by Nicholls & Whitford (1976); proposed high-Al and olivine tholeiite primary magmas in the continental margin (Tatsumi et al., 1983), and proposed "high-Al"

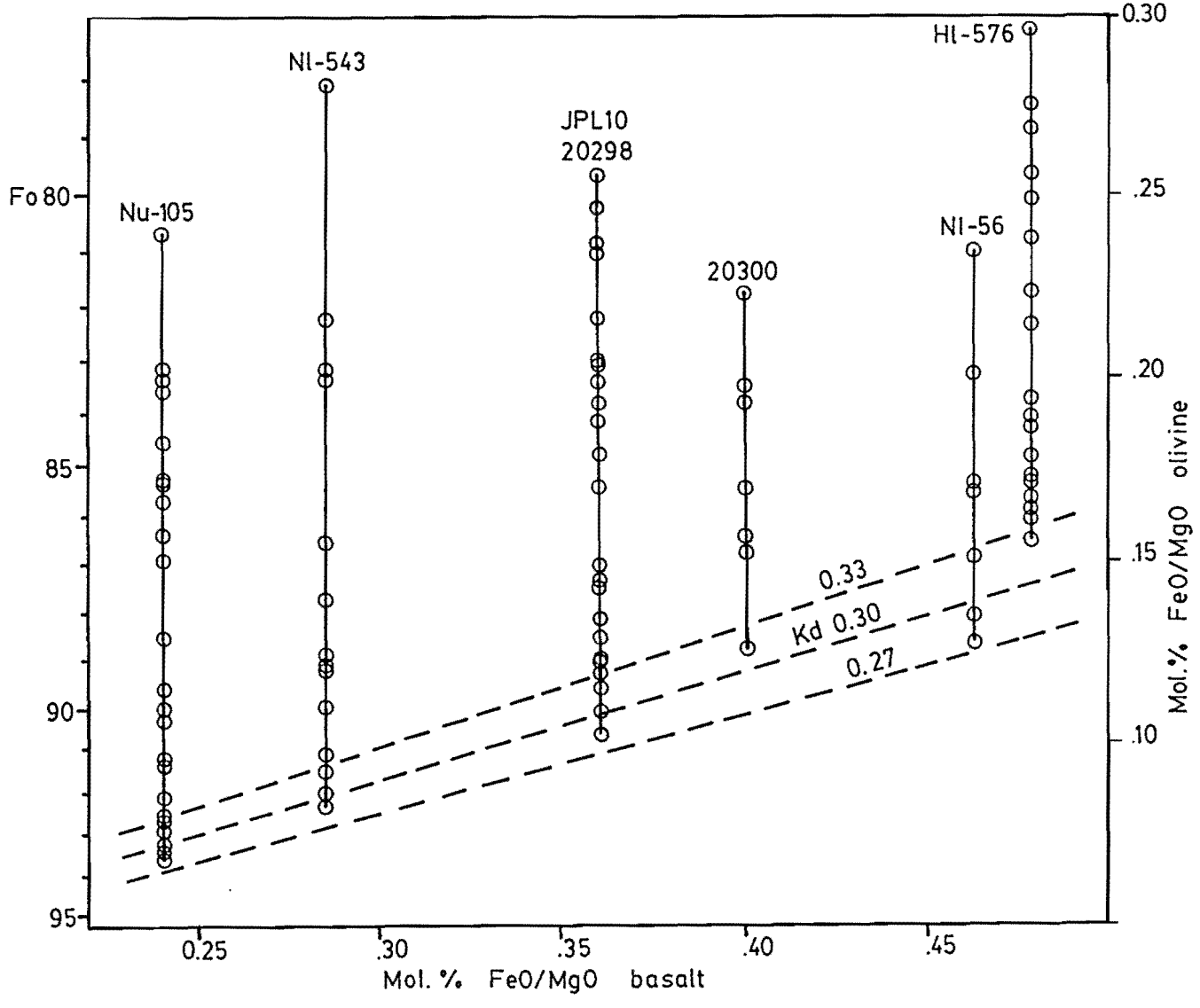

Figure VII.1 Relationship between FeO/MgO ratios of bulk rock compositions of the 1982-83 Galunggung high-Mg basalts and the cores of their olivine phenocryst (circles). Sample numbers : Nu-105, Nl-543, Nl-56 and Hl-576 are from Oshima-Oshima basalts, NE Japan (Yamamoto, 1988).

Table VII.4 A comparison between Galunggung high-Mg basalts erupted in 1982-83 (1) and possible primary magmas according to Nicholls & Whitford (1976, 2) and proposed high-Al (3) and olivine tholeiite primary magmas (4, Tatsumi et al., 1983) in volcanic arc, and proposed high-Al primary magmas of ocean floor basalts (5, Frey et al., 1974; 6, Langmuir et al., 1977).

	1	2	3	4	5	6
SiO_2	50.0 - 49.0	49.4 - 49.1	49.39	49.71	49.7	49.1
TiO_2	0.8 - 0.7	1.0 - 0.9	0.85	0.74	0.72	0.62
Al_2O_3	16.4 - 15.1	18.0 - 17.2	15.70	14.97	16.4	16.5
FeO*	8.3 - 9.2	9.5 - 9.7	9.76	10.57	7.89	8.78
MgO	10.0 - 12.5	8.4 - 10.3	12.5	13.03	10.1	10.3
CaO	10.9 - 11.7	10.2 - 9.7	9.43	9.0	13.0	12.4
Na_2O	2.4 - 1.9	2.8 - 2.6	2.33	1.56	1.98	1.92
K_2O	0.4 - 0.3	0.3 - 0.3	0.34	0.28	0.01	0.07
Ni	119 - 193				200	232
Cr	418 - 711				479	410
Mg#	69 - 75	64 - 68	71.4	71.37	71.7	69.9

olivine tholeiite primary magmas from mid-oceanic ridge basalts (MORB) (BVSP, 1981). The proposed primary MORB values are basaltic glasses quoted by Frey et al. (1974, DSDP Leg 3, 3-18-7-1) and Langmuir et al. (1977, Table 1, 527-1-1, in the FAMOUS area). Although Falloon & Green (1987b) have argued that most primitive MORB glasses were derived from picritic basalt by olivine fractionation, they agree that the most primitive one (3-18-7-1) is primary and a ternary diagram plot (Fig. VII.2) shows that most Galunggung high-Mg basalts fall within the field of primary magma.

The difference in Ca content between the Galunggung high-Mg basalts and the proposed primary magmas of Tatsumi et al. (1983) and BVSP (1981) may relate to the pressure in the magma source. Higher Ca contents may be yielded in lower pressure environments. K contents in the 1982-83 Galunggung high-Mg basalts are higher than in the MORB primary magmas. This correlates with the slightly higher Rb contents. Although both reflect depleted magma sources the differences may reflect mantle heterogeneity (e.g. Hart, 1988; Wood et al., 1979) in different tectonic settings.

VII.2.4.1.2 Depth of Origin

Figure VII.2 suggests that the source of the Galunggung low-K high-Mg basalts is located at about 50 km depth (15 Kb). This is similar to the primary high-Al basalt of Tatsumi et al. (1983) and is consistent with a suggestion (Whitford, 1975b) that the depth of primary magmas beneath Java is < 70 km.

The high content of Ca in olivines (> 0.11 % CaO) and Al in Cr-

Figure VII.2 Ternary diagram projection from plagioclase onto plane olivine (OLV) - diopside (DI) - quartz (Q) for Galunggung high-Mg basalts and proposed primary basaltic magmas from Mid-Oceanic Ridge Basalts (MORB; Frey et al., 1974; Langmuir et al., 1977), and continental plate margin (Tatsumi et al., 1983). This projection is calculated following the methods of Walker et al. (1979) and Grove et al. (1982) by converting wt. % oxides into mole % as in the following manner :

$$DI = CaO - Al_2O_3 + Na_2O + K_2O$$

$$OLV = (FeO + MgO + MnO + 2\ Fe_2O_3 + Al_2O_3 - CaO - Na_2O_3 - K_2O)/2$$

$$Q = SiO_2 - (\ Al_2O_3 + FeO + MgO + MnO + 3\ CaO + 11\ Na_2O + 11\ K_2O + 2\ Fe_2O_3)/2$$

Shown also are the 1 Atm (Walker et al., 1979) and approximate 10, 15 and 20 Kb (Stolper, 1980) cotectics.

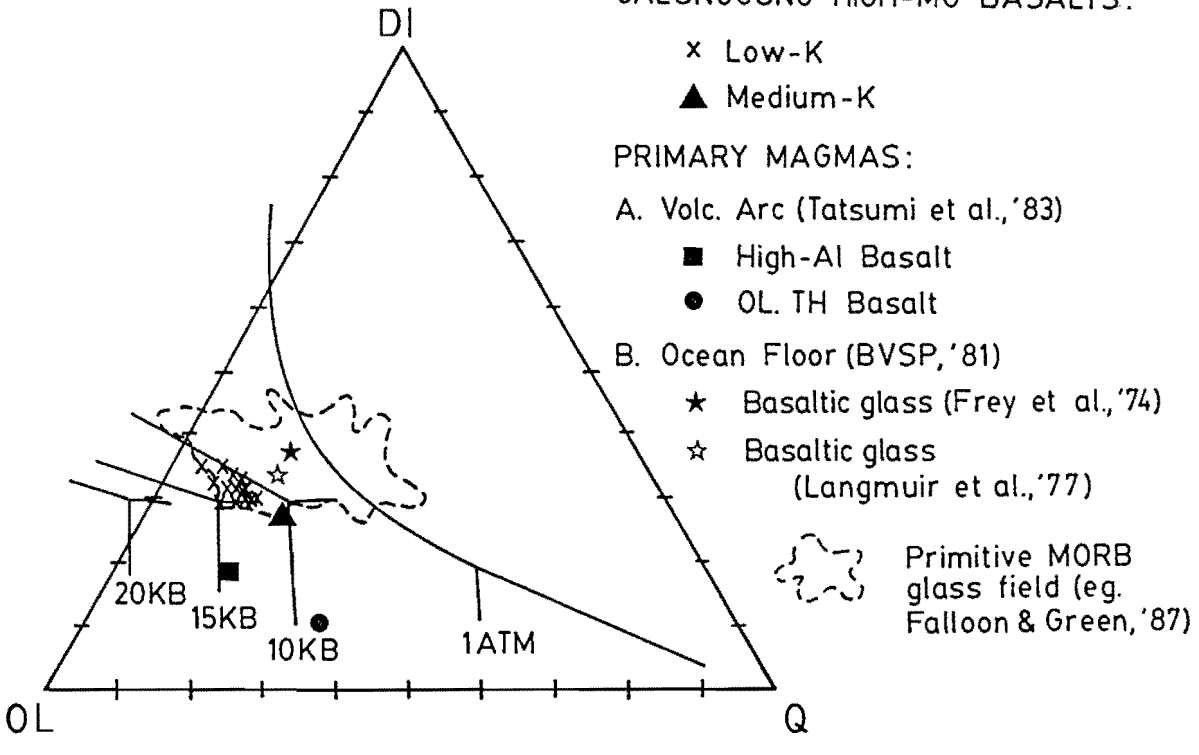

GALUNGGUNG HIGH-MG BASALTS:

× Low-K

▲ Medium-K

PRIMARY MAGMAS:

A. Volc. Arc (Tatsumi et al., '83)

■ High-Al Basalt

● OL. TH Basalt

B. Ocean Floor (BVSP, '81)

★ Basaltic glass (Frey et al., '74)

☆ Basaltic glass (Langmuir et al., '77)

Primitive MORB glass field (eg. Falloon & Green, '87)

spinels (12 - 20 % Al_2O_3), suggests that the minerals crystallised at low pressure (< 10 Kb ?) (Simkin & Smith, 1970; Sigurdsson & Schilling, 1976; Nye & Reid, 1986). Because plagioclase is not stable at a depth of > 40 km, the presence of the mineral supports the conclusion that crystallisation took place at high levels, en route to the surface.

VII.2.4.2 Medium-K High-Mg Basalt

VII.2.4.2.1 Identification of Liquid

Although the medium-K high-Mg basalt that forms Old Galunggung cryptodome is altered, it has apparently only diopsidic pyroxene and calcic plagioclase as phenocryst phases. Neither olivine nor orthopyroxene occur. The absence of olivine is also reflected by higher K and Rb contents in the bulk rock in comparison with low-K high-Mg basalt (Table VI.1-2) and high Mg content as well as Cr content in the diopsidic pyroxene (Fig. V.10). Normal zoning and lack of reaction rims around the clinopyroxenes suggest that the phenocrysts are in equilibrium with the groundmass crystals and the bulk rock may represent a liquid composition. The absence of olivine may therefore indicate a different source magma from the low-K high-Mg basalts. Figure VII.2 compares the composition of medium-K high-Mg basalt with low-K high-Mg basalt and proposed primary magmas from published data.

So far, olivine-poor high-Mg basalts are recognised only as pyroxene and basaltic komatiites (e.g. Arndt et al., 1977; Arth et

al., 1977). They are characterised by high Si (50 - 55 % SiO_2), low normative olivine and quartz, and high Mg contents (10 - 20 % MgO) (Arndt et al., 1977; Williams, 1972; Sun & Nesbitt, 1978). Table VII.5 gives a comparison between medium-K high-Mg basalt of the Old Galunggung cryptodome and the pyroxene and basaltic komatiites. The high-Mg basalt has lower Fe but higher Ti, Al, K and incompatible trace element abundances than the two komatiites. However, Brook & Hart (1974), and Nisbet & Walker (1982) suggest that Archean komatiites with eruption temperatures > 1650 ^{o}C and depth of the mantle source ~ 300 km (100 Kb) do not occur in modern times because of lower geothermal gradients corresponding to a cooling planet. A speculative suggestion is that the medium-K high-Mg basaltic magma beneath Galunggung was formed at a much shallower depth than the komatiites.

VII.2.4.2.2 Depth of Origin

According to Jaques & Green (1980), pyroxene (or olivine -poor) high-Mg basalts might represent primary magmas segregated from residual peridotite at about 25 - 40 % melting in the plagioclase peridotite stability field, probably at 5 Kb pressure; whereas Aoki & Shiba (1973) propose a depth of 20 - 25 km for plagioclase lherzolite.

Figure VII. 2 suggests that the Galunggung medium-K high-Mg basalt melted out at about 10 Kb pressure or 30 km deep. This is in the uppermost mantle beneath Galunggung (crustal thickness is 20 - 25 km thick; Katili, 1975), which probably comprises plagioclase lherzolite.

Table VII.5 Comparison of bulk rock chemical composition between medium-K high-Mg basalt of Old Galunggung cryptodome (20258) and olivine-poor pyroxenitic komatiite (P9-185) and basaltic komatiite (P9-108) lavas from Munro Township, Ontario (Arndt et al., 1977; Arth et al., 1977). na = not analysed.

	20258	P9-185	P9-108
SiO_2	47.06	47.20	50.40
TiO_2	0.87	0.43	0.57
Al_2O_3	15.67	11.90	12.00
FeO*	8.50	11.11	11.21
MnO	0.26	0.20	0.17
MgO	10.32	12.60	10.20
CaO	11.26	9.90	11.10
Na_2O	1.46	1.90	0.56
K_2O	0.56	0.01	0.28
P_2O_5	0.11	na	na
Nd	21	3.21	3.21
Rb	18	0.2	8
Sr	188	75	97
Ba	44	20	56
Sc	na	35	44
Mg#	71.08	69.64	64.80
Normative			
Ab	12.85	16.87	4.91
An	35.95	25.09	30.44
Di	17.29	21.41	21.41
Hy	16.65	17.10	32.55
Ol	10.13	16.37	-
Q	-	-	5.39

VII.3 Partial Melting to Produce Galunggung Primary Magma

VII.3.1 Experimental Studies

Geophysical evidence suggests that except for the outer core the mantle and crust normally consist of solid material. Thus any magma must originate by melting or partial melting of pre-existing solid rock. Melting may be induced by a local kinetic control (e.g. sudden local heating or pressure release and melt separation, BVSP, 1981), or by the influx of a mobile constituent causing rapid melt separation.

Experimental studies (e.g. Jaques & Green, 1980) indicate that the most primitive volcanic rocks, picrite and komatiite, are produced by 40 - 60 % partial melting within the spinel lherzolite field. The melt then migrates away from the source region probably leaving some form of refractory residue behind. However, partial melting at depth to give rise to large bodies of magma is not a process which can be observed directly.

The experimental study of Jaques & Green (1980) also suggests that olivine tholeiites are produced by moderate to large degrees of partial melting (10 - 30 %) at pressures > 7 - 8 Kb within the spinel peridotite field, whereas high degrees of partial melting at low pressure (< 5 Kb, within the plagioclase peridotite field) yields olivine-poor tholeiite. These results will be examined using quantitative partial melting models for the 1982-83 Galunggung high-Mg basalts.

Equations describing the behaviour of trace elements during partial melting were formulated by Schilling & Winchester (1967) and

Gast (1968). Shaw (1970) later described three possible partial melting models : 1. Continuous removal of melt from the residual solid, 2. Continuous removal of melt from residual solid followed by collection of this melt in a single completely mixed chamber. 3. Continuous equilibrium of the liquid phase with the residual solid until removal of the liquid from the solid (" batch" melting). When small fractions of material are melted, the equations for each mechanism yield similar results. When large fractions of material are melted (> 25 %) results from the three equations differ considerably. As the continuous removal of infinitesimal amounts of liquid (no. 1 & 2) is often considered physically unlikely, mechanism 3 may be the most geologically realistic for large bodies of magma of uniform composition (Arth, 1976).

The mathematical approach modified from equation 15 of Shaw (1970) has been reported by Arth (1976) and Hertogen & Gijbels (1976), as :

$C_l/C_o = 1/D + F\ (1 - D)$, where :

C_o = Concentration of a trace element in the initial solid

C_l = Concentration of a trace element in the liquid

D = Bulk solid-liquid distribution coefficient

$(D = \Sigma\ X^i\ K^i)$

F = Degree of melting

X^i = Mass fraction of phase i in the solid

K^i = Solid-liquid partition coefficient of a trace element for phase i.

Table VII.6 Trace element distribution coefficients. Data from Arth (1976), Cox et al. (1981), Graham & Hackett (1987), Ewart & Hawkesworth (1987), Geist et al. (1985), Hertogen & Gijbels (1976) and McBirney (1985). OLV = olivine, CPX = clinopyroxene, PLG = plagioclase, MAG = magnetite.

	OLV	CPX	PLG	MAG
Ba	0.001 - 0.1	0.001	0.15 - 0.3	0.001
Rb	0.001	0.001	0.03 - 0.08	0.001
Sr	0.001	0.08	1.2 - 2.2	0.001
Ni	7 - 15	1.7 - 2.1	0.04	4 - 15
Cr	1.2	1.7 - 5.5	0.01	30 - 100
Zr	0.01 - 0.023	0.01 - 0.25	0.02	0.02

VII.3.2 Modelling for the Low-K High-Mg Basalt

It has already been argued that Galunggung high-Mg basalts represent primary melt compositions which have not changed in composition since they were generated by partial melting of a peridotite source. This section discusses the degree of partial melting.

The compositions of spinel lherzolite and garnet lherzolite proposed by Maaløe & Aoki (1977) are chosen for modelling. Initial concentrations of trace elements are for ultramafic rocks from the compilation of Wedepohl (1975). Distribution coefficients are given in Table VII.6. Only values for Rb, Sr, Zr, La, Ce and Nd are quoted in Table VII.7 because of the high degree of uncertainty for partition coefficient of other trace elements in mineral phases (Hertogen & Gijbels, 1976). Although the spinel lherzolite and garnet lherzolite differ in modal mineralogy and mineral proportions, they give a relatively similar result for the degree of melting. Table VII.7 presents that degree of partial melting from the peridotitic upper mantle composition for the low-K high-Mg basalts is about 15 %. This is close to the 20 % melting of peridotite to produce primary magma beneath Java (Whitford, 1975b) and 10 - 15 % melting of spinel lherzolite to yield basic rocks from Guntur volcano (Purbawinata, 1988).

VII.3.3 Are Subducted Components Involved in the Galunggung Magma Source ?

In volcanic rocks of convergent plate settings, the involvement

Table VII.7 Degree of melting calculations using spinel lherzolite (spi-lh) and garnet lherzolite (gnt-lh) of Aoki & Maaløe (1977), initial concentration of trace elements of ultra-mafic rocks (Wedepohl, 1975) and distribution coefficient from Table VII.6. See text for further explanation. / references in

	F (degree of melting x 100 %)			
Element	20334		Mean of 18 high-Mg basalts	
	spi-lh	gnt-lh	spi-lh	gnt-lh
Rb	19.91	18.87	16.59	15.51
Sr	10.33	10.67	9.63	9.87
Zr	11.94	11.99	10.16	10.21
La	18.19	17.50	17.83	17.14
Ce	26.27	27.20	20.51	21.41
Nd	10.27	9.57	11.21	10.52
Average	16.15	15.97	14.32	14.11

of subducted altered oceanic crust and sediments in magma source is a subject of debate. Two different models are currently proposed in the literature. The first model states that melting peridotite does not necessarily relate to the subduction slab (e.g. Plank & Langmuir, 1988; Falloon et al., 1989), whereas the second model argues that subducted components occur in the melt (e.g. Gill, 1981; Nye & Reid, 1986; Ujike, 1988).

The first model is supported by geochemical and isotope studies of some volcanoes in the Sunda Arc (Foden, 1983; Foden & Varne, 1980; Wheller, 1986; Wheller et al., 1987; Wheller & Varne, 1986a, b; Wolff et al., 1986). The low-K (< 0.3 % K_2O) and low Sr but high Nd isotope ratios ($^{87}Sr/^{86}Sr$ = 0.7040, $^{143}Nd/^{144}Nd$ = 0.5129 from Batur volcano; Wheller, 1986; $^{87}Sr/^{86}Sr$ ratios from Rinjani volcano : 0.70386 - 0.7042 and Tambora volcano : 0.70385 - 0.70389; Foden & Varne, 1980) which form a wide field within the "mantle array" defined by MORB and OIB (DePaolo & Wasserburg, 1976; O'Nions et al., 1977; Allegre et al., 1979; Zindler et al., 1982) indicate that their genesis has not involved incorporation of recently subducted, continent-derived sialic material. On the basis of similarities in composition and isotopes, Falloon et al. (1989) have argued that high alkali Quaternary eastern Sunda Arc volcanics are similar to Christmas Island basalts which represent hot spot volcanism behind the subduction zone. A very low Sr isotopic ratio from New Britain ($^{87}Sr/^{86}Sr$ = 0.70319; DePaolo & Johnson, 1979), where the only high-Mg basalts comparable to those in Galunggung are present, also suggests a homogeneous magma source that does not relate to oceanic crust and a subduction zone. In addition, an evaluation of the global variations in the major element chemistry of arc basalts (Plank & Langmuir, 1988) provides further evidence that

the mantle wedge, and not the slab, melts beneath arc volcanic fronts.

The Galunggung high-Mg basalts have low-alkali contents and incompatible element abundances reflecting a depleted magma source. They can be compared with N type MORB, and spidergrams of trace element concentrations in the Galunggung high-Mg basalts, normalised to primordial mantle composition, show a flat pattern. These data may suggest that the Galunggung magma source may not be related to the subducted slab. Melt could be generated by melting of a hydrous peridotite mantle (McBirney, 1969; Kushiro et al., 1968; Mysen, 1973) by kinetic energy (BVSP, 1981) or decompression (Scott & Stevenson, 1989). This is possibly indicated by intermediate - deep tectonic earthquakes. Blot & Priam (1963) reported the 10 July 1960 eruption of Lopevi volcano in Vanuatu was preceded 4 months earlier by a deep earthquake ($h = 250$ km, $M = 7.25$), the focus of which was just under the volcano. Each of the large volcanic eruptions recorded between 1910 and 1962 followed a deep focus earthquake of magnitude > 7, whereas moderate eruptions were preceded by earthquakes of magnitude between 5.75 and 6.75. During the year before the eruption, notable tectonic earthquakes occurred in areas related to Manam volcano's location in New Britain (Taylor, 1963). And few shocks occurred on the Manam volcano during first two years of the current eruptive cycle.

At Galunggung the 1982-83 eruptions were preceded by tectonic earthquakes on 2 November 1979 and 16 April 1980 which had magnitudes of 6.4 (Priyantono et al., 1980). The epicentre of the earthquakes were however located about 100 km south of Galunggung at a depth between 33 and 65 km. At this location, the subducted slab is at a depth of 80 km, whereas beneath Galunggung it is at 130 km (Hatherton & Dickinson, 1969).

A speculative possibility is that the energy of the earthquake moved from the focal depth to the north and triggered upper mantle material beneath Galunggung volcano to produce partial melting. The magma movement is possibly similar to a "mantle diapir" model proposed by McBirney (1985). However, this hypothesis still requires a detailed (geophysical) study of the upper mantle characteristics which are poorly understood at the present time.

The second model is based on the presence of high-Mg basalts containing high alkali contents, incompatible element and $^{87}Sr/^{86}Sr$ isotope ratios reflecting enriched upper mantle as a common feature in volcanic arcs. In the Sunda Arc, the involvement of subducted components in the magma sources is discussed by Whitford (1975b), Whitford et al. (1981) and Whitford & Jezek (1982). Low-K volcanic rocks on Java (including Galunggung) have Sr isotope ratios from 0.7041 to 0.7045 (av. 0.7043; Whitford, 1975 b). These values are higher than Indian Ocean basalts (0.7034; Subbarao & Hedge, 1973).

Recently, Gill & Williams (1989) have proposed a new technique using the Th/U isotope ratio to test sediment - subduction models. They argue that the involvement of subducted components is reflected by high correlation of $^{230}Th/^{232}Th$ and $^{238}U/^{232}Th$. Another new method is also reported by Morris et al. (1989) by using $^{10}Be/Be$ and B/Be isotope ratios. They have stated that $^{10}Be/Be$ is enriched in pelagic sediments, whereas B/Be is enriched in altered oceanic basalts. On the basis of the two techniques, subducted components are recognised in the New Britain magma source.

Low Th/U isotope ratio (< 0.8) of the Galunggung high-Mg basalts is one of the lowest ratios yet found has been reported (Williams et al., 1983; Gill, 1987, pers. comm.; Gill & Williams, 1989).

Although having lowest values, Sunda Arc volcanics lie on a mixing line between $^{230}Th/^{232}Th$ and $^{238}U/^{232}Th$ indicating an involvement of subducted components. Thus, if subducted components are involved in the Galunggung magma source, their proportion must be very small. More isotope studies are required to clarify this problem.

Melt is generated by following the model of Tatsumi et al. (1983, Fig. 5). In the model, the downgoing slab does not melt but is a source of water which has an important influence on melting of mantle wedge material. The water has dissolved in it some chemical components of oceanic sediments and altered basaltic rocks. In the Northeastern Japan Arc, subducted components are reflected by high alkali and incompatible element abundances (Ujike, 1988; Yamamoto, 1988). In Galunggung, however, the water may carry only a faint oceanic crustal chemical signature. The mantle peridotite melt is less dense than the overlying mantle materials and begins to ascend as a mantle diapir. The mantle diapir has a temperature of about 1320°C at a depth of 35 - 70 km. This is consistent with the highest crystallisation temperature in Galunggung high-Mg basalt (1313°C) and depth of the magma source (50 km).

Overall, the volume of erupted high-Mg basalts at Galunggung is much smaller than the low-Mg basalts. This may be due to the deeper location (30 - 50 km) of the sources of the former, which may well result in high-Mg basaltic magmas becoming more fractionated en route to the surface, particularly if the magma resided in a shallower magma chamber (< 25 km) to produce low-Mg basalts and more evolved rocks. Thus, the eruption of high-Mg basalts is caused by rapid magma ascent from the mantle. Francis et al. (1983) have suggested that high-Mg lavas are most likely to reach the surface after the physical integ-

rity of the crust has been disrupted by rifting but before large and abundant magma chambers are established. A study on both Vanuatu and Solomon Islands, where picrite - olivine basalts occur, suggests extensive fracturing of the overriding plate, with the fracture pattern conforming remarkably well to a simple collision model (Collot et al., 1985). These fractures associated with collision may have provided relatively rapid access to the surface for the magma (Ramsay et al., 1984; Crawford et al., 1987).

VII.4 Crystal Fractionation from Galunggung High-Mg basalts to More Evolved Rocks

VII.4.1 Introduction

If crystals and liquid are separated before the magma solidifies completely, the remaining liquid continues to crystallise to form a rock with a chemical composition different from that of the original liquid. This, in essence, is the basic principle of crystal fractionation (McBirney, 1985).

Three mechanisms of crystal-liquid separation have been applied to crystallising basaltic parental magmas, (1) gravitative crystal settling, (2)"liquid-liquid fractionation"(McBirney, 1985), and (3) flowage differentiation (Bhattacharji & Smith, 1964; BVSP, 1981).

The first mechanism suggests that crystals fall towards the base of a tranquil magma chamber with a terminal settling velocity (Stoke's Law) that is related to the crystal radius, crystal-liquid density contrast and liquid velocity (depends on order of nucleation).

Consequently, olivine should be the first mineral to sink, followed by pyroxene and magnetite, whereas plagioclase (having a neutral density compared with most basic magmas) remains in situ.

However, the thermal characteristics and viscosity of molten magma, together with heat flux of the chamber and chamber geometry and size indicate that convective circulation must normally occur in basaltic magma reservoirs (Bartlett, 1969). In the Skaegaard intrusion, McBirney & Noyes (1979) have found that plagioclase, which was lighter than the liquid, is a major component of rocks on the floor, while mafic minerals that were heavier than the liquid accumulated under the roof. On the basis of cumulate textures, preferred orientations of crystals, and layering at the margins of the Skaegaard intrusion McBirney & Noyes (1979) suggest that crystal-liquid fractionation is caused by "in situ" crystallisation. This statement is supported by experimental studies of the crystallisation behaviour of hot, saturated aqueous solutions which indicate that crystallisation at the margins of a magma chamber causing compositional variations is caused by "liquid-liquid fractionation" (McBirney, 1985) or "convective fractionation" (Sparks et al., 1984). Recently, Langmuir (1989) demonstrated that geochemical trends in magmas formed by "in situ" crystallisation can be very different from those formed by equilibrium or perfect crystal fractionation. He concludes that "in situ" crystallisation causes more change in the incompatible elements relative to the major elements than does crystal fractionation. Also, MgO, FeO and An normative trends differ between "in situ" crystallisation and crystal fractionation models.

The third mechanism which is also termed "flow segregation" by McBirney (1985) is a process by which solid particles are concentrated

towards the centre of liquid flowing in a narrow conduit. If the flow is arrested and the magma solidifies in situ, it forms a dyke with phenocrysts concentrated toward the centre. This is due to the "dispersive shear pressure" (McBirney, 1985) which tends to drive crystals out of the zone of maximum shear and into the interior of the flow. Such crystal-liquid segregation is less common in lava flows and is very difficult to identify in fragmental pyroclastic material.

VII.4.2 Least Squares Fractionation Model

Least squares methods by which the proportions of mineral and liquid phases in a crystal fractionation scheme may be quantified have been described by Bryan, 1969; Bryan et al., 1969; Chayes, 1968; Stormer & Nicholls, 1978; Wright & Doherty, 1970; and Geist et al., 1985. These techniques yield the best least-squares fit to a proposed daughter or model composition. The best-fit models are those for which the sum of the squares of the residuals is minimised when minerals removed from the parental composition give a composition close to the specified daughter.

Calculations for Galunggung volcanic rocks use the GPP program of Geist et al., 1985, which is principally based on the crystal fractionation scheme of Wright & Doherty (1970).

Three models are presented to explain the compositional variation of Galunggung volcanic rocks from low-K high-Mg basalt to rhyolite (pumice).

Model 1 (Table VII.8) consists of 3 steps : (1) from high-Mg basalt to high-Mg basaltic andesite, (2) from high-Mg basaltic ande-

Table VII. 8 Crystal fractionation modelling. Model 1 : from low-K high-Mg basalt to high-Mg basaltic andesite (step 1), from high- to low-Mg basaltic andesite (step 2), and from low-Mg basaltic andesite to rhyolite (step 3). OL = olivine, CP = clinopyroxene, PL = plagioclase, OP = orthopyroxene, MA = magnetite, AM = amphibole, and CALC = calculated.

Step 1

	Parent	Daughter		Mineral composition			
	20298	VB 16	CALC	OL	CP	PL	MA
SiO_2	49.37	53.19	53.19	40.17	51.74	47.93	0.14
TiO_2	.82	.77	.81	-	.57	-	9.33
Al_2O_3	15.92	17.73	17.73	.06	4.30	32.78	4.86
FeO	8.94	7.98	7.97	11.99	5.94	.63	.46
MnO	.17	.16	.18	.23	.17	.04	.46
MgO	10.81	6.58	6.58	47.29	14.70	.09	3.99
CaO	11.30	9.76	9.77	.24	22.40	16.01	.08
Na_2O	2.21	3.12	3.15	-	0.18	2.47	-
K_2O	.35	.57	.59	.02	-	.05	-
P_2O_5	.10	.14	.17	-	-	-	-
Rb	6	13	10.4				
Sr	215	247	247.9				
Zr	49	69	80.6				
Ba	48	116	80.9				
Cr	558	203	207.4				
Ni	152	59	65.7				

	Sol'n	% cumulate
20298	1.000	
OL	- .101	23.8
CP	- .144	34.0
PL	- .152	35.7
MA	- .027	6.4
VB 16	.575	

R. Squared = .005

Crystal removed = 42.5 %

Step 2

	Parent	Daughter		Mineral composition			
	VB 16	20294	CALC	OL	CP	PL	MA
SiO_2	53.19	57.05	57.04	40.65	52.74	50.01	0.14
TiO_2	.77	.70	.70	-	.20	.02	9.93
Al_2O_3	17.73	18.41	18.41	.04	2.63	30.99	4.86
FeO	7.98	7.00	7.00	10.06	4.17	.74	80.53
MnO	.16	.15	.17	.20	.17	.04	.46
MgO	6.58	3.92	3.92	48.85	16.51	.11	3.99
CaO	9.76	8.16	8.17	.20	23.37	14.54	.08
Na_2O	3.12	3.68	3.75	-	.19	3.48	-
K_2O	.57	.76	.81	-	.01	.07	-
P_2O_5	.14	.16	.20	-	-	-	-
Rb	13	18	18.6				
Sr	247	273	270.5				
Zr	69	86	97.0				
Ba	116	176	163				
Cr	203	38	38.1				
Ni	59	20	20.9				

	Sol'n	% cumulate
VB 16	1.000	
OL	- .049	15.8
CP	- .082	26.4
PL	- .152	48.9
MA	- .027	8.8
20294	.690	

R. Squared = .009

Crystal removed = 31.0 %

Step 3

	Parent	Daughter		Mineral composition					
	20294	20244	CALC	OL	CP	PL	MA	OP	AM
SiO_2	57.05	71.41	71.41	37.64	51.42	53.89	0.13	52.06	42.28
TiO_2	.70	.24	.24	.01	.40	.03	11.66	.20	2.34
Al_2O_3	18.41	15.37	15.35	.02	1.79	28.60	3.54	1.20	13.44
FeO	7.00	2.47	2.47	22.69	10.86	.54	81.92	20.41	11.71
MnO	.15	.09	.14	.36	.37	-	.42	.79	.11
MgO	3.92	.90	.90	39.14	14.52	.09	2.24	23.86	15.02
CaO	8.16	3.16	3.16	.14	20.36	11.85	.09	1.48	12.30
Na_2O	3.68	4.10	4.20	-	.26	4.90	-	-	2.58
K_2O	.76	2.16	2.00	.01	.02	.09	-	-	.21
P_2O_5	.16	.09	.45	-	-	-	-		

Rb	18	70	46.3
Sr	273	226	236.9
Zr	86	106	237.0
Ba	176	315	431.7
Cr	38	12	2.8
Ni	20	5	8.8

	Sol'n	% cumulate
20294	1.000	
OL	- .005	.8
CP	- .068	10.5
PL	- .419	65.0
MA	- .038	6.0
OP	- .065	10.0
AM	- .049	7.6
20244	.356	

R.squared = .166

Crystal removed = 64.4 %

site to low-Mg basaltic andesite, and (3) from low-Mg basaltic andesite to rhyolite. These steps represent the compositional sequence of the 1982-83 Galunggung eruption. "Transitional" high-Mg basalt is not included in the calculation because it is very close to both high-Mg basalt and basaltic andesite. Sample 20298 was chosen to represent the Galunggung high-Mg basalts because its composition is very close to the average composition of the high-Mg basalts.

Model 2 (Table VII.9) also has 3 steps : (1) from high-Mg basalt to low-Mg basalt, (2) from low-Mg basalt to low-Mg basaltic andesite, and (3) from low-Mg basaltic andesite to rhyolite. This model is related to the pre-1982 Galunggung volcanic rocks.

Low-Mg basaltic andesite in model 1 has olivine, orthopyroxene, clinopyroxene, magnetite, amphibole and plagioclase mineral phases, whereas in model 2, it has only orthopyroxene, clinopyroxene, magnetite and plagioclase.

Model 3 (Table VII.10) shows that medium-K high-Mg basalt of Old Galunggung cryptodome fails to be a parental rock for high-Mg basaltic andesite (step 1) or low-Mg basalt (step 2). This is in agreement with its petrography and geochemistry data which differ from other Galunggung volcanic rocks. So, the medium-K high-Mg basalt is considered as a single primitive rock.

In steps 1 and 2 of model 1, four mineral phases (olivine, clinopyroxene, magnetite and plagioclase) are subtracted from parental rocks at each step of the two models to obtain the calculated daughter liquid. From high-Mg basalt to high-Mg basaltic andesite (step 1 of model 1), olivine, clinopyroxene and plagioclase are the main fractionating phases (23.8 %, 34.0 %, and 35.7 %, respectively), whereas in the second step there is an increase in the percentage of magnetite

Table VII. 9 Crystal fractionation modelling. Model 2 : from low-K high-Mg basalt to low-Mg basalt (step 1), from low-Mg basalt to low-Mg basaltic andesite (step 2), and from low-Mg basaltic andesite to rhyolite (step 3). Abbreviations as for Table VII.8

Step 1

	Parent	Daughter		Mineral composition			
	20298	L 35	CALC	OL	CP	PL	MA
SiO_2	49.37	52.99	52.97	40.59	51.03	46.34	0.24
TiO_2	.82	.95	1.00	-	.98	.01	2.01
Al_2O_3	15.92	19.51	19.52	.03	3.37	34.04	23.20
FeO	8.94	8.18	8.18	9.10	8.78	.56	64.03
MnO	.17	.16	.17	.17	.21	.01	.50
MgO	10.81	4.50	4.51	49.92	14.49	.13	9.85
CaO	11.30	9.63	9.65	.19	20.77	17.33	.17
Na_2O	2.21	3.33	3.41	-	.35	1.55	-
K_2O	.35	.59	.59	-	.35	1.55	-
P_2O_5	.10	.16	.17	-	-	-	-
Rb	6	11	10.2				
Sr	215	267	272.7				
Zr	49	80	83.3				
Ba	48	109	80.6				
Cr	558	29	25.7				
Ni	152	16	13.1				

	Sol'n	% cumulate
20298	1.000	
OL	- .104	25.0
CP	- .190	45.7
PL	- .098	23.7
MA	- .024	5.6
L 35	.584	

R.squared = .011

Crystal removed = 41.6 %

Step 2

	Parent	Daughter		Mineral composition			
	L 35	20347	CALC	OL	CP	PL	MA
SiO_2	52.99	56.12	56.12	38.73	51.83	47.81	0.16
TiO_2	.95	.73	.79	-	.47	.06	17.44
Al_2O_3	19.51	19.03	19.03	.03	2.67	32.78	2.62
FeO	8.18	7.44	7.43	22.97	9.05	.61	76.98
MnO	.16	.15	.16	.42	.33	.03	.44
MgO	4.50	3.55	3.57	37.84	14.84	.09	2.26
CaO	9.63	8.24	8.25	-	20.49	16.08	.06
Na_2O	3.33	3.82	3.91	-	.34	2.49	-
K_2O	.59	.75	.77	.01	.01	.06	.03
P_2O_5	.16	.16	.22	-	-	-	-
Rb	11	17	14.6				
Sr	267	286	270.8				
Zr	80	84	104.6				
Ba	109	155	141.3				
Cr	29	11	11.5				
Ni	16	9	8.4				

	Sol'n	% cumulate
L 35	1.000	
OL	- .029	11.5
CP	- .047	18.7
PL	- .155	62.3
MA	- .019	7.5
20347	.751	

R. squared = .014

Crystal removed = 24.9 %

Step 3

	Parent	Daughter		Mineral composition			
	20347	20244	CALC	OP	CP	PL	MA
SiO_2	56.12	71.41	71.06	54.21	49.99	52.63	0.15
TiO_2	.73	.24	- 2.89	.17	.52	2.07	12.45
Al_2O_3	19.03	15.37	16.14	.78	4.77	26.66	3.31
FeO	7.44	2.47	2.91	19.52	9.25	3.13	81.82
MnO	.15	.09	.01	.69	.49	.07	.47
MgO	3.55	.90	1.33	23.11	14.42	.15	1.81
CaO	8.24	3.16	3.41	1.52	20.19	10.00	-
Na_2O	3.82	4.10	4.17	-	.30	5.04	-
K_2O	.75	2.16	2.20	-	.08	.24	-
P_2O_5	.16	.09	.57	-	-	-	-

	Sol'n	% cumulate
20347	1.000	
OP	- .070	9.8
CP	- .098	13.6
PL	- .517	72.0
MA	- .033	4.5
20244	.751	

R. Squared = 11.87

Crystal removed = 71.8 %

Table VII. 10 Crystal fractionation modelling. Model 3 : from med-K high-Mg basalt to high-Mg basaltic andesite (step 1), and from med-K high-Mg basalt to low-Mg basalt. Abbreviations as for Table VII.8

Step 1

	Parent	Daughter		Mineral composition		
	20258	VB 16	CALC	CP	PL	
SiO_2	48.99	53.19	51.22	50.68	48.51	
TiO_2	.91	.77	.93	.40	.04	
Al_2O_3	16.31	17.73	20.02	4.88	32.24	
FeO	8.85	7.98	9.01	5.16	.90	R. squared = 24.134
MnO	.27	.16	.25	.33	-	
MgO	10.74	6.58	9.75	15.51	.42	
CaO	11.72	9.76	11.26	22.83	15.10	
Na_2O	1.52	3.12	1.86	.22	2.60	
K_2O	.58	.57	.65	-	.19	
P_2O_5	.11	.14	.12	-	-	

Step 2

	Parent	Daughter		Mineral composition		
	20258	L 35	CALC	CP	PL	
SiO_2	48.99	52.98	50.94	50.68	48.51	
TiO_2	.91	.95	.89	.40	.04	
Al_2O_3	16.31	19.51	22.07	4.88	32.24	
FeO	8.85	8.18	8.54	5.16	.90	R. squared = 30.174
MnO	.27	.16	.22	.33	-	
MgO	10.74	4.50	8.52	15.51	.42	
CaO	11.72	9.63	10.82	22.83	15.10	
Na_2O	1.52	3.33	2.03	.22	2.60	
K_2O	.58	.59	.65	-	.19	
P_2O_5	.11	.16	.12	-	-	

and plagioclase fractionated. These values are reasonable in term of modal mineral occurrences. No orthopyroxene is involved in the model implying that orthopyroxene observed in core of clinopyroxene phenocrysts in the high-Mg basaltic andesite is not in equilibrium with the host rock. Differences in measured trace element abundances of Cr, Ni, Ba, Rb, Sr and Zr between observed and calculated values are generally minor. Trace element distribution coefficients used in the models are given in Table VII.6.

High percentages of removed crystals (64.4 %) occur in the fractionation of low-Mg basaltic andesite to rhyolite (step 3 of model 1). Fractionated plagioclase is dominant, while amphibole and olivine are also involved.

In model 2, clinopyroxene is the main fractionating phase (45.7 %) from high-Mg basalt to low-Mg basalt (step 1), whereas from low-Mg basalt to low-Mg basaltic andesite it is plagioclase (62.3 %). However, the basaltic andesite fails to produce rhyolite (step 3). This implies that although minor, amphibole and olivine are important phases in the crystal fractionation.

VII.4.3 Discussion on Fractionation of Galunggung Rocks.

This section discusses fractionation processes, whether they occur in a magma chamber or in a conduit system and their depth. Two fractionation systems have occurred in Galunggung, (1) high-Mg basalt - "transitional" high-Mg basalt - high-Mg basaltic andesite - low-Mg basaltic andesite, and (2) high-Mg basalt - low-Mg basalt - low-Mg basaltic andesite. Least squares fractionation models indicate that

the fractionation involves olivine, clinopyroxene, plagioclase and magnetite. Langmuir (1989) demonstrated that an "in situ" crystallisation trend differs from that of Rayleigh crystal fractionation. Information on the geometry of the magma chamber is necessary in order to quantitatively model the "in situ" crystallisation process (Ragland & Butler, 1972; Morse, 1979 & 1982), and clearly this is not available for Galunggung. However, changes in the incompatible trace elements in Galunggung rocks are compatible with major element modelling and this implies that the "in situ" crystallisation model does not apply to Galunggung. Overall, the close-fit between the measured and calculated compositions at each step in the crystal fractionation models 1 and 2 indicates that the major and trace element data are mutually consistent. This supports the hypothesis that closed system crystal fractionation of basaltic magma was the main process by which the Galunggung basaltic andesite rocks formed.

Although there is a fractionation from high-Mg basalt through low-Mg basalt to low-Mg basaltic andesite, the most common rocks erupted from Galunggung are low-Mg basalt and low-Mg basaltic andesite. This implies that the low-Mg basalt and basaltic andesite were formed in a magma chamber beneath Galunggung volcano. High-Mg basaltic magmas coming from the upper mantle entered the magma chamber and were fractionated to become low-Mg basalts and low-Mg basaltic andesites before eruption. The mineral chemistry of the low-Mg basalts, particularly the Ca content of olivines (> 0.11 % CaO), and Al content of orthopyroxenes and magnetites (< 2.5 % and 2.5 - 4.5 % Al_2O_3, respectively), suggest that the minerals crystallised at low pressure (< 10 Kb ?) (Simkin & Smith, 1970; Cox & Jamieson, 1974; Deer et al., 1978a,b, 1982; Osborn & Watson, 1977). The common low-Mg basalts on Galunggung

may also imply that the rocks were derived from a shallow depth magma chamber.

Sibbett (1988) has studied the depth of intrusions under stratovolcanoes in the Circum-Pacific and Western Cascades, USA, and concludes that shallow magma chambers are typically 4 to 9 km deep, whereas subvolcanic stocks are emplaced at depths of 1 to 4 km. A study of the October 1974 low-Mg basaltic tephra from Fuego volcano in Guatemala (Rose et al., 1978) indicated that crystallisation began at a depth of 5 km, and based on the presence of pargasitic amphibole, the magma pressure was estimated at 2 - 3 Kb.

Bulk rock compositions of the low-Mg basalts are projected in the pseudoternary system diopside-olivine-silica (Walker et al., 1979) from plagioclase (Figure VII.3). Also shown are the projected 1 atm cotectics determined by Walker et al. (1979), as well as higher pressure (10, 15 and 20 Kb) cotectics reported by Stolper (1980). Most of the low-Mg basalts occur at less than 10 Kb. These are similar to low-Mg basalts from other island arc volcanoes which are probably generated by fractionation at < 5 Kb (Crawford et al., 1987).

In the 1982-83 eruption, Galunggung volcanic rocks systematically changed from low-Mg basaltic andesite - high-Mg basaltic andesite - "transitional" high-Mg basalt - high-Mg basalt. No low-Mg basalt was produced in this event. This is not common in Galunggung and suggests that there was no magma chamber formed. The magma came directly from upper mantle and was affected by crystal fractionation en route to the surface. Consequently, the most fractionated magma was erupted first, followed by less evolved magmas and ended by a relatively unmodified magma.

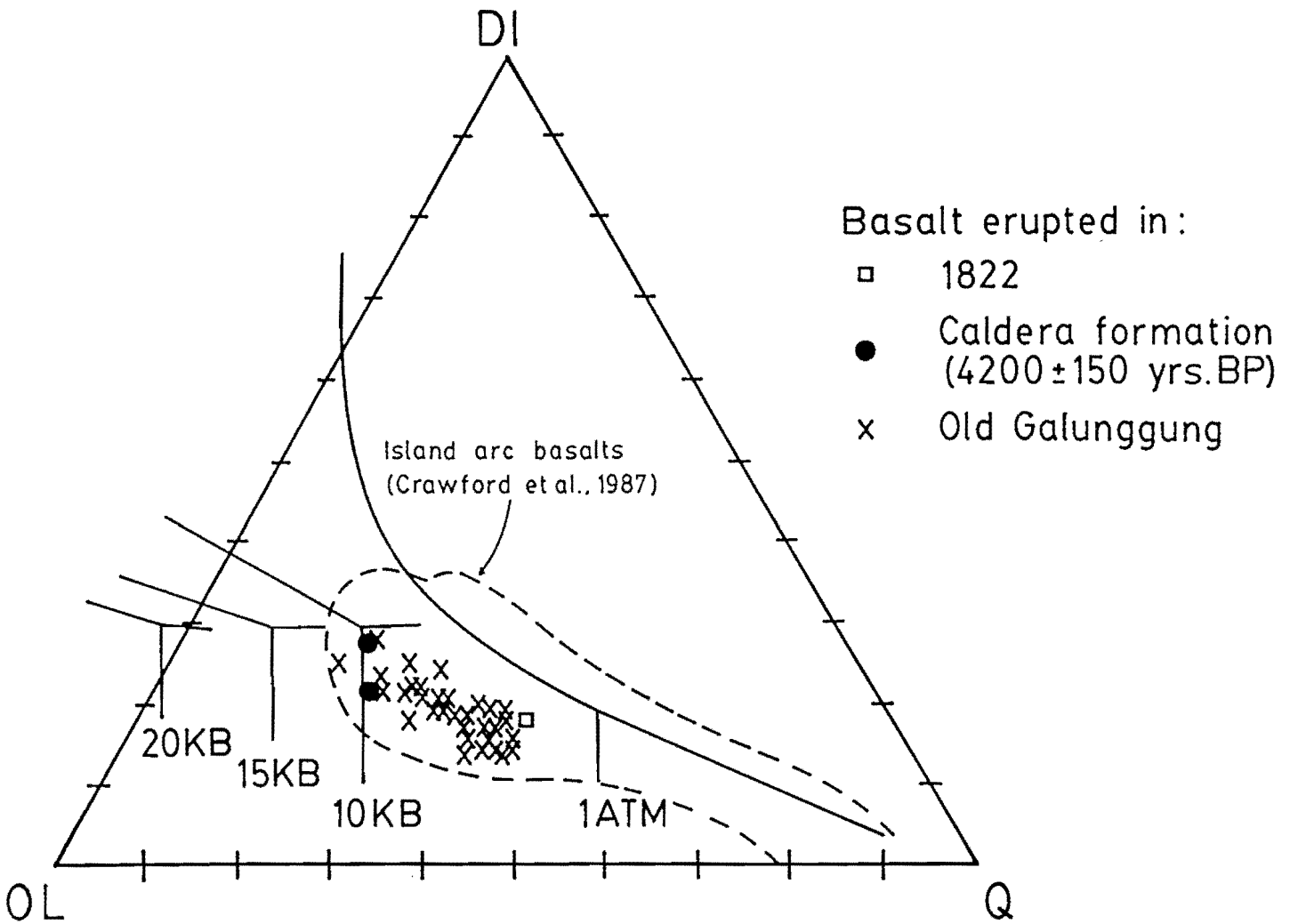

Figure VII.3 Ternary diagram projection from plagioclase onto plane olivine (OLV) - diopside (DI) - quartz (Q) for low-Mg basalts of Galunggung. Shown also are the 1 Atm (Walker et al., 1979) and approximate 10, 15 and 20 Kb (Stolper, 1980) cotectics.

VII.4.4 Calcic Plagioclase in Low-Mg Basalt

Although Mg contents of olivine and clinopyroxene in low-Mg basalts are low, the compositions of plagioclase phenocryst cores are very calcic, similar to those in high-Mg basalts. Rose et al. (1978) reported plagioclase with An_{95-89} in the October 1974 low-Mg basaltic tephra from Fuego volcano, Guatemala. A similar case also occurs in Guntur volcanic products (Purbawinata, 1988, pers. comm.). According to Crawford et al. (1987), fractionation of olivine (+ Cr-spinel) and clinopyroxene in high-Mg basalts drives liquids to low-Mg basaltic compositions with < 7 % MgO, but plagioclase nucleation is delayed by their low but significant (< 1 % ?) H_2O content. They conclude that the calcic plagioclase in the low-Mg basalts is accumulative. This is supported by higher proportion of modal plagioclase (average 24 %) than the subtracted plagioclase (15.5 %) in model 2 step 2.

VII.4.5 Origin of Gabbro and Amphibole

Since the Galunggung caldera forming-event gabbro clasts have been erupted as either accidental blocks or in cores of volcanic bombs. Similarly, amphiboles are found in the gabbro and in volcanic bombs erupted since caldera formation. Three types of gabbro clasts and three types of amphibole crystals are described in previous chapters. The first type of gabbro clasts and amphiboles having poikilitic texture and opaque rims imply late stage rapid crystallisation. This

suggests that the minerals precipitated at a shallow depth (5 - 8 km; Bardinzeff & Bonin, 1987; Johnson, 1977; Lambert & Wyllie, 1970; Stewart, 1975). However, amphiboles having poikilitic texture are also found together with euhedral amphibole phenocrysts that crystallised earlier (Giret et al., 1980), at a considerable depth. This is supported by the absence of amphibole groundmass crystals.

Amphiboles in Galunggung rocks are pargasite according to the classification of Leake (1978). Experimental studies indicate (Holloway, 1973; Holloway & Ford, 1975) that pargasite can be stable phase at 2 - 8 Kb in magmatic temperatures. Holloway & Ford (1975) also suggest that pargasites which crystallised at high pressure have low H_2O but high F contents, whereas amphiboles crystallised at low pressure contain high H_2O but low F contents. Galunggung amphiboles contain high Al (12 - 14 % Al_2O_3) suggesting high water pressure (Kay & Kay, 1985b) as suggested for amphibole and gabbro clast studies from other areas (e.g. Becker, 1977; Yamazaki et al., 1965; Foden, 1983).

Hammarstrom & Zen (1986) suggest that amphiboles from shallow intrusions have total Al $\leq$ 2.0. Galunggung amphiboles, however, have total Al > 2.0 (Table V.5) reflecting a high pressure crystallisation. Using the formula of Hammarstrom & Zen (1986), P = - 3.92 + 5.03 total Al, amphiboles from Galunggung gabbro clasts and volcanic bombs are plotted together with amphibole data collected from the literature in Figure VII.4. Amphiboles in gabbro clasts give similar pressure values (7 - 9 Kb) to those in the volcanic bombs which may indicate that the amphiboles crystallised in the same environment. The average pressure of about 8 Kb or 24 km deep is comparable to the hornblende in an ultrabasic rock from India (Deer et al., 1978a). In the same way, amphiboles in gabbro clasts from Central Japan (Yamazaki et al.,

Figure VII.4 Amphibole geobarometer following the method of Hammarstrom & Zen (1986) where P Kb = - 3.92 + 5.03 total Al.


Gabbro clasts and volcanic bombs from Galunggung


High pressure intrusive rocks (Deer et al., 1978a; Hammarstrom & Zen, 1986)


Low pressure intrusive rocks (Hammarstrom & Zen, 1986)


Hornblende gabbroic inclusions (Yamazaki et al., 1965)


Mt. Hood andesites (produced experimentally at T = 920 ^{o}C and P = 18 Kb) (Allen et al., 1975)


Mt. Hood andesites (produced experimentally at T = 920 ^{o}C and P = 10 Kb) (Allen et al., 1975)


Paricutin andesites (produced experimentally at T = 930 ^{o}C and P = 5.8 Kb) (Eggler, 1972)


Ultra-basic rocks (Deer et al., 1978a)


Andesitesitic volcanic rocks (Eggler, 1972; Garcia & Jacobson, 1979; Jakes & White, 1972; Stewart, 1975)

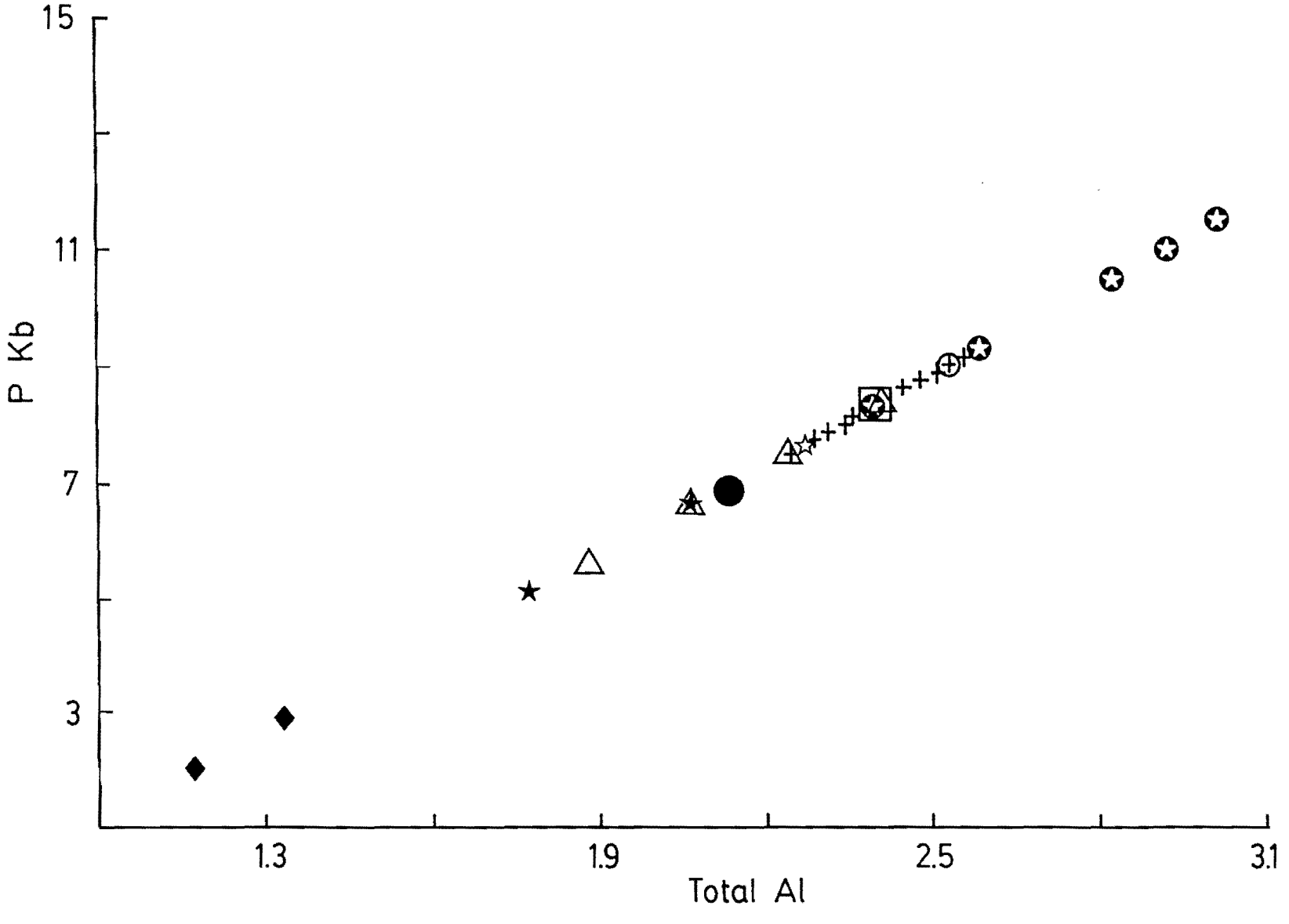
15
11
7
3
P Kb
1.3
1.9
2.5
3.1
Total Al

1965), West Germany (Becker, 1977), Mt. Pelée (Bourdier et al., 1985), Mt. Soufriere (Lewis, 1973) and amphiboles in Rinjani andesites (Foden, 1983) also show high pressure crystallisation (Table V.5). On the other hand, amphibole inclusions in plagioclase phenocrysts of the 1983 lava flow are not in equilibrium with the host rock and give a very low pressure like amphiboles in Rabaul pumice (Heming & Carmichael, 1973).

Foden (1983) proposed a hypothesis of amphibole gabbro formation beneath Rinjani volcano as follows :

"In its early stages an island arc may be built up on oceanic crust, perhaps only 10 km thick, and basaltic liquids which rise up against the base of this crust will cool at pressures markedly less than 7 Kb and are unlikely to crystallise the critical amphibole gabbro assemblage. In this young oceanic arc, crystallisation of a combination of the phases olivine, clinopyroxene and plagioclase will tend to yield low-MgO, basaltic andesite differentiates, but not abundant andesite. As the arc develops, the thickening basalt pile will gradually depress the base of its crust, which will also accrete downwards due to the emplacement of anhydrous gabbroic plutons and accumulate assemblages of combinations of olivine, clinopyroxene and plagioclase. Once the crust has developed and thickened to the stage where its base is at 20 - 25 km, then amphibole-gabbro assemblages may be precipitated and andesitic liquids produced. Hence, as an arc develops through time, there is an enlarged potential for the production of andesitic liquids formed as a result of the increasing opportunity for basaltic parent liquidus to cool under those conditions where the plagioclase and amphibole liquidi intersect closest to that basaltic liquidus."

This hypothesis is however not applicable for Galunggung and other volcanoes in Western Sunda arc because :

1. The presence of granite and metamorphic basement rocks beneath Western Sunda Arc (see chapter II) means that Java is not an island arc. 2. Galunggung amphibole-rich gabbro is associated with low-Mg basalts and basaltic andesites. Andesites are not observed at Galunggung nor is there any evidence of an anhydrous gabbro pluton. And 3. Galunggung geochemical evolution suggests that most evolved basaltic andesite is not followed by andesitic rocks but is terminated by an eruption of high-Mg basalt.

In addition, Foden's hypothesis implies that the amphibole-bearing gabbro occurs as a large-widespread intrusion in the lower crust. However, the volume of ejected amphibole gabbro clasts in any volcanic rock is small and the intrusion is geophysically undetectable. These imply that the amphibole gabbro is a small intrusion restricted in a local area. A model for amphibole gabbro formation in Galunggung is presented in Figure VII.5. The formation of amphibole in a rising magma body is also suggested by Witt & Seck (1989) for amphibolite xenoliths from the Rhenish Massif, West Germany. The model implies that Galunggung primary magma was relatively hydrous. Anhydrous mineral crystallisation would concentrate water in the magma resulting in a high water pressure. Amphibole would crystallise when a sufficiently high water pressure (> 7 Kb) was attained. This interpretation is in agreement with long dormant periods before Galunggung caldera formation and before historic eruptions in 1822, 1894 and 1982-83. On the other hand, amphibole is not observed in Old Galunggung rocks and the 1918 lava dome. This may be because any gas in the magma had already escaped so high water pressures were never attained.

Figure VII.5 Schematic model for gabbro formation in Galunggung.

A. A fairly wet magma body derived from about 50 km beneath Galunggung volcano, rises to lower crustal levels (< 24 km). Anhydrous minerals, olivine and clinopyroxene, begin to crystallise, and water remains in the residual melt, particularly at the top of the magma body (because of its lower density). Because of continuing anhydrous mineral crystallisation, the water pressure increases to about 7 - 8 kb, when amphiboles (green, euhedral prismatic crystals) crystallise.

B. The top part of the magma body has solidified, but liquid underneath continues to migrate upward. Pressure from below causes cracks to form in the solidified material, while anhydrous minerals continue to crystallise and to concentrate water in the magma. Water-rich liquid, having a lower density than the main basaltic magma and solidified green amphibole bearing gabbro, tends to occupy the highest level of the magma body by flowing along the cracks. At higher levels in the crust, temperature decreases sharply and amphiboles are oxidised as they crystallise, to form brown amphiboles with opaque rims at the crystal margins.

C. The magma movement also causes deformation in the crust that becomes more intense with time. This enables meteoric water to interact with the magma at shallow depths, and hydrostatic pressure increases sharply. A combination of tectonic, magmatic and hydrologic processes (Newhall & Dzurisin, 1988) could then trigger the catastrophic eruption causing caldera formation. Both types of amphibole and gabbro clasts were erupted and occur in pyroclastic flow deposits associated with that event.

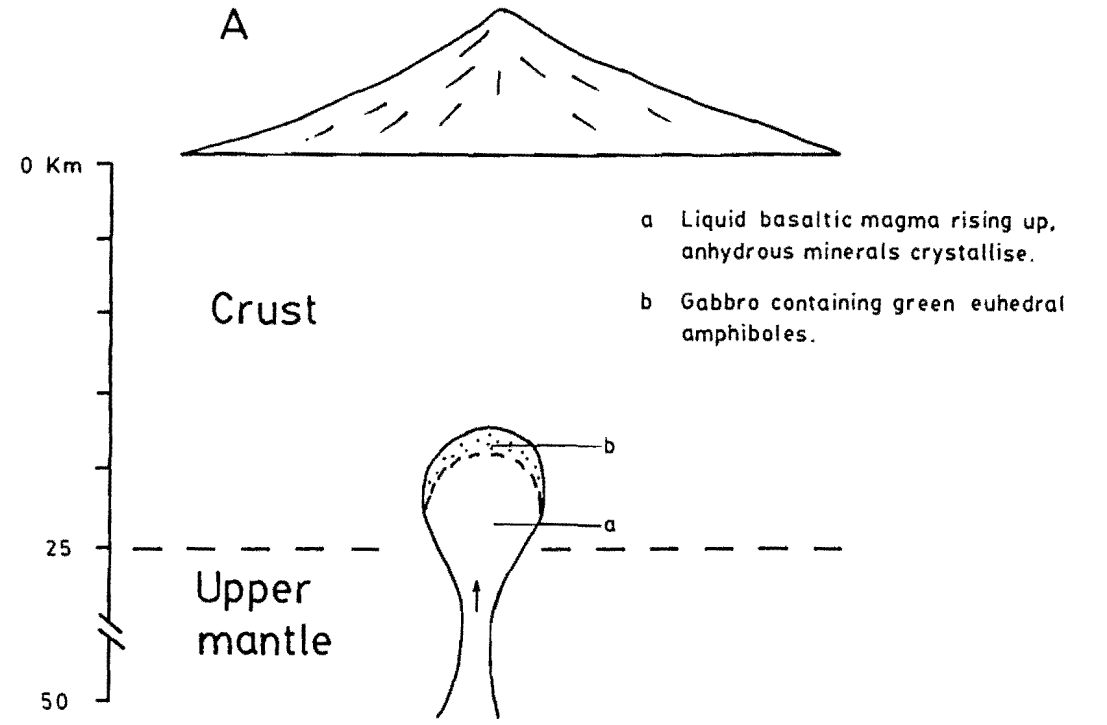
A
0 Km
Crust
25
Upper
mantle
50
a Liquid basaltic magma rising up, anhydrous minerals crystallise.
b Gabbro containing green euhedral amphiboles.
b
a

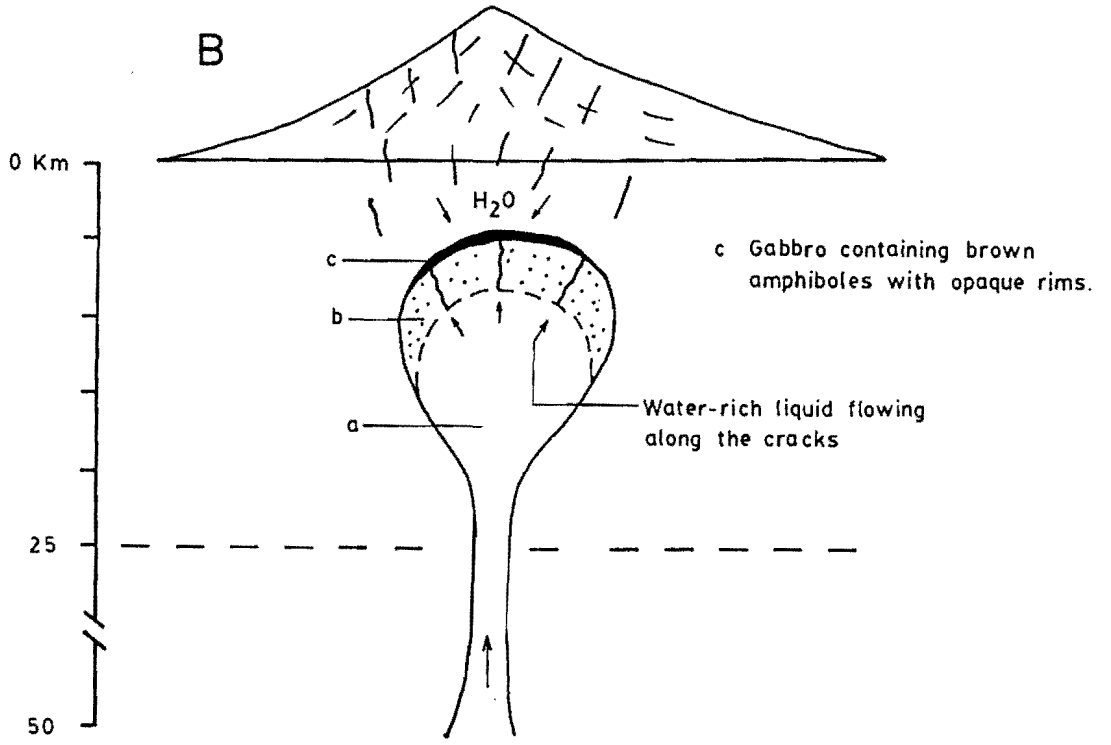
B
0 Km
H_2O
c
b
a
25
50
c Gabbro containing brown amphiboles with opaque rims.
Water-rich liquid flowing along the cracks

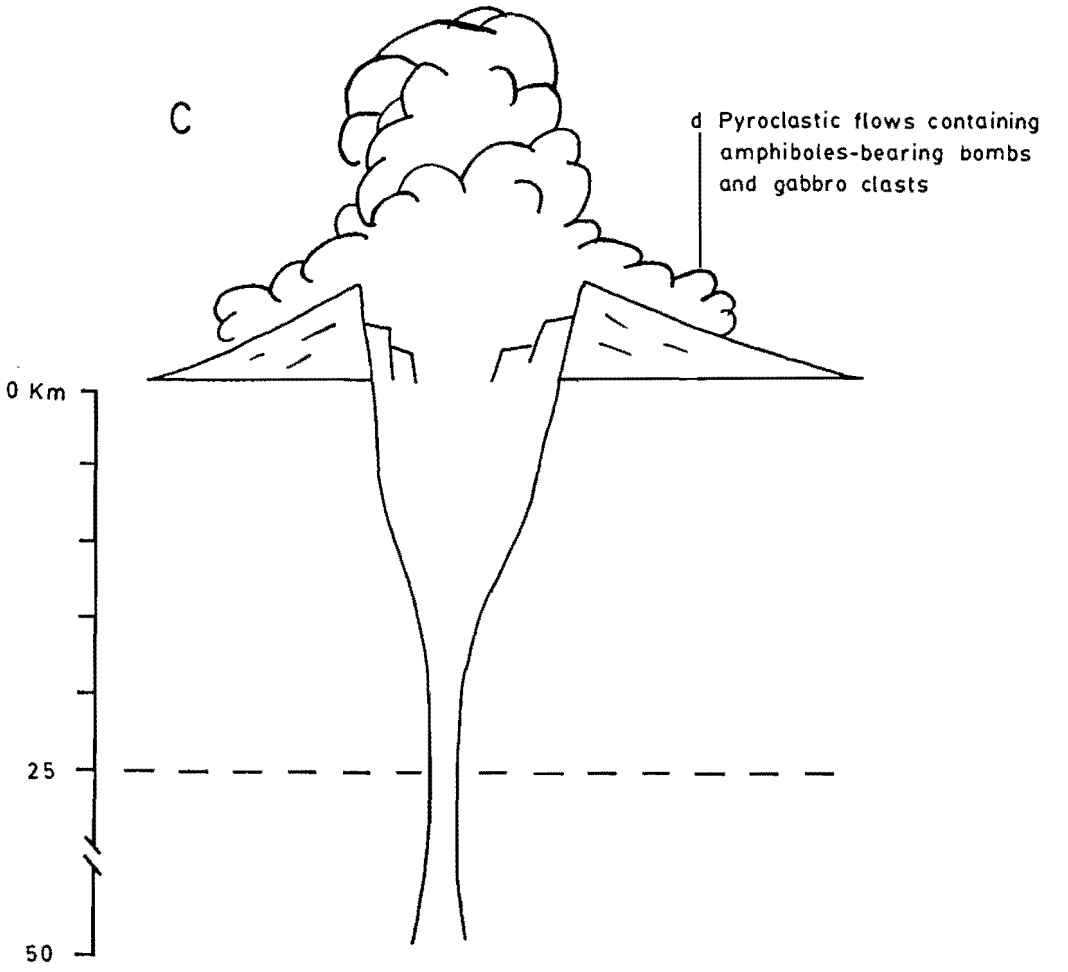

Destructive eruption during caldera formation

Degassing may thus be caused by frequent but relatively small eruptions. This indicates that during Old Galunggung volcanic activity, which can be considered as a constructive period, eruptions were more frequent but less destructive than the following volcanic activities. Degassing also occurred in the magma of the 1918 lava dome extrusion which was only separated by a short period of dormancy from the 1894 eruption.

VII.4.6 Origin of Rhyolite

On 16 September 1982, a Galunggung eruption ejected rhyolite pumice clasts blanketed by basaltic material. Although volcanic glass in the pumice is fresh, feldspars are mostly replaced by dusty opaque materials. Compared with feldspars in the 1883 Krakatau pumice, feldspars in the Galunggung pumice are strongly altered. Bulk rock chemical composition (Table VI.5) gives a very high silica content (> 71 % SiO_2), much higher than the commonly observed Galunggung evolved rocks (57 % SiO_2).

Some possibilities for the origin of rhyolite pumice clasts are listed below :

a. Xenoliths coming from another source.

b. Crustal melt generated by basalt intrusion.

c. Extreme crystal fractionation of Galunggung basaltic magma.

d. Partial melting of pre-existing dacite rock.

Neither pre-1982 Galunggung rocks nor other volcanic rocks around Galunggung have rhyolite compositions. Where crustal melt has been invoked, such as in Taupo Volcanic Zone (Graham & Hackett, 1987) metamorphic xenoliths derived from the sedimentary rock are present. Huppert & Sparks (1988a,b) propose that granitic magmas can be generated by intrusion of basalt into continental crust. They estimate that basalt sills 10 to 1500 m thick require only 1 to 270 years to solidify and would form voluminous overlying layers of convecting silicic magma. They also predict that dacitic volcanic rocks and granodiorite/tonalite plutons would be the dominant rock types. However, in this situation rhyolite should be erupted at the beginning of eruption followed by dacite and andesite rocks before basaltic andesite and basalt are erupted. At Galunggung rhyolite pumice clasts were erupted in the final stages of eruption in association with basalt, while dacite and andesite are not observed. Moreover, ejected intrusive rocks are gabbro not granodiorite.

Compared with most observed Galunggung volcanic rocks, rhyolite pumice is much higher in silica, alkali and incompatible elements. When plotted on a spider diagram the rhyolite has a similar pattern to that of most Galunggung volcanic rocks (Fig. VI.16), indicating that Galunggung rhyolite could be derived from Galunggung basaltic magma by crystal fractionation and least squares mixing calculations (Table VII.8, model 1, step 3) involving amphibole fractionation also show that Galunggung basaltic andesite can be a parental composition to the rhyolite. Trace element modelling does not however fit well; some trace elements calculated are too high and others are too low compared with the observed concentrations (Table VII.8, step 3 of model 1). Crystal fractionation of basaltic magma has been suggested for other

volcanoes in Sunda arc (e.g. Camus et al., 1987, Wheller & Varne, 1986a, b, Foden, 1983) but these have a complete sequence from basalt - andesite - dacite - rhyolite. The absence of andesite and dacite rocks in Galunggung and the poor fit for trace elements in modelling therefore do not support the crystal fractionation model.

According to Conrad et al. (1988) rhyolite can result from melting of preexisting dacite in the crust; and there is Miocene dacite exposed to the south of Galunggung volcano (see chapter II, section 3.3). Dacite could remelt as the high temperature (1300^{o}C, see Table VII.2) high-Mg basalts were erupted in the final stages of eruption. Such a model is supported by the presence of the dusty opaque materials replacing plagioclase phenocrysts. However an isotopic study is really necessary before the proposed origin could be verified.

VII.5 Summary

Two primary liquids have been identified at Galunggung volcano : (1) low-K high-Mg basalt, and (2) medium-K high-Mg basalt. The low-K high-Mg basalt is derived from 15 % melting of spinel peridotite at about 50 km depth, whereas, the medium-K high-Mg basalt is segregated from plagioclase peridotite (30 km depth) at 25 - 40 % melting (Jaques & Green, 1980). The low-K high-Mg basalt is the predominant magma source of Galunggung volcanic rocks.

Two fractionation systems occur from (1) low-K high-Mg basalt - "transitional" high-Mg basalt - high-Mg basaltic andesite - low-Mg basaltic andesite, and (2) low-K high-Mg basalt - low-Mg basalt -

low-Mg basaltic andesite. The first sequence occurred in 1982-83 eruption. The rapid ascend and uncommon event suggest that the magma came directly from upper mantle and was fractionated in a conduit system during migration. The second sequence represents very common rocks erupted before 1982. Low-K high-Mg basaltic magma was fractionated in a magma chamber to become low-Mg basalt - basaltic andesite before eruption. The medium-K high-Mg basalt is a single primary magma ascending diapirically in a conduit system. The evolution of Galunggung magma is summarised in Figure VII.6.

Figure VII.6 Schematic model of evolution of Galunggung magma.

I Old Galunggung

IA. Low-K high-Mg basaltic magmas from the spinel peridotite field moved upward into the crust, and were fractionated in a magma chamber (about 10 km depth) to become low-Mg basalts and basaltic andesites. Very frequent and relatively small eruptions from the magma chamber built Galunggung stratovolcano.

IB. A medium-K high-Mg basaltic magma migrated diapirically from the plagioclase peridotite field to a high level, formed a cryptodome beneath the crater and the Old Galunggung activity terminated.

II Syn- and post- Galunggung caldera formation

IIA. A low-K high-Mg basaltic magma derived from the spinel peridotite ascended relatively slowly enabling water to be concentrated to yield a high water pressure. The magma was fractionated to become low-Mg basalt and basaltic andesite, and hydrous (amphibole) minerals crystallised. Gabbro solidified at the top of the magma body. Because the Old Galunggung cryptodome plugged the existing vent, a new vent developed on the SE flank. During caldera formation, the low-Mg basalt - basaltic andesite and amphibole gabbro clasts were erupted. In the pre-1982 historic eruptions, magmas followed the same evolutionary path.

IIB. In the early 1980's, a new generation of low-K high-Mg basaltic magma moved diapirically from its source. The magma did not form a chamber. However, en route to the surface, the upper parts were affected by crystal fractionations of olivine, clinopyroxene, plagioclase and Ti-magnetite. The magma was erupted in 1982-83 and produced firstly low-Mg basaltic andesite followed by high-Mg basaltic andesite, "transitional" high-Mg basalt, and finally high-Mg basalt. Pumice clasts of rhyolite composition may be derived from remelting of Miocene dacite.

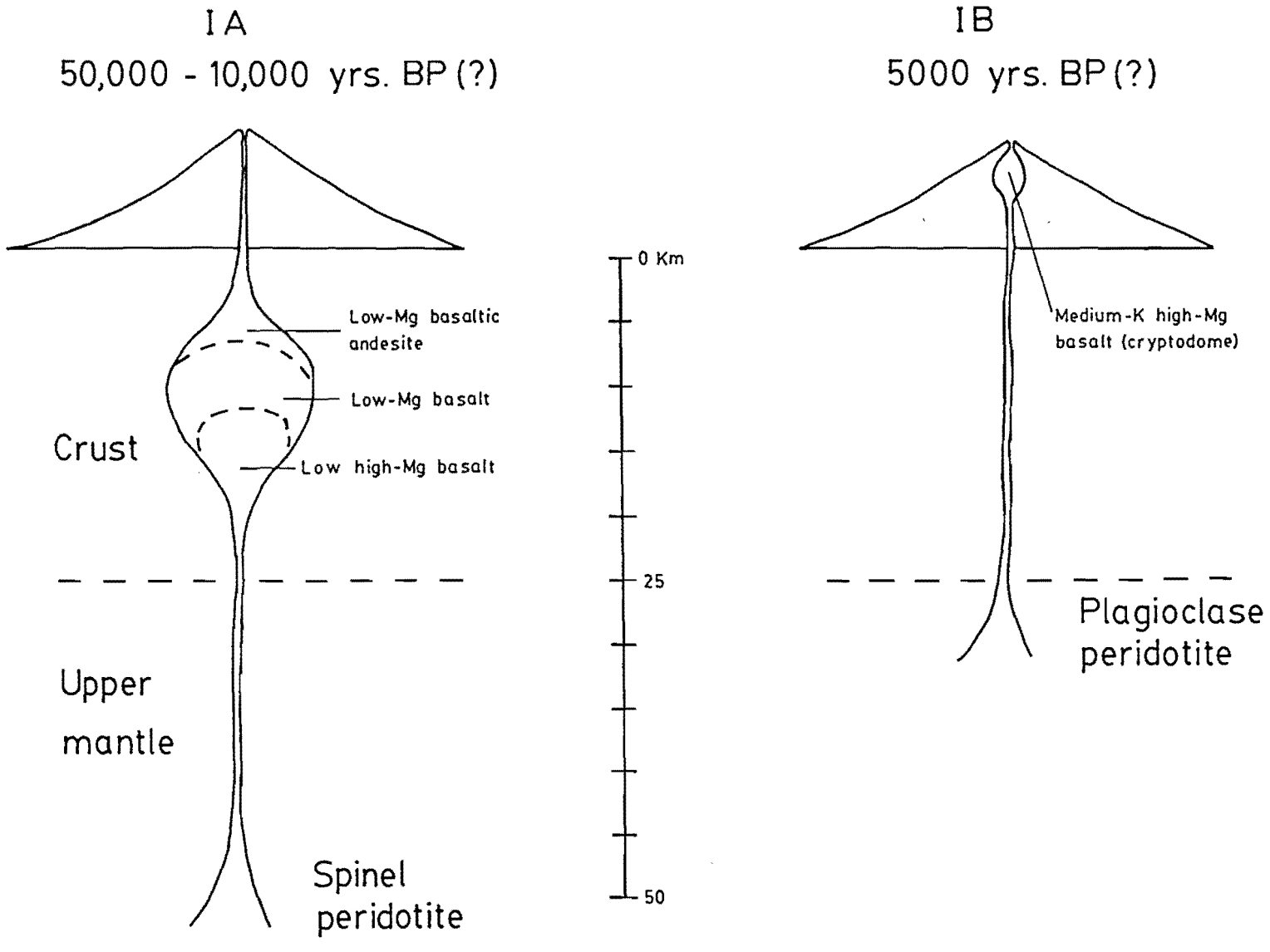
I A
50,000 - 10,000 yrs. BP (?)
I B
5000 yrs. BP (?)
0 Km
25
50
Low-Mg basaltic andesite
Low-Mg basalt
Low high-Mg basalt
Crust
Upper mantle
Spinel peridotite
Medium-K high-Mg basalt (cryptodome)
Plagioclase peridotite

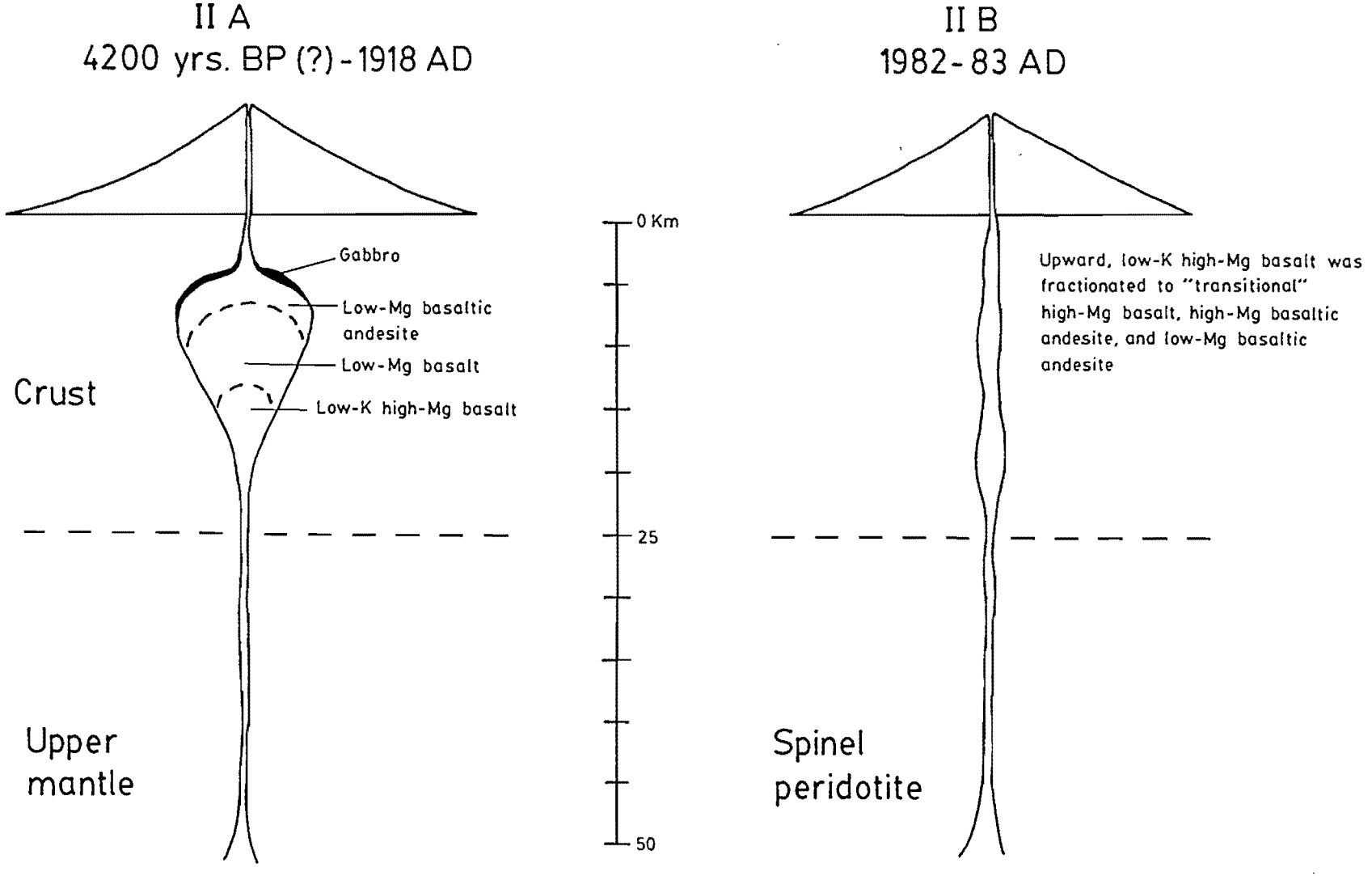
II A
4200 yrs. BP (?) - 1918 AD
Gabbro
Low-Mg basaltic andesite
Low-Mg basalt
Low-K high-Mg basalt
Crust
Upper mantle
0 Km
25
50
II B
1982 - 83 AD
Upward, low-K high-Mg basalt was fractionated to "transitional" high-Mg basalt, high-Mg basaltic andesite, and low-Mg basaltic andesite
Spinel peridotite

VIII VOLCANIC HAZARD ASSESSMENT

VIII.1 Introduction

A volcanic hazard assessment should provide information on direct and indirect hazards from future volcanic eruptions, and portray them on maps, so as to reduce loss of life and property damage. The district of Tasikmalaya, where Galunggung is located, covers an area of 2,748 km^2 and has a population of 1,594,331 people or ca. 580 people/km^2 (Aruman, 1982). It, like the area surrounding other Indonesian active volcanoes, is important economically. Galunggung usually erupts with a periodicity of more than 50 years so people living in the surrounding area tend to forget past volcanic disasters, and with time the population and land-use tends to increase and to move closer to the hazard source. The longer the period of dormancy the more explosive the next eruption is likely to be, but the closer the population tends to be to the summit of the volcano.

Volcanic hazard refers to any potentially damaging or destructive volcanic event, whereas volcanic risk refers to the expectable consequences of a volcanic event in terms of deaths or injury to people, the damage of property, or other kinds of economic loss. Desirable components of a volcanic hazard assessment are the specific time or period during which an event or events are anticipated, an estimate of the frequency of such events, the frequency with which certain areas will be affected, and the extents of those areas. Important components of a volcanic risk assessment include an inventory of the number of people who could be affected by a volcanic event, as

well as the economic activities and public services that would be affected. This chapter is concerned primarily with assessments and map portrayals of volcanic hazards, and does not consider volcanic risk assessment.

Two types of volcanic hazard can be recognised. Those events which occur on average less than once per century, so that people are unlikely to experience them in their lifetime. These are considered as long-term hazards. Those events that occur more than once per century, so that people living on or near the volcano are likely to experience them at least once during their lifetimes are termed short-term hazards. Both types of hazard are present at Galunggung and should be planned for in different ways.

Two types of volcanic hazard maps are used in Indonesia. Established hazard maps are used for volcanoes which erupt very often so their characteristics are already known, e.g. Merapi (Pardyanto et al., 1978). Preliminary hazard maps are made of volcanoes with few known eruptions. Galunggung volcano comes into the second category. Zonation of each type of map is given in Table VIII.1

The validity of these maps is based on the following assumptions :

1. Eruptions occur in the main crater from which volcano has erupted in the past, and not from other unexpected points such as flank eruptions.
2. The eruption column will be vertical.
3. Eruption will not form a caldera.
4. Morphology of the volcano does not change considerably.

Table VIII.1 Zonation of volcanic hazard map in Indonesia, (Kusumadinata, 1979).

I. Established hazard map :

1. *Forbidden zone or closed zone* is an area situated closest to the danger source, that is easily affected by pyroclastic flows and ballistic blocks and bombs, and therefore should be permanently abandoned.

2. *First danger zone* is an area which was in danger during previous eruptions although it may not be affected by pyroclastic flows. During paroxysms, however, it may be destroyed by ballistic blocks and bombs

3. *Second danger area* comprises the areas situated in or close to valleys originating from the summit, and which may be invaded by rain lahar. This zone may be eventually divided into "alert zone" and "abandoned zone". The first is an area situated near a topographic high, e.g., a hill which can provide an evacuation area in case of lahars.

II. Preliminary hazard map :

1. *Danger zone* is an area that has to be absolutely abandoned in case of signs of increased activity. The situation may be afterwards investigated by a competent volcanologist.

2. *Alert Zone* is an inhabited area where people have to be on their alert, and evacuation from this zone may also be necessary, depending on the development of the volcano's activity.

VIII.2 Existing Volcanic Hazard Maps of Galunggung

Volcanic hazard mapping and monitoring of Galunggung volcano has been carried out over many years.

Müller (1839) mapped areas damaged by the 1822 eruption (Fig.III.12). This map could be considered as the first volcanic hazard map of Galunggung. He identified three damaged areas :

1. That affected by pyroclastic flow and pyroclastic surge on 8 October.
2. An area invaded by rain-generated lahars on 12 October.
3. An area damaged by extensions of lahar and flood.

A second volcanic hazard map, based on historic eruptions and topography of the area, was made by Kusumadinata (1967, 1979). He considered the danger area to have a radius of 3 km but expanded along river valleys due to such hazards as lava flows, pyroclastic flows and lahars (Fig. VIII.1). The total danger area was about 57.0 km^2. Kusumadinata identified an alert zone with a radius of 5 km from the crater which also extended along the river valleys covering 157.5 km^2.

A third volcanic hazard map was produced by staff of the Volcanological Survey of Indonesia (VSI) on the basis of damage caused by the 1982-83 eruption (Fig. VIII.2).

Galunggung volcano had been visited many times since the 1822 eruption with regular observations since 1918 (e.g., van Es, 1924; Taverne, 1924; Stehn, 1935; Adiwinata, 1950; Kusumadinata, 1959; Suryo, 1959a,b; Alzwar, 1969; Tulus et al., 1979; and Rasjid, 1982). Since the 1982-83 eruption, continuous monitoring has been carried out from a permanent observatory with visual and seismic methods.

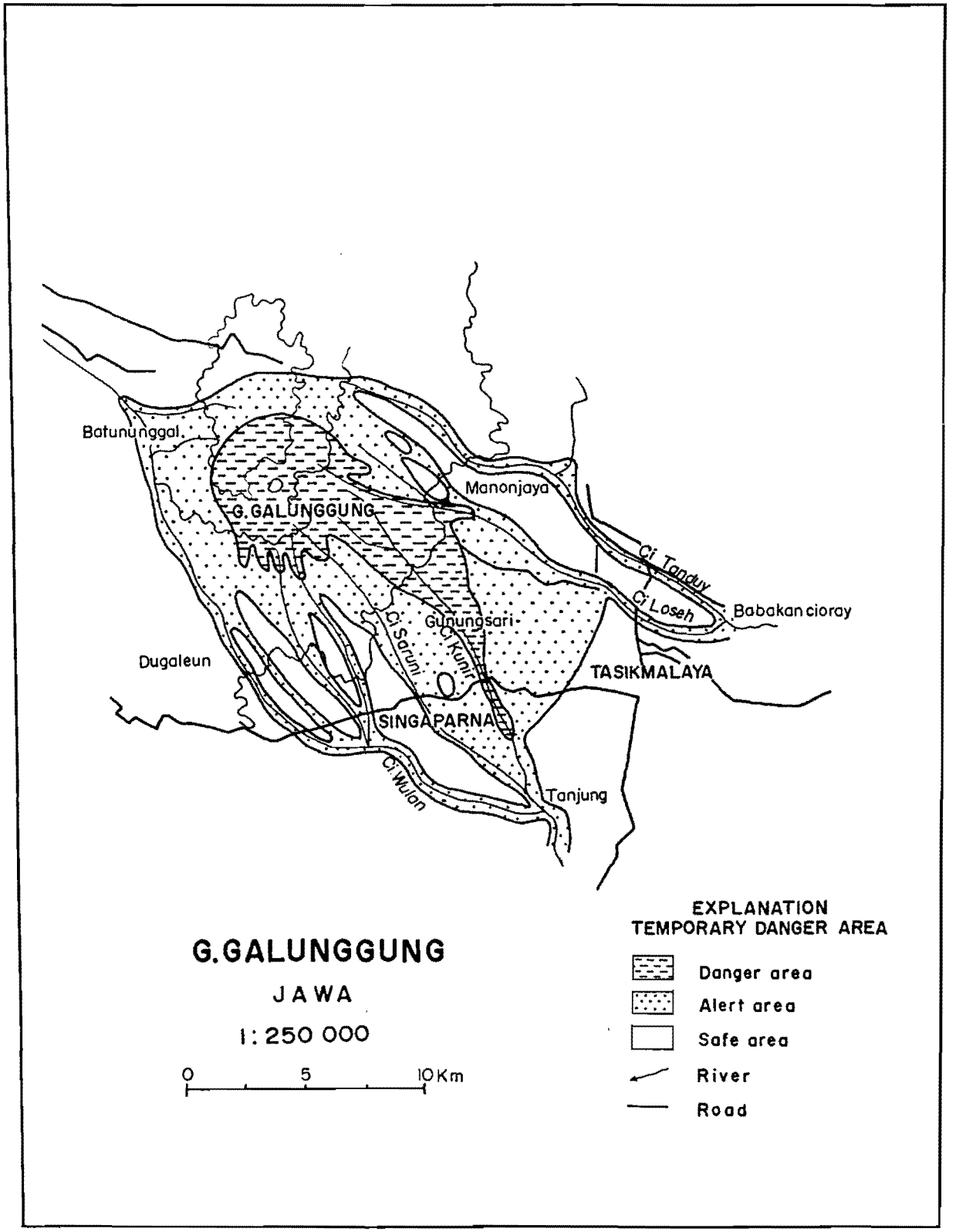

Figure VIII.1 Preliminary volcanic hazard map of Galunggung volcano (Kusumadinata, 1979).

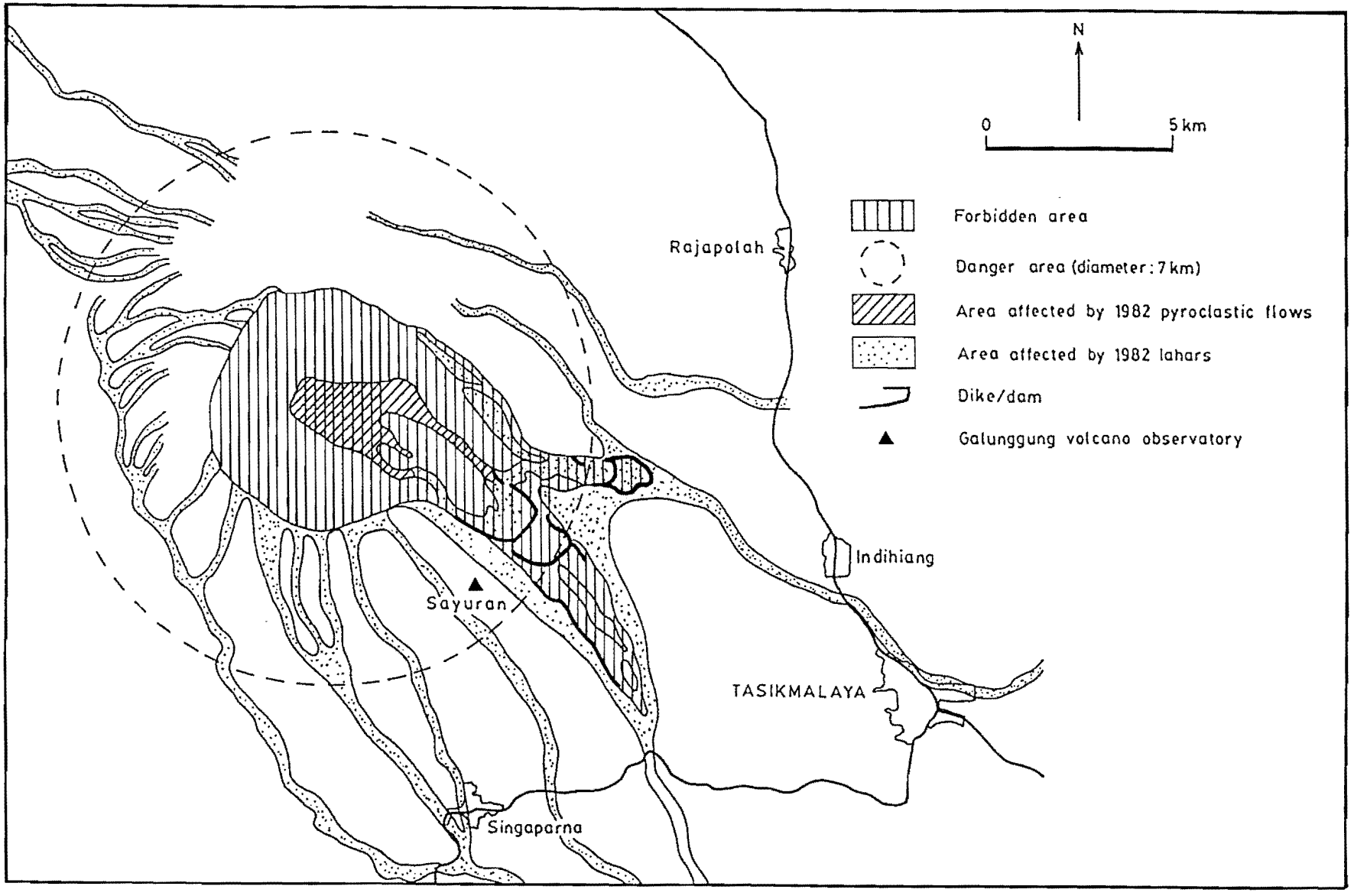

Figure VIII.2 Preliminary volcanic hazard map of the 1982-83 Galunggung eruption (VSI, 1985).

VIII.3 Potential Volcanic Hazards

Potential future volcanic hazards on Galunggung are identified on the basis of what has happened in the past, the types of explosive eruption and types of volcanic product (Table VIII.2). Possible consequences can then be assessed.

Both effusive and explosive eruptions have occurred at Galunggung. An effusive eruption occurs when magma reaches on the surface and produces a lava dome or a lava flow, while the type of explosive eruption depends on intensity and are termed Bandaian, Peléean, Vulcanian and Strombolian in decreasing order of intensity. Most types have been observed in historic eruptions. Their effects have been observed and can also be compared with eruptions elsewhere (e.g. Blong, 1984; Macdonald, 1972; Simkin et al., 1981).

Volcanic products which directly or indirectly endanger people and land-use around the volcano are volcanic debris avalanche, pyroclastic flow, pyroclastic surge, pyroclastic fall, lahar and lava. These are described in chapter III. In this section, the effects of each type of product are discussed in terms of their volcanic hazards.

VIII.3.1 Volcanic Debris Avalanches

Debris avalanches are probably the most destructive volcanic event because they can drastically alter the topography of the area affected. A large landslide of rock debris from a volcano side (or

Table VIII.2 Types of eruption and products of Galunggung volcanic activity. 4011 People were killed in the 1822 eruption and 79 houses were damaged by the 1894 eruption. In the 1982-83 eruption, 35000 people were evacuated and loss of economical value was about US $ 100 million.

Activity	Types of eruption	Volcanic product	Total volume (m^3)
1982-83 Eruption 5 April - 7 January Lahars	Peléean Vulcanian Strombolian Non-explosive	Pyroclastic flows Pyroclastic surges Pyroclastic falls Lava flow	270 x 10^6 (Katili & Sudradjat, 1984)
1918 Eruption 16 - 19 July	Non-Explosive	Lava dome	~ 21 x 10^6
1894 Eruption 7 - 9 October	Vulcanian	Pyroclastic falls Lahars	2 x 10^6 (Fennema, 1896)
1822 Eruption 8 October 13.00 - 15.00	Peléean	Debris avalanches Pyroclastic flows Pyroclastic surges Pyroclastic falls Lahars (12 Oct.)	100 x 10^6 (Neumann van Padang, 1951); 56 x 10^6 (Kusumadinata, 1979)
Caldera formation (4200 ± 150 yrs. BP)	Bandaian	Debris avalanches Pyroclastic flows Pyroclastic surges Pyroclastic falls Lahars	~ 20 x 10^9
Old Galunggung stratovolcano (50,000 - 5000 yrs. BP)	Peléean Vulcanian Strombolian (?) Non-explosive	Pyroclastic flows Pyroclastic surges Pyroclastic falls Lavas & lahars	~ 56.5 x 10^9

sides) may be triggered by a volcanic explosion or by a severe earthquake and can move at high speed beyond the base of the volcano (Crandell & Nichols, 1987).

In 1888, structural collapse of part of Bandai-san volcano in Japan was caused by steam (phreatic ?) explosions that triggered a massive avalanche of rocks debris from the volcano (Sekiya & Kikuchi, 1889). The avalanche involved 1.2 km^3 of the volcano, travelled up to 10 km away from the source with a velocity of about 21 m/sec. The deposits covered an area of 20 km^2 and killed 461 persons. Eruptions of Bezymianny on 30 March 1956 (Gorshkov, 1959) and Shiveluch on 12 November 1964 (Gorshkov & Dubik, 1970) also produced debris avalanches. At Shiveluch volcano the debris avalanches had a volume of at least 1.5 km^3 and covered 96 km^2. A collapse of the north flank of Mount St. Helens in 1980 that was caused by a magnitude-4 earthquake accompanying magmatic injection and phreatic eruptions (Voight et al., 1981) produced debris avalanches which move up to 22 km westward at about 50 m/sec., and covered an area of 60 km^2.

Many large pre-historic debris avalanches have been reported, for instance at Mount Egmont, New Zealand (Neall, 1976; Ui et al., 1986a), Mount Shasta, USA (Crandell et al., 1984; Crandell & Nichols, 1987; Schuster & Crandell, 1984), and at Japan volcanoes (e.g. Ui et al., 1986b; Endo et al., 1986).

Debris avalanches are also common on slopes of volcanoes in Java, such as Gede-Pangrango and Guntur in West Java, Sundoro and Sumbing in Central Java, and Raung in East Java. On Raung volcano, a debris avalanche slid up to 48 km away from the source and formed three horse shoe-shaped depressions. So far, this is the furthest a debris avalanche has travelled in Indonesia. The last recorded vol-

canic debris avalanche in Indonesia occurred at Papandayan volcano in West Java on 11 - 12 August 1772 and 0.14 km^3 of the deposit covered an area of 18 km^2 killing 2957 people (e.g. Frank et al., 1987; Glicken et al., 1987; Kusumadinata, 1979; Neumann van Padang, 1951). The 1883 Krakatau eruption when the volcanic cones of Danan, Perbuwatan and one third Rakata were destroyed probably produced a submarine debris avalanche (Francis, 1985; Verbeek, 1885).

A gigantic debris avalanche occurred during Galunggung caldera formation (4200 ± 150 yrs. BP) which travelled about 23 km to the ESE of the volcano. This was a Bandaian type of eruption and represented the most destructive type of eruption to occur at Galunggung. More than one third of the SE part of the volcano slid onto Tasikmalaya high-plain to form a fan-shaped hummocky topography covering about 170 km^2. A smaller debris avalanche was reported by Junghuhn (1853) during the 1822 Peléean eruption. At present the 1822 debris avalanche deposit forms a ridge (2 km length and 250 m width) extending from the crater to ESE-ward, and is well exposed in Ci Banjaran valley.

Hazards caused by volcanic debris avalanches are those of burial and building damage. Ground deformation monitoring system may detect part of the volcano that is deforming so that evacuation of people in the threatened area can be arranged. If there is a lake in the crater, a lahar and/or flood may also be generated.

VIII.3.2 Pyroclastic Flows

Pyroclastic flows are hot, dry masses which move rapidly down the slope of a volcano. The mass consists of gas and mixed solid mate-

rials from ash (< 2 mm in diameter) through lapilli (2 - 64 mm) to block and bomb (> 64 mm) sized material. Their temperature varies from 200 - 800°C and velocity ranges from 15 - 40 m/sec. (Matahelumual, 1982). Pyroclastic flows erupted from Mt. Pelée in May 1902 (Trechmann, 1938), and Asama in 1783 (Aramaki, 1956) have temperatures of 1075 and 900°C, respectively. The heat is preserved for many years in a thicker pyroclastic flow deposit. Very high velocity pyroclastic flows were reported at Mayon eruption in 1968 (63 km/sec., Moore & Melson, 1969), and Mount St. Helens in 1980 (170 km/sec., Moore & Sisson, 1981).

Relatively moderate to small pyroclastic flows moved along valleys, and in the lowlands surrounding the volcano the flows spread onto peripheral fans. These are common in Peléean and Vulcanian eruptions, but usually have volumes < 1 km^3. Pyroclastic flows generated during observed eruptions in Indonesia usually travel up to 8 km from source, but occasionally as far as 15 km (Suryo & Clarke, 1985).

Large pyroclastic flows, on the other hand, travel radially outwards to roughly equal distances in all directions, frequently traversing quite deeply incised valleys and climbing over obstructions tens of metres high, even tens of kilometres from the source (e.g. Blong, 1984). These flows are associated with collapse of a Plinian eruption column such as the 1815 Tambora and the 1883 Krakatau eruptions, and can reach up to 150 km, cover areas more than 100 km^2, and have volumes exceeding 10 km^3. These pyroclastic flows may occur in Bandaian eruptions although the flows are more likely to be directed.

There are two origins for pyroclastic flow at Galunggung : 1. by vertical expulsion of rock debris from the crater, followed by fall

back and flowage down slope of the volcano, and 2. by a laterally directed explosion at the base of a dome (when the dome was present). Galunggung historic pyroclastic flows moved down from the crater to ESE along the caldera depression. Peléean eruptions produced pyroclastic flows which travel more than 4 km; much further than those associated with Vulcanian eruptions (< 3 km), and much further than ballistic bombs and blocks ejected by vertical eruptions. Secondary steam explosions occurred when the pyroclastic flows entered the water or when water (usually from rivers) flowed through the hot pyroclastic flow deposits.

General hazards caused by pyroclastic flows are those of burial, fire and building damage. Evacuation of people in the area likely to be destroyed is the best way.

VIII.3.3 Pyroclastic Surges

Three types of pyroclastic surges; ground surge, ash cloud and base surge, have been described in chapter III. The first two types of pyroclastic surge are hot because they involve incandescent volcanic debris, whereas the third is a cold pyroclastic surge. They typically move very fast and in a sector of less than 180 degrees. However, the collapse of a vertical eruption column may be followed by the outward movement radially from the volcano. Movement itself is not constrained by topography.

Pyroclastic flows formed at Mayon volcano during eruptions in 1968 were bordered by seared zones as much as 2 km wide in which all animal life and most plant life were killed (Moore & Melson, 1969).

These seared zones were probably caused by pyroclastic surges of hot ash that accompanied the pyroclastic flows. Similar seared zones bordered pyroclastic flows at Mt. Lamington during the climactic eruption on 21 January 1951. These zones locally extended nearly 4 km beyond the limits of the pyroclastic flows (Taylor, 1958).

During the 8 April 1982 Galunggung eruption, an ash cloud type of pyroclastic surge rose above a pyroclastic flow moved rapidly ESE-ward and burned houses at Pasirngemplong village (3.5 km from the crater), while the pyroclastic flow turned to follow Ci Banjaran valley (see Fig.III.24A). In the houses, bottle glasses were deformed suggesting that the temperature was more than 700^{o}C (Blong, 1984). A larger pyroclastic surge occurred in the 1822 eruption and moved eastward up to 18 km away from the crater (see Fig. III.12). These pyroclastic surges were similar to that which destroyed the city of St. Pierre (e.g. Macdonald, 1972, p. 144) when Mt. Pelée erupted on 8 May 1902 (Fig. III.24B). The straight path followed by the pyroclastic surge at Mt. St. Helens (Fig. III.24C) that occurred on 9 May 1986 (Mellors et al., 1988) can also be compared, although it was much shorter and was generated by dome collapsed.

Ground surge and ash cloud pyroclastic surges flow so fast that their path is unpredictable. So, escape is not possible once they have been generated. Zones that may be affected should therefore be evacuated at the start of an eruption.

Base surges commonly occur in volcanic areas having maars, such as Gamalama in Ternate, and Lamongan in East Java (Bronto et al., 1982, 1986a). However, they are not impossible at Galunggung, particularly as there is a lake in the crater. These surges may occur during phreatic events, in the early stages of eruptions. Velocities of 50 to

300 km/hr. can be inferred from the vertical heights ascended by some surges, but they seem to lose their energy quickly during movement, rapidly decelerate, and typically stop within distances of less than 10 km from their source. This may be due to the presence of water and low temperature (< 100^{o}C).

Base surges can cause destruction or removal of structures and vegetation by rock debris moving at high speed, severe abrasion and impact by rock fragments. So, evacuation of people from zones that are likely to be affected is necessary, and also, for long- term planning, avoidance of such zones for building and occupation.

VIII.3.4 Pyroclastic Falls

The main hazards of pyroclastic falls are : 1. ballistic blocks and bombs, and 2. ash- to lapilli-falls.

Ballistic blocks and bombs are often thrown to a considerable height and this can cause severe damage, because of high velocity of impact (Houghton et al., 1988). The travel distance of the projectiles depends on the eruption size. During Strombolian eruptions, bombs are ejected only a short distance from the vent (usually < 3 km; Matahelumual, 1982), whereas in Vulcanian eruptions the coarse particles may be thrown 7 km or more. Some of them reached 8 km from the vent during the 1963 eruption of Agung volcano in Bali (Kusumadinata, 1979), and in 1783, at Asama volcano, red hot pumice bombs 50 cm in diameter landed at a distance of 11 km from the crater (Aramaki, 1956). Sparks & Wilson (1976) have shown that magmatic particles larger than about 5 mm will fail to maintain thermal equilibrium with

the surrounding gas dispersion; that is, they remain hotter than the convecting cloud, the rate of cooling being dependent on particle radius. These hot particles started fires in villages and in the forest. In the 1982-83 Galunggung eruption, ballistic blocks and bombs fell up to 7 km from the vent during Vulcanian eruptions but decreased to 3 km in Strombolian eruptions; the coarse particles destroying houses by impact, not fires.

Ash- to lapilli-falls can be distributed in wide wedge or oval-shaped areas. Galunggung historic eruptions in 1894 and 1982 show that fine material reached up to 200 km downwind (WNW) from the vent (see Fig. III.18). Older deposits were also mostly deposited on the western slope of the volcano indicating that this is the predominant downwind direction. Thickness of the pyroclastic fall deposits decreases with distance, e.g. the deposits erupted in 1982-83 are about 30 m thick around the crater, but decreases to 60 cm in a distance of 7 km and to 5 cm at approximately 50 km NNW of the vent. The area covered by pyroclastic falls having > 5 cm in thickness is about 600 km^2 (Katili & Sudradjat, 1984).

Burial by pyroclastic fall deposits may cause failure and collapse of roofs, and in a typical Indonesian village, more than 20 cm of ash will cause building to collapse. The chief danger of pyroclastic falls to health is on the respiratory system and irritation to eyes. Ash particles having < 10 micron in size can be inhaled and the respiratory system will be affected into two ways : 1. "asphyxia" and "silicosis" (Sudradjat, 1982). Silicosis is a disease caused by fibrous free-silica minerals ("pulmonary fibrous") which may crystallise as quartz, tridymite or cristobalite. Cristobalite is particularly dangerous because of it is the sharpest. During the 1980 St.

Helens eruption, ash particles (67 % SiO_2) of < 10 micron in size contain 3 - 7 % free-silica of quartz and cristobalite, but none of them were fibrous. Ash particles of the 1982-83 Galunggung eruption that have 49 - 57 % SiO_2 contain neither free-silica nor fibrous free-silica minerals. It was nevertheless suggested to evacuate people living in radius of 7 km around the volcano during Peléean and Vulcanian eruptions, and in a radius of 3 km during Strombolian eruptions. Effects of ash on human respiratory system can be reduced if people stay indoors and breathe through filter masks or damp cloths (Crandell & Nichols, 1987), and to protect eyes, goggles must be worn. It is not advisable to drive vehicles while ash is falling because of the danger of becoming stranded by ash-caused engine failure or of having an accident because of poor visibility. In the air, ash is not identified by radar systems of airplanes, and two accidents occurred during the 1982 Galunggung eruptions. So both domestic and international airlines must be informed, to avoid similar accidents. Ash may also carry acids which can corrode metals, damage or kill agricultural crops and contaminate unprotected water supplies. It may also clog filters in water supply systems.

Damp or wet pyroclastic fall deposits are generally more hazardous than dry ones for two reasons. First, wet ash is much heavier and hence more likely to cause collapse when it falls on the roof of buildings. Second, wet ash may adhere to electric power and telephone lines. Fine-grained moist ash deposits are highly cohesive (Blong, 1984), and those < 0.1 mm in diameter have a tendency to form a surface crust affecting plant respiration.

VIII.3.5 Lavas

Non-explosive eruptions may produce lava domes or lava flows. A lava dome is formed when pasty lava is extruded through a vent and is too viscous to flow sideways more than a few tens or hundred of metres (e.g. Crandell & Nichols, 1987). Movement is chiefly upward in the centre of the dome, which causes the sides to become unstable. This instability means that the height of domes is generally limited to only a few hundred metres.

Lava domes may form within the summit crater of a volcano, on its flanks, or at one or more vents along a fissure on or beyond the base of a volcano. In Galunggung, a lava dome extrusion (e.g. the 1918 lava dome) is unlikely to endanger people because of the high and complete nature of the crater rim. However, when the crater rim is dissected (such as on Merapi in Central Java and Semeru in East Java) or the lava dome develops outside the crater it will threaten people living directly downslope and their property. This is because gas explosions within the dome and unstable sides of the growing dome may break away and form pyroclastic flows.

Domes may also form shallow intrusions which are termed cryptodomes. The hydrostatic pressure of molten rock causes the overlying roof of the intrusion to swell upwards. The cryptodome itself is not dangerous. However, it may allow pressure to build up and make the next eruption more explosive, particularly when the dome is emplaced directly under the main crater.

Lava flows in Indonesia are usually of blocky type which move slowly enough for people to get out of their way. However, lava flows may start forest fires, and because of irregularity of channel val-

leys, sudden collapse of lava accumulation can produce pyroclastic flows. Distances reached by lava flows are determined by the volume of lava erupted and its viscosity, and the topography and slope over which they move. The 1983 lava flow of Galunggung was restricted to the crater floor because of its small volume and the lack of an outlet from the crater.

VIII.3.6 Lahars

There are several kinds of lahar but at Galunggung lahars caused by rain on unconsolidated pyroclastic flows are most important. The lahars mostly travel to the ESE because of topography and threaten wide densely populated areas downslope. They occur both during eruptions and for many months or even several years after the eruptions terminate. The size depends on the amounts of pyroclastic deposits (as a source material), adequate water (to give the debris mobility) and a slope. When the pyroclastic deposits decrease but a lot of water is continuously supplied (as in prolonged periods of heavy rain falls), floods extend the damage areas.

Distances reached by lahars also depend on their volume, water content, and gradient and shape of a valley. A steep and narrow valley will permit a lahar of a given volume and water content to move a great distance, whereas a broad valley of low gradient will encourage a lahar to slow, spread, and stop within a shorter distance. In the 1982-83 Galunggung eruptions, lahars flowed in river valleys whose sides have a slope > 30 %, and then spread onto peripheral fans on the more gentle slope and plain areas up to 17 km to the ESE (Ci Tandui catch-

ment area), to the south (Ci Wulan) and NNW (Ci Manuk). The lahars covered areas of about 70 km^2 (Hamidi, 1985), and had a volume of more than 20 x 10^6 m^3. Lahars which developed in 1822 were much longer (40 km to ESE) and as were those in 1894 which followed a similar path.

The velocity of a lahar is determined by gradient, the solid-to-water ratio, and by channel shape. The highest speeds reported are from the slopes of volcanoes, where movement is similar to that of a debris avalanche. Lahars caused by the eruption of Mount St. Helens on 18 May 1980 had inferred speeds on steep slopes of more than 165 km/hr. (Janda et al., 1981). In Japan, lahars of Tokachidake volcano were reported to have a velocity up to 180 km/hr (Murai, 1963) and an average speed of 58 km/hr. (Tada & Tsuya, 1927). A lahar from Cotopaxi volcano in Equador in 1877 was estimated to have had an average velocity of 27 km/hr over a distance of 300 km (Macdonald, 1975).

Lahars caused by an eruption of Kelut volcano in East Java in 1919 have an average speed of 64 km/hr, and in 1966, about 43 km/hr in the upper 9 km of their source, and 23 km/hr in the next 15 km (Kusumadinata, 1979). At Galunggung, observed lahars have a velocity greater than that of floods which are generally less than 30 km/hr.

Because of topography and the presence of waterfalls on the Galunggung caldera wall, a crater lake is always likely to form after an eruption period terminates. The water accumulation in the crater may cause either a phreatic explosion or an explosion lahar. This depends on the intensity of interaction between water and hot magma body underneath, and headward erosion towards the crater. Historic records indicate that a crater lake formed after the 1894 eruption. However, a lava dome extrusion in 1918 was not preceded by a phreatic explosion or an explosion lahar such as on Kelut volcano at East Java.

This was probably due to low gas content of the 1918 Galunggung magma as has been discussed in chapter VII. After the 1918 eruption the lake drained out through Ci Banjaran and when the 1982-83 eruption occurred there was insufficient water to produce a lahar.

Lahars threaten people, agriculture and engineering sites. They move down the valley at high speed and then spread across the surrounding plain areas, burying highways and buildings. Because of their high bulk density, lahars can displace and carry very large and heavy objects, such as houses and bridges. Lahars also cause river channels to shift, and may form lakes by damming tributary valleys. Dikes and other lahar-control structures have been built on valley floor to limit the effect of lahars in Indonesian active volcanoes, such as Galunggung, Merapi, Kelut and Agung.

VIII.4 Background Information Necessary for Volcanic Hazard Assessment

Volcanic hazard assessment is generally based on a volcano's eruptive record during historic time, as well as known prehistoric activity.

Historic records are generally found in old documents, newspapers, and sometimes in local history and legends. On the basis of archaeological data (Sunardjo et al., 1978) the district of Tasikmalaya has been occupied since 526 AD, but more reliable indicators suggest it was established in 1111 AD. Although the capital of the district moved many times there is no information to indicate any volcanic eruptions during its early history. This may correlate with

carbon dating (590 ± 150 yrs. BP, see Fig. III.14) and a report from the Resident of Priangan (West Java) that before the 1822 eruption, Galunggung volcano was covered by dense forest and there was no indication that it was an active volcano (van Es, 1924).

Historic eruptions occurred in 1822, 1894, 1918 and 1982-83 (Table VIII.2). All of them are described in chapter III and indicate that Galunggung eruptions vary in type, duration and volcanic products. The eruption cycles are mostly separated by long periods of dormancy (> 50 years) except for that between the 1894 and 1918 eruptions (24 years). However, this short dormancy was followed by a non-violent extrusion of a lava dome. This may imply that if the next eruption occurs after only a short dormancy period it will not be an explosive one. However, if the present inactive period continues for a long time period the next eruption will be destructive.

Volcanic events in prehistoric times are interpreted from studies of the products of past eruptions, volcanic stratigraphy and radiocarbon dating. These studies suggest that Old Galunggung volcanic activity was similar to the historic eruptions but with a larger eruption occurring during Galunggung caldera formation.

On the basis of petrological and geochemical studies, two major magmatic cycles from low-Mg basalt and basaltic andesite to high-Mg basalt are identified at Galunggung. The first cycle extends through Old Galunggung activity and the second one is from Galunggung caldera-forming event to the 1982-83 eruption. The two cycles are probably separated by a considerable period of dormancy.

If future magmatic generation is consistent with past volcanic events in which two magmatic cycles were each ended by an eruption of high-Mg basalts, a new cycle is likely to occur after a long inactive

period. This enables gas to accumulate and produce a high water pressure environment and hydrous mineral (amphibole) precipitation. Bardinzeff & Bonin (1987) reported that amphibole is a common mineral in explosive volcanic products. This is in agreement with frequently observed amphiboles in pyroclastic flow deposits erupted during Galunggung caldera formation, but the mineral is not found in Galunggung effusive rocks. According to Bardinzeff & Bonin (1987), amphiboles can be dissolved (break-down) suddenly because of modification of the thermodynamic conditions such as a rapid magma ascent. This break-down of amphibole liberates water in the magma to increase hydrostatic pressure and create an explosive eruption.

In addition, the presence of rhyolite pumice, which is commonly associated with violent eruptions, requires further attention. Although the origin of Galunggung rhyolite pumice is not yet clear, any rhyolite eruption may be destructive. Evidently, caldera formation may occur more than one time in a volcanic area. Studies on Toba (e.g. Aldiss & Ghazali, 1984; Chesner & Rose, 1987; Stauffer, 1987), and Krakatau (e.g. Bronto et al., 1986b; Camus et al., 1987; Simkin & Fiske, 1983; van Bemmelen, 1949; Verbeek, 1885) reported that at least two caldera formations are identified. However, the eruptions were separated by a very long dormancy. Surveillance is always necessary to guard against such events.

VIII.5 Preparation of Hazard-Zonation Maps

The ways in which volcanic hazards are portrayed on maps differ from one scientific organisation to another. Hazard-zonation maps for

specific volcanic products have been proposed by many volcanologists (e.g. Crandell, 1980; Crandell & Nichols, 1987; Miller et al., 1978). Hazard-zonation maps have also been made on the basis of eruption type (e.g. Houghton et al., 1987). In Indonesia, established volcanic hazard maps have been prepared for volcanoes which erupt frequently.

Most potentially hazardous volcanic products suggest evacuation to reduce volcanic risk but as all areas surrounding Indonesian active volcanoes are densely populated and have very high economic values this is difficult. One radical solution is to permanently evacuate all people in the high risk zones and resettle them in more sparsely populated areas. However, this is not really practicable (Zen, 1983), because people have their livelyhood around their homes. This is compounded by the fact that the area surrounding the volcano is generally much more fertile and hence more intensely settled than other places. Furthermore, no prediction statement can be regarded as 100 % certain and an evacuation without the expected eruption would cause volcanologists to lose credibility in the eyes of the public.

On the basis of studies of past volcanic events and a realistic view of what is possible in Indonesia, four categories of volcanic hazards on Galunggung are distinguished :

1. First degree hazard

This is the most destructive event, when a big eruption, either Bandaian or Plinian - ultra-Plinian, is expected. This could produce a voluminous debris avalanche, pyroclastic flow, pyroclastic surge, pyroclastic fall, lahar or combination of processes. It requires closing a zone with a radius of above 30 km in the Tasikmalaya plain and surrounding areas, and the whole area of West Java should be considered as a danger zone. Evacuation of the whole area is the only real-

istic course to take.

2. Second degree hazard

A second degree hazard would be caused by Peléean eruptions producing large pyroclastic flows and surges, accompanied by rain lahars. Also, there is the possibility of flank eruptions and poison gases that may appear along fractures in the Galunggung caldera depression. Explosion lahars from the crater are possible although they were not recorded in the historic volcanic events. The most affected areas would be to the ESE, extending from the horseshoe-shaped Galunggung caldera. Evacuation is suggested for the people living in this area. Pyroclastic falls may not require evacuation of people living at a distance, however warnings must be given to people in areas likely to be affected.

3. Third degree hazard

This would be caused by predominantly vertical explosions producing pyroclastic falls, although small pyroclastic flows and surges may occur near to the vent. However, rain lahars would threaten wide areas, particularly when the eruption is of long duration. Ballistic projectiles of blocks and bombs may reach up to 7 km from the vent and threaten people living in the area. The possibility of burial away from the volcano depends on the wind direction. Warnings need to be given to people both on the ground and those dealing with aircraft navigation. Hazards caused by phreatic explosions and base surges are included in this category.

4. Fourth degree hazard

This is caused by Strombolian eruptions, lava flows, and lava domes in the crater. Affected areas are probably the smallest, particularly around the crater and for a short distance along stream chan-

nels relating to the crater.

To estimate the hazard degree in the future, monitoring systems and identification of paroxysmal events are the most important factors. Paroxysms that reflect the most powerful eruption in the period occur when plugs, or the bulk of a plug, are instantaneously ejected. There may be more than one paroxysm, e.g. in the eruption of Agung volcano, Bali in 1963 (Kusumadinata, 1979, 1981). This possibility may not be expected if the magma is strongly fractionated which could lead to a paroxysmal event occurring near the beginning of an eruption period. Simkin & Siebert (1984) noted that most paroxysmal phases occur within days of the beginning of an eruption. The likely reason for this is that near the roof of a magma body, the most evolved magma (richest in SiO_2) interacts with meteoric water and other cold country rocks to produce high hydrostatic pressure. Pressure increases with increasing water supply and increasing strength of cap rocks or the occurrence of a plug. The increasing pressure causes fractures to develop. At first, steam rises upwards through the fractures and is erupted. This is followed by phreatic explosions, then phreatomagmatic explosions, and finally purely magmatic materials are erupted.

VIII.6 Hazard-Zonation Maps

Although the writer considers that a long-term hazard is most likely after the 1982-83 eruption, smaller eruptions may occur in the short-term. This section concerns short-term hazards, while further research is needed to determine what to do in event of a first degree (long-term) hazard.

Three volcanic hazard maps have been produced for Galunggung (Fig. VIII.3-5) representing second, third and fourth degrees hazard maps, respectively. Each consists of a closed zone and a danger zone. The third and fourth degree hazard maps also have an alert zone.

The closed zone is an area situated closest to the danger source, that is most likely to be affected by pyroclastic flows, pyroclastic surges, ballistic projectiles, thick pyroclastic falls, and lahars and floods directly derived from pyroclastic deposits in the Galunggung caldera depression.

The danger zone is an extension of the closed zone that is mainly affected by pyroclastic falls, lahars and floods originating from flanks and down slopes of the volcano. Lahar and flood hazards in the danger zone are often as dangerous as in the closed zone because if the first lahar enters a stream channel (although very small) or even an irrigation channel in the closed zone, this could cause a big lahar and flood in the danger zone. This hazard will then threaten the plains which are highly populated. In general, areas along river valleys and up to an elevation of 25 m above the river bottom must be abandoned.

The duration of lahar hazard in the danger zone is shorter than in the closed zone because the volume of source material in the danger zone (mainly pyroclastic fall deposits) is smaller and is distributed over a wider area. Furthermore, fine ash particles are cohesive and become rapidly indurated. This reduces erosion intensity in pyroclastic fall deposits. After the eruption terminates lahars and floods in the danger zone are restricted to river valleys while erosion becomes more intensive and stream lines begin to establish. This is the time to allow people living in the danger zone to return home, thus reduc-

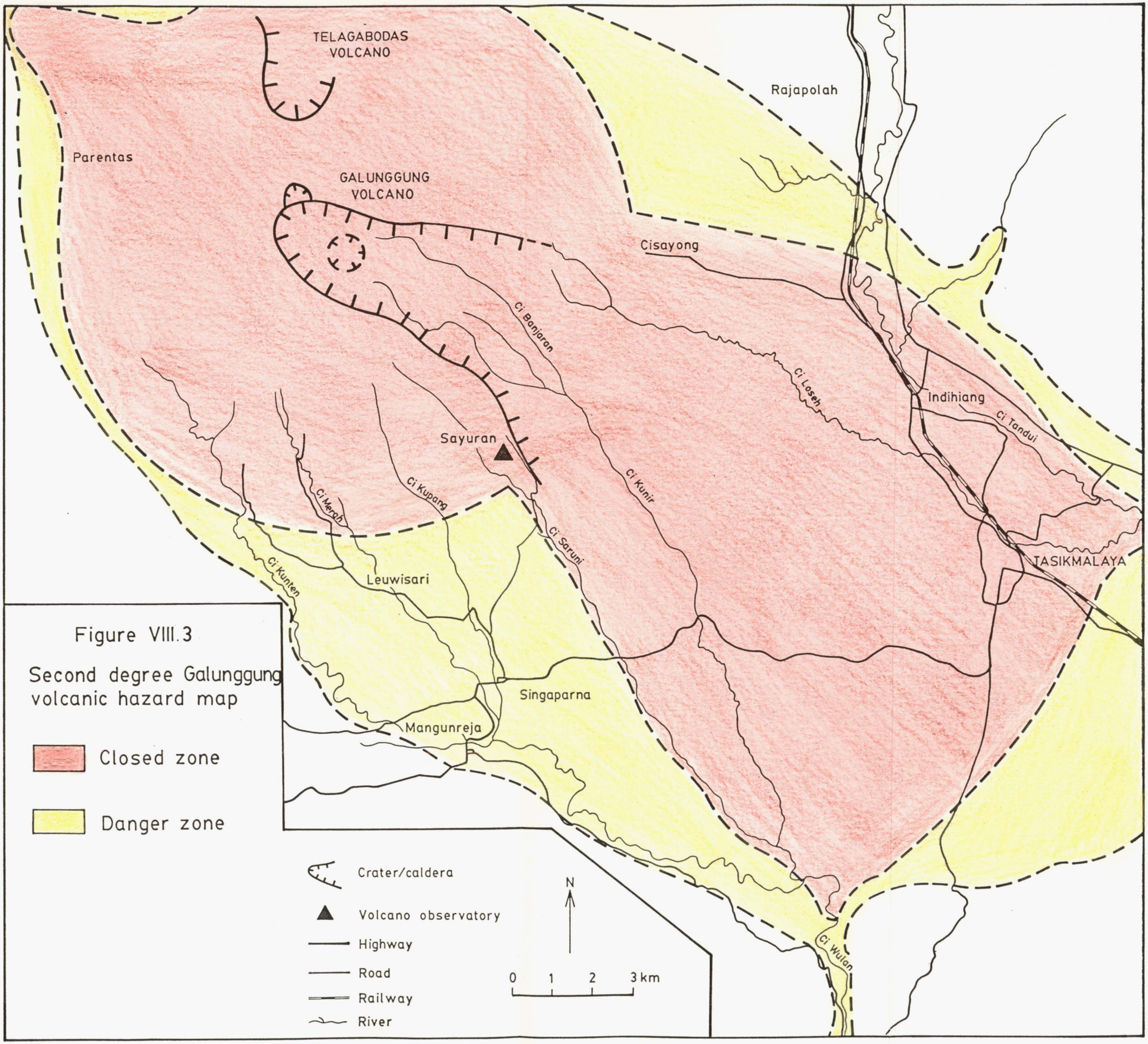
TELAGABODAS
VOLCANO
Parentas
GALUNGGUNG
VOLCANO
Rajapolah
Cisayong
Ci Banjaran
Ci Loseh
Indihiang
Ci Tandui
Sayuran
Ci Kupang
Ci Merah
Ci Kunir
Ci Saruni
Ci Kunten
Leuwisari
TASIKMALAYA
Singaparna
Mangunreja
Ci Wulan
Figure VIII.3
Second degree Galunggung volcanic hazard map
Closed zone
Danger zone
Crater/caldera
Volcano observatory
Highway
Road
Railway
River
N
0 1 2 3 km

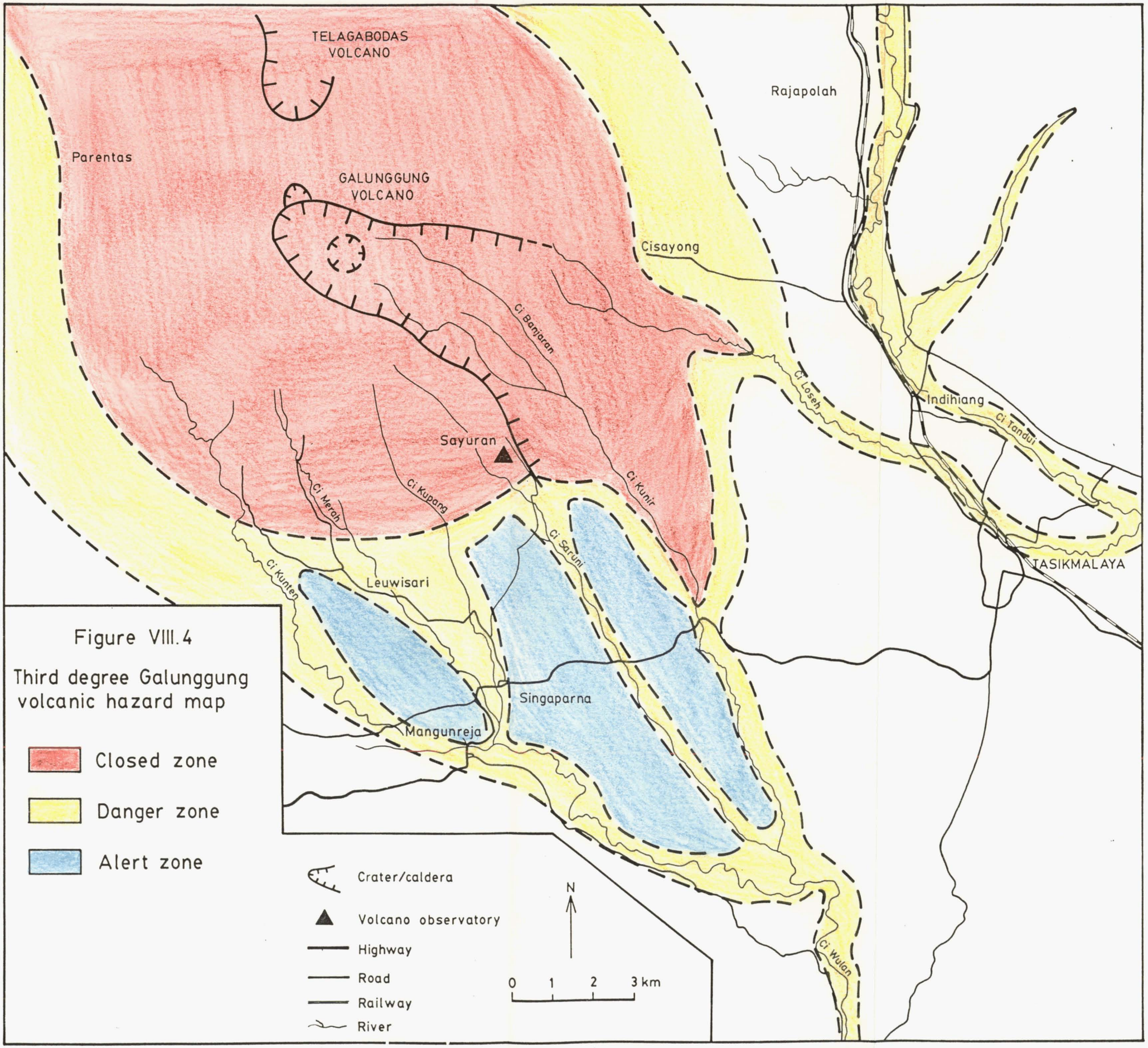
TELAGABODAS VOLCANO
Parentas
GALUNGGUNG VOLCANO
Rajapolah
Cisayong
Ci Banjaran
Ci Loseh
Indihiang
Ci Tandui
Sayuran
Ci Merah
Ci Kupang
Ci Kunir
Ci Saruni
Ci Kunten
Leuwisari
TASIKMALAYA
Singaparna
Mangunreja
Ci Wulan
Figure VIII.4
Third degree Galunggung volcanic hazard map
Closed zone
Danger zone
Alert zone
Crater/caldera
Volcano observatory
Highway
Road
Railway
River
N
0 1 2 3 km

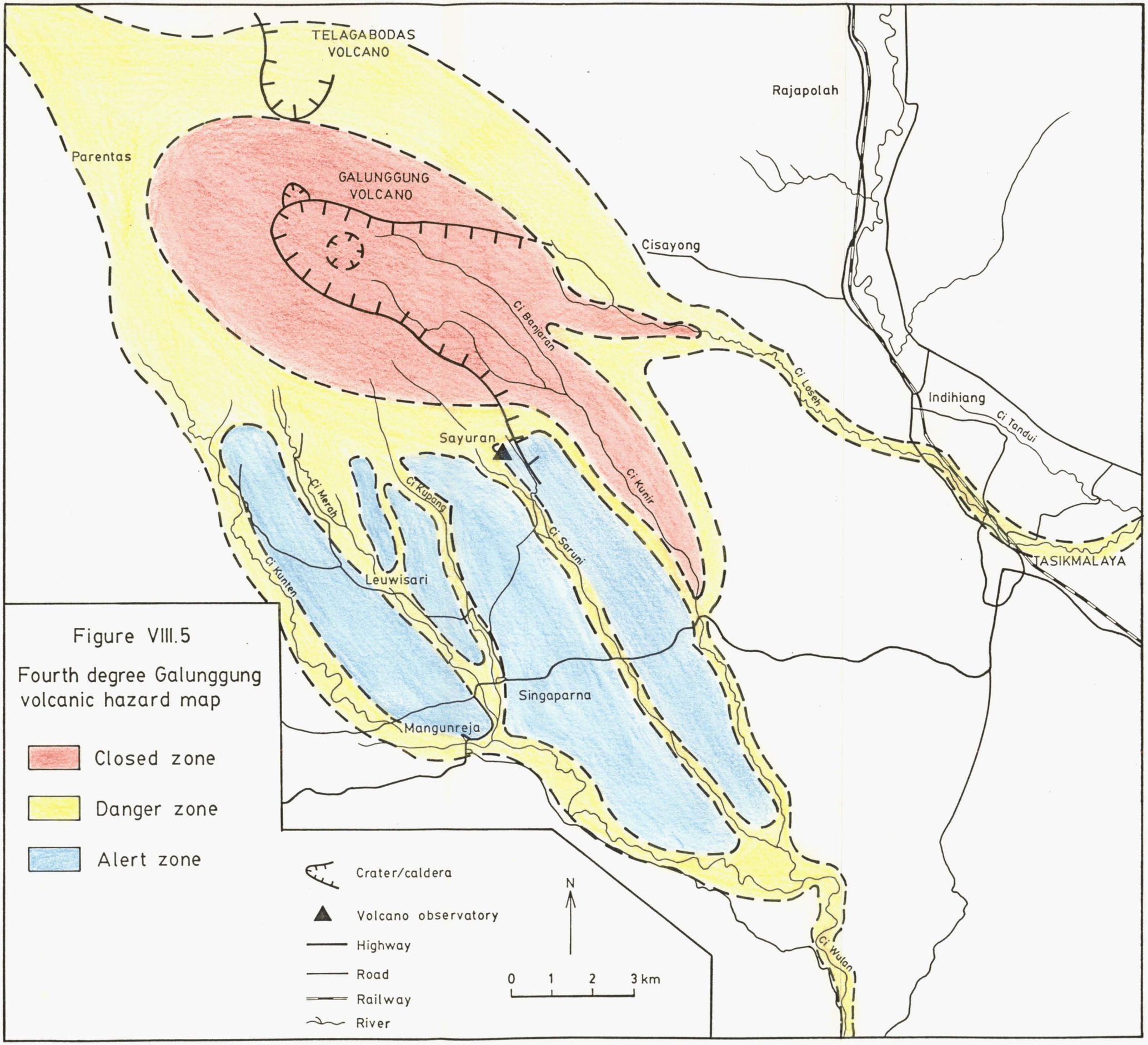
TELAGABODAS
VOLCANO
Parentas
GALUNGGUNG
VOLCANO
Rajapolah
Cisayong
Ci Banjaran
Ci Loseh
Indihiang
Ci Tandui
Sayuran
Ci Merah
Ci Kupang
Ci Kunir
Ci Saruni
Ci Kunten
Leuwisari
TASIKMALAYA
Singaparna
Mangunreja
Ci Wulan
Figure VIII.5
Fourth degree Galunggung volcanic hazard map
Closed zone
Danger zone
Alert zone
Crater/caldera
Volcano observatory
Highway
Road
Railway
River
N
0 1 2 3 km

ing the cost in evacuation areas. On the other hand, thick lahar deposits cover both plains and river valleys in the closed zone and this area is not habitable for a considerable duration.

The alert zone is a relatively high area in the danger zone that will not be threatened by lahars although may be affected by pyroclastic falls. To minimise traffic accidents and panic, the area can be used for temporary evacuation. However, if it is considered that bridges along the main road will be destroyed by lahars, the people must be evacuated.

The closed zone of the second degree volcanic hazard map covers an area of 14 km in diameter from the vent. Extensions occur 20 km SE-ward diverging from the Galunggung caldera depression and 10 km to the NW. The danger zone surrounds the closed zone. This zone is narrow in high level areas and rarely population, but becomes abroad in the plains because of high population. The danger zone also extends along the main stream channels. (Fig. VIII.3).

In the third degree volcanic hazard map (Fig. VIII.4), the closed zone threatened by ballistic projectiles and thick pyroclastic falls deposits is similar to that in the second degree volcanic hazard map. Extensions of the closed zone to the southeast up to 12 km away from the crater. This covers the plains area between the Galunggung caldera depression and the hummocky topography downslope. The most probable hazard in this area are lahars which flow along the main stream channel of Ci Kunir in the west and Ci Loseh in the east. Debris avalanche hills are quite effective as natural barriers to the lahars and for temporary evacuation of the population (for hills 30 to 50 m high above the plain). However, to restrict the lahars moving along the main rivers, engineering sites are suggested. Check dams and

sand pockets should be built at a narrow and deep rivers between the hills, and dikes should be built along the banks of main stream channels.

It must be realised that eruptions may last for long periods (e.g. 9 months in 1982-83). This will result in a large amount of pyroclastic fall debris which can feed large rain lahars. So, all areas near to the closed zone must be considered a possible danger zone. Pyroclastic falls (ash to lapilli in size) can affect a very wide area, depending on the downwind direction. Most pyroclastic falls in the past were deposited in NW - SE direction. People in the affected area must stay in strong buildings and wait for evacuation if necessary. In terms of lahar and flood hazards, requirements would be similar to that of a second degree hazard.

In addition, volcanic hazard maps for surrounding volcanoes must also be provided. Evidently, lahars flowed down from Guntur volcano (30 km west of Guntur) when Galunggung erupted in 1982-83. This was caused by Galunggung ash being deposited on Guntur volcano. When heavy rainfalls occurred, it mixed with the pyroclastic flow deposits to cause rain lahars.

In the fourth degree volcanic hazard map (Fig. VIII.5) the closed zone would be threatened mainly by ballistic projectiles and ash to lapilli pyroclastic falls which are likely affected by NW - SE downwind direction. This zone covers an oval-shaped area having a shortest diameter of 6 km and the longest one of 10 km. The area extends SE-ward along the main stream channels of Ci Kunir and Ci Loseh for lahar and flood hazards. The danger zone is also an elliptical area with the shortest diameter of 10 km and the longest one of 14 km. This danger zone also extends both NW- and SE-wards, along the

main stream channels. The alert zone area is probably secure enough, provided the eruption was not of long duration.

All these volcanic hazard maps should be immediately available when indications of eruption are observed. Which map is used depends on the monitoring data. People living in the hazard area must be aware of the danger, and taught how to recognise eruption precursors so they can report to the local authority or volcanologist at the observatory immediately. They must also know when to evacuate and when they may return. Moreover, because Galunggung does not erupt very often, the people must be repeatedly told of the danger as previous activity is soon forgotten.

On the basis of the volcanic hazard maps, evacuation can be arranged in all directions away from the Galunggung volcano. For instance, people living in Tasikmalaya and surrounding areas must evacuate to the east whereas those in Indihiang and Singaparna must go to the north and west, respectively. All detailed arrangements must be planned well in advance of an actual event.

IX CONCLUSIONS

IX.1 Location, Physiography and Geological Setting

Galunggung volcano is located in the district of Tasikmalaya, West Java, Indonesia, and is bordered by Quaternary volcanoes on the west, north and east sides and Tertiary rocks in the south. The volcano covers an area about 275 km^2 and is elliptical in outline with a major diameter (NW-SE) of 27 km and a minor diameter of 13 km.

Physiographically, the Galunggung area is divided into an Old Galunggung volcanic cone, a horseshoe-shaped caldera and a hilly area. The cone reaches an altitude of 2168 m and has an inactive circular crater, 500 m across and 100-150 m deep. The horseshoe-shaped caldera opens to the ESE and is 9 km long and 2-7 km wide. The height of the caldera wall decreases from about 1000 m on the NNW side to 10 m in the ESE side. There is an active crater inside the caldera, which has a circular form, approximately 1000 m across and 150 m deep. A cinder cone, 250 x 165 m across and 30 m above crater floor, was formed during the final stages of the 1982-83 eruption. In December 1986, this cinder cone was completely covered by rain water. The hilly area is located on Tasikmalaya plain at the ESE foot of Galunggung volcano, directly opposite the open horseshoe-shaped caldera. The numerous conical hills are 5 - 50 m high and have 5 - 15^{o} slopes. There are three main drainage patterns; Ci Manuk to the north, Ci Tandui to the east and Ci Wulan to the south.

Galunggung volcano is built on a basement of Permo-Triassic metamorphic rocks, Cretaceous granites and Tertiary volcanic and sedi-

mentary rocks. The oldest rocks (Cretaceous - Eocene age) in West Java are a melange complex comprising metamorphosed basic (gabbros and pillow lavas) and sedimentary rocks. The Tertiary volcanic rocks are dacite in the lower part, andesite in the middle and basalt at the top. Crustal thickness is about 25 km so the Western Sunda Arc where Galunggung is situated cannot be considered an island arc.

IX.2 Geology and Stratigraphy

Galunggung volcanic rocks are included within the Galunggung Group and can be divided into the Old Galunggung Formation, the Tasikmalaya Formation and the Cibanjaran Formation. The first formation represents rocks of Old Galunggung stratovolcano (50,000 - 10,000 yrs. BP ?), the second formation covers rocks erupted during Galunggung caldera forming event (4200 ± 150 yrs. BP) and the third one comprises rocks erupted in 1822, 1894, 1918 and 1982-83.

Old Galunggung volcano erupted frequently to build a stratovolcano consisting mainly of lava flows, pyroclastic flows, pyroclastic falls and lahars with a total rock volume of about 56.5 km^3. This activity ended by intrusion of a cryptodome under the crater. This blocked the existing vent and subsequent activity moved to the weakest part of the old cone to the ESE resulting in the caldera forming-event. This destructive eruption formed a horseshoe-shaped caldera and ejected more than 20 km^3 of material comprising debris avalanche, pyroclastic flow, pyroclastic fall, pyroclastic surge and lahar deposits. Historic eruptions separated by relatively long dormant periods produced less volume (< 0.4 km^3) but also comprising debris aval-

anche, pyroclastic flow, pyroclastic fall, pyroclastic surge, lava and lahar deposits. Regional tectonic activity is likely one of important parameters to trigger Galunggung eruption.

More detailed studies of pyroclastic and lahar deposits leading to volcanic hazard assessment are suggested.

IX.3 Petrology and Geochemistry

Galunggung lavas and volcanic bombs comprise basalt (49 - 53 % SiO_2) to basaltic andesite (53 - 57 % SiO_2) having porphyritic texture with medium-sized phenocrysts in a fine-grained or glassy groundmass. Modal analyses indicate 15 - 40 % phenocrysts, mainly plagioclase (average 18 %) and clinopyroxene (1.6 %) although a few lavas do not have clinopyroxene phenocrysts. Olivine is common in basic rocks (1 - 4 %) except for Old Galunggung cryptodome, whereas orthopyroxene occurs frequently in the most evolved rocks (up to 4 %). Amphibole is not observed in Old Galunggung rocks but is fairly common in bombs of pyroclastic flow deposits and amphibole gabbro clasts ejected during Galunggung caldera forming event. The mineral is occasionally found in basaltic andesites of historic eruptions. Magnetite microphenocrysts are rare in Old Galunggung rocks whereas Cr-spinel inclusions in olivine phenocrysts and microphenocrysts in rocks erupted in 1982-83 only. Olivine and clinopyroxene vary from anhedral embayed, hollow, elongated skeletal crystals to euhedral crystals, whereas plagioclase contains glass inclusions.

Most olivine compositions in pre-1982 eruption rocks have low forsterite contents ($< Fo_{80}$). On the other hand, olivines in the

1982-83 eruption rocks have $Fo_{80 - 90}$. These are accompanied by high Ni and Ca contents (up to 0.44 % NiO and > 0.11 % CaO, respectively) in the mineral. Most clinopyroxenes in Galunggung rocks are augite ($Ca_{43-32}Mg_{45-41}Fe_{23-12}$). Diopsidic compositions occur in the Old Galunggung cryptodome and rocks erupted in the final stages of the 1982-83 eruption. Cr and Mg contents in the diopsides of the cryptodome are correlative because olivine is absent.

All orthopyroxenes are hypersthene and are relatively homogeneous in composition ($Ca_{4-3}Mg_{70-61}Fe_{36-26}$) with a low Al content (< 2.5 % Al_2O_3). Pigeonites occur as fine-grained groundmass crystals and as coronas around olivine crystals, together with orthopyroxene. These represent rapid metastable crystallisation at high temperature during quenching.

Two kinds of spinel, Cr-spinel and Ti-magnetite, are present in Galunggung rocks. Cr-spinels have high Cr (up to 50 % Cr_2O_3, Cr/(Cr + Al) = 0.5 - 0.7) but low Al (< 20 % Al_2O_3) and Fe^{3+} (Fe^{3+}/(Cr + Al + Fe^{3+}) < 0.2) contents. Magnetites contain 9 - 19 % TiO_2 (Ti-magnetites) and low Al (< 5 % Al_2O_3) contents. The replacement of Cr-spinel by magnetite is illustrated by decreasing Cr but increasing Fe^{3+} ratios.

Three phases of amphibole crystal are identified : 1. euhedral, 2. rimmed by opaque materials, and 3. having poikilitic texture. However, chemically, all are pargasite with a high Al content (Al > 2.0).

Plagioclases are commonly normally zoned. The phenocryst cores have An_{95-80} and their rims and groundmass crystals are An_{79-45}.

All minerals in Galunggung rocks suggest that crystallisation occurred at high temperature (1000 - 1300^{o}C) but low pressure (< 10

Kb) in the crust and some of them crystallised shortly before eruption.

On the basis of Mg contents, Galunggung rocks are divided into : 1. high-Mg basalt (12.5 - 10 % MgO), 2. "Transitional" high-Mg basalt (9 - 6.5 % MgO), and low-Mg basalt (< 6 % MgO). Similarly, the basaltic andesites are divided into high-Mg basaltic andesite (7 - 6 % MgO) and low-Mg basaltic andesite (< 5 % MgO). The high-Mg basalts are subdivided into low-K high-Mg basalt (< 0.4 % K_2O) and medium-K high-Mg basalt (0.6 % K_2O). Low-Mg basalts - basaltic andesites represent volcanic rocks erupted before 1982, except for the Old Galunggung cryptodome (medium-K high-Mg basalt). Whereas a sequence from low-K high-Mg basalt - "transitional" high-Mg basalt - high-Mg basaltic andesite - low-Mg basaltic andesite was erupted in 1982-83.

Alkali and incompatible elements increase but Mg, Fe, Ca and compatible elements decrease with increasing SiO_2. The high-Mg basalts represent the most primitive Galunggung rocks in having the highest Mg number (Mg# = 75 - 69), Ni (up to 193 ppm), and Cr (711 ppm) but lowest incompatible elements. The "primitiveness" of the basalts is also reflected by their $^{230}Th/^{232}Th$ (= 0.68) which is one of the lowest ratios yet found. Comparable high-Mg basalt from New Britain volcanic have $^{87}Sr/^{86}Sr$ = 0.70319.

IX.4 Petrogenesis

The Galunggung primitive high-Mg basalts represent liquid compositions which have been derived from upper mantle peridotites. The low-K high-Mg basalt originated from spinel-peridotite by 15 % melting

at about 50 km depth. The medium-K high-Mg basalt was from plagioclase-peridotite by 25 - 40 % melting at about 30 km depth. Eruption of these primitive magmas probably result from rapid movement to the surface as mantle "diapirs". Partial melting mantle peridotite was possibly caused by : (1) kinetic control causing sudden pressure release and local heating, or (2) the involvement of water from subducted slab in the upper mantle. The first hypothesis requires a detailed geophysical study to test the characteristics of the upper mantle materials, whereas the second hypothesis needs more radiogenic isotope data.

During Old Galunggung volcanic activity, low-K high-Mg basalt magma moved upward and formed a magma chamber in the crust at about 10 km deep. Crystal fractionation of this magma, involving olivine, clinopyroxene, plagioclase and magnetite, formed low-Mg basalts and basaltic andesites. Frequent small eruptions of low-Mg basalts and basaltic andesites built Old Galunggung stratovolcano. This activity ended when a medium-K high-Mg basalt was erupted rapidly and formed a cryptodome.

In the following stage, another low-K high-Mg basalt, derived from spinel peridotite rose into the crust. Gas was trapped and high water pressure was attained. Consequently, amphiboles crystallised in evolved rocks. In addition, amphibole gabbro solidified in the roof of the magma body. These rocks were erupted during Galunggung caldera forming-event (4200 ± 150 yrs. BP) and in 1822 and 1894 but not in 1918 because the 1918 lava dome did not have high enough water pressure.

In 1982-83, a new generation of low-K high-Mg basalt magma was rapidly erupted. Crystal fractionation of olivine, clinopyroxene, plagioclase and magnetite in a conduit system altered composition at

the top and middle parts but not significantly the lower part of the magma body. During the eruptive sequence firstly low-Mg basaltic andesite was erupted, then high-Mg basaltic andesite, "transitional" high-Mg basalt, and finally the low-K high-Mg basalt. So, two major magmatic cycles, from low-Mg basaltic andesite to high-Mg basalt have occurred in Galunggung volcanic rocks.

Rhyolite pumice, composed of glass, altered feldspar and quartz was erupted in September 1982. This is considered to be a product of remelting of Miocene dacite by the high temperature (1300^{o}C) Galunggung high-Mg basalt magma. However, isotopic study is needed to confirm this hypothesis.

IX.5 Volcanic Hazard Assessment

Galunggung eruptions vary from non-violent lava dome/ lava flow extrusions to destructive explosive (Strombolian, Peléean and Bandaian) events. During explosive eruptions pyroclastic flows, surges and falls are erupted while heavy rainfall causes the pyroclastic deposits to become lahars. Each volcanic product creates hazards for people living in affected areas. Four categories of hazard can be devised for Galunggung : first, second, third and fourth degree hazards. The first degree hazard relates to long-term hazards and requires further study. In this thesis volcanic hazard maps are presented for second, third and fourth degree hazards. Each locates a closed zone, and for third and fourth degree hazards a danger zone and an alert zone. Evacuation routes are suggested away from the volcano as all arrangements must be planned well in advance of an actual

event. It is noted that volcanic hazard maps should also be provided for surrounding volcanoes.

ACKNOWLEDGMENTS

I wish to thank my supervisors : Prof. J.W. Cole, who has done more than his duty as supervisor, and Dr. S.D. Weaver who co-supervised the study and provided constructive criticism of the manuscript, assistance on geochemical analyses and setting up computer programming for geochemical data. The advice and discussion on tectonic and petrographic aspects with Dr. J.D. Bradshaw and Dr. D. Shelley respectively (UC, Univ. of Canterbury) and on petrogenesis with Dr. J.A. Gamble (VUW, Victoria Univ. of Wellington) are gratefully acknowledged. I also acknowledge the Ministry of External Relations & Trade, New Zealand Government for the financial support, and the Indonesian Government, particularly Dr. A. Sudradjat (Previous Director of Volcanological Survey of Indonesia), Ir. W.S. Modjo (Director of VSI), Ir. A.C. Effendi and Ir. T. Suhanda who assigned me to study overseas and gave permission to bring the data out from Indonesia. Thanks to Ir. M.A. Purbawinata (Geol. Dept., Univ. of Otago, Dunedin), Ir. R. Sukhyar (Earth Sciences Dept., Monash Univ., Melbourne) and other colleagues at the Department of Geology, VUW who are currently studying abroad, for their constructive discussions and assistance. VSI staff, both in the main office and Galunggung volcano observatory are also acknowledged.

The efforts of the technical staff are much appreciated. Thanks go to : Dr. D.W. Lewis (Geol. Dept., UC) for setting up the computer program, A. Alloway, S. Brown (Geol. Dept., UC) and K. Palmer (Geol. Dept. VUW) for assisting with sample preparation, running XRF and electron microprobe analyses; J. Carter (Geol. Dept., VUW) and K. Holder (Geol. Dept., UC) for producing thin sections; A. Downing (Geol. Dept., UC) for photographic work; T. Robinson (Zoology Dept., UC) for laser printing; and D. Jones, A. Nicholas, W. Nuthall and J. McTurk for various assistance.

The assistance provided by people at establishments elsewhere is appreciated : Dr. T.J. Casadevall (USGS Volcanologist) for carbon dating; Dr. J.P. Lockwood, Dr. R.I. Tilling (USGS Volcanologists) and Prof. J.B. Gill (Univ. of California, Santa Cruz) for providing geochemical and isotopic data from Galunggung rocks, for constructive discussion on petrogenesis (Prof. Gill); Dr. A.F. Glazner (Geol. Dept., Univ. of North Carolina, Chapell Hill) for geothermometry calculations; Dr. R.W. Johnson (BMR, Canberra) for data from New Britain

volcanics; Dr. S. Martodjojo (ITB, Bandung) for data on geological setting; Dr. C.J. Nye (Alaska Div. of Geol. & Geophys. Surv., Fairbanks) for electron microprobe analyses from a Galunggung rock sample; Dr. R. Sewell (NZ Geol. Surv., Christchurch) for assisting with computer programs and geochemical calculations, and Dr. van der Lingen (NZ Geol. Surv., Christchurch) for translating Dutch papers and discussions concerning the stratigraphy of "melange" deposits.

I wish to thank Prof. H. Schmincke (IAVCEI Secretary General), Dr. S.T. Malling (UNESCO, Jakarta), Drs. Sujanto (Head of Observation & Volcanic Mapping Project, VSI, Bandung), Dr. C.G. Newhall (USGS Volcanologist) for their financial support and encouragement in improving my knowledge by attending international geological conferences during my study.

I also thank all Geology Department post-graduate students (UC), and staff members of NZ Geological Survey, Christchurch Office for helping to improve my written English.

Finally, I am grateful to my wife Maryuni, daughters Anelia and Intan, and parents for their support, encouragement and understanding.

REFERENCES

Adiwinata, R.S., 1950, Kawah Gn. Galunggung meletus (bitu), Geol. Surv. Indon., Bandung, unpubl.

Adnawidjaja, M.I. & Rothpletz, W., 1958, Laporan G. Galunggung 15 Januari 1958, Geol Surv. Indon., Bandung, unpubl.

Aldiss, D.T. & Ghazali, S.A., 1984, The regional geology and evolution of the Toba volcano - tectonic depression, Indonesia, **J. Geol. Soc. London, 141, 487 - 500.**

Allegre, C.J., Othman, D.B., Polve, M. & Richard, P., 1979, The Nd-Sr isotopic correlation in mantle minerals and geodynamic consequences, **Phys. Earth Planet. Inter.**, 19, 293 - 306.

Allen, J.C., Boettcher, A.L. & Marland, G., 1975, Amphiboles in andesite and basalt : I. Stability as a function of P-T-fO_2, **Am. Miner.**, 60, 1069 - 1085.

Alzwar, M., 1969, Pengamatan G. Galunggung tgl. 23 - 24 Juli 1969, Geol. Surv. Indon., Bandung, unpubl.

Anderson, A.T., 1974, Evidence for a picritic volatile-rich magma beneath Mt. Shasta, California, **J. Petrol.**, 15, 243 - 267.

Aoki, K.I. & Fujimaki, H., 1982, Petrology and geochemistry of calc-alkaline andesite of presumed upper mantle origin from Hinomigata, Japan, **Am. Miner.**, 67, 1 - 13.

Aoki, K. & Shiba, I., 1973, Pyroxenes from lherzolite inclusions of Itinome-gata, Japan, **Lithos**, 6, 41 - 51.

Aramaki, S., 1956, The 1783 activity of Asama volcano, Japan, **J. Geol. Geograph.**, 27, p. 189-229.

Aramaki, S. & Ui, T., 1982, Andesite in Japan, In : R.S. Thorpe (Ed.), **Andesite**, John Wiley, New York, pp. 259 - 292.

Arculus, R.J. & Johnson, R.W., 1978, Criticism of generalised models for the magmatic evolution of arc-trench system, **Earth Planet. Sci. Lett.**, 39, 118 - 126.

Arculus, R.J. & Johnson, R.W., 1981, Island-arc magma sources: a geochemical assessment of the rocks of slab derived components and crustal contamination, **Geochem. J.**, 15, 109 - 133.

Armstrong, R.L., 1971, Isotopic and chemical constraints on models of magma genesis in volcanic arcs, **Earth Planet. Sci. Lett.**, 12, 137 - 142.

Arndt, N.T., Naldrett, A.J. & Pyke, D.R., 1977, Komatiitic and iron-rich tholeiitic lavas of Munro Township, NE Ontario, **J. Petrol.**, 18, 319 - 369.

Arpandi, D. & Padmosukismo, S., 1975, The Cibulakan Formation as one of the most prospective stratigraphic units in the North West Java basinal area, Proceed. Petrol. Assoc., 4th Annual Conv., Jakarta.

Arth, J.G., 1976, Behavior of trace elements during magmatic processes - A summary of theoretical models and their applications, **J. Res. U.S. Geol. Surv.**,4, 41 - 47.

Arth, J.G., Arndt, N.T. & Naldrett, A.J., 1977, Genesis of Archean komatiites from Munro Township, Ontario : Trace element evidence, **Geology**, 5, 590 - 594.

Aruman, H.H.B., 1982, 1982 Galunggung volcanic risk, a speech presented on the Galunggung National Workshop in Bandung, Indonesia, 20 - 25 Sept. 1982, unpubl.

Atlas, L., 1952, The polymorphism of $MgSiO_3$ and solid state equilibria in the system $MgSiO_3$ - $CaMgSi_2O_6$, **J. Geol.**, 60, 125 - 147.

Augustithis, S.S., 1978, **Atlas of the textural pattern of basalts and their significance**, Elsevier Sci. Publ. Co., New York, 323 p.

Bardintzeff, J.M. & Bonin, B., 1987, The amphibole effect : A possible mechanism for triggering explosive eruptions, **J. Volc. Geoth. Res.**, 33, 255 - 262.

Barlett, R.W., 1969, Magma convection, temperature distribution, and differentiation, **Amer. J. Sci.**, 267, 1067-1082.

Barry, R.G. & Chorley, R.J., 1982, **Atmosphere, weather and climate**, Methuen & Co Ltd., 4th ed., London, 407 p.

Barsdell, M., Smith, I.E.M. & Sporli, K.B., 1982, The origin of reversed geochemical zoning in the Northern New Hebrides volcanic arc, **Contr. Min. Petr.**, 81, 148 - 155.

Basaltic Volcanism Study Project (BVSP), 1981, **Basaltic volcanism on the terrestrial planets**, Pergamon Press, New York, 1286 p.

Bates, R.L. & Jackson, J.A., Eds., 1980, **Glossary of geology**, American Geological Institute, second edition, Falls Church, Virginia, 751 p.

Becker, H.J., 1977, Pyroxenites and Hornblendites from the Maar-Type volcanoes of the Westeifel, Federal Republic of Germany, **Contr. Min. Petr.**, 65, 45 - 52.

Ben-Avraham, Z., 1978, The evolution of marginal basins and adjacent shelves in East and Southeast Asia, **Tectonophysic**, 45, 269-288.

Ben-Avraham, Z. & Emery, K.O., 1973, Structural framework of the Sunda Shelf, **Amer. Assoc. Pet. Geol. Bull.**, 57, 2323 - 2366.

Bence, A.E. & Albee, A.L., 1968, Empirical correction factors for the electron microanalysis of silicates and oxides, **J. Geology**, 76, 382 - 403.

Berg, J.H. & Klewin, K.W., 1988, High-MgO lavas from Keweenawan mid-continent rift near Mamainse Point, Ontario, **Geology**, 16, 1003 - 1006.

Best, M.G., 1975, **Igneous and metamorphic petrology**, W.H. Freeman & Co., San Fransisco, 630 p.

Bhattacharji, S. & Smith, C.H., 1964, Flowage differentiation, **Science**, 145, 150 - 153.

Blong, R.J., 1984, **Volcanic hazards : A Sourcebook on the Effects of Eruptions**, Academic Press, Orlando, Florida, 424 p.

Bloomer, S.H. & Fisher, R.L., 1987, Petrology and geochemistry of igneous rocks from Tonga-trench - A non-accreting plate boundary, **J. Geology**, 95, 469 - 495.

Blot, C. & Priam, R., 1963, Volcanisme et seesmicite dan's l' Archipel des Non velles - He'brides, **Bull. Volc.**, 26, 167 - 180.

Bolliger, W. & de Ruiter, P.A.C., 1975, Geology of the South Central Java offshore Area : **Proc. of Indon. Petrol. Assoc.**, Jakarta, pp. 67 - 81.

Bonatti, E. & Michael, P.J., 1989, Mantle peridotites from continental rifts to ocean basins to subduction zones, **Earth Planet. Sci. Lett.**, 91, 297 - 311.

Bonin,B., 1986, **Ring Complex Granites and Anorogenic Magmatism**, Elsevier, Amsterdam, 188 p.

Borgia, A., Poore, C., Carr, M.J., Melson, M.G. & Alvarado, G.E., 1988, Structural, stratigraphic and petrologic aspects of the Arenal - Chato volcanic system, Costa Rica : Evolution of a young stratovolcanic complex, **Bull. Volcanol.**, 50, 86 - 105.

Bourdier, J.L., Gourgaud, A. & Vincent, P.M., 1985, Magma mixing in a main stage of formation of Montagne Pelée : The Saint Vincent - type scoria flow sequence (Martinique, F.W.I), **J. Volc. Geoth. Res.**, 25, 309 - 332.

Bowin, C.O., 1973, Origin of Ninetyeast Ridge from studies near the equator, **J. Geophys. Res.**, 78, 6029 - 6043.

Bronto, S., 1982, Geologi G. Galunggung, 11th Ann. Conven. Indon. Assoc. Geol., manuscript, 15 p.

Bronto, S., 1987a, Reducing Galunggung volcanic risk, abstract, **Hawaii Sympos. on How Volc. Work, Diamond Jubilee (1912 - 1987), Hilo, Hawaii**, p. 25.

Bronto, S., 1987b, Galunggung eruption, Indonesia - 1982/83, abstract, **Ann. Conf. Geol. Soc. New Zealand Inc., Dunedin, New Zealand.**

Bronto, S., Effendi, A.C. & Kaswanda, O., 1983, Ladu dan pengaruhnya, hasil letusan gunungapi Galunggung 1982, Volc. Surv. Indon., Bandung, unpubl.

Bronto, S., Hadisantono, R.D. & Lockwood, J.P., 1982, **Geologic Map of Gamalama volcano, Ternate, North Maluku**, Volc. Surv. Indon., Bandung.

Bronto, S., Situmorang, T. & Effendi, W., 1986a, **Geologic map of Lamongan volcano, East Java, Indonesia**, Volc. Surv. Indon., Bandung.

Bronto, S., Sukhyar, R. & Effendi, A.C., 1986b, **Geologic map of Krakatau volcano, Sunda Strait, Indonesia**, Volc. Surv. Indon., Bandung.

Bronto, S., Sutawidjaja, I.S. & Hadisantono, R.D., 1986c, **Geologic Map of Guntur volcano, West Java, Indonesia**, Volc. Surv. Indon., Bandung.

Bronto, S., Erfan, R.D. & Zaennudin, M., 1984, Geologic map of Arjuno-Welirang Volcanic Complex, East Java, Indonesia, Volc. Surv. Indon., Bandung, in prep.

Brooks, C.K., 1976, The Fe_2O_3/FeO ratio of basalt analyses : an appeal for a standardised procedure, **Bull. Geol. Soc. Denmark**, 25, 117 -120.

Brooks, C. & Hart, S.R., 1974, On the significance of komatiite, **Geology**, 2, 107 - 110.

Brophy, J.G. & Marsh, B.D., 1986, On the origin of high-alumina arc basalt and the mechanics of melt extraction, **J. Petrol.**, 27, 76 3 - 789.

Brouwer, H.A., 1925, **The Geology of the Netherlands East Indiest**, The Macmillan Co., New York, 160 p.

Brown, G. M., Holland, J.G., Sigurdsson, H., Tomblin, J.F. & Arculus, R.J., 1977, Geochemistry of the Lesser Antilles volcanic island arc, **Geochim. Cosmochim. Acta**, 41, 785 - 801.

Brownlow, A.H., 1979, **Geochemistry**, Prentice-Hall, Inc., Englewood Cliffs, N.J. 07632, Wellington, 498 p.

Bryan, W.B., 1969, Some applications of linear least squares calculations to petrographic problem, Abstr. - AGU 5th Annual Meeting, **Amer. Geophys. Union Trans.**, 50, p. 354.

Bryan, W.B., Finger, L.W. & Chayes, F., 1969, Estimating proportions in petrographic mixing equations by least - square approximation, **Science**, 163, 926 - 927.

Bryan, W.B., Thompson, G., Frey, F.A. & Dickey, J.S., 1976, Inferred geologic settings and differentiation in basalts from Deep Sea Drilling Project, **J. Geophys. Res.**, 81, 4285 - 4304.

Budhitrisna, T., 1982, Geologic map of the Tasikmalaya Quadrangle, West Java, Geol Res. Dev. Centre, in prep.
Campbell, I.H. & Borley, G.D., 1974, The Geochemistry of pyroxenes from the lower layered series of the Jimberlana intrusion, Western Australia, **Contr. Min. Petr.**, 47, 281 - 297.
Camus, G., Gourgand, A. & Vincent, P.M., 1987, Petrologic evolution of Krakatau (Indonesia) : implications for a future activity, **J. Volc. Geoth. Res.**, 33, 299 - 316.
Carmichael, I.S.E., 1967, The iron-titanium oxides of salic volcanic rocks and their associated ferromagnesium minerals, **Contr. Min. Petr.**, 14, 36 - 64 .
Cas, R.A.F. & Wright, J.V., 1987, **Volcanic successions, modern and ancient**, Allen & Unwin, London, 528 p.
Casadevall, T.J., 1986, Volcanic hazard and the crater lake of Galunggung Volcano, West Java, Indonesia, Preliminary report, unpubl.
Cattermole, P., 1982, Meru - a Rift Valley giant, **Volcano news**, 11, 1 - 3.
Charlton, T.R., 1986, A plate tectonic model of the Eastern Indonesia collision zone, **Nature**, 319, 394 - 396.
Chase, C.G., 1978, Plate kinematics : The Americas, East Africa, and the rest of the world, **Earth Planet. Sci. Lett.**, 37, 353 - 368.
Chayes, F., 1968, A least squares approximation for estimating the amounts of petrographic partition products, **Mineralog. et Petrog. Acta**, 14, 111 - 114.
Chesner, C.A. & Rose, W.I., 1987, Pre-eruptive conditions of magma bodies giving rise to the Toba tuffs, Sumatra, abstract, **Hawaii Sympos. on How Volc. Work, Hilo, Hawaii**, Jan. 19-25, p.36.
Clarke, D.B., 1970, Tertiary basalts of Baffin Bay : possible primary magma from mantle, **Contr. Min. Petr.**, 25, 203 - 224.
Clarke, D.B. & O'Hara, M.J., 1979, Nickel, and the existence of high-MgO liquids in nature, **Earth Planet. Sci. Lett.**, 44, 153 - 158.
Coish, R.A. & Taylor, L.A., 1979, The effects of cooling rate on texture and pyroxene chemistry in DSDP Leg 34 Basalt : A microprobe study, **Earth Planet. Sci. Lett.**, 42, 389 - 398.
Cole, J.W., 1973, High-alumina basalts of Taupo volcanic zone, New Zealand, **Lithos**, 6, 53 - 64.
Collot, J.Y., Daniel, J. & Burne, R.W., 1985, Recent tectonics associated with the subduction/collision of the D'Entre-casteaux zone in the central New Hebrides, **Tectonophysics**, 112, 325 - 356.
Conrad, W.K., Nicholls, I.A. & Wall, V.J, 1988, Water- Saturated and -Undersaturated Melting of Metaluminous and Peraluminous Crustal Compositions at 10 Kb : Evidence for the origin of Silicic Magmas in the Taupo Volcanic Zone, New Zealand, and Other Occurrences, **J. Petrol.**, 29, 765 - 803.
Coombs, D.S., 1987, The Dunedin Volcano, GSNZ Field Trip A1, 3 Dec. 1987, **Geol. Soc. New Zealand miscell. publ.**, 37 B, 1 - 28.
Coote, A., 1987, Cenozoic volcanism in the Waiau area, North Canterbury, MSc thesis, Univ. of Canterbury, Christchurch, New Zealand.
Cox, K.G., 1978, Komatiites and other high-magnasia lavas : some problems, **Phil. Trans. Roy. Soc. Lond.**, A288, 599 - 609.
Cox, K.G. & Bell, J.D., 1972, A crystal fractionation model for the basaltic rocks of the New Georgia Group, British Solomon Islands, **Contrib. Miner. Petrol.**, 37, 1 - 13.
Cox, K.G., Bell, J.D. & Pankhurst, R.J., 1981, **The Interpretation of Igneous Rocks**, George Allen & Unwin (publ.) Ltd., London, 450 p.

Cox, K.G., Gass, I.G. & Mallick, D.I.J., 1970, The peralkaline volcanic suite of Aden and Little Aden, South Arabia, **J. Petrol.**, 11, 433 - 461.

Cox, K.G. & Jamieson, B.G., 1974, The olivine-rich lavas of the Nuanetsi : a study of polybaric evolution, **J. Petrol.**, 15, 269-301.

Cox, K.G., Johnson, R.L., Monkman, L.J., Stillman, C.J., Vail, J.R., Wood, D.N., 1965, The Geology of the Nuanetsi Igneneous Province, **Phil. Trans. Roy. Soc. London**, 257, 71 - 218.

Crandell, D.R., 1980, Recent eruptive history of Mount Hood, Oregon, and potential hazards from future eruptions, **U.S. Geol. Surv. Bull.**, 1492, 81 p.

Crandell, D.R., Miller, C.D., Glicken, H., Christiansen, R.L. & Newhall, C.G., 1984, Catastrophic debris avalanche from ancestral Mount Shasta volcano, California, **Geology**, 12, 143 - 146.

Crandell, D.R. & Nichols, D.R., 1987, **Volcanic Hazards at Mount Shasta, California**, U.S. Geol. Surv., 21 p.

Crawford, A.J., Falloon, T.J. & Eggins, S., 1987, The origin of island arc high-alumina basalts, **Contr. Min. Petr.**, 97, 417 - 430.

Davies, T.A., Luyendyk, B.P., Eds., 1973, **Initial reports of the Deep Sea Drilling Project**, vol. 26, U.S. Govt. Print. Office, Washington, 1129 p.

Decker, R.W. & Decker, B., 1981, The eruptions of Mount St. Helens, **Scientific American**, 244, 52 - 64.

Deer, W.A., Howie, R.A. & Zussman, J., 1978a, **An Introduction to the Rock-Forming Minerals**, Longman Group Ltd., London, 528 p.

Deer, W.A., Howie, R.A. & Zussman, J., 1978b, **Rock-Forming Minerals, Volume 2A, Single-Chain Silicates**, Longman Group Ltd., London, 668 p.

Deer, W.A., Howie, R.A. & Zussman, J., 1982, **Rock-Forming Minerals, Volume 1A, Orthosilicates**, Longman Group Ltd., London. 919 p.

De Kock, H., 1895, Verslag van de assisstent resident van Tasikmalaya omtrent de uitbarstingen van de Galoenggoeng in October 1894 en haar gevolgen, Geol. Surv. Indon., Bandung, unpubl.

Delaney, J.M. & Helgeson, H.C., 1978, Calculation of the thermodynamic consequences of dehydration of subducting ocenic crust to 100 Kb and > 800^{o}C, **Amer. J. Sci.**, 278, 638 - 686.

Delong, S.E., Perfit, M.R., Mcculloch, M.T. & Ach, J., 1985, Magmatic evolution of Semisopochnoi Island, Alaska : Trace element and isotopic constraints, **J. Geology**, 93, 609 - 618.

DePaolo, D.J. & Johnson, R.W., 1979, Magma genesis in the New Britain island-arc : Constraints from Nd and Sr isotopes and trace-element patterns, **Contr. Min. Petr.**, 70, 367 - 379.

DePaolo, D.J. & Wasserburg, G.J., 1976, Inferences about magma sources and mantle structure from variations of $^{143}Nd/^{144}Nd$, **Geophys. Res. Lett.**, 3, 743 - 746.

DePaolo, D.J. & Wasserburg, G.J., 1977, The sources of island arcs as indicated by Nd and Sr isotopic studies, **Geophys. Res. Lett.**, 4, 465 - 468.

Dietrich, V., Emmermann, R., Keller, J. & Puchelt, H., 1977, Tholeiitic basalts from the Tyrrhenian Sea floor, **Earth Planett. Sci. Lett.**, 36, 285 - 296.

Dixon, T.H. & Batiza, R., 1979, Petrology and chemistry of recent lavas in the Northern Marianas : Implication for the origin of island arc basalts, **Contr. Min. Petr.**, 70, 167 - 181.

Djajawinangun, A., 1963, Pemeriksaan G. Galunggung pada tgl. 28 April 1963, Geol. Surv. Indon., Bandung, unpubl.

Djuri, 1973, **Geologic map of the Arjawinangun Quadrangle, Java**, 10/XIII-D, scale 1 : 100,000, Geol. Surv. Indon., Bandung.
Donaldson, C.H., 1976, An experimental investigation of olivine morphology, **Contr. Min. Petr.**, 57, 187 - 213.
Donaldson, C.H. & Henderson, C.M.B., 1988, A new interpretation of round embayments in quartz crystals, **Miner. Mag.**, 52, 27 - 33.
Dupuy, C., Barsczus, H.G., Liotard, J.M. & Dostal, J., 1988, Trace element evidence for the origin of ocean island basalts : an example from the Austral Island (French Polynesia), **Contr. Min. Petr.**, 98, 293 - 302.
Dupuy, C., Dostal, J. & Traineau, H., 1985, Geochemistry of volcanic rocks from Mt. Pelée, Martinique, **J. Volc. Geoth. Res.**, 26, 147 -165.
Eggler, D.H., 1972, Amphibole stability in H_2O-undersaturated calc-alkaline melts, **Earth Planet. Sci. Lett.**, 15, 28 - 34.
Eichelberger, J.C., 1978, Andesite in island arcs and continental margins : Relationship to crustal evolution, **Bull. Volc.**, 41, 480 - 500.
Elthon, D., 1979, High magnesia liquids as the parental magma for ocean floor basalts, **Nature**, 278, 514 - 518.
Elthon, D. & Scarfe, C.M., 1980, High-pressure phase equilibria of a high-magnesia basalt : implications for the origin of mid-ocean ridge basalts, **Carnegie Inst. Washington Year Book**, 79, 277-281.
Endo, K., Kobayashi, T. & Sumita, M., 1986, Debris avalanche deposits by the 1984 collapse of Ontake volcano, Central Japan, abstract, **Internat. Volc. Cong., Auckl.-Hamil.-Rot., N.Z.**, 1-9 Feb., p.239.
Escher, B.G., 1919, Programma van Werkzaamheden, **Natuurk. Tijdschr. Nedrl. Ind.**, 79, 99 - 116.
Escher, B.G., 1920, L'eruption du Goenoeng Galoenggoeng en Juillet 1918, **Natuurk. Tijdschr. Nederl. Ind.**, 80, 260 - 263.
Escher, B.G., 1925 L'eboulement prehistorique de Tasikmalaya et le volcan Galounggoung (Java), **Leid. Geol. Meded.**, 1, 8 - 21.
Escher, B.G., 1930, Le Eboulement prehistorique de Tasikmalaya et le volcan Galoenggoeng Java, **Vulkanol. Zeitschr.**, 21, 67 - 68.
Evance, B.W. & Leake, B.E., 1960, The composition and origin of stripped amphibolites of Connemara, Ireland, **J. Petrol.**, 1, 337 - 363.
Ewart, A., 1976, Mineralogy and chemistry of modern orogenic lavas -some statistics and implications, **Earth Planet. Sci. Lett.**, 31, 417 - 432.
Ewart, A., 1982, The mineralogy and petrology of Tertiary - Recent orogenic volcanic rocks : with special reference to the andesite - basaltic compositional range, in R.S. Thorpe (ed.), **Andesites : Orogenic Andesites and Related Rocks**, John Wiley Sons Ltd., New York, pp. 25 - 95.
Ewart, A. & Bryan, W.B., 1972, Petrography and geochemistry of the igneous rocks from Ena, Tongan Islands, **Geol. Soc. Amer. Bull.**, 83, 3281 - 3298.
Ewart, A., Bryan, W.B. & Gill, J.B., 1973, Mineralogy and geochemistry of the young volcanic islands of Tonga, SW Pacific, **J. Petrol.**, 14, 429 - 465.
Ewart, A. & Hawkesworth, C.J., 1987, The Pleistocene - Recent Tonga - Kermadec arc lavas : interpretation of new isotopic and rare earth data in terms of a depleted mantle source model, **J. Pettrol.**, 28, 495 - 530.
Fabries, J., 1979, Spinel- olivine geothermometry in peridotites from ultramafic complexes, **Contr. Min. Petr.**, 69, 329 - 336.

Falloon, T.J. & Green, D.H., 1987, Anhydrous partial melting of MORB pyrolite and other peridotite compositions at 10 kbar : implica-cations for the origin of primitive MORB glasses, **Miner. Petrol.**, 37, 181 - 219.

Falloon, T.J., Green, D.H. & Crawford, A.J., 1987, Dredged igneous rocks from the northern termination of the Tofua magmatic arc, Tonga and adjacent Lau Basin, **Austral. J. Earth. Sci.**, 34, 487 - 506.

Falloon, T.J., Varne, R., Morris, J.D & Hart, S.R., 1989, Alkaline volcanics from Christmas Island and nearby seamounts : magmatism of the northeast Indian Ocean, Continental Magmatism Abstracts, IAVCEI General Assembly, Santa Fe, New Mexico, USA, June 25 - July 1, **New Mexico Bureau of Mines & Miner. Resour.**, 131, p. 86.

Fennema, R., 1896, Kort bericht over de uitbarsting van den vulkaan Galoenggoeng op 18 en 19 October 1894, **Natuurk. Tijdschr. Nederl. Ind.**, 55, 427 - 440.

Figee, S. & Onnen, H., 1897, Vulkanische verschijusclen in het jaar 1895, **Natuurk. Tijdschr. Nederl. Ind.**, 56, 81 - 91.

Fisher, R.V. & Schmincke, H.U, 1984, **Pyroclastic rocks**, Berlin, Springer - Verlag, 472 p.

Fisk, M.R. & Bence, A.E., 1979, Experimental studies of spinel crys-tallization in FAMOUS basalt 527-1-1, **EOS, Trans. Amer. Geophys. Union**, 60, p.420.

Fisk, M.R. & Bence, A.E., 1980, Experimental crystallization of chrome spinel in FAMOUS basalt 527-1-1, **Earth Planet. Sci. Lett.**, 48, 111 - 123.

Fitch, T.J., 1970, Earthquake mechanisms and island-arc tectonics in the Indonesian - Philippine region, **Bull. Seismol. Soc. Amer.**, 60, 565 - 591.

Fitch, T.J., 1972, Plate convergence, transcurrent faults and internal deformation adjacent to Southeast Asia and the Western Pacific, **J. Geophys. Res.**, 77, 4432 - 4460.

Fleet, A.J., Henderson, P. & Kempe, D.R.C., 1976, Rare earth element and related chemistry of some drilled southern Indian Ocean ba-salts and volcanogenic sediments, **J. Geophys. Res.**, 81, 23, 4257 - 4268.

Fleet, M.E., MacRae, N.D. & Herzberg, C.T., 1977, Partition of nickel between olivine and sulfide : A test for immiscible sulfide liq-uids, **Contr. Min. Petr.**, 65, 191 - 198.

Flood, R.H. & Vernon, R.H., 1988, Microstructural evidence of orders of crystallization in granitoid rocks, **Lithos**, 21, 237 - 245.

Foden, J.D., 1983, The petrology of the calcalkaline lavas of Rinjani volcano, east Sunda arc : a model for island arc petrogenesis, **J. Petrol.**, 24, 98 - 130.

Foden, J., 1986, The petrology of Tambora volcano, Indonesia : a model for the 1815 eruption, **J. Volc. Geoth. Res.**, 27, 1 - 41.

Foden, J.D. & Varne, R., 1980, The petrology and tectonic setting of Quaternary - recent volcanic centres of Lombok and Sumbawa, Sunda Arc, **Chem. Geol.**, 30, 201 - 226.

Fodor, R.V., 1987, Low- and high- TiO_2 flood basalts of southern Bra-zil : origin from picritic parentage and a common mantle source, **Earth Planet. Sci. Lett.**, 84, 423 - 430.

Fodor, R.V. & Keil, K., 1975, Contributions to mineral chemistry of Hawaiian rocks, **Contr. Min. Petr.**, 50, 173 - 195.

Francis, D., 1985, The Baffin Bay lavas and the value of picrites as analogues of primary magmas, **Contr. Min. Petr.**, 89, 144 - 154.

Francis, D.M., Ludden, J.N. & Hyves, A.J., 1983, Magma evaluation in a Proterozoic rifting environment, **J. Petrol.**, 24, 556 - 582.

Francis, P.W., 1985, The origin of the 1883 Krakatau tsunamis, **J. Volc. Geoth. Res.**, 25, 349 - 363.

Frank, D., Lubis, H., Casadevall, T.J., Glicken, H. & Suparman, 1987, Influence of hydrothermal alteration on volcanic hazards at Papandayan volcano, West Java, Indonnesia, abstract, **Hawaii Sympos. on How Volc. Work., Hilo, Hawaii**, Jan. 19-25, p. 80.

Frey, F.A., Bryan, W.A. & Thompson, G., 1974, Atlantic Ocean floor : Geochemistry and petrology of basalts from Legs 2 and 3 of the Deep Sea Drilling Project, **J. Geophys. Res.**, 79, 5507 - 5529.

Gast, P.W., 1968, Trace element fractionation and the origin of tholeiitic and alkaline magma types, **Geochim. Cosmochim. Acta**, 32, 1057 - 1086.

Garcia, M.O. & Jacobson, S.S., 1979, Crystal clots, amphibole fractionation and the evolution of calc-alkaline magma, **Contr. Min. Petr.**, 69, 319 - 327.

Geist, D.J., Baker, B.H. & McBirney, A.R., 1985, GPP : A program package for creating and using geochemical data files (Version for IBM - PC and compatible microcomputer), **Center for Volcanology, Univ. of Oregon**, Eugene, Oregon, 97403, 33 p.

Geological Survey of Indonesia, 1942, Rapport G. Galoenggoeng dari tgl. 20 sampai 24 December 1941, Bandung, unpubl.

Geological Survey of Indonesia, 1977, **Geological map of Java and Madura**, scale 1 : 2,000,000, Geol. Surv. Indon., Bandung.

Gerlach, D.C. & Grove, T.L., 1982, Petrology of Medicine Lake Highland Volcanics : Characterization of endmembers of magma mixing, **Contr. Min. Petr.**, 80, 147 - 159.

Gill, J.B., 1970, Geochemistry of Viti Levu, Fiji, and its evaluation as an island arcs, **Contr. Min. Petr.**, 27, 179 - 203.

Gill, J.B., 1976, Evolution of the mantle : Geochemical evidence from alkali basalt : comment, **Geology**, 4, 625 - 626.

Gill, J.B., 1981, **Orogenic Andesites and Plate Tectonics**, Springer - -Verlag, 390 p.

Gill, J.B. & Williams, R., 1989, Th isotopes and U-series disequilibria in subduction-related volcanic rocks, Continental Magmatism Abstracts, IAVCEI General Assembly, Santa Fe, New Mexico, USA, June 25 - July 1, **New Mexico Bureau of Mines & Miner. Resour.**, p. 107.

Giret, A., 1979, Genese des roches feldspathoidiques par la destabilisation des amphiboles : Le Massif des Montagnes Vertes, Kerguelen, C.R. Acad. Sci., **Paris, 289**, 379 - 382.

Giret, A., Bonin, B. & Leger, J.M., 1980, Amphibole compositional trends in oversaturated and undersaturated alkaline plutonic ring - complexes, **Canad. Miner.**, 18, 481 - 495.

Glazner, A.F., 1984, Activities of olivine and plagioclase components in silicate melts and their application to geothermometry, **Contr. Min. Petr.**, 88, 260 - 268.

Glicken, H., 1982, Criteria for identification of large volcanic debris avalanche (abstract), **EOS, Trans. Amer. Geophys. Union**, 63, p. 1141.

Glicken, H., 1983, Rockslide-debris avalanche of May 18, 1980 Mount St. Helens volcano, Dissertation Prospectus, Dept. Geol. Sci., Univ. of California, Santa Barbara.

Glicken, H., 1986, Rock-slide debris avalanche of May 18, 1980, Mount St. Helens volcano, PhD Dissertation, Univ. of California, Santa Barbara.

Glicken, H., Asmoro, P., Lubis, H., Frank, D. & Casadevall, T.J., 1987, The 1772 debris avalanche and eruption at Papandayan volcano, Indonesia, and hazards from future similar events, abstract, **Hawaii Sympos. on How Volc. Work, Hilo, Hawaii**, Jan. 19-25, p.91.

Glicken, H., Voight, B. & Janda, R.J., 1981, Rockslide-debris avalanche of May 18, 1980, Mount St. Helens volcano, abstract, **IAVCEI Sympos. Arc Volcanism, Tokyo and Hakone**, 109 - 110.

Goldscmidt, V.M., 1954, **Geochemistry**, Clarendon press, Oxford, 730 p.

Gorshkov, G.S., 1959, Gigantic eruption of the Bezymianny volcano, **Bull. Volc.**, 20, 77 - 109.

Gorshkov, G.S., 1963, Directed volcanic blast, **Bull. Volc.**, 26, 83 - 88.

Gorshkov, G.S. & Dubik, Y.M., 1970, Gigantic directed blast at Shiveluch volcano (Kamchatka), **Bull. Volc.**, 34, 261 - 307.

Gorton, M.P., 1977, The geochemistry and origin of Quaternary volcanism in New Hebrides, **Geochim. Cosmochim. Acta**, 41, 1257 - 1270.

Graham, I.J. & Hackett, W.R., 1987, Petrology of calc-alkaline lavas from Ruapehu volcano and related vents, Taupo volcanic zone, New Zealand, **J. Petrol.**, 28, 531 - 567.

Green, D.H., 1970, The origin of basaltic and nephelinitic magmas, **Trans. Leicester Lit. Phil. Soc.**, 64, 26 - 54.

Green, D.H., 1971, Composition of basaltic magmas as indicator of conditions of origin : application to oceanic volcanism, **Phil. Trans. Roy. Soc. Lond.**, A, 268, 707 - 724.

Green, D.H., Hibberson, W.O. & Jaques, A.L., 1979, Petrogenesis of mid-ocean ridge basalts, in : M.W. McElhinny (ed.), **The Earth : its origin, structure and evolution**, Academic Press, pp. 265-299.

Green, D.H. & Ringwood, A.E., 1967, The genesisi of basaltic magmas, **Contr. Min. Petr.**, 15, 103 - 190.

Green, D.H. & Ringwood, A.E., 1970, Mineralogy of peridotite compositions under upper mantle conditions, **Phys. Earth Planet. Inter.**, 3, 359 - 371.

Green, T.H., 1980, Island-arc and continent- building magmatism - a review of key geochemical parameters and genetic processes, **Tectonophysiscs**, 63, 367 - 385.

Green, T.H. & Pearson, N.J., 1986, Ti-rich accessory phase saturation in hydrous mafic - felsic compositions at high P, T, **Chem. Geol.**, 54, 185 - 201.

Green, T.H. & Ringwood, A.E., 1968, Genesis of the calc-alkaline igneous rock suite, **Contr. Min. Petr.**, 18, 105 - 162.

Griffin, W.L., 1973, Lherzolite nodules from the Fen alkaline complex, Norway, **Contr. Min. Petr.**, 38, 135 - 146.

Grove, T.L. & Baker, M.B., 1984, Phase equilibrium controls on the tholeiitic versus calc-alkaline differentiation trends, **J. Geophys. Res.**, 89, 3253 - 3274.

Grove, T.L., Gerlach, D.C. & Sando, T.W., 1982, Origin of calc-alkaline series lavas at Medicine Lake volcano by fractionation, assimilation and mixing, **Contr. Min. Petr.**, 80, 160 - 182.

Gudmundsson, A., 1988, Formation of collapse calderas, **Geology**, 16, 808 - 810.

Gust, D.A. & Perfit, M.R., 1987, Phase relations of a high-Mg basalt from the Aleutian island arc : Implications for primary island arc basalts and high-Al basalts, **Contr. Min. Petr.**, 97, 7 - 18.

Hackett, W.R., 1985, Geology and petrology of Ruapehu volcano and related vents, PhD thesis, Victoria University of Wellington, Wellington, New Zealand.

Hadian, R., Hamidi, S., Reksowirogo, L.D. & Kusumadinata, K., 1974, Data dasar gunungapi Indonesia, v.1 Jawa, Geol. Surv. Indon., Bandung, unpubl.

Hadikusumo, D., 1959, Laporan singkat kegiatan G. Galunggung dalam bulan Mei 1959, Geol. Surv. Indon., Bandung, unpubl.

Hamidi, S., 1985, Evaluasi lahar G. Galunggung, perkembangan dan urutan terjadinya sampai Januari 1985, Volc. Surv. Indon., Bandung, unpubl.

Hamilton, W., 1970, Tectonic map of Indonesia, a progress report, **U.S. Geol. Surv.**, Denver, Colo., 29 p.

Hamilton, W., 1973, Tectonics of the Indonesian region, **Geol. Soc. Malaysia Bull.**, 6, 3 - 10.

Hamilton, W., 1977, Subduction in the Indonesian Region. Island arcs, deep sea trenches and back-arc basins, **Maurice Ewing Series**, 1, 15 - 31.

Hamilton, W., 1979, Subduction in the Indonesian Region, **USGS Prof. Paper**, 1078, 345 p.

Hammarstrom, J.M. & Zen, E., 1986, Aluminium in hornblende : An empirical igneous geobarometer, **Amer. Min.**, 71, 1297 - 1313.

Hart, S.R., 1988, Heterogeneous mantle domains : signatures, genesis and mixing chronologies, **Earth Planet. Sci. Lett.**, 90, 273 - 296.

Hart, S.R. & Davis, K.E., 1978, Nickel partitioning between olivine and silicate melt, **Earth Planet. Sci. Lett.**, 40, 203 - 219.

Harvey, P.K., Taylor, D.M, Hendry, R.D. & Bancroft, F., 1973, An accurate fusion method for the analysis of rocks and chemically related materials by X-ray fluorescence spectometry, **X-Ray Spectometry**, 2, 33 - 44.

Hatch, F.H., Wells, A.K. & Wells, M.K., 1972, **Petrology of the Igneous Rocks**, Thomas Murby & Co., London, 551 p.

Hatherton, T. & Dickinson, W.R., 1969, The relationship between andesitic volcanism and seismicity in Indonesia, the Lesser Antilles, and other island arcs, **J. Geophys. Res.**, 74, 5301 - 5310.

Hawkesworth, C.J. O'nions, R.K., Pankhurst, R.J., Hamilton, P.J. & Evensen, N.M., 1977, A geochemical study of island-arc and back-arc tholeiites from the Scotia Sea, **Earth Planett. Sci. Lett.**, 36, 253 - 262.

Hayes, D.E., Frakes, L.A. & others, eds., 1975, **Initial reports of the deep sea drilling project**, 28, U.S. Govt. Print. Off., Washington, D.C., 1017 p.

Hedberg, H.D. (ed.), 1976, **International Stratigraphic Guide. A Guide to Stratigraphic Classification, Terminology, and Procedure**, John Wiley and Sons, New York, 200 p.

Heier, K.S., 1962, The possible origin of amphibolites in an area of high metamorphic grade, **Norsk Geol. Tiddissk.**, 42, 157 - 165.

Heming, R.F., 1974, Geology and petrology of Rabaul caldera, **Geol. Soc. Amer. Bull.**, 85, 1253 - 1264.

Heming, R.F. & Carmichael, I.S.E., 1973, High-temperature pumice flow from the Rabaul caldera Papua, New Guinea, **Contr. Min. Petr.**, 38, 1 - 20.

Hermes, O.D. & Schilling, J.G., 1976, Olivine from Reykjanes ridge and Iceland tholeiites, and its significance to the two-mantle source model, **Earth Planet. Sci. Lett.**, 28, 345 - 355.

Hertogen, J. & Gijbels, R., 1976, Calculation of trace element frac-fractionation during partial melting, **Geochim. Cosmochim. Acta**, 40, 313 - 322.

Hofmann, A.W., 1986, Nb in Hawaiian magmas : constraints on source composition and evolution, **Chem. Geol.**, 57,17 - 30.

Hofmann, A.W. Jochum, K.P., Seufert, M. & White, W.M., 1986, Nb and Pb in oceanic basalts : new constraints on mantle evolution, **Earth Planet. Sci. Lett.**, 79, 33 - 45.

Holloway, J.R., 1973, The system pargasite-H_2O-CO_2 : a model for melting of a hydrous mineral with a mixed-volatile fluid-I. Experimental results to 8 kbar, **Geochim. Cosmochim. Acta**, 37, 651-666.

Holloway, J.R. & Ford, C.E., 1975, Fluid-absent melting of the fluorohydroxy amphibole pargasite to 35 kilobars, **Earth Planet. Sci. Lett.**, 25, 44 - 48.

Hoover, J.D. & Presnall, D.C., 1982, Melting relations of simplified peridotite in the SiO_2-CaO-Al_2O_3-MgO-Na_2O (SCAMN) system from 1 atm to 20 kb-II. Results and application to basalt generation, abstract, **Geol. Soc. Amer. Abstr. with Programms**, 14, 517.

Houghton, B.F., Latter, J.H. & Hackett, W.R., 1987, Volcanic hazard assessment for Ruapehu composite volcano, Taupo Volcanic Zone, New Zealand, **Bull. Volc.**, 49, 737 - 751.

Houghton, B.F., Latter, J.H. & Froggatt, P.C., 1988, Volcanic Hazard in New Zealand. Identifying the problem and practical measures to to mitigate the risk, **Geol. Soc. N.Z. miscell. publ.**, 41 d.

Huppert, H.E. & Sparks, R.S.J., 1988 a, The fluid dynamics of crustal melting by injection of basaltic sills, **Trans. Royal Soc. Edinburgh : Earth Sciences**, 79, 237 - 243.

Huppert, H.E. & Sparks, R.S.J., 1988 b, The generation of granitic magmas by intrusion of basalt into continental crust, **J. Petrol.**, 29, 599 - 624.

Hutchison, C.S., 1973, Tectonic evolution of Sundaland : A phanerozoic synthesis, **Geol. Soc. Malaysia Bull.**, 6, 61 - 86.

Irvine, T.N., 1967, Chromian spinel as a petrogenetic indicator, 2. Petrologic applications, **Can. J. Earth Sci.**, 4, 71 - 103.

Irvine, T.N., 1979, Rocks whose composition is determined by crystal accumulation and sorting. In H.S. Yoder Jr. (ed.), **The evaluation of the igneous rocks**, Princeton Univ. Press, New Jersey, 245-306.

Irvine, T.N. & Baragar, W.R.A., 1971, A guide to the chemical classification of the common volcanic rocks, **Canad. J. Earth Sci.**, 8, 523 - 548.

Irving, A.J., 1978, A review of experimental studies of crustal/liquid trace element partitioning, **Geochim. Cosmochim. Acta**, 42, 743 - 770.

Ito, K. & Kennedy, G.C., 1967, Melting and phase relations in a natural peridotite to 40 kilobars, **Amer. J. Sci.**, 265, 519 - 538.

Jacobsen, S.B., 1988, Isotopic and chemical constraints on mantle - crust evolution, **Geochim. Cosmochim. Acta**, 52, 1341 - 1350.

Jakes, P.J. & Gill, J., 1970, Rare earth elements and the island arc tholeiitic series, **Earth Planet. Sci. Lett.**, 9, 17 - 28.

Jakes, P.J. & White, A.J.R., 1971, Composition of island arcs and continental growth, **Earth Planet. Sci. Lett.**, 12, 224 - 230.

Jakes, P.J. & White, A.J.R., 1972, Major and trace elements abundances in volcanic rocks of orogenic areas, **Geol. Soc. Amer. ull.**, 83, 29 - 40.

Janda, R.J., Scott, K.M., Nolan, K.M. & Martinson, H.A., 1981, Lahar movement, effects, and deposits. In P.W. Lipman & D.R. Mullineaux (eds.), **The 1980 eruptions of Mount St. Helens, Washington**, U.S. Geol. Surv. Prof. Paper, 1250, 461 - 478.

Jaques, A.L. & Green, D.H., 1980, Anhydrous melting of peridotite at 0 - 15 Kb pressure and the genesis of tholeiitic basalts, **Contr. Min. Petr.**, 73, 287 - 310.

Johnson, R.W., 1977, Distribution and major - element chemistry of Late Cenozoic volcanoes at the Southern margin of the Bismarck Sea, Papua New Guinea, **Bur. Miner. Res. Aust. Rept.**, 188, 170 p.

Johnson, R.W. & Chappell, B.W., 1979, Chemical analyses of rocks from the Late Cenozoic volcanoes of north - central New Britain and the Witu Islands, Papua New Guinea, **Bur. Miner. Res. Aust. Rept.**, 209, BMR Microform M.F.76.

Johnson, R.W., Jaques, A.L., Hickey, R.L., McKee, C.O. & Chappell, B. W., 1985, Manam Island Papua New Guinea : Petrology and geochemistry of a low-TiO_2 basaltic island - arc volcano, **J. Petrol.**, 26, 283 - 323.

Johnson, R.W., Mackenzie, D.W. & Smith, I.E.M., 1978, Volcanic rock associations at convergent plate boundaries : reappraisal of the concept using case histories from Papua pua New Guinea, **Geol. Soc. Amer. Bull.**, 89, 96 - 106.

Johnson, B.D., Powell, C.McA. & Veevers, J.J., 1976, Spreading history of the eastern Indian Ocean and Greater Indias's northward flight from Antarctica and Australia, **Geol. Soc. Amer. Bull.**, 87, 1560 -1566.

Johnstone, M.R., 1975, **Sheet N159 and pf. N158, Tinui - Awatoitoi** (1st ed.) " **Geological Map of New Zealand, 1 : 63360**", DSIR, Wellington, N.Z.

Junghuhn, F.,1850, Galoenggoeng, **Java II**,124-160.

Junghuhn, F., 1853, **Java, deszelfs, gedaante, bekleeding en inwendige structuur**, Amsterdam 2nd ed. 4 Parts.

Juwarna, H., Wirakusumah, A.D., Sutoyo & Bronto, S., 1986, **Geologic map of Galunggung volcano, West Java, Indonesia**, Volc. Surv. Indon., Bandung, Indonesia.

Karig, D.E., 1975, Basin genesis in the Philippine Sea, **Initial reports of the Deep Sea Drilling Program**, 31, U.S. Govt. Print. Off., 857 - 879.

Karig, D.E., Moore, G.F. & Hehanusa, P.E., 1979, Cenozoic evolution of the Sunda Arc in the Central Sumatra region, in J. Watkins & L. Montadert (eds.) : Geological and Geophysical Investigations of Continental Slopes and Rises, **Am. Assoc. Petrol. Geol. Mem.**, 29, 223 - 237.

Karig, D.E., Moore, G.F., Curray, J.R. & Lawrence, M.B., 1980, Morphology and shallow structure of the lower trench slope off Nias island, Sunda Arc, in Hayes, D.E., (ed.) : The tectonic and geologic evolution of Southeast Asian and islands, **Geophysical Monograph** : 23, 179 - 208.

Karig, D.E. & Sharman, G.F.III, 1975, Subduction and accretion in trenches, **Geol. Soc. Amer. Bull.**, 86, 377 - 389.

Kartakusumah, R.S., 1984, Preliminary radiocarbon data of charcoal sample on one hillock of 'Ten Thousand Hills' Tasikmalaya, **Geosurv. Newslett.**, 16, 39 - 40.

Kastowo, 1975, **Geologic map of the Majenang Quadrangle, Java**, 10/XIV-B, scale 1 : 100,000, Geol. Surv. Indon., Bandung.

Katili, J.A., 1969, Permian volcanism and its relation to the tectonic development of Sumatra, **Bull. Volc.**, 33, 530 - 540.
Katili, J.A., 1970, Large transcurrent faults in Southeast Asia, with special reference to Indonesia, **Geol. Rundsch.**, 59, 581 - 600.
Katili, J.A., 1971, A review of geotectonic theories and tectonic maps of Indonesia, **Earth Sci. Rev.**, 7, 143 - 163.
Katili, J.A., 1973 a, On fitting certain geological and geophysical features of the Indonesian island arcs to new global tectonics, **Univ. of Western Australia Press**, 287 - 305.
Katili, J.A., 1973 b, Geochronology of West Indonesia and its implications on plate tectonics, **Tectonophysics**, 19, 195 - 212.
Katili, J.A., 1975, Volcanism and plate tectonics in the Indonesian island arcs, **Tectonophysics**, 26, 165 - 188.
Katili, J.A. & Hehuwat, F., 1967, On the occurrence of large transcurrent faults in Sumatra, Indonesia, **J. Geosciences**, Osaka City Univ., 10, 5 - 17.
Katili, J.A. & Sudradjat, A., 1984, **Galunggung. The 1982-1983 Eruption**, Volc. Surv. Indon., Bandung, 102.
Katsui, Y., Oba, Y., Y., Ando, S., Nishimura, S., Masuda, Y., Kurasawa, H. & Fujimaki, H., 1978, Petrochemistry of the Quaternary volcanic rocks of Hokkaido, North Japan, **Jour. Fac. Sci., Hokkaido Univ.**, Ser.IV, v.18, n.3, 449-484.
Kay, R., Hubbard, N.J. & Gast, P.W., 1970, Chemical characteristics and origin of oceanic ridge volcanic rocks, **J. Geophys. Res.**, 75, 75, 1585 - 1613.
Kay, M.S. & Kay, Kay, R.W., 1985a, Aleutian tholeiitic and calc-alkaline magma series I : The mafic phenocrysts, **Contr. Min. Petr.**, 90, 276 - 290.
Kay, M.S. & Kay, R.W., 1985b, Role of crystal cumulates and the oceanic crust in the formation of the lower crust of the Aleutian arc, **Geology**, 13, 461 - 464.
Kay, R.W., 1977, Geochemical constraints on the origin of Aleutian magmas, in : M. Talwani & W.C. Pitman III (eds.), **Island Arcs, Deep Sea Trenches and Arc Basins** 229 - 242, Maurice Ewing Series 1, Amer. Geophys. Union, Washington, D.C.
Kay, R.W., 1978, Aleutian magnesian andesites : melts from subducted Pacific Ocean crust, **J. Volc. Geoth. Res.**, 4, 117 - 132.
Kay, R.W., 1984, Elemental abundances relevant to identification of magma sources, **Phil. Trans. R. Soc. Lond.**, A 310, 535 - 547.
Kay, R.W. & Kay, S.M., 1988, Crustal recycling and the Aleutian arc, **Geochim. Cosmochim. Acta**, 52, 1351 - 1359.
Kay, R.W., Sun, S. S. & Lee-Hu, C.N., 1978, Pb and Sr isotopes in volcanic rocks from the Aleutian Islands and Pribilof Islands, Alaska, **Geochim. Cosmochim. Acta**, 42, 263 - 273.
Kemmerling, G.L.L., 1921, De Galoenggoeng, **Natuurk. Tijdschr. Nederl. Ind.**, 81, 39 - 40.
Kerr, P.F., 1977, **Optical Mineralogy**, McGraw-Hill Book Co., New York, 492 p.
Kienle, J., Kyle, P.R., Self, S., Motyka, R.J. & Lorennz, V., 1980, Ukinrek Maars, Alaska, I. April 1977 eruption sequence, petrology and tectonic setting, **J. Volc. Geoth. Res.**, 7, 11 - 37.
King, L.C., 1962, **The morphology of the earth**, Hafner, New York, 577 p.
Kirsanov, I.T., Koloskov, A.V., Kutyev, F.Sh. & Erlich, E.N., 1979, Rock forming and accessory minerals of the basalt - andesite - basalt rock series of Kamchatka, **Bull. Volc.**, 42, 131 - 147.

Knutson, J. & Green, T.H., 1975, Experimental duplication of a high-pressure megacryst/ cumulate assemblage in a near saturated hawaiite, **Contr. Min. Petr.**, 52, 121 -132.

Koesoemadinata, R.P. & Pulunggono, A., 1975, Geology of the Southern Sunda shelf in reference to the tectonic framework of Tertiary sediment basins of Western Indonesia, **J. Indo. Assoc. Geol.**, 2, 1 - 11.

Koolhoven, W.C.B., 1935, Het primaire voorkomen van den Zuid Borneo diamant, **Verh. Geol. Mijnbouw Ned. Kol. Geol. Ser.**, 11, 189-132.

Kretz, R., 1982, Transfer and exchange equilibria in a portion of the pyroxene quadrilateral as deduced from natural and experimental data, **Geochim. Cosmochim. Acta**, 46, 411-422.

Krishnamurthy, P. & Cox, K.G., 1977, Picrite basalts and related lavas from the Deccan Traps of Western India, **Contr. Min. Petr.**, 62, 53 - 75.

Kuno, H., 1954, Study of orthopyroxenes from volcanic rocks, **Am. Miner.**, 39, 30 - 46.

Kuno, H., 1966, Lateral variation of basalt magma type across continental margins and island arcs, **Bull. Volc.**, 29, 195 - 222.

Kushiro, I. & Nakamura, Y., 1970, Petrology of some lunar crystalline rocks, Proc. Apollo 11 Lunar Science Conference, 1, 607 - 626.

Kushiro, I., Syono, Y. & Akimoto, S., 1968, Melting of a peridotite nodule at high pressures and high water pressures, **J. Geophys. Res.**, 73, 6023 - 6029.

Kushiro, I. & Yoder, H.S.Jr., 1966, Anorthite - forsterite and anorthite - enstatite relations and their bearing on the basalt - eclogite transformation, **J. Petrol.**, 7, 337-362.

Kusnaeny, K., 1977, X-ray microanalyses of the ignimbrites of Toba, **Proc. Reg. Conf. Min. Res. SE Asia, Jakarta**, 175 - 184.

Kusumadinata, K., 1959, G. Galunggung (32) 16 April 1959; G. Galunggung (32) 14 - 16 Mei 1959; G. Galunggung (32). Laporan bulan Mei 1959, Geol. Surv. Indon., Bandung, unpubl.

Kusumadinata, K., 1967, Daerah bahaya sementara G. Galunggung berdasarkan peta dan pustaka, Volc. Surv. Indon., unpbl.

Kusumadinata, K., Ed., 1979, **Catalogue of references on Indonesian volcanoes with eruptions in historical time**, Volc. Surv. Indon., Bandung, 820 p.

Kusumadinata, K., 1981, 13 Agung (54), **Bull. Volc. Surv. Indon.**, 104, 6 - 41.

Lacroix, A., 1904, **La Montagne Pelée et ses eruptions**, Masson et Cie, Paris, 662 p.

Lambert, I.B. & Wyllie, P.J., 1968, Stability of hornblende and a model for the low-velocity zone, **Nature**, 219, p. 1240 .

Lambert, I.B. & Wyllie, P.J., 1970, Melting in the deep crust and upper mantle and the nature of the low velocity layer, **Phys. Earth Planet. Int.**, 3, p. 316.

Lambert, I.B. & Wyllie, P.J., 1972, Melting of gabbro (quartz eclogite) with excess water to 35 kilobars, with geological applications, **J. Geology**, 80, 693 - 708.

Langmuir, C.H., 1989, Geochemical consequenses of in situ crystallization, **Nature**, 340, 199 - 205.

Langmuir, C.H., Bender, J.F., Bence, A.E., Hanson, G.N. & Taylor, S.R., 1977, Petrogenesis of basalts from the FAMOUS area : Mid-Atlantic Ridge, **Earth Planet. Sci. Lett.**, 36, 133 - 156.

Langmuir, C.H. & Hanson, G.N., 1980, An evaluation of major element heterogeneity in the mantle sources of basalts, **Phil. Trans. Roy . Soc. Lond., A 297, 383 - 407.**

Larsen, E.S., Irving, J., Gonyer, F.A. & Larsen, E.S., 1936, Petrologic results of a study of the minerals from the Tertiary rocks of the San Juan region, Colorado, **Amer. Min.**, 21, 694 - 700.

Larson, R.L., 1975, Late Jurrasic sea-floor spreading in the Eastern Indian Ocean, **Geology**, 4, 69 - 71.

Larson, R.L., Carpenter, G.B. & Diebold, J.B., 1978, A Geophysical study of the Warton Basin near the Investigator Fracture Zone, **J. Geophys. Res.**, 83, 773 - 782.

Leake, B.E., 1978, Nomenclature of amphiboles, **Am. Miner.**, 63, 1023 - 1052.

Le Bas, M.J., Le Maitre, R.W., Streckeisen, A. & Zanettin, B, 1986, A chemical classification of volcanic rocks based on the total alkali - silica diagram, **J. Petrol.**, 27, 745 - 750.

Leeman, W.P., Vitaliano, C.J. & Prinz, M., 1976, Evolved lavas from the Snake River Plain : Craters of the Moon National Monument, Idaho, **Contr. Min. Petr.**, 56, 35 - 60.

LEMIGAS, 1975, Peta anomali gaya berat bebas udara di Jawa Barat Selatan, unpubl. rept.

Le Pichon, X. & Heirtzler, J.R., 1968, Magnetic anomalies in the Indian Ocean and sea floor spreading, **J. Geophys. Res.**, 73, 2101 - 2117.

Lewis, J.F., 1973, Mineralogy of the Ejected Blocks of the Soufriere volcano St. Vincent : Olivine, Pyroxene, Amphibole and magnetite Paragenesis, **Contr. Min. Petr.**, 38, 197 - 220.

Lindsley, D.H., 1983, Pyroxene thermometry, **Am. Miner.**, 68, 477 - 493.

Lipman, P.W., 1967, Mineral and chemical variations within an ash-flow sheet from Aso Caldera, southwestern Japan, **Contr. Min. Petr.**, 16, 300 - 327.

Lockwood, J.P. & Lipman, P.W., 1980, Recovering datable charcoal beneath young lavas : Lesson from Hawaii, **Bull. Volc.**, 43, 609 - 615.

Lofgren, G.E., 1983, Effect of heterogeneous nucleation on basaltic textures : A dynamic crystallization study, **J. Petrol.**, 24, 229 - 255.

Lofgren, G.E., 1989, Dynamic crystallization of chondrule melts of porphyritic olivine composition : Textures experimental and natural, **Geochim. Cosmochim. Acta**, 53, 461 - 470.

Lofgren, G.E. & Russell, W.J., 1986, Dynamic crystallization of chondrule melts of porphyritic and radial pyroxene composition, **Geochim. Cosmochim. Acta**, 50, 1715 - 1726.

Longhi, J. & Pan, V., 1988, A reconnaisance study of phase boundarie s in low-alkali basaltic liquids, **J. Petrol.**, 29, 115 - 147.

Lopez-Escobar, L., Frey, F.A. & Vergara, M., 1977, Andesites and high alumina basalts from the Central - South Chile High Andes : geochemical evidence bearing on their petrogenesis, **Contr. Min. Petr.**, 63, 199 - 228.

Lowrie, A., Bracey, D.R. & Vogt, P.R., 1972, Geophysical surveys in the Eastern Indian Ocean and Caroline Basin : preliminary results, abstract, **Trans. Amer. Geophys. Union**, 53,p. 413.

Luhr, J.F., Carmichael, I.S.E. & Varekamp, J.C., 1984, The 1982 eruptions of El Chichon volcano, Chiapas, Mexico : Mineralogy and petrology of the anhydrite-bearing pumices, **J. Volc. Geoth. Res.**, 23, 69 - 108.

Lyell, C., 1872, Galongoon, Java, 1822, in : **Principles of Geology**, John Murray, Albermarle St., p. 56 - 58.

Maaløe, S. & Aoki, K., 1977, The major element composition of the mantle estimated from the composition of lherzolites, **Contr. Min. Petr.**, 63, 161 - 173.

Maaløe, S. & Steel, R., 1980, Mantle composition derived from the composition of lherzolites, **Nature**, 285, 321 p.

Macdonald, G.A., 1972, **Volcanoes**, Prentice-Hall, Inc., Englewood Cliffs, New Jersey, 510 p.

Macdonald, G.A., 1975, Hazards from volcanoes, in : Bolt, B.A., Horn, W.L., Macdonald, G.A. & Scott, R.F., **Geological Hazards**, Springer -Verlag, New York, p. 63 - 131.

Markl, R.G., 1974, Evidence for the breakup of eastern Gondwanaland by the early Cretaceous, **Nature**, 251, 196 - 200.

Martodjojo, S., 1984, Evolusi Cekungan Bogor, Jawa Barat, PhD thesis, Fakultas Pasca Sarjana, Institute Teknologi Bandung, Bandung, Indonesia.

Martodjojo, S., Suparka, S. & Hadiwisastro, S., 1978, Status Formasi Ciletuh dalam evolusi Jawa Barat, **Geologi Indonesia**, 5, 29 - 38.

Masuda, Y. & Katsui, Y., 1975, Rare-earth and trace elements in the Quaternary volcanic rocks of Hokkaido, Japan, **Chem. Geol.**, 15, 251 - 271.

Matahelumual, J., 1982, Gunungapi dan Bahayanya di Indonesia, **Bull. Volc. Surv. Indon.**, 105, 69 p.

Maury, R.C., 1976, Contamination (par l'encaissant et les enclaves) et crstallisation fractionnée de séries volcaniques alcalines, continentales (Massif Central Français) et océaniques (Pacifique Central) : l'origine des laves acides, Thèse Doctorat d'état, Université Paris sud Orsay.

McBirney, A.R., 1969, Compositional variations in Cenozoic Calc - Alkaline suites of Central America, in : A.R. McBirney (ed.), Proc. Andes. Confer. Confer., **Oregon Dep. Geol. Miner. Resour. Bull.**, 65, 185-189.

McBirney, A.R., 1985, **Igneous Petrology**, Freeman, Cooper & Co., California, 504 p.

McBirney, A.R. & Noyes, R.M., 1979, Crystallization and layering of the Skaegaard intrusion, **J. Petrol.**, 20, 487 - 554.

Medaris, Jr. L.G., 1972, High-pressure peridotites in Southwestern Oregon, **Geol. Soc. Amer. Bull.**, 83, 41 - 58.

Mellors, R.A., Waitt, R.B. & Swanson, D.A., 1988, Generation of pyroclastic flows and surges by hot-rock avalanches from the dome of Mount St. Helens Volcano, USA, **Bull. Volcan.**, 50, 14 - 25.

Miller, C.D., 1982, Reconnaissance investigations at Merapi and Galunggung volcanoes, Dieng Plateau and Kamojang geothermal areas, Java, Indonesia, Volc. Surv. Indon., 1 - 7, unpbl.

Miller, C.D., Mullineaux, D.R. & Hall, M.L., 1978, Reconnaissance map of potential volcanic hazards from Cotopaxi volcano, Equador, **U.S. Geol. Surv. Miscell. Invest. Map I - 1072.**

Mimura, K., Kawachi, S., Fujimoto, U., Taneichi, M., Hyuga, T., Ichikawa, S. & Koizumi, M., 1982, Debris avalanche hills and their natural remanent magnetization - Nirazaki debris avalanche, Central Japan, **J. Geol. Soc. Jpn.**, 88, 653 - 663.

Minster, J.B. & Jordan, T.H., 1978, Present-day plate motions, **J. Geophys. Res.**, 83, 5331 - 5354.

Miyashiro, A., 1974, Volcanic rock series in island arcs and active continental margins, **Amer. J. Sci.**, 274, 321 - 355.

Miyashiro, A., 1975, Island arc volcanic rock series : a critical review, **Petrologie**, 3, 177 - 187.
Miyashiro, A. & Shido, F., 1975, Tholeiitic and calc-alkalic series in relation to the behavior of titanium, vanadium, chromium, and nickel, **Amer. J. Sci.**, 275, 265 - 277.
Mizuno, Y., 1975, Piedmont geomorphology of Iwaki volcano, **Tohoku Univ. Sci. Rep.**, ser. 7, 25, 159 - 164.
Moore, G.F. Curray, J.R., Moore, D.G. & Karig, D.E., 1980, Variation in geologic structure along the Sunda fore arc, Northeastern Indian Ocean, in Hayes, D.E. (Ed.) : The tectonic and geologic of Southeast Asian Seas and Islands, **Geophys. Monograph**, 23, 145 -160.
Moore, G.F. & Karig, D.E., 1980, Structural geology of Nias Island, Indonesia : Implications for subduction zone tectonics, **Amer. J. Sci.**, 280, 193 - 223.
Moore, J.G., 1967, Base surge in recent volcanic eruptions, **Bull. Volc.**, 30, 337 - 363.
Moore, J.G., 1970, Water content of basalt erupted on the ocean floor, **Contr. Min. Petr.**, 28, 272 - 279.
Moore, J.G. & Melson, W.G., 1969, Nuee ardentes of the 1968 eruption of Mayon volcano, Philippines, **Bull. Volc.**, 33, 600 - 620.
Moore, J.G. & Sisson, T.W., 1981, Deposits and effects of the May 18 pyroclastic surge, in : P.W. Lipman & D.R. Mullineaux (eds.), **The 1980 eruptions of Mount St. Helens**, U.S. Geol. Surv. Prof. Paper, 1250, 421 - 438.
Morimoto, N., Fabries, J., Fergusson, A.K., Ginzburg, I.V., Ross, M., Seifert, F.A., Zussman, J., Aoki, K. & Gottardi, G., 1988, Nomenclature of pyroxenes, **Miner. Mag.**, 52, 535 - 550.
Moriya, I., 1980, "Bandaian Eruption" and landforms associated with it, Collection of articles in memory of retirement of Prof. Nishimura from Tohoku Univ., 214 - 219.
Morrice, M.G. & Gill, J.B., 1986, Spatial patterns in the Mineralogy of island arc magma series : Sangihe arc, Indonesia, **J. Volc. Geoth. Res.**, 29, 311 - 353.
Morris, J.D., Tera, F., Gill, J.B., Leeman, W.P. & Johnson, R.W., 1989, Beryllium isotopes, Boron-Beryllium systematics and uranium uranium series disequilibria in the New Britain Arc, Continental Magmatism Abstracts, IAVCEI General Assembly, Santa Fe, New Mexico, USA, June 25-July 1, **New Mexico Bureau of Mines & Miner. Resour.**, 131, p.196.
Morris, J.D., Jezek, P.A., Hart, S.R. & Gill, J.B., 1980, The Halmahera island arc, Molluca Sea collision zone, Indonesia : A geochemical survey, in Hayes, D.E. (Ed.) : The tectonic and geologic evolution of Southeast Asian Seas and Islands, part 2, **Geophys. Monograph**, 27, 373 - 387.
Morse, S.A., 1979, Kiglapait geochemistry I : Systematics, sampling, and density, **J. Petrol.**, 20, 555 - 590.
Morse, S.A., 1981, Kiglapait geochemistry IV : The major elements, **Geochim. Cosmochim. Acta**, 45, 461 - 479.
Morse, S.A., 1982, Kiglapait geochemistry V : Strontium, **Geochim. Cosmochim. Acta**, 46, 223 - 234.
Müller, S., 1939, Landstreek, verwoest door de uitbarsting van den Galoenggoeng op 8 en 12 Oct. 1822, **Vulkanol. Meded**, 6, Plaat III.
Murai, I., 1961, A study of the textural characteristics of pyroclastic flow deposits in Japan, **Bull. Earthq. Res. Inst., Tokyo Univ.**, 39, 133 - 248.

Murai, I., 1963, A brief note on the eruption of the Tokachi-dake volcano of June 29 and 30, 1962, **Bull. Earthq. Res. Inst., Tokyo Univ.**, 41, 185 - 208.

Murck, B.W. & Campbell, I.H., 1986, The effect of temperature, oxygen fugacity and melt composition on the behaviour of chromium in basic and ultrabasic melts, **Geochim. Cosmo. Acta**, 50, 1871 - 1887.

Musper, K.A.F., 1937, Geologische kaart van Sumatra, schaal 1 : 200,000, Toelichting by blad 16 (Lahat), **Dienst. Mijn. Ned. Ind.**, 5, 110.

Myers, J.D., Marsh, B.D. & Sinha, K., 1986, Geochemical and strontium isotopic characteristics of parental Aleutian arc magmas : Evidence from the basaltic lavas of Atka, **Contr. Min. Petr.**, 94, 1 -11.

Mysen, B., 1973, Melting in a hydrous mantle; phase relations of mantle peridotite with controlled water and oxygen fugacities, **Carnegie. Inst. Wash. Yerb.**, 72, 467 - 478.

Mysen, B.O. & Kushiro, I., 1979, Pressure dependence of nickel partitioning between forsterite and aluminous silicate melts, **Earth Planet. Sci. Lett.**, 42, 383 - 388.

Nakamura, K., 1977, Volcanoes as possible indicators of tectonic stress orientation - principle and proposal, **J. Volc. Geoth. Res.**, 2, 1 - 16.

Nakamura, Y., 1978, Geology and petrology of Bandai and Nekoma volcanoes, **Tohoku Univ. Sci. Rep.**, ser. 3, 14, 67 - 119 .

Naldrett, A.J. & Turner, A.R., 1977, The geology and petrogenesis of a greenstone belt and related nickel sulfide mineralisation at Yakabindie, Western Australia, **Precambrian Res.**, 5, 43 - 103.

Neal, C.R., 1988, The origin and composition of metasomatic fluids and amphibole beneath Malaita, Solomon Island, **J. Petrol.**, 29, 149 -179.

Neall, V.E., 1976, Lahars - global occurrences and annotated bibliography, **Geol. Dept., Victoria Univ. of Wellington**, Pub. 5, 18 pp.

Neumann van Padang, M., 1951, **Catalogue of the active volcanoes of the world including solfatara fields, Part 1**, Internat. Volc. Assoc., Napoli, 271 p.

Newcomb, K.R. & McCann, W.R., 1987, Seismic history and seismotectonics of the Sunda Arc, **J. Geophys. Res.**, 92, 421 - 439.

Newhall, C.G., 1982, A prehistoric debris avalanche from Mount St. Helens, abtract, **EOS, Trans. Amer. Geophys. Union**, 63, 1141.

Newhall, C.G. & Dzurisin, D., 1988, Historical unrest at large Quaternary calderas of the world, **U.S. Geol. Surv. Bull.**, 1855, 1108 p.

Nicholls, I.A. & Whitford, D.J., 1976, Primary magmas associated with Quaternary volcanism in the Western Sunda Arc, Indonesia, in : R. W. Johnson (Ed.), **Volcanism in Austra lasia**, Elsevier, Amsterdam, pp. 77 - 90.

Nicholls, I.A. & Whitford, D.J., 1978, Geochemical zonation in the Sunda volcanic arc and the origin of K-rich lavas, **Bull. Aust. Soc. Explor. Geophys.**, 9, 3, 93 - 97.

Nicholls, I.A. & Whitford, D.J., 1983, Potassium-rich volcanic rocks of the Muriah Complex, Java, Indonesia : Products of multiple magma sources ?, **J. Volcan. Geoth. Res.**, 18, 337 - 359.

Nicholls, I.A., Whitford, D.J., Harris, K.L. & Taylor, S.R., 1980, Variation in the geochemistry of mantle sources for tholeiitic and calc-alkaline mafic magmas, Western Sunda volcanic arc, Indonesia, **Chem. Geol.**, 30, 177 - 199.

Nielsen, R.L. & Dungan, M.A., 1983, Low pressure mineral - melt equilibria in natural anhydrous mafic system, **Contr. Min. Petr.**, 84, 310 - 326.

Ninkovich, D., Shackleton, N.J., Abdel-Monem, A.A., Obradovich, J.D. & Izett, G., 1978, K-Ar age of the Late Pleistocene eruption of Toba, N. Sumatra, **Nature**, 276, 574 - 577.

Nisbet, E.G. & Pearce, J.A., 1977, Clinopyroxene composition in mafic lavas from different tectonic settings, **Contr. Min. Petr.**, 63, 149 - 160.

Nisbet, E.G. & Walker, D., 1982, Komatiites and the structure of the Archean mantle, **Earth Planet. Sci. Lett.**, 60, 105 - 113.

Nockolds, S.R., 1940, The Garabal Hill-Glen fine igneous complex, **Q.J. Geol. Soc. London**, 96, 451 - 511.

Nohda, S., 1984, Classification of island arcs by Nd - Sr isotopic data, **Geochem. J.**, 18, 1 - 9.

Norrish, K. & Hutton, J.T., 1969, An accurate X-ray spectrographic method for the analysis of a wide range of geological samples, **Geochim. Cosmochim. Acta**, 33, 431 - 453.

Nye, C.J. & Reid, M.R., 1986, Geochemistry of primary and least fractionated lavas from Okmok volcano, Central Aleutians : Implications for arc magma genesis, **J. Geophys. Res.**, 91, 10271 - 10287.

Oba, N., Tomita, K., Yamamoto, M., Bronto, S., Istidjab, M., Sudradjat, A. & Suhanda, T., 1983, Geochemical study of some volcanic products from Galunggung volcano, West Java, Indonesia, **Rept. Fac. Sci. (Earth Sci. & Biol.), Kagoshima Univ.**, 16, 1 - 20.

Oba, Y., 1972, Petrology of the Late Pliocene basalt of the western part of Hokkaido, **J. Fac. Sci., Hokk. Univ.**, Ser. 4, 15, 11 - 26.

Oba, Y, 1975, Late Neogene basaltic rocks from the Kitami-Monbetsu district, northeast Hokkaido, **J. Fac. Sci., Hokk. Univ.**, ser. 4, 16, 501 - 510.

O'Hara, M.J., 1968, Are ocean floor basalts primary ?, **Nature**, 220, 683 - 686.

O'Hara, M.J., 1977, Geochemical evolution during fractional crystallisation of a periodically refilled magma chamber, **Nature**, 266, 503 - 507.

O'Hara, M.J. & Mathew, R.E., 1981, Geochemical evolution in advancing, periodically replenished, periodically tapped, continuously fractionated magma chamber, **J. Geol. Soc. Lond.**, 138, 237 - 277.

O'Neill, H.St.C. & Wall, V.J., 1987, The olivine - orthopyroxene - spinel oxygen geobarometer, the nickel precipitation curve, and curve, and the oxygen fugacity of the earth's upper mantle , **J. Petrol.**, 28, 1169 - 1191.

O'Nions, R.K., Hamilton, P.J. & Evensen, N.M., 1977, Variations in in $^{143}Nd/^{144}Nd$ and $^{87}Sr/^{86}Sr$ ratios in oceanic basalts, **Earth Planet. Sci. Lett.**, 34, 13 - 22.

Osborn, E.F., 1959, Role of oxygen pressure in the crystallisation and differentiation of basaltic magma, **Amer. J. Sci.**, 257, 609 - 647.

Osborn, E.F. & Watson, E.B., 1977, Studies of phase relations in subalkaline volcanic rock suite, **Carnegie Inst. Washington, Ann. Rept. Dir. Geophys. Lab**, 1976-77, 472 - 478.

Padmosukismo, S. & Yahya, I., 1974, The basement conviguration of the North West Java Basinal Area, Proceedings, Indon. Petrol. Assoc., Jakarta.

Papike, J.J., 1987, Chemistry of the rock-forming silicates : ortho, ring, and single - chain structures, **Rev. Geophys.**, 25, 1483 -1526.

Papike, J.J., 1988, Chemistry of the rock-forming silicates : multiple - chain, sheet, and framework structures, **Rev. Geophys.**, 26, 407 - 444.

Papike, J.J., Cameron, K.L. & Baldwin, K., 1974, Amphiboles and pyroxenes : Characterization of other than quadrilateral components and estimates of ferric iron from microprobe data, abstract, **Geol. Soc. Amer., Abstract with programs**, 6, 1053-1054.

Pardyanto, L., Reksowirogo, L.D., Mitrohartono, F.X.S. & Hardjowasito, S.H., 1978, **Volcanic hazard map, Merapi volcano Central Java, Central Java, scale 1 : 100,000**, Geol. Surv. Indon., Bandung.

Partosentiko, S., 1972, Laporan peninjauan G. Papandayan dan G. Galunggung bulan April 1972, Geol. Surv. Indon., Bandung, unpubl.

Parsons, I., (ed.), 1986, **Origins of Igneous Layering**, D. Reidel Publ. Co., Boston, 666 p.

Pearce, J.A., 1982, Trace element characteristics of lavas from destructive plate boundaries, in : Thorpe, R.S. (Ed.), **Andesites**, Chichester, J. Wiley & Sons, pp 525 - 548.

Pearce, J.A. & Cann, J.R., 1973, Tectonic setting of basic volcanic rocks determined using trace element analyses, **Earth Planet. Sci. Lett.**, 19, 290 - 300.

Pearce, J.A. & Norry, M.J., 1979, Petrogenetic implications of Ti, Zr, Y and Nb variations in volcanic rocks, **Contr. Min. Petr.**, 69, 33 47.

Peccerillo, A. & Taylor, S.R., 1976, Geochemistry of Eocene calc-alkaline volcanic rocks from the Kastamonu area, northern Turkey, **Contr. Min. Petr.**, 58, 63 - 81.

Perfit, M., 1979, The petrochemistry and strontium isotopic composition of mafic basalts from the Aleutian Islands, Abstract with program, **Geol. Soc. Amer.**, 10, 39 - 40.

Perfit, M.R. Gust, D.A., Bence, A.E., Arculus, R.J. & Taylor, S.R., 1980a, Chemical characteristics of island-arc basalts : Implications for mantle sources, **Chem. Geol.**, 30, 227 - 256.

Perfit, M.R., Brueckner, H., Lawrence, J.R. & Kay, R.W., 1980b, Trace element and isotopic variations in a zoned pluton and associated volcanic rocks, Unalaska Island, Alaska : a model for fractionation in the Aleutian calc-alkaline suite, **Contr. Min. Petr.**, 73, 69 - 87.

Pe-Piper, G., 1988, Calcic amphiboles of mafic rocks of the Jeffer Brook plutonic complex, Nova Scotia, Canada, **Am. Miner.**, 73, 993 - 1006.

Pe-Piper, G. & Jansa, L.F., 1988, The origin of complex mantling relationships in clinopyroxene from the New England seamounts, **Canad. Miner.**, 26, 109 - 116.

Petroeschevsky, W.A., 1925, Toestand van de Galoenggoeng on de 1^{e} en 2^{e} September 1925, 23 Ocktober 1925, Geol. Surv. Indon., Bandung, unpubl.

Philpotts, J.A., Martin, W. & Schuetzler, C.C., 1971, Geochemical aspects of some Japanese lavas, **Earth Planet. Sci. Lett.**, 12, 89 - 96.

Plank, T. & Langmuir, C.H., 1988, An evaluation of the global variations in the major element chemistry of arc basalts, **Earth Planet. Sci. Lett.**, 90, 349 - 370.

Presnall, D.C., 1966, The join forsterite - diopside - iron oxide and its bearing on the crystallization of basaltic and ultramafic magmas, **Amer. J. Sci.**, 264, 753 - 809.

Presnall, D.C. Dixon, J.R., O'Donell, T.H. & Dixon, S.A., 1979, Generation of mid-ocean ridge tholeiites, **J. Petrol.**, 20, 3 - 35.
Presnall, D.C. & Hoover, J.D., 1984, Composition and depth of origin of primary mid-ocean ridge basalts, **Contr. Min. Petr.**, 87, 170 -178.
Presnall, D.C. & Hoover, J.D., 1986, Composition and depth of origin of primary mid-ocean ridge basalts - reply to D. Elthon, **Contr. Min. Petr.**, 94, 257 - 261.
Prevot, M. & Mergoil, J., 1973, Crystallization trend of titanomagnetite in an alkali basalts from Sain-Clement (Massif Central, France), **Min. Mag.**, 39, 474 - 481.
Priyantono, T. Effendi, I. & Budiono, K., 1980, The earthquakes of 2 November, 1979 and 16 April, 1980 in the Garut and Tasikmalaya areas, West Java, **Bull. Geol. Res. Dev. centre**, 3, 13 - 18.
Purbawinata, M.A., 1988, Some geochemical aspects from Guntur - Gandapura volcanic centre, West Java, Indonesia, abstract, **Geol. Soc. New Zealand Inc., Annual Conf., 28 Nov. - 1 Dec. 1988, Hamilton, N.Z.**, p. 124.
Ragland, P.C. & Butler, J.R., 1972, Crystallization of the West Farrington pluton, North Carolina, USA, **J. Petrol.**, 13, 381 - 404.
Rama Murthy, V. & Griffin, W.L., 1970, K/Rb fractionation by plagioclase feldspars, **Chem. Geol.**, 6, 265 - 271.
Ramsay, W.R.H., Crawford, A.J. & Foden, J.D., 1984, Field setting, mineralogy, chemistry, and genesis of arc picrites, New Georgia, Solomon Islands, **Contr. Min. Petr.**, 88, 386 - 402.
Rasjid, S.A., 1982, Pengamatan gempabumi di G. Galunggung, 10th **Ann. Conv. Indon. Assoc. Geol.**, 278 - 288, manuscript.
Reagan, M.K., Meijer, A. & Hickey, R., 1981, Geology and Geochemistry of early arc volcanic rocks from Guam, **EOS, Trans. Amer. Geophys. Union**, 62, 45, p. 1091.
Reid, M. & Nye, C., 1981, Geochemistry of least fractionated basalts from Okmok volcano, Central Aleutians, **EOS, Trans. Amer. Geophys. Union**, 62, 45, p. 1092.
Ringwood, A.E., 1974, The petrological evolution of island arc systems, **J. Geol. Soc. Lond.**, 130, 183 - 204.
Ringwood, A.E., 1975, **Composition and Petrology of the Earth's Mantle**, McGraw Hill, New York, 618 p.
Robinson, P., 1980, The composition space of terrestrial pyroxenes internal and external limits, in C.T. Prewitt (ed.), **Reviews in Mineralogy**, v. 7, pyroxenes.
Rock, N.M.S., Syah, H.H., Davis, A.E., Hutchison, D., Styles, M.T. & Lena, R., 1982, Permian to Recent volcanism in Northern Sumatra, Indonesia : a preliminary study of its distribution, chemistry, and peculiarities, **Bull. Volc.**, 45, 127 - 152.
Rochanan, S., Sobana, R., Effendi, S. & Martono, A., 1984, Topographic map of Galunggung crater, **Volc. Surv. Indon.**, unpubl. report.
Roeder, P.L., 1974, Activity of iron and olivine solubility in basaltic liquids, **Earth Planet. Sci. Lett.**, 23, 397 - 410.
Roeder, P.L., Campbell, I.H. & Jamieson, H.E., 1979, A re-evaluation of the olivine - spinel geothermometer, **Contr. Min. Petr.**, 68, 325 - 334.
Roeder, P.L. & Emslie, R.F., 1970, Olivine-liquid equilibrium, **Contr. Min. Petr.**, 29, 275 - 289.
Roobol, M.J. & Smith, A.L., 1976, Mount Pelée, Martinique : a pattern of alternating eruptive styles, **Geology**, 4, 521 - 524.

Rose, W.I.Jr., Anderson, A.T. Jr., Woodruff, L.G. & Bonis, S.B., 1978, The October 1974 basaltic tephra from Fuego volcano : Description and history of the magma body, **J. Volc. Geoth. Res.**, 4, 3 - 53.

Rubin, K.H., Wheller, G.E., Tanzer, M.O., Macdougall, J.D., Varne, R. & Finkel, R., ^{238}U Decay series systematics of the young lavas from Batur volcano, Sunda Arc, in prep.

Sabine, P.A., Harrison, R.K. & Lawson, R.I., 1985, Classification of volcanic rocks of the British Isles on the total alkali oxide - silica diagram, and the significance of alteration, **British Geol. Surv. Rept.**, 17, 1 - 9.

Samsu, B., 1975, Jatibarang volcanic, the prospections volcanic horizon, Indon. Petrol. Assoc., unpubl.

Sano, S., Untung, M. & Fujii, K., 1978, Epilogue : Some gravity features of Island Arcs of Jawa and Japan and their tectonic implications, in M. Untung & Y. Sato (eds.) : **Gravity and Geological Studies in Jawa, Indonesia**, Geol. Surv. Indon., spec. publ. n. 6, pp. 183 - 207.

Sato, H., 1977, Nickel content of basaltic magmas : Identification of primary magmas and a measure of the degree of olivine fractionation, **Lithos**, 10, 113 - 120.

Scarfe, C.M. & Fujii, T., 1987, Petrology of crystal clots in the pumice of Mount St. Helens' March 19, 1982 eruption; significant role of Fe-Ti oxide crystallization, **J. Vol. Geoth. Res.**, 34, 1 - 14.

Schilling, J.G. & Winchester, J.W., 1967, Rare-earth fractionation and magmatic process, in S.K. Runcorn (ed.), **Mantles of the Earth and Terrestrial Planets**, London & New York, Interscience Publisher, p. 267 - 283.

Schroeder, B., Thompson, G., Sulanowska, M. & Ludden, J.N., 1980, Analysis of geologic materials using an automated X-ray fluorescence system, **X-Ray Spectometry**, 9, 198 - 205.

Schuster, R.L. & Crandell, D.R., 1984, Catastrophic debris avalanches from volcanoes, **Proceed. of the IV Internat. Sympos. on landslides, Toronto**, 1, 567 - 572.

Schweitzer, E.L., Papike, J.J. & Bence, A.D., 1979, Statistical analysis of clinopyroxenes from deep-sea basalts, **Am. Miner.**, 64, 501 - 513.

Sclater, J.G. & Fisher, R.L., 1974, Evolution of the East Central Indian Ocean, with emphasis on the tectonic setting of the Ninetyeast Ridge, **Geol. Soc. Amer. Bull.**, 85, 683 - 702.

Scott, D. & Stevenson, D.J., 1989, A self-consistent model of melting, magma migration and buoyancy-driven circulation beneath mid-ocean ridges, abstract, **EOS, Trans. Amer. Geophys. Union**, 70, p.48.

Sekiya, S. & Kichuchi, Y., 1889, The eruption of Bandai-san, **Imper. Univ. of Japan, College of Sci. Jour.**, 3, 91 - 172.

Self, S., Rampino, M.R. & Newton, M.S. & Wolff, J.A., 1984, Volcanological study of the great Tambora eruption of 1815, **Geology**, 12, 659 - 663.

Sewell, R.J., Weaver, S.D., Falloon, T.J. & Gibson, I.C., 1986, Petrogenesis of alkali olivine - basalt magmas, Banks. Peninsula, abstract, New Zealand, Internat. Volc. Conggr., Auckl.- Hamilt. - Rotorua, N.Z., 1 - 9 Feb., p. 203.

Sharaskin, A.Y., Bogdanov, N.A. & Zakariadze, G.S., 1981, Geochemistry and timing of the marginal basin and arc-magmatism of the Philippine Sea, **Phil. Trans. Roy. Soc. Lond.**, A 300, 287 - 297.

Shaw, D.M., 1970, Trace element fractionation during anatexis, **Gechim. Cosmochim. Acta**, 34, 237 - 243.
Shelley, D., 1981, **Manual of optical mineralogy**, Elsevier, New York, 239 p.
Shelley, D., 1988, Radial dikes of Lyttelton volcano - their structure, form, and petrography, **N.Z. J. Geol. Geophys.**, 31, 65 - 75.
Shervais, J.W., 1982, Ti-V plots and the petrogenesis of modern and ophiolitic lavas, **Earth Planet. Sci. Lett.**, 59, 101 - 118.
Shibata, T., Thompson, G. & Frey, F.A., 1979, Tholeiitic and alkali basalts from the Mid-Atalntic Ridge at 43°N, **Contr. Min. Petr.**, 70, 127 - 141.
Shimazaki, H., Bunno, M. & Ozawa, T., 1984, Sadanagaite and magnesio - sadanagaite, new silica - poor members of cal cic amphibole from Japan, **Am. Miner.**, 69, 465 - 471.
Sibbett, B.S., 1988, Size, depth and related structures of intrusions under stratovolcanoes and associated geothermal systems, **Earth Sci. Rev.**, 25, 291 - 309.
Siebert, L., 1984, Large volcanic debris avalanches : Characteristics teristics of source areas, deposits, and associated eruptions, **J. Volc. Geoth. Res.**, 22, 163 - 197.
Sigurdsson, H., 1982, In the volcano, **Nat. Hist.**, 91 (3), 61 - 67.
Sigurdsson, H. & Schilling, J.G., 1976, Spinels in Mid-Atlantic Ridge basalts : Chemistry and occurrence, **Earth Planet. Sci. Lett.**, 29, 7 - 20.
Simkin, T. & Fiske, R.S., 1983, **Krakatau 1883 : The volcanic eruption and its effects**, Smithsonian Institution Press, Washington, D.C., 464 p.
Simkin, T. & Siebert, L., 1984, Explosive eruptions in space and time : Duration, intervals, and a comparison of the world's active volcanic belts, in : **Explosive Volcanism : Inception, Evaluation, and Hazards**, Geophys. Study Comm. Nat. Res. Counc., National Academy Press, Washington, D.C., pp. 110 - 121.
Simkin, T., Siebert, L., McClelland, L., Bridge, D., Newhall, C.G. & Latter, J.H., 1981, **Volcanoes of the world : A Regional Directory Gazetteer, and Chronology of Volcanism during the last 10,000 years**, Hutchison & Ross, Strondsburg, Pennsylvania, 240 p.
Simkin, T. & Smith, J.V., 1970, Minor-element distribution in olivine, **J. Geol.**, 78, 304 - 325.
Smith, I.E. & Mitchell, P.A., 1989, High magnesium lavas in the Late Cenozoic volcanic arc associations of Papua New Guinea, **Geology**, in prep.
Smith, R.L., 1960a, Ash flows, **Geol. Soc. Amer. Bull.**, 71, 795 - 842.
Smith, R.L., 1960b, Zones and zonal variations in welded ash-flows, **U.S. Geol. Surv. Prof. Pap.**, 354-F, 149 - 159.
Siswowidjojo, S., 1987, Eruptions of Galunggung volcano in West Java, Indonesia, in 1982/1983 and its volcanological implications, PhD thesis, Univ. Tokai, Japan.
Siswowidjojo, S., 1988, Seismicity and other phenomena associated with the eruption of Galunggung volcano in West Java, Indonesia, **Proceed. at Kagoshima Internat. Confer. on Volcanoes**, July 23 -28.
Soekamto, R., 1975, **Geological map of the Jampang and Balekambang Quadrangle, Java**, 9/XIV-A & B, scale 1 : 100,000, Geol. Surv. Indon., Bandung.
Somantri, O., 1955, Gunung Galunggung mengeluarkan asap, Geol. Surv. Indon., Bandung, unpubl.

Soya, T. & Katsui, Y., 1981, The Zenkoji debris avalanche of Usu volcano, Hokkaido, Japan, abstract, **IAVCEI Sympos. (Arc Volcanism)**, p. 347.

Sparks, R.S.J., 1976, Grain size variations in ignimbrite and implications for the transport of pyroclastic flows, **Sedimentology**, 23, 147 - 188.

Sparks, R.S.J., 1989, In situ differentiation in magma, **Nature**, 340, p.187.

Sparks, R.S.J., Huppert, H.E. & Turner, J.S., 1984, The fluid dynamics of evolving magma chambers, **Phil. Trans. Roy. Soc. London**, A310, 511 - 534.

Sparks, R.S.J., Self, S. & Walker, G.P.L., 1973, Products of ignimbrite eruptions, **Geology**, 1, 115 - 118.

Sparks, R.S.J. & Walker, G.P.L., 1973, The ground surge deposit, a third kind of pyroclastic rock, **Nature**, 241, 62 - 64.

Sparks, R.S.J. & Wilson, L., 1976, A model for the formation of ignimbrite by gravitational column collapse, **J. Geol. Soc. London**, 132, 441 - 451.

Stanton, R.L. & Bell, J.D., 1969, Volcanic and associated rocks of the New Georgia Group, British Solomon Island Protectorate, **Overseas Geol. Min. Res.**, 10, 113 - 145.

Stauffer, P.H., 1987, Pleistocene volcanic ash on the Malay Penninsula : Evidence for magnitude and age of a catastrophic eruption of Toba, Sumatra, abstr., **Hawaii Sympos. on How Volc. Work, Hilo, Hawaii**, January 19 - 25, p. 241.

Stehn, Ch.E., 1923, Maandrapport over de maand Juni 1923, Geol. Surv. Indon., Bandung, unpubl.

Stehn, Ch.E., 1935, De Galoenggoeng, Geol. Surv. Indon., Bandung, unpubl.

Stern, C.R., 1974, Melting products of olivine tholeiite basalt in subduction zone, **Geology**, 4, 227 - 230.

Stern, R.J. & Ito, E., 1983, Trace-element and isotopic constraints on the source of magmas in the active volcano and Mariana Island Arcs, Western Pacific, **J. Volc. Geoth. Res.**, 18, 461 - 482.

Stevens, N.C., Oba, Y. & Katsui, Y., 1978, Some trace-element data on Pliocene basaltic rocks from two districts in Hok kaido, **J. Fac. Sci., Univ. Hokk.**, ser. IV, 18, 3, 485 - 489.

Stewart, D.C., 1975, Crystal clots in calc-alkaline andesites as break-down products of high-Al amphiboles, **Contr. Min. Petr.**, 53, 195 - 204.

Stolper, E., 1980, A phase diagram for mid-ocean ridge basalts : Preliminary results and implications for petrogenesis, **Contr. Min. Petr.**, 74, 13 - 27.

Stormer, J.C., 1973, Calcium zoning in olivine and its relationship to silica activity and pressure, **Geochim. Cosmochim. Acta**, 37, 1815 - 1821.

Stormer, J.C. Jr. & Nicholls, J., 1978, XLFRAC : A program for the the interactive testing of magmatic differentiation models, **Computers and Geosci.**, 4, 143 - 159.

Streickeisen, A., 1978, Classification and nomenclature of volcanic rocks, lamprophyres, carbonatites and melilitic rocks, **Neues Jahrbuch fur mineralogie**, 134, 1 - 14.

Streickeisen, A., 1980, Classification and nomenclature of volcanic rocks, lamprophyres, carbonatites and melilitic rocks, **Geol. Rundschau**, 69, 194 - 207.

Subbarao, K.V. & Hedge, C.E., 1973, K, Rb, Sr and $^{87}Sr/^{86}Sr$ in rocks from the mid-Indian Oceanic ridge, **Earth Planet. Sci. Lett.**, 18, 223 - 228.

Sudradjat, A., 1982, Catatan mengenai pengaruh abu gunungapi terhadap kesehatan, Volc. Surv. Indon., Bandung, unpubl.

Sudradjat, A., 1984, Penyelidikan Gunungapi di Indonesia, Volc. Surv. Indon., Bandung, n.825, Unpubl.

Sudradjat, A. & Martono, A., 1983, Preliminary topographic survey of the 1982-83 cinder cone of Mt. Galunggung, Volc. Surv. Indon., Bandung, unpubl.

Sudradjat, A. & Tilling, R., 1984, Volcanic hazards in Indonesia : The 1982-83 eruption of Galunggung, Episodes, 7, 13 - 19.

Sun, S.S. & Nesbitt, R.W., 1978, Petrogenesis of Archean ultra basic volcanics : evidence from REE, **Contr. Min. Petr.**, 65, 301-325.

Sunardjo, R.H., Permadi, A., Marlina, I., Suryawan, J. & Ekadjadi, E., 1978, **Harijadi Tasikmalaya**, Pemerintah Daerah Kab. Tasikmalaya, 125 p.

Suryo, I., 1959a, Laporan pemeriksaan Gunung Galunggung, 16 April 1959, Geol. Surv. Indon., Bandung, unpubl.

Suryo, I., 1959b, Gunung Galunggung, **Bull. Volc. Surv. Indon.**, 102, 21 - 23.

Suryo, I. & Clarke, M.C.G., 1985, The occurrence and mitigation of volcanic hazards in Indonesia as exemplified at the Mount Merapi, Mount Kelut and Mount Galunggung volcanoes, **Q.J. Eng. Geol. London**, 18, 79 - 98.

Suwijanto, 1978, Hubungan antara kegempaan dengan kelurusan struktur pada citra landsat di daerah Jawa Barat, suatu tinjauan, **Riset**, LIPI, 1, 1 - 8.

Syahbuddin, A., Sumantri, Y.R., Kartanegara, L. & Asikin, S, 1986, Pola perkembangan tektonik Cekungan Rangkasbitung, Jawa Barat, selama Tersier sebagai akibat dari letaknya yang berada di antara Cekungan Bogor, Cekungan Jawa Baratdaya dan Cekungan Sumatra Selatan, XVth Annual Convent. Indon. Assoc. Geol., 9 - 10 Dec., Yogyakarta, manuscript.

Syarifuddin, M.Z., Purbawinata, M.A. & Suhanda, T., 1983, Petrografi dan analysis kimia bom gunungapi skoria dan lapili letusan G. Galunggung April 1982 - Januari 1983, Tasikmalaya, Jawa Barat, Volc. Surv. Indon., Bandung, unpubl.

Tada, F. & Tsuya, H., 1927, The eruption of the Tokachidake volcano, Hokkaido, on May 24, 1926, **Earthq. Res. Inst., Tokyo Univ.**, 2, 49 - 84.

Takahashi, E. & Kushiro, I., 1983, Melting of a dry peridotite at high pressures and basalt magma genesis, **Am. Miner.**, 68, 859 - 879.

Tatsumi, Y., Sakuyama, M., Fukuyama, H. & Kushiro, I., 1983, Generation of arc basalt magmas and thermal structure of the mantle wedge in subduction zones, **J. Geophys. Res.**, 88, 5815 - 5825.

Taverne, N.J.M., 1922, Maandrapport over de maand Februari 1922, De Galoenggoeng, Geol. Surv. Indon., Bandung, unpubl.

Taverne, N.J.M., 1924, De Galoengggoeng en Telaga Bodas, **Vulkanol. Meded.**, 6, 27 - 63.

Taylor, G.A., 1958, The 1951 eruption of Mount Lamington, Papua, **Austral. Bur. Min. Res., Geol. & Geophys. Bull.**, 38, 117 p.

Taylor, G.A., 1963, Seismic and tilt phenomena preceding a Peléean type eruption from a basaltic volcano, **Bull. Volc.**, 26, 5 - 11.

Taylor, S.R., Kaye, M., White, A.J.R., Duncan, A.R. & Ewart, A., 1969, Genetic significance of Co, Cr, Ni, Sc and V content of andesites, **Geochim. Cosmochim. Acta**, 33, 275 - 286.

Thayib, E.S., Said, E.L., Siswojo, & Projomarsono, S., 1977, The status of the Melange Complex in Ciletuh Area, South - West Java : **Proceed. Indon. Petrol. Assoc.**, Jakarta.

Thompson, G., Bryan, W.B., Frey, F.A. & Sung, C.M., 1972, Petrology and geochemistry of basalts and related rocks from sites 214, 215, 216, DSDP Leg 22, Indian Ocean, in : **Initial Reports of the Deep Sea Drilling Project XXII**, U.S. Govt. Print Off., Washington, D.C., pp. 459 - 473.

Thorton, C.P. & Tuttle, O.F., 1960, Chemistry of igneous rocks I Differentiation Index, **Amer. J. Sci.**, 258, 664 - 684.

Tilling, R.I., (Ed.), 1989, **Volcanic Hazards**, Amer. Geophys. Union, Washington, D.C., 123 p.

Tjia, H.D., Hadian, R., Sumailani, A.R., and Martono, A., 1980, The nature of "Umsini Volcano", Irian Jaya, Indonesia, **Bull. Volc.**, 43-3, 595-600.

Tootell, B., 1985, **'All Four Engines Have Failed. The true and triumphant story of flight BA 009 and the 'Jakarta incident'**, Hutchinson Group (NZ) Ltd, Auckland, 178 p.

Trechmann, C.T., 1938, Relics of the Mt. Pelée eruption of May, 1902, **Nature**, 141, 435 - 437.

Tulus, Suryadi, B., Subagiyo & Aidil, 1979, Laporan pemeriksaan kawah G. Galunggung, G. Guntur, G. Papandayan dan G. Gede di Jawa Barat, 6 - 8 Nopember 1979, Volc. Surv. Indon., Bandung, unpubl.

Ui, T., 1983, Volcanic dry avalanche deposits - identification and comparison with non volcanic debris stream deposits, in : S. Aramaki & I. Kushiro (Eds.), Arc Volcanism, **J. Volc. Geoth. Res.**,18, 135 - 150.

Ui, T. & Glicken, H., 1986, Internal structural variations in a debris -avalanche deposit from ancestral Mount Shasta, California, USA, **Bull. Volc.**, 48, 189 - 194.

Ui, T. Kawachi, S. & Neall, V.E., 1986a, Fragmentation of debris avalanche material during flowage - evidence from the Pungarehu Formation, Mount Egmont, New Zealand, **J. Volc. Geoth. Res.**, 27, 255 - 264.

Ui, T., Yamamoto, H., Suzuki-Kamata, K., 1986b, Characterization of debris avalanche deposits in Japan, **J. Volc. Geoth. Res.**, 29, 231 - 243.

Ujike, O., 1988, Probable mineralogic control on the mantle metasomatic fluid composition beneath the Northeast Japan arc, **Geochim. Cosmochim. Acta**, 52, 2037 - 2046.

Untung, M., 1974, **Bouguer anomaly map of Java and Madura, scale 1 : 2,000,000**, Geol. Surv. Indon., Bandung.

Van Bemmelen, R.W., 1949, **Geology of Indonesia**, vol. I A, Martinus Nijhoff, the hague, 732 p.

Van den Elysinga, R.R., 1822, Professor Reinwardt op de berg Galoenggoeng, Indie, ter bevordering der kennis van Nederlands Oostersche bezetingen, **Bukittinggi**, 2, p. 422.

Van der Capellen, R., 1823, Bataav Cour 22 Februari.

Van der Lingen, G.J. & Pettinga, J.R., 1980, The Makara Basin : a Miocene slope - basin along the New Zealand sector of the Australian - Pacific obliquely convergent plate boundary, **Spec. Publ. int. Ass. Sediment.**, 4, 191 - 215.

Van Es, L.J.C., 1924, De uitbarsting van den Galoenggoeng op den 17 den Juli 1918 envolgende dagen, benevens een herziene beschrijving van de uitbarstingen van 1822 en 1894, **Vulkanol. Meded.**, 6, 1 - 24.

Van Es, L.J.C. & Taverne, N.J.M., 1924, De Galoenggoeng en Telaga Bodas, **Vulkanol. Meded.**, 6, 33 - 41.

Veevers, J.J. & Heirtzler, J.R (Eds.), 1974, **Initial reports of the Deep Sea Drilling Project, XXVII**, U.S. Govt. Print. Off., Washington, D.C., 1060 p.

Vening Meinesz, F.A., 1954, Indonesian Archipelago : A geophysical study, **Bull. Geol. Soc. Amer.**, 65 : 143 - 164.

Verbeek, R.D.M., 1884, The Krakatau eruption, **Nature**, 30, 10 - 15.

Verbeek, R.D.M., 1885, **Krakatau**, Govt. Press, Batavia, 495 p.

Verbeek, R.D.M. & Fennema, R., 1885, De Telaga Bodas - Galoenggoeng vulkaan, **Geol. beschrijving van Java en Madoera**, 687 - 700.

Verbeek, R.D.M. & Fennema, R., 1896, **Geologische beschrijving van Java en Madoera**, Amsterdam.

Veth, P.J., 1903, Galoenggoeng, **Java**, 3, 368 - 369.

Visser, S.W., 1919, Vulkanische verschijnselen waargenomen gedurande het jaar 1918, **Natuurk. Tijdschr. Nederl. Ind.**, 79, 129 - 130.

Visser, S.W., 1921, Vulkanische verschijnselen in het jaar 1920, **Natuurk. Tijdschr. Nederl. Ind.**, 81, p. 90.

Viljoen, M.J. & Viljoen, R.P., 1969, The geology and geochemistry of the lower ultramafic unit of the Onverwacht Group and a proposed new class of igneous rock, **Upper Mantle Project Spec. Publs. Geol. Soc. S. Africa**, 2, 221 - 244.

Voight, B., Glicken, H., Janda, R.J. & Douglass, P.M., 1981, Catastrophic rockslide avalanche of May 18. In : P.W. Lipman and D.R. Mullineaux (Eds.), **The 1980 Eruptions of Mount St. Helens, Washington**, U.S. Geol. Surv.Pap., 98, 347 - 377.

Volcanological Survey of Indonesia (VSI), 1983, Annual report, Bandung, unpubl.

Volcanological Survey of Indonesia (VSI), 1985, Preliminary volcanic hazard map of the 1982-83 Galunggung eruption, Bandung, unpubl.

Von der Borch, C.C. & Sclater, J.G. (Eds.), 1972, **Initial reports of the Deep Sea Drilling Project, XXII**, D.C., U.S. Govt. Print. Off., Washington, D.C., 890 p.

Wager,L.R. & Brown, G.M., 1968, **Layered Igneous Rocks**, Oliver & Boyd, Edinburgh & London, 588 p.

Walker, D., Shibata, T. & DeLong, S.E., 1979, Abyssal Tholeiites from the Oceanographer Fracture Zone, **Contr. Min. Petr.**, 70, 111 -125.

Wass, S.Y., 1988, Multiple origins of clinopyroxenes in alkali basaltic rocks, **Lithos**, 12, 115 - 132.

Watanabe, T., Grapes, R. & Palmer, K., 1981, Quantitative analyses of rock forming minerals by JXA - 733 Electron Probe X-ray microanalyses, **JEOL News**, 19E-1, 15 - 19.

Watson, E.B. & Ryerson, F.J., 1986, Partitioning of zirconium between clinopyroxene and magmatic liquids of intermediate composition, **Geochim. Cosmochim. Acta**, 50, 2523 - 2526.

Weaver, S.D., Saunders, A.D., Pankhurst, R.J. & Tarney, J., 1979, A geochemical study of magmatism associated with the initial stages of back-arc spreading, **Contr. Min. Petr.**, 68, 151 - 169.

Weaver, S.D., Sewell, R.J. & Dorsey, C., 1985, Extinct volcannoes : A guide to the geology of Banks Peninsula, **Geol. Soc. of New Zealand**, Guide book no.7.

Wedepohl, K.H., 1975, The contribution of chemical data to assumptions about the origin of magmas from the mantle, **Fortschritte der Mineralogie**, 52, 141 - 172.

Wheller, G.E., 1986, Petrogenetic studies of basalt - andesite - dacite volcanism at Batur volcano, Bali, and of the causes of K - variation in Sunda - Banda arc basalts, PhD thesis, Univ. of Tasmania.

Wheller, G.E. & Varne, R. 1986a, Genesis of dacitic magmatism at Batur volcano, Bali, Indonesia : implications for the origins of stratovolcano calderas, **J. Volc. Geoth. Res.**, 28, 363 - 378.

Wheller, G.E. & Varne, R., 1986b, Petrogenesis of basalt - andesite - dacite volcanism at the active Batur volcano, Bali, Eastern Sunda Arc, and the origins of stratovolcano calderas, abstract, in : **Internat. Volcanol. Conggress, Auckl. - Hamil. - Rotorua, New Zealand**, 1 - 9 Feb., 359.

Wheller, G.E., Varne, R., Foden, J.D. & Abbott, M.J., 1987, Geochemistry of Quaternary volcanism in the Sunda - Banda arc, Indonesia, and three - component genesis of island - arc basaltic magmas, **J. Volc. Geoth. Res.**, 32, 137 - 160. White, R.W., 1966, Ultramafic inclusions in basaltic rocks from Hawaii, **Contr. Min. Petr.**, 12, 245 - 314.

Whitford, D.J., 1975a, Geochemistry and petrology of volcanic rocks from the Sunda arc, Indonesia, and their petrogenetic implications, Ph.D. thesis, Australian National Univ., Canberra, 449 p.

Whitford, D.J., 1975b, Strontium isotopic studies of the volcanic rocks of the Sunda arc, Indonesia, and their petrogenetic implications, **Geochim. Cosmochim. Acta**, 39, 1287 - 1302.

Whitford, D.J. & Jezek, P.A., 1982, Isotopic constraints on the role of subducted sialic material in Indonesian island-arc magmatism, **Geol. Soc. Amer. Bull.**, 93, 504 - 513.

Whitford, D.J. & Nicholls, I.A., 1973, Report on Geochemical investigations of the volcanic rocks of Java, Dept. Geophys. Geochem., Australian National University, Canberra.

Whitford, D.J. & Nicholls, I.A., 1976, Potassium variation in lavas across the Sunda Arc in Java and Bali, In : R.W. Johnson (Ed.), **Volcanism in Australiasia**, Elsevier, Amsterdam, 63 - 75.

Whitford, D.J., Nicholls, D,J. & Taylor, S.R., 1979, Spatial variations in the geochemistry of Quaternary lavas across the Sunda Arc in Java and Bali, **Contr. Min. Petr.**, 70, 341 - 356.

Whitford, D.J., White, W.M. & Jezek, P.A., 1981, Neodymium isotopic composition of Quaternary island arc lavas from Indonesia, **Geochim. Cosmochim. Acta**, 45, 989-995.

Wilkinson, J.F.G., 1986, Classification and average chemical compositions of common basalts and andesites, **J. Petrol.**, 27, 31 - 62.

Williams, D.A.C., 1972, Archean ultramafic, mafic, and associated ated rocks, Mt. Monger, Western Australia, **J. Geol. Soc. Aust.**, 19, 163 - 188.

Williams, H., Turner, F.J. & Gilbert, C.M., 1982, **Petrography : An Introduction to the Study of Rocks in Thin Sections**, W.H. Freeman and Company, San Francisco, 626 p.

Williams, R.W., Gill, J.B. & Bruland, K.W., 1983, Th and U decay series nuclides in historic arc lavas from Java, Japan and Mt. St. Helens, abstract, **EOS, Trans Amer. Geophys. Union**, 64, p. 906.

Wilson, C.J.N., 1984, The role of fluidisation in the emplacement of pyroclastic flows, 2 : experimental results and their interpretation, **J. Volc. Geoth. Res.**, 20, 55 - 84 .

Wilson, J.T., 1972, The physical study of earth and the scientific revolution it has caused, **Internat. Union Pure Appl. Phys.**, 50th anniv. meeting, Washington, D.C.

Wilson, L., 1980, Relationship between pressure, volatile content and ejecta velocity in three types of volcanic explosion, **J. Volc. Geoth. Res.**, 8, 297 - 313.

Wilson, L., Sparks, R.S.J., Huang, T.C. & Watkins, N.D., 1978, The control of eruption column heights by eruption energetics and dynamics, **J. Geophys. Res.**, 83, 1829-1836.

Wirakusumah, A.D., 1982, Perbukitan sepuluh ribu di Tasikmalaya, **Berita Geologi**, 23, 211 - 213.

Wirakusumah, A.D., Juwarna, H. & Bronto, S., 1981, Laporan kemajuan pemetaan geologi daerah G. Galunggung, Jawa Barat, **Volc. Surv. Indon.**, unpubl. report.

Witt, G. & Seck, H.A., 1989, Origin of amphibole in recrystallised and porphyroclastic mantle xenoliths from Rhenish Massif : implications for the nature of mantle metasomatism, **Earth Planet. Sci. Lett.**, 91, 327 - 340.

Wohletz, D.H. & Sheridan, M.F., 1979, A model of pyroclastic surge, **Geol. Soc. Am. Spec. Pap.**, 180, 177 - 194.

Wolff, J.A., Newton, M.S. & Self, S., 1986, Petrogenesis of the Tambora 1815 magma, abstract, **Internat. Volc. Conggr., Aukl. - Ham. -Rot., N.Z.**, 1 - 9 Feb., p.224.

Wones, D.R. & Gilbert, M.C., 1982, Amphiboles in the igneous environment, in : D.R. Veblen & P.H. Ribbe (eds.), **Amphiboles : Petrology and Experimental phase relations**, Reviews in Mineralogy, 9 B, 355 - 390.

Wood, B.J. & Kleppa, O.J., 1981, Thermochemistry of forsterite - fayalite olivine solutions, **Geochim. Cosmochim. Acta**, 45, 529 - 534.

Wood, D.A., Tarney, J., Varet, J., Saunders, A.D., Bougault, H., Joron, J.L., Treuil, M. & Cann, J.R., 1979, Geochemistry of basalts drilled in the North Atalntic by Ipod leg 49 : implications for mantle heterogeneity, **Earth Planet. Sci. Lett.**, 42, 77 - 97.

Woodhead, J.D., 1988, The origin of geochemical variations in Mariana lavas : a general model for petrogenesis in intra-oceanic island arcs ?, **J. Petrol.**, 29, 805 - 830.

Wright, T.L. & Doherty, P.C., 1970, A linear programming and least - squares computer method for solving petrologic mixing problems, **Geol. Soc. Amer. Bull.**, 81, 1995 - 2008.

Wright, J.V., Smith, A.L. & Self, S., 1980, A working terminology of pyroclastic deposits, **J. Volc. Geoth. Res.**, 8, 315 - 336.

Wright, J.V. & Walker, G.P.L., 1981, Eruption, transport and deposition of ignimbrite : a case study from Mexico, **J. Volc. Geoth. Res.**, 9, 111 - 131.

Wyllie, P.J., 1971, Role of water in magma generation and initiation of diapiric uprise in the mantle, **J. Geophys. Res.**, 76, 77 - 97.

Wyllie, P.J., 1988, Magma genesis, plate tectonics and chemical differentiation of the earth, **Reviews of Geophysics**, 26, 370 - 404.

Yamamoto, M., 1984, Origin of calc-alkaline andesite from Oshima-Oshima volcano, North Japan, **J. Fac. Sci., Hokkaido Univ.**, IV, 21, 77 - 131.

Yamamoto, M., 1988, Picritic primary magma and its source mantle for Oshima-Oshima and back-arc side volcanoes, Northeast Japan arc, **Contr. Min. Petr.**, 99, 352 - 359.

Yamazaki, T., Onuki, H. & Tiba, J., 1965, Significance of hornblende gabbroic inclusions in calc-alkali rocks, **Instit. Min. Pet. Econ. Geol., Tohoku Univ., Japan**, 55, 87 - 103.

Yeats, R.S., Forbes, W.C., Heath, G.R. & Scheidegger, K.F., 1972, Petrology and geochemistry of DSDP Leg 16 basalts, Eastern Equatorial Pacific, in : **Initial reports of the DSDP, XVI**, U.S. Govt. Print. Off., Washington, D.C., 617 - 645.

Zen, M.T., 1983, Mitigating volcanic disaster in Indonesia. In : H Tazieff and J. Clabroux (Eds.), **Forecasting Volcanic Events**, Elsevier, Amsterdam, pp. 219 - 236.

Zindler, A., Jagoutz, E. & Goldstein, S., 1982, Nd, Sr and Pb isotopic systematics in a three-component mantle : a new perspective, **Nature**, 298, 519 - 523.

APPENDICES

Appendix 1.1 Sketch of stratigraphic position of rock samples in the SW wall of Galunggung caldera.

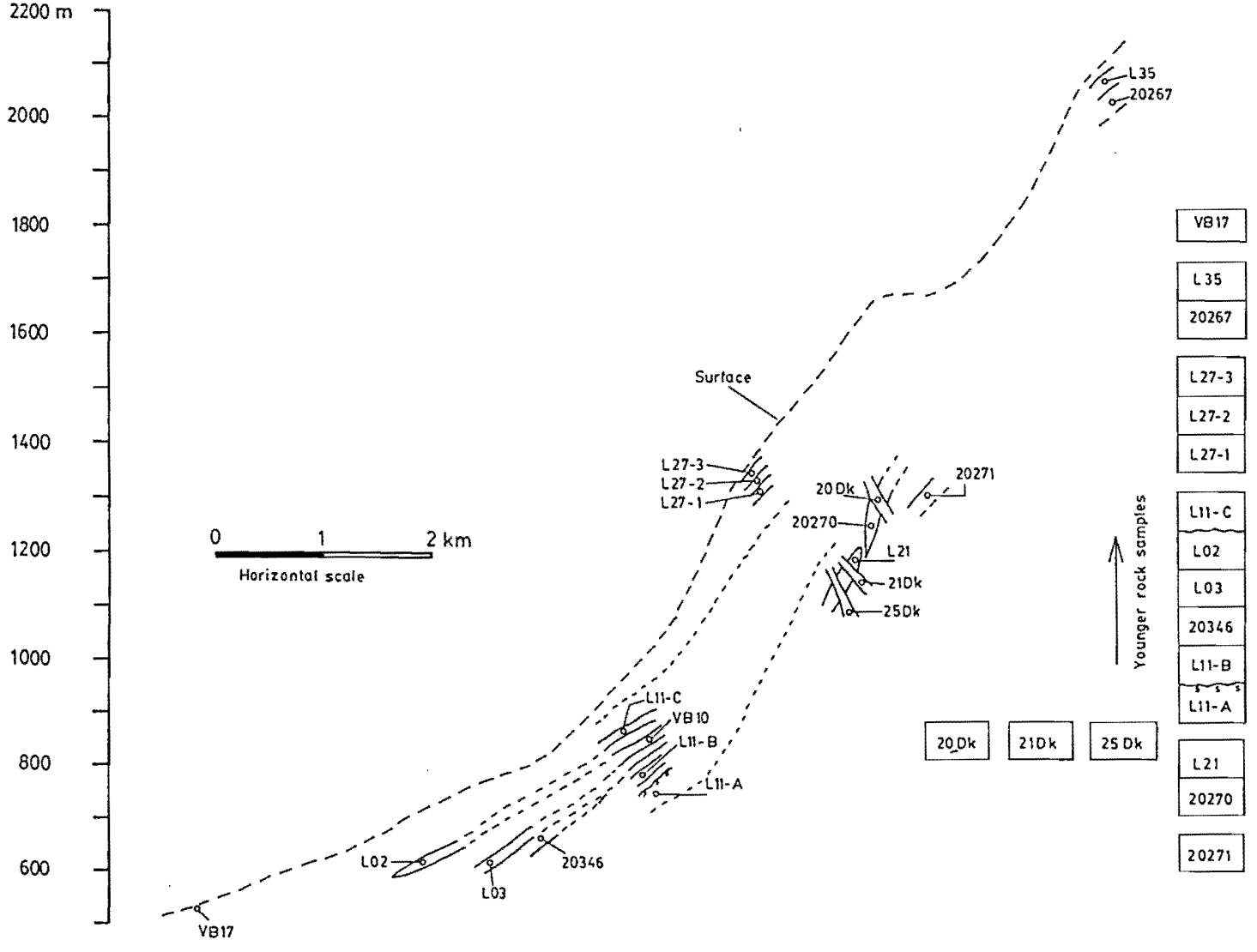

Appendix 1.2 Sketch of stratigraphic position of rock samples in the NE wall of Galunggung caldera.

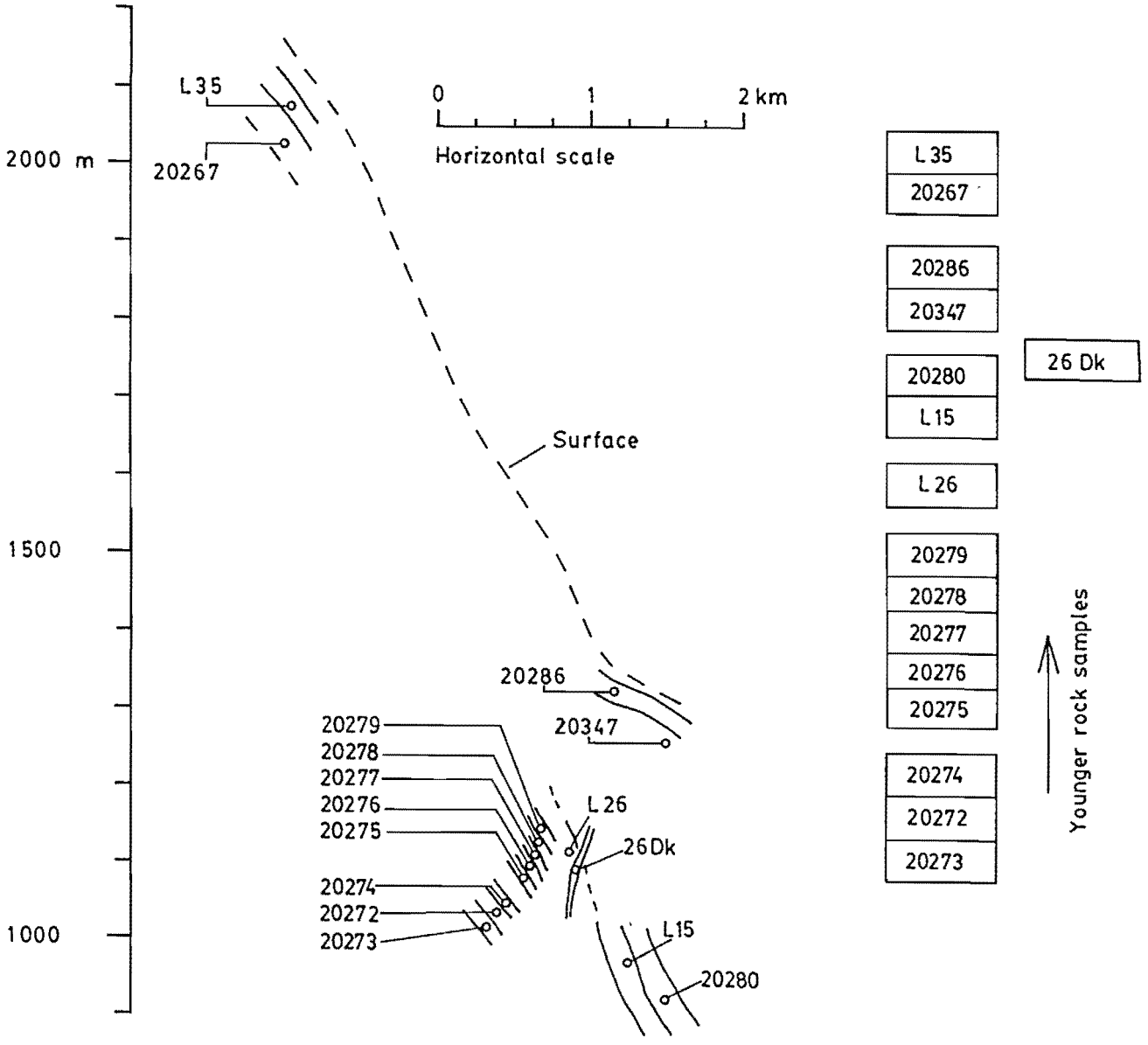

Appendix 1.3 Stratigraphic correlation in the SW wall of Galunggung caldera.

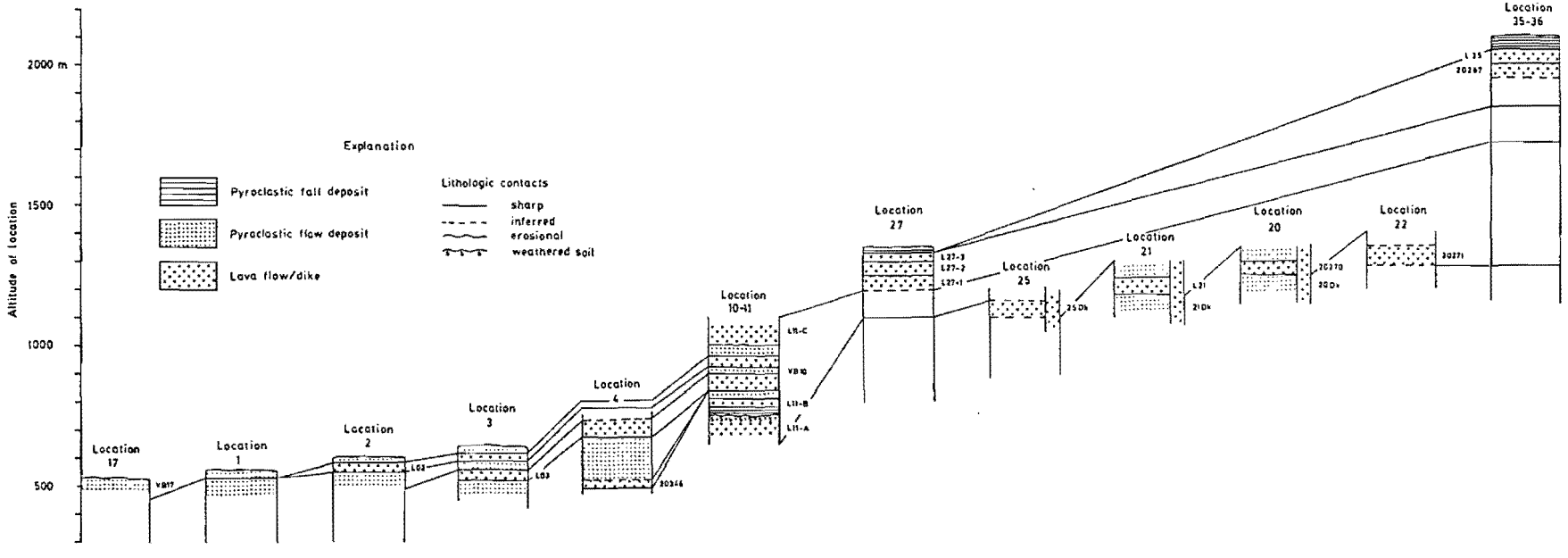

Appendix 1.4 Stratigraphic correlation in the NE wall of Galunggung caldera.

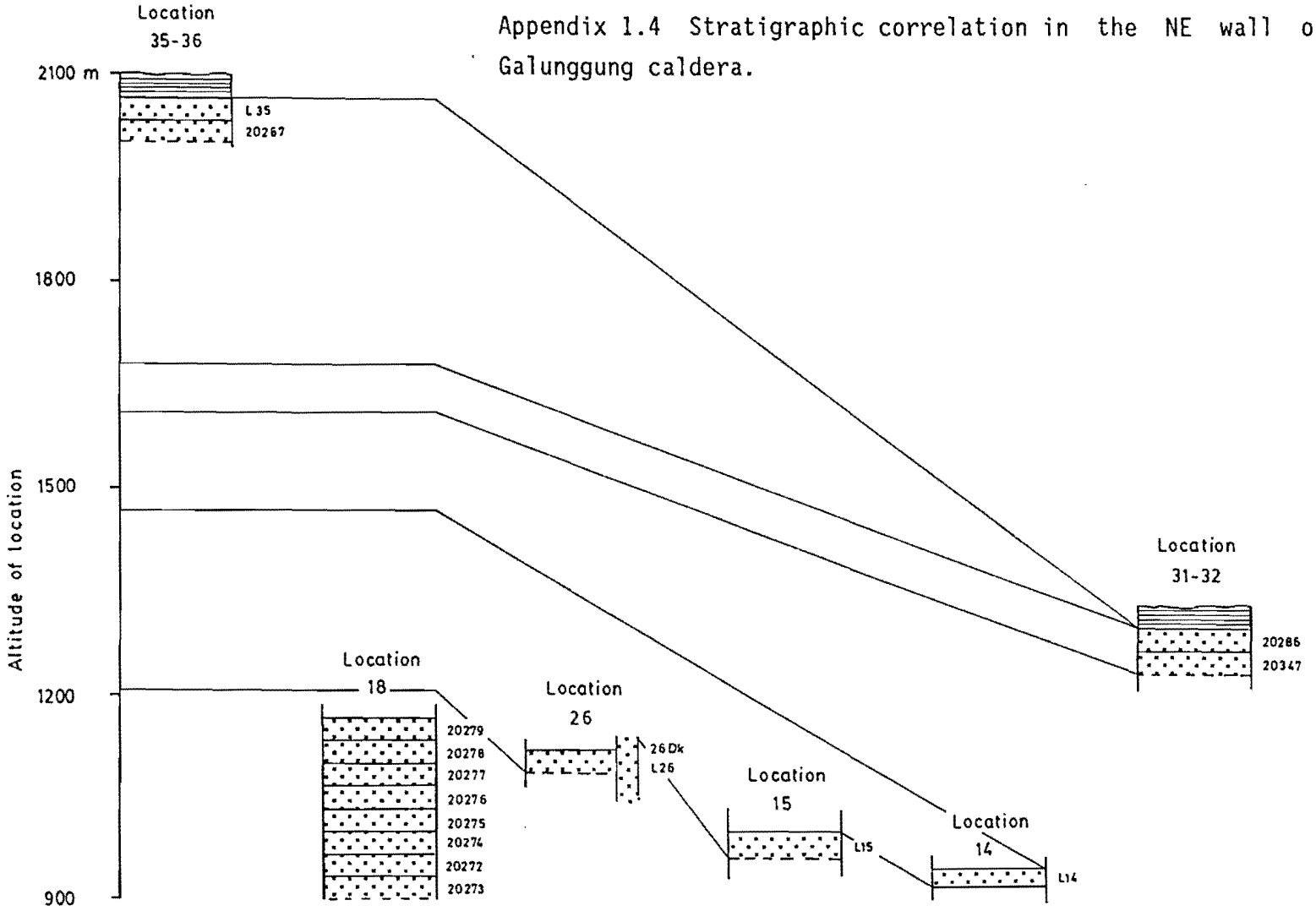

Appendix 1.5 Lithologic section at location 1.

Thickness (m)	Lithologic column	Name	Description and sample code
17.3	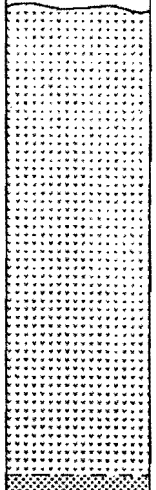	Pyroclastic flow deposit	Light grey to brown, structureless, loose to indurated, poorly sorted, abundant ash and lapilli with some blocks and bombs of basaltic andesite.
1.5		Fluvial deposit	Silt to sand, planar, cross bedding, rounded to subrounded gravels.
> 1.0		Lahar deposit	Light grey, structureless, to < 20 cm across. indurated, unsorted, abundant ash-lapilli, some subangular - subrounded boulders floating in the matrix.

Appendix 1.6 Lithologic section at location 2.

Thickness (m)	Lithologic column	Name	Description and sample code
8.5	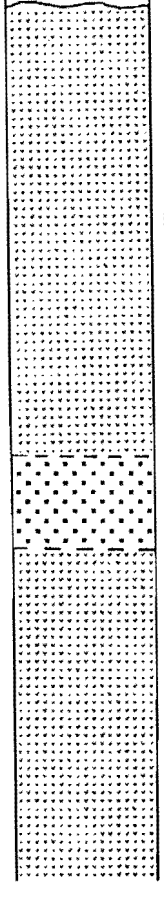	Pyroclastic flow deposit	Light brown, indurated, structureless, poorly sorted, abundant ash-lapilli with some blocks and bombs; forms a vertical cliff, contact with lava flow below is not clear.
3.0		Lava flow	Light grey, porphyr.; pyrox. & plag. in aphanetic groundmass; wedging downward. L02.
25.0		Pyroclastic flow deposit	Light brown, massive, indurated, structureless, poorly sorted, abundant ash-lapilli with some blocks and bombs of basaltic andesite; forms a vertical cliff.

Appendix 1.7 Lithologic section at location 3.

Thickness (m)	Lithologic column	Name	Description and sample code
25.0	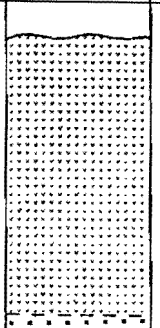	Pyroclastic flow deposit	Light brown, massive, indurated, structureless, poorly sorted, abundant ash-lapilli with some blocks and bombs of basaltic andesite; forms a vertical cliff.
7.5	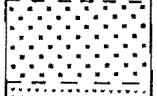	Lava flow	Light grey, porphyr.; pyrox. plag. in aphanetic groundmass. L02.
3.5		Pyroclastic flow deposit	
17.5	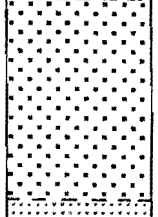	Lava flow	Basaltic andesite, grey, porphyr., pyrox. & plag. in aphan. groundmass. The lava is blocky at the bottom but changes to brecciated then to massive in the middle that is columnar jointed. L03.
24.0	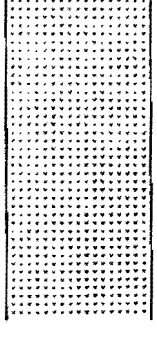	Pyroclastic flow deposit	

Appendix 1.8 Lithologic section at location 4.

Thickness (m)	Lithologic column	Name	Description and sample code
> 15.0	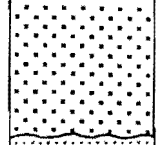	Lava flow	L 03
2.5	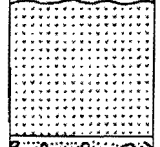	Pyroclastic flow deposit	Dark brown, structureless, abundant ash, weathered.
2.5	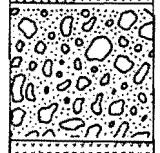	Lahar deposit	Dark brown, fragmental, structureless, poorly sorted; andesitic boulders floating in the matrix.
1.5	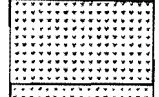	Pyroclastic flow deposit	Dark brown, bomb-rich in ash, unsorted.
2.7	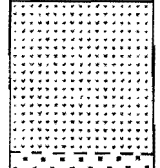	Pyroclastic flow deposit	Dark brown, structureless, abundant ash with some bombs and blocks of basaltic andesite.
5.0	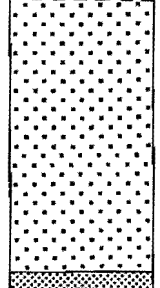	Lava flow	Andesite, grey, porphyr., pyrox. & plag. in groundmass, slightly altered. L04.
> 2.0		Fluvial deposit	Reworked deposit, indurated, sand - gravel, planar structure.

Appendix 1.9 Lithologic section at location 10-11.

Thickness (m)	Lithologic column	Name	Description and sample code
> 14.0		Lava flow	Basal. andes., porphyr.; pyrox. & plag. in aphan. gdm.; channel-filling. L11-C.
3.0		Pyroclastic flow deposit	Light brown, structureless, abundant ash, some andesitic blocks.
5.0		Lava flow	Basal. andes., porphyr., pyrox. & plag. in aphan. gdm, wedging downward. L02.
10.0		Pyroclastic flow deposit	Light brown, structureless, abundant ash with some breadcrust bombs and andesitic blocks. VB10.
5.0		Lava flow	Basal. andes., porphyr., pyrox. & plag. in aphan. gdm. L03.
3.0		Pyroclastic flow	Light brown, structureless, unsorted, abundant ash.
2.0		Lava flow	Basal. andes., porphyr., pyrox. & plag. L11-B.
1.0		Pyroclastic fall deposit	Unconsolid. sand-lapilli, grad. bed.
> 6.0		Lava flow	Basal. andes., porphyr., pyrox. & plag., having paleo soil at the top. L11-A.

Appendix 1.10 Lithologic section at location 18.

Thickness (m)	Lithologic column	Name	Description and sample code
> 5.0		Blocky lava	Lava flows consisting massive and blocky-brecciated units All massive lavas are dark, slightly altered, vesiculer, porphyritic, phenocrysts : plagioclase & pyroxene (1 - 2 mm) in aphan. groundmass. Vesicles are filled by bluish grey second. material. A gradual change occurs from blocky through brecciated to massive lavas. This makes contact between one to another single lava flow is obscure. Blocky-brecciated lavas are brownish red, thicker than the massive unit. Above this section, there are still numerous lava flows up to the top, but they could not be assessed. Collected massive lavas (9) from lower (20273) to upper (20279) flows.
0.6		Massive lava	
2.5		Blocky lava	
1.5		Massive lava	
5.5		Blocky lava	
1.9		Massive lava	
1.5		Blocky lava	
1.1		Massive lava	
2.5		Blocky lava	
1.1		Massive lava	
1.2		Blocky lava	
2.0		Massive lava	
0.3		Blocky lava	
1.7		Massive lava	
3.0		Blocky lava	
6.0		Massive lava	
5.0		Blocky lava	
10.0		Massive lava	
> 3.0		Blocky lava	

Appendix 1.11 Lithologic section at location 14.

Thickness (m)	Lithologic column	Name	Description and sample code
1.0		1982-83 Pyroclastic fall deposit	Grey brown (lower) to black (upper), ash to lapilli, normal grad. bed., intercalated pyroclastic surge dep.
2.0		1982 Pyroclastic flow deposit	Brownish grey, loose, structureless, dominant ash with few glassy breadcrust bombs.
1.0		1982 Pyroclastic flow deposit	Light grey, loose, structureless, dominant ash, few andesitic blocks and bombs.
6.5 - 3.5		1982 Bomb-rich pyroclastic flow deposit	Dark, breadcrust bomb-rich (10 - 80 cm), abundant ash in thin layers, some andesitic blocks near the vent. 20291.
3.3 - 0.3		1982 Lahar deposit	Reddish brown, unsorted, densely indurated, dominant ash (silt-sand), few blocks and bombs (10 - 15 cm).
3.5 - 1.4		1982 Bomb-rich pyroclastic flow deposit	Dark, breadcrust bomb-rich with some andesitic blocks (up to 1.5 m), unsorted, loose material. 20290, X-14.
1.3 - 0.2		Pyroclastic fall deposit	Brown ash, graded bedding.
1.7 - 0.5		1982 Pyroclastic flow deposit	Brown, unsorted, predominant andesitic blocks, unconsolidated.
1.0		Lahar deposit	Dark grey altered, some boulders in silt groundmass, wood and charcoal.
		Lava flow	Old Galunggung lava flow, blocky in the lower & upper parts but massive in the middle. 20280.

Appendix 1.12 Lithologic section at location 16.

Thickness (m)	Lithologic column	Name	Description and sample code
3.0 - 1.5		1982-83 Pyroclastic fall deposit	Dark, ash-lapilli, few bombs and blocks, grad. bed.; alternating with pyr. flow deposit. at lower part.
4.0 - 1.5		1982 Pyroclastic flow deposit	Grey-brown, poorly sorted, abundant ash, few bombs & blocks, unconsolidated.
5.0 - 4.5			Ditto, bombs & bombs are 20 - 30 cm in diameter. VB 16.
7.0 - 3.0		1982 Bomb-rich pyroclastic flow deposit	Black, bomb-rich in the middle and abundant ash at lower and upper parts, loose.
2.0		Lahar deposit	Poorly sorted, dense, contains wood pieces
4.5 - 2.5		1982 Pyroclastic flow deposit	Brownish grey, unsorted, abundant blocks, loose.
3.5 - 1.5		1982 Bomb-rich pyroclastic flow deposit	Black, bomb-rich in the middle and abundant ash at lower and upper parts, loose.
2.0		Lahar deposit	Poorly sorted, dense, contains wood pieces
3.0		1982 Pyroclastic flow deposit	Brownish grey, unsorted, abundant blocks, loose.
2.0			
8.0		1822 Volcanic debris avalanche deposit	Abundant blocks, unsorted, indurated at most upper part and others are loose. 20243.
10.0		1822 Pyroclastic flow deposit	Dark grey, slightly altered, abundant ash. 20342.

Appendix 1.13 Lithologic section at location 30.

Thickness (m)	Lithologic column	Name	Description and sample code
1.5	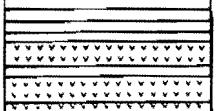	1982-83 Pyroclastic deposit	Pyr. flow & fall dep. at lower part, dominant pyr. fall dep. at upper part
2.0	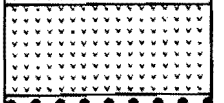	Pyroclastic flow deposit	Brownish grey, unsorted, structureless, loose, dominant ash. VB30C.
4.0	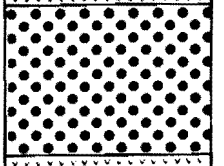	Bomb-rich pyroclastic flow deposit	Black, predominant bombs up to 1 m across, unsorted, loose.
4.0	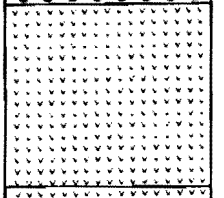	1982 Pyroclastic flow deposit	Abundant blocks at lower and predominant bombs at upper parts, aver. 15 cm across, unconsolidated. VB30B.
2.0	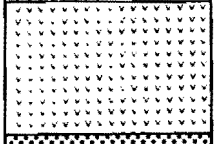	1822 Pyroclastic flow deposit	Dark grey, abundant ash, slightly altered, indurated. VB30 A.
1.0	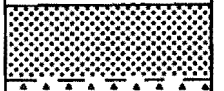	Fluvial deposit	Sand-size, cross bed., wood of 590 ± 150 yrs. BP in age.
> 10.0	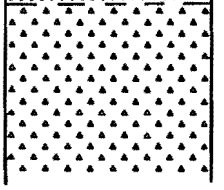	Volcanic debris avalanche deposit	Unsorted, weathered, partly indurated; a product of Galunggung caldera formation.

Appendix 1.14 Stratigraphic correlation of the 1982-83 volcanic deposit in the Ci Banjaran downstream.

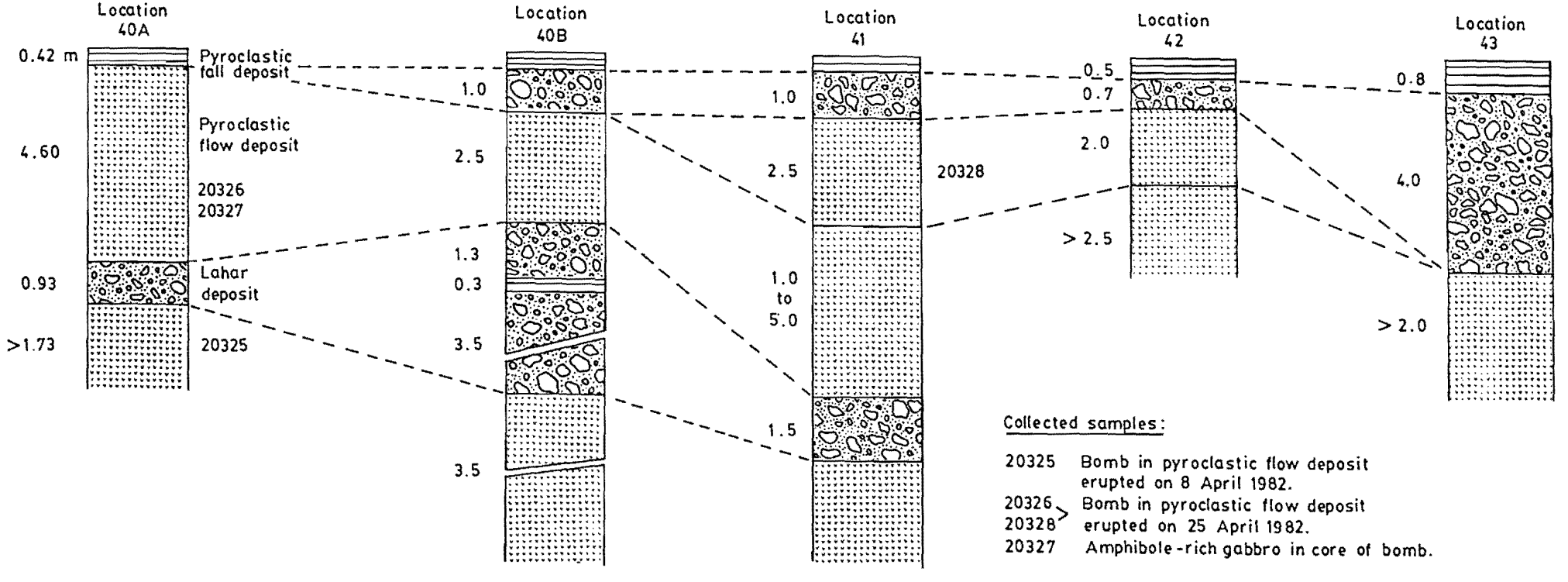

Appendix 1.15 Stratigraphic correlation of the 1982-83 volcanic deposit in the Ci Kunir valley.

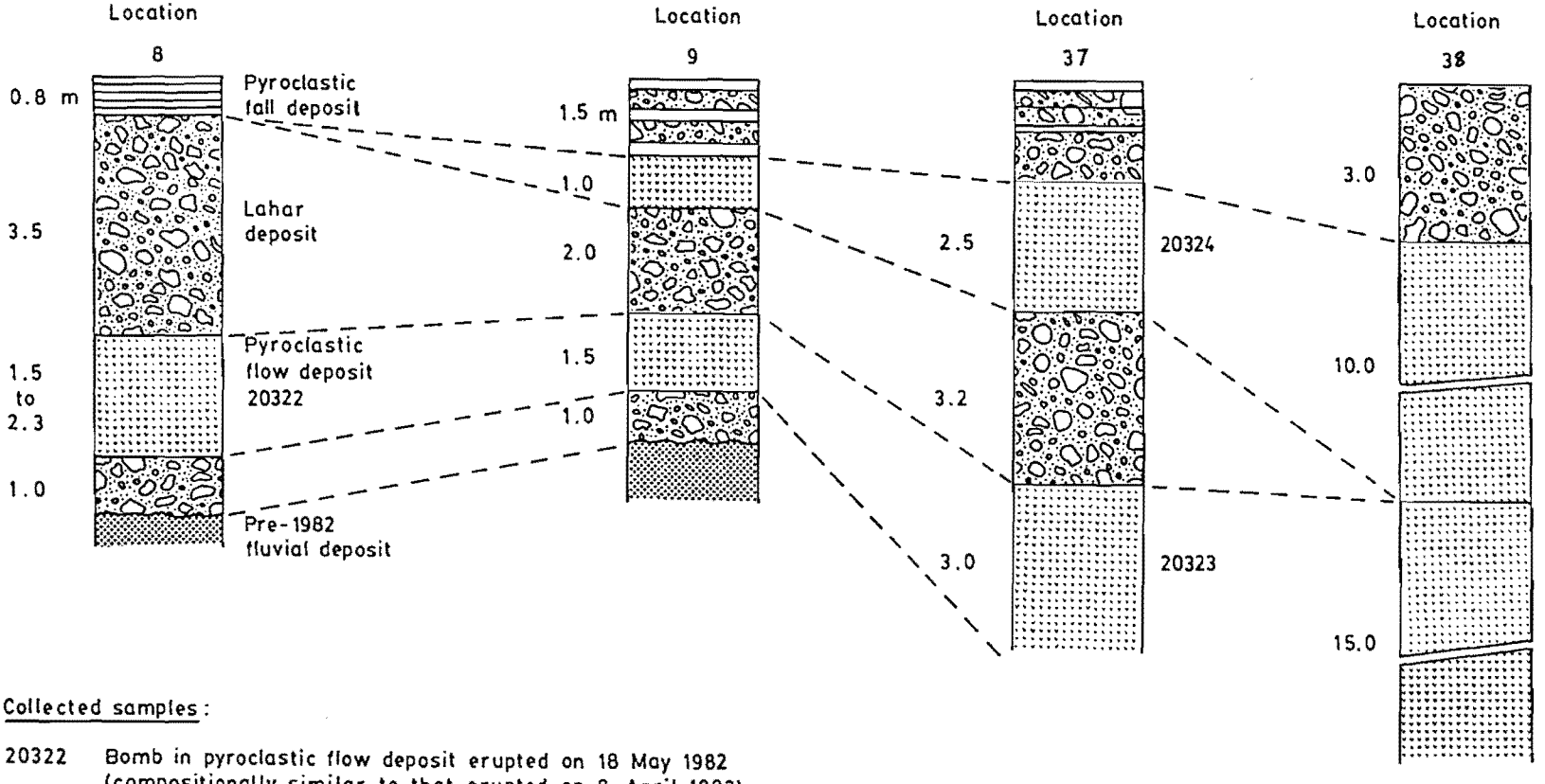

Collected samples:

20322 Bomb in pyroclastic flow deposit erupted on 18 May 1982 (compositionally similar to that erupted on 8 April 1982).

20323 Bomb in pyroclastic flow deposit erupted on 18 May 1982.

20324 Bomb in pyroclastic flow deposit erupted in June 1982.

Appendix 1.16 Lithologic section of the 1982-83 pyroclastic deposits at location 59, west of active crater.

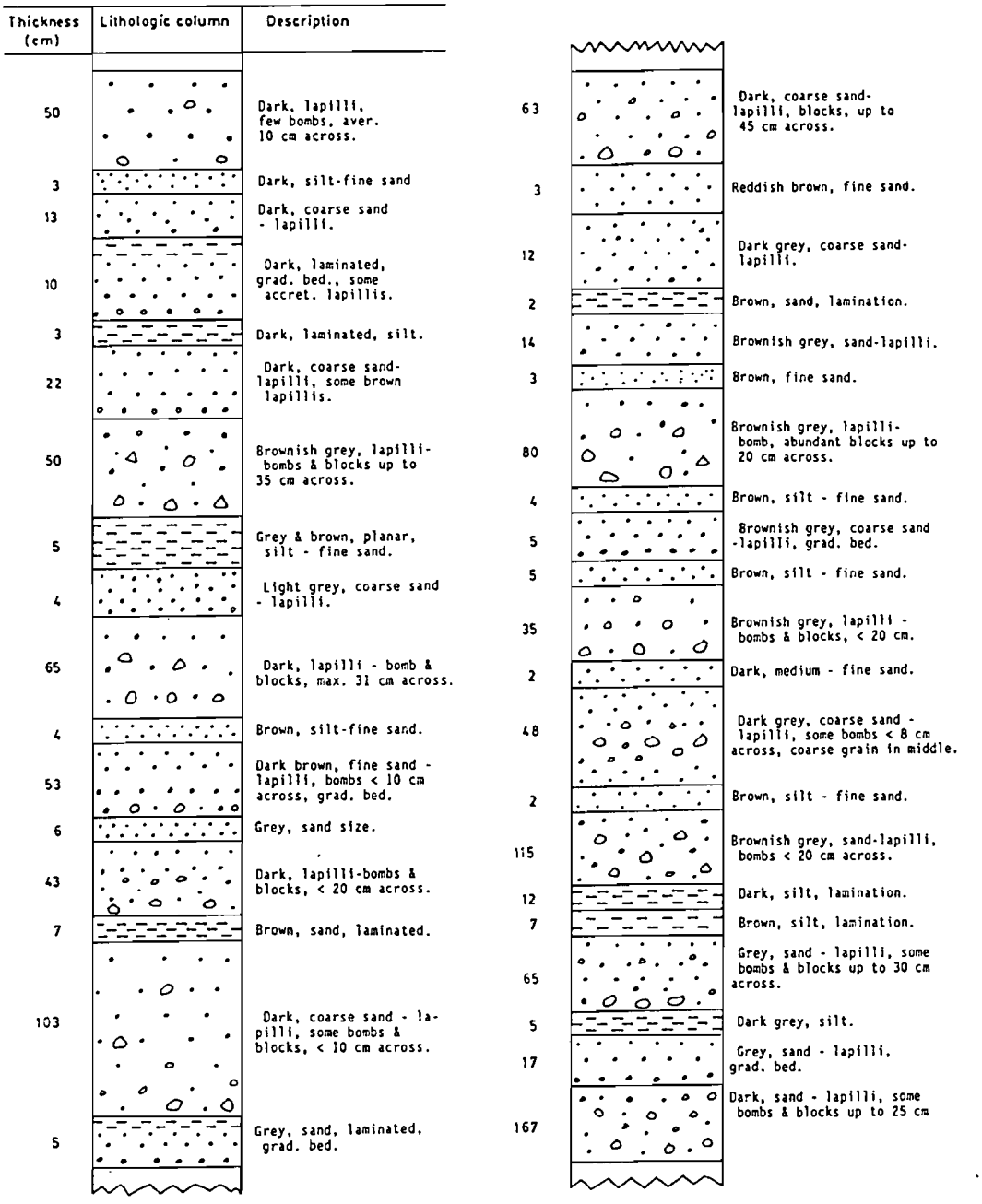

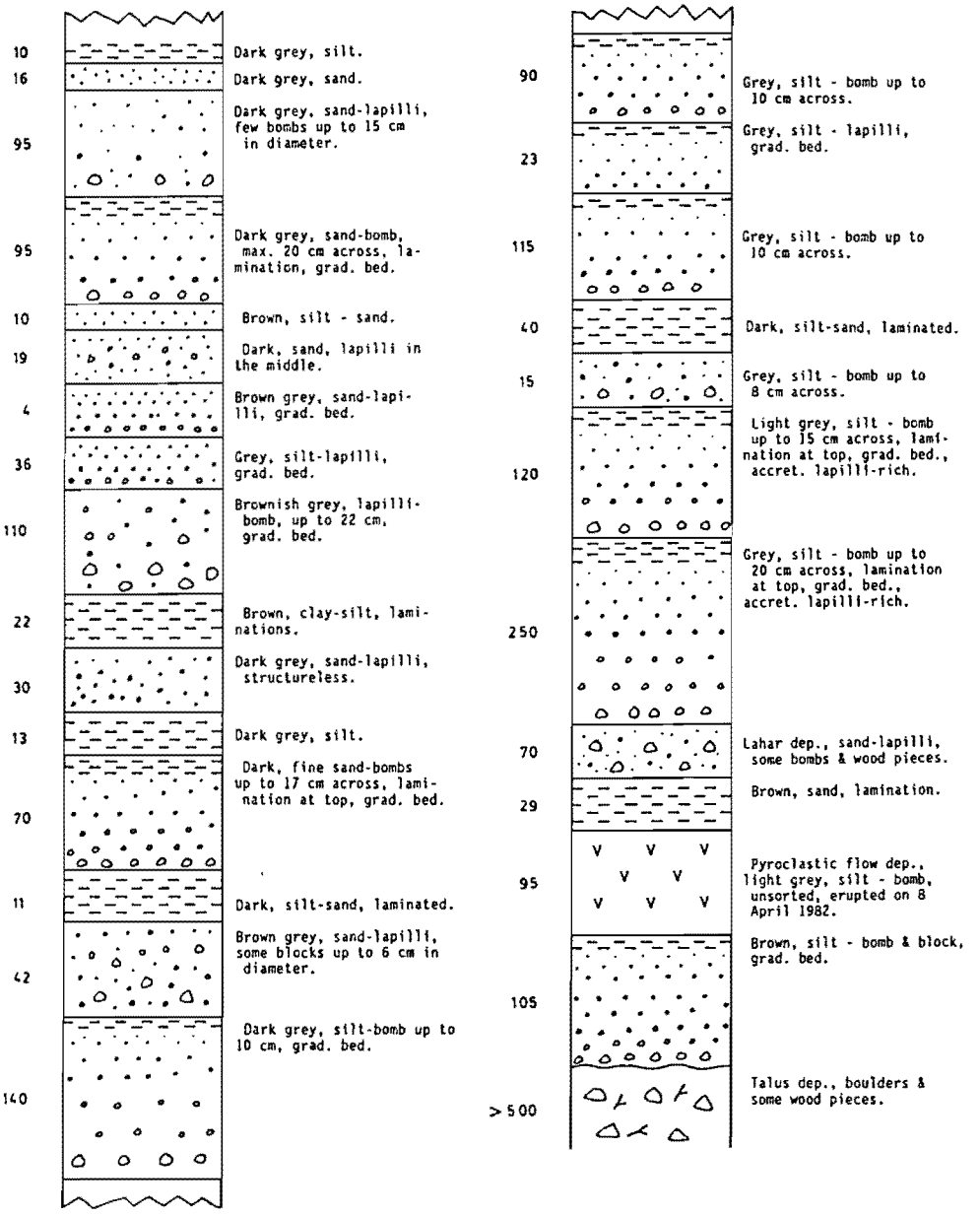
10
Dark grey, silt.
16
Dark grey, sand.
95
Dark grey, sand-lapilli, few bombs up to 15 cm in diameter.
95
Dark grey, sand-bomb, max. 20 cm across, lamination, grad. bed.
10
Brown, silt - sand.
19
Dark, sand, lapilli in the middle.
4
Brown grey, sand-lapilli, grad. bed.
36
Grey, silt-lapilli, grad. bed.
110
Brownish grey, lapilli-bomb, up to 22 cm, grad. bed.
22
Brown, clay-silt, laminations.
30
Dark grey, sand-lapilli, structureless.
13
Dark grey, silt.
70
Dark, fine sand-bombs up to 17 cm across, lamination at top, grad. bed.
11
Dark, silt-sand, laminated.
42
Brown grey, sand-lapilli, some blocks up to 6 cm in diameter.
140
Dark grey, silt-bomb up to 10 cm, grad. bed.
90
Grey, silt - bomb up to 10 cm across.
23
Grey, silt - lapilli, grad. bed.
115
Grey, silt - bomb up to 10 cm across.
40
Dark, silt-sand, laminated.
15
Grey, silt - bomb up to 8 cm across.
120
Light grey, silt - bomb up to 15 cm across, lamination at top, grad. bed., accret. lapilli-rich.
250
Grey, silt - bomb up to 20 cm across, lamination at top, grad. bed., accret. lapilli-rich.
70
Lahar dep., sand-lapilli, some bombs & wood pieces.
29
Brown, sand, lamination.
95
Pyroclastic flow dep., light grey, silt - bomb, unsorted, erupted on 8 April 1982.
105
Brown, silt - bomb & block, grad. bed.
>500
Talus dep., boulders & some wood pieces.

Appendix 1.17 Strikes of lineaments and faults in Tasikmalaya region (in N ... ^{o}E).

A. Data from Geologic map of the Tasikmalaya quadrangle, West Java (Budhitrisna, 1982).

1. 60	2. 343	3. 312	4. 90	5. 87	6. 304
7. 317	8. 316	9. 330	10. 77	11. 79	12. 312
13. 281	14. 290	15. 326	16. 347	17. 274	18. 280
19. 296	20. 313	21. 72	22. 315	23. 280	24. 322
25. 290	26. 305	27. 320	28. 339	29. 297	30. 308
31. 306	32. 289	33. 58	34. 339	35. 277	36. 270
37. 42	38. 307	39. 59	40. 292	41. 74	42. 68
43. 90	44. 65	45. 90			

B. Data from landsat image.

1. 299	2. 336	3. 315	4. 304	5. 329	6. 304
7. 295	8. 320	9. 307	10. 290	11. 344	12. 315
13. 312	14. 326	15. 10	16. 349	17. 354	18. 340
19. 336	20. 302	21. 334	22. 329	23. 299	24. 310
25. 3	26. 321	27. 20	28. 308	29. 334	30. 13
31. 357	32. 58	33. 59	34. 81	35. 358	36. 350
37. 354	38. 47	39. 324	40. 320	41. 312	42. 322
43. 82					

Appendix 1.18 Sample collections.

1) XRF Lab of Geology Department, University of Canterbury

2) Samples were analysed at XRF Lab of Geology Department, Victoria University of Wellington

No.	Field no.	Lab no.[1]	University no.	Location	Explanation
1	VB 17[2]	-	13243	17	Basaltic andesite bomb in Old Galunggung pyroclastic flow deposit.
2	L35[2]	-	13244	35	Basalt, Old Galunggung lava flow.
3	L36	20267	13245	36	ditto
4	L27-3[2]	-	13246	27-3	Basaltic andesite, Old Galunggung lava flow.
5	L27-2[2]	-	13247	27-2	Basalt, Old Galunggung lava flow.
6	L27-1[2]	-	13248	27-1	ditt o
7	L11-C[2]	-	13249	11	ditto
8	L02[2]	-	13250	2	ditto
9	VB10[2]	-	13251	10	Basalt bomb in Old Galunggung pyroclastic flow deposit.
10	L03[2]	-	13252	3	Basaltic andesite, Old Galunggung lava flow.
11	L04	20346	13253	4	ditto
12	L11-B[2]	-	13254	11	Basalt, Old Galunggung lava flow.
13	L11-A[2]	-	13255	11	ditto
14	L21[2]	-	13256	21	ditto
15	L20	20270	13257	20	ditto
16	L22	20271	13258	22	ditto
17	L31[2]	20286	13259	31	ditto
18	L32	20347	13260	32	Basaltic andesite, Old Galunggung lava flow.
19	L14	20280	13261	14	Basalt, Old Galunggung lava flow.
20	L15[2]	-	13262	15	Basaltic andesite, Old Galunggung lava flow.
21	L26[2]	-	13263	26	ditto
22	L18-7	20279	13264	18	Basalt, Old Galunggung lava flow.
23	L18-6	20278	13265	18	ditto
24	L18-5	20277	13266	18	ditto
25	L18-4	20276	13267	18	ditto
26	L18-3	20275	13268	18	ditto
27	L18-1	20274	13269	18	ditto
28	L18-8	20272	13270	18	ditto
29	L18-9	20273	13271	18	ditto
30	L28[2]	-	13272	28	ditto
31	L34[2]	20285	13273	34	ditto
32	L50	20348	13274	50	ditto
33	L51	20349	13275	51	ditto
34	L52	20350	13276	52	ditto
35	L33-A	20266	13277	33	ditto
36	L33-C	20265	13278	33	ditto
37	L33-D	20263	13279	33	ditto
38	L33-E	20264	13280	33	ditto
39	GG-1	20260	13281	61	Basaltic andesite lava flow in debris avalanche deposit of caldera formation.
40	GG-2	20353	13282	61	Basalt bomb in debris avalanche deposit of caldera formation.

41	GG-3	20261	13283	61	Basaltic andesite bomb in debris avalanche deposit of caldera formation.
42	GG-4	20262	13284	61	Basalt lava flow in debris avalanche deposit of caldera formation.
43	GG[2)]	20288	13285	61	Basaltic andesite lava flow in debris avalanche deposit of caldera formation.
44	SKMH[2)]	20287	13286	62	Basalt lava flow in debris avalanche deposit of caldera formation.
45	LPdark[2)]	-	13287	63	ditto
46	LPgrey[2)]	-	13288	63	ditto
47	X 14[2)]	-	13289	14	Basalt lava fragment in 1982 pyroclastic flow deposit.
48	DB	20243	13290	16	Basalt lava fragment in 1822 debris avalanche deposit.
49	F14	20343	13291	14	Basaltic andesite lava fragment in 1982 lahar deposit.
50	GB-A	20351	13292	58	Basal lava flow in debris avalanche deposit of caldera formation.
51	GB-B	20352	13293	58	ditto
52	20 Dk	20284	13294	20	Basalt, Old Galunggung dike.
53	21 Dk[2)]	-	13295	21	Basaltic andesite, Old Galunggung dike.
54	25 Dk	20283	13296	25	Basalt, Old Galunggung dike.
55	26 Dk[2)]	-	13297	26	ditto
56	33-1 Dk	20281	13298	33	Basaltic andesite dike in debris avalanche deposit of caldera formation.
57	33-2 Dk	20282	13299	33	Basalt dike in debris avalanche deposit of caldera formation.
58	L24	20258	13300	24	Basalt, Old Galunggung cryptodome.
59	VB6[2)]	20289	13301	6	Basaltic andesite bomb in pyroclastic flow deposit of caldera formation.
60	VB6-1	20345	13302	6	ditto
61	VB6-2A	20344	13303	6	Basalt bomb in pyroclastic flow deposit of caldera formation.
62	VB6-2B	20254	13304	6	Basalt bomb in pyroclastic flow of caldera formation.
63	VB6-3A	20253	13305	6	Basaltic andesite bomb in pyroclastic flow deposit of caldera formation.
64	VB6-3C	20255	13306	6	ditto
65	VB6-3B	20252	13307	6	Thermal metamorphosed gabbro clast in pyroclastic flow deposit of caldera formation.
66	GPA	20256	13308	6	Gabbro clast in pyroclastic flow deposit of caldera formation.
67	GHA	20257	13309	6	ditto
68	VB6-3D	-	13310 13311 Gabbro	6	Thermal metamorphosed andesitic clast in pyroclastic flow deposit of caldera
69	VB30-A[2)]	-	13312	30	Basaltic andesite bomb in 1822 pyroclastic flow deposit.
70	VB4A	20250	13313	16	ditto
71	OB16	20342	13314	4	Basalt bomb in 1822 pyroclastic flow deposit.
72	1894 A	20245	13315	60	Basaltic andesite bomb in 1894 pyroclastic fall deposit.
73	1894 B	20246	13316	60	ditto
74	4AK [2)]	20292	13317	-	1918 basaltic andesite lava dome collected by MA Purbawinata.
75	4AH [2)]	20293	13318	-	ditto
76	VB13A[2)]	20294	13319	13	Basaltic andesite bomb in 8 April 1982 pyroclastic flow deposit.

77	VB40-1	20325	13320	40	ditto
78	WL[2)]	20290	13321	14	ditto
79	B-8	20322	13322	8	8 April (?) basaltic andesite bomb in May 1982 pyroclastic flow deposit.
80	WL-1	20249	13323	14	Basaltic andesite bomb in 25 April 1982 pyroclastic flow deposit.
81	VB14A[2)]	20291	13324	14	ditto
82	VB13B[2)]	20295	13325	13	ditto
83	VB40-2	20326	13326	40	ditto
84	VB41-3	20328	13327	41	ditto
85	40/LG/82	20336	13328	-	1982 Basaltic andesite scoria lapilli collected by VSI (Volcanological Survey of Indonesia).
86	WL-2	20340	13329	16	Basaltic andesite bomb in 25 April 1982 pyroclastic flow deposit.
87	VB16-2	20341	13330	16	ditto
88	VB30B[2)]	-	13331	30	ditto
89	VB16-3	20248	13332	16	Basaltic andesite bomb in 6 May pyroclastic flow deposit.
90	VB13C[2)]	20296	13333	13	ditto
91	VB16[2)]	-	13334	16	ditto
92	VB30C[2)]	-	13335	30	ditto
93	VB13D[2)]	20297	13336	13	Basalt bomb in 18 May 1982 pyroclastic flow deposit.
94	B37-1	20323	13337	37	ditto
95	B37-2	20324	13338	37	Basalt bomb in June 1982 pyroclastic flow deposit.
96	Mlgt	20329	13339	-	Basalt bomb in pyroclastic fall deposit collected from Malaganti by S. Rasyid.
97	Jul-82	20330	13340	-	Basalt, sand size ash erupted on 13-14 July 1982 collected by VSI.
98	Aug-82	20331	13341	-	Basalt, silt size ash erupted on 26 August 1982, collected by VSI.
99	41A/LG	20332	13342	-	Basalt, coarse sand size ash erupted on 4 September 1982 collected by VSI.
100	P.82	20244	13343	19	Rhyolite pumice erupted on 16 September 1982.
101	66/LG	20335	13344	-	Basalt, fusiform bomb erupted on 16 September 1982.
102	VB82[2)]	20298	13345	14	ditto
103	64/LG	20334	13346	-	Basalt, sand size ash erupted in September 1982 collected by VSI.
104	45/LG	20333	13347	-	Basalt, scoria lapilli erupted on 25 September 1982 collected by VSI.
105	B82-3	20321	13348	39	Basalt, cowdung bomb erupted in September (?) 1982.
106	81/LG	20337	13349	-	Basalt, coarse sand size ash erupted on 18 November 1982 collected by VSI.
107	107/LG	20338	13350	-	Basalt, fine lapilli erupted in December (?) 1982 collected by VSI.
108	121/LG	20339	13351	-	Basalt, bomb erupted on 3 December 1982, collected by VSI.
109	L19[2)]	20299	13352	19	Basalt, fusiform bomb erupted in September (?) 1982.
110	L1983	20300	13353	-	Basalt lava flow extruded on 1-7 January 1983, collected by R. Sukhyar.
111	G40	20327	13354	40	Gabbro clast in breadcrust bomb in 25 April 1982 pyroclastic flow deposit.
112	VB19	-	13355	19	Gabbro in fusiform bomb erupted in September (?) 1982
113	FCB	-	13356	40	Basaltic andesite clast having plagioclase megacryst with olivine inclusions .

APPENDIX 2 Petrographic Terminology and Descriptions

84 Rock samples with 145 thin sections have been examined under microscope. Selected modal analyses are estimated using point counting techniques. Each examined thin section is counted to 1000 points in three interval stages. Sample numbers follow field and lab numbers. A confirmation to the numbers of Canterbury University is given in Appendix 1-18.

Standard terminology is used in this study, and definitions are given after Best (1975), Cox et al. (1981), Hatch et al. (1972) and Williams et al. (1982).

Porphyritic texture is when large crystals (phenocrysts) set in a finer grained matrix (**groundmass**). **Phenocrysts** are solid phases which were in equilibrium with the liquid. Petrogenetically, they must be differed from **cumulates** (crystals settled out of a magma) and **xenocrysts** (foreign crystals).

Crystal grains which are completely bounded by their own rational crystal faces are called **euhedral**; those only partly bounded by crystal faces are called **subhedral**; and those have irregular shape, are referred to as **anhedral**. The grain is said to be **fine** if the average diameter of individual grains is 1 mm or less; **medium** for those are 1 - 5 mm; **coarse** for those are 5 mm - 3 cm; and **very coarse** for those are more than 3 cm.

Rocks in which the phenocrysts are gathered in clots are called **glomeroporphyritic** texture. A large grain crystal encloses numerous fine grain of various minerals is said to have a **poikilitic** texture. Groundmass can be composed of wholly crystals (**holocrystalline**), crystal and glass (**hypocrystalline**) or predominantly glass (**vitrophyric**). If the individual component crystals can be distinguished with a microscope, the texture is termed **microcrystalline**.

In groundmass, interstices between feldspars are occupied by ferromagnesian (**mafic**) granules, usually olivine, pyroxene and magnetite. The resultant is called **intergranular**; if glass is present between the crystals, the texture is **intersertal**. The feldspars may show a subparallel manner (flow oriented), the texture is **pilotaxitic**; whereas **trachytoid** is used when feldspars give a parallel pattern (typical texture in the high-silica orthopyroxene basaltic andesite of Galunggung).

Fine grains of orthopyroxene or orthopyroxene, clinopyroxene and magnetite surrounding anhedral rounded olivine are termed **coronas**. This may also be seen around orthopyroxene and consists of clinopy-

roxene. Minerals (and mineraloids) are secondary when they were resulted from alteration or reconstruction of primary minerals. Alteration may be caused by hydrothermal, weathering, or thermal metamorphism processes.

Intrusive rocks usually are composed wholly of crystals (holocrystalline). This texture has specific terms depending on the common occurrences in the rocks, e.g gabbroic, granitic and diabasic. Rock fragments clearly of foreign origin are xenoliths. These are readily recognized by having granoblastic texture that is a secondary texture formed essentially equidimensional (or saccaroidal) crystals, because of thermal metamorphism when the rock fragments fell into magma.

Abreviations in the petrographic descriptions are alphabetically listed as follows :

Acic.	Acicular	Mag.	Magnetite
Alb.	Albite	Max.	Maximum
Alter.	Alteration	Med.	Medium
Amp	Amphibole	Microcryst.	Microcrystalline
Andes.	Andesite	Olv	Olivine
Aggreg.	Aggregate	Opx	Orthopyroxene
Anhed.	Anhedral	Oscill.	Oscillatory
Assoc.	Associated	Phenoc.	Phenocryst
Aver.	Average	Pleoc.	Pleochroic
Bas.	Basaltic	Plg	Plagioclase
Bowl.	Bowlingite	Pilotax.	Pilotaxitic
Carb.	Carbonate	Poikil.	Poikilitic
Carls.	Carlsbad	Porphyr.	Porphyritic
Chlor.	Chlorite/chloritic	Px	Pyroxene
Compos.	Composition	Recryst.	Recrystallisation
Cpx	Clinopyroxene	RN	Rock name
Cr-sp	Cr-spinel	RT	Rock type
Cryst.	Crystal	Sec. min.	Secondary mineral
Euhed.	Euhedral	SN	Sample number
Gdm.	Groundmass	Subhed.	Subhedral
Glomer.	Glomeroporphyritic	Tab.	Tabular
Holoc.	Holocrystalline	Text.	Textur
Hypoc.	Hypocrystalline	Trachyt.	Trachytoid
Inclus.	Inclusion	Vesic.	Vesicle
Intergran.	Intergranular	Vitrophyr.	Vitrophyric
Intersert.	Intersertal	Volc.	Volcanic
Loc.	Location		

1. SN : VB 17 RN : Bas. andes. RT : Volc. bomb Loc. : 17

Text. Med.-fine grained, hypoc. porphyr., few glomer.

Phenoc. Plg, euhed.-subhed., 0.5-1.5 mm (max. 6.0 mm), normal zoned, twinned (Carls.-Alb. & Alb.), abundant. Few plg phenoc. have a wide unzoned core & olv inclus. Opx, anhed.-subhed., 0.3-1.0 mm, weakly pleoc. (colourless-pale brown), few jacketed by cpx, rare. Cpx, anhed., up to 2.0 mm, rare.

Gdm. Plg, mag, cpx, olv (< 0.1 mm), abundant brown glass.

2. SN : L 35 RN : Basalt RT : Lava flow Loc. : 35

Text. Med.-fine grained, hypoc. porphyr.

Phenoc. Olv, subhed. tab. (4.0 mm) & rounded (0.8 mm), rare. Cpx, euhed.-subhed., 0.1 - 1.6 mm, some have mag & plg inclus., common. Opx microcryst., 0.2 - 0.5 mm, several jacketed by cpx & assoc. with mag, rare. Mag. microcryst. < 0.5 mm, very rare. Plg, euhed.-subhed., 0.5-2.0 mm (max. 5.5 mm), normally zoned, twinned (Alb. & Carls.-Alb.), inclus.: glass, px & mag, abundant.

Gdm. Olv, cpx, mag, acicular - lath-like plg, and brown glass.

3. SN : 20267 RN : Basalt RT : Lava flow Loc. : 36

Text. Fine grained, hypoc. porphyr., glomer. (OPX & CPX).

Phenoc. Olv, euh.-subhed., 0.5 - 1 mm, mostly altered, few replaced by opx, alteration : green bowl. & carb., rare. Cpx, euhed.-anhed., up to 2 mm, rare normally zoned, inclus. : plg & mag, common. Opx, subhed., 0.5 - 1 mm, very rare. Mag microcryst., common. Plg, euhed.-subhed., aver. 1 mm, normally zoned, twinned (Alb. & Carls.-Alb.), glass inclus., abundant.

Gdm. Px, ubiquitous mag, plg laths, green altered (olv ?), a small amount of pale brown glass.

4. SN : L27-3 RN : Bas. andes. RT : Lava flow Loc. : 27-3

Text. Med.-fine grained, hypoc. porphyr., glomer. (cpx).

Phenoc. Olv, anhed. rounded, max. 0.5 mm, cpx coronas, very rare. Opx, subhed., up to 1.5 mm, weakly pleoc. (colourless - pale brown), assoc. with mag, very rare. Cpx, rounded - subhed., up to 2.4 mm, inclus. : olv & mag, rare. Plg, euhed. - subhed., 1 - 2 mm, normally - oscillatory zoned, twinned (Carls.-Alb. & Alb.), inclus. : glass & rare cpx, abundant.

Gdm. Olv, cpx, mag & plg in dusty glass.

5. SN : L27-2 RN : Basalt RT : Lava flow Loc. : 27-2

Text. Med.-fine grained, porphyr., glomer. (olv, cpx &plg).

Phenoc. Olv, anhed. rounded, 0.1 - 0.7 mm (aver. 0.4 mm), cpx coronas, rare. Cpx, subhed.-anhed. rounded, 0.3 - 4.2 mm, inclus. : olv, mag & plg, very rare. Plg, euhed. - subhed., 1 - 2 mm, twinned (Carls._Alb. & Carls.), normally zoned, inclus. : glass partly crystallised to cpx, abundant.

Gdm. Cpx, mag & plg, abundant.

6. SN : L27-1 RN : Basalt RT : Lava flow Loc. : 27-1

Text. Med.-fine grained, hypoc. porphyr., glomer. (olv, cpx & plg, < 3 mm).

Phenoc. Olv, anhed. rounded, up to 2 mm, very rare. Cpx, subhed.-anhed., up to 2.8 mm, inclus. : olv, cpx, plg & glass, common. Plg, euhed.-subhed., 1-2 mm (max. 4 mm), twinned (Alb. & Carls.-Alb.), normally zoned, glass inclus.

Gdm. Olv, cpx, mag & plg in light brown glass.

7. SN : L11-C RN : Basalt RT : Lava flow Loc. : 11

Text. Med. fine grained, porphyr.

Phenoc. Olv, subhed. rounded-tab., 0.5 - 3 mm, partly altered to reddish brown iddingsite (?), carb. & chlor. (?), very rare. Cpx, rounded-subhed., 0.5 - 2 mm, inclus. : olv, mag, plg & glass, very rare. Plg, euhed.-subhed., 0.5 - 2 mm, twinned (Carls.-Alb. & Alb.), normally zoned, glass inclus., abundant.

Gdm. Cpx, mag & plg, abundant.

8. SN : L02 RN : Basalt RT : Lava flow Loc. : 2

Text. Med.-fine grained, hypoc. porphyr.

Phenoc. Olv, anhed. rounded, 0.1 - 0.5 mm, px coronas, partly altered to reddish brown iddingsite (?), rare mag inclus. Cpx, subhed.-anhed., 0.3 - 2 mm, inclus. : plg, mag & glass. Plg, euhed.-subhed., 0.2 - 2 mm, normally zoned, twinned (Carls.-Alb. & Alb.), inclus.: glass & rare cpx.

Gdm. Cpx, mag, plg, intersertal, dusty glass.

9. SN : VB 10 RN : Basalt RT : Volc. bomb Loc. : 10

Text. Med.-fine grained, vitrophyr., glomer. (cpx), pilotax.

Phenoc. Olv, subhed.- rounded, up to 2.5 mm, rare. Cpx, subhed.-rounded, 0.2 - 1.5 mm, twinned, inclus. : olv, mag & plg, common. Plag, euhed.-subhed., 0.5 - 1.5 mm, normally zoned, twinned (carls.-Alb. & Alb.), inclus. : glass & rare cpx, abundant .

Gdm. Cpx, mag & plg in abundant brown glass.

10. SN : L03 RN : Bas. andes. RT : Lava flow Loc. : 3

Text. Med.-fine grained, porphyr., glomer. (cpx, opx & mag), poikil.

Phenoc. Olv, euhed., 1.5 mm, partly altered to green bowl., very rare. Cpx, euhed.-subhed., 1.5 - 3.5 mm, inclus. : mag & plg, very rare. Opx, subhed., 1 mm, very rare. Plg, euhed.-subhed., 0.5 - 2.0 mm, twinned (carls.-Alb. & Alb.), oscill. & normally zoned, glass inclus.

Gdm. Cpx, mag, acic. - lath-like plg.

11. SN : 20346 RN : Bas. andes. RT : Lava flow Loc. : 4

Text. Med.-fine grained, hypoc. porphyr., pilotax.

Phenoc. olv, anhed., 0.3 - 0.6 mm, max. 0.9 mm elongated, px coronas, mag coronas, mag inclus., rare. Plg, euhed.-subhed., 0.5 - 2 mm (aver. 1 mm), flow oriented, normally zoned, twinned (Alb. & Carls.-Alb.), abundant.

Gdm. Cpx, mag & plg laths.

12. SN : L11-B RN : Basalt RT : Lava flow Loc. : 11

Text. Med.-fine grained, hypoc. porphyr.

Phenoc. Olv, anhed. rounded-subrounded, up to 0.3 mm, alteration : green bowl. & carb., rare. Cpx, subhed., 0.2 mm, very rare. Plg, euhed., 0.5 - 2 mm, flow oriented, normally zoned, twinned (Alb. & Carls.-Alb.), glass inclus.

Gdm. Cpx, mag, Acic. - lath-like plg, dusty light brown glass.

13. SN : L11-A RN : Basalt RT : Lava flow Loc. : 11

Text. Med.-fine grained, porphyr.

Phenoc. Olv, euhed.- anhed. rounded, 0.2 - 1.5 mm, partly to pale brown bowl. & reddish brown iddingsite (?), rare. Plg, euhed.- subhed., 0.3 - 2.5 mm, normally zoned, twinned (Alb. & Carls.-Alb.), glass inclus.

14. SN : L 21 RN Basalt RT : Lava flow Loc. : 21

Text. Med.-fine grained, porphyr., glomer. (cpx, mag & plg), poikil.

Phenoc. Olv, anhed., 0.6 - 3 mm, altered to green bowl., rare. Cpx, euhed. - anhed., up to 4 mm (aver. 1 mm), inclus. : mag & plg, common. Plg, euhed. - subhed., 0.5 - 2 mm (aver. 1 mm), twinned (Alb. & Carls.-Alb.), normally zoned, abundant.

Gdm. Partly altered olv, cpx, mag and tab. plag, dusty glass.

15. SN : 20270 RN : Basalt RT : Lava flow Loc. : 20

Text. Med.-fine grained, porphyr., pilotax.

Phenoc. Olv, tab. - subrounded, 0.1 - 1.5 mm, mag inclus., alteration : bowl. & carb. Plg, euhed.- subhed., 0.2 - 1.8 mm (aver. 1 mm), twinned (Alb. & Carls.-Alb.), normally zoned, glass inclus.

Gdm. Olv, cpx, mag & plag. laths.

16. SN : 20271 RN : Basalt RT : Lava flow Loc. : 22

Text. Med.-fine grained, hypoc. porphyr.

Phenoc. Opx, anhed., up to 2.5 mm, mostly altered : carb. & mag. Cpx, subhed.- anhed., 1 - 1.5 mm, inclus. : mag & plg. Plg, euhed.- subhed., 0.5 - 1 mm, twinned (carls.-Alb. & Alb.), normally zoned, glass inclus.

Gdm. Cpx, mag, acic. - lath-like plg microcryst., dusty glass, alteration : chlor.

17. SN : 20286 RN : Basalt RT : Lava flow Loc. : 31

Text. Med.-fine grained, porphyr.

Phenoc. Olv, tab. subhed.- anhed. rounded, 0.2 - 1.8 mm, px coronas, rare. Cpx, subhed.- anhed., 1 - 2.5 mm, inclus. : olv, plg & glass, common. Plg, euhed.- subhed., 0.5 - 2.0 mm (aver. 1 - 1.5 mm), twinned (Alb. & Carls.-Alb.), normally zoned, glass inclus.

Gdm. Olv, cpx, mag & plg microcryst.

18. SN : 20347 RN : Bas. andes. RT : Lava flow Loc. : 32

Text. Med.- fine grained, porphyr., glomer. (opx, cpx, mag), trachyt.

Phenoc. Opx, subhed., 0.2 - 1.7 mm, weakly pleoc. (neutral - light brown), assoc. with mag, some in cpx cores, common. Cpx, euhed.- subhed., 0.2 - 2 mm, common. Plg, euhed.- subhed., 0.2 - 1.5 mm, twinned (Alb. & Carls.-Alb.), normally zoned, minute glass inclus.

Gdm. Mag & acic. - lath-like plg, strong flow oriented.

19. SN : 20280 RN : Basalt RT : Lava flow Loc.: 14

Text. Med.- fine grained, porphyr., glomer. (olv & mag, opx & mag).

Phenoc. Olv, anhed. rounded, 0.2 - 0.5 mm (max. 1 mm), coronas : px & plg, alteration : chlor. & carb. Opx, subhed., 0.3 - 0.5 mm, very rare. Cpx, subhed., 0.5 - 2 mm, inclus. : mag, plg & glass. Plg, euhed.- subhed., 0.5 - 1 mm (max. 2 mm), twinned (Alb. & Carls.-Alb.), normally zoned, glass inclus.

Gdm. Mag, plg & altered mafics (olv & px ?).

20. SN : L 15 RN : Bas. andes. RT : Lava flow Loc. : 15

Text. Med.- fine grained, hypoc. porphyr., glomer. (opx & cpx).

Phenoc. Olv, euhed. - anhed., 0.2 - 0.5 mm (max. 1.5 mm), px coronas, alteration : chlor. & carb. Opx, subhed., 0.5 - 1 mm, jacketed by cpx, very rare. Cpx, euhed. - anhed., 0.5 - 2.5 mm, inclus. : plg & mag. Plg, euhed. - subhed., 0.5 - 1.5 mm, flow oriented, twinned (Alb. & Carls.-Alb.), normally zoned. very common.

Gdm. Px, mag & acic. plg microcryst., glass.

21. SN : L 26 RN : Bas. andes. RT : Lava flow Loc. : 26

Text. Fine grained, hypoc. porphyr., glomer. (opx, cpx & plg), poikil. (cpx).

Phenoc. Opx, subhed., 0.3 - 0.5 mm, rimmed by cpx, common., Cpx, anhed., aver. 1 mm, inclus. : plg & mag. Mag, subhed., up to 0.5 mm, very rare. Plg, euhed. - subhed., aver. 1 mm, twinned (Alb. & Carls.- Alb.), normally zoned.

Gdm. Opx, cpx, mag, plg & glass.

22. SN : 20279 RN : Basalt RT : Lava flow Loc. : 18

Text. Med.- fine grained, porphyr. glomer. (plg).

Phenoc. Altered mafics (olv & Cpx ?), subhed., aver. 1 mm, sec. min. : chlor. around carb. Plg, euhed. - subhed., aver. 1.5 mm, normally zoned, twinned (Carls.-Alb. & Alb.), glass inclus.

Gdm. Cpx, mag & lath-like plg microcryst.

23. SN : 20278 RN : Basalt RT : Lava flow Loc. : 18

Text. Fine grained, porphyr., glomer. (plg).

Phenoc. Mafics (olv & cpx ?), subhed., aver. 0.5 mm, completely altered : chlor. & carb. Plg, euhed. - subhed., aver. 1 mm, twinned (Carls. - Alb. & Alb.), normally zoned.

Gdm. Cpx, mag & plg microcryst.

24. SN : 20277 RN : Basalt RT : Lava flow Loc. : 18

Text. Med. - fine grained, porphyr., intergran. (gdm).

Phenoc. Mafics (olv & cpx ?), subhed., 0.1 - 0.5 mm, completely altered : chlor. around carb. Plg, euhed. - subhed., 1 - 2 mm, twinned (Alb. & Carls.- Alb.), normally - oscill. zoned, a small number of glass inclus.

Gdm. Cpx, mag & plg, alteration : green chlor.

25. SN : 20276 RN : Basalt RT : Lava flow Loc. : 18

Text. Med. - fine grained, hypoc. porphyr.

Phenoc. Altered mafics (olv & cpx ?), subhedral, 0.1 - 0.5 mm, sec. min. : chlor. & mag. Plg, euhed. - subhed., aver. 1. 5 mm, twinned (Carls. - Alb. & Alb.), normally zoned.

Gdm. Cpx, mag & plg microcryst., brown glass.

26. SN : 20275 RN : Basalt RT : Lava flow Loc. : 18

Text. Med. - fine grained, porphyr., intergran. (gdm).

Phenoc. Altered olv : bowl. (?); opx & rounded cpx, rare. Plg, euhed. - subhed., 0.5 - 2 mm, twinned (Carls. - Alb. & Alb.), normally zoned, a small number of glass inclus .

Gdm. Cpx, mag & lath-like plg microcryst.

27. SN : 20274 RN : Basalt RT : Lava flow Loc. : 18

Text. Med. - fine grained, hypoc. porphyr.

Phenoc. Altered mafics (olv & cpx ?), subhed., aver. 1 mm, sec. min. : chlor. carb. Plg, euhed. - subhed., 1 - 1.5 mm, twinned (Carls. - Alb. & Alb.), normally zoned.

Gdm. Cpx, mag & plg microcryst, dusty glass.

28. SN : 20272 RN : Basalt RT : Lava flow Loc. : 18

Text. Med. - fine grained, hypoc. porphyr., glomer. (plg).

Phenoc. Altered mafics (olv & cpx ?), subhedral, aver. 1 mm, sec. min. : chlor., carb. & mag (0.005 mm). Plg, euhed., 1 - 2 mm, normally zoned, twinned (carls. _ Alb. & Alb.).

Gdm. Cpx, mag & plg microcryst., brown glass.

29. SN : 20273 RN : Basalt RT : Lava flow Loc. : 18

Text. Med.- fine grained, hypoc. porphyr., glomer. (cpx & plg).

Phenoc. Altered olv (?) : chlor. & carb., subhed., 0.1 - 0.5 mm. Cpx, sub-rounded, 1 - 2.5 mm, inclus. : mag & plg, rare. Plg, euhed. - subhed., 1 - 2 mm, twinned (Carls. - Alb. & Alb.), normally zoned, inclus. : cpx & glass.

Gdm. Cpx, mag & plg microcryst., brown glass.

30. SN : L 28 RN : Basalt RT : Lava flow Loc. : 28

Text. Med. - fine grained, hypoc. porphyr., glomer. (opx & cpx).

Phenoc. Olv, euhed. - rounded, up to 1 mm, rare. Opx, subhed. - anhed., 1 mm, rimmed by cpx, rare. Cpx, subhed., aver. 1 mm (max. 2.5 mm), inclus. : mag & plg. Plg, euhed. - subhed., 0.5 - 1.5 mm, flow oriented, twinned (Carls. - Alb. & Alb.), normally zoned, a smallnumber of glass inclus.

Gdm. Cpx, mag & plg microcryst., dusty glass.

31. SN : 20348 RN : Basalt RT : Lava flow Loc. : 50

Text. Med. - fine grained, hypoc. porphyr.

Phenoc. Olv, anhed., 0.1 - 1 mm, px coronas, rare. Cpx, subhed., 0.5 - 2 mm, inclus. : olv, mag & plg. Opx, subhed., cpx coronas, assoc. with mag. Plg, euhed. - subhed., 0.1 - 3 mm, twinned (Alb. & Carls. - Alb.), normally zoned, inclus. : glass & cpx .

Gdm. Rounded olv, mag, px & lath-like plg microcryst., pale brown glass.

32 SN : 20266 RN : Basalt RT : Lava flow Loc. : 33

Text. Med. - fine grained, porphyr., glomer. (olv, cpx & plg).

Phenoc. Olv, subhed., 0.2 - 1.2 mm (max. 4 mm), partly altered to bowl, rare. Cpx, euhed. - subhed., 0.1 - 1.9 mm, weakly pleoc. (neutral - pale green), inclus. : mag, olv, plg, common. Plg, euhed. - subhed., 0.5 - 3.0 mm, flow oriented, twinned (Alb. & Carls. - Alb.), normally zoned, glass inclus, abundant. Few plg have a wide unzoned core, without glass inclus.

Gdm. Olv, cpx, mag & plg; alteration : chlor. & carb.

33. SN : 20265 RN : Basalt RT : Lava flow Loc. : 3 3

Text. Med. - fine grained, hypoc. porphyr.

Phenoc. Olv, euhed. tab - subrounded, 1 - 2 mm, altered : bowl. & carb, common. Cpox, subhed., aver. 1 mm, rare. Plg, euhed. - subhed., aver. 1 mm, twinned (Carls. - Alb. & Alb.), normally zoned.

Gdm. Cpx & plg microcryst., dusty glass.

34. SN : 20263 RN : Basalt RT : Lava flow Loc. : 33

Text. Med.- fine grained, hypoc. porphyr.

Phenoc. Altered olv to bowl. (?), euhed. - subhed., 0.5 - 1 mm, common. Cpx, partly altered, subhedral, 0.5 - 2 mm, common. Plg, euhed. - subhed., 1 - 2 mm, twinned (Carls.- Alb. & Alb.), normally zoned, abundant.

Gdm. Cpx, mag & plg microcryst., brown glass.

35. SN : 20264 RN : Basalt RT : Lava flow Loc. : 33

Text. Med.- fine grained, hypoc. porphyr.

Phenoc. Altered mafics (olv & cpx), subhed., aver. 0.5 mm, very common, sec. min. : chlor., carb. & opaque. Plg, euhed. - subhed., 0.5 - 1.5 mm (max. 3 mm), twinned (Carls.- Alb. & Alb.), normally zoned, abundant.

Gdm. Px, mag & plg microcryst., brown glass.

36. SN : 20285 RN : Basalt RT : Lava flow Loc. : 34

Text. Med.- fine grained, porphyr., glomer. (olv & px).

Phenoc. Olv, tab. & subrounded, 0.1 - 1.5 mm, px coronas, rare. Cpx, euhed. - subhed., 0.1 - 2.5 mm (max. 4 mm), mag inclus., common. Opx, subhed., up to 1 mm, in aggreg. or cpx cores, very rare. Mag, anhed., 0.2 - 0.5 mm, very rare. Plg, euhed. - subhed., 0.1 - 2 mm, normally zoned, twinned (Carls. - Alb. & Alb.), inclus. : glass, rare cpx, abundant.

Gdm. Olv, cpx, mag & lath-like plg microcryst. (< 0.05 mm), glass.

37. SN : 20287 RN : Basalt RT : Lava flow Loc. : 62

Text. Med.- fine grained, porphyr., glomer. (px, plg, 1 - 3 mm).

Phenoc. Olv, anhed. rounded, 0.2 - 1 mm, px coronas, mag. inclus., alter. : bowl., very rare. Cpx, subhed. - anhed., 0.5 - 1.5 mm (max. 4 mm), rare normal zoning, inclus. : rare olv, mag & plg, common. Opx, subhed.- anhed., 0.3 - 0.5 mm, weakly pleoc. (neutral - pale brown), in aggreg. with mag microcryst. whick surround anhed. olv, very rare. Plag, euhed. - subhed., 0.5 - 2 mm (aver. 1 mm), normally zoned, twinned (Alb. & Carls. - Alb.), abundant.

Gdm. Olv, cpx, mag & plg microcryst., glass; alter. : carb. & chlor.

38. SN : 20288 RN : Bas. andes. RT : Lava flow Loc. : 61

Text. Med.- fine grained, porphyr., glomer. (opx, cpx, mag), trachyt. (gdm.).

Phenoc. Opx, euhed.- subhed., 0.3 - 1 mm, weakly pleoc. (neutral - light brown), in aggreg. with mag, few as cpx cores, common. Cpx, subhed. - anhed., 0.3 - 1.5 mm, normally zoned, rare. Plg, euhed.- subhed., 0.5 - 1 mm (max. 4 mm), flow oriented, twinned (Alb. & Carls.- Alb.), normally zoned, glass inclus., abundant.

Gdm. Mag & acic. plg microcryst., glass.

39. SN : LP RN : Basalt RT : Lava flow Loc. : 63

Text. Med.- fine grained, porphyr., intersert. (gdm.).

Phenoc. Olv, subhed.- anhed. rounded, 0.5 - 1.5 mm, partly altered : green bowl. & reddish brown iddingsite, rare. Cpx, subhed.- anhed. rounded, 1.5 - 3.5 mm, inclus. : olv, mag & plg, rare. lg, euhed.- subhed., 1 - 1.5 mm, normally zoned, twinned (Carls. - Alb. & Alb.), a small number glass inclus., abundant.

Gdm. Cpx, mag & plg microcryst.

40. SN : X-14 RN : Basalt RT : Lava fragment in 1982 pyroclastic flow deposit Loc. : 14

Text. Med.- fine grained, porphyr.

Phenoc. Plg, euhed.- subhed., 1 - 2 mm, twinned (Carls. - Alb. & Alb.), normally zoned, a small number glass inclus., abundant.

Gdm. Cpx, mag & plg microcryst., brown glass.

41. SN : 21 Dk RN : Bas. andes. RT : Dike Loc. : 21

Text. Med.- fine grained, hypoc. porphyr., glomer. (opx, cpx, mag), poikil. (cpx), trachyt. (gdm.).

Phenoc. Opx, euhed., 1 - 2 mm, weakly pleoc. (colourless - pale brown), rare. Cpx, euhed. - subhed., up to 4 mm, oscill. normal zoning, inclus. : mag, plg, rare. Plg, euhed.- subhed., 1 - 1.5 mm, twinned (Carls. - Alb. & Alb.), normally zoned, abundant.

Gdm. Px, mag & lath-like plg microcryst., brown glass.

42. SN : 20283 RN : Basalt RT : Dike Loc. : 25

Text. Med.- fine grained, hypoc. porphyr.

Phenoc. Cpx, subhed. - anhed., 0.2 - 0.3 mm, very rare. Plg, euhed.- subhed., 1 - 2 mm, twinned (Carls. - Alb. & Alb.), normally zoned, a small number glass inclus., abundant, few plg having a wide unzoned core.

Gdm. Cpx, mag & plg microcryst. in abundant glass.

43. SN : 26 Dk RN : Basalt RT : Dike Loc. : 26

Text. Med.- fine grained, porphyr., glomer. (cpx), intergran. (gdm.).

Phenoc. Olv, anhed. rounded, 0.1 - 0.5 mm, very rare. Cpx, subhed., in aggreg. (2 mm), very rare. Plg, euhed. - subhed., 1 - 2 mm (max. 5 mm), twinned (Carls. - Alb. & Alb.), normally zoned, abundant.

Gdm. Cpx, mag & plg microcryst., a little glass; alter. : green chlor.

44. SN : 20281 RN : Basalt RT : Dike Loc. : 33

Text. Med.- fine grained, porphyr., glomer. (cpx, 2 mm), intersert. (gdm.).

Phenoc. Olv, anhed. subrounded, 0.5 - 1.5 mm (aver. 1 mm), completely altered to bowl., rare. Cpx, anhed., aver. 1 mm, max. 2 mm, inclus. : mag & plg, rare. Plg, euhed.- subhed., 1 - 2 mm, twinned (Carls. - Alb. & Alb.), normally zoned, a small number glass inclus., abundant.

Gdm. Cpx, mag & plg microcryst., alter. : chlor.

45. SN : 20282 RN : Basalt RT : Dike Loc. : 33

Text. Med.- fine grained, porphyr.

Phenoc. Olv, anhed., aver. 1.5 mm, alter. : bowl., rare. Cpx, rounded, 1.5 mm, plg inclus., rare. Plg, euhed.- subhed., 1 - 2 mm, twinned (Alb. & Carls.- Alb.), normally zoned, a small number glass inclus., abundant.

Gdm. Cpx, mag & acic. - lath-like plg microcryst.

46. SN : 20258 RN : Basalt RT : Cryptodome Loc. : 24

Text. Med. - fine grained, porphyr.

Phenoc. Cpx, euhed. - anhed., 2 - 4 mm (max. 7 mm), normally zoned, common. Plg, euhed, - subhed., 0.5 - 1.5 mm, normally zoned, twinned (Alb. & Carls. - Alb.), glass inclus., common.

Gdm. Cpx & plg microcryst., alter. : clay, carb. (1 - 4 mm wide in fracture) & pyrite.

47. SN : 20253 RN : Bas. andes. RT : Volc. bomb Loc. : 6

Text. Med.- fine grained, hypoc. porphyr., pilotax. (gdm), vesic.

Phenoc. Olv, subhed., 0.5 - 1 mm, px coronas, rare. Cpx, euhed. - subhed., 0.5 - 1 mm (max. 5 mm), partly replaced opx assoc. with mag, rare oscill. - normally zoned, inclus. : olv, mag & plg, rare. Amp, brown, strongly pleoc. (pale green - pale brown), anhed., 0.5 - 1 mm (max. 7 mm), rimmed or completely replaced by opaque, rare. Plg, euhed. - subhed., 0.5 - 2 mm, twinned (Carls. - Alb. & Alb.), normallly - oscill. zoned, a small number glass inclus., abundant. Few plg have a wide unzoned core.

Gdm. Anhed. olv, cpx, mag & lath-like plg microcryst. in brown glass.

48. SN : 20289 RN : Bas. andes. RT : Volc. bomb Loc. : 6

Text. Very coarse - fine grained, hypoc. porphyr., glomer. (opx, cpx, mag & plg, 1 - 2 mm), poikil. (amp), vesic.

Phenoc. Olv, anhed. rounded, 0.5 - 0.8 mm, a megacryst : 8 mm, very rare. Opx, subhed., 0.5 - 1 mm, weakly pleoc. (neutral - pale brown), in aggreg. or cpx core, rare. Cpx, euhed.- anhed., 0.2 - 1 mm, inclus. : plg & mag, common. Amp,

euhed. - subhed., long prismatic, up to 4 cm, strongly pleoc. (green - light brown), without opaque rimm, enclosed min. : opx, cpx, mag & plg, very common. Plg, euhed. - subhed., 2 - 4 mm (max. 10 mm), oscill. - normal zoned, twinned (Carls. - Alb. & Alb.), a small number glass inclus., some have a wide unzoned core, abundant.

Gdm. Cpx, mag & plg microcryst. in abundant glass.

49. SN : 20255 Rn : Bas. andes. Rt : Vocl. bomb. Loc. : 6

Text. Med. - fine grained, hypoc. porphyr., glomer. (opx, cpx & mag), vesic.

Phenoc. Olv, subhed. - anhed., rounded, 0.5 - 1 mm (max. 2 mm), mag inclus., very rare. Opx, subhed., 1 - 2 mm, weakly pleoc. (neutral - pale brown), in aggreg. with mag, rare. Cpx, subhed., 0.5 - 1.5 mm, in aggreg., twinned, oscill. - normally zoned, rare. Amp, anhed., aver. 1 mm, opaque rimm, pleoc. (light brown - brown), very rare. Plg, euhed. - subhed., 0.3 - 1 mm (max. 2 mm), twinned (Carls. - Alb. & Alb.), oscill. - normally zoned, glass inclus., abundant.

Gdm. Px, mag & lath-like plg microcryst., in pale brown glass.

50. SN : 20344 RN : Basalt RT : Volc. bomb Loc. : 6

Text. Med. - fine grained, hypoc. porphyr., glomer. (up to 7 mm), poikil.(cpx), vesic.

Phenoc. Olv, subhed. - anhed., 0.05 - 0.5 mm, embayed, mag. inclus., rare. Opx, subhed., aver. 1 mm, weakly pleoc. (neutral - pale brown), very rare. Cpx, subhed. - anhed., 0.05 - 1 mm (max. 3.4 mm), normally zoned, inclus. : olv, mag & plg, rare. Plg, euhed. - subhed., 0.5 - 2 mm, twinned (Carls. - Alb. & Alb.), normally - oscill. zoned, glass inclus., abundant. Few plg have a wide unzoned core.

Gdm. Olv, cpx & plg microcryst. in dark glass.

51. SN : 20254 RN : Basalt RT : Volc. bomb Loc. : 6

Text. Med. - fine grained, hypoc. porphyr., vesic.

Phenoc. Plg, euhed. - subhed., 0.5 - 2.5 mm (aver. 1 mm), twinned (Carls. - Alb. & Alb.), normally-oscill. zoned, flow oriented, glass inclus., abundant.

Gdm. Cpx, mag & plg microcryst. in glass.

52. SN : 20345 RN : Bas. andes. RT : Volc. bomb Loc. : 6

Text. Fine grained, vitrophyr., glomer., vesic.

Phenoc. Olv, anhed. rounded, up to 0.1 mm, very rare. Opx, subhed., 0.3 - 1 mm, in aggreg. or cpx core, very rare. Cpx, euhed. - subhed., 0.05 - 1 mm, in aggreg., inclus. : mag & plg, rare. Amp, subhed., 1 mm, pleoc. (pale brown -

brown), thin opaque rim, very rare. Plg, euhed. - subhed., 0.5 - 1 mm, twinned (Carls. - Alb. & Alb.), glass inclus., few wide unzoned cores, abundant.

Gdm. Olv, cpx, mag & plg microcryst. in abundant dark brown glass.

53. SN : 20252 RN : Gabbro RT : Intrusive clast Loc. : 6

Text. Coarse grained, poikil. - granoblastic, contact with basalt.

Compos. Amp, anhed., 3 - 40 mm, pleoc. (green - brown), without opaque rimm, enclosed min. cpx, mag & plg, granular - saccaroidal crystals < 0.1 mm),very common. Cpx, anhed., 1.5 3 mm, rare. Opx, anhed, < 1 mm, very rare.

Basalt's text. Med. - fine grained, hypoc. porphyr., glomer. (cpx & opx), poikil.

Phenoc. Opx, subhed. - anhed., 0.5 - 1 mm, weakly pleoc. (neutral - pale brown), rare. Cpx, euhed. - subhed., aver. 1 mm, common. Amp., euhed. - subhed., 0.5 - 1 mm, pleoc. (green - brown), common. Mag, anhed., 0.1 - 0.5 mm, rare. Plg, euhed. - subhed., 0.5 - 1 mm, twinned (Carls. - Alb. & Alb.), normally zoned, very common. Few plg (up to 3 mm) have a wide unzoned core.

Gdm. Cpx, amp, plag & mag microcryst. in glass.

In contact between gabbro and basalt, 1 - 2 mm thick, text. : holocryst., microgabbroic, composed : cpx, opx, mag & plg.

54. SN : VB6 -3D RN : Andesite RT : Lava fragment Loc. : 6

Text. Fine grained, intergran., granoblastic.

Compos. Plg, cpx, mag & very rare biotite.

55. SN : 20256 RN : Gabbro RT : Intrusive clast Loc. : 6

Text. Coarse - med. grained (3 - 10 mm), gabbroic, poikil. (amp), injected by basalt.

Compos. Amp, pleoc. (green - pale brown), anhed., short prismatic, thin opaque rim, enclosed min. : olv, cpx, mag & plg, very common. Plg, euhed. - subhed., aver. 1 mm, twinned (Alb.), wide unzoned cores, very common. Cpx, subhed. - anhed., 0.5 - 1 mm, common.

Basalt's text. Fine grained, hypoc. porphyr.

Phenoc. Olv, subhed. - anhed., elongated, tab., skeletal, 0.5 - 1 mm (max. 2 mm), px coronas, mag inclus., common. Opx, subhed., 0.5 mm, weakly pleoc. (neutral - pale brown), in cpx core, mag inclus., very rare. Cpx, euhed. - anhed., 0.5 - 1 mm, common. Plg, euhed. - subhed., 0.5 - 1 mm, max. 2 mm, twinned (Alb. & Carls. - Alb.), normally - oscill. zoned, very common.

Gdm. Olv, cpx, mag & lath-like plg microcryst. in glass.

56. SN : 20257 RN : Gabbro RT : Intrusive clast Loc. : 6

Text. Coarse - med. grained, gabbroic, injected by basalt.

Compos. Amp, pleoc. (green - pale brown), long prismatic, 1 - 6 mm (max. 2.5 cm), thin opaque rim, very common. Plg, subhed., up to 10 mm, normally zoned thin rim, abundant. Mag, anhed., 0.5 - 1.5 mm, rare.

Basalt Very fine anhed. elongated cpx, acic. plg, dusty opaque and glass.

57. SN : 20327 RN : Gabbro RT : Intrusive clast in bomb Loc. : 40

Text. Coarse - med. grained, gabbroic, poikil. (amp), injected by basalt.

Compos. Olv, anhed. rounded, 0.5 - 1 mm, rare. Amp, anhed, 2 - 10 mm, pleoc. (green - brown), thin opaque rim, enclosed min. : olv, mag & plg, abundant. Cpx, anhed., 0.5 - 1 mm, rare. Plg, subhed., 1 - 5 mm, twinned (Carls. - Alb.), wide unzoned cores, abundant.

Basalt Very fine grained, elongated - acic. cpx & plg, dusty opaque & glass.

58. SN : VB 19 RN : Gabbro RT : Intrusive clast in bomb Loc. : 9

Text. Coarse - med. grained, gabbroic, poikil. (amp), injected by basalt.

Compos. Amp, anhed., 1 - 5 mm, pleoc. (pale green - light brown), thin opaque rim, enclosed min. : olv, cpx, mag & plg, very common. Plg, subhed, 0.5 - 1 mm, twinned (Alb. & Carls. - Alb.), wide unzoned cores, interlocking, abundant.

Basalt's text. Med. - fine grained, porphyr., glomer. (2 mm).

Phenoc. Olv, subhed. - anhed., elongated & rounded, 0.1 - 1 mm, px coronas, spnl inclus., common. Cpx, euhed. - anhed., up to 1 mm, common. Plg, euhed. - subhed., 1 - 1.5 mm, twinned (Carls. - Alb. & Alb.), normally - oscill. zoned, glass inclus., very common.

Gdm. Olv, cpx, mag & plg microcryst. in glass, abundant.

59. SN : FCB RN : Bas. andes. RT : Lava fragment Loc. : 40

Text. Fine grained, hypoc. porphyr., trachyt. (gdm), glomer. (plg, 10 mm), poikil. (cpx).

Phenoc. Olv, anhed. rounded, aver. 0.3 mm, very rare. Opx, euhed. - subhed., 0.5 - 1 mm, flow oriented, weakly pleoc. (neutral - pale brown), assoc. with mag microcryst., few in cpx core, common. Cpx, euhed. - subhed., 0.5 - 1.5 mm, enclosed min. : mag & plg, rare. Plg, euhed. - subhed., aver. 1 mm, twinned (Carls. - Alb. & Alb.), normally - oscill. zoned, glass inclus., flow oriented, abundant.

Gdm. Acic. plg & mag microcryst. in glass, abundant.

Plg megacryst Twinned (Alb. & pericline), extinction angle : 35 ^{o} (An_{60},

labradorite), inclus. : subrounded olv, 0.1 - 0.8 mm.

60. SN : 20250 RN : Bas. andes. RT : 1822 Bomb Loc. : 4

Text. Med. - fine grained, hypoc. porphyr., glomer. (cpx, 3 mm), vesic.

Phenoc. Cpx, subhed., 0.5 - 1 mm, inclus. : mag & plg, rare. Opx, euhed. - subhed., aver. 0.5 mm (max. 1 mm), in aggreg. & cpx core, very rare. Plg, euhed. - subhed., 0.5 - 1.5 mm, twinned (Carls. - Alb. & Alb.), normally-oscill. zoned, bundance glass inclus., abundant.

Gdm. Olv, opx, cpx, mag & plg microcryst. (< 0.05 mm) in dark brown glass.

61. SN : 20342 RN : Basalt RT : 1822 Bomb Loc. : 16

Text. Med. - fine grained, hypoc. porphyr., glomer. (cpx, mag & plg).

Phenoc. Olv, subhed. - anhed. rounded, aver. 1 mm, px coronas, partly altered : carb. & chlor., rare. Cpx, subhed. - anhed., 0.5 - 1.5 mm, in aggreg. (up to 3 mm). Opx, subhed. -anhed., 0.3 - 0.5 mm, in cpx core, very rare. Amp, anhed., 1 - 2 mm, pleoc. (brown - pale brown), opaque rimm. Plg, euhed. - subhed., 0.5 - 2 mm, twinned (Carls. - Alb. & Alb.), normally - oscill. zoned, common.

Gdm. Olv, cpx, mag & lath-like plg microcryst. in brown glass.

62. SN : VB30A RN : Bas. andes. RT : 1822 Bomb Loc. : 16

Text. Med. - fine grained, hypoc. porphyr., glomer., poikil.(amp).

Phenoc. Olv, subhed. tab. (3 mm) - anhed. rounded (1 mm), px coronas, very rare. Opx, euhed. prismatic, o.5 - 1.4 mm, in cpx core, rare. Cpx, subhed., 0.5 - 1 mm (max. 2 mm), in aggreg. (up to 4 mm), olv inclus., rare. Amp, anhed., 0.8 mm, pleoc. (brown - light brown), enclosed min. : plg & mag, very rare. Plg, euhed. - subhed., 0.5 - 2 mm, twinned (Carls. - Alb. & Alb.), normally - oscill. zoned, glass inclus., abundant. A plg-rich aggreg. (3 mm), enclosed min. : cpx, opx & mag, a hollow in centre.

Gdm. Cpx, mag & acic. - lath-like plg microcryst. in brown glass.

63. SN : 20245 RN : Bas. andes. RT : 1894 Bomb Loc. : 60

Text. Fine grained, hypoc. porphyr., glomer. (cpx, opx & mag), trachyt. (gdm).

Phenoc. Cpx, subhed., 0.5 - 1 mm, in aggreg. common. Opx, subhed., 0.5 - 1 mm, in aggreg. & cpx core, rare. Olv, anhed., 0.3 mm, very rare. Very fine grained opaque (mag ?), anhed, vesicular-filling. Amp, anhed., 0.1 mm, opaque rim, very rare. Plg, euhed. - subhed., 0.5 - 1.5 mm, twinned (Carls. - Alb. & Alb.), normally - oscill. zoned, glass inclus., very common.

Gdm. Olv, cpx, mag & acic. plg microcryst. in brown glass.

64. SN : 20246 RN : Basalt RT : 1894 Bomb Loc. : 60

Text. Med. - fine grained, hypoc. porphyr., glomer., pilotax. (gdm).

Phenoc. Olv, anhed., up to 1.5 mm, partly altered : bowl. & carb., rare. Cpx, subhed. - anhed., 1 - 2 mm, enclosed min. : mag, rare. Opx, anhed., 0.3 - 0.5 mm, in aggreg., very rare. Plg, euhed. - subhed., 0.5 - 2 mm, twinned (Carls. - Alb. & Alb.), normally - oscill. zoned, abundant.

Gdm. Olv, cpx, mag & acic. plg microcryst. in brown glass. Sec. min. : carb. & chlor.

65. SN : 20292 RN : Bas. andes. RT : 1918 Lava dome

Text. Med. - fine grained, hypoc. porphyr., glomer. (cpx), pilotax. (gdm).

Phenoc. Olv, anhed. rounded, 0.2 - 0.5 mm, opaque rim, very rare. Opx, euhed. - subhed., 0.3 - 1 mm, weakly pleoc. (neutral - light brown), jacketed by cpx, in aggreg., rare. Cpx, subhed., 0.3 - 1 mm (max. 3 mm), in aggreg., common. Plg, euhed. - subhed., 0.2 - 1 mm (max. 4 mm), normally - oscill. zoned, twinned (Crals. - Alb. & Alb.), few wide unzoned cores, abundant.

Gdm. Px, mag & acic. plg microcryst. in glass.

66. SN : 20293 RN : Bas. andes. RT : 1918 Lava dome

Text. Med. - fine grained, hypoc. porphyr.

Phenoc. Olv, subrounded, 0.7 - 0.9 mm, altered : bowl., very rare. Opx, euhed. - subhed., 0.2 - 0.5 mm, weakly pleoc. (neutral - pale brown), cpx rim, rare. Cpx, subhed. - rounded, 0.2 - 0.5 mm, max. 2 mm, normally zoned, rare. Plg, euhed. - subhed., 0.5 - 2 mm, twinned(Carls. - Alb. & Alb.), normally - oscill. zoned, flow oriented, inclus. : glass, px & mag, abundant.

Gdm. Cpx, mag & lath-like plg microcryst. in dusty glass.

67. SN : 20322 RN : Bas. andes. RT : 1982 Bomb Loc. : 8

Text. Fine grained, hypoc. vitrophyr., glomer. (up to 3 mm, olv, cpx, opx, mag & plg), trachyt. (gdm), granoblastic (xenolith), vesic.

Phenoc. Olv, euhed. - subhed. : tab. - subrounded, 0.1 - 0.6 mm, inclus. : glas, cr-sp, very rare. Cpx, euhed. - subhed., 0.5 - 1 mm, fairly common. Amp., anhed. elongated, up to 7 mm, pleoc. (green - pale brown), thin opaque rim, rare. Plg, euhed. - subhed., 0.3 - 1 mm, twinned (Carls. - Alb. & Alb.), normally - oscill. zoned, a small number glass inclus., very common. Andes. xenolith (3 mm), compos. : cpx, mag & plg saccaroidal crystals.

Gdm. Mag, cpx & acic. plg microcryst. in glass, abundant.

68. SN : 20325 RN : bas. andes. RT : 1982 Bomb Loc. : 40

Text. Fine grained, hypoc. vitrophyr., glomer. (up to 3 mm, composed : cpx, opx, mag & plg), trachyt. (gdm), vesic.

Phenoc. Olv, anhed. rounded, aver 0.1 mm, cr-sp inclus., px coronas, very rare. Opx, euhed. - subhed., 0.5 - 1 mm, assoc. with mag, in cpx core, in aggreg., rare. Cpx, euhed. - subhed., 0.5 - 1 mm, common. Amp, subrounded, 3 mm, pleoc. (pale green - pale brown), thin opaque rim, rare. Plg, euhed. - subhed., 0.5 - 1 mm, twinned (Carls. - Alb. & Alb.), normally - oscill. zoned, glass inclus., very common.

Gdm. Cpx, mag & acic. plg microcryst. in glass, abundant.

69. SN : 20294 RN : Bas. andes. RT : 1982 Bomb Loc. : 13

Text. Med. - fine grained, hypoc. vitrophyr., glomer. (up to 3 mm), trachyt. (gdm), vesic.

Phenoc. Olv, anhed. subrounded, 0.5 - 1 mm, in aggreg. (2 mm), cr-sp inclus., px coronas, very rare. Opx, euhed. - subhed., 0.4 - 0.8 mm (max. 1.5 mm), weakly pleoc. (neutral - pale brown), jacketed by cpx, inclus. : plg & mag, rare. Cpx, subhed. - anhed., 0.5 - 1.3 mm, twinned, in aggreg., inclus. : mag & glass, common. Amp, anhed., 0.3 - 3 mm, pleoc. (pale brown - greenish brown), opaque rim, rare. Mag, anhed., 0.1 - 0.3 mm, assoc. with px, very rare. Plg, euhed. - subhed., 0.3 - 1 mm (max. 1.5 mm), normally - oscill. zoned, twinned (Carls. - Alb. & Alb.), glass inclus., very common.

Gdm. Mag, rare cpx & acic. plag microcryst in glass, abundant.

70. SN : 20290 RN : Bas. andes. RT : 1982 Bomb Loc. : 14

Text. Med. - fine grained, hypoc. porphyr.., glomer. (up to 3 mm, cpx, opx, mag & plg), vesic.

Phenoc. Olv, anhed. : subrounded - elongated, skeletal, 0.3 - 1.8 mm (aver. 1 mm), px coronas, cr-sp inclus., rare. Opx, subhed. - anhed., 0.3 - 1.5 mm, weakly pleoc. (neutral - pale brown), jacketed by cpx, inclus. : mag & plg, rare. Cpx, euhed. - anhed., 0.2 - 1.7 mm, normally zoned, in aggreg., very common. Amp, pleoc. (brown - pale brown), anhed., 1 mm, opaque rim, very rare. Plg, euhed. - subhed., 0.5 - 2 mm, twinned (Carls. - Alb. & Alb.), normally - oscill. zoned, inclus. : glass & mag, in aggreg., few wide unzoned cores, very common.

Gdm. Cpx, mag & lath-like plg microcryst. in glass, abundant.

71. SN : 20291 RN : Bas. andes. RT : 1982 Bomb Loc. : 14

Text. Med. - fine grained, hypoc. porphyr., glomer. (cpx, opx, mag & plg), poikil. (amp).

Phenoc. Olv, subhed. - anhed., aver 0.5 mm (max. 1.4 mm), px coronas, cr-sp inclus., rare. Opx, subhed., 0.1 - 1.5 mm, pleoc. (neutral - pale brown), in aggreg., in cpx core, inclus. : plg & mag, rare. Cpx, subhed. - anhed., up to 2.3 mm, twinned, normally zoned, in aggreg., common. Amp, anhed., pleoc. (green-pale brown), 7 mm, enclosed min. : plg, cpx, opx & mag, rare. Plah, euhed. -

subhed., 0.5 - 2 mm, twinned (Carls. - Alb. & Alb.), oscill. - normally zoned, glass inclus., few wide unzoned cores with ammpo inclus. (0.6 mm), abundant.

Gdm. Cpx, mag & lath-like plg microcryst. in brown glass.

72. SN : VB30B RN : Bas. andes. RT : 1982 Bomb Loc. : 30

Text. Fine grained, hypoc. porphyr., pilotax. (gdm), glomer. (up to 7 mm, cpx, mag & plg, vesic.

Phenoc. Olv, anhed. : elongated - subrounded, 0.4 - 1 mm, px coronas, cr-sp inclus., rare. Opx, subhed., 0.2 - 0.5 mm, weakly pleoc. (neutral - pale brown), in cpx core, very rare. Cpx, subhed. - anhed., 0.7 - 1 mm, twinned, in aggreg., inclus. : glass & plg, fairly common. Amp, anhed., 1.5 mm, opaque rim, plag inclus., very rare. Plg, euhed. - subhed., 0.5 - 1 mm (3 mm), twinned (Carls. - Alb. & Albite), oscill. - normally zoned, in aggreg., glass inclus., very common .

Gdm. Olv, cpx, mag & lath-like plg microcryst. in brown glass, abundant.

73. SN : 20295 RN : Bas. andes. RT : 1982 Bomb Loc. : 13

Text. Fine grained, hypoc. porphyr., glomer. (2 mm, cpx, opx, mag & plg), vesic.

Phenoc. Olv, subhed. - anhed. : elongated, skeletal & rounded, 0.2 - 0.5 mm (max. 2.5 mm), px coronas, cr-sp inclus., rare. Opx, subhed., 0.2 - 0.5 mm (max. 1.2 mm), in cpx core, very rare. Cpx, subhed. - anhed., 0.2 - 0.8 mm (max. 1.5 mm), in aggreg., normally zoned, twinned, inclus. : mag & plg, fairly common. Plg, euhed. - subhed., 0.3 - 0.7 mm (max. 1.5 mm), oscill. - normally zoned, twinned (Carls. - Alb. & Alb.), in aggreg., glass inclus., very common.

Gdm. Olv, cpx mag & lath-like plg microcryst. in brown glass, abundant.

74. SN : VB30C RN : Basalt RT : 1982 Bomb Loc. : 30

Text. Fine grained, hypoc. porphyr., glomer. (up to 3 mm; olv, cpx, opx, mag & plg), vesic.

Phenoc. Olv, subhed., 0.1 - 0.5 mm (max. 2 mm), cr-sp inclus., in aggreg., rare. Opx, subhed., 0.3 - 0.5 mm, weakly pleoc. (neutral - pale brown), assoc. with mag, in cpx core, in aggreg., very rare. Cpx, euhed. - subhed., 0.3 - 1 mm, twinned, normally zoned, in aggreg., glass inclus., common. Plg, euhed. - subhed., 0.5 - 1 mm (max. 1.5 mm), oscill. - normally zoned, twinned (Carls. - Alb. & Alb.), glass inclus., common.

Gdm. Olv, cpx, mag & acic. - lath-like plg microcryst. in brown glass.

75. SN : 20296 RN : Basalt RT : 1982 Bomb Loc. : 30

Text. Med. - fine grained, hypoc. porphyr., glomer. (2 mm; cpx, mag & plg), vesic.

Phenoc. Olv, subhed. - anhed. : elongated, skeletal & rounded, 0.15 - 1 mm (

max. 2 mm), px coronas, cr-sp inclus., common. Opx, anhed., 0.4 - 0.8 mm, weakly pleoc. (neutral - pale brown), in aggreg., in cpx core, very rare. Cpx, subhed. - anhed., 0.2 - 0.5 mm (max. 2 mm), in aggreg., common. Mag, anhed., 0.1 - 0.3 mm, assoc. with cpx & opx, very rare. Plg, euhed. - subhed., 0.5 - 2 mm, normally - oscill. zoned, twinned (Carls.-Alb. & Alb.), in aggreg., glass inclus., few wide unzoned cores, very common.

Gdm. Olv, cpx, mag & acic. - lath-like plg microcryst. in dark glass.

76. SN : VB 16 RN : Basalt RT : 1982 Bomb Loc. : 16

Text. Med. - fine grained, hypoc. porphyr., glomer. (2 mm; olv, cpx, opx, mag & plg), pilotax. (gdm), vesic.

Phenoc. Olv, subhed. - anhed. : elongated, skeletal, & rounded, 0.1 - 1. 5 mm, in aggreg., cr-sp inclus., px coronas, fairly common. Opx, euhed. - subhed., 0.5 - 1 mm, assoc. with mag microcryst., in aggreg., jacketed by cpx, rare. Cpx, euhed. - subhed., 0.3 - 1 mm, in aggreg., fairly common. Amp, anhed., 0.5 - 1 mm, pleoc. (brown - pale brown), opaque rimm, very rare. Plg, euhed. - subhed., 0.5 - 1.5 mm, twinned (Carls. _ Alb. & Alb.), normally - oscill. zoned, glass inclus., few wide unzoned cores, very common.

Gdm. Olv, cpx, mag & acic. - lath-like plg microcryst in brown glass.

77. SN : 20297 RN : Basalt RT : 1982 Bomb Loc. : 13

Text. Med. - fine grained, hypoc. porphyr., vesic.

Phenoc. Olv, subhed. - anhed. : elongated, skeletal & rounded, 0.1 - 1 mm (max. 4 mm), px coronas, cr-sp inclus., fairly common. Opx, subhed. - anhed., 0.4 - 0.8 mm (max. 1 mm), in cpx core, assoc. with mag microcryst, very rare. Cpx, subhed. - anhed., 0.3 - 0.6 mm (max. 1.2 mm), twinned, inclus. : mag & glass, fairly common. Plg, euhed. - subhed., 0.3 - 1 mm (max. 2 mm), normally - oscill. zoned, twinned (Carls. - Alb. & Alb.), glass inclus., very common.

Gdm. Olv, cpx, mag & acic. - lath-like plg microcryst. in glass.

78. SN : 20324 RN : Basalt RT : 1982 Bomb Loc. : 38

Text. Med. - fine grained, hypoc. porphyr., glomer. (up to 2 mm; olv, cpx, opx, mag & plg), poikil. (olv, cpx), vesic.

Phenoc. Olv, subhed. - anhed. : tab., rounded, embayed, elongated & skeletal, 0.2 - 1 mm (max. 2.5 mm), hollow, coronas : px, mag & plg, cr-sp inclus., very common. Cpx, subhed. - anhed., vary up to 3 mm, normally zoned, hollow, inclus. : glass, plg & mag, rare olv; in aggreg. (2 - 4 mm), common. Opx, anhed., 0.1 - 0.3 mm, in aggreg. & cpx core, very rare. Plg, euhed. - subhed., 0.5 - 2 mm (aver. 1 mm), oscill. - normally zoned, twinned (Carls. - Alb. & Alb.), glass inclus., very common.

Gdm. Olv, cpx, mag & acic. - lath-like plg microcryst. in dark brown glass.

79. SN : 20335 RN : Basalt RT : 1982 Bomb

Text. Med. - fine grained, hypoc. porphyr., interlocking (olv, cpx & plg), poikil. (cpx), vesic.

Phenoc. Olv, euhed. - anhed. : tab., embayed, elongated, rounded & skeletal, 0.5 - 1 mm (max. 2 mm), hollow, cr-sp inclus., very common. Cpx, euhed. - anhed., 0.5 - 1 mm, normally zoned, hollow, olv inclus., interlocking in aggreg. (up to 3 mm), very common. Plg, euhed. - subhed., 0.5 - 1 mm (max. 3 mm), twinned (Carls. - Alb. & Alb.), oscill. - normally zoned, glass inclus., few wide unzoned cores, common.

Gdm. Olv, cpx, mag & lath-like plg microcryst. in brown glass.

80. SN : 20298 RN : Basalt RT : 1982 Bomb Loc. : 14

Text. Med. - fine grained, hypoc. porphyr., glomer. interlocking (olv, cpx & plg), poikil. (cpx).

Phenoc. Olv, euhed. - anhed. : skeletal, embayed, rounded & skeletal, up to 2 mm, cr-sp inclus., common. Cpx, euhed. - anhed., embayed, hollow, 0.5 - 1 mm, in aggreg. (2 mm), common. Plg, euhed. - subhed., 0.5 - 1 mm, twinned (Carls. - Alb. & Alb.), normally - oscill. zoned, glass inclus., in aggreg. (3 mm), very common.

Gdm. Olv, cpx, mag & lath-like plg microcryst. in brown glass.

81. : 20339 RN : Basalt RT : 1982 Bomb

Text. Med. - fine grained, hypoc. porphyr., glomer. interlocking (olv, cpx & plg, up to 2 mm), poikil. (cpx).

Phenoc. Olv, euhed. - anhed. : embayed, skeletal, elongated & rounded, up to 2 mm; cr-sp inclus., common. Cpx, euhed. - anhed., embayed, hollow, 0.5 - 1 mm (max. 1.75 mm), olv inclus., very common. Plg, euhed. - subhed., aver. 1 mm (max. 3 mm), twinned (Carls. - Alb. & Alb.), normally - oscill. zoned, glass inclus., interlocking, very common .

Gdm. Olv, cpx, plg & mag microcryst. in brown glass.

82. SN : 20299 RN : Basalt RT : 1982 Bomb Loc. : 19

Text. Med. - fine grained, hypoc. porphyr., glomer. interlocking (up to 3 mm; olv, cpx & plg), vesic.

Phenoc. Olv, euhed. - anhed. : tab, skeletal, elongated & subrounded, hollow, up to 2 mm; cr-sp inclus., common. Cpx, euhed. - subhed., 0.5 - 1 mm (max. 2 mm), hollow, normally zoned, in aggreg., very common. Opx, in cpx core, very rare. Plg, euhed. - subhed., 0.5 - 1 mm (max. 1.5 mm), normally - oscill. zoned, glass inclus., very common.

Gdm. Olv, cpx, mag & plg microcryst. in brown glass.

83. SN : 20300 RN : Basalt RT : 1983 Lava flow Loc. : 19

Text. Med. - fine grained, hypoc. porphyr., interlocking (olv, cpx, plg), poikil. (cpx), vesic.

Phenoc. Olv, euhed. - subhed. : tab., embayed, up to 2.5 mm; cr-sp inclus., opaque rim, very common. Cpx, euhed. - subhed., hollow, up to 2 mm, normally zoned, very common. Plg, euhed. - subhed., aver. 1 mm, twinned (Carls. - Alb. & Alb.), normally - oscill. zoned, inclus. : glass & cpx, common.

Gdm. Olv, cpx, mag & plg microcryst. in brown glass.

84. SN : 20244 RN : Rhyolite RT : Pumice Loc. : 19

Text. Fine grained, hypocryst. porphyr., pumiceous, injected by basalt.

Phenoc. Feldspars, subhed. - anhed, 0.5 - 1 mm, altered : dusty opaque, common. Quartz, euhed., 0.8 - 1 mm, rare.

Gdm. Feldspar, opaque & glass, abundant.

Basalt Fine grained, vitrophyr. Phenoc. : olv, euhed. - subhed., 0.2 - 0.4 mm, cr-sp inclus.; cpx, euhed., up to 1 mm; plg : subhed., 0.5 - 1 mm, twinned (Carls. - Alb.), normally zoned, glass inclus. Gdm. : olv, cpx & plg microcryst. in dark brown glass.

APPENDIX 3 Mineral Chemistry

3.1 Analytical Method

All mineral analyses (893 analysed from 28 rock samples) were made using the Jeol 733 Superprobe (JXA-733) of the Analytical Facility, Geology Department, Victoria University of Wellington. Polished mounts were first carbon-coated, then analysed with an accelerating potential of 25 kV and specimen current of 1.2×10^{-8} amps and beam diameter increased from 3 to 10 microns to reduce Na-loss.

The instrument was initially calibrated against pure oxide and/or mineral standards. Analyses are corrected empirically using the method of Bence and Albee (1968), with alpha correction factors after Kushiro and Nakamura (1970). Additional corrections are made for dead-time, background and probe current drift (Watanabe et al, 1981). In analyses of unknowns, three 10s counts were made on peaks, and single 10s counts on each of two background positions. For glasses, count time was reduced to a single 10s count and two 5s counts on background.

Analytical precision and accuracy was estimated from replicate analyses of mineral standards including Amelia albite, OR-1 (orthoclse), PX-1 (pyroxene), Kakanui augite and Engels hornblende. Statistical parameters for two of these are given in Table 3.1 (compiled by K.Palmer, 1983). For unknowns, only those analyses with oxide totals in the range 98.5 % to 101.0 % were accepted (except for spinels and amphiboles), unless the amount of any non analysed component (i.e. trace elements, volatiles) could not be accurately assessed. For a mineral of known stoichiometry, agreement with the accepted cation total was used to test accuracy.

16 Olivine analyses (analyses number 1126C - 1139C) and 8 Cr-spinel analyses (analyses number 5121 - 5128) of Nye (1988, pers. comm.) are included. These data were resulted from rock sample JPL10 (Gill, 1987, pers. comm.) which is comparable to rock samples 20298 and 20335 as fusiform bombs of high-Mg basalt erupted on 16 September 1982.

Table 3.1 Electron microprobe analyses of two mineral standards.

	PX-1 (21)			OR-1 (18)		
	MEAN	p	REF.	MEAN	p	REF.
SiO_2	53.98	1.22	53.94	64.63	.55	64.39
TiO_2	.23	.06	.26	nd	-	nd
Al^2O_3	.61	.10	.66	18.53	.05	18.58
Cr_2O_3	.23	.08	.21	nd	-	nd
FeO	2.90	.53	2.93	nd	-	nd
MnO	.08	.09	.07	nd	-	nd
MgO	16.80	.37	16.93	nd	-	nd
CaO	24.70	.55	24.55	nd	-	nd
BaO	nd	-	nd	.91	.38	.82
Na_2O	.22	.06	.24	1.05	.11	1.14
K_2O	nd	-	nd	14.90	.62	14.92
Total	99.75		99.79	100.02		99.85

Notes : Analysis by K. Palmer (1983). Number of repeated analyses is given in brackets after the mineral name. Precision (p) is given as one standard deviation. REF = Goldich et al. (1967); n.d. = not detected, (Palmer, 1988, pers. comm.).

3.2 Sample codes

Because of a limitation in the number of available characters in the computer program, sample numbers of rocks analysed in the Analytical Laboratory at the Department of Geology, University of Canterbury are abbreviated. Two first digits in all samples, 20-, are replaced by G. For example 20271-01 becomes G271-01.

For samples analysed in the Analytical Laboratory at the Geology Department, Victoria University of Wellington, numbers are similar to the field number, e.g. VB16. Thus mineral analysis data are listed as VB16-01 etc.

3.3 Numbers of ions

Olivine is analysed on the basis of 4 oxygens, whereas pyroxene (orthopyroxene, clinopyroxene and pigeonite) is analysed on the basis of 6 oxygens. Amphibole is analysed on the basis of 23 oxygens. Plagioclase, Cr-spinel and magnetite are based on 32 oxygens.

3.4 Abbreviations

OLV = Olivine	MAG = Magnetite
OPX = Orthopyroxene	CHR = Cr-spinel
PIG = Pigeonite	HBD = Amphibole
CPX = Clinopyroxene	PLG = Plagioclase

	VB17-01	VB17-02	VB17-03	VB17-04	VB17-05	VB17-06	VB17-07	VB17-08	VB17-09	VB17-10
	OLV	OPX	OPX	CPX	MAG	PLG	PLG	PLG	PLG	PLG
Oxide										
SiO2	38.260	53.168	53.231	52.139	.153	44.745	43.387	43.742	45.748	45.350
Al2O3	.012	.551	.589	1.801	4.188	34.872	35.572	35.115	33.730	34.210
TiO2	.037	.282	.277	.722	11.650	.036	-	-	.037	.014
Feo	21.809	20.811	21.016	13.307	74.783	.498	.511	.516	.681	.689
MnO	.266	.631	.692	.433	.313	-	-	-	.006	-
MgO	38.425	21.898	21.482	14.202	2.623	.040	.011	.044	.074	.036
CaO	.172	1.961	1.898	16.851	.119	18.881	19.429	19.024	17.205	17.977
NaO	-	-	-	.299	-	.793	.678	.844	1.747	1.546
K2O	.026	.022	.024	.026	.018	-	-	.011	.039	.028
NiO	-	-	.038	.075	.065	.003	.023	-	.030	.054
Cr2O3	-	-	-	.003	.044	.029	.026	.019	-	-
Cl	-	-	-	-	.006	.023	-	.025	.010	.011
Total	99.007	99.323	99.246	99.859	93.961	99.919	99.638	99.340	99.307	99.915
Cation										
Si	1.003	1.988	1.994	1.960	.053	8.291	8.089	8.171	8.510	8.405
Al	-	.024	.026	.080	1.713	1.615	7.817	7.730	7.395	7.473
Ti	.001	.008	.008	.020	3.041	.005	-	-	.005	.002
Fe	.478	.651	.658	.418	21.708	.077	.080	.081	.106	.107
Mn	.006	.020	.022	.014	.092	-	-	-	.001	-
Mg	1.502	1.221	1.200	0.796	1.357	.011	.003	.012	.021	.010
Ca	.005	.079	.076	.679	.044	3.748	3.881	3.907	3.429	3.570
Na	-	-	-	.022	-	.285	.245	.306	.630	.556
K	.001	.001	.001	.001	.008	-	-	.003	.009	.007
Ni	-	-	.001	.002	.018	-	.003	-	.010	.008
Cr	-	-	-	-	.012	.004	.004	.003	-	-
Cl	-	-	-	-	.004	.007	-	.004	.001	.003
Total	2.996	3.992	3.986	3.992	28.051	20.044	20.123	20.116	20.116	20.141
Fe/Fe+Mg	.242	.348	.354	.345	.941	.876	.963	.868	.837	.915
Mg#	75.800	-	-	-	-	-	-	-	-	-
Ca#	-	4.000	3.900	35.600	-	-	-	-	-	-
An	-	-	-	-	-	92.900	94.100	92.490	84.300	86.400

VB17-01 Olivine inclusion in plagioclase
VB17-02 Orthopyroxene microcryst
VB17-03 Orthopyroxene microphenocryst
VB17-04 Clinopyroxene microcryst
VB17-05 Magnetite groundmass
VB17-06 Plagioclase phenocryst core
VB17-07 Plagioclase phenocryst core
VB17-08 Plagioclase phenocryst core
VB17-09 Plagioclase phenocryst core
VB17-10 Plagioclase microcryst

	VB17-11	VB17-12	VB17-13	VB17-14	VB17-15	VB17-16	VB17-17	L35-01	L35-02	L35-03
	PLG	PLG	PLG	PLG	PLG	PLG	PLG	OLV	OLV	OLV
Oxide										
SiO2	43.775	52.091	48.570	52.008	51.606	52.345	53.608	38.837	36.829	37.220
Al2O3	35.582	30.173	31.896	29.624	29.676	29.943	28.761	.033	.033	-
TiO2	-	.040	.006	.040	.065	.072	.078	.001	-	.013
Feo	.536	.586	.584	.580	.642	.700	.669	23.035	30.172	29.438
MnO	-	.043	.001	-	-	.001	.035	.420	.578	.610
MgO	.034	.104	.081	.122	.087	.127	.089	37.942	31.745	32.151
CaO	18.850	13.212	15.179	12.785	12.925	12.805	11.544	-	.176	.178
NaO	.774	4.121	3.010	4.235	4.204	4.423	5.027	-	.033	-
K2O	.014	.046	.046	.057	.078	.071	.080	.011	.009	.003
NiO	.018	.062	.044	-	.015	-	.063	-	-	-
Cr2O3	.083	.013	.056	-	-	-	.075	-	.068	-
Cl	.002	-	-	-	.014	.010	-	.016	.054	-
Total	99.666	100.493	99.472	99.451	99.311	100.496	100.030	100.295	99.698	99.614
Cation										
Si	8.143	9.444	8.960	9.512	9.467	9.487	9.729	1.009	1.002	1.008
Al	7.801	6.447	6.935	6.386	6.416	6.396	6.151	.001	.001	-
Ti	-	.006	.001	.006	.009	.010	.011	-	-	-
Fe	.083	.089	.090	.089	.099	.106	.101	.501	.686	.667
Mn	-	.007	-	-	-	-	.005	.009	.013	.014
Mg	.009	.028	.022	.033	.024	.034	.024	1.470	1.287	1.298
Ca	3.757	2.566	3.000	2.505	2.540	2.487	2.245	-	.005	.005
Na	.279	1.449	1.077	1.502	1.495	1.554	1.769	-	.002	-
K	.003	.011	.011	.013	.018	.016	.018	-	-	-
Ni	.003	.009	.007	-	.005	-	.009	-	-	-
Cr	.012	.002	.008	-	-	-	.011	-	.001	-
Cl	.001	-	-	-	.002	.003	-	.001	.002	-
Total	20.092	20.056	20.111	20.047	20.076	20.093	20.073	2.991	3.001	2.992
Fe/Fe+Mg	.899	.760	.801	.728	.806	.755	.807	.254	.348	.339
Mg*	-	-	-	-	-	-	-	74.600	65.200	66.100
Ca*	-	-	-	-	-	-	-	-	-	-
An	93.000	63.700	73.400	62.300	62.700	61.300	55.700	-	-	-

VB17-11 Plagioclase microcryst
VB17-12 Plagioclase phenocryst rim
VB17-13 Plagioclase phenocryst mantle
VB17-14 Plagioclase phenocryst rim
VB17-15 Plagioclase phenocryst rim
VB17-16 Plagioclase microphenocryst
VB17-17 Plagioclase microphenocryst
L35-01 Anhedral olivine phenocryst
L35-02 Anhedral olivine phenocryst
L35-03 Anhedral olivine phenocryst

	L35-04	L35-05	L35-06	L35-07	L35-08	L35-09	L35-10	L35-11	L35-12	L35-13
	OPX	CPX	CPX	CPX	CPX	CPX	CPX	CPX	CPX	CPX
Oxide										
SiO2	53.756	50.923	50.762	50.203	52.394	52.220	50.045	51.388	51.719	52.233
Al2O3	.585	2.684	2.405	5.627	1.891	2.088	3.484	2.219	2.625	2.424
TiO2	.268	.860	.631	.743	.448	.428	.943	.641	.471	.618
FeO	19.344	8.591	8.998	6.493	8.539	9.100	11.622	10.030	9.029	9.301
MnO	.670	.321	.299	.140	.314	.327	.422	.362	.323	.333
MgO	22.864	14.762	15.203	13.702	15.407	15.062	13.757	15.087	14.812	14.683
CaO	1.870	20.815	20.510	23.056	20.191	20.376	18.847	19.184	20.445	19.935
NaO	.039	.319	.336	.297	.264	.327	.349	.351	.338	.370
K2O	-	-	.001	.013	.001	-	-	.028	.010	-
NiO	.020	.069	-	-	-	-	.019	-	.087	.027
Cr2O3	-	.011	.093	.179	.032	.086	.037	-	.148	.052
Cl	.014	-	-	.006	.004	.013	-	.002	-	-
Total	99.430	99.355	99.239	100.458	99.485	100.026	99.524	99.291	100.007	99.975
Cation										
Si	1.993	1.909	1.909	1.825	1.951	1.942	1.890	1.930	1.925	1.941
Al	.026	.119	.107	.244	.082	.092	.155	.098	.115	.106
Ti	.007	.024	.018	.021	.012	.012	.027	.018	.013	.017
Fe	.600	.269	.283	.201	.265	.283	.367	.315	.281	.289
Mn	.021	.010	.010	.002	.010	.010	.014	.012	.010	.010
Mg	1.264	.825	.852	.753	.855	.835	.775	.845	.822	.814
Ca	.074	.836	.826	.910	.805	.812	.763	.772	.815	.794
Na	.003	.023	.025	.021	.019	.024	.026	.026	.024	.027
K	-	-	-	-	-	-	-	.001	-	-
Ni	.001	.002	-	-	-	-	.001	-	.003	.001
Cr	-	-	.003	.004	.001	.086	.001	-	.004	.002
Cl	.001	-	-	-	-	.013	-	-	-	-
Total	3.989	4.019	4.031	3.981	4.000	4.012	4.018	4.016	4.014	4.001
Fe/Fe+Mg	.322	.246	.249	.210	.237	.253	.322	.272	.255	.262
Mg*	-	-	-	-	-	-	-	-	-	-
Ca*	3.800	43.100	41.900	48.800	41.602	41.900	39.800	39.700	42.272	41.636
An	-	-	-	-	-	-	-	-	-	-

	L35-14	L35-15	L35-16	L35-17	L35-18	L35-19	L35-20	L35-21	L35-22	L35-23
	CPX	MAG	MAG	PLG	PLG	PLG	PLG	PLG	PLG	PLG
Oxide										
SiO2	51.264	.174	.123	45.038	44.353	51.941	52.324	51.907	52.627	52.577
Al2O3	2.499	4.040	3.622	34.980	35.415	29.373	29.741	29.855	29.782	29.419
TiO2	.610	11.744	11.685	-	.002	.068	.051	.040	.066	.114
FeO	9.312	73.668	76.176	.506	.468	.747	.811	.823	.848	.807
MnO	.364	.507	.431	.082	.059	-	-	.010	-	-
MgO	14.717	3.300	2.815	.044	.079	.062	.068	.050	.030	.042
CaO	19.975	.054	-	18.464	18.826	13.524	12.672	12.971	12.625	12.533
NaO	.326	-	-	1.020	.661	3.857	4.283	4.204	4.376	4.183
K2O	-	.037	.019	.036	.020	.159	.186	.200	.234	.117
NiO	-	.114	.041	.074	.021	-	-	-	.034	.116
Cr2O3	.035	.065	.111	-	-	-	.065	.011	-	-
Cl	.001	-	.020	.046	-	-	.001	.009	.016	-
Total	99.102	93.701	95.042	100.291	99.905	99.731	100.201	100.078	100.636	99.908
Cation										
Si	1.927	.060	.042	8.315	8.217	9.500	9.513	9.463	9.531	9.575
Al	.111	1.650	1.474	7.611	7.733	6.322	6.373	6.414	6.356	6.314
Ti	.017	3.060	3.034	-	-	.009	.007	.005	.009	.016
Fe	.293	21.346	21.999	.078	.073	.114	.123	.125	.128	.123
Mn	.012	.149	.126	.013	.009	-	-	.001	-	-
Mg	.824	1.704	1.449	.012	.022	.017	.018	.014	.008	.011
Ca	.804	.020	-	3.652	3.737	2.650	2.468	2.533	2.450	2.445
Na	.024	-	-	.365	.238	1.368	1.510	1.486	1.537	1.477
K	-	.016	.008	.009	.005	.037	.043	.046	.054	.027
Ni	-	.032	.011	.011	.003	-	-	-	.005	.027
Cr	.001	.018	.030	-	-	-	.009	.002	-	-
Cl	-	-	.012	.014	-	-	-	.003	.005	-
Total	4.012	28.054	28.187	20.081	20.037	20.027	20.066	20.093	20.082	20.005
Fe/Fe+Mg	.262	.926	.938	.865	.768	.871	.871	.902	.941	.916
Mg*	-	-	-	-	-	-	-	-	-	-
Ca*	35.600	-	-	-	-	-	-	-	-	-
An	-	-	-	90.710	93.890	65.350	61.380	62.310	60.630	61.910

L35-04 Orthopyro ene in core of clinopyroxene
L35-05 Clinopyro ene phenocryst
L35-06 Clinopyro ene phenocryst
L35-07 Clinopyro ene phenocryst
L35-08 Clinopyro ene phenocryst
L35-09 Clinopyro ene phenocryst
L35-10 Clinopyro ene phenocryst
L35-11 Clinopyro ene phenocryst
L35-12 Clinopyroxene phenocryst
L35-13 Clinopyroxene phenocryst

L35-14 Clinopyroxene groundmass
L35-15 Magnetite microphenocryst
L35-16 Magnetite microphenocryst
L35-17 Plagioclase phenocryst core
L35-18 Plagioclase phenocryst core
L35-19 Plagioclase phenocryst rim
L35-20 Plagioclase phenocryst rim
L35-21 Plagioclase groundmass
L35-22 Plagioclase groundmass
L35-23 Plagioclase inclusion

	VB10-01	VB10-02	VB10-03	VB10-04	VB10-05	VB10-06	VB10-07	VB10-08	VB10-09	VB10-10
	OLV	OLV	OLV	OLV	OLV	OLV	CPX	CPX	CPX	PIG
Oxide										
SiO2	37.594	37.785	37.443	37.373	37.334	38.630	52.237	52.270	50.939	52.460
Al2O3	.019	.037	.028	.024	.049	.018	1.484	2.518	3.393	.579
TiO2	.037	.033	.103	.063	.044	-	.721	.514	.572	.403
FeO	26.216	25.709	26.410	26.123	26.576	21.805	11.709	7.760	7.837	21.521
MnO	.423	.417	.433	.453	.477	.341	.456	.178	.281	.629
MgO	35.314	35.100	34.973	35.190	34.468	38.308	14.618	14.930	14.516	19.806
CaO	.175	.161	.151	.144	.292	.191	18.703	20.847	21.108	3.837
NaO	-	-	-	-	-	-	.331	.282	.308	.013
K2O	.004	.006	.013	-	.009	.014	-	-	.085	-
NiO	.014	.046	.097	-	.079	.060	-	-	-	-
Cr2O3	.009	-	-	-	-	-	.014	.150	.224	.027
Cl	-	-	.011	.001	.010	.007	-	-	.003	-
Total	99.805	99.293	99.663	99.372	99.337	99.375	100.272	99.450	99.268	99.275
Cation										
Si	1.000	1.007	.999	.999	1.001	1.009	1.952	1.943	1.905	1.983
Al	.001	.001	.001	.001	.001	.001	.065	.110	.150	.026
Ti	.001	.001	.002	.002	.001	-	.020	.014	.016	.011
Fe	.583	.573	.589	.583	.596	.476	.366	.241	.245	.680
Mn	.010	.009	.010	.001	.011	.008	.014	.006	.009	.020
Mg	1.400	1.395	1.391	1.401	1.377	1.491	.815	.827	.809	1.116
Ca	.005	.005	.004	.004	.008	.005	.749	.830	.846	.155
Na	-	-	-	-	-	-	.024	.020	.022	.001
K	-	-	-	-	-	-	-	-	.004	-
Ni	-	.001	.002	-	.002	.001	-	-	-	-
Cr	-	-	-	-	-	-	-	.004	.007	.001
Cl	-	-	.001	-	-	-	-	-	-	-
Total	2.999	2.992	2.999	2.991	2.997	2.992	4.006	3.996	4.014	3.993
Fe/Fe+Mg	.294	.291	.298	.294	.302	.242	.310	.226	.232	.379
Mg*	70.600	70.900	70.200	70.900	69.800	75.800	-	-	-	-
Ca*	-	-	-	-	-	-	38.500	43.600	44.300	7.900
An	-	-	-	-	-	-	-	-	-	-

VB10-01 Subhedral olivine phenocryst
VB10-02 Anhedral olivine phenocryst
VB10-03 Rounded olivine phenocryst
VB10-04 Rounded olivine phenocryst
VB10-05 Subhedral olivine phenocryst
VB10-06 olivine inclusion in clinopyroxene
VB10-07 Clinopyroxene phenocryst
VB10-08 Clinopyroxene phenocryst
VB10-09 Clinopyroxene phenocryst
VB10-10 Pigeonite groundmass

	VB10-11	VB10-12	VB10-13	VB10-14	VB10-15	VB10-16	VB10-17	VB10-18	VB10-19	VB10-20
	PIG	MAG	MAG	MAG	PLG	PLG	PLG	PLG	PLG	PLG
Oxide										
SiO2	52.606	.140	.157	.176	46.733	46.894	47.107	47.620	47.511	47.786
Al2O3	.543	2.598	2.502	2.643	33.956	33.400	33.000	32.642	33.268	32.060
TiO2	.424	15.626	16.639	16.328	.005	.039	.052	.057	-	.018
FeO	22.156	73.101	73.448	72.376	.632	.641	.676	.606	.609	.631
MnO	.653	.437	.420	.441	-	-	.067	.029	-	-
MgO	18.739	2.954	2.155	2.232	-	.072	.094	.085	.061	.093
CaO	4.043	.159	.060	.087	17.137	16.747	16.354	16.015	16.544	15.768
NaO	.062	-	-	-	1.735	2.066	2.161	2.483	1.952	2.623
K2O	-	.003	.032	.070	-	-	.037	.056	-	-
NiO	-	-	.024	.055	.009	-	.002	-	-	.118
Cr2O3	.040	.005	.056	.012	-	-	.011	.024	.046	-
Cl	-	-	.017	-	-	-	.009	.003	-	.043
Total	99.267	95.023	95.511	94.421	100.206	99.860	99.570	99.620	99.990	99.139
Cation										
Si	1.995	.047	.053	.060	8.591	8.650	8.711	8.792	8.731	8.866
Al	.040	1.037	.994	1.060	7.356	7.261	7.192	7.103	7.205	7.011
Ti	.020	3.981	4.218	4.180	.001	.005	.007	.008	-	.002
Fe	1.170	20.710	20.706	20.603	.097	.099	.104	.094	.096	.098
Mn	.035	.125	.120	.127	-	-	.011	.005	-	-
Mg	1.765	1.492	1.083	1.133	-	.020	.026	.023	.016	.026
Ca	.272	.058	.022	.032	3.375	3.310	3.240	3.168	3.259	3.134
Na	.007	-	-	-	.618	.739	.775	.889	.693	.943
K	-	.001	.014	.031	-	-	.009	.013	-	-
Ni	-	-	.006	.015	.001	-	-	-	-	.018
Cr	.002	.001	.015	.003	-	-	.002	.003	.005	-
Cl	-	-	.010	-	-	-	.003	.001	-	.013
Total	5.306	27.453	27.241	27.244	20.040	20.084	20.080	20.099	20.005	20.112
Fe/Fe+Mg	.399	.933	.950	.948	1.000	.833	.801	.800	.849	.791
Mg*	-	-	-	-	-	-	-	-	-	-
Ca*	8.400	-	-	-	-	-	-	-	-	-
An	-	-	-	-	84.500	81.700	80.500	77.800	82.500	76.900

VB10-11 Pigeonite groundmass
VB10-12 Magnetite microphenocryst
VB10-13 Magnetite microphenocryst
VB10-14 Magnetite groundmass
VB10-15 Plagioclase phenocryst core
VB10-16 Plagioclase phenocryst core
VB10-17 Plagioclase phenocryst core
VB10-18 Plagioclase microphenocryst
VB10-19 Plagioclase phenocryst core
VB10-20 Plagioclase microphenocryst

	VB10-21	VB10-22	VB10-23	G271-01	G271-02	G271-03	G271-04	G271-05	G271-06	G271-07
	PLG	PLG	PLG	OLV	OLV	OPX	OPX	OPX	CPX	CPX
Oxide										
SiO2	47.174	55.624	53.010	37.107	37.328	52.084	52.148	53.440	50.437	50.828
Al203	32.835	28.004	28.955	-	.013	1.960	2.205	.807	2.812	2.409
TiO2	-	.104	.072	-	-	.259	.404	.342	.616	.571
Feo	.520	.721	.838	26.120	25.756	18.324	18.223	17.794	10.646	10.851
MnO	.021	.002	-	.422	.634	.511	.547	.543	.355	.402
MgO	.059	.009	.118	36.048	36.569	24.846	25.137	25.088	14.683	15.221
CaO	16.552	10.669	12.460	.117	.332	1.807	1.813	1.753	19.293	18.225
NaO	2.158	5.334	4.570	.030	-	.041	.044	.017	.344	.496
K2O	.050	.192	.101	.019	.094	.013	-	-	-	.003
NiO	.070	.002	-	.099	.085	.065	-	.015	.027	-
Cr203	-	-	.053	.095	.019	.009	.006	-	-	.083
Cl	.015	.006	-	.029	-	-	.034	-	-	.083
Total	99.454	100.757	100.176	100.086	100.830	99.919	100.561	99.799	99.213	99.172
Cation										
Si	8.733	9.978	9.633	.986	.984	1.919	1.912	.961	1.905	1.918
Al	7.164	5.921	6.201	-	-	.085	.088	.035	.125	.107
Ti	-	.014	.010	-	-	.007	.011	.009	.017	.016
Fe	.080	.108	.127	.581	.567	.565	.559	.546	.336	.342
Mn	.003	-	-	.009	.014	.016	.017	.017	.011	.013
Mg	.016	.026	.032	1.428	1.437	1.365	1.374	1.373	.827	.856
Ca	3.283	2.051	2.426	.003	.009	.071	.071	.069	.781	.737
Na	.775	1.855	1.610	.001	-	.003	.003	.001	.025	.036
K	.012	.044	.023	-	.003	.001	-	-	-	-
Ni	.010	-	-	.002	.002	.002	-	-	.001	-
Cr	-	-	.008	.002	-	-	-	-	-	.002
Cl	.005	.002	-	.001	-	-	.002	-	-	.005
Total	20.083	19.999	20.070	3.013	3.016	4.033	4.037	4.012	4.028	4.034
Fe/Fe+Mg	.831	.804	.800	.283	.289	.293	.289	.285	.289	.286
Mg*	-	-	-	71.700	71.100	-	-	-	-	-
Ca*	-	-	-	-	-	3.800	3.500	3.500	39.900	37.800
An	80.700	51.900	59.800	-	-	-	-	-	-	-

	G271-08	G271-09	G271-10	G271-11	G271-12	G271-13	G271-14	G271-15	G271-16	G271-17
	CPX	CPX	CPX	CPX	CPX	OPX	MAG	MAG	MAG	MAG
Oxide										
SiO2	50.833	50.732	50.830	51.055	51.760	52.534	.130	.106	.106	.118
Al203	2.405	3.232	2.809	2.773	1.959	1.772	3.789	3.841	5.570	2.853
TiO2	.651	.655	.619	.604	.548	.402	13.819	14.606	11.197	16.782
Feo	10.299	10.644	10.871	10.670	11.275	18.149	75.287	74.992	74.272	74.720
MnO	.280	.376	.389	.358	.382	.394	.384	.378	.351	.432
MgO	15.052	14.625	15.210	14.887	16.040	23.998	1.623	1.955	3.854	1.550
CaO	19.174	18.951	18.724	18.934	17.818	1.868	.079	.001	.032	.030
NaO	.379	.326	.295	.426	.276	.003	-	-	.016	.098
K2O	-	.005	-	.039	.021	-	-	.009	-	-
NiO	-	-	.031	.008	-	.041	.052	-	-	.101
Cr203	.014	.023	.075	-	.011	.041	.157	.131	.038	.115
Cl	.074	-	.032	.003	-	-	.010	.007	.021	.024
Total	99.161	99.569	99.885	99.757	100.090	99.202	99.098	99.703	99.703	100.199
Cation										
Si	1.917	1.904	1.905	1.914	1.931	1.944	.044	.036	.036	.039
Al	.107	.143	.124	.123	.086	.077	1.524	1.523	2.208	1.121
Ti	.018	.018	.017	.017	.015	.011	3.547	3.697	2.832	4.205
Fe	.325	.334	.341	.334	.352	.562	21.488	21.107	20.889	20.823
Mn	.009	.012	.012	.011	.012	.012	.111	.108	.100	.122
Mg	.846	.818	.850	.832	.892	1.324	.826	.981	1.932	.770
Ca	.775	.762	.752	.760	.712	.074	.029	-	.011	.011
Na	.028	.024	.021	.031	.020	-	-	-	.010	.063
K	-	-	-	.002	.001	-	-	.004	-	-
Ni	-	-	.001	-	-	.001	.014	-	-	.027
Cr	-	.001	.002	-	-	.001	.042	.035	.010	.030
Cl	.005	-	.002	-	-	-	.006	.004	.012	.013
Total	4.030	4.017	4.027	4.025	4.021	4.006	27.632	27.494	28.040	27.225
Fe/Fe+Mg	.277	.290	.286	.287	.283	.298	.963	.956	.915	.964
Mg*	-	-	-	-	-	-	-	-	-	-
Ca*	39.400	39.600	38.500	39.200	36.200	3.753	-	-	-	-
An	-	-	-	-	-	-	-	-	-	-

VB10-21 Plagiocla e phenocryst core
VB10-22 Plagiocla e groundmass
VB10-23 Plagiocla e groundmass
G271-01 Anhedral livine microphenocryst
G271-02 Anhedral livine microphenocryst
G271-03 Orthopyro ene microphenocryst
G271-04 Orthopyro ene microphenocryst
G271-05 Orthopyro ene microphenocryst
G271-06 Anhedral clinopyroxene phenocryst
G271-07 Anhedral clinopyroxene phenocryst

G271-08 Anhedral clinopyroxene phenocryst
G271-09 Clinopyroxene phenocryst core
G271-10 Clinopyroxene phenocryst core
G271-11 Clinopyroxene inclusion in clinopyroxene
G271-12 Clinopyroxene microphenocryst
G271-13 Orthopyroxene groundmass
G271-14 Magnetite microphenocryst
G271-15 Magnetite microphenocryst
G271-16 Magnetite microphenocryst
G271-17 Magnetite microphenocryst

	G271-18	G271-19	G271-20	G271-21	G271-22	G271-23	G271-24	G271-25	G271-26	G271-27
	PLG	PLG	PLG	PLG	PLG	PLG	PLG	PLG	PLG	PLG
Oxide										
SiO2	45.904	45.101	43.181	44.611	52.214	49.532	44.223	50.480	51.121	45.882
Al2O3	34.633	35.102	36.030	35.550	29.840	31.564	35.665	30.597	31.064	34.675
TiO2	.008	.015	.020	-	.001	.002	.006	.026	.067	.042
FeO	.498	.588	.332	.459	.748	.598	.465	.800	.746	.615
MnO	.038	-	.021	-	.002	.037	.085	-	-	.006
MgO	.055	.052	.029	.045	.118	.058	.088	.123	.050	.058
CaO	17.753	18.267	19.329	19.390	13.032	15.314	18.975	13.845	14.073	17.912
NaO	1.339	1.067	.538	.694	4.085	3.056	.678	3.853	3.473	1.226
K2O	-	.001	.005	.002	.077	.043	.042	.098	-	.011
NiO	-	-	.038	.052	.034	-	-	-	.025	-
Cr2O3	-	.009	-	.014	-	.040	.051	.029	.032	-
Cl	-	.002	-	-	.010	.013	-	.002	.002	-
Total	100.228	100.204	99.523	100.817	100.162	100.257	100.278	99.853	100.653	100.427
Cation	Cation									
Si	8.447	8.320	8.048	8.203	9.494	9.061	8.172	9.251	9.270	8.432
Al	7.511	7.632	7.914	7.704	6.395	6.805	7.767	6.609	6.639	7.510
Ti	.001	.002	.003	-	-	0.000	.001	.004	.009	.006
Fe	.077	.091	.052	.071	.114	.091	.072	.123	.113	.095
Mn	.006	-	.003	-	-	.006	.013	-	-	.001
Mg	.015	.014	.008	.012	.032	.016	.024	.034	.014	.016
Ca	3.500	3.610	3.860	3.820	2.539	3.001	3.757	2.719	2.734	3.527
Na	.478	.382	.194	.248	1.440	1.084	.243	1.369	1.221	.437
K	-	-	.001	.001	.018	.010	.010	.023	-	.003
Ni	-	-	.006	.008	.005	-	-	-	.004	-
Cr	-	.001	-	.002	-	.006	.007	.004	.005	-
Cl	-	.001	-	-	.003	.004	-	.001	.001	-
Total	20.035	20.053	20.090	20.068	20.040	20.084	20.066	20.135	20.010	20.027
Fe/Fe+Mg	.835	.865	.867	.852	.780	.853	.748	.785	.893	.855
Mg*	-	-	-	-	-	-	-	-	-	-
Ca*	-	-	-	-	-	-	-	-	-	-
An	87.980	90.430	86.700	93.880	93.690	73.280	93.690	66.140	69.130	88.910

	G271-28	G271-29	G271-30	G286-01	G286-02	G286-03	G286-04	G286-05	G286-06	G286-07
	PLG	PLG	PLG	OLV	OLV	OLV	OLV	CPX	CPX	CPX
Oxide										
SiO2	50.320	52.018	53.593	37.640	37.177	38.321	36.580	50.171	51.885	50.760
Al2O3	31.679	29.926	28.678	.004	-	.002	.005	5.564	3.285	3.570
TiO2	.073	.009	.060	.016	.042	.022	.060	.734	.398	.671
FeO	.702	.724	.936	25.006	26.718	24.738	30.416	6.424	4.441	8.043
MnO	.013	.072	.034	-	.626	.364	.422	.137	.147	.213
MgO	.077	.124	.153	37.489	35.723	36.925	32.306	14.583	16.072	14.970
CaO	14.391	13.481	11.699	.199	.131	.154	.211	22.481	22.845	21.318
NaO	3.296	3.868	4.892	-	-	-	-	.278	-	.300
K2O	.041	.075	.141	-	.360	-	-	-	-	.020
NiO	.036	-	.047	.022	.116	.036	.030	.036	-	.031
Cr2O3	-	-	-	-	-	-	.010	.169	.619	.138
Cl	-	-	.039	.015	.001	-	.017	-	-	-
Total	100.628	100.297	100.272	100.391	100.570	100.562	100.057	100.577	99.692	100.034
Cation										
Si	9.142	9.455	9.721	.988	.986	1.002	.992	1.846	1.908	1.887
Al	6.783	6.411	6.131	-	-	-	-	.241	.142	.156
Ti	.010	.001	.008	-	.001	-	.001	.020	.011	.019
Fe	.107	.110	.142	.549	.593	.541	.690	.198	.137	.250
Mn	.002	.011	.005	0.000	.014	.008	.010	.004	.005	.007
Mg	.021	.034	.041	1.467	1.413	1.440	1.306	.800	.881	.830
Ca	2.801	2.626	2.274	.006	.004	.004	.006	.886	.900	.849
Na	1.161	1.363	1.720	-	-	-	-	.020	-	.022
K	.009	.017	.033	-	.001	-	-	-	-	.001
Ni	.005	-	.007	-	.002	.001	.001	.001	-	.004
Cr	-	-	-	-	-	-	-	.005	.018	.004
Cl	-	-	.012	.001	-	-	.001	-	-	-
Total	20.042	20.028	20.094	3.012	3.014	2.997	3.007	4.021	4.001	4.025
Fe/Fe+Mg	.837	.766	.775	.277	.296	.273	.346	.198	.134	.232
Mg*	-	-	-	72.300	70.400	72.700	65.400	-	-	-
Ca*	-	-	-	-	-	-	-	46.900	46.800	43.900
An	70.540	65.550	56.470	-	-	-	-	-	-	-

G271-18 G271-28 Plagioclase microphenocryst
G271-19 G271-29 Plagioclase microphenocryst rim
G271-20 G271-30 Plagioclase groundmass
G271-21 G286-01 Olivine phenocryst
G271-22 G286-02 Olivine phenocryst
G271-23 G286-03 Olivine microphenocryst core
G271-24 G286-04 Olivine microphenocryst coreoned cor
G271-25 G286-05 Clinopyroxene phenocryst coreed core
G271-26 G286-06 Clinopyroxene phenocryst coreed core
G271-27 G286-07 Clinopyroxene phenocryst rim

G271-28 Plagioclase microphenocryst
G271-29 Plagioclase microphenocryst rim
G271-30 Plagioclase groundmass
G286-01 Olivine phenocryst
G286-02 Olivine phenocryst
G286-03 Olivine microphenocryst cor
G286-04 Olivine microphenocryst cor
G286-05 Clinopyroxene phenocryst co e
G286-06 Clinopyroxene phenocryst core
G286-07 Clinopyroxene phenocryst rim

	G286-08	G286-09	G286-10	G286-11	G286-12	G286-13	G286-14	G286-15	G286-16	G286-17
	CPX	CPX	CPX	CPX	PIG	PIG	MAG	PLG	PLG	PLG
Oxide										
SiO2	51.973	51.531	51.401	51.158	52.499	51.959	.099	45.561	46.770	45.330
Al203	1.589	1.633	2.082	1.916	.976	.594	.931	34.510	34.112	34.658
TiO2	.583	.553	.607	.756	.624	.382	19.279	-	-	.006
Feo	10.812	11.684	10.072	15.760	19.980	23.666	75.234	.645	.620	.532
MnO	.456	.496	.439	.401	.628	.705	.497	.033	-	-
MgO	16.145	16.565	14.727	13.840	20.006	16.988	.660	.091	.069	.072
CaO	18.461	16.387	19.684	15.416	4.221	4.746	.030	17.429	17.272	18.040
NaO	.217	.239	.290	.237	.035	.062	-	1.650	1.687	1.182
K2O	-	-	.003	.012	.024	.037	-	.024	.038	.026
NiO	-	.054	.001	.029	.037	.025	-	-	-	-
Cr203	-	-	.028	.029	.046	-	.133	-	.046	.014
Cl	.009	.027	-	-	.003	.025	-	.007	-	-
Total	100.245	99.169	99.334	99.554	99.079	99.189	99.931	99.950	100.614	99.860
Cation										
Si	1.935	1.939	1.933	1.945	1.976	1.992	.033	8.422	8.568	8.385
Al	.070	.072	.092	.085	.043	.027	.368	7.518	7.365	7.556
Ti	.016	.016	.017	.021	.018	.010	4.865	-	-	.001
Fe	.337	.368	.317	.501	.629	.759	21.115	.100	.095	.082
Mn	.014	.016	.014	.013	.020	.022	.141	.005	-	-
Mg	.896	.929	.826	.784	1.123	.972	.330	.025	.019	.020
Ca	.737	.660	.793	.628	.170	.195	.011	3.452	3.390	3.575
Na	.016	.017	.021	.018	.003	.004	-	.592	.599	.424
K	-	-	-	-	.001	.001	-	.006	.009	.006
Ni	-	.002	-	.001	.001	.001	-	-	-	-
Cr	-	-	.001	.001	.001	-	.350	-	.007	.002
Cl	.001	.002	-	-	-	.001	-	.002	-	-
Total	4.022	4.020	4.014	3.997	3.986	3.984	26.900	20.120	20.051	20.051
Fe/Fe+Mg	.273	.284	.277	.390	.359	.439	.985	.799	.835	.805
Mg*	-	-	-	-	-	-	-	-	-	-
Ca*	37.100	33.400	40.700	32.600	8.800	10.000	-	-	-	-
An	-	-	-	-	-	-	-	85.230	84.790	89.260

G286-08 Clinopyro ene groundmass
G286-09 Clinopyro ene groundmass
G286-10 Clinopyro ene groundmass
G286-11 Clinopyroxene groundmass
G286-12 Pigeonite groundmass
G286-13 Pigeonite groundmass
G286-14 Magnetite groundmass
G286-15 Plagioclase phenocryst core
G286-16 Plagioclase phenocryst core
G286-17 Plagioclase phenocryst core

	G286-18	G286-19	G286-20	G286-21	G286-22	G286-23	G286-24	G347-01	G347-02	G347-03
	PLG	PLG	PLG	PLG	PLG	PLG	PLG	OPX	OPX	OPX
Oxide										
SiO2	52.043	45.530	56.645	45.775	52.596	52.904	53.228	54.206	52.333	53.378
Al203	29.271	34.462	26.662	34.575	29.785	29.310	29.055	.780	1.358	1.139
TiO2	.161	.016	.102	.006	-	.093	.060	.171	.157	.176
Feo	.740	.506	.772	.496	.712	.932	1.052	19.523	19.439	19.731
MnO	.043	-	-	.018	-	.008	.015	.689	.708	.599
MgO	.092	.061	.082	.042	.060	.069	.065	23.106	23.176	23.357
CaO	12.797	18.170	9.542	18.123	12.818	12.139	12.161	1.524	1.554	1.545
NaO	4.240	1.234	5.657	1.314	4.241	4.592	4.582	-	.171	.068
K2O	.145	.017	.288	-	.158	.177	.177	-	.003	-
NiO	.143	.061	-	-	-	-	-	.040	-	-
Cr203	-	-	-	.067	.008	.033	-	-	.198	-
Cl	-	.012	-	.001	-	.002	-	-	.131	.008
Total	99.675	100.069	99.750	100.417	100.378	100.259	100.395	100.039	99.228	100.001
Cation										
Si	9.522	8.410	10.227	8.421	9.536	9.605	9.651	1.994	1.953	1.970
Al	6.312	7.502	5.673	7.496	6.365	6.271	6.209	.034	.060	.050
Ti	.022	.002	.014	.001	-	.013	.008	.005	.004	.005
Fe	.113	.078	.117	.076	.108	.141	.160	.601	.606	.609
Mn	.007	-	-	.003	-	.001	.002	.021	.022	.019
Mg	.025	.017	.022	.011	.016	.019	.018	1.267	1.290	1.285
Ca	2.509	3.596	1.846	3.572	2.490	2.361	2.362	.060	.061	.061
Na	1.504	.442	1.980	.469	1.491	1.616	1.611	-	.012	.005
K	.034	.004	.066	-	.036	.041	.041	-	-	-
Ni	.021	.009	-	-	-	-	-	.001	-	-
Cr	-	-	-	.010	.001	.005	-	-	.006	-
Cl	-	.004	-	-	-	.001	-	-	.008	.001
Total	20.069	20.064	19.945	20.060	20.044	20.074	20.062	3.984	4.022	4.003
Fe/Fe+Mg	.818	.823	.841	.869	.869	.883	.901	.322	.320	.322
Mg*	-	-	-	-	-	-	-	-	-	-
Ca*	-	-	-	-	-	-	-	3.100	3.100	3.100
An	62.000	88.970	47.430	88.390	61.990	58.760	58.840	-	-	-

G286-18 Plagioclase phenocryst rim
G286-19 Plagioclase phenocryst core
G286-20 Plagioclase phenocryst rim
G286-21 Plagioclase microphenocryst core
G286-22 Plagioclase microphenocryst
G286-23 Plagioclase groundmass
G286-24 Plagioclase groundmass
G347-01 Orthopyroxene phenocryst core
G347-02 Orthopyroxene phenocryst core
G347-03 Orthopyroxene phenocryst core

	G347-04	G347-05	G347-06	G347-07	G347-08	G347-09	G347-10	G347-11	G347-12	G347-13
	OPX	OPX	OPX	OPX	OPX	OPX	OPX	OPX	PIG	PIG
Oxide										
SiO2	53.639	53.200	53.476	53.817	53.878	53.259	53.299	53.024	52.656	53.146
Al2O3	.735	1.211	1.244	.777	1.354	1.710	1.457	1.358	.480	2.162
TiO2	.191	.235	.174	.203	.167	-	.277	.261	.219	.383
FeO	19.354	19.973	19.188	19.608	19.203	18.549	19.003	19.846	26.743	23.851
MnO	.731	.662	.615	.722	.522	.577	.414	.699	1.004	.921
MgO	23.708	23.136	23.622	23.222	23.535	24.195	23.814	23.084	15.712	15.464
CaO	1.569	1.483	1.580	1.613	1.290	1.508	1.633	1.661	3.065	3.600
NaO	-	.046	.044	.047	.048	.105	.013	.055	.052	.066
K2O	.012	-	-	-	-	.020	-	-	.043	.036
NiO	.046	-	.006	.001	-	-	-	.004	.025	.095
Cr2O3	.009	.051	.021	.007	-	-	.086	-	-	.031
Cl	.004	-	.011	-	-	.073	.006	.007	-	-
Total	99.998	99.997	99.981	100.017	99.997	99.996	100.002	99.999	99.999	99.755
Cation										
Si	1.977	1.966	1.969	1.984	1.648	1.956	1.960	1.960	2.019	2.011
Al	.032	.053	.054	.034	.049	.074	.063	.059	.022	.096
Ti	.005	.007	.005	.006	.004	-	.008	.007	.006	.011
Fe	.591	.617	.591	.605	.491	.570	.584	.614	.857	.755
Mn	.023	.021	.019	.023	.014	.018	.013	.022	.033	.030
Mg	1.303	1.275	1.296	1.276	1.073	1.325	1.305	1.272	.898	.873
Ca	.062	.059	.062	.064	.042	.059	.064	.066	.126	.146
Na	-	.003	.003	.003	.003	.007	.001	.004	.004	.005
K	.001	-	-	-	-	.001	-	-	.002	.002
Ni	.001	-	-	-	-	-	-	-	.001	.003
Cr	-	.002	.001	-	-	-	.003	-	-	.001
Cl	-	-	.001	-	-	.004	-	-	-	-
Total	4.002	4.002	4.001	3.994	3.325	4.015	4.001	4.005	3.967	3.932
Fe/Fe+Mg	.314	.326	.313	.321	.314	.301	.309	.325	.488	.464
Mg*	-	-	-	-	-	-	-	-	-	-
Ca*	3.100	3.000	3.100	3.100	3.300	2.600	3.000	3.300	6.600	8.100
An	-	-	-	-	-	-	-	-	-	-

G347-04 Orthopyroxene phenocryst core
G347-05 Orthopyroxene phenocryst core
G347-06 Core of intergrown orthopyroxene phenocryst
G347-07 Core of intergrown orthopyroxene phenocryst
G347-08 Core of intergrown orthopyroxene phenocryst
G347-09 Core of intergrown orthopyroxene phenocryst
G347-10 Core of intergrown orthopyroxene phenocryst
G347-11 Core of intergrown orthopyroxene phenocryst
G347-12 Pigeonite groundmass
G347-13 Pigeonite groundmass

	G347-14	G347-15	G347-16	G347-17	G347-18	G347-20	G347-21	G347-22	G347-23	G347-24
	OPX	OPX	PIG	CPX	CPX	CPX	PLG	PLG	PLG	PLG
Oxide										
SiO2	53.516	53.239	51.749	49.970	50.089	52.019	49.333	51.400	49.976	48.920
Al2O3	.805	1.469	.807	4.771	4.877	2.401	31.959	30.286	31.130	32.093
TiO2	.098	.270	.358	.518	.712	.440	-	.018	-	.023
FeO	19.577	19.425	25.806	9.249	6.878	9.391	.488	.571	.486	.471
MnO	.771	.547	1.012	.485	.234	-	-	.010	.016	.042
MgO	23.839	23.513	16.592	14.410	14.061	14.628	.043	.039	.054	.065
CaO	1.606	1.503	3.491	20.183	22.908	20.816	15.479	13.312	14.351	15.403
NaO	.001	.026	.094	.297	.221	.305	2.836	4.098	3.508	2.877
K2O	.001	.006	-	.081	.008	-	.062	.110	.081	.042
NiO	-	-	.090	-	-	-	-	.011	-	-
Cr2O3	-	-	-	.028	-	-	.034	-	-	-
Cl	.010	-	-	.056	.010	-	.006	-	.004	.022
Total	100.224	99.998	99.999	100.048	99.998	100.000	100.240	99.855	99.606	99.958
Cation										
Si	1.971	1.961	1.983	1.865	1.860	1.936	9.018	9.387	9.175	8.973
Al	.035	.064	.036	.210	.213	.105	6.885	6.519	6.735	6.938
Ti	.003	.007	.010	.015	.020	.012	-	.002	-	.003
Fe	.603	.598	.827	.289	.214	.292	.075	.087	.075	.072
Mn	.024	.017	.033	.015	.007	-	-	.002	.002	.006
Mg	1.309	1.291	.948	.802	.779	.812	.012	.011	.015	.018
Ca	.063	.059	.143	.807	.912	.830	3.032	2.605	2.823	3.027
Na	-	.002	.007	.022	.016	.022	1.005	1.451	1.248	1.023
K	-	-	-	.004	-	-	.015	.026	.019	.010
Ni	-	-	.003	-	-	-	-	.002	-	-
Cr	-	-	-	.001	-	-	.005	-	-	-
Cl	.001	-	-	-	.001	-	.002	-	.001	.007
Total	4.009	4.001	3.991	4.028	4.022	4.010	20.048	20.090	20.093	20.078
Fe/Fe+Mg	.315	.317	.466	.265	.215	.265	.863	.892	.836	.803
Mg*	-	-	-	-	-	-	-	-	-	-
Ca*	3.300	3.000	7.300	42.200	47.700	43.000	-	-	-	-
An	-	-	-	-	-	-	74.830	63.820	69.020	74.560

G347-14 Orthopyroxene phenocryst core
G347-15 Orthopyroxene microphenocryst
G347-16 Pigeonite groundmass
G347-17 Clinopyroxene phenocryst
G347-18 Clinopyroxene phenocryst
G347-20 Clinopyroxene phenocryst
G347-21 Plagioclase phenocryst core
G347-22 Plagioclase phenocryst rim
G347-23 Plagioclase phenocryst rim
G347-24 Plagioclase phenocryst core

	G347-25	G347-26	G347-27	G347-28	G347-29	G347-30	G347-31	G347-32	G347-33	G347-34
	PLG	PLG	PLG	PLG	PLG	PLG	PLG	PLG	PLG	MAG
Oxide										
SiO2	52.811	52.239	49.250	50.024	46.797	53.419	51.470	52.546	53.007	.138
Al2O3	30.141	29.400	32.044	31.172	33.428	29.361	30.370	26.618	29.076	3.141
TiO2	.171	.024	-	.061	-	.074	.021	2.069	.074	11.823
FeO	.260	.667	.714	.649	.763	.532	.711	3.128	.728	77.719
MnO	.027	-	.006	.126	.001	.016	-	.069	-	.446
MgO	.062	.056	.061	.060	.045	.080	.034	.148	.011	1.722
CaO	12.440	12.742	15.348	14.239	16.937	12.460	13.647	9.986	12.037	-
NaO	4.388	4.309	2.955	3.488	1.977	4.519	4.103	5.033	4.920	-
K2O	.099	.128	.048	.186	.042	.102	.125	.236	.255	-
NiO	.210	.009	.012	-	.030	-	-	.041	.101	-
Cr2O3	.010	-	.056	-	-	.009	.255	-	-	.023
Cl	.003	-	-	-	.001	.009	.084	.004	.016	.006
Total	100.622	99.574	100.494	100.005	100.021	100.581	100.820	99.878	100.225	99.283
Cation										
Si	9.530	9.549	8.993	9.161	8.631	9.645	9.343	9.668	9.634	.048
Al	6.411	6.334	6.896	6.728	7.266	6.248	6.497	5.772	6.228	1.293
Ti	.023	.003	-	.008	-	.010	.003	.286	.010	3.107
Fe	.039	.102	.109	.099	.118	.080	.108	.481	.111	22.711
Mn	.004	-	.001	.020	-	.002	-	.011	-	.132
Mg	.017	.015	.017	.016	.012	.021	.009	.041	.003	.897
Ca	2.405	2.496	3.003	2.794	3.347	2.410	2.694	1.969	2.344	-
Na	1.535	1.527	1.046	1.238	.707	1.582	1.444	1.796	1.734	-
K	.023	.030	.011	.043	.010	.023	.029	.055	.059	-
Ni	.030	.001	.002	-	.004	-	-	.006	.015	-
Cr	.001	-	.008	-	-	.001	.037	-	-	.006
Cl	.001	-	-	-	-	.003	.026	.001	.005	.004
Total	20.020	20.059	20.084	20.108	20.095	20.026	20.150	20.086	20.143	28.199
Fe/Fe+Mg	.703	.869	.868	.858	.904	.789	.921	.922	.973	.962
Mg*	-	-	-	-	-	-	-	-	-	-
Ca*	-	-	-	-	-	-	-	-	-	-
An	74.560	61.580	73.400	68.560	82.360	60.020	64.270	51.540	56.660	-

G347-25 Plagioclase phenocryst mantle
G347-26 Plagioclase phenocryst rim
G347-27 Plagioclase phenocryst core
G347-28 Plagioclase phenocryst rim
G347-29 Core of intergrown plagioclase phenocryst
G347-30 Rim of intergrown plagioclase phenocryst
G347-31 Rim of intergrown plagioclase phenocryst
G347-32 Plagioclase groundmass
G347-33 Plagioclase groundmass
G347-34 Magnetite microphenocryst

	G347-35	G347-36	G266-01	G266-02	G266-03	G266-04	G266-05	G266-06	G266-07	G266-08
	MAG	MAG	OLV	OLV	OLV	CPX	CPX	CPX	PIG	PIG
Oxide										
SiO2	.139	.204	37.532	37.843	36.938	51.421	50.614	51.848	52.953	53.460
Al2O3	3.135	3.515	.051	.001	.032	2.379	4.173	2.056	.975	.603
TiO2	11.042	10.923	.054	.002	-	.663	.808	.796	.395	.329
FeO	77.971	77.379	25.939	25.168	30.620	9.599	9.818	9.368	20.186	19.972
MnO	.402	.382	.405	.182	.473	.321	.216	.287	.576	.739
MgO	1.565	1.728	35.644	36.613	31.665	14.885	14.058	15.020	19.541	20.812
CaO	.034	.068	.210	.146	.237	19.244	19.920	20.262	5.173	3.964
NaO	-	-	-	-	.008	.378	.388	.301	.109	.081
K2O	.009	.002	.038	-	-	-	.005	.015	.013	.017
NiO	-	.056	.099	.045	.002	.070	-	-	-	.017
Cr2O3	.085	.019	.022	-	-	.166	.002	.037	.078	.015
Cl	.008	-	-	-	.006	.102	-	.011	-	-
Total	98.753	98.612	99.994	100.000	99.981	99.228	100.002	100.001	99.999	100.009
Cation										
Si	.049	.072	.996	.998	1.002	1.931	1.887	1.932	1.980	1.990
Al	1.307	1.460	.002	-	.001	.105	.183	.090	.043	.026
Ti	2.938	2.895	.001	-	-	.019	.023	.022	.011	.009
Fe	23.069	22.805	.576	.555	.695	.301	.306	.292	.631	.622
Mn	.120	.114	.009	.004	.011	.010	.007	.008	.018	.023
Mg	.825	.908	1.410	1.440	1.281	.833	.782	.834	1.089	1.154
Ca	.013	.026	.006	.004	.007	.774	.796	.808	.207	.158
Na	-	-	-	-	-	.027	.028	.021	.008	.006
K	.004	.001	.001	-	-	-	-	-	.001	.001
Ni	-	.016	.002	.001	-	.002	-	-	-	.001
Cr	.024	.005	-	-	-	.005	-	.001	.002	-
Cl	.005	-	-	-	-	.007	-	-	-	-
Total	28.355	28.301	3.003	3.002	2.998	4.015	4.012	3.927	3.991	3.991
Fe/Fe+Mg	.965	.962	.290	.278	.352	.266	.281	.259	.367	.350
Mg*	-	-	71.000	72.200	64.800	-	-	-	-	-
Ca*	-	-	-	-	-	40.400	42.100	41.600	10.600	8.100
An	-	-	-	-	-	-	-	-	-	-

G347-35 Magnetite microphenocryst in clot
G347-36 Magnetite microphenocryst in clot
G266-01 Olivine phenocryst core
G266-02 Olivine phenocryst core
G266-03 Olivine microphenocryst
G266-04 Clinopyroxene phenocryst core
G266-05 Clinopyroxene phenocryst core
G266-06 Anhedral clinopyroxene microphenocryst
G266-07 Pigeonite groundmass
G266-08 Pigeonite groundmass

	G266-09	G266-10	G266-11	G266-12	G266-13	G266-14	G266-15	G266-16	G266-17	G266-18
	PIG	PIG	PIG	MAG	PLG	PLG	PLG	PLG	PLG	PLG
Oxide										
SiO2	52.281	53.297	52.980	.153	48.221	44.704	52.078	45.653	51.004	51.272
Al2O3	1.361	.497	.588	1.572	32.525	35.397	29.687	34.639	30.095	30.079
TiO2	.608	.247	.343	19.149	.020	-	.044	.172	.005	.037
FeO	18.994	20.671	20.992	73.267	.688	.485	.816	.471	.939	.721
MnO	.727	.611	.731	.483	.014	-	.033	.055	.044	.038
MgO	18.513	20.648	20.075	1.300	.049	.053	.105	.081	.260	.107
CaO	7.419	3.811	4.173	.004	16.027	18.888	13.065	18.080	13.730	13.415
NaO	.074	.102	.074	-	2.513	.849	3.534	1.303	3.747	3.859
K2O	.010	.009	.001	-	.003	.014	.079	.015	.086	.098
NiO	.001	-	.021	.041	.036	-	-	.136	-	-
Cr2O3	.012	.090	.022	.069	-	-	-	.019	.005	.011
Cl	-	.015	-	-	-	-	-	.015	.021	.006
Total	100.000	99.998	100.000	99.018	100.096	100.390	99.441	100.639	99.936	99.643
Cation										
Si	1.960	1.989	1.984	.051	8.854	8.243	9.520	8.389	9.335	9.388
Al	.060	.022	.025	.620	7.039	7.693	6.396	7.502	6.492	6.491
Ti	.017	.007	.009	4.819	.003	-	.006	.024	.001	.005
Fe	.596	.645	.657	20.515	.106	.075	.125	.072	.144	.110
Mn	.023	.019	.022	.137	.002	0.000	.005	.009	.007	.006
Mg	1.035	1.149	1.120	.648	.013	.014	.029	.022	.071	.029
Ca	.298	.153	.168	.001	3.153	3.732	2.559	3.560	2.693	2.632
Na	.005	.007	.006	-	.895	.304	1.253	.464	1.330	1.370
K	.001	-	-	-	.001	.003	.018	.004	.020	.023
Ni	-	-	-	.011	.005	-	-	.020	-	-
Cr	-	.003	-	.018	-	-	-	.003	.001	.002
Cl	-	.001	-	-	-	-	-	.005	.007	.002
Total	3.995	3.995	3.991	26.811	20.071	20.064	19.911	20.073	20.099	20.058
Fe/Fe+Mg	.365	.360	.370	.969	.888	.838	.813	.766	.670	.791
Mg*	-	-	-	-	-	-	-	-	-	-
Ca*	15.266	7.782	8.541	-	-	-	-	-	-	-
An	-	-	-	-	77.870	92.400	66.810	88.380	66.610	63.390

G266-09 Pigeonite groundmass
G266-10 Pigeonite groundmass
G266-11 Pigeonite groundmass
G266-12 Magnetite microphenocryst
G266-13 Plagioclase phenocryst core
266-14 Plagioclase phenocryst core
G266-15 Plagioclase phenocryst rim
G266-16 Plagioclase phenocryst core
G266-17 Plagioclase phenocryst rim
G266-18 Plagioclase phenocryst rim

	G266-19	G266-20	G266-21	G285-01	G285-02	G285-03	G285-04	G285-05	G285-06	G285-07
	PLG	PLG	PLG	OLV	OLV	OLV	OLV	OLV	OLV	OLV
Oxide										
SiO2	53.208	47.671	53.980	38.236	37.033	38.319	38.225	36.842	35.906	35.663
Al2O3	28.615	32.552	27.352	.033	.029	.002	.018	.003	.005	.017
TiO2	.006	.007	.091	.004	.007	-	.027	.034	.015	.001
FeO	.815	.987	1.486	20.624	27.212	20.609	21.358	30.205	34.518	38.105
MnO	.027	.041	.008	.291	.507	.302	.363	.601	.595	.835
MgO	.130	.144	.199	39.750	34.287	39.690	39.016	31.673	28.073	24.487
CaO	11.839	15.997	11.152	.174	.176	.166	.128	.144	.250	.253
NaO	4.853	2.413	5.130	-	-	-	-	-	-	-
K2O	.132	.070	.223	.013	-	-	-	-	.007	-
NiO	-	.023	.031	.098	.067	.083	.041	-	.093	.015
Cr2O3	-	-	.051	-	-	-	.066	-	-	.044
Cl	.046	.004	.003	-	-	.019	.011	-	.009	.018
Total	99.671	99.909	99.706	99.223	99.318	99.190	99.253	99.502	99.471	99.438
Cation										
Si	9.708	8.792	9.862	.996	.996	.998	.999	1.003	1.001	1.013
Al	6.153	7.075	5.890	.001	.001	-	.001	-	-	.001
Ti	.001	.001	.013	-	-	-	.001	.001	-	-
Fe	.124	.152	.227	.449	.612	.449	.467	.688	.805	.905
Mn	.004	.006	.001	.006	.012	.007	.008	.014	.014	.020
Mg	.035	.040	.054	1.544	1.375	1.541	1.520	1.286	1.167	1.037
Ca	2.314	3.161	2.183	.005	.005	.005	.004	.004	.007	-
Na	1.717	.863	1.817	-	-	-	-	-	-	.008
K	.031	.016	.052	-	-	-	-	-	-	-
Ni	-	.003	.005	.002	.001	.002	.001	-	.002	-
Cr	-	-	.007	-	-	-	.001	-	-	.001
Cl	.014	.001	.001	-	-	.001	-	-	-	.001
Total	20.102	20.111	20.112	3.004	3.003	3.003	3.000	2.996	2.999	2.987
Fe/Fe+Mg	.778	.794	.807	.225	.308	.466	.235	.349	.408	.466
Mg*	-	-	-	77.500	69.200	77.400	76.500	65.100	59.200	53.400
Ca*	-	-	-	-	-	-	-	-	-	-
An	56.970	78.240	53.870	-	-	-	-	-	-	-

G266-19 Plagioclase phenocryst rim
G266-20 Plagioclase groundmass
G266-21 Plagioclase groundmass
G285-01 Olivine phenocryst core
G285-02 Olivine phenocryst core
G285-03 Olivine phenocryst core
G285-04 Olivine phenocryst core
G285-05 Rounded olivine phenocryst core
G285-06 Rounded olivine phenocryst core
G285-07 Anhedral olivine microphenocryst

	G285-08	G285-09	G285-10	G285-11	G285-12	G285-13	G285-14	G285-15
	OLV	OLV	CPX	CPX	CPX	CPX	CPX	PIG
Oxide								
SiO2	35.191	35.260	50.853	51.725	51.449	52.178	52.120	52.503
Al2O3	.037	.036	2.633	1.724	2.328	2.020	2.318	.520
TiO2	-	.044	.670	.427	.599	.545	.579	.418
FeO	37.509	39.120	10.072	10.973	10.001	8.879	8.967	21.100
MnO	.670	.754	.319	.433	.328	.388	.386	.555
MgO	25.694	24.633	14.609	15.425	14.026	14.788	14.731	19.512
CaO	.237	.264	19.636	18.139	20.028	20.506	20.618	4.402
Na2O	-	-	.383	.281	.333	.288	.317	-
K2O	-	-	-	.014	0.000	.037	.015	-
NiO	.051	.007	.033	-	.017	.015	.019	-
Cr2O3	.051	.020	.178	-	-	.101	-	-
Cl	-	.008	.051	-	.005	.024	.031	-
Total	99.440	100.146	99.437	99.141	99.114	99.769	100.101	99.010
Cation								
Si	.998	1.000	1.913	1.947	1.938	1.945	1.937	1.988
Al	.001	.001	.117	.076	.103	.089	.102	.023
Ti	-	.001	.019	.012	.017	.015	.016	.012
Fe	.890	.928	.317	.345	.315	.277	.279	.668
Mn	.016	.018	.010	.014	.010	.012	.012	.018
Mg	1.086	1.041	.819	.866	.788	.822	.816	1.101
Ca	.007	.008	.791	.732	.808	.819	.821	.179
Na	-	-	.028	.021	.024	.021	.023	-
K	-	-	-	.001	-	.002	.001	-
Ni	.001	-	.001	-	.001	-	.001	-
Cr	.001	-	.005	-	-	.003	-	-
Cl	-	-	.003	-	-	.002	.002	-
Total	3.001	2.999	4.024	4.013	4.006	4.007	4.009	3.989
Fe/Fe+Mg	.450	.471	.279	.285	.286	.252	.255	.378
Mg*	55.000	52.900	-	-	-	-	-	-
Ca*	-	-	40.840	37.400	42.060	42.440	42.580	9.100
An	-	-	-	-	-	-	-	-

G285-08 Anhedral olivine microphenocryst
G285-09 Olivine groundmass
G285-10 Clinopyroxene phenocryst core
G285-11 Clinopyroxene phenocryst core
G285-12 Clinopyroxene phenocryst core
G285-13 Clinopyroxene phenocryst core
G285-14 Clinopyroxene phenocryst core
G285-15 Pigeonite groundmass

	G285-16	G285-17	G285-18	G285-19	G285-20	G285-21	G285-22	G285-23	G285-24	G285-25
	PIG	CPX	PIG	PIG	PIG	MAG	PLG	PLG	PLG	PLG
Oxide										
SiO2	53.698	49.617	52.862	51.732	50.222	.125	51.467	53.063	46.449	45.615
Al2O3	1.030	3.311	.619	1.087	.857	2.740	30.478	29.366	33.545	33.789
TiO2	.412	1.276	.379	.576	.538	14.685	.069	.038	-	.012
FeO	23.019	11.956	20.723	21.316	21.834	74.833	.666	.782	.614	.491
MnO	.712	.483	.700	.643	.773	.326	-	.040	-	-
MgO	16.933	13.115	19.833	18.206	17.570	2.145	.092	.077	.051	.057
CaO	4.266	19.050	3.928	5.942	7.125	.019	13.859	12.252	17.184	18.137
Na2O	.128	.370	.077	.093	.178	.008	3.636	4.652	1.767	1.277
K2O	.027	.078	-	-	-	.016	.095	.156	.004	.019
NiO	-	-	.007	-	.063	.055	-	-	-	-
Cr2O3	-	.028	-	-	.092	.189	-	-	-	.030
Cl	.004	-	-	-	.088	.001	.002	-	.043	-
Total	100.229	99.284	99.128	99.595	99.340	98.877	100.364	100.426	99.657	99.427
Cation										
Si	2.018	1.887	1.992	1.962	1.934	.043	9.355	9.616	8.596	8.477
Al	.046	.148	.027	.049	.039	1.105	6.529	6.265	7.316	7.400
Ti	.012	.036	.010	.016	.016	3.778	.009	.005	-	.002
Fe	.724	.379	.654	.676	.703	21.409	.101	.119	.095	.076
Mn	.023	.015	.022	.021	.025	.095	.025	.006	-	-
Mg	.946	.744	1.114	1.029	1.008	1.094	2.699	.021	.014	.016
Ca	.172	.775	.159	.241	.294	.007	1.281	2.379	3.407	3.611
Na	.009	.027	.006	.007	.013	.005	.022	1.635	.634	.460
K	.001	.004	-	-	-	.007	-	.036	.001	.004
Ni	-	-	-	-	.002	.015	-	-	-	-
Cr	-	.001	-	-	.003	.051	-	-	-	.004
Cl	-	-	-	-	.006	.001	.001	-	.014	-
Total	3.953	4.016	3.984	4.001	4.042	27.608	20.023	20.082	20.077	20.051
Fe/Fe+Mg	.433	.338	.370	.396	.411	.951	.802	.850	.872	.828
Mg*	-	-	-	-	-	-	-	-	-	-
Ca*	9.220	40.510	8.160	12.250	14.480	-	-	-	-	-
An	-	-	-	-	-	-	67.440	58.740	84.290	88.610

G285-16 Pigeonite groundmass
G285-17 Clinopyroxene groundmass
G285-18 Pigeonite groundmass
G285-19 Coronas of pigeonite surrounding olivine
G285-20 Coronas of pigeonite surrounding olivine
G285-21 Rounded magnetite microphenocryst
G285-22 Plagioclase phenocryst mantle
G285-23 Plagioclase phenocryst rim
G285-24 Plagioclase phenocryst core
G285-25 Plagioclase phenocryst core

	G285-26	G285-27	G285-28	G285-29	G287-01	G287-02	G287-03	G287-04	G287-05	G287-06
	PLG	PLG	PLG	PLG	OLV	OLV	OLV	OLV	OLV	OLV
Oxide										
SiO2	51.974	46.981	53.642	57.227	37.187	36.767	37.838	39.132	38.934	36.757
Al2O3	29.950	33.380	29.228	26.488	-	.015	.037	.020	.016	.014
TiO2	.090	-	.011	.066	.007	.010	.029	-	.016	.030
FeO	.606	.552	.759	.901	28.494	27.478	21.719	20.203	20.724	29.624
MnO	.019	.011	-	-	.504	.451	.316	.333	.301	.479
MgO	.077	.060	.090	.062	34.109	34.888	40.138	40.847	40.521	32.959
CaO	13.134	17.028	12.180	9.568	.181	.154	.182	.130	.148	.176
Na2O	3.946	1.830	4.497	5.612	.029	.008	-	-	-	-
K2O	.118	.004	.138	.590	.009	.008	-	-	-	.033
NiO	.019	-	-	-	-	-	-	-	.112	.091
Cr2O3	.017	-	.003	-	.081	.017	-	-	-	.040
Cl	.011	-	-	.014	-	.014	-	.014	.010	.012
Total	99.961	99.846	100.548	100.528	100.601	99.810	100.259	100.679	100.782	100.215
Cation										
Si	9.467	8.662	9.685	10.271	.993	.986	.981	1.000	.997	.992
Al	6.430	7.254	6.219	5.603	-	-	.001	.001	-	-
Ti	.012	-	.001	.009	-	-	.001	-	-	.001
Fe	.092	.085	.115	.135	.636	.616	.471	.432	.444	.669
Mn	.003	.002	-	-	.011	.010	.007	.007	.007	.011
Mg	.021	.016	.024	.017	1.358	1.395	1.552	1.556	1.547	1.326
Ca	2.563	3.364	2.356	1.840	.005	.004	.005	.004	.004	.005
Na	1.394	.654	1.574	1.953	.001	-	-	-	-	-
K	.027	.001	.032	.135	-	-	-	-	-	.001
Ni	.003	-	-	-	-	-	-	-	.002	.002
Cr	.003	-	-	-	.002	-	-	-	-	.001
Cl	.003	-	-	.004	-	.001	-	.001	-	.001
Total	20.018	20.038	20.007	19.967	3.007	3.014	3.018	3.000	3.003	3.008
Fe/Fe+Mg	.816	.838	.826	.891	.319	.306	.233	.217	.223	.335
Mg*	-	-	-	-	68.100	69.400	76.700	78.300	77.700	66.500
Ca*	-	-	-	-	-	-	-	-	-	-
An	64.330	83.700	59.460	46.840	-	-	-	-	-	-

	G287-07	G287-08	G287-09	G287-10	G287-11	G287-12	G287-13	G287-14	G287-15	G287-16
	OLV	OLV	OLV	OLV	OLV	OLV	OLV	OPX	OPX	OPX
Oxide										
SiO2	36.055	37.554	38.624	37.434	37.118	38.731	35.725	53.846	52.170	52.457
Al2O3	.010	.016	.019	.006	.034	.021	.030	1.540	1.044	.807
TiO2	-	.032	-	.023	.026	-	.026	.190	.344	.254
FeO	31.463	32.203	20.570	28.027	28.766	21.121	30.722	17.160	19.113	19.335
MnO	.615	.609	.264	.447	.539	.301	.520	.370	.524	.509
MgO	31.551	30.292	40.616	33.519	33.254	39.598	32.212	25.830	24.214	24.305
CaO	.179	.206	.180	.144	.147	.148	.191	1.710	1.732	1.759
Na2O	.018	-	.017	.020	-	.022	.008	-	.015	-
K2O	.016	.008	-	-	-	-	-	-	.013	.009
NiO	.013	-	.062	.036	-	.036	.029	.040	-	.046
Cr2O3	.007	.026	.025	.022	-	-	-	.014	.069	.067
Cl	.018	.006	.010	-	-	.003	.007	-	.008	-
Total	99.945	100.952	100.387	99.678	99.884	99.981	99.470	100.700	99.246	99.548
Cation										
Si	.986	1.015	.993	1.005	.999	1.002	.979	1.949	1.942	1.948
Al	-	-	.001	-	.001	.001	.001	.066	.046	.035
Ti	-	.001	-	-	.001	-	.001	.005	.010	.007
Fe	.720	.728	.442	.630	.648	.457	.704	.520	.595	.601
Mn	.014	.014	.006	.010	.012	.007	.012	.011	.017	.016
Mg	1.287	1.220	1.557	1.342	1.335	1.527	.316	1.394	1.344	1.346
Ca	.005	.006	.005	.004	.004	.004	.006	.066	.069	.070
Na	.001	-	.001	.001	-	.001	-	-	.001	-
K	.001	-	-	-	-	-	-	-	.001	-
Ni	-	-	.001	.001	-	.001	-	.001	-	.001
Cr	-	.001	.001	-	-	-	-	-	.002	.002
Cl	.001	-	-	-	-	-	-	-	-	-
Total	3.015	2.985	3.007	2.994	3.000	2.999	3.020	4.013	4.026	4.026
Fe/Fe+Mg	.359	.374	.221	.319	.327	.230	.349	.272	.307	.309
Mg*	64.100	62.600	77.900	68.100	67.300	77.000	65.100	-	-	-
Ca*	-	-	-	-	-	-	-	3.300	3.400	3.400
An	-	-	-	-	-	-	-	-	-	-

G285-26 Plagioclase phenocryst rim
G285-27 Core of intergrown plagioclase phenocryst
G285-28 rim of intergrown plagioclase phenocryst
G285-29 Plagioclase microphenocryst
G287-01 Olivine phenocryst core
G287-02 Olivine phenocryst core
G287-03 Olivine phenocryst core
G287-04 Olivine phenocryst core
G287-05 Olivine phenocryst core
G287-06 Anhedral olivine microphenocryst

G287-07 Anhedral olivine microphenocryst
G287-08 Anhedral olivine microphenocryst
G287-09 Anhedral olivine microphenocryst
G287-10 Euhedral olivine microphenocryst
G287-11 Euhedral olivine microphenocryst
G287-12 Olivine inclusion in rounded clinopyroxene
G287-13 Olivine groundmass
G287-14 Orthopyroxene phenocryst core
G287-15 Orthopyroxene phenocryst core
G287-16 Intergrown orthopyroxene phenocryst

	G287-17	G287-18	G287-19	G287-20	G287-21	G287-22	G287-23	G287-24	G287-25	G287-26
	OPX	OPX	OPX	OPX	OPX	OPX	CPX	CPX	CPX	CPX
Oxide										
SiO2	53.799	53.776	53.211	52.215	52.589	52.264	51.824	50.784	51.083	52.181
Al2O3	2.214	1.540	2.156	2.050	1.374	1.317	3.852	3.376	3.616	2.763
TiO2	.313	.207	.378	.291	.257	.377	.450	.753	.761	.457
FeO	17.747	16.474	17.454	17.311	18.948	19.132	5.030	9.008	9.890	8.716
MnO	.091	.423	.389	.632	.487	.542	.173	.210	.350	.237
MgO	24.840	25.418	25.190	25.252	24.769	24.123	15.547	14.780	14.700	15.656
CaO	1.520	1.595	1.602	1.535	1.648	1.786	22.860	20.660	19.580	20.164
Na2O	.029	.027	.022	.048	-	.004	.221	.330	.380	.272
K2O	-	.008	.008	.010	-	.017	.008	-	-	.005
NiO	.220	-	-	-	.059	-	.008	.090	.010	.040
Cr2O3	-	-	.023	.053	-	.070	.175	-	-	-
Cl	.010	-	.012	.007	.001	-	-	.010	-	-
Total	100.783	99.468	100.445	99.404	100.132	99.632	100.148	100.001	100.370	100.491
Cation										
Si	1.950	1.963	1.934	1.923	1.936	1.937	1.901	1.893	1.897	1.925
Al	.094	.066	.092	.089	.060	.058	.167	.148	.158	.120
Ti	.009	.006	.010	.008	.007	.011	.012	.021	.021	.013
Fe	.537	.503	.531	.533	.583	.593	.154	.281	.307	.269
Mn	.003	.013	.012	.020	.015	.017	.005	.007	.011	.007
Mg	1.340	1.383	1.365	1.386	1.359	1.333	.850	.821	.814	.861
Ca	.059	.062	.062	.061	.065	.071	.898	.825	.779	.797
Na	.002	.002	.002	.003	-	-	.016	.024	.027	.019
K	-	-	-	-	-	.001	-	-	-	-
Ni	.006	-	-	-	.002	-	-	.003	-	.001
Cr	-	-	.001	.002	-	.002	.005	-	-	-
Cl	-	-	.001	-	-	-	-	-	-	-
Total	3.998	3.999	4.010	4.026	4.027	4.023	4.009	4.024	4.016	4.012
Fe/Fe+Mg	.286	.267	.280	.278	.300	.308	.154	.255	.274	.238
Mg*	-	-	-	-	-	-	-	-	-	-
Ca*	3.000	3.200	3.100	3.000	3.200	3.500	47.100	42.700	40.800	41.200
An	-	-	-	-	-	-	-	-	-	-

G287-17 Intergrown orthopyroxene phenocryst
G287-18 Intergrown orthopyroxene phenocryst
G287-19 Intergrown orthopyroxene phenocryst
G287-20 Intergrown orthopyroxene phenocryst
G287-21 Intergrown orthopyroxene phenocryst
G287-22 Intergrown orthopyroxene phenocryst
G287-23 Clinopyroxene phenocryst core
G287-24 Clinopyroxene phenocryst core
G287-25 Clinopyroxene phenocryst rim
G287-26 Core of anhedral clinopyroxene phenocryst

	G287-27	G287-28	G287-29	287-30	G287-31	G287-32	G287-33	G287-34	G287-35	G287-36
	CPX	PIG	PIG	CPX	PIG	MAG	MAG	MAG	MAG	PLG
Oxide										
SiO2	50.371	52.787	53.677	51.649	51.804	.111	.121	.142	.153	47.850
Al2O3	4.788	.707	.472	1.600	.508	3.036	4.655	.709	4.557	32.890
TiO2	.585	.424	.247	.885	.359	13.271	11.567	12.764	10.882	.030
FeO	7.619	23.065	20.199	14.568	26.026	76.806	74.257	79.599	74.299	-
MnO	.133	.634	.718	.507	.792	.386	.386	.336	.400	.064
MgO	14.089	18.259	21.664	14.711	17.073	1.938	3.150	.255	3.622	.080
CaO	22.079	4.477	3.528	15.423	3.610	-	.043	.104	.015	16.390
Na2O	.252	.050	.033	.275	.082	.007	-	.029	.230	2.190
K2O	-	-	.002	.004	.018	.009	.010	-	.001	.020
NiO	-	-	.078	-	.048	.041	.040	.093	.030	-
Cr2O3	.094	-	-	.006	.012	.173	.264	.010	.512	.090
Cl	.002	-	-	.022	.015	.015	-	-	.020	-
Total	100.012	100.403	100.618	99.650	100.347	99.801	98.638	98.246	99.012	99.604
Cation										
Si	1.870	1.988	1.985	1.951	1.980	.038	.041	.051	.052	8.810
Al	.210	.031	.021	.071	.023	1.228	1.880	.303	1.840	7.140
Ti	.016	.012	.007	.025	.010	3.425	2.981	3.482	2.800	.004
Fe	.237	.726	.625	.460	.832	22.043	21.281	24.147	21.270	-
Mn	.004	.020	.022	.016	.026	.112	.112	.103	.115	.010
Mg	.780	1.025	1.194	.829	.973	.991	1.607	.138	1.850	.022
Ca	.878	.181	.140	.624	.148	-	.016	.040	.006	3.232
Na	.018	.004	.002	.020	.006	.005	.003	.020	.153	.781
K	-	-	-	-	.001	.004	.003	-	.001	.005
Ni	-	-	.002	-	.001	.011	.011	-	.008	-
Cr	.003	-	-	-	-	.047	.071	.027	.139	.013
Cl	-	-	-	.001	.001	.009	-	.006	.010	-
Total	4.016	3.987	3.999	3.999	4.002	27.913	28.003	28.318	28.244	20.010
Fe/Fe+Mg	.233	.415	.343	.357	.461	.957	.930	.994	.920	-
Mg*	-	-	-	-	-	-	-	-	-	-
Ca*	46.200	9.300	7.100	32.300	7.500	-	-	-	-	-
An	-	-	-	-	-	-	-	-	-	80.440

G287-27 Core of anhedral clinopyroxene phenocryst
G287-28 Pigeonite groundmass
G287-29 Pigeonite groundmass
G287-30 Clinopyroxene groundmass
G287-31 Pigeonite groundmass
G287-32 Magnetite microphenocryst in clot
G287-33 Magnetite microphenocryst
G287-34 Magnetite groundmass
G287-35 Magnetite inclusion in clinopyroxene clots
G287-36 Plagioclase phenocryst core

	287-37	G287-38	287-39	G287-40	G287-41	G287-42	G287-43	G287-44	G287-45	G287-46
	PLG	PLG	PLG	PLG	PLG	PLG	PLG	PLG	PLG	PLG
Oxide										
SiO2	44.250	53.960	44.240	45.890	54.438	52.792	53.570	52.869	54.894	55.172
Al2O3	35.058	28.220	35.484	34.510	28.422	29.288	28.732	28.772	28.048	27.700
TiO2	.023	.080	.043	.050	.094	.053	.069	.051	.122	.083
FeO	.495	.900	.183	.583	.910	.657	.705	.773	1.010	.970
MnO	-	-	-	-	.033	-	.015	.033	-	.096
MgO	.032	.140	.044	.010	.116	.054	.050	.111	.101	.110
CaO	18.930	11.810	19.041	18.044	11.925	12.720	11.680	12.598	11.460	11.610
Na2O	.640	4.750	.620	1.175	4.764	4.489	4.916	4.342	4.980	5.040
K2O	.002	.120	.014	.020	.165	.147	.216	.102	.180	.180
NiO	.130	-	-	-	-	.044	.003	.028	-	-
Cr2O3	.013	-	-	-	.121	.022	.014	.057	.010	-
Cl	.001	.010	-	-	.011	-	-	-	-	-
Total	99.574	99.990	99.669	100.282	100.998	100.267	99.970	99.734	100.805	100.961
Cation										
Si	8.233	9.800	8.207	8.448	9.790	9.587	9.732	9.650	9.880	99.230
Al	7.690	6.040	7.760	7.488	6.030	6.269	6.152	6.187	5.950	5.870
Ti	.003	.010	.006	.005	.013	.007	.009	.007	.016	.011
Fe	.077	.137	.028	.091	.137	.100	.107	.118	.151	.146
Mn	-	-	-	-	.005	-	.002	.005	-	.015
Mg	.009	.038	.012	.005	.031	.015	.014	.030	.027	.029
Ca	3.773	2.300	3.790	3.557	2.300	2.475	2.273	2.463	2.210	2.238
Na	.229	.167	.222	.421	1.662	1.581	1.731	1.536	1.740	1.756
K	.001	.028	.003	.005	.038	.034	.050	.024	.041	.041
Ni	.019	-	-	-	-	.006	-	.004	-	-
Cr	.002	-	-	-	.017	.003	.002	.008	.001	-
Cl	-	.004	-	-	.003	-	-	-	-	-
Total	20.034	20.030	20.021	20.020	20.025	20.077	20.073	20.029	20.016	20.029
Fe/Fe+Mg	.897	.783	.700	.970	.815	.873	.888	.796	.849	.835
Mg*	-	-	-	-	-	-	-	-	-	-
Ca*	-	-	-	-	-	-	-	-	-	-
An	94.250	57.480	94.390	89.300	57.490	60.510	56.070	61.220	55.400	55.460

G287-37 Plagioclase phenocryst core
G287-38 Plagioclase phenocryst rim
G287-39 Plagioclase phenocryst core
G287-40 Plagioclase phenocryst core
G287-41 Plagioclase phenocryst rim
G287-42 Rim of plagioclase phenocryst clots
G287-43 Rim of plagioclase phenocryst clots
G287-44 Plagioclase microphenocryst
G287-45 Plagioclase groundmass
G287-46 Plagioclase groundmass

	G288-01	G288-02	G288-03	G288-04	G288-05	G288-06	G288-07	G288-08	21DK-01	21DK-02
	OPX	OPX	OPX	OPX	OPX	CPX	PLG	PLG	OPX	OPX
Oxide										
SiO2	53.740	52.814	53.094	52.586	52.510	51.230	47.474	54.180	53.362	52.920
Al2O3	1.185	1.366	1.490	1.127	1.190	2.331	33.205	28.674	1.413	1.622
TiO2	.240	.356	.330	.294	.260	.644	-	.054	.210	.284
FeO	18.511	18.287	18.450	19.996	18.850	11.720	.572	.714	18.910	19.301
MnO	.453	.450	.500	1.050	.510	.430	-	.015	.550	.532
MgO	24.900	24.300	24.060	23.520	24.345	14.460	.040	.071	23.540	22.920
CaO	1.642	1.730	1.717	1.874	1.680	18.560	16.540	10.990	1.590	1.710
Na2O	.050	.030	.030	.029	.020	.330	2.020	5.120	.024	.040
K2O	.010	.012	-	.022	.040	.020	.031	.200	-	.020
NiO	.060	.012	.320	.042	.040	-	.020	-	-	-
Cr2O3	-	.004	-	-	-	.012	-	-	.011	.060
Cl	-	0.000	.013	-	-	.010	-	.016	.010	-
Total	100.791	99.351	100.004	100.540	99.445	99.747	99.902	100.034	99.620	99.409
Cation										
Si	1.960	1.952	1.952	1.943	1.947	1.930	8.740	9.810	1.970	1.962
Al	.051	.060	.064	.049	.052	.103	7.200	6.120	.061	.071
Ti	.007	.010	.009	.008	.007	.020	-	.007	.006	.008
Fe	.564	.565	.568	.618	.584	.369	.085	.108	.583	.598
Mn	.014	.014	.015	.033	.016	.014	-	.002	.017	.017
Mg	1.351	1.340	1.319	1.296	1.345	.811	.011	.019	1.294	1.267
Ca	.064	.068	.068	.074	.067	.748	3.259	2.133	.063	.068
Na	.003	.002	.002	.002	.001	.024	.720	1.800	.002	.003
K	-	-	-	.001	-	.001	.005	.045	-	.001
Ni	.002	-	.008	.001	.001	-	-	-	-	.002
Cr	-	-	-	-	-	-	-	-	-	.002
Cl	-	-	.001	-	-	-	-	.005	-	-
Total	4.013	4.010	4.006	4.026	4.021	4.016	20.016	20.047	3.996	3.996
Fe/Fe+Mg	.294	.297	.301	.323	.303	.313	.889	.850	.311	.321
Mg*	-	-	-	-	-	-	-	-	-	-
Ca*	3.200	3.400	3.400	3.700	3.300	38.500	-	-	3.500	3.200
An	-	-	-	-	-	-	81.790	53.670	-	-

G288-01 Orthopyroxene phenocryst core
G288-02 Orthopyroxene phenocryst core
G288-03 Orthopyroxene phenocryst core
G288-04 Orthopyroxene phenocryst core
G288-05 Orthopyroxene phenocryst core
G288-06 Clinopyroxene jacketing orthopyroxene
G288-07 Plagioclase phenocryst core
G288-08 Plagioclase phenocryst rim
21DK-01 Orthopyroxene clots
21DK-02 Orthopyroxene microphenocryst

	21DK-03	21DK-04	21DK-05	21DK-06	21DK-07	21DK-08	21DK-09	21DK-10	21DK-11	21DK-12
	CPX	CPX	MAG	MAG	PLG	PLG	PLG	PLG	PLG	PLG
Oxide										
SiO2	51.512	50.257	.111	.130	45.095	49.632	50.640	45.290	52.060	49.070
Al2O3	2.094	3.741	3.411	3.360	34.650	31.570	31.660	34.910	30.520	32.460
TiO2	.572	.750	12.631	13.540	.023	.050	.020	.024	.052	.052
FeO	10.577	10.500	76.325	75.140	.544	.630	.573	.482	.680	.480
MnO	.390	.354	.404	.431	.017	.032	-	-	.020	.080
MgO	14.109	13.812	2.006	1.530	.054	.050	.070	.045	.062	.060
CaO	19.360	19.480	.021	.031	18.210	14.513	14.680	18.270	13.470	15.580
Na2O	.340	.340	.131	.012	1.012	2.930	3.044	1.060	3.830	2.660
K2O	.020	.010	-	.012	.016	.050	.063	.039	.070	.044
NiO	.002	.024	-	.013	-	-	-	-	-	-
Cr2O3	.110	.054	.231	.052	.019	.020	-	.051	.040	-
Cl	.040	.008	.133	.009	.054	0.000	.002	-	.010	-
Total	99.126	99.330	95.403	94.247	99.694	99.477	100.752	100.171	100.814	100.486
Cation										
Si	1.944	1.894	.038	.045	8.360	9.120	9.180	8.354	9.410	8.950
Al	.093	.166	1.386	1.375	7.570	6.832	6.760	7.590	6.500	6.980
Ti	.016	.021	3.274	5.536	.003	.005	-	.003	.005	.007
Fe	.334	.331	22.002	21.819	.084	.096	.085	.074	.101	.073
Mn	.012	.011	.118	.127	.003	.005	-	-	.005	.012
Mg	.794	.776	1.031	.791	.015	.015	.016	.012	.015	.016
Ca	.783	.786	.008	.012	3.620	2.860	2.853	3.611	2.610	3.044
Na	.025	.025	.087	-	.364	1.050	1.072	.038	1.340	.940
K	.001	-	-	.006	.004	.011	.016	.009	.015	.010
Ni	-	.001	-	.004	-	-	-	-	-	-
Cr	.003	.002	.063	.014	.003	-	-	.007	.005	-
Cl	.002	.001	.078	.005	.017	-	-	-	.005	-
Total	4.007	4.014	28.084	27.733	20.047	19.983	19.984	20.039	20.010	20.030
Fe/Fe+Mg	.296	.299	.955	.965	.850	.877	.824	.858	.860	.822
Mg*	-	-	-	-	-	-	-	-	-	-
Ca*	40.700	41.300	-	-	-	-	-	-	-	-
An	-	-	-	-	90.770	73.030	72.390	90.300	65.810	76.210

21DK-03 Clinopyroxene phenocryst
21DK-04 Clinopyroxene phenocryst
21DK-05 Magnetite microphenocryst clots
21DK-06 Magnetite microphenocryst clots
21DK-07 Plagioclase phenocryst core
21DK-08 Plagioclase phenocryst mantle
21DK-09 Plagioclase phenocryst mantle
21DK-10 Plagioclase phenocryst core
21DK-11 Plagioclase phenocryst rim
21DK-12 Core of plagioclase microphenocryst

	21DK-13	21DK-14	21DK-15	21DK-16	21DK-17	21DK-18	21DK-19	21DK-20	26DK-01	26DK-02
	PLG	PLG	PLG	PLG	PLG	PLG	PLG	PLG	OLV	OLV
Oxide										
SiO2	50.150	49.040	49.370	52.420	52.600	49.610	52.227	55.844	36.900	36.240
Al2O3	31.180	31.940	31.740	29.914	29.060	31.490	30.001	27.440	.020	.010
TiO2	.040	.033	.014	.040	.030	.032	.027	.030	-	.050
FeO	.580	.550	.580	.590	.680	.740	.567	1.154	28.960	28.090
MnO	.034	-	.010	.034	.052	-	-	-	.490	.480
MgO	.070	.050	.080	.090	.101	.070	.083	.135	33.560	33.450
CaO	14.310	14.950	15.020	13.010	12.350	14.850	13.170	10.440	.200	.140
Na2O	3.370	2.830	3.060	4.070	4.390	2.910	4.090	5.400	-	-
K2O	.080	.050	.070	.100	.100	.050	.080	.302	-	-
NiO	.020	-	.010	.010	.024	.010	-	-	.020	.130
Cr2O3	.054	-	.010	-	.022	.040	.060	.010	-	.040
Cl	.040	-	-	-	.020	-	-	.011	-	-
Total	99.928	99.443	99.964	100.278	99.429	99.802	100.305	100.766	100.150	98.630
Cation										
Si	9.180	9.023	9.050	9.509	9.620	9.100	9.480	10.040	.992	.989
Al	6.730	6.930	6.860	6.400	6.260	6.810	6.420	5.810	.001	
Ti	.005	.005	.002	.005	.005	.004	.005	.004	-	.001
Fe	.088	.084	.090	.089	.104	.113	.085	.173	.651	.641
Mn	.005	-	.001	.005	.008	.019	-	-	.011	.011
Mg	.019	.013	.022	.023	.027	2.920	.020	.036	1.350	1.360
Ca	2.810	2.950	2.950	2.530	2.420	1.033	2.560	2.010	.006	.004
Na	1.200	1.011	1.090	1.430	1.560	.011	1.440	1.880	-	-
K	.018	.011	.016	.022	.023	.002	.016	.069	-	-
Ni	.002	-	.001	-	.004	.005	-	-	-	.003
Cr	.008	-	.001	-	.003	-	.010	.001	-	.001
Cl	.012	-	-	-	.005	-	-	.003	-	-
Total	20.067	20.020	20.072	20.010	20.040	20.012	20.030	20.030	3.007	3.010
Fe/Fe+Mg	.822	.863	.802	.795	.790	.857	.793	.828	.326	.320
Mg*	-	-	-	-	-	-	-	-	67.400	68.000
Ca*	-	-	-	-	-	-	-	-	-	-
An	69.800	74.250	72.800	63.500	60.490	73.660	63.740	50.760	-	-

21DK-13 Plagioclase phenocryst mantle
21DK-14 Core of plagioclase microphenocryst
21DK-15 Mantle of plagioclase microphenocryst
21DK-16 Rim of plagioclase microphenocryst
21DK-17 Plagioclase groundmass
21DK-18 Plagioclase groundmass
21DK-19 Plagioclase inclusion in plagioclase
21DK-20 Plagioclase inclusion in clinopyroxene
26DK-01 Olivine phenocryst core
26DK-02 Olivine phenocryst core

	260K-03	260K-04	260K-05	260K-06	260K-07	260K-08	260K-09	260K-10	260K-11	260K-12
	OLV	OLV	OLV	OLV	OLV	OLV	CPX	CPX	CPX	CPX
Oxide										
SiO2	36.890	36.810	36.280	36.740	36.402	36.402	50.550	51.811	49.985	50.430
Al2O3	.043	.043	.030	.030	.023	.022	2.870	2.450	2.633	1.803
TiO2	-	-	.030	.060	.050	.067	.670	.582	1.231	.844
FeO	28.201	28.720	28.900	28.740	28.140	32.461	9.814	10.500	14.020	15.260
MnO	.560	.450	.540	.540	.541	.067	.232	.298	.474	.524
MgO	33.420	33.680	33.760	33.480	33.560	30.094	14.970	15.350	12.642	16.013
CaO	.210	.264	.160	.230	.210	.232	19.790	19.210	18.374	14.480
Na2O	-	.060	-	.030	-	.037	.341	.280	.366	.251
K2O	-	-	.010	-	.080	.041	.020	.010	.014	.004
NiO	-	.040	.060	.030	-	.022	.050	-	.002	.043
Cr2O3	-	.050	-	-	.022	-	.020	-	-	.027
Cl	-	.070	.060	.050	-	.045	-	-	.074	-
Total	99.324	100.187	99.830	99.930	99.028	99.490	99.327	100.491	99.815	99.679
Cation										
Si	.997	.990	.982	.991	.989	.999	1.902	1.924	1.904	1.926
Al	.001	.001	.001	.001	.001	.001	.127	.107	.118	.081
Ti	-	-	.001	.001	.001	.001	.019	.016	.035	.024
Fe	.638	.646	.654	.648	.639	.745	.309	.326	.447	.487
Mn	.013	.010	.012	.012	.012	.014	.007	.009	.015	.016
Mg	1.350	1.350	1.360	1.350	1.360	1.231	.840	.850	.718	.912
Ca	.006	.008	.005	.007	.006	.007	.798	.764	.750	.593
Na	-	.003	-	.001	-	.002	.025	.020	.027	.018
K	-	-	-	-	.003	.001	.001	-	.001	-
Ni	-	.001	.001	.001	-	-	.001	-	-	.001
Cr	-	.001	-	-	-	-	-	-	-	.001
Cl	-	.003	.003	.002	-	.002	-	-	.005	-
Total	3.002	3.014	3.020	3.010	3.011	3.003	4.029	4.017	4.020	4.059
Fe/Fe+Mg	.321	.324	.324	.325	.320	.377	.269	.277	.384	.348
Mg*	67.900	67.600	67.800	67.500	68.000	62.300	-	-	-	-
Ca*	-	-	-	-	-	-	40.800	39.200	38.900	29.500
An	-	-	-	-	-	-	-	-	-	-

260K-03 Olivine phenocryst core
260K-04 Olivine phenocryst core
260K-05 Olivine phenocryst core
260K-06 Olivine phenocryst core
260K-07 Olivine phenocryst core
260K-08 Olivine groundmass
260K-09 Clinopyroxene phenocryst core
260K-10 Clinopyroxene clots
260K-11 Clinopyroxene groundmass
260K-12 Clinopyroxene groundmass

	260K-13	260K-14	260K-15	260K-16	260K-17	260K-18	260K-19	260K-20	260K-21	260K-22
	PLG	PLG	PLG	PLG	PLG	PLG	PLG	PLG	PLG	PLG
Oxide										
SiO2	46.193	50.923	55.480	47.860	46.152	55.114	48.042	48.651	54.520	55.453
Al2O3	34.142	30.412	26.420	32.520	34.695	27.835	33.539	32.432	24.153	27.550
TiO2	.076	.062	.050	.034	.047	.087	-	-	.260	.074
FeO	.597	.940	.910	.730	.578	1.002	.763	.653	3.050	.940
MnO	.017	-	.020	.040	.058	-	-	.102	.090	-
MgO	.063	.170	.117	.080	.074	.152	.081	.092	1.560	.130
CaO	17.700	14.370	10.720	16.500	17.989	11.202	16.891	16.171	11.060	10.910
Na2O	1.653	3.730	5.550	2.380	1.344	4.861	2.059	2.547	4.910	5.380
K2O	.050	.105	.270	.060	.047	.157	.032	.091	.234	.260
NiO	.052	-	-	.090	-	.063	-	-	-	.009
Cr2O3	-	-	-	.030	.046	.054	-	.019	-	-
Cl	-	.001	.030	-	.048	-	.008	.020	-	.050
Total	100.543	100.713	99.567	100.324	101.078	100.527	101.415	100.778	99.837	100.756
Cation										
Si	8.490	9.268	10.103	8.800	8.439	9.933	8.723	8.882	10.036	9.980
Al	7.400	6.524	5.670	7.042	7.476	5.912	7.177	6.978	5.240	5.845
Ti	.011	.008	.007	.005	.007	.012	-	-	.035	.010
Fe	.092	.143	.138	.112	.088	.151	.116	.100	.470	.141
Mn	.003	-	.003	.005	.009	-	-	.016	.014	-
Mg	.017	.046	.032	.023	.020	.041	.022	.025	.429	.034
Ca	3.490	2.802	2.092	3.250	3.524	2.163	3.286	3.163	2.182	2.104
Na	.589	1.316	1.959	.849	.476	1.699	.725	.901	1.752	1.880
K	.012	.024	.063	.014	.011	.036	.007	.021	.055	.059
Ni	.008	-	-	.013	-	.009	-	-	-	.001
Cr	-	-	-	.004	.007	.008	-	.003	-	-
Cl	-	-	.008	-	.015	-	.002	.006	-	.014
Total	22.102	20.131	20.074	20.109	20.072	19.963	20.057	20.095	20.213	20.068
Fe/Fe+Mg	.841	.755	.813	.832	.814	.787	.841	.800	.523	.806
Mg*	-	-	-	-	-	-	-	-	-	-
Ca*	-	-	-	-	-	-	-	-	-	-
An	85.290	67.650	50.850	79.000	87.860	55.490	81.780	77.430	54.700	52.070

260K-13 Plagioclase phenocryst core
260K-14 Plagioclase phenocryst mantle
260K-15 Plagioclase phenocryst rim
260K-16 Plagioclase phenocryst mantle
260K-17 Plagioclase phenocryst core
260K-18 Plagioclase phenocryst rim
260K-19 Core of plagioclase phenocryst in clot
260K-20 Mantle of plagioclase phenocryst in clot
260K-21 Rim of plagioclase phenocryst
260K-22 Plagioclase groundmass

	260K-23	260K-24	260K-25	260K-26	260K-27	260K-28	G282-01	G282-02	G282-03	G282-04
	PLG	PLG	PLG	PLG	PLG	PLG	CPX	CPX	CPX	PIG
Oxide										
SiO2	54.460	51.735	46.163	47.046	44.413	52.223	50.413	50.607	50.172	52.070
Al2O3	26.960	30.984	34.810	32.650	34.980	30.393	3.463	2.800	3.230	.560
TiO2	.100	-	.050	.031	-	.054	.830	.584	.750	.300
FeO	.960	.583	.593	.672	.662	.672	9.510	10.000	9.840	21.310
MnO	.010	.035	-	.005	.075	-	.270	.291	.281	.730
MgO	.114	.122	.058	.080	.068	.074	14.060	14.990	14.620	20.120
CaO	10.680	14.124	18.567	16.630	18.093	13.720	20.114	19.680	19.880	4.220
Na2O	5.410	3.660	1.173	2.141	1.351	3.394	.421	.360	.400	.120
K2O	.290	.080	.041	.044	.042	.066	-	-	.020	.013
NiO	-	.030	.016	.105	-	-	.040	-	.040	.030
Cr2O3	-	-	.002	.009	-	.027	.060	-	-	-
Cl	-	-	.005	.004	.010	-	-	-	.030	.013
Total	98.984	101.353	101.475	99.417	99.694	100.623	99.181	99.312	99.263	99.486
Cation										
Si	9.980	9.317	8.413	8.730	8.260	9.412	1.900	1.910	1.890	1.970
Al	5.824	6.580	7.476	7.140	7.670	6.460	.154	.124	.143	.025
Ti	.014	-	.007	.004	-	.007	.023	.017	.021	.008
Fe	.147	.088	.090	.104	.103	.101	.299	.315	.310	.674
Mn	.001	.005	0.000	.001	.012	-	.009	.009	.009	.023
Mg	.031	.033	.016	.002	.019	.020	.789	.841	.821	1.134
Ca	2.100	2.725	3.630	3.304	3.600	2.650	.811	.794	.803	.171
Na	1.920	1.276	.415	.770	.487	1.390	.031	.026	.029	.009
K	.068	.018	.010	.010	.010	.015	-	-	.001	.001
Ni	-	.004	.002	.016	-	-	.001	-	.001	.001
Cr	-	-	-	.001	-	.004	.002	-	-	-
Cl	-	-	.001	.001	.003	-	-	-	.002	.001
Total	20.090	20.042	20.056	20.094	20.161	20.053	4.017	4.030	4.032	4.016
Fe/Fe+Mg	.825	.729	.851	.825	.845	.837	.275	.272	.274	.373
Mg*	-	-	-	-	-	-	-	-	-	-
Ca*	-	-	-	-	-	-	42.500	40.500	41.300	8.500
An	51.310	67.880	89.510	80.900	87.880	65.370	-	-	-	-

260K-23 Plagioclase groundmass
260K-24 Rim of plagioclase inclusion
260K-25 Core of plagioclase inclusion
260K-26 Core of plagioclase inclusion
260K-27 Core of plagioclase inclusion
260K-28 Rim of plagioclase inclusion
G282-01 Clinopyroxene phenocryst
G282-02 Anhedral clinopyroxene phenocryst
G282-03 Anhedral clinopyroxene phenocryst in clot
G282-04 Pigeonite groundmass

	G282-05	G282-06	G282-07	G282-08	G282-09	G282-10	G282-11	G282-12	G258-01	G258-02
	PLG	PLG	PLG	PLG	PLG	PLG	PLG	PLG	CPX	CPX
Oxide										
SiO2	47.820	47.790	54.810	51.720	45.410	51.840	53.940	51.180	50.550	50.150
Al2O3	32.350	33.300	27.179	29.910	34.790	29.920	28.610	30.370	4.860	4.660
TiO2	.072	.060	.110	.030	.040	.075	-	.060	.400	.680
FeO	.640	.580	1.270	.750	.620	.814	.653	.730	5.140	5.920
MnO	-	-	.010	.013	-	-	.044	.010	.330	.330
MgO	.070	.060	.190	.090	.060	.099	.124	.060	15.470	15.440
CaO	15.940	16.380	10.750	13.277	17.780	13.080	12.101	13.690	22.770	22.560
Na2O	2.540	2.210	5.170	3.996	1.260	3.910	4.780	3.660	.220	.310
K2O	.060	.035	.264	.120	.010	.121	.100	.070	-	-
NiO	.012	-	.019	-	.050	-	-	-	-	.070
Cr2O3	.040	.002	-	.020	.050	.040	-	-	.390	.370
Cl	.010	-	.020	.003	.010	.010	.023	.010	-	-
Total	99.554	100.417	99.792	99.929	100.080	99.909	100.375	99.840	100.130	100.490
Cation										
Si	8.840	8.750	9.970	9.440	8.380	9.460	9.760	9.350	1.860	1.850
Al	7.040	7.180	5.830	6.434	7.570	6.430	6.100	6.540	.211	.202
Ti	.010	.008	.015	.004	.005	.010	-	.008	.011	.019
Fe	.098	.880	.194	.114	.095	.124	.099	.111	.158	.182
Mn	-	-	.001	.002	-	-	.007	.002	.010	.010
Mg	.020	.016	.051	.024	.016	.027	.033	.016	.849	.849
Ca	3.160	3.213	2.095	2.597	3.520	2.560	2.350	2.680	.898	.891
Na	.909	.784	1.822	1.414	.450	1.380	1.680	1.300	.016	.022
K	.013	.008	.061	.028	.003	.028	.023	.017	-	-
Ni	.002	-	.003	-	.007	-	-	-	-	.002
Cr	.005	-	-	.002	.008	.005	-	-	.011	.011
Cl	.003	-	.005	.001	.004	.003	.007	.001	-	-
Total	20.100	20.049	20.047	20.060	20.055	20.024	20.050	20.026	4.025	4.037
Fe/Fe+Mg	.832	.847	.792	.829	.860	.821	.747	.872	.157	.177
Mg*	-	-	-	-	-	-	-	-	-	-
Ca*	-	-	-	-	-	-	-	-	46.900	46.100
An	77.390	80.220	52.660	64.300	88.590	64.430	57.980	67.120	-	-

G282-05 Plagioclase phenocryst mantle
G282-06 Plagioclase phenocryst core
G282-07 Plagioclase phenocryst rim
G282-08 Plagioclase phenocryst rim
G287-09 Core of plagioclase in clot
G282-10 Rim of plagioclase in clot
G282-11 Plagioclase microphenocryst
G282-12 Plagioclase inclusion
G258-01 Clinopyroxene phenocryst core
G258-02 Clinopyroxene phenocryst core

	G258-03	G258-04	G258-05	G258-06	G258-07	G258-08	G258-09	G258-10	G258-11	G258-12
	CPX	CPX	CPX	CPX	CPX	CPX	CPX	CPX	CPX	CPX
Oxide										
SiO2	53.360	49.600	53.008	51.060	50.370	52.871	53.750	49.245	53.890	52.804
Al2O3	2.350	6.480	2.400	4.980	5.750	1.877	2.196	4.877	1.895	2.946
TiO2	.210	.630	.280	.810	.640	.171	.131	1.024	.181	.213
FeO	4.070	5.590	3.800	6.330	5.350	3.306	3.734	7.369	3.045	3.807
MnO	.090	.203	.300	.194	-	.094	.001	.494	.108	-
MgO	16.820	14.250	16.790	14.750	14.694	17.552	16.970	14.440	17.337	16.480
CaO	22.810	22.140	23.140	21.150	22.573	22.984	22.660	21.561	22.758	23.033
Na2O	.205	.330	.143	.464	.086	.215	.271	.319	.201	.221
K2O	-	-	.021	-	.014	-	-	.020	-	.004
NiO	-	.096	.140	.210	.246	.034	-	.054	.002	-
Cr2O3	.435	.531	.365	.400	-	.668	.403	.530	.761	.741
Cl	.020	.009	-	.012	-	-	-	-	-	.005
Total	100.370	99.859	100.387	100.360	99.723	99.771	100.116	99.933	100.178	100.254
Cation										
Si	1.942	1.832	1.932	1.880	1.857	1.935	1.955	1.840	1.955	1.924
Al	.101	.282	.103	.216	.250	.081	.094	.214	.081	.127
Ti	.006	.018	.008	.022	.018	.005	.002	.029	.005	.006
Fe	.124	.173	.116	.195	.165	.101	.114	.230	.092	.116
Mn	.003	.006	.009	.006	-	.003	-	.016	.003	-
Mg	.912	.785	.912	.808	.808	.957	.920	.803	.938	.895
Ca	.889	.876	.904	.832	.892	.901	.880	.862	.885	.899
Na	.014	.024	.010	.033	.006	.015	.019	.023	.014	.016
K	-	-	.001	-	.001	-	-	.001	-	-
Ni	-	.003	.004	.006	.007	.001	-	.002	-	-
Cr	.013	.016	.011	.012	-	.019	.011	.016	.022	.021
Cl	.001	.001	-	.001	-	-	-	-	-	-
Total	4.004	4.001	4.009	4.006	4.003	4.018	3.936	4.033	3.995	4.004
Fe/Fe+Mg	.120	.180	.113	.194	.170	.096	.110	.223	.090	.115
Mg*	-	-	-	-	-	-	-	-	-	-
Ca*	46.100	47.600	46.600	45.200	47.800	45.900	46.100	45.110	46.100	47.100
An	-	-	-	-	-	-	-	-	-	-

G258-03 Clinopyroxene phenocryst core
G258-04 Clinopyroxene phenocryst core
G258-05 Clinopyroxene phenocryst core
G258-06 Clinopyroxene phenocryst core
G258-07 Euhedral clinopyroxene phenocryst
G258-08 Clinopyroxene microphenocryst
G258-09 Clinopyroxene microphenocryst
G258-10 Clinopyroxene phenocryst rim
G258-11 Anhedral clinopyroxene microphenocryst
G258-12 Anhedral clinopyroxene phenocryst

	G258-13	G258-14	G258-15	G258-16	G258-17	G258-18	G258-19	G258-20	G258-21	G258-22
	CPX	CPX	CPX	CPX	CPX	CPX	CPX	CPX	PLG	PLG
Oxide										
SiO2	49.180	50.100	49.640	49.610	52.492	50.587	51.924	49.821	44.730	44.217
Al2O3	6.550	5.161	5.990	6.031	3.210	6.470	3.750	5.366	34.830	35.003
TiO2	.865	.550	.624	.593	.332	.632	.430	.635	.020	.010
FeO	6.880	5.611	5.800	5.528	3.990	5.126	4.411	6.266	.620	.535
MnO	.053	.107	.087	.144	.121	.093	.074	.048	-	.027
MgO	14.102	14.724	14.154	14.980	16.085	14.048	15.695	14.399	.080	.110
CaO	21.680	22.631	22.465	22.532	22.710	22.227	22.877	22.356	18.200	18.430
Na2O	.365	.458	.387	.248	.214	.196	.195	.246	1.130	.950
K2O	-	.016	-	-	.030	-	-	-	.020	.063
NiO	.060	-	.083	.048	.061	.043	.006	-	.055	-
Cr2O3	.326	.568	.505	.230	.712	.250	.686	.823	-	-
Cl	.014	.026	-	-	-	.009	.007	-	-	.003
Total	100.075	99.952	99.735	99.944	99.957	99.681	100.055	99.960	99.685	99.348
Cation										
Si	1.821	1.853	1.839	1.831	1.920	1.860	1.902	1.845	8.310	8.243
Al	.286	.225	.261	.262	.138	.280	.162	.234	7.620	7.690
Ti	.024	.015	.017	.016	.009	.017	.012	.018	.002	.001
Fe	.213	.174	.180	.171	.122	.158	.135	.194	.096	.083
Mn	.002	.003	.003	.005	.004	.003	.002	.002	-	.004
Mg	.778	.812	.782	.824	.877	.770	.857	.795	.023	.031
Ca	.860	.897	.892	.891	.890	.875	.898	.887	3.620	3.680
Na	.026	.033	.028	.018	.015	.014	.014	.018	.408	.343
K	-	.001	-	-	.001	-	-	-	.005	.015
Ni	.002	-	.002	.001	.002	.001	-	-	.008	-
Cr	.010	.017	.015	.007	.021	.007	.020	.024	-	-
Cl	.001	.002	-	-	-	.001	-	-	-	.001
Total	4.022	4.030	4.019	4.027	3.999	3.986	4.003	4.017	20.090	20.091
Fe/Fe+Mg	.215	.176	.187	.172	.122	.170	.136	.196	.805	.732
Mg*	-	-	-	-	-	-	-	-	-	-
Ca*	46.400	47.600	48.000	47.100	47.000	48.400	47.500	47.230	-	-
An	-	-	-	-	-	-	-	-	89.760	91.130

G258-13 Clinopyroxene phenocryst
G258-14 Anhedral clinopyroxene phenocryst
G258-15 Anhedral clinopyroxene phenocryst
G258-16 Anhedral zoned clinopyroxene phenocryst
G258-17 Anhedral zoned clinopyroxene phenocryst
G258-18 Core of zoned clinopyroxene phenocryst
G258-19 Mantle of zoned clinopyroxene phenocryst
G258-20 Rim of zoned clinopyroxene phenocryst
G258-21 Plagioclase phenocryst core
G258-22 Plagioclase phenocryst core

	G258-23	G258-24	G258-25	G258-26	G258-27	G258-28	G256-01	G256-02	G256-03	G256-04
	PLG	PLG	PLG	PLG	PLG	PLG	OLV	OLV	OLV	OLV
Oxide										
SiO2	46.612	45.583	48.342	50.126	49.114	48.270	38.970	37.557	39.900	37.860
Al2O3	34.314	35.076	32.124	31.615	31.776	32.220	.035	.025	.050	.030
TiO2	-	.003	.044	.076	.064	.037	.030	-	.070	.040
FeO	.438	.348	.895	.946	.668	.621	18.490	24.600	12.820	25.340
MnO	.011	.014	-	-	-	.020	.244	.424	.211	.440
MgO	.097	.044	.422	.176	.154	.148	41.570	36.521	46.332	35.930
CaO	17.358	18.093	15.043	14.338	15.023	15.792	.198	.135	.171	.140
Na2O	1.264	.975	2.591	3.161	2.966	2.240	.020	.140	-	.003
K2O	.028	.013	.186	.103	.112	.109	-	-	-	.003
NiO	.057	-	-	-	-	-	.091	.042	.130	.082
Cr2O3	-	.006	.133	-	.142	.003	.041	.189	.011	-
Cl	-	.001	-	-	.029	.001	.018	.112	-	-
Total	100.179	100.156	99.780	100.541	100.048	99.461	99.707	99.745	99.695	99.868
Cation										
Si	8.558	8.389	8.900	9.128	9.007	8.904	.999	.994	.996	1.002
Al	7.425	7.608	6.970	6.784	6.870	7.004	.001	.001	.001	.001
Ti	-	-	.006	.008	.009	.005	.001	-	.001	.001
Fe	.067	.053	.138	.144	.102	.096	.396	.545	.268	.561
Mn	.002	.004	-	-	-	.003	.005	.010	.004	.010
Mg	.027	.011	.166	.048	.042	.041	1.590	1.442	1.724	1.417
Ca	3.414	3.568	2.967	2.800	2.952	3.121	.005	.004	.005	.004
Na	.450	.337	.925	1.112	1.054	.801	.001	.007	.005	-
K	.007	.003	.044	.024	.026	.026	-	-	-	-
Ni	.008	-	-	-	-	-	.002	.001	.003	.002
Cr	-	.001	.019	-	.021	-	.001	.004	-	-
Cl	-	.001	-	-	.009	-	.001	.005	-	-
Total	19.960	19.975	20.084	20.048	20.089	20.002	3.001	3.012	3.002	2.997
Fe/Fe+Mg	.716	.828	.544	.751	.709	.702	.200	.274	.134	.283
Mg*	-	-	-	-	-	-	80.000	72.600	86.600	71.800
Ca*	-	-	-	-	-	-	-	-	-	-
An	88.190	91.300	75.380	71.140	73.210	79.050	-	-	-	-

G258-23 Plagioclase phenocryst core
G258-24 Plagioclase phenocryst core
G258-25 Plagioclase phenocryst mantle
G258-26 Plagioclase phenocryst mantle
G258-27 Plagioclase microphenocryst
G258-28 Plagioclase phenocryst mantle
G256-01 Olivine phenocryst core
G256-02 Olivine phenocryst rim
G256-03 Anhedral olivine phenocryst
G256-04 Anhedral olivine phenocryst

	G256-05	G256-06	G256-07	G256-08	G256-09	G256-10	G256-11	G256-12	G256-13	G256-14
	OLV	OLV	OLV	OLV	OLV	OLV	OLV	OLV	OLV	OLV
Oxide										
SiO2	37.610	40.131	37.793	38.412	37.532	38.070	37.510	37.910	38.037	37.640
Al2O3	.005	.030	.015	.020	.012	.010	.003	-	-	.025
TiO2	.007	-	.036	.030	.005	.003	-	.001	.030	.125
FeO	26.430	10.310	25.348	20.620	29.311	21.370	24.730	25.080	24.692	25.481
MnO	.440	.164	.570	.304	.452	.390	.352	.380	.370	.562
MgO	34.980	48.650	36.033	40.070	32.579	40.370	37.430	36.770	36.462	36.575
CaO	.180	.180	.144	.200	.181	.187	.109	.107	.158	.146
Na2O	-	.011	-	-	-	-	-	.002	.189	-
K2O	-	-	-	-	-	-	.002	.009	.001	.027
NiO	.030	.274	.015	.140	.029	-	.055	.043	.095	.116
Cr2O3	-	.020	.023	-	-	.034	-	-	.263	.097
Cl	.002	.007	.010	-	-	-	.006	.002	.183	.004
Total	99.684	99.777	99.987	99.796	100.101	100.434	100.197	100.304	100.480	100.798
Cation										
Si	1.002	.991	.999	.995	1.009	.984	.987	.997	1.000	.989
Al	-	.001	-	.001	-	-	-	-	-	.001
Ti	-	-	.001	.001	-	-	-	-	.001	.002
Fe	.589	.213	.561	.447	.659	.462	.544	.552	.543	.560
Mn	.010	.003	.013	.007	.010	.009	.008	.008	.008	.013
Mg	1.390	1.790	1.421	1.547	1.310	1.555	1.469	1.442	1.429	1.433
Ca	.005	.005	.004	.005	.005	.005	.003	.003	.004	.004
Na	-	.001	-	-	-	-	-	-	.010	-
K	-	-	-	-	-	-	-	-	-	.001
Ni	.001	.005	-	.003	.001	-	.001	.001	.002	.002
Cr	-	-	-	-	-	.001	-	-	.005	.002
Cl	-	-	-	-	-	-	-	-	.008	-
Total	2.998	3.009	3.000	3.006	2.991	3.016	3.013	3.003	3.010	3.008
Fe/Fe+Mg	.298	.106	.283	.224	.335	.229	.270	.277	.275	.281
Mg*	70.200	89.400	72.000	77.600	66.500	77.100	73.000	72.300	72.500	71.900
Ca*	-	-	-	-	-	-	-	-	-	-
An	-	-	-	-	-	-	-	-	-	-

G256-05 Anhedral olivine phenocryst
G256-06 Anhedral olivine phenocryst
G256-07 Anhedral olivine phenocryst
G256-08 Olivine groundmass
G256-09 Olivine groundmass
G256-10 Olivine inclusion in clinopyroxene
G256-11 Olivine inclusion in amphibole
G256-12 Olivine inclusion in amphibole
G256-13 Olivine inclusion in amphibole
G256-14 Olivine inclusion in plagioclase

	G256-15	G256-16	G256-17	G256-18	G256-19	G256-20	G256-21	G256-22	G256-23	G256-24
	OLV	OLV	OLV	OLV	OLV	OLV	OPX	OPX	CPX	CPX
Oxide										
SiO2	37.740	37.443	39.804	36.920	39.962	37.230	53.940	53.491	53.501	51.676
Al2O3	.020	-	.017	.016	.036	.040	.817	1.712	1.770	2.945
TiO2	.020	.012	.186	-	.011	.020	.183	.324	.430	.633
FeO	25.740	25.603	12.940	26.590	12.730	25.240	19.455	19.996	9.396	9.026
MnO	.435	.470	.150	.479	.159	.403	.766	.674	.276	.164
MgO	35.580	35.870	46.950	35.013	46.812	35.971	22.915	22.643	16.077	15.004
CaO	.130	.142	.180	.143	.211	.159	1.512	1.805	18.939	19.824
NaO	-	-	-	-	.018	-	.001	-	.220	.172
K2O	-	.017	.006	-	-	.001	-	-	.002	-
NiO	.070	.015	.302	-	.176	.126	.014	-	-	.052
Cr2O3	-	-	.068	-	-	-	.075	.004	-	-
Cl	-	.013	-	-	-	-	-	-	-	-
Total	99.735	99.585	100.603	99.161	100.115	99.190	99.678	100.649	100.611	99.496
Cation										
Si	1.002	.996	.987	.992	.993	.993	1.993	1.963	1.965	1.926
Al	.001	-	-	-	.001	.001	.036	.073	.077	.129
Ti	-	-	.003	-	-	-	.005	.009	.012	.018
Fe	.572	.570	.268	.598	.003	.563	.601	.613	.290	.281
Mn	.010	.011	.003	.011	1.734	.009	.024	.021	.009	.005
Mg	1.408	1.423	1.735	1.403	.006	1.431	1.262	1.239	.880	.834
Ca	.004	.004	.005	.004	.001	.005	.060	.070	.745	.791
Na	-	-	-	-	-	-	-	-	.016	.012
K	-	.001	-	-	-	-	-	-	-	-
Ni	.001	-	.006	-	.004	.003	-	-	-	.002
Cr	-	-	.001	-	-	-	.002	-	-	-
Cl	-	.001	-	-	-	-	-	-	-	-
Total	2.997	3.005	3.009	3.008	3.007	3.006	3.983	2.661	3.992	3.998
Fe/Fe+Mg	.289	.286	.134	.299	.132	.282	.323	.331	.247	.252
Mg*	71.100	71.400	86.600	70.100	86.800	71.800	-	-	-	-
Ca*	-	-	-	-	-	-	3.000	3.600	38.700	41.390
An	-	-	-	-	-	-	-	-	-	-

	G256-25	G256-26	G256-27	G256-28	G256-29	G256-30	G256-31	G256-32	G256-33	G256-34
	CPX	CPX	CPX	CPX	CPX	CPX	CPX	CPX	CPX	CPX
Oxide										
SiO2	53.063	49.797	50.061	49.971	49.100	52.375	49.943	50.152	55.363	49.991
Al2O3	2.379	5.259	3.930	4.286	5.662	2.713	5.532	5.479	3.608	4.004
TiO2	.518	.629	.950	.725	.759	.298	.533	.621	.804	.673
FeO	7.441	4.834	9.619	6.756	6.834	4.433	4.728	5.126	10.038	8.620
MnO	.270	.023	.311	.118	.146	.201	.047	-	.350	.531
MgO	15.475	14.885	14.015	14.649	14.216	16.487	14.480	14.930	12.252	14.582
CaO	20.826	23.281	20.384	22.319	22.385	22.821	23.500	23.215	16.802	20.902
NaO	.179	.285	.319	.278	.380	.163	.211	.182	.906	.323
K2O	.013	-	-	-	.011	.028	.017	.015	.277	-
NiO	.030	.004	-	-	-	.048	-	-	.034	.041
Cr2O3	.076	1.107	-	.153	.239	.472	.718	.683	.033	-
Cl	.015	.072	-	.098	.019	.007	-	-	.019	.005
Total	100.285	100.176	99.589	99.353	99.751	100.046	99.709	100.403	100.486	99.672
Cation										
Si	1.950	1.837	1.979	1.867	1.830	1.920	1.846	1.842	2.021	1.872
Al	.103	.229	.174	.189	.249	.117	.241	.237	.155	.177
Ti	.014	.017	.027	.020	.021	.008	.015	.017	.022	.019
Fe	.229	.149	.302	.211	.213	.136	.146	.157	.306	.270
Mn	.008	.001	.010	.004	.005	.006	.001	-	.011	.016
Mg	.848	.819	.784	.816	.790	.901	.798	.818	.667	.814
Ca	.820	.920	.820	.894	.894	.896	.931	.914	.657	.838
Na	.013	.020	.023	.020	.027	.012	.015	.013	.064	.024
K	.001	-	-	-	.001	.001	.001	.001	.013	-
Ni	.001	-	-	-	-	.001	-	-	.001	.001
Cr	.002	.032	-	.004	.007	.014	.021	.020	.001	-
Cl	.001	.004	-	.006	.001	-	-	-	.001	-
Total	3.990	4.030	4.019	4.031	4.037	4.013	4.016	4.019	3.919	4.031
Fe/Fe+Mg	.212	.154	.278	.206	.212	.131	.155	.162	.315	.249
Mg*	-	-	-	-	-	-	-	-	-	-
Ca*	43.000	49.000	42.800	46.400	47.000	46.000	50.000	48.000	46.100	46.400
An	-	-	-	-	-	-	-	-	-	-

G256-15 Anhedral olivine microphenocryst
G256-16 Anhedral olivine microphenocryst
G256-17 Olivine phenocryst core
G256-18 Olivine phenocryst rim
G256-19 Olivine microphenocryst core
G256-20 Anhedral olivine microphenocryst
G256-21 Orthopyroxene phenocryst
G256-22 Orthopyroxene microphenocryst
G256-23 Clinopyroxene phenocryst
G256-24 Clinopyroxene groundmass

G256-25 Clinopyroxene microphenocryst
G256-26 Clinopyroxene microphenocryst
G256-27 Clinopyroxene microphenocryst
G256-28 Clinopyroxene microphenocryst
G256-29 Clinopyroxene phenocryst
G256-30 Clinopyroxene phenocryst
G256-31 Clinopyroxene phenocryst
G256-32 Clinopyroxene phenocryst
G256-33 Clinopyroxene phenocryst
G256-34 Anhedral clinopyroxene phenocryst

	G256-35	G256-36	G256-37	G256-38	G256-39	G256-40	G256-41	G256-42	G256-43	G256-44
	CPX	CPX	CPX	CPX	CPX	CPX	CPX	CPX	CPX	CPX
Oxide										
SiO2	49.330	49.464	51.308	51.694	52.040	50.787	50.709	50.572	51.057	50.221
Al2O3	5.064	5.184	2.277	1.894	1.726	2.904	3.690	3.587	3.738	4.180
TiO2	.820	.777	.396	.423	.418	.562	.470	.523	.681	.931
FeO	7.630	7.257	10.215	9.931	9.974	10.228	8.038	7.535	8.776	7.006
MnO	.205	.198	.432	.395	.336	.372	.162	.162	.233	.125
MgO	14.140	14.388	14.237	14.505	15.303	14.119	14.823	14.848	14.661	14.700
CaO	22.027	22.310	20.561	20.445	20.155	20.335	22.261	22.069	20.840	21.620
NaO	.261	.298	.330	.310	.284	.271	.235	.218	.252	.542
K2O	.012	.014	-	.009	.004	.010	-	-	-	.031
NiO	.060	.011	.076	.068	-	.018	-	.071	-	-
Cr2O3	.091	.036	.020	.025	-	-	-	.015	.073	-
Cl	-	.005	-	.010	.002	-	-	-	-	-
Total	99.640	99.942	99.852	99.709	100.242	99.606	100.388	99.600	100.311	99.356
Cation										
Si	1.844	1.841	1.926	1.939	1.939	1.910	1.882	1.887	1.893	1.874
Al	.223	.227	.101	.084	.076	.129	.161	.158	.163	.184
Ti	.023	.022	.011	.012	.012	.016	.013	.015	.019	.026
Fe	.238	.226	.321	.312	.311	.322	.249	.235	.272	.219
Mn	.006	.006	.014	.013	.011	.012	.005	.005	.007	.004
Mg	.788	.798	.797	.811	.850	.791	.820	.826	.810	.818
Ca	.882	.890	.827	.822	.804	.819	.885	.882	.828	.864
Na	.019	.021	.024	.023	.020	.020	.017	.016	.018	.039
K	.001	.001	-	-	-	-	-	-	-	.001
Ni	.002	-	.002	.002	-	-	-	.002	-	-
Cr	.003	.001	-	.001	-	-	-	-	.002	-
Cl	-	-	-	.001	-	-	-	-	-	-
Total	4.030	4.034	4.023	4.019	4.022	4.019	4.032	4.027	4.014	4.029
Fe/Fe+Mg	.232	.221	.287	.277	.268	.289	.233	.222	.251	.211
Mg*	-	-	-	-	-	-	-	-	-	-
Ca*	46.100	46.000	42.000	42.000	41.000	42.100	45.200	45.300	43.200	45.350
An	-	-	-	-	-	-	-	-	-	-

	G256-45	G256-46	G256-47	G256-48	G256-49
	MAG	MAG	MAG	MAG	MAG
Oxide					
SiO2	.127	.109	.133	.139	.134
Al2O3	3.656	2.956	4.495	4.495	6.478
TiO2	10.792	12.653	10.120	10.108	6.911
FeO	76.245	76.822	75.455	75.668	74.970
MnO	.446	.282	.289	.322	.178
MgO	2.483	2.235	3.404	3.321	4.609
CaO	.043	-	.077	.088	.037
NaO	-	-	.026	-	.133
K2O	.006	-	.002	.010	.001
NiO	.037	.045	.099	.063	.049
Cr2O3	.005	-	.008	.066	.156
Cl	-	-	.007	.009	.089
Total	93.840	95.101	94.116	93.619	93.745
Cation					
Si	.045	.037	.046	.048	.047
Al	1.517	1.205	1.842	1.840	2.649
Ti	2.858	3.296	2.646	2.639	1.803
Fe	22.453	22.267	21.936	21.972	21.754
Mn	.133	.008	.085	.095	.052
Mg	1.303	1.157	1.764	1.719	2.384
Ca	.016	-	.029	.033	.014
Na	-	-	.017	-	.090
K	.002	-	.001	.005	-
Ni	.011	.002	.028	.018	.014
Cr	.001	-	.002	.018	.090
Cl	-	-	.004	.005	.052
Total	28.339	27.972	28.399	28.391	28.902
Fe/Fe+Mg	.945	.951	.926	.927	.901
Mg*	-	-	-	-	-
Ca*	-	-	-	-	-
An	-	-	-	-	-

G256-35 Euhedral clinopyroxene phenocryst
G256-36 Euhedral clinopyroxene phenocryst
G256-37 Clinopyroxene phenocryst
G256-38 Clinopyroxene phenocryst in clot
G256-39 Clinopyroxene phenocryst in clot
G256-40 Clinopyroxene in gabbro
G256-41 Clinopyroxene in gabbro
G256-42 Clinopyroxene in gabbro
G256-43 Clinopyroxene in gabbro
G256-44 Clinopyroxene inclusion in amphibole

G256-45 Magnetite microphenocryst
G256-46 Magnetite inclusion in clinopyroxene
G256-47 Magnetite inclusion in clinopyroxene
G256-48 Magnetite inclusion in clinopyroxene
G256-49 Magnetite inclusion in amphibole

	G256-50	G256-51	G256-52	G256-53	G256-54	G256-55	G256-56	G256-57	G256-58	G256-59
	MAG	HBD	HBD	HBD	HBD	HBD	HBD	PLG	PLG	PLG
Oxide										
SiO2	.146	41.288	42.394	41.339	43.152	41.637	42.053	48.929	51.119	54.353
Al2O3	6.095	13.026	13.230	13.251	13.242	12.885	13.262	32.800	30.773	26.305
TiO2	7.261	2.175	2.055	2.069	2.107	2.388	2.098	.025	-	.239
FeO	75.090	11.340	10.906	10.989	11.151	11.355	11.007	.598	.593	2.438
MnO	.290	.230	.159	.136	.145	.147	.159	-	.002	.051
MgO	4.563	14.209	14.344	14.235	14.302	14.180	14.087	.042	.090	1.051
CaO	.021	11.740	11.508	11.668	11.791	11.647	11.619	14.653	13.790	11.546
Na2O	.032	2.373	2.461	2.496	2.601	2.489	2.447	2.750	3.808	3.696
K2O	-	.196	.166	.186	.208	.223	.224	.031	.081	.390
NiO	.062	.064	-	.036	.073	.020	-	.024	.098	-
Cr2O3	.061	.032	.011	-	-	.015	-	-	-	-
Cl	-	.018	-	.009	-	-	-	.010	.015	.028
Total	93.619	96.691	97.234	96.414	98.773	96.987	96.956	99.861	100.369	100.097
Cation										
Si	.051	6.400	6.491	6.699	6.513	6.428	6.470	8.955	9.301	9.915
Al	2.498	2.380	2.387	2.421	2.355	2.344	2.404	7.075	6.599	5.655
Ti	1.899	.254	.237	.241	.239	.275	.243	.004	-	.033
Fe	21.841	1.470	1.396	1.425	1.408	1.464	1.416	.091	.090	.372
Mn	.085	.030	.020	.018	.019	.020	.021	-	-	.008
Mg	2.366	3.284	3.274	3.289	3.218	3.264	3.231	.012	.024	.286
Ca	.008	1.950	1.888	1.938	1.906	1.928	1.915	2.873	2.688	2.257
Na	.021	.713	.730	.750	.762	.744	.730	.976	1.343	1.307
K	-	.039	.032	.036	.040	.044	.044	.007	.019	.091
Ni	.017	.008	-	.004	.008	.004	-	.003	.014	-
Cr	.017	.004	.001	-	-	-	-	-	-	-
Cl	-	.005	-	.002	-	-	-	.003	.005	.009
Total	28.803	16.537	16.456	17.147	16.468	16.515	16.474	19.999	20.085	19.932
Fe/Fe+Mg	.902	.309	.299	.302	.304	.310	.305	.888	.788	.565
Mg*	-	-	-	-	-	-	-	-	-	-
Ca*	-	-	-	-	-	-	-	-	-	-
An	-	-	-	-	-	-	-	74.510	66.370	61.750

G256-50 Magnetite inclusion in amphibole
G256-51 Amphibole
G256-52 Amphibole
G256-53 Amphibole
G256-54 Amphibole
G256-55 Amphibole
G256-56 Amphibole
G256-57 Plagioclase phenocryst core
G256-58 Plagioclase phenocryst core
G256-59 Plagioclase phenocryst core

	G256-60	G256-61	G256-62	G256-63	G256-64	G256-65	G256-66	G256-67	G256-68	G256-69
	PLG	PLG	PLG	PLG	PLG	PLG	PLG	PLG	PLG	PLG
Oxide										
SiO2	46.395	47.586	45.179	45.172	44.117	50.045	45.345	53.262	53.326	47.473
Al2O3	33.451	33.232	34.333	35.035	35.822	31.116	35.042	29.112	29.157	33.765
TiO2	.007	.013	.022	.048	.060	.002	.042	.039	.040	.013
FeO	.474	.410	.524	.606	.663	.714	.527	.899	.779	.753
MnO	.042	-	-	-	-	-	.034	-	.038	-
MgO	.074	-	.038	.050	.061	.104	.060	.128	.006	.082
CaO	17.214	16.460	18.078	18.013	18.645	14.338	18.704	12.685	12.273	16.205
Na2O	1.835	2.394	1.204	1.072	.912	3.547	.921	4.400	4.620	1.983
K2O	.004	-	.007	.034	-	.059	.017	.100	.136	.038
NiO	-	-	-	.025	-	.056	.023	.020	-	-
Cr2O3	-	.120	.016	-	.006	-	.072	-	-	-
Cl	-	.073	-	-	-	-	-	.001	.009	-
Total	99.495	100.289	99.401	100.055	100.287	99.979	100.787	100.646	100.445	100.312
Cation										
Si	8.596	8.732	8.399	8.341	8.152	9.165	8.325	9.633	9.654	8.695
Al	7.305	7.187	7.522	7.621	7.802	6.716	7.582	6.206	6.221	7.289
Ti	.001	.002	.003	.005	.008	-	.006	.005	.005	.002
Fe	.073	.063	.082	.096	.102	.109	.081	.136	.118	.115
Mn	.007	-	-	-	-	-	.005	-	.006	-
Mg	.020	-	.010	.015	.017	.028	.016	.035	.018	.022
Ca	3.417	3.236	3.601	3.563	3.692	2.813	3.679	2.458	2.381	3.180
Na	.659	.852	.434	.384	.327	1.259	.328	1.543	1.622	.704
K	.001	-	.002	.005	-	.014	.004	.023	.032	.009
Ni	-	-	-	.005	-	.008	.003	.003	-	-
Cr	-	.017	.002	-	.001	-	.010	-	-	-
Cl	-	.023	-	-	-	-	-	-	.003	-
Total	20.080	20.112	20.054	20.035	20.101	20.113	20.039	20.042	20.059	20.016
Fe/Fe+Mg	.783	1.000	.886	.872	.859	.794	.831	.798	.869	.838
Mg*	-	-	-	-	-	-	-	-	-	-
Ca*	-	-	-	-	-	-	-	-	-	-
An	83.810	79.160	89.200	90.160	91.860	68.840	91.720	61.080	59.009	81.680

G256-60 Plagioclase phenocryst core
G256-61 Plagioclase phenocryst core
G256-62 Plagioclase in gabbro
G256-63 Plagioclase in gabbro
G256-64 Plagioclase in gabbro
G256-65 Plagioclase microphenocryst
G256-66 Corroded plagioclase microphenocryst
G256-67 Plagioclase phenocryst rim
G256-68 Plagioclase groundmass
G256-69 Plagioclase groundmass

	G256-70	G256-71	G256-72	G257-01	G257-02	G257-03	G257-04	G257-05	G257-06	G257-07
	PLG	PLG	PLG	OPX	OPX	OPX	OPX	OPX	OPX	OPX
Oxide										
SiO2	56.912	60.008	44.459	53.086	53.716	55.161	53.190	52.922	53.279	53.599
Al2O3	26.114	24.039	34.828	1.916	1.745	.996	2.139	2.322	1.279	1.300
TiO2	.110	.177	.008	.171	.190	.251	.297	.296	.166	.117
FeO	.048	1.075	.552	17.611	15.456	13.636	15.197	15.323	17.616	16.914
MnO	.052	.010	.010	.351	.342	.289	.290	.354	.551	.566
MgO	.118	.140	.042	25.194	26.787	27.889	26.816	26.654	25.504	25.911
CaO	9.961	8.474	18.648	1.441	1.649	1.710	1.457	1.485	1.536	1.611
Na2O	4.997	5.411	.973	.052	.017	-	-	.019	.003	-
K2O	.413	.707	.012	-	-	.001	-	-	.020	.017
NiO	-	.082	-	-	-	.057	-	-	-	.038
Cr2O3	.020	-	-	.048	-	-	-	-	.038	.011
Cl	.014	.005	.002	.020	.047	.009	-	-	.001	-
Total	99.757	100.129	99.535	99.889	99.950	99.999	99.386	99.376	99.993	100.084
Cation										
Si	10.286	10.743	8.273	1.942	1.944	1.975	1.933	1.926	1.949	1.953
Al	5.562	5.072	7.638	.083	.075	.042	.092	.100	.055	.056
Ti	.015	.024	.001	.005	.004	.007	.008	.008	.004	.003
Fe	.158	.161	.086	.539	.468	.408	.462	.466	.539	.515
Mn	.008	.001	.002	.001	.010	.009	.009	.011	.017	.017
Mg	.032	.037	.012	1.374	1.446	1.489	1.453	1.446	1.391	1.407
Ca	1.929	1.625	3.718	.056	.064	.066	.057	.058	.060	.063
Na	1.751	1.878	.351	.004	.001	-	-	.001	-	-
K	.095	.162	.003	-	-	-	-	-	-	.001
Ni	-	.012	-	-	-	.002	-	-	-	.001
Cr	.003	-	-	.001	-	-	-	-	-	-
Cl	.004	.002	.001	.001	.003	.001	-	-	-	-
Total	19.844	19.718	20.084	4.016	4.015	3.998	4.013	4.017	4.015	4.017
Fe/Fe+Mg	.833	.811	.879	.282	.245	.215	.241	.244	.279	.268
Mg*	-	-	-	-	-	-	-	-	-	-
Ca*	-	-	-	3.200	3.330	3.350	3.000	3.000	3.000	3.000
An	51.100	46.390	91.310	-	-	-	-	-	-	-

	G257-08	G257-09	G257-10	G257-11	G257-12	G257-13	G257-14	G257-15	G257-16	G257-17
	PIG	PIG	CPX	CPX	CPX	CPX	CPX	CPX	CPX	CPX
Oxide										
SiO2	53.153	53.742	50.683	51.017	51.108	50.799	50.259	51.392	51.243	52.340
Al2O3	1.244	.703	2.668	2.725	2.615	3.754	3.489	2.746	2.540	2.073
TiO2	.563	.314	.773	.427	.497	1.261	.696	.484	.525	.458
FeO	18.022	17.612	10.277	9.379	8.897	12.706	8.726	9.371	8.876	8.716
MnO	.642	.440	.326	.273	.385	.403	.173	.463	.452	.310
MgO	22.756	23.543	15.204	15.472	15.393	16.573	15.828	15.247	14.936	15.672
CaO	3.644	2.718	19.571	20.441	20.849	14.245	19.780	20.274	20.910	20.245
Na2O	-	.031	.339	.348	.280	.285	.137	.286	.275	.215
K2O	.004	-	-	-	-	.002	-	.023	.130	-
NiO	.033	-	.013	-	.033	-	-	-	.149	-
Cr2O3	-	.033	-	.040	.033	.003	-	.017	.006	-
Cl	-	-	-	-	-	-	-	-	-	.002
Total	100.061	99.136	99.854	100.122	100.088	100.031	99.089	100.304	100.041	100.031
Cation										
Si	1.959	1.986	1.900	1.902	1.905	1.889	1.884	1.911	1.913	1.940
Al	.054	.031	.118	.120	.115	.165	.154	.120	.112	.091
Ti	.016	.009	.022	.012	.014	.035	.020	.014	.015	.013
Fe	.555	.544	.322	.292	.277	.395	.273	.291	.277	.270
Mn	.020	.014	.010	.009	.012	.013	.006	.015	.014	.010
Mg	1.250	1.297	.850	.860	.855	.919	.884	.845	.831	.866
Ca	.144	.108	.786	.817	.833	.568	.794	.808	.836	.804
Na	-	.002	.025	.027	.020	.021	.010	.021	.020	.015
K	-	-	-	-	-	-	-	.001	.006	-
Ni	.001	-	-	-	.001	-	-	-	.004	-
Cr	-	.001	-	.001	.001	-	-	-	-	-
Cl	-	-	-	-	-	-	-	-	-	-
Total	3.999	3.991	4.032	4.038	4.033	4.004	4.025	4.026	4.029	4.010
Fe/Fe+Mg	.308	.296	.275	.254	.245	.301	.236	.256	.250	.238
Mg*	-	-	-	-	-	-	-	-	-	-
Ca*	7.300	5.500	39.939	41.300	42.135	30.000	40.600	42.000	42.700	41.200
An	-	-	-	-	-	-	-	-	-	-

G256-70 Plagioclase groundmass
G256-71 Plagioclase groundmass
G256-72 Plagioclase inclusion in horblende
G257-01 Anhedral orthopyroxene microphenocryst
G257-02 Anhedral orthopyroxene microphenocryst
G257-03 Clinopyroxene phenocryst core
G257-04 Anhedral orthopyroxene microphenocryst
G257-05 Orthopyroxene groundmass
G257-06 Orthopyroxene groundmass
G257-07 Orthopyroxene groundmass

G257-08 Pigeonite inclusion in plagioclase groundmass
G257-09 Pigeonite inclusion in plagioclase groundmass
G257-10 Clinopyroxene groundmass
G257-11 Clinopyroxene groundmass
G257-12 Clinopyroxene groundmass
G257-13 Clinopyroxene groundmass
G257-14 Clinopyroxene groundmass
G257-15 Clinopyroxene microphenocryst
G257-16 Clinopyroxene groundmass
G257-17 Clinopyroxene groundmass

	G257-18	G257-19	G257-20	G257-21	G257-22	G257-23	G257-24	G257-25	G257-26	G257-27
	CPX	CPX	CPX	OPX	MAG	HBD	HBD	HBD	HBD	HBD
Oxide										
SiO2	51.188	51.924	52.959	53.685	.153	41.502	41.653	41.943	41.631	41.409
Al2O3	3.529	2.915	1.304	.911	6.519	13.613	13.623	14.191	13.013	13.889
TiO2	.545	.709	.778	.566	12.779	2.135	2.108	2.353	2.103	2.237
FeO	8.869	8.426	12.249	19.197	70.245	10.435	11.653	10.293	10.176	11.568
MnO	.411	.253	.265	-	.541	.227	.298	.016	.128	.154
MgO	15.387	16.109	15.664	22.977	3.811	14.996	14.036	14.276	14.879	13.983
CaO	20.179	19.274	16.661	2.102	.277	12.185	11.653	12.185	11.987	11.635
Na2O	.361	.255	.305	.056	.110	2.608	2.661	2.491	2.552	2.500
K2O	.024	-	.013	-	.072	.292	.173	.233	.237	.258
NiO	-	-	.010	.012	-	-	.072	.107	-	-
Cr2O3	.097	-	.050	-	.001	.077	.361	.146	.017	.043
Cl	.024	-	-	.008	-	.049	.010	-	.003	.027
Total	100.615	99.864	100.258	99.514	94.508	98.119	98.301	98.235	96.724	97.703
Cation										
Si	1.893	1.920	1.968	1.983	.051	6.328	6.361	6.359	6.416	6.352
Al	.154	.127	.057	.040	2.551	2.446	2.451	2.536	2.363	2.512
Ti	.015	.020	.022	.016	3.191	.245	.242	.268	.244	.260
Fe	.274	.261	.381	.593	19.503	1.330	1.488	1.305	1.312	1.484
Mn	.013	.008	.008	-	.152	.029	.039	.002	.017	.020
Mg	.848	.888	.868	1.265	1.886	3.408	3.196	3.226	3.418	3.196
Ca	.800	.764	.663	.083	.099	1.127	1.906	1.979	1.897	1.912
Na	.026	.018	.022	.004	.071	.771	.788	.733	.763	.744
K	.001	-	.001	-	.031	.056	.033	.045	.047	.052
Ni	-	-	-	-	-	-	.009	.013	-	-
Cr	.003	-	.001	-	-	.009	.044	.018	.002	.004
Cl	.002	-	-	-	-	.012	.003	-	.001	.008
Total	4.028	4.006	3.992	3.984	27.534	15.761	16.561	16.484	16.480	16.552
Fe/Fe+Mg	.244	.227	.305	.319	.912	.281	.318	.288	.277	.317
Mg*	-	-	-	-	-	-	-	-	-	-
Ca*	41.300	39.800	34.500	4.300	-	-	-	-	-	-
An	-	-	-	-	-	-	-	-	-	-

	G257-28	G257-29	G257-30	G257-31	G257-32	G257-33	G257-34	G257-35	G257-36	G257-37
	HBD	HBD	HBD	HBD	HBD	PLG	PLG	PLG	PLG	PLG
Oxide										
SiO2	40.638	41.509	41.792	41.805	41.219	45.608	45.110	44.942	45.947	45.081
Al2O3	13.934	13.824	13.215	13.436	14.024	33.838	34.873	35.208	34.112	34.568
TiO2	2.329	2.118	1.792	1.861	2.156	.027	.090	-	.072	.033
FeO	11.551	11.257	11.502	11.300	10.160	.444	.422	.583	.614	.659
MnO	.204	.153	.352	.130	.143	.023	-	.030	-	-
MgO	14.060	14.688	14.255	14.131	14.864	.073	.061	.050	.044	.028
CaO	11.727	11.933	11.744	11.693	12.104	18.372	18.873	18.952	18.189	18.901
Na2O	2.663	2.543	2.284	2.420	2.557	1.169	.897	1.062	1.447	1.035
K2O	.276	.305	.307	.219	.163	.019	.026	-	.035	-
NiO	.006	-	.116	-	-	.052	.140	-	.029	-
Cr2O3	-	.059	-	-	.093	.156	-	.005	-	.067
Cl	.007	.013	-	.012	.013	.045	.014	.001	.005	-
Total	97.394	98.402	97.360	97.008	97.494	99.825	100.506	100.833	100.494	100.372
Cation										
Si	6.271	6.321	6.434	6.439	6.305	8.454	8.312	8.263	8.459	8.327
Al	2.535	2.481	2.398	2.440	2.528	7.392	7.573	7.629	7.401	7.525
Ti	.270	.242	.208	.216	.248	.004	.012	-	.010	.005
Fe	1.491	1.433	1.481	1.456	1.299	.068	.065	.090	.095	.102
Mn	.027	.020	.046	.017	.019	.004	-	.005	-	-
Mg	3.235	3.335	3.271	3.245	3.389	.019	.017	.014	.012	.008
Ca	1.939	1.947	1.937	1.929	1.984	3.649	3.726	3.733	3.588	3.740
Na	.797	.750	.681	.723	.759	.420	.321	.378	.516	.371
K	.054	.059	.060	.043	.031	.004	.006	-	.008	-
Ni	.001	-	.014	-	-	.008	.021	-	.004	-
Cr	-	.007	-	-	.011	.022	-	.001	-	.010
Cl	.002	.003	-	.003	.003	.014	.004	-	.001	-
Total	16.622	16.598	16.530	16.511	16.576	20.058	20.057	20.112	20.094	20.087
Fe/Fe+Mg	.315	.301	.312	.310	.277	.774	.796	.867	.887	.929
Mg*	-	-	-	-	-	-	-	-	-	-
Ca*	-	-	-	-	-	-	-	-	-	-
An	-	-	-	-	-	89.590	91.930	90.800	87.260	90.970

G257-18 Clinopyroxene groundmass
G257-19 Clinopyroxene phenocryst core
G257-20 Clinopyroxene phenocryst rim
G257-21 Orthopyroxene as rim of clinopyroxene phenocryst
G257-22 Magnetite groundmass
G257-23 Amphibole
G257-24 Amphibole
G257-25 Amphibole
G257-26 Amphibole
G257-27 Amphibole

G257-28 Amphibole
G257-29 Amphibole
G257-30 Amphibole
G257-31 Amphibole
G257-32 Amphibole
G257-33 Plagioclase in gabbro
G257-34 Plagioclase in gabbro
G257-35 Plagioclase in gabbro
G257-36 Plagioclase phenocryst core
G257-37 Plagioclase phenocryst core

	G257-38	G257-39	G257-40	G257-41	G257-42	G257-43	G257-44	G257-45	G289-01	G289-02
	PLG	PLG	PLG	PLG	PLG	PLG	PLG	PLG	OLV	OLV
Oxide										
SiO2	45.181	45.608	54.592	54.231	55.628	45.570	45.427	45.504	38.747	38.310
Al2O3	34.500	33.838	28.215	28.078	27.042	34.891	34.458	32.124	.046	.031
TiO2	.006	.027	.086	.156	.131	.019	.002	.368	.017	-
FeO	.979	.444	.777	.722	.785	.670	.712	1.667	18.801	18.718
MnO	.019	.023	.032	.050	.006	.044	-	.017	.206	.321
MgO	.020	.073	.112	.083	.089	.053	.005	1.230	42.563	43.096
CaO	18.688	18.372	11.033	10.610	10.461	18.179	18.468	17.143	.146	.147
Na2O	1.116	1.169	5.361	5.951	5.497	1.261	.908	1.661	.012	.022
K2O	.008	.019	.113	.191	.200	.017	.011	.053	.021	.053
NiO	-	.052	-	.018	.056	.043	.029	.062	.153	.086
Cr2O3	.063	.156	-	-	.043	.021	-	-	.027	.001
Cl	.024	.045	-	.014	-	.007	-	-	.035	.010
Total	100.604	99.825	100.321	100.102	99.938	100.775	100.021	99.828	100.775	100.795
Cation										
Si	8.337	8.454	9.863	9.839	10.068	8.366	8.399	8.483	.985	.975
Al	7.503	7.392	6.008	6.004	5.768	7.550	7.509	7.058	.001	.001
Ti	.001	.004	.012	.021	.018	.003	-	.052	-	-
Fe	.151	.068	.117	.110	.119	.103	.110	.260	.400	.398
Mn	.003	.004	.005	.008	.001	.007	-	.003	.004	.007
Mg	.005	.019	.030	.022	.024	.014	.001	.342	1.614	1.635
Ca	3.695	3.649	2.136	2.062	2.028	3.576	3.658	3.424	.004	.004
Na	.399	.420	1.878	2.093	1.929	.449	.326	.600	.001	.001
K	.002	.004	.026	.044	.046	.004	.003	.012	.001	.002
Ni	-	.008	-	.003	.008	.006	.004	.009	.003	.002
Cr	.009	.022	-	-	.006	.003	-	-	.001	-
Cl	.007	.014	-	.004	-	.002	-	-	.002	-
Total	20.114	20.058	20.074	20.211	20.015	20.083	20.010	20.243	3.015	3.026
Fe/Fe+Mg	.965	.774	.796	.830	.831	.876	.987	.432	.199	.196
Mg*	-	-	-	-	-	-	-	-	80.000	80.000
Ca*	-	-	-	-	-	-	-	-	-	-
An	90.210	89.590	52.870	49.110	50.660	88.760	91.750	84.840	-	-

	G289-03	G289-04	G289-05	G289-06	G289-07	G289-08	G289-09	G289-10	G289-11	G289-12
	OLV	OLV	OPX	OPX	OPX	CPX	CPX	CPX	CPX	CPX
Oxide										
SiO2	38.177	38.300	53.433	52.347	51.617	47.624	51.877	50.681	49.642	50.408
Al2O3	.014	.035	.850	1.608	1.592	6.529	1.557	4.059	3.892	3.630
TiO2	.064	-	.126	.254	.279	.958	.332	.677	.649	.620
FeO	19.462	18.835	19.282	19.610	20.448	7.596	9.879	9.384	9.703	8.298
MnO	.217	.342	.774	.654	.747	.143	.367	.373	.373	.281
MgO	42.848	42.878	24.612	24.651	22.671	13.720	15.000	13.813	14.243	14.469
CaO	.130	.136	1.451	1.445	1.890	22.624	20.731	21.243	21.109	22.126
Na2O	-	-	.006	.001	.046	.265	.245	.284	.331	.234
K2O	.023	.042	.019	.022	-	.008	-	-	.025	-
NiO	.122	.037	-	.017	.007	-	.046	-	.031	-
Cr2O3	-	-	-	.012	.098	.019	-	-	-	-
Cl	-	-	-	.056	.060	-	-	.003	-	.008
Total	101.057	100.605	100.553	100.677	99.454	99.485	100.034	100.518	99.998	100.075
Cation										
Si	.972	.977	1.960	1.924	1.933	1.789	1.940	1.885	1.864	1.880
Al	-	.001	.037	.070	.070	.289	.069	.178	.172	.160
Ti	.001	-	.003	.007	.008	.027	.009	.019	.018	.017
Fe	.415	.402	.591	.603	.641	.239	.309	.292	.305	.259
Mn	.005	.007	.024	.020	.024	.005	.012	.012	.012	.009
Mg	1.627	1.630	1.346	1.351	1.266	.769	.836	.766	.797	.805
Ca	.004	.004	.057	.057	.076	.911	.831	.846	.849	.884
Na	-	-	-	-	.003	.019	.018	.020	.024	.017
K	.001	.001	.001	.001	-	-	-	-	.001	-
Ni	.002	.001	-	-	-	-	.001	-	.001	-
Cr	-	-	-	-	.003	.001	-	-	-	-
Cl	-	-	-	.003	.004	-	-	-	-	-
Total	3.027	3.023	4.019	4.038	4.028	4.048	4.025	4.018	4.044	4.031
Fe/Fe+Mg	.203	.198	.305	.309	.336	.237	.270	.276	.277	.243
Mg*	80.000	80.000	-	-	-	-	-	-	-	-
Ca*	-	-	3.000	3.000	4.000	47.000	42.000	44.000	43.000	45.000
An	-	-	-	-	-	-	-	-	-	-

G257-38 Plagioclase phenocryst core
G257-39 Plagioclase phenocryst core
G257-40 Plagioclase groundmass
G257-41 Plagioclase groundmass
G257-42 Plagioclase groundmass
G257-43 Plagioclase inclusion in amphibole
G257-44 Plagioclase inclusion in amphibole
G257-45 Plagioclase inclusion in amphibole
G289-01 Olivine phenocryst
G289-02 Olivine phenocryst

G289-03 Olivine phenocryst
G289-04 Olivine phenocryst
G289-05 Core of orthopyroxene phenocryst in cumulate
G289-06 Core of orthopyroxene phenocryst in cumulate
G289-07 Core of orthopyroxene jacketed by clinopyroxene
G289-08 Clinopyroxene phenocryst core
G289-09 Clinopyroxene jacketing orthopyroxene
G289-10 Core of clinopyroxene phenocryst in cumulate
G289-11 Core of clinopyroxene phenocryst in clots
G289-12 Clinopyroxene inclusion in amphibole

	G289-13	G289-14	G289-15	G289-16	G289-17	G289-18	G289-19	G289-20	G289-21	G289-22
	MAG	MAG	MAG	HBD	HBD	HBD	HBD	PLG	PLG	PLG
Oxide										
SiO2	.139	.095	.105	41.514	41.412	41.167	40.765	44.220	44.661	44.718
Al2O3	2.888	3.257	3.326	12.309	12.990	12.657	14.331	34.987	35.478	34.682
TiO2	11.542	11.756	11.533	2.228	2.168	2.327	1.913	.017	.005	.123
FeO	78.781	78.544	78.653	12.755	11.965	12.668	9.815	.515	.467	.662
MnO	.479	.550	.544	.248	.314	.219	.106	.046	.020	.003
MgO	1.578	1.826	1.962	14.187	14.235	14.048	15.145	.061	.039	.014
CaO	.044	.042	-	11.534	11.485	11.388	12.290	18.704	19.047	18.222
Na2O	-	-	-	2.529	2.477	2.620	2.593	.955	.829	1.036
K2O	-	-	.020	.114	.260	.252	.320	.040	.025	-
NiO	.096	.033	-	-	.050	.022	.030	.003	.010	.015
Cr2O3	.082	.067	-	.021	-	.079	.009	-	.066	.052
Cl	.017	-	-	.024	.030	-	.021	.009	-	.023
Total	95.646	96.169	96.143	97.463	97.385	97.448	97.338	99.557	100.748	99.551
Cation										
Si	.049	.033	.036	6.424	6.196	6.377	6.248	8.233	8.213	8.314
Al	1.189	1.326	1.355	2.243	2.288	2.310	2.588	7.677	7.711	7.600
Ti	3.032	3.053	2.997	.260	.244	.271	.220	.002	.001	.017
Fe	23.014	22.686	22.728	1.652	1.496	1.641	1.259	.080	.072	.103
Mn	.142	.161	.159	.032	.400	.029	.011	.007	.003	.001
Mg	.822	.940	1.011	3.272	3.176	3.244	3.640	.017	.011	.004
Ca	.016	.016	-	1.912	1.840	1.900	2.020	3.731	3.753	3.630
Na	-	-	-	.760	.626	.787	.772	.345	.295	.373
K	-	-	.009	.024	.048	.050	.064	.009	.006	-
Ni	.027	.009	-	-	.008	.003	.004	.001	.001	.002
Cr	.023	.018	-	.004	-	.009	-	-	.010	.008
Cl	.010	-	-	.008	.008	-	.004	.003	-	.007
Total	28.323	28.242	28.294	16.591	16.330	16.621	16.650	20.106	20.076	20.059
Fe/Fe+Mg	.966	.960	.957	.335	.320	.336	.267	.825	.869	.965
Mg*	-	-	-	-	-	-	-	-	-	-
Ca*	-	-	-	-	-	-	-	-	-	-
An	-	-	-	-	-	-	-	91.334	92.570	90.680

G289-13 Magnetite groundmasss
G289-14 Magnetite inclusion in orthopyroxene
G289-15 Magnetite inclusion in orthopyroxene
G289-16 Amphibole
G289-17 Amphibole
G289-18 Amphibole
G289-19 Amphibole
G289-20 Plagioclase phenocryst core
G289-21 Plagioclase phenocryst core
G289-22 Core of plagioclase phenocryst in cumulate

	G289-23	G289-24	G289-25	G289-26	G250-01	G250-02	G250-03	G250-04	G250-05	G250-06
	PLG	PLG	PLG	PLG	OLV	OLV	OLV	OLV	OPX	OPX
Oxide										
SiO2	48.860	53.542	48.513	45.576	37.459	37.390	36.749	37.932	52.378	53.102
Al2O3	32.728	28.916	31.596	34.840	-	.018	.026	.036	.735	.795
TiO2	-	.052	-	.052	-	.010	.012	.016	.280	.298
FeO	.517	.449	.519	.588	25.411	27.429	29.065	26.885	21.122	19.901
MnO	.005	-	-	-	.395	.452	.541	.565	.632	.547
MgO	.042	.037	.037	.026	35.595	34.562	33.087	34.623	21.839	22.445
CaO	15.734	11.770	15.228	18.524	.119	.152	.173	.155	2.373	1.969
Na2O	2.657	4.841	5.063	.913	.097	.035	-	-	.002	-
K2O	.014	.073	.003	.050	-	-	.009	-	-	-
NiO	-	.028	.021	.036	.019	.111	-	-	-	.042
Cr2O3	.033	-	.078	.008	.162	-	.032	.049	.058	-
Cl	.025	-	.046	.006	.122	-	-	.036	.007	-
Total	100.615	99.708	99.103	100.618	99.380	100.160	99.694	100.298	99.427	99.101
Cation										
Si	8.906	9.730	8.986	8.374	.999	.997	.994	1.007	1.966	1.982
Al	7.031	6.193	6.897	7.545	-	.001	.001	.001	.033	.035
Ti	-	.007	-	.007	-	-	-	-	.008	.008
Fe	.079	.068	.080	.090	.567	.612	.657	.597	.663	.621
Mn	.001	-	-	-	.009	.010	.012	.013	.020	.017
Mg	.011	.010	.010	.007	1.415	1.374	1.334	1.369	1.222	1.249
Ca	3.073	2.292	3.022	3.647	.003	.004	.005	.005	.095	.079
Na	.939	1.706	1.100	.325	.005	.002	-	-	-	-
K	.003	.017	.001	.012	-	-	-	-	-	-
Ni	-	.004	.003	.005	-	.002	-	-	-	.001
Cr	.005	-	.011	.001	.003	-	.001	.001	.002	-
Cl	.008	-	.014	.002	.006	-	-	.001	-	-
Total	20.055	20.027	20.125	20.016	3.007	3.003	3.005	2.994	4.009	3.992
Fe/Fe+Mg	.874	.873	.887	.927	.286	.308	.330	.303	.352	.332
Mg*	-	-	-	-	71.400	69.200	67.000	69.700	-	-
Ca*	-	-	-	-	-	-	-	-	4.700	4.000
An	76.540	57.090	73.300	91.540	-	-	-	-	-	-

G289-23 Mantle of plagioclase pheno ryst in cumulate
G289-24 Rim of plagioclase phenocryst in cumulate
G289-25 Plagioclase groundmass
G289-26 Plagioclase inclusion
G250-01 Anhedral olivine phenocryst
G250-02 Anhedral olivine microphenocryst
G250-03 Anhedral olivine microphenocryst
G250-04 Anhedral olivine phenocryst
G250-05 Orthopyroxene phenocryst core
G250-06 Orthopyroxene phenocryst core

	G250-07	G250-08	G250-09	G250-10	G250-11	G250-12	G250-13	G250-14	G250-15	G250-16
	OPX	OPX	OPX	OPX	CPX	MAG	MAG	MAG	MAG	PLG
Oxide										
SiO2	53.025	52.446	53.252	52.920	51.303	.112	.143	.146	.157	47.187
Al2O3	.616	2.098	1.355	.925	2.556	3.574	4.736	3.256	3.814	33.354
TiO2	.303	.377	.286	.356	.555	11.480	9.240	12.824	11.862	.033
FeO	21.273	19.804	18.895	19.627	10.847	75.746	76.758	75.767	74.670	.587
MnO	.588	.493	.632	.594	.338	.254	.414	.391	.345	.036
MgO	22.171	23.069	23.489	22.941	14.449	2.851	3.246	2.912	3.156	.063
CaO	1.909	1.947	1.973	1.888	19.449	.018	.002	.020	.024	16.676
Na2O	.024	.002	.025	.019	.288	-	-	-	.012	2.146
K2O	-	-	.037	-	-	.016	.017	.008	-	.024
NiO	.093	-	.025	.076	.030	.004	.043	.008	.008	.003
Cr2O3	.003	.063	-	.002	-	.093	.079	.073	-	.051
Cl	-	.011	-	-	.007	.027	.017	-	-	.019
Total	100.005	100.310	99.970	99.347	99.823	94.175	94.695	95.405	94.048	100.179
Cation										
Si	1.975	1.934	1.962	1.969	1.924	.039	.050	.050	.054	8.677
Al	.027	.091	.059	.041	.113	1.469	1.940	1.313	1.557	7.228
Ti	.008	.010	.008	.010	.016	3.011	2.415	3.301	3.090	.005
Fe	.663	.611	.582	.611	.340	22.090	22.309	21.688	21.630	.090
Mn	.019	.015	.020	.019	.011	.075	.122	.113	.101	.006
Mg	1.231	1.268	1.290	1.273	.808	1.482	1.682	1.486	1.630	.017
Ca	.076	.077	.078	.075	.781	.007	.001	.007	.009	3.285
Na	.002	-	.002	.001	.021	-	-	-	.008	.765
K	-	-	.002	-	-	.007	.008	.004	-	.006
Ni	.003	-	.001	.002	.001	.001	.012	.002	.002	-
Cr	-	.002	-	-	-	.026	.022	.020	-	.007
Cl	-	.001	-	-	-	.016	.010	-	-	.006
Total	4.004	4.010	4.003	4.001	4.015	28.222	28.569	27.984	28.081	20.092
Fe/Fe+Mg	.350	.325	.311	.324	.296	.937	.930	.936	.930	.839
Mg*	-	-	-	-	-	-	-	-	-	-
Ca*	3.800	4.065	3.900	3.791	40.258	-	-	-	-	-
An	-	-	-	-	-	-	-	-	-	80.990

G250-07 Core of i tergrown orthopyroxene
G250-08 Core of orthopyroxene in rounded crystal clots
G250-09 Core of intergrown orthopyroxene
G250-10 Euhedral orthopyroxene phenocryst core
G250-11 Anhedral clinopyroxene phenocryst core
G250-12 Magnetite microphenocryst in cumulate
G250-13 Magnetite microphenocryst in cumulate
G250-14 Magnetite microphenocryst in cumulate
G250-15 Magnetite microphenocryst in cumulate
G250-16 Plagioclase phenocryst core

	G250-17	G250-18	G250-19	G250-20	G250-21	G250-22	G250-23	G250-24	B30A-01	B30A-02
	PLG	PLG	PLG	PLG	PLG	PLG	PLG	PLG	OLV	OPX
Oxide										
SiO2	49.267	53.622	50.142	52.064	52.622	49.342	51.968	51.766	40.389	SiO2
Al2O3	32.246	29.126	31.764	29.700	29.185	31.986	30.349	30.157	.038	Al2O3
TiO2	-	.064	.039	.047	.030	.013	.008	.072	.029	TiO2
FeO	.526	.626	.606	.430	.753	.715	.626	.846	11.300	FeO
MnO	.041	.019	-	.001	.010	.002	-	-	.175	MnO
MgO	.061	.093	.060	.077	.108	.067	.090	.104	47.575	MgO
CaO	15.208	11.744	14.839	13.018	11.880	14.985	13.688	13.065	.243	CaO
Na2O	2.869	4.795	3.182	4.240	4.697	2.983	3.770	4.173	-	Na2O
K2O	.069	.072	.002	.088	.112	.049	.054	.085	.007	K2O
NiO	-	.030	-	-	-	.018	-	.016	.169	NiO
Cr2O3	.043	.018	-	-	-	-	-	.083	.067	Cr2O3
Cl	-	-	.003	.010	.001	-	-	.055	.007	Cl
Total	100.330	100.208	100.637	99.676	99.398	100.158	100.552	100.423	99.999	Total
Cation										
Si	8.995	9.704	9.113	9.504	9.620	9.026	9.416	9.411	.998	Si
Al	6.938	6.212	6.804	6.390	6.288	6.896	6.481	6.461	.001	Al
Ti	-	.009	.005	.006	.004	.002	.001	.010	.001	Ti
Fe	.080	.095	.092	.066	.115	.109	.095	.129	.233	Fe
Mn	.006	.003	-	-	.002	-	-	-	.004	Mn
Mg	.016	.025	.016	.021	.029	.018	.024	.028	1.752	Mg
Ca	2.975	2.277	2.889	2.546	2.327	2.937	2.657	2.545	.006	Ca
Na	1.016	1.682	1.121	1.501	1.665	1.058	1.324	1.471	-	Na
K	.016	.017	-	.020	.026	.011	.012	.020	-	K
Ni	-	.004	-	-	-	.003	-	.002	.003	Ni
Cr	.006	.003	-	-	-	-	-	.012	.001	Cr
Cl	-	-	.001	.003	-	-	-	.017	-	Cl
Total	20.049	20.030	20.042	20.058	20.077	20.060	20.011	20.105	3.001	Total
Fe/Fe+Mg	.830	.791	.849	.757	.796	.858	.796	.820	.118	Fe/Fe+Mg
Mg*	-	-	-	-	-	-	-	-	88.200	Mg*
Ca*	-	-	-	-	-	-	-	-	-	Ca*
An	74.240	57.270	72.040	62.600	57.910	73.310	66.540	63.060	-	An

G250-17 Plagioclase phenocryst mantle
G250-18 Plagioclase phenocryst rim
G250-19 Plagioclase phenocryst mantle
G250-20 Plagioclase phenocryst rim
G250-21 Plagioclase phenocryst rim
G250-22 Plagioclase microphenocryst core
G250-23 Plagioclase microphenocryst rim
G250-24 Plagioclase groundmass
B30A-01 Anhedral olivine phenocryst
B30A-02 Orthopyroxene phenocryst core

	B30A-03	B30A-04	B30A-05	B30A-06	B30A-07	B30A-08	B30A-09	B30A-10	B30A-11	B30A-12
	OPX	OPX	CPX	CPX	CPX	CPX	CPX	CPX	OPX	OPX
Oxide										
SiO2	53.238	53.695	52.079	51.901	51.799	52.185	51.624	51.493	53.955	52.897
Al2O3	1.029	1.321	1.875	6.479	1.907	1.762	2.057	3.532	1.784	.819
TiO2	.232	.205	.411	.327	.403	.365	.487	.509	.303	.261
FeO	20.819	19.333	9.514	8.670	9.419	9.044	10.331	6.128	17.583	22.138
MnO	.647	.709	.349	.245	.348	.350	.365	.179	.418	.831
MgO	22.424	23.189	15.561	11.672	14.904	15.687	13.880	15.429	23.842	20.208
CaO	1.575	1.505	19.362	19.864	20.666	19.613	20.351	22.031	1.980	2.410
Na2O	.023	.026	.224	.786	.252	.206	.324	.191	.071	.219
K2O	-	.007	-	.005	-	.051	.020	.011	.011	.130
NiO	-	-	-	.077	-	.001	.037	-	.028	.027
Cr2O3	-	-	.033	.037	-	.091	.054	.014	.011	.056
Cl	.013	.008	.012	.032	.008	.036	-	-	.013	.003
Total	100.000	99.998	99.419	100.095	99.708	99.391	99.529	99.518	99.999	99.999
Cation										
Si	1.975	1.976	1.946	1.913	1.938	1.949	1.942	1.906	1.970	1.984
Al	.045	.057	.083	.282	.084	.078	.091	.154	.077	.036
Ti	.006	.006	.012	.009	.011	.010	.014	.014	.008	.007
Fe	.646	.595	.297	.267	.295	.283	.325	.190	.537	.694
Mn	.020	.022	.011	.008	.011	.011	.012	.006	.013	.026
Mg	1.240	1.272	.867	.641	.831	.873	.778	.851	1.298	1.130
Ca	.063	.059	.775	.785	.828	.785	.820	.874	.077	.097
Na	.002	.002	.016	.056	.018	.015	.024	.014	.005	.016
K	-	-	-	-	-	.002	.001	.001	.001	.006
Ni	-	-	-	.002	-	-	.001	-	.001	.001
Cr	-	-	.001	.001	-	.003	.002	-	-	.002
Cl	.001	.001	.001	.002	.001	.002	-	-	.001	-
Total	3.998	3.991	4.009	3.967	4.018	4.011	4.010	4.000	3.987	4.001
Fe/Fe+Mg	.342	.319	.255	.294	.262	.244	.295	.182	.293	.381
Mg*	-	-	-	-	-	-	-	-	-	-
Ca*	3.200	3.000	40.000	46.000	42.000	40.000	42.400	46.000	4.000	4.982
An		-	-	-	-	-	-	-	-	-

B30A-03 Core of orthopyroxene phenocryst in cumulate
B30A-04 Core of orthopyroxene phenocryst in cumulate
B30A-05 Clinopyroxene phenocryst core
B30A-06 Clinopyroxene phenocryst core
B30A-07 Clinopyroxene phenocryst core
B30A-08 Clinopyroxene phenocryst core
B30A-09 Clinopyroxene phenocryst core
B30A-10 Clinopyroxene microphenocryst
B30A-11 Orthopyroxene groundmass
B30A-12 Orthopyroxene groundmass

	B30A-13	B30A-14	B30A-15	B30A-16	B30A-17	B30A-18	B30A-19	B30A-20	B30A-21	B30A-22
	CPX	CPX	CPX	OPX	MAG	PLG	PLG	PLG	PLG	PLG
Oxide										
SiO2	51.660	52.542	51.457	52.381	.114	44.576	46.951	44.915	51.749	46.068
Al2O3	2.959	1.890	2.215	2.410	3.482	35.065	33.335	35.014	30.028	33.751
TiO2	.428	.300	.531	.196	11.024	.013	.034	-	-	.033
FeO	5.492	10.294	10.252	18.898	77.510	.500	.435	.410	.527	.613
MnO	.181	.478	.339	.641	.416	.052	-	-	-	-
MgO	15.843	13.581	13.555	22.813	2.028	.052	.029	.032	.054	.005
CaO	21.904	20.112	20.385	1.628	-	18.721	16.987	18.782	13.183	17.357
Na2O	.211	.371	.334	-	-	1.028	2.035	.992	4.228	1.632
K2O	.027	.007	.019	.063	.008	.082	.035	-	.083	.025
NiO	.062	.029	.038	.084	.111	-	-	-	-	.071
Cr2O3	.289	.040	-	-	.010	.016	.077	-	.118	-
Cl	.047	.051	-	-	-	.012	.107	-	.090	.009
Total	99.104	99.695	99.125	99.116	94.705	100.126	100.026	100.145	100.061	99.564
Cation										
Si	1.918	1.969	1.943	1.945	.040	8.254	8.656	8.298	9.435	8.540
Al	.129	.083	.099	.105	1.439	7.652	7.243	7.624	6.452	7.374
Ti	.012	.008	.015	.006	2.907	.002	.005	-	-	.005
Fe	.170	.323	.324	.586	22.727	.077	.067	.063	.080	.095
Mn	.006	.015	.011	.019	.124	.008	-	-	-	-
Mg	.877	.759	.763	1.263	1.060	.014	.008	.009	.015	.001
Ca	.871	.807	.825	.064	-	3.714	3.355	3.718	2.575	3.447
Na	.015	.027	.024	-	-	.369	.728	.355	1.495	.586
K	.001	-	.001	.003	.004	.019	.008	-	.019	.006
Ni	.002	.001	.001	.003	.031	-	-	-	-	.011
Cr	.008	.001	-	-	.003	.002	.011	-	.017	-
Cl	.003	.003	-	-	-	.007	.033	-	.028	.003
Total	4.013	3.997	4.005	3.994	28.334	20.119	20.114	20.067	20.116	20.068
Fe/Fe+Mg	.163	.298	.298	.317	.955	.845	.894	.876	.845	.987
Mg*	-	-	-	-	-	-	-	-	-	-
Ca*	45.000	42.400	42.000	3.313	-	-	-	-	-	-
An	-	-	-	-	-	90.540	82.010	91.280	62.930	85.340

B30A-13 Clinopyroxene groundmass
B30A-14 Clinopyroxene inclusion in plagioclase
B30A-15 Clinopyroxene inclusion in plagioclase
B30A-16 Orthopyroxene surrounding anhedral olivine phenocryst
B30A-17 Magnetite microphenocryst
B30A-18 Plagioclase phenocryst core
B30A-19 Plagioclase phenocryst core
B30A-20 Plagioclase phenocryst core
B30A-21 Plagioclase phenocryst rim
B30A-22 Plagioclase microphenocryst core

	B30A-23	B30A-24	B30A-25	B30A-26	G292-01	G292-02	G292-03	G292-04	G292-05	G292-06
	PLG	PLG	PLG	PLG	OLV	OLV	OPX	OPX	OPX	OPX
Oxide										
SiO2	49.523	51.874	47.682	58.897	36.787	36.750	52.941	42.784	53.552	52.713
Al2O3	31.636	29.851	33.044	24.049	.008	.006	1.050	.755	.883	1.509
TiO2	-	.085	-	.319	-	.035	.120	.229	.302	.303
FeO	.625	.617	.545	1.456	30.091	29.488	19.700	19.107	18.247	19.249
MnO	.083	-	.100	.032	.526	.640	.457	.511	.470	.579
MgO	.092	.103	.067	.180	32.617	31.883	23.371	24.426	24.046	23.533
CaO	14.875	12.968	16.457	8.357	.201	.044	1.926	1.817	1.868	1.915
Na2O	3.125	4.261	2.365	5.112	-	-	.039	-	.069	.062
K2O	.120	.102	.077	.729	-	.079	.020	-	-	-
NiO	-	.020	-	.022	.040	-	-	.045	-	.009
Cr2O3	-	-	.045	-	.025	-	-	-	.073	-
Cl	-	.091	.009	-	-	-	.012	-	.043	.008
Total	100.078	99.972	100.392	99.153	100.295	98.925	99.636	99.674	99.553	99.881
Cation										
Si	9.069	9.463	8.747	10.666	.993	1.004	1.964	1.954	1.974	1.948
Al	6.828	6.418	7.144	5.133	-	-	.046	.033	.038	.066
Ti	-	.012	-	.043	-	.001	.003	.006	.008	.008
Fe	.096	.094	.084	.220	.680	.674	.611	.592	.562	.595
Mn	.013	-	.016	.005	.012	.015	.014	.016	.015	.018
Mg	.025	.028	.018	.049	1.313	1.299	1.293	1.348	1.321	1.297
Ca	2.918	2.534	3.234	1.622	.006	.001	.077	.072	.074	.076
Na	1.109	1.507	.841	1.795	-	-	.003	-	.005	.004
K	.028	.024	.018	.168	-	.003	.001	-	-	-
Ni	-	.003	-	.003	.001	-	-	.001	-	-
Cr	-	-	.006	-	.001	-	-	-	.002	-
Cl	-	.028	.003	-	-	-	.001	-	.003	.001
Total	20.086	20.110	20.111	19.705	3.006	2.996	4.012	4.023	4.003	4.013
Fe/Fe+Mg	.792	.770	.820	.819	.341	.342	.321	.305	.299	.315
Mg*	-	-	-	-	65.900	65.800	-	-	-	-
Ca*	-	-	-	-	-	-	4.000	4.000	4.000	4.000
An	71.960	62.340	79.010	45.240	-	-	-	-	-	-

	G292-07	G292-08	G292-09	G292-10	G292-11	G292-12	G292-13	G292-14	G292-15	G292-16
	OPX	OPX	OPX	OPX	CPX	CPX	CPX	CPX	MAG	MAG
Oxide										
SiO2	52.723	52.137	51.797	51.620	50.842	51.223	50.629	51.119	.063	.170
Al2O3	1.735	1.294	1.753	1.048	2.283	1.683	2.564	2.611	3.582	4.128
TiO2	.396	.260	.369	.229	.584	.465	.755	.560	11.194	11.957
FeO	18.807	19.156	19.778	18.848	11.164	11.813	11.362	11.011	76.548	76.275
MnO	.449	.622	.605	.495	.351	.557	.349	.363	.494	.440
MgO	23.615	24.549	23.396	23.947	14.495	15.638	14.739	14.938	2.668	3.032
CaO	1.904	1.699	1.711	1.754	19.408	18.310	18.429	18.804	.005	.066
Na2O	.025	.008	.030	.050	.344	.300	.283	.381	-	-
K2O	-	-	-	-	.045	.023	-	.067	-	-
NiO	.008	-	-	.062	-	-	.004	.038	.042	-
Cr2O3	-	-	.028	.030	.026	.029	-	.117	.137	.017
Cl	.020	-	-	.051	.081	.007	-	.071	.025	-
Total	99.682	99.725	99.467	98.133	99.621	100.047	99.114	100.080	94.758	96.085
Cation										
Si	1.947	1.932	1.929	1.944	1.918	1.924	1.914	1.914	.022	.058
Al	.076	.057	.077	.047	.102	.075	.114	.115	1.470	1.649
Ti	.011	.007	.010	.006	.017	.013	.021	.016	2.931	3.048
Fe	.581	.594	.616	.594	.352	.371	.359	.345	22.288	21.625
Mn	.014	.020	.019	.016	.011	.018	.011	.012	.146	.126
Mg	1.300	1.356	1.299	1.344	.815	.876	.831	.834	1.385	1.532
Ca	.075	.067	.068	.071	.785	.737	.746	.755	.002	.024
Na	.002	.001	.002	.004	.025	.022	.021	.028	-	-
K	-	-	-	-	.002	.001	-	.003	-	-
Ni	-	-	-	.002	-	-	-	.001	.012	-
Cr	-	-	.001	.001	.001	.001	-	.003	.038	.005
Cl	.001	-	-	.003	.005	-	-	.004	.015	-
Total	4.007	4.033	4.022	4.031	4.033	4.037	4.018	4.030	28.308	28.067
Fe/Fe+Mg	.309	.304	.322	.306	.302	.298	.302	.293	.942	.934
Mg*	-	-	-	-	-	-	-	-	-	-
Ca*	4.000	3.000	3.000	3.000	40.000	37.000	38.000	39.000	-	-
An	-	-	-	-	-	-	-	-	-	-

B30A-23 Plagioclase microphenocryst mantle
B30A-24 Plagioclase microphenocryst rim
B30A-25 Plagioclase groundmass core
B30A-26 Plagioclase groundmass rim
G292-01 Olivine phenocryst in cumulate
G292-02 Olivine microphenocryst
G292-03 Orthopyroxene phenocryst core
G292-04 Orthopyroxene phenocryst core
G292-05 Anhedral orthopyroxene phenocryst core
G292-06 Core of orthopyroxene phenocryst in cumulate

G292-07 Core of orthopyroxene phenocryst in cumulate
G292-08 Core of orthopyroxene phenocryst in cumulate
G292-09 Anhedral orthopyroxene phenocryst
G292-10 Orthopyroxene groundmass
G292-11 Clinopyroxene phenocryst core
G292-12 Anhedral clinopyroxene phenocryst core
G292-13 Clinopyroxene microphenocryst
G292-14 Clinopyroxene groundmass
G292-15 Magnetite microphenocryst
G292-16 Magnetite microphenocryst in cumulate

	G292-17	G292-18	G292-19	G292-20	G292-21	G292-22	G292-23	G292-24	G292-25	G292-26
	MAG	GLASS	PLG	PLG	PLG	PLG	PLG	PLG	PLG	PLG
Oxide										
SiO2	.127	55.572	45.767	43.959	45.700	53.401	44.097	53.104	53.163	51.517
Al2O3	2.236	25.871	34.802	35.712	33.885	28.860	35.416	28.870	29.070	30.150
TiO2	12.769	.034	-	.036	.013	-	.010	.062	.058	.012
FeO	76.628	1.193	.496	.393	.568	.705	.357	.594	.638	.673
MnO	.460	-	.030	.111	.025	-	.113	.050	.017	-
MgO	2.059	.228	.058	.046	.059	.088	.028	.061	.084	.038
CaO	.045	9.505	19.035	19.047	18.061	11.914	18.989	12.503	12.008	12.761
Na2O	-	5.666	.700	.782	1.317	4.713	.849	4.525	4.549	4.274
K2O	.027	.476	.053	.080	.024	.130	.011	.104	.076	.155
NiO	-	-	-	-	-	-	-	-	.008	.001
Cr2O3	.206	-	-	.005	-	.074	.051	.064	-	-
Cl	.017	-	-	.021	.014	.069	.001	-	.012	-
Total	94.573	98.545	100.942	100.191	99.668	99.953	99.923	99.937	99.684	99.582
Cation										
Si	.045	10.206	8.384	8.140	8.479	9.707	8.181	9.661	9.677	9.426
Al	.924	5.600	7.513	7.793	7.406	6.183	7.743	6.189	6.236	6.502
Ti	3.367	.005	-	.005	.002	-	.001	.008	.008	.002
Fe	22.470	.183	.076	.061	.088	.107	.055	.090	.097	.103
Mn	.137	-	.005	.017	.004	-	.018	.008	.003	-
Mg	1.076	.062	.016	.013	.016	.024	.008	.017	.023	.010
Ca	.017	1.870	3.736	3.779	3.589	2.320	3.774	2.436	2.342	2.502
Na	-	2.017	.249	.281	.474	1.661	.305	1.596	1.605	1.516
K	.012	.111	.012	.019	.006	.030	.003	.024	.018	.036
Ni	-	-	-	-	-	-	-	-	.001	-
Cr	.057	-	-	.001	-	.011	.007	.009	-	-
Cl	.010	-	-	.007	.005	.021	-	-	.004	-
Total	28.114	20.054	19.990	20.115	20.064	20.063	20.097	20.038	20.013	20.097
Fe/Fe+Mg	.954	.746	.828	.828	.844	.818	.877	.841	.809	.909
Mg*	-	-	-	-	-	-	-	-	-	-
Ca*	-	-	-	-	-	-	-	-	-	-
An	-	-	93.430	92.650	88.200	57.840	92.450	60.060	59.070	61.720

	G292-27	G292-28	G292-29	G292-30	G300-01	G300-02	G300-03	G300-04	G300-05	G300-06
	PLG	PLG	PLG	PLG	OLV	OLV	OLV	OLV	OLV	OLV
Oxide										
SiO2	53.017	52.813	50.479	53.179	39.413	38.664	37.879	38.338	36.915	37.043
Al2O3	28.797	29.280	29.971	28.900	.009	.035	.020	.018	.036	.007
TiO2	.024	.006	-	.053	.035	-	.008	.032	.010	.002
FeO	.778	.662	.773	.619	14.139	15.798	20.843	15.831	29.423	25.519
MnO	-	-	-	.024	.115	.232	.454	.226	.579	.451
MgO	.032	.065	.032	.077	46.562	44.853	40.517	44.958	33.204	36.286
CaO	12.304	12.554	14.101	12.295	.249	.230	.216	.207	.311	.215
Na2O	4.631	4.516	3.680	4.589	.026	-	.012	-	-	-
K2O	.037	.010	.016	.108	-	.019	.025	.011	.004	.013
NiO	-	.003	-	.019	.014	.120	.154	.163	.074	.075
Cr2O3	-	.022	-	.022	.026	.006	.001	-	.048	.007
Cl	.038	.078	-	.002	.012	-	-	-	-	-
Total	99.658	100.010	99.053	99.887	100.602	99.956	100.129	99.783	100.603	99.619
Cation										
Si	9.674	9.607	9.320	9.671	.982	.979	.981	.973	.991	.986
Al	6.193	6.277	6.522	6.198	-	.001	.001	.001	.001	-
Ti	.003	.001	-	.007	.001	-	-	.001	-	-
Fe	.119	.101	.119	.094	.295	.335	.452	.336	.661	.568
Mn	-	-	-	.004	.002	.005	.010	.005	.013	.010
Mg	.009	.018	.009	.021	1.729	1.693	1.565	1.701	1.329	1.440
Ca	2.405	2.477	2.789	2.399	.007	.006	.006	.006	.009	.006
Na	1.638	1.593	1.317	1.616	.001	-	.001	-	-	-
K	.009	.002	.004	.025	-	.001	.001	-	-	-
Ni	-	-	-	.003	-	.003	.003	.003	.002	.002
Cr	-	.003	-	.003	.001	-	-	-	.001	-
Cl	.012	.024	-	-	.001	-	-	-	-	-
Total	20.062	20.073	20.080	20.041	3.018	3.023	3.019	3.026	3.007	3.014
Fe/Fe+Mg	.932	.850	.932	.817	.146	.165	.224	.165	.332	.283
Mg*	-	-	-	-	85.400	83.500	77.600	83.500	66.800	71.700
Ca*	-	-	-	-	-	-	-	-	-	-
An	59.350	60.830	67.860	59.381	-	-	-	-	-	-

G292-17 Magnetite inclusion
G292-18 Volcanic glass inclusion in plagioclase
G292-19 Plagioclase phenocryst core
G292-20 Plagioclase phenocryst core
G292-21 Plagioclase phenocryst core
G292-22 Plagioclase phenocryst rim
G292-23 Plagioclase phenocryst core
G292-24 Plagioclase phenocryst mantle
G292-25 Plagioclase phenocryst rim
G292-26 Plagioclase microphenocryst core

G292-27 Plagioclase microphenocryst rim
G292-28 Plagioclase microphenocryst
G292-29 Plagioclase microphenocryst
G292-30 Plagioclase groundmass
G300-01 Olivine phenocryst core
G300-02 Olivine phenocryst core
G300-03 Olivine phenocryst rim
G300-04 Anhedral olivine phenocryst core
G300-05 Anhedral olivine phenocryst rim
G300-06 Olivine phenocryst rim

	G300-07	G300-08	G300-09	G300-10	G300-11	G300-12	G300-13	G300-14	G300-15	G300-16
	OLV	OLV	OLV	OLV	OLV	OLV	OLV	OLV	OLV	OLV
Oxide										
SiO2	39.159	36.002	37.042	38.251	36.761	37.070	39.472	38.652	36.711	39.581
Al203	.041	-	.032	.012	.053	1.062	.036	.006	.017	.021
TiO2	-	.021	.012	-	.019	.006	-	-	.018	.114
FeO	15.587	31.871	26.037	21.045	30.146	27.384	11.028	17.389	32.568	12.886
MnO	.235	.826	.418	.403	.534	.538	.188	.324	.511	.018
MgO	45.158	29.878	36.310	39.858	32.907	33.132	49.234	43.790	30.106	47.146
CaO	.222	.454	.251	.190	.443	.875	.212	.174	.309	.227
Na20	-	-	-	.024	.006	.055	-	-	-	-
K20	.018	.004	-	.001	-	.054	.019	.024	-	-
NiO	.248	-	.043	.100	.025	.063	.233	.197	.126	.436
Cr203	.022	-	.001	.027	.063	.027	-	.012	.009	-
Cl	.003	.011	.007	.033	.002	.041	.009	-	-	-
Total	100.694	99.067	100.153	99.945	100.961	100.365	100.432	100.568	100.374	100.429
Cation										
Si	.983	.997	.983	.992	.987	.989	.973	.980	1.003	.983
Al	.001	-	.001	.001	.002	.033	.001	-	.001	.001
Ti	-	-	-	-	-	.001	-	-	-	.002
Fe	.327	.738	.578	.457	.677	.611	.227	.369	.744	.268
Mn	.005	.019	.009	.009	.012	.012	.004	.007	.012	-
Mg	1.689	1.234	1.437	1.541	1.317	1.317	1.810	1.655	1.226	1.746
Ca	.006	.013	.007	.005	.013	.025	.006	.005	.009	.006
Na	-	-	-	.001	-	.003	-	-	-	-
K	.001	-	-	-	-	.002	.001	.001	-	-
Ni	.005	-	.001	.002	-	.001	.005	.004	.003	.009
Cr	-	-	-	.001	.001	.001	-	-	-	-
Cl	-	.001	-	.001	-	.002	-	-	-	-
Total	3.017	3.003	3.017	3.011	3.009	2.997	3.027	3.020	2.997	3.014
Fe/Fe+Mg	.162	.374	.287	.229	.339	.317	.112	.182	.378	.133
Mg*	83.800	62.600	71.300	77.100	66.100	68.300	88.800	81.800	62.200	86.700
Ca*	-	-	-	-	-	-	-	-	-	-
An	-	-	-	-	-	-	-	-	-	-

G300-07 Olivine phenocryst core
G300-08 Olivine phenocryst mantle
G300-09 Olivine groundmass
G300-10 Olivine groundmass
G300-11 Olivine inclusion in plagioclase phenocryst
G300-12 Olivine inclusion in plagioclase phenocryst
G300-13 Olivine phenocryst core
G300-14 Olivine phenocryst core
G300-15 Olivine phenocryst rim
G300-16 Olivine phenocryst core

	G300-17	G300-18	G300-19	G300-20	G300-21	G300-22	G300-23	G300-24	G300-25	G300-26
	OLV	OLV	OLV	OLV	OLV	CPX	CPX	CPX	CPX	CPX
Oxide										
SiO2	39.767	36.913	39.411	36.038	36.476	50.251	49.375	49.449	50.828	49.013
Al203	.030	-	.014	.022	.030	2.770	2.613	5.009	4.200	5.331
TiO2	.018	-	.042	.074	.125	.531	1.110	.645	.746	.776
FeO	13.160	27.136	15.736	32.408	30.650	9.155	16.047	6.079	5.893	5.968
MnO	.209	.612	.315	.618	.554	.159	.601	.098	.130	.121
MgO	46.638	34.462	44.474	29.674	31.027	15.186	13.046	14.925	14.640	14.465
CaO	.209	.158	.235	.283	.343	20.097	15.759	22.646	22.939	22.946
Na20	-	.008	-	.053	-	.290	.392	.259	.257	.261
K20	.005	.054	.058	.012	-	-	.056	-	.011	.008
NiO	.163	.105	.181	.023	.249	.091	.036	.034	.019	.048
Cr203	.017	.045	-	.042	-	.171	.052	.627	.721	.558
Cl	.004	.002	-	-	-	-	.010	-	.002	.022
Total	100.220	99.496	100.466	99.247	99.456	98.699	99.097	99.772	100.387	99.516
Cation										
Si	.990	.993	.991	.997	.999	1.900	1.901	1.838	1.874	1.829
Al	.001	-	-	.001	.001	.123	.119	.219	.182	.234
Ti	-	-	.001	.002	.003	.015	.032	.018	.021	.022
Fe	.274	.610	.331	.750	.702	.289	.517	.189	.182	.186
Mn	.004	.014	.007	.014	.013	.005	.020	.003	.004	.004
Mg	1.730	1.381	1.667	1.224	1.266	.856	.749	.827	.804	.805
Ca	.005	.005	.006	.008	.010	.814	.650	.902	.906	.917
Na	-	-	-	.003	-	.021	.029	.019	.018	.019
K	-	.002	.002	-	-	-	.003	-	.001	-
Ni	.003	.002	.004	.001	.005	.003	.001	.001	.001	.001
Cr	-	.001	-	.001	-	.005	.002	.018	.021	.016
Cl	-	-	-	-	-	-	.001	-	-	.001
Total	3.007	3.008	3.009	3.002	2.998	4.032	4.023	4.034	4.014	4.035
Fe/Fe+Mg	.137	.306	.166	.380	.357	.253	.408	.186	.184	.188
Mg*	86.300	69.400	83.400	62.000	64.300	-	-	-	-	-
Ca*	-	-	-	-	-	41.446	33.574	47.000	48.000	48.000
An	-	-	-	-	-	-	-	-	-	-

G300-17 Olivine phenocryst core
G300-18 Olivine phenocryst rim
G300-19 Olivine phenocryst core
G300-20 Olivine phenocryst groundmass
G300-21 Olivine microphenocryst
G300-22 Clinopyroxene as inner coronas of olivine phenocryst
G300-23 Clinopyroxene as outer coronas of olivine phenocryst
G300-24 Clinopyroxene phenocryst core
G300-25 Clinopyroxene phenocryst core
G300-26 Clinopyroxene phenocryst rim

	G300-27	G300-28	G300-29	G300-30	G300-31	G300-32	G300-33	G300-34	G300-35	G300-36
	CPX	CPX	CPX	CPX	CPX	CPX	CPX	CPX	CPX	CPX
Oxide										
SiO2	51.405	51.388	49.315	49.980	49.331	49.228	49.902	51.562	51.813	51.219
Al2O3	3.527	2.359	5.870	4.665	5.789	5.718	4.886	1.589	3.033	3.586
TiO2	.433	.623	.673	.489	.800	.792	.676	.408	.575	.557
FeO	5.725	9.218	5.522	.814	5.500	6.072	5.654	10.411	5.374	6.735
MnO	.181	.232	.130	.090	.148	.091	.119	.392	.283	.290
MgO	16.091	15.035	14.394	14.982	14.853	14.717	14.579	16.210	15.599	15.335
CaO	22.108	20.332	22.881	23.848	23.326	23.779	23.297	19.069	22.493	22.212
Na2O	.205	.273	.196	.213	.222	.213	.201	.208	-	.178
K2O	-	-	-	.026	.011	-	.011	.016	.150	-
NiO	.043	.025	.001	-	.048	-	.015	-	.183	.046
Cr2O3	.372	.082	.690	.437	.709	.174	.546	.040	-	.146
Cl	-	-	-	.019	-	.004	.015	.044	-	-
Total	100.090	99.568	99.673	99.561	100.738	100.788	99.901	99.949	99.505	100.304
Cation										
Si	1.892	1.923	1.830	1.855	1.815	1.815	1.831	1.928	1.917	1.891
Al	.153	.104	.257	.204	.250	.248	.211	.070	.132	.156
Ti	.012	.018	.019	.013	.022	.022	.019	.011	.016	.015
Fe	.176	.288	.171	.150	.169	.187	.156	.326	.166	.208
Mn	.006	.007	.004	.003	.004	.003	.004	.012	.009	.009
Mg	.883	.839	.796	.829	.814	.809	.798	.904	.860	.844
Ca	.872	.815	.909	.948	.919	.939	.916	.764	.892	.879
Na	.015	.020	.014	.015	.016	.015	.014	.015	-	.013
K	-	-	-	.001	-	-	-	.001	.007	-
Ni	.001	.001	-	-	.001	-	-	-	.005	.001
Cr	.011	.002	.020	.013	.021	.005	.016	.001	-	.004
Cl	-	-	-	.001	-	-	.001	.003	-	-
Total	4.021	4.017	4.020	4.032	4.031	4.044	3.966	4.035	4.005	4.020
Fe/Fe+Mg	.166	.256	.177	.153	.172	.188	.425	.265	.162	.198
Mg*	-	-	-	-	-	-	-	-	-	-
Ca*	45.000	42.000	48.000	49.000	48.000	48.000	49.000	38.000	46.000	45.000
An	-	-	-	-	-	-	-	-	-	-

G300-27 Clinopyroxene phenocryst core
G300-28 Clinopyroxene phenocryst rim
G300-29 Clinopyroxene phenocryst core
G300-30 Clinopyroxene groundmass
G300-31 Clinopyroxene groundmass
G300-32 Clinopyroxene groundmass
G300-33 Clinopyroxene phenocryst core
G300-34 Clinopyroxene phenocryst rim
G300-35 Clinopyroxene phenocryst core
G300-36 Clinopyroxene phenocryst rim

	G300-37	G300-38	G300-39	G300-40	G300-41	G300-42	G300-43	G300-44	G300-45	G300-46
	CPX	CPX	CPX	CPX	CHR	CHR	CHR	CHR	CHR	HBD
Oxide										
SiO2	50.329	51.246	52.165	51.813	.136	.182	.117	.147	.063	48.942
Al2O3	4.048	3.340	3.235	1.822	13.407	16.308	14.274	12.584	20.006	4.909
TiO2	.865	.611	.171	.703	1.164	.560	.603	.995	.460	2.559
FeO	7.488	8.755	4.633	13.656	37.004	21.033	29.406	32.738	26.175	20.768
MnO	.211	.324	.214	.562	.290	.010	.155	.164	-	.402
MgO	14.265	15.065	16.384	15.667	5.692	13.299	7.822	7.466	12.342	9.218
CaO	22.209	19.859	22.678	15.663	.098	-	.028	.030	-	8.776
Na2O	.302	.306	.187	.238	-	-	-	.025	.064	1.193
K2O	.015	.017	.060	.118	.004	.019	-	-	-	1.182
NiO	-	.043	-	.009	-	.433	.168	.126	-	-
Cr2O3	.236	.336	.543	-	41.564	47.951	46.222	44.661	39.293	-
Cl	-	.014	.017	-	.021	.023	.012	-	.081	.029
Total	99.968	99.915	100.287	100.251	99.381	99.765	98.808	98.936	98.483	97.979
Cation										
Si	1.873	1.905	1.909	1.940	.033	.044	.032	.041	.016	7.667
Al	.178	.146	.140	.080	3.881	4.608	4.572	4.098	.127	.906
Ti	.024	.017	.005	.020	.215	.101	.123	.207	.090	.299
Fe	.233	.272	.142	.428	6.839	3.794	6.684	7.565	5.689	2.723
Mn	.007	.010	.007	.018	.060	.002	.036	.038	-	.054
Mg	.792	.835	.894	.874	2.084	4.753	3.169	3.075	4.781	2.154
Ca	.886	.791	.889	.628	.026	-	.008	.009	-	1.475
Na	.022	.022	.013	.017	-	-	-	.013	.032	.360
K	.001	.001	.003	.006	.001	.006	-	-	-	.234
Ni	-	.001	-	-	-	.083	.037	.028	-	-
Cr	.007	.010	.016	-	8.072	9.089	9.932	9.757	8.074	-
Cl	-	.001	.001	-	.009	.010	.005	-	.036	.006
Total	4.022	4.012	4.018	4.012	21.222	22.488	24.598	24.832	24.845	15.878
Fe/Fe+Mg	.227	.246	.137	.328	.766	.539	.678	.711	.543	.558
Mg*	-	-	-	-	-	-	-	-	-	-
Ca*	46.000	41.500	46.000	32.200	-	-	-	-	-	-
An	-	-	-	-	-	-	-	-	-	-

G300-37 Clinopyroxene microphenocryst core
G300-38 Clinopyroxene microphenocryst rim
G300-39 Clinopyroxene microphenocryst core
G300-40 Clinopyroxene microphenocryst rim
G300-41 Cr-spinel microphenocryst
G300-42 Cr-spinel inclusion in olivine phenocryst
G300-43 Cr-spinel inclusion in olivine phenocryst
G300-44 Cr-spinel inclusion in olivine phenocryst
G300-45 Cr-spinel inclusion in olivine phenocryst
G300-46 Amphibole inclusion in plagioclase phenocryst

	G300-47	G300-48	G300-49	G300-50	G300-51	G300-52	G300-53	G300-54	G300-55	G300-56
	HBD	HBD	HBD	HBD	HBD	HBD	HBD	PLG	PLG	PLG
Oxide										
SiO2	49.201	52.214	50.253	51.577	53.442	45.475	42.635	45.678	44.445	52.510
Al2O3	4.813	6.626	6.571	6.946	6.119	3.573	3.652	34.000	34.488	28.489
TiO2	2.596	2.935	3.030	2.746	3.076	2.601	4.250	-	.040	.281
FeO	20.869	17.979	20.782	17.731	18.084	22.136	28.550	.491	.569	1.318
MnO	.381	.387	.405	.466	.598	.540	.596	.057	.017	.068
MgO	8.849	6.881	6.081	6.983	6.682	11.599	6.797	.101	.111	.123
CaO	8.514	8.767	8.273	9.068	7.934	10.053	8.990	18.704	18.371	11.813
Na2O	.563	.477	.502	.669	.635	.481	1.054	1.108	1.110	5.999
K2O	1.123	.674	.706	.546	1.087	.186	.552	.011	.028	.277
NiO	-	.105	-	.011	.034	-	.007	.046	.002	-
Cr2O3	.016	-	-	.233	-	.077	.039	.037	-	-
Cl	.017	.026	.015	.062	.019	-	.019	-	-	.008
Total	96.943	97.070	96.616	97.039	97.710	96.721	97.141	100.234	99.180	100.887
Cation										
Si	7.758	8.004	7.869	7.925	8.131	7.330	7.120	8.436	8.300	9.558
Al	.894	1.197	1.212	1.257	1.097	.679	.720	7.400	7.591	6.112
Ti	.306	.338	.357	.317	.352	.315	.533	-	.006	.039
Fe	2.754	2.305	2.271	2.278	2.301	2.984	3.988	.076	.089	.201
Mn	.048	.050	.053	.060	.077	.074	.083	.009	.003	.011
Mg	2.082	1.572	1.419	1.560	1.515	2.787	1.691	.028	.031	.033
Ca	1.440	1.440	1.388	1.493	1.293	1.736	1.608	3.701	3.676	2.304
Na	.174	.142	.152	.199	.187	.150	.340	.397	.040	2.117
K	.227	.131	.141	.107	.211	.039	.116	.003	.007	.064
Ni	-	.012	-	.001	.004	-	-	.007	-	-
Cr	-	-	-	.028	-	.009	.004	.005	-	-
Cl	.006	.006	.004	.016	.005	-	.004	-	-	.003
Total	15.689	15.197	15.316	15.241	15.173	16.103	16.207	20.061	20.103	20.441
Fe/Fe+Mg	.570	.594	.657	.588	.603	.517	.702	.731	.742	.857
Mg*	-	-	-	-	-	-	-	-	-	-
Ca*	-	-	-	-	-	-	-	-	-	-
An	-	-	-	-	-	-	-	90.250	89.990	51.370

G300-47 Amphibole inclusion in plagioclase phenocryst
G300-48 Amphibole inclusion in plagioclase phenocryst
G300-49 Amphibole inclusion in plagioclase phenocryst
G300-50 Amphibole inclusion in plagioclase phenocryst
G300-51 Amphibole inclusion in plagioclase phenocryst
G300-52 Amphibole inclusion in plagioclase phenocryst
G300-53 Amphibole inclusion in plagioclase phenocryst
G300-54 Plagioclase phenocryst core
G300-55 Plagioclase phenocryst core
G300-56 Very thin rim of plagioclase phenocryst

	G300-57	G300-58	G300-59	G300-60	G300-61	G300-62	G300-63	G300-64	G300-65	G298-01
	PLG	PLG	PLG	PLG	PLG	PLG	PLG	PLG	PLG	OLV
Oxide										
SiO2	45.848	49.095	52.635	45.568	46.518	45.710	52.792	49.887	50.345	39.093
Al2O3	34.517	31.166	29.383	34.771	34.366	34.260	29.472	30.716	30.412	.035
TiO2	.029	.049	.100	.054	-	-	.205	.082	.072	.025
FeO	.566	.860	.846	.576	.581	.761	.961	.799	1.039	15.231
MnO	-	.019	.043	.034	.035	.027	-	-	.062	.291
MgO	.113	.122	.143	.108	.087	.078	.123	.128	.122	45.443
CaO	18.018	15.366	13.431	18.557	17.848	17.923	12.968	15.046	14.568	.178
Na2O	1.280	2.882	3.822	1.143	1.235	1.179	4.017	3.231	3.331	.006
K2O	-	.049	.113	.033	.013	.042	.144	.097	.085	.013
NiO	-	-	-	.008	-	-	.220	-	-	.131
Cr2O3	-	.013	.047	-	.212	.029	-	.034	.033	.059
Cl	-	.022	-	-	.101	.034	-	.007	.005	.011
Total	100.371	99.643	100.564	100.852	100.997	100.043	100.903	100.009	100.078	100.517
Cation										
Si	8.434	9.051	9.540	8.362	8.505	8.447	9.542	9.154	9.228	1.472
Al	7.484	6.771	6.277	7.520	7.406	7.461	6.278	6.643	6.569	.002
Ti	.004	.007	.014	.007	-	-	.028	.011	.010	.001
Fe	.087	.133	.128	.088	.089	.118	.145	.123	.159	.479
Mn	-	.003	.007	.005	.005	.004	-	-	.010	.009
Mg	.031	.034	.039	.030	.024	.021	.033	.035	.033	2.550
Ca	3.551	3.035	2.608	3.649	3.496	3.549	2.511	2.958	2.861	.007
Na	.456	1.030	1.343	.407	.438	.423	1.408	1.143	1.184	-
K	-	.012	.026	.008	.003	.010	.033	.023	.020	.001
Ni	-	-	-	.001	-	-	.032	-	-	.004
Cr	-	.002	.007	-	.031	.004	-	.005	.005	.002
Cl	-	.007	-	-	.031	.011	-	.002	.001	.001
Total	20.048	20.084	19.989	20.077	20.028	20.047	20.011	20.096	20.079	4.527
Fe/Fe+Mg	.737	.797	.769	.749	.789	.846	.815	.778	.827	.158
Mg*	-	-	-	-	-	-	-	-	-	84.200
Ca*	-	-	-	-	-	-	-	-	-	-
An	88.620	74.440	65.580	89.790	88.800	89.126	63.540	71.730	70.380	-

G300-57 Core of euhedral plagioclase microphenocryst
G300-58 Rim of euhedral plagioclase microphenocryst
G300-59 Very thin outer rim of plagioclase phenocryst
G300-60 Plagioclase phenocryst core
G300-61 Core of plagioclase microphenocryst
G300-62 Plagioclase phenocryst core
G300-63 Plagioclase phenocryst rim
G300-64 Plagioclase groundmass
G300-65 Plagioclase groundmass
G298-01 Olivine phenocryst core

	G298-02	G298-03	G298-04	G298-05	G298-06	G298-07
	OLV	OLV	OLV	OLV	OLV	OLV
Oxide						
SiO2	38.839	37.198	39.845	39.258	36.834	37.519
Al2O3	.029	.005	.058	.020	.150	-
TiO2	-	-	-	.041	.021	-
FeO	18.621	27.404	11.892	15.993	29.226	26.520
MnO	.412	.589	.229	-	.468	.420
MgO	40.960	33.596	46.901	44.052	32.664	34.455
CaO	.207	.231	.234	.201	.241	.236
Na2O	.039	-	-	-	-	-
K2O	.071	-	.020	-	.013	.006
NiO	.159	.107	.258	.093	.046	.085
Cr2O3	-	.063	.047	-	-	.029
Cl	.043	.005	.015	-	-	.002
Total	99.380	99.198	99.499	99.658	99.527	99.277
Cation						
Si	1.001	1.003	.994	.994	.998	1.005
Al	.001	-	.002	.001	-	-
Ti	-	-	-	.001	-	-
Fe	.401	.618	.248	.339	.663	.594
Mn	.009	.013	.005	-	.011	.010
Mg	1.574	1.351	1.744	1.663	1.320	1.376
Ca	.006	.007	.006	.005	.007	.007
Na	.002	-	-	-	-	-
K	.002	-	.001	-	-	-
Ni	.003	.002	.005	.002	.001	.002
Cr	-	.001	.001	-	-	.001
Cl	.002	-	.001	-	-	-
Total	3.002	2.996	3.006	3.005	3.001	2.995
Fe/Fe+Mg	.203	.314	.125	.169	.334	.302
Mg*	79.700	68.600	87.500	83.100	66.600	69.800
Ca*	-	-	-	-	-	-
An	-	-	-	-	-	-

G298-02 Olivine phenocryst core
G298-03 Olivine phenocryst rim
G298-04 Olivine phenocryst core
G298-05 Olivine phenocryst core
G298-06 Olivine microphenocryst
G298-07 Olivine microphenocryst

	G298-08	G298-09	G298-10	G298-11	G298-12	G298-13	G298-14	G298-15	G298-16	G298-17
	OLV	CPX	CPX	CPX	CPX	CPX	CHR	CHR	PLG	PLG
Oxide										
SiO2	38.159	51.238	52.789	51.218	50.424	52.793	.089	.111	44.994	44.344
Al2O3	.009	4.259	2.256	3.618	3.329	1.996	16.857	3.743	34.769	35.846
TiO2	.064	.560	.373	.526	.971	.571	.656	12.413	.050	-
FeO	21.477	5.879	5.506	5.737	8.680	8.763	31.169	65.390	.463	.491
MnO	.399	.168	.146	.118	.211	.240	.115	.352	.031	-
MgO	38.768	14.560	15.947	15.343	14.321	16.316	9.127	3.797	.031	.041
CaO	.242	22.184	21.943	22.014	20.528	18.707	.025	.077	18.739	18.971
Na2O	.081	.181	.180	.345	.350	.191	-	-	.881	.621
K2O	.062	-	-	-	.001	-	-	.005	.004	.006
NiO	.103	.052	.036	-	.039	.008	.076	.012	-	-
Cr2O3	.171	.608	.325	.461	.458	.202	39.478	10.068	-	.055
Cl	.124	.004	.021	.100	.020	-	-	-	-	-
Total	99.661	99.692	99.521	99.480	99.331	99.788	97.591	95.968	99.962	100.376
Cation										
Si	.996	1.894	1.947	1.899	1.892	1.951	.024	.036	8.323	8.176
Al	-	.186	.097	.158	.147	.087	5.404	1.438	7.584	7.792
Ti	.001	.016	.010	.015	.027	.016	.134	3.042	.005	-
Fe	.469	.182	.169	.178	.272	.271	7.090	17.822	.069	.075
Mn	.009	.005	.004	.004	.007	.007	.027	.097	.005	-
Mg	1.509	.802	.876	.848	.801	.898	3.701	1.845	.011	.011
Ca	.007	.879	.867	.878	.825	.741	.007	.027	4.461	3.749
Na	.004	.013	.013	.025	.025	.013	-	-	.315	.224
K	.002	-	-	-	-	-	-	.002	-	-
Ni	.002	.002	.001	-	.001	-	.017	.003	-	-
Cr	.004	.018	.009	.014	.014	.006	8.490	2.594	-	.011
Cl	.005	-	.001	.006	.001	-	-	-	-	-
Total	3.009	3.996	3.994	4.020	4.014	3.990	24.894	26.907	20.773	20.038
Fe/Fe+Mg	.237	.185	.162	.173	.254	.232	.657	.906	.892	.869
Mg*	76.700	-	-	-	-	-	-	-	-	-
Ca*	-	47.000	45.000	46.000	43.000	39.000	-	-	-	-
An	-	-	-	-	-	-	-	-	93.400	94.360

G298-08 Olivine microphenocryst
G298-09 Clinopyroxene phenocryst core
G298-10 Clinopyroxene phenocryst core
G298-11 Clinopyroxene phenocryst core
G298-12 Clinopyroxene groundmass
G298-13 Clinopyroxene groundmass
G298-14 Cr-spinel inclusion in olivine phenocryst
G298-15 Cr-spinel inclusion in olivine phenocryst
G298-16 Plagioclase phenocryst core
G298-17 Plagioclase phenocryst core

	G298-18	G298-19	G298-20	G298-21	G298-22	G298-23	G298-24	G298-25	G298-26	G298-27
	PLG	PLG	PLG	PLG	PLG	PLG	PLG	PLG	PLG	PLG
Oxide										
SiO2	46.460	46.655	54.962	46.311	45.321	46.593	45.934	50.825	51.023	52.575
Al2O3	34.015	33.475	27.096	34.013	34.467	32.917	33.966	29.828	30.530	28.980
TiO2	.031	.023	.191	.009	.011	.076	.043	.065	.029	.131
FeO	.459	.682	1.269	.556	.521	1.009	.558	.906	.904	.948
MnO	-	.001	.038	.007	.021	.036	.116	-	.001	-
MgO	.118	.121	.171	.125	.080	.146	17.874	.106	.102	.138
CaO	17.169	16.657	10.725	17.314	18.098	16.365	1.457	13.260	13.647	12.238
Na2O	1.640	1.818	5.037	1.552	1.124	1.809	.009	3.859	3.726	4.438
K2O	.016	.045	.328	.048	.023	.106	-	.146	.128	.237
NiO	-	-	.023	.017	-	.011	-	.033	.026	-
Cr2O3	.064	-	-	-	.010	.037	.019	.067	.067	-
Cl	.026	.007	.006	.005	-	-		.019	-	.021
Total	99.997	99.482	99.844	99.957	99.677	99.107	99.975	99.113	100.184	99.706
Cation										
Si	8.558	8.634	9.990	8.540	8.399	8.669	8.487	9.372	9.309	9.606
Al	7.384	7.301	5.804	7.392	7.528	7.218	7.397	6.482	6.565	6.240
Ti	.004	.003	.026	.001	.002	.011	.006	.009	.004	.018
Fe	.071	.106	.193	.086	.081	.157	.086	.140	.138	.145
Mn	-	-	.006	.001	.003	.006	-	-	-	-
Mg	.032	.033	.046	.034	.022	.041	.032	.029	.028	.037
Ca	3.388	3.303	2.089	3.421	3.594	3.262	3.539	2.620	2.668	2.396
Na	.586	.652	1.775	.555	.404	.653	.522	1.380	1.318	1.572
K	.004	.011	.076	.011	.005	.025	.002	.034	.030	.055
Ni	-	-	.003	.002	-	.002	-	.005	.004	-
Cr	.009	-	-	-	.001	.005	-	.010	.010	-
Cl	.008	.002	.002	.001	-	-	.006	.006	-	.006
Total	20.044	20.045	20.010	20.044	20.039	20.048	20.076	20.086	20.073	20.076
Fe/Fe+Mg	.686	.760	.807	.717	.785	.794	.730	.828	.833	.794
Mg*	-	-	-	-	-	-	-	-	-	-
Ca*	-	-	-	-	-	-	-	-	-	-
An	85.170	83.280	53.020	85.800	89.780	82.790	87.100	69.950	66.430	59.560

G298-18 Plagioclase phenocryst core
G298-19 Plagioclase phenocryst mantle
G298-20 Plagioclase phenocryst rim
G298-21 Plagioclase phenocryst core
G298-22 Plagioclase phenocryst core
G298-23 Plagioclase phenocryst rim
G298-24 Plagioclase microphenocryst
G298-25 Plagioclase groundmass
G298-26 Plagioclase groundmass
G298-27 Plagioclase groundmass

	G297-01	G297-02	G297-03	G297-04	G297-05	G297-06	G297-07	G297-08	G297-09	G297-10
	OLV	OLV	OLV	OPX	OPX	OPX	OPX	CPX	CPX	CPX
Oxide										
SiO2	39.110	37.969	37.112	52.923	53.104	53.799	53.277	49.795	50.875	49.928
Al2O3	-	.002	.012	1.414	1.139	.210	.636	5.087	3.764	4.689
TiO2	.008	-	.013	.276	.247	.964	.140	.549	.453	.533
FeO	13.016	21.642	5.811	19.981	19.716	19.865	19.816	5.405	4.554	4.999
MnO	.170	.364	.453	.780	.760	.699	.752	-	.081	.114
MgO	48.053	39.612	36.403	23.524	24.156	23.447	24.023	14.450	15.636	15.195
CaO	.213	.172	.197	1.539	1.520	1.516	1.581	23.889	23.582	24.305
Na2O	.014	.004	.016	.010	.048	.018	.032	.242	.172	.186
K2O	.011	-	-	.001	.003	.002	-	-	-	-
NiO	-	.109	.079	-	-	-	.093	-	-	.054
Cr2O3	-	.043	-	.036	.033	.001	.072	.190	.625	.123
Cl	.068	.012	.004	.009	.030	.086	.009	.005	.008	-
Total	100.663	99.929	100.100	100.494	100.756	100.608	100.430	99.641	99.749	100.127
Cation										
Si	.970	.988	.984	1.949	1.949	1.974	1.964	1.849	1.879	1.846
Al	-	-	-	.061	.049	.006	.028	.223	.164	.204
Ti	-	-	-	.008	.007	.042	.004	.015	.013	.015
Fe	.270	.477	.573	.615	.605	.610	.611	.168	.141	.155
Mn	.004	.008	.010	.024	.024	.022	.023	-	.003	.004
Mg	1.778	1.531	1.440	1.292	1.322	1.283	1.320	.800	.861	.837
Ca	.006	.005	.006	.061	.060	.060	.062	.951	.933	.963
Na	.001	-	.001	.001	.003	.001	.002	.017	.012	.013
K	-	-	-	-	-	-	-	-	-	-
Ni	.001	.002	.002	-	-	.002	.003	-	-	.001
Cr	-	.001	-	.001	.001	-	.002	.006	.018	.004
Cl	-	.001	-	.001	.002	-	-	-	-	-
Total	3.030	3.013	3.016	4.013	4.022	4.000	4.019	4.030	4.024	4.042
Fe/Fe+Mg	.132	.238	.285	.323	.314	.322	.316	.173	.140	.156
Mg*	86.800	76.200	71.500	-	-	-	-	-	-	-
Ca*	-	-	-	3.000	3.000	3.000	3.000	50.000	48.000	49.000
An	-	-	-	-	-	-	-	-	-	-

G297-01 Olivine microphenocryst
G297-02 Olivine groundmass
G297-03 Olivine inclusion in clinopyroxene cumulate
G297-04 Orthopyroxene in core of clinopyroxene cumulates
G297-05 Orthopyroxene in core of clinopyroxene cumulate
G297-06 Orthopyroxene in core of intergrown clinopyroxene
G297-07 Orthopyroxene in core of clinopyroxene phenocryst
G297-08 Clinopyroxene phenocryst core
G297-09 Clinopyroxene phenocryst rim
G297-10 Clinopyroxene phenocryst core

	G297-11	G297-12	G297-13	G297-14	G297-15	G297-16	G297-17	G297-18	G297-19	G297-20
	CPX	CPX	CPX	CPX	CPX	MAG	MAG	MAG	PLG	PLG
Oxide										
SiO2	51.669	51.792	51.370	51.087	51.007	.152	.117	.110	45.827	44.430
Al2O3	1.676	1.777	1.775	2.369	3.004	3.824	4.476	4.241	34.787	35.716
TiO2	.274	.291	.383	.502	.463	10.774	10.218	10.246	.027	.077
FeO	10.522	9.856	10.484	9.259	5.780	77.260	77.899	78.184	.469	.485
MnO	.530	.473	.497	.321	.179	.376	.297	.324	-	.066
MgO	14.516	15.574	14.979	14.672	16.197	2.523	2.554	2.861	.068	.056
CaO	20.202	20.215	20.711	20.960	22.827	-	.004	.027	18.583	19.245
Na2O	.262	.274	.253	.290	.111	-	-	-	1.134	.848
K2O	-	.001	-	.008	.010	.004	-	.008	.029	-
NiO	.007	.016	-	.025	-	-	.004	.089	.012	.105
Cr2O3	-	.035	-	.032	.122	.062	.171	-	.025	-
Cl	-	-	.023	.003	-	-	.015	-	-	.001
Total	99.658	100.303	100.474	99.528	99.700	94.909	95.756	96.097	100.962	101.029
Cation										
Si	1.943	1.930	1.921	1.980	1.891	.039	.030	.028	8.392	8.162
Al	.074	.078	.078	.105	.131	1.160	1.345	1.271	7.508	7.733
Ti	.008	.007	.011	.014	.013	2.085	1.959	1.959	.004	.011
Fe	.331	.307	.328	.291	.179	14.962	14.946	14.960	.072	.074
Mn	.017	.015	.016	.010	.006	.082	.064	.700	-	.010
Mg	.814	.865	.835	.821	.895	.968	.971	1.084	.019	.015
Ca	.814	.807	.830	.843	.907	-	.001	.007	3.646	3.788
Na	.019	.019	.018	.021	.008	-	-	.001	.403	.302
K	-	-	-	-	-	.001	-	.002	.007	-
Ni	-	-	-	.002	-	-	.001	.018	.002	.015
Cr	-	-	-	.001	.004	.013	.034	-	.004	-
Cl	-	-	.001	-	-	-	.007	-	-	-
Total	3.534	4.028	4.039	4.027	4.033	19.310	19.358	20.030	20.054	20.112
Fe/Fe+Mg	.289	.262	.282	.261	.167	.939	.939	.932	.795	.828
Mg*	-	-	-	-	-	-	-	-	-	-
Ca*	42.000	41.000	42.000	43.000	46.000	-	-	-	-	-
An	-	-	-	-	-	-	-	-	89.900	93.000

G297-11 Clinopyroxene phenocryst in cumulate
G297-12 Core of clinopyroxene in cumulate
G297-13 Core of clinopyroxene in cumulate
G297-14 Rim of clinopyroxene phenocryst in cumulate
G297-15 Rim of clinopyroxene phenocryst in cumulate
G297-16 Magnetite in cumulate
G297-17 Magnetite in cumulate
G297-18 Magnetite in cumulate
G297-19 Plagioclase phenocryst core
G297-20 Plagioclase phenocryst core

	G297-21	G297-22	G297-23	G297-24	G297-25	G297-26	G297-27	VB16-01	VB16-02	VB16-03
	PLG	PLG	PLG	PLG	PLG	PLG	PLG	OLV	OLV	OLV
Oxide										
SiO2	49.646	45.472	45.236	46.984	45.515	47.848	58.460	40.046	38.818	40.413
Al2O3	31.655	34.731	35.476	33.005	34.179	32.673	25.483	.024	.061	.040
TiO2	.032	-	-	-	.054	.008	.197	.111	-	-
FeO	.674	.428	.549	.780	.650	.595	1.373	10.765	16.245	9.998
MnO	-	-	-	.073	.045	.023	-	.217	.352	.196
MgO	.064	.059	.034	.089	.066	.079	.175	47.871	43.151	48.572
CaO	15.418	18.898	19.307	17.543	18.141	16.258	10.077	.181	.291	.200
Na2O	2.907	.931	.805	1.624	1.302	2.463	4.393	-	-	-
K2O	.045	.008	.014	.008	.006	.027	.353	.057	.028	.003
NiO	-	-	.023	-	.024	.060	.026	.350	.139	.281
Cr2O3	.047	.026	-	-	-	.052	-	-	.126	.023
Cl	-	.006	.004	-	.012	.078	.013	-	.036	-
Total	100.488	100.559	101.448	100.105	99.993	100.163	100.549	99.622	99.246	99.725
Cation										
Si	9.058	8.364	8.263	8.664	8.422	8.798	10.542	.993	.992	.996
Al	6.807	7.529	7.637	7.173	7.454	7.080	5.370	.001	.002	.001
Ti	.004	-	-	-	.008	.001	.026	.002	-	-
Fe	.103	.066	.084	.120	.101	.092	.205	.223	.347	.206
Mn	-	-	-	.011	.007	.004	-	.005	.008	.004
Mg	.017	.016	.009	.024	.018	.022	.047	1.769	1.644	1.785
Ca	3.014	3.724	3.778	3.466	3.597	3.203	1.930	.005	.008	.005
Na	1.028	.332	.285	.581	.467	.878	.523	-	-	-
K	.011	.002	.003	.002	.001	.006	.080	.002	.001	-
Ni	-	-	.003	-	.004	.009	.004	.007	.003	.006
Cr	.007	.004	-	-	-	.008	-	-	.003	-
Cl	-	.002	.001	-	.004	.024	.004	-	.002	-
Total	20.050	20.039	20.064	20.041	20.082	20.124	19.642	3.006	3.008	3.003
Fe/Fe+Mg	.856	.804	.901	.832	.848	.808	.815	.112	.174	.104
Mg*	-	-	-	-	-	-	-	88.800	82.600	89.600
Ca*	-	-	-	-	-	-	-	-	-	-
An	74.000	91.000	92.900	85.600	88.500	78.400	76.200	-	-	-

G297-21 Plagioclase phenocryst rim
G297-22 Plagioclase phenocryst core
G297-23 Plagioclase phenocryst core
G297-24 Plagioclase inclusion in cumulate
G297-25 Plagioclase inclusion in cumulate
G297-26 Plagioclase microphenocryst
G297-27 Plagioclase groundmass
VB16-01 Olivine phenocryst core
VB16-02 Olivine phenocryst rim
VB16-03 Anhedral olivine phenocryst core

	VB16-04	VB16-05	VB16-06	VB16-07	VB16-08	VB16-09	VB16-10	VB16-11	VB16-12	VB16-13
	OLV	OLV	OLV	OLV	OLV	OLV	OLV	OPX	OPX	OPX
Oxide										
SiO2	39.918	39.186	38.108	39.016	39.192	39.676	38.290	53.015	53.109	54.415
Al2O3	.060	.033	.048	.039	.013	.044	.022	1.390	.923	1.146
TiO2	-	-	.014	.118	.032	.020	.036	.245	.319	.345
FeO	13.043	14.333	22.165	17.530	14.117	13.235	18.280	19.291	18.803	18.277
MnO	.230	.278	.427	.214	.335	.209	.306	.688	.577	.471
MgO	46.151	44.960	38.801	42.450	45.541	46.574	42.687	23.006	23.655	23.676
CaO	.279	.208	.192	.198	.220	.263	.139	1.601	1.992	2.231
Na2O	.008	-	.037	.008	.001	.072	-	.044	.028	.027
K2O	-	.042	-	-	.051	.040	-	-	.028	.006
NiO	.183	.121	.096	.158	.147	.136	.057	-	.005	-
Cr2O3	.104	.070	.121	-	-	.037	-	-	.142	-
Cl	.012	-	.030	-	.008	.059	-	-	-	-
Total	99.988	99.232	100.039	99.731	99.657	100.363	99.817	99.280	99.582	100.593
Cation										
Si	.995	.991	.993	.996	.987	.988	.981	1.968	1.965	1.981
Al	.002	.001	.001	.001	-	.001	.001	.061	.040	.049
Ti	-	-	-	.002	.001	-	.001	.007	.009	.009
Fe	.272	.303	.483	.374	.297	.276	.392	.599	.582	.557
Mn	.005	.006	.009	.005	.007	.004	.007	.022	.018	.015
Mg	1.715	1.696	1.507	1.615	1.710	1.729	1.631	1.273	1.305	1.285
Ca	.007	.006	.005	.005	.006	.007	.004	.064	.079	.087
Na	-	-	.002	-	-	.003	-	.003	.002	.002
K	-	.001	-	-	.002	.001	-	-	.001	-
Ni	.004	.002	.002	.003	.003	.003	.001	-	-	-
Cr	.002	.001	.002	-	-	.001	-	-	.004	-
Cl	.001	-	.001	-	-	.002	-	-	-	-
Total	3.003	3.008	3.007	3.002	3.013	3.016	3.018	3.996	4.006	3.986
Fe/Fe+Mg	.137	.152	.243	.188	.148	.137	.194	.320	.308	.302
Mg*	86.300	84.800	75.700	81.200	85.200	86.300	80.600	-	-	-
Ca*	-	-	-	-	-	-	-	3.000	3.982	4.475
An	-	-	-	-	-	-	-	-	-	-

VB16-04 Anhedral microphenocryst core
VB16-05 Anhedral olivine phenocryst rim
VB16-06 Rim of olivine phenocryst in cumulate
VB16-07 Anhedral olivine microphenocryst core
VB16-08 Anhedral olivine microphenocryst core
VB16-09 Anhedral olivine microphenocryst core
VB16-10 Anhedral olivine microphenocryst core
VB16-11 Orthopyroxene phenocryst core in cumulate
VB16-12 Coronas of orthopyroxene surrounding olivine
VB16-13 Coronas of orthopyroxene surrounding olivine microphenocryst

	VB16-14	VB16-15	VB16-16	VB16-17	VB16-18	VB16-19	VB16-20	VB16-21	VB16-22	VB16-23
	OPX	PIG	OPX	OPX	CPX	CPX	CPX	CPX	CPX	CPX
Oxide										
SiO2	53.100	53.086	52.866	53.097	50.488	52.367	52.356	50.601	52.895	51.097
Al2O3	1.245	1.141	1.303	.955	3.219	3.558	2.611	2.754	2.633	3.110
TiO2	.265	.401	.430	.236	.523	.489	.203	.559	.443	.573
FeO	18.770	18.713	18.638	19.821	9.045	5.568	4.139	9.866	4.835	8.649
MnO	.673	.635	.585	.587	.149	.172	.164	.301	.139	.393
MgO	23.516	22.925	23.663	23.554	15.111	15.305	16.393	14.400	16.154	14.431
CaO	1.966	2.574	2.027	1.427	19.587	22.811	23.200	20.164	22.428	20.933
Na2O	.060	-	.018	.034	.320	.095	.192	.336	.298	.303
K2O	.056	.020	-	-	-	.050	.005	.019	-	-
NiO	-	.018	-	.128	.069	-	-	.042	.028	.029
Cr2O3	.087	-	.009	-	-	.077	.479	.036	.613	.006
Cl	.006	-	-	-	-	-	.026	-	.123	-
Total	99.745	99.513	99.539	99.841	98.510	100.493	99.767	99.078	100.589	99.525
Cation										
Si	1.961	1.967	1.955	1.965	1.905	1.915	1.924	1.911	1.930	1.912
Al	.054	.050	.057	.042	.143	.153	.113	.123	.112	.137
Ti	.007	.011	.012	.007	.015	.013	.006	.016	.012	.016
Fe	.580	.580	.576	.614	.285	.170	.127	.312	.147	.271
Mn	.021	.020	.018	.018	.005	.005	.005	.010	.004	.012
Mg	1.295	1.266	1.305	1.300	.850	.835	.898	.811	.879	.805
Ca	.078	.102	.080	.057	.792	.894	.913	.816	.877	.839
Na	.004	-	.001	.002	.023	.007	.014	.025	.021	.022
K	.003	.001	-	-	-	.002	-	.001	-	-
Ni	-	.001	-	.004	.002	-	-	.001	.001	.001
Cr	.003	-	-	-	-	.002	.014	.001	.018	-
Cl	-	-	-	-	-	-	.002	-	.007	-
Total	4.007	3.998	4.005	4.008	4.020	3.998	4.016	4.024	4.008	4.015
Fe/Fe+Mg	.309	.314	.306	.321	.251	.170	.124	.278	.144	.252
Mg*	-	-	-	-	-	-	-	-	-	-
Ca*	3.951	5.183	4.042	2.866	40.994	47.000	47.000	42.000	46.000	44.000
An	-	-	-	-	-	-	-	-	-	-

VB16-14 Coronas of orthopyroxene surrounding olivine microphenocryst
VB16-15 Coronas of pigeonite surrounding olivine microphenocryst
VB16-16 Coronas of orthopyroxene surrounding olivine microphenocryst
VB16-17 Inner rim of orthopyroxene phenocryst
VB16-18 Clinopyroxene as outer rim of orthopyroxene phenocryst
VB16-19 Clinopyroxene phenocryst core
VB16-20 Clinopyroxene phenocryst core
VB16-21 Clinopyroxene phenocryst core
VB16-22 Anhedral clinopyroxene microphenocryst
VB16-23 Anhedral clinopyroxene microphenocryst

	VB16-24	VB16-25	VB16-26	VB16-27	VB16-28	VB16-29	VB16-30	VB16-31	VB16-32	VB16-33
	CPX	CPX	CPX	CPX	CPX	OPX	OPX	CPX	MAG	MAG
Oxide										
SiO2	47.428	51.317	51.434	51.004	50.913	52.963	53.006	52.342	.133	.135
Al2O3	7.434	3.441	3.555	2.279	3.964	1.324	1.040	1.419	3.823	4.574
TiO2	1.163	.413	.538	.532	.852	.393	.446	.466	10.650	9.344
FeO	6.074	4.841	5.038	10.149	8.891	17.894	18.621	11.443	76.123	75.769
MnO	.131	.172	.115	.439	.337	.575	.637	.441	.380	.429
MgO	13.547	15.616	15.434	14.096	14.244	23.836	23.316	15.839	2.640	3.758
CaO	22.621	22.804	23.407	20.357	21.166	2.130	2.149	17.384	-	.079
Na2O	.282	.177	-	.287	.335	.383	.115	.249	-	-
K2O	.048	.064	.025	-	.009	.010	.076	-	.003	.003
NiO	.041	-	.074	.015	.070	.040	.063	-	.027	.006
Cr2O3	.396	.394	-	-	.020	-	-	-	.013	-
Cl	.064	-	-	.005	.010	.047	.006	-	.006	-
Total	99.229	99.239	99.621	99.165	100.810	99.595	99.474	99.582	93.797	94.098
Cation										
Si	1.777	1.902	1.900	1.927	1.884	1.955	1.964	1.959	.047	.047
Al	.328	.150	.155	.101	.173	.058	.045	.063	1.584	1.879
Ti	.033	.012	.015	.015	.024	.011	.012	.013	2.816	2.449
Fe	.190	.150	.156	.321	.275	.552	.577	.358	22.387	22.080
Mn	.004	.005	.004	.014	.010	.018	.020	.014	.113	.127
Mg	.757	.863	.850	.794	.786	1.312	1.288	.884	1.384	1.952
Ca	.908	.905	.926	.824	.839	.084	.085	.697	-	.030
Na	.020	.013	-	.021	.024	.027	.008	.018	-	-
K	.002	.003	.001	-	-	-	.004	-	.001	.001
Ni	.001	-	.002	-	.002	.001	.002	-	.008	.002
Cr	.012	.012	-	-	-	-	-	-	.004	-
Cl	.004	-	-	-	-	.003	-	-	.004	-
Total	4.036	4.014	4.008	4.018	4.017	4.022	4.007	4.006	28.347	28.566
Fe/Fe+Mg	.201	.148	.155	.288	.259	.296	.309	.288	.942	.916
Mg*	-	-	-	-	-	-	-	-	-	-
Ca*	49.000	47.000	47.800	42.000	44.000	4.273	4.315	-	-	-
An	-	-	-	-	-	-	-	-	-	-

VB16-24 Clinopyroxene in cumulate with olivine
VB16-25 Clinopyroxene in cumulate with olivine
VB16-26 Clinopyroxene in cumulate with olivine
VB16-27 Core of clinopyroxene phenocryst in cumulate
VB16-28 Clinopyroxene phenocryst rim
VB16-29 Orthopyroxene groundmass
VB16-30 Orthopyroxene groundmass
VB16-31 Clinopyroxene phenocryst rim
VB16-32 Magnetite groundmass
VB16-33 Magnetite microphenocryst in cumulate

	VB16-34	VB16-35	VB16-36	VB16-37	VB16-38	VB16-39	VB16-40	VB16-41	VB16-42	VB16-43
	PLG	PLG	PLG	PLG	PLG	PLG	PLG	PLG	PLG	PLG
Oxide										
SiO2	45.355	47.829	45.175	45.432	47.616	47.443	46.646	51.748	50.068	52.026
Al2O3	34.508	32.915	34.570	34.196	32.563	32.986	33.830	29.955	31.023	30.162
TiO2	-	.054	.023	.016	-	.031	-	.056	.018	.159
FeO	.545	.641	.547	.546	.625	.631	.574	.599	.745	.732
MnO	-	.008	.029	.009	.035	-	-	.087	.039	.011
MgO	.022	.091	.042	.006	.091	.085	.008	.145	.112	.146
CaO	18.116	16.399	18.197	17.923	15.909	16.488	17.230	13.431	14.561	13.293
Na2O	1.175	2.331	1.312	1.227	2.449	2.261	1.752	4.026	3.483	4.037
K2O	-	.059	.034	-	.052	.006	-	.145	.069	.122
NiO	.004	.002	-	-	-	-	-	-	-	.069
Cr2O3	.075	.043	.009	-	-	-	.043	.021	.121	.002
Cl	-	.012	.001	-	.110	.027	.007	-	.135	-
Total	99.801	100.386	99.939	99.354	99.449	99.957	100.090	100.212	100.373	100.760
Cation										
Si	8.397	8.770	8.364	8.492	8.811	8.737	8.588	9.423	9.156	9.419
Al	7.530	7.113	7.543	7.489	7.101	7.159	7.341	6.429	6.686	6.436
Ti	-	.007	.003	.002	-	.004	-	.008	.002	.022
Fe	.084	.098	.085	.085	.097	.097	.088	.091	.114	.111
Mn	-	.001	.005	.001	.006	-	-	.013	.006	.002
Mg	.006	.025	.012	.002	.025	.023	.002	.039	.031	.039
Ca	3.593	3.222	3.610	3.568	3.154	3.253	3.399	2.620	2.853	2.579
Na	.422	.829	.471	.442	.879	.807	.625	1.421	1.235	1.417
K	-	.014	.008	-	.012	.001	-	.034	.016	.028
Ni	.001	-	-	-	-	-	-	-	-	.010
Cr	.011	.006	.001	-	-	-	.006	.003	.018	-
Cl	-	.004	-	-	.035	.008	.002	-	.042	-
Total	20.044	20.089	20.101	20.032	20.119	20.092	20.053	20.081	20.157	20.063
Fe/Fe+Mg	.931	.799	.880	.981	.794	.807	.976	.699	.788	.738
Mg*	-	-	-	-	-	-	-	-	-	-
Ca*	-	-	-	-	-	-	-	-	-	-
An	84.990	79.540	88.480	88.978	77.973	80.100	84.470	64.290	69.520	64.090

VB16-34 Plagioclase phenocryst having a wide unzoned core
VB16-35 Plagioclase phenocryst having a wide unzoned core
VB16-36 Plagioclase phenocryst core
VB16-37 Plagioclase phenocryst core
VB16-38 Plagioclase phenocryst rim
VB16-39 Plagioclase groundmass
VB16-40 Plagioclase phenocryst core
VB16-41 Plagioclase phenocryst rim
VB16-42 Plagioclase groundmass
VB16-43 Plagioclase groundmass

	G291-01	G291-02	G291-03	G291-04	G291-05	G291-06	G291-07	G291-08	G291-09	G291-10
	OLV	OLV	OLV	OLV	OLV	OLV	OLV	OLV	OLV	OLV
Oxide										
SiO2	39.920	40.611	39.662	38.033	39.135	39.404	37.549	38.387	37.832	37.299
Al2O3	.031	.010	.006	.022	.008	.041	.025	.024	.030	.027
TiO2	-	.017	.041	-	-	-	-	-	.019	.013
FeO	10.303	10.947	11.206	10.228	14.408	11.522	18.482	20.617	24.238	24.670
MnO	.184	.238	.214	.115	-	.238	.395	.284	.414	.404
MgO	49.088	47.187	47.976	50.841	45.770	48.277	42.405	40.927	38.159	37.255
CaO	.203	.218	.192	.174	.195	.177	.225	.149	.118	.135
Na2O	.018	-	-	.085	.011	.002	-	.007	-	.009
K2O	.009	.011	.042	-	-	.014	.008	-	-	-
NiO	.144	.201	.181	.213	.153	.178	.114	-	.094	.011
Cr2O3	.035	.038	-	.126	-	-	.033	.024	-	-
Cl	.027	-	-	.062	.005	.016	-	.013	-	-
Total	99.962	99.478	99.520	99.899	99.684	99.870	99.236	100.430	100.905	99.824
Cation										
Si	.984	1.006	.986	.944	.985	.979	.972	.987	.986	.986
Al	.001	-	-	.001	-	.001	.001	.001	.001	.001
Ti	-	-	.001	-	-	-	-	-	.001	-
Fe	.212	.227	.233	.212	.303	.239	.400	.443	.529	.545
Mn	.004	.005	.005	.002	-	.005	.009	.006	.009	.009
Mg	1.804	1.743	1.779	1.881	1.718	1.788	1.636	1.569	1.483	1.468
Ca	.005	.006	.005	.005	.005	.005	.006	.004	.003	.004
Na	.001	-	-	.004	.001	-	-	-	-	-
K	-	-	.001	-	-	-	-	-	-	-
Ni	.003	.004	.004	.004	.003	.004	.002	-	.002	-
Cr	.001	.001	-	.002	-	-	.001	-	-	-
Cl	.001	-	-	.003	-	.001	-	.001	-	-
Total	3.017	2.993	3.013	3.059	3.015	3.022	3.027	3.013	3.014	3.014
Fe/Fe+Mg	.105	.115	.116	.101	.150	.118	.196	.220	.263	.271
Mg*	89.500	88.500	88.400	89.900	85.000	88.200	80.400	78.000	73.700	72.900
Ca*	-	-	-	-	-	-	-	-	-	-
An	-	-	-	-	-	-	-	-	-	-

G291-01 Olivine phenocryst core
G291-02 Anhedral olivine phenocryst core
G291-03 Olivine phenocryst core
G291-04 Olivine phenocryst core
G291-05 Olivine phenocryst core
G291-06 Anhedral olivine phenocryst core
G291-07 Rounded olivine phenocryst rim
G291-08 Anhedral olivine phenocryst core
G291-09 Rounded olivine phenocryst
G291-10 Rounded olivine phenocryst

	G291-11	G291-12	G291-13	G291-14	G291-15	G291-16	G291-17	G291-18	G291-19	G291-20
	OLV	OLV	OLV	OLV	OLV	OLV	OLV	OPX	OPX	OPX
Oxide										
SiO2	37.650	40.436	40.019	39.980	37.997	39.714	38.796	52.387	52.585	53.197
Al2O3	.012	.028	-	.020	.031	.007	.029	.913	.720	.725
TiO2	.039	.021	-	.005	-	-	.025	.364	.182	.157
FeO	24.000	10.455	11.563	11.446	22.171	11.972	16.995	20.561	19.647	18.822
MnO	.483	.135	.219	.345	.315	.192	.321	.738	.765	.659
MgO	37.818	49.141	48.029	48.222	39.408	48.218	42.801	23.576	24.194	24.822
CaO	.121	.199	.129	.266	.276	.208	.225	1.533	1.532	1.460
Na2O	-	.006	-	.011	-	.005	-	-	.039	.042
K2O	-	.004	-	.087	.016	.005	.019	.004	.008	.003
NiO	.122	.272	.183	.155	.027	.302	.069	.045	-	.073
Cr2O3	-	.071	.023	-	.037	.025	.056	-	.027	.012
Cl	.002	.003	.026	.009	-	.003	-	.006	-	-
Total	100.247	100.772	100.192	100.547	100.280	100.651	99.336	100.125	99.699	99.972
Cation										
Si	.988	.989	.989	.986	.987	.981	.993	1.945	1.953	1.959
Al	-	.001	-	.001	.001	-	.001	.040	.031	.031
Ti	.001	-	-	-	-	-	-	.010	.005	.004
Fe	.527	.214	.239	.236	.482	.247	.364	.638	.610	.580
Mn	.011	.003	.005	.007	.007	.004	.007	.023	.024	.021
Mg	1.479	1.791	1.770	1.772	1.526	1.775	1.632	1.305	1.339	1.363
Ca	.003	.005	.003	.007	.008	.006	.006	.061	.061	.058
Na	-	-	-	.001	-	-	-	-	.003	.003
K	-	-	-	.003	.001	-	.001	-	-	-
Ni	.003	.005	.004	.003	.001	.006	.001	.001	-	.002
Cr	-	.001	-	-	.001	-	.001	-	.001	-
Cl	-	-	.001	-	-	-	-	-	-	-
Total	3.011	3.010	3.012	3.016	3.012	3.019	3.006	4.023	4.028	4.022
Fe/Fe+Mg	.263	.107	.119	.118	.240	.122	.182	.329	.313	.298
Mg*	73.700	89.300	88.100	88.200	76.000	87.800	81.800	-	-	-
Ca*	-	-	-	-	-	-	-	3.000	3.000	3.000
An	-	-	-	-	-	-	-	-	-	-

G291-11 Anhedral olivine phenocryst
G291-12 Subhedral olivine phenocryst
G291-13 Subhedral olivine phenocryst
G291-14 Olivine phenocryst core
G291-15 Olivine phenocryst rim
G291-16 Olivine microphenocryst core
G291-17 Olivine microphenocryst rim
G291-18 Orthopyroxene phenocryst core
G291-19 Orthopyroxene phenocryst in cumulate
G291-20 Orthopyroxene phenocryst in cumulate

	G291-21	G291-22	G291-23	G291-24	G291-25	G291-26	G291-27	G291-28	G291-29	G291-30
	OPX	OPX	OPX	CPX	CPX	CPX	OPX	PIG	CPX	CPX
Oxide										
SiO2	53.248	51.901	53.000	49.143	50.187	51.374	52.231	52.354	51.446	51.615
Al2O3	.779	1.581	1.275	5.048	3.291	2.855	1.949	1.671	2.369	2.796
TiO2	.198	.211	.247	.876	.707	.337	.429	.417	.366	.464
FeO	19.562	19.689	20.691	8.227	9.404	4.499	18.130	18.954	10.468	8.288
MnO	.591	.680	.732	.210	.344	.087	.638	.689	.379	.306
MgO	24.134	24.011	22.246	14.686	14.885	16.009	24.427	22.707	14.155	15.033
CaO	1.477	1.541	1.931	20.912	20.931	23.252	2.096	2.721	20.396	21.469
Na2O	.002	.041	.018	.263	.276	.145	.017	.336	.294	.262
K2O	.016	.002	.015	.011	-	-	.013	.017	.002	-
NiO	-	-	.022	.027	.027	.072	.010	-	.050	.042
Cr2O3	.041	-	-	-	-	.467	-	-	.014	.121
Cl	.001	.004	.017	.012	-	-	.002	-	-	.033
Total	100.050	99.660	100.192	99.414	100.053	99.096	99.942	99.867	99.939	100.427
Cation										
Si	1.964	1.929	1.965	1.841	1.878	1.907	1.923	1.941	1.929	1.913
Al	.034	.069	.056	.223	.145	.125	.085	.073	.105	.122
Ti	.005	.006	.007	.025	.020	.009	.012	.012	.010	.013
Fe	.603	.612	.642	.258	.294	.140	.558	.588	.328	.257
Mn	.018	.021	.023	.007	.011	.003	.020	.022	.012	.010
Mg	1.327	1.330	1.230	.820	.830	.886	1.341	1.255	.791	.831
Ca	.058	.061	.077	.839	.839	.925	.083	.108	.819	.852
Na	-	.003	.001	.019	.020	.010	.001	.024	.021	.019
K	.001	-	.001	.001	-	-	.001	.001	-	-
Ni	-	-	.001	.001	.001	.002	-	-	.002	.001
Cr	.001	-	-	-	-	.014	-	-	-	.004
Cl	-	-	.001	.001	-	-	-	-	-	.002
Total	4.013	4.032	4.002	4.034	4.039	4.020	4.024	4.023	4.019	4.023
Fe/Fe+Mg	.313	.315	.343	.239	.262	.136	.294	.319	.293	.236
Mg*	-	-	-	-	-	-	-	-	-	-
Ca*	3.000	3.000	3.905	43.600	42.500	47.339	4.000	5.474	42.000	44.000
An	-	-	-	-	-	-	-	-	-	-

G291-21 Orthopyroxene phenocryst in cumulate
G291-22 Core of orthopyroxene jacketed by clinopyroxene
G291-23 Orthopyroxene phenocryst core
G291-24 Clinopyroxene phenocryst
G291-25 Clinopyroxene surrounding olivine
G291-26 Clinopyroxene groundmass
G291-27 Lathlike orthopyroxene groundmass
G291-28 Lathlike pigeonite groundmass surrounding olivine
G291-29 Clinopyroxene phenocryst core
G291-30 Clinopyroxene phenocryst core

	G291-31	G291-32	G291-33	G291-34	G291-35	G291-36	G291-37	G291-38	G291-39	G291-40
	CPX	CPX	CPX	CPX	CPX	CPX	CPX	CPX	CPX	CPX
Oxide										
SiO2	49.310	52.304	49.422	50.183	47.604	51.474	49.422	50.049	50.183	52.335
Al2O3	4.989	2.371	5.591	4.923	6.226	3.472	4.455	3.532	4.731	2.467
TiO2	1.057	.218	.721	.595	1.252	.500	.979	.666	.662	.327
FeO	9.520	5.635	5.563	6.119	9.370	6.891	9.615	9.576	4.886	3.972
MnO	.332	.160	.213	.154	.174	.116	.348	.323	.085	.098
MgO	14.076	16.254	14.516	14.582	13.258	15.962	14.336	14.700	15.127	16.611
CaO	20.443	22.719	22.809	23.001	21.306	21.296	20.935	20.766	23.536	23.966
Na2O	.403	.194	.349	.252	.366	.187	.329	.318	.198	.200
K2O	-	.007	.045	.010	.003	.009	-	.004	-	.004
NiO	-	.039	-	-	.003	-	-	.044	.048	-
Cr2O3	.006	.142	.410	.247	-	.073	.073	.036	.825	.380
Cl	-	.013	.103	.019	.004	-	.001	-	.013	-
Total	100.137	100.056	99.742	100.086	99.564	99.980	100.494	100.012	100.294	100.360
Cation										
Si	1.843	1.926	1.835	1.857	1.796	1.900	1.845	1.875	1.849	1.915
Al	.220	.103	.245	.215	.277	.151	.196	.156	.205	.106
Ti	.030	.006	.020	.017	.036	.014	.027	.019	.018	.009
Fe	.298	.174	.173	.189	.296	.213	.300	.300	.151	.122
Mn	.011	.005	.007	.005	.006	.004	.011	.010	.003	.003
Mg	.784	.892	.804	.804	.746	.878	.798	.821	.831	.906
Ca	.819	.896	.907	.912	.861	.842	.837	.833	.929	.936
Na	.029	.014	.025	.018	.027	.013	.024	.023	.014	.014
K	-	-	.002	-	-	-	-	-	-	-
Ni	-	.001	-	-	-	-	-	.001	.001	-
Cr	-	.004	.012	.007	-	.002	.002	.001	.024	.011
Cl	-	.001	.006	.001	-	-	-	-	.001	-
Total	4.032	4.022	4.036	4.026	4.044	4.017	4.041	4.040	4.026	4.025
Fe/Fe+Mg	.275	.163	.177	.191	.284	.195	.273	.268	.153	.118
Mg*	-	-	-	-	-	-	-	-	-	-
Ca*	43.000	47.000	48.000	48.000	45.000	44.000	43.000	44.377	48.537	47.600
An	-	-	-	-	-	-	-	-	-	-

G291-31 Clinopyroxene phenocryst rim
G291-32 Clinopyroxene phenocryst in cumulate
G291-33 Clinopyroxene phenocryst in cumulate
G291-34 Clinopyroxene phenocryst in cumulate
G291-35 Clinopyroxene groundmass
G291-36 Clinopyroxene groundmass
G291-37 Clinopyroxene microcryst as inner olivine coronas
G291-38 Coronas of clinopyroxene surrounding olivine
G291-39 Curved clinopyroxene as the outest coronas surrounding olivine
G291-40 Clinopyroxene as the outest coronas surrounding olivine

	G291-41	G291-42	G291-43	G291-44	G291-45	G291-46	G291-47	G291-48	G291-49	G291-50
	CPX	OPX	MAG	MAG	MAG	MAG	HBD	HBD	HBD	HBD
Oxide										
SiO2	50.512	52.551	.148	.193	.156	.149	41.956	41.805	41.665	41.727
Al2O3	3.794	.892	3.534	3.464	3.586	2.804	12.463	12.597	13.177	12.747
TiO2	.856	.367	11.254	10.507	11.104	12.501	2.094	2.095	2.168	2.146
FeO	8.565	21.044	76.269	77.254	77.501	72.899	10.926	11.017	10.909	11.061
MnO	.259	.684	.422	.415	.472	.380	.166	.148	.119	.129
MgO	15.363	21.665	2.556	2.475	2.373	2.534	14.930	14.952	15.286	14.824
CaO	20.309	2.410	.006	.001	.037	.134	11.545	11.670	11.634	11.749
Na2O	.358	.020	.022	-	-	-	2.524	2.473	2.431	2.511
K2O	.006	.017	-	.003	-	-	.223	.221	.180	.217
NiO	-	-	-	.073	-	-	-	-	.023	.037
Cr2O3	.025	.019	.029	.055	.011	4.496	.044	.057	.055	.087
Cl	-	.011	.005	.011	-	-	-	-	-	.006
Total	100.048	99.680	94.245	94.451	95.240	95.897	96.870	97.033	97.647	97.241
Cation										
Si	1.877	1.966	.052	.068	.054	.050	6.470	6.441	6.372	6.420
Al	.166	.039	1.457	1.434	1.467	1.118	2.265	2.287	2.375	2.311
Ti	.024	.010	2.960	2.776	2.900	3.180	.243	.243	.249	.248
Fe	.266	.658	22.311	22.697	22.506	20.623	1.409	1.419	1.395	1.423
Mn	.008	.021	.125	.124	.139	.109	.022	.019	.016	.017
Mg	.851	1.209	1.333	1.296	1.229	1.278	3.432	3.434	3.485	3.401
Ca	.809	.096	.002	-	.014	.049	1.907	1.926	1.906	1.937
Na	.026	.001	.015	-	-	-	.754	.739	.721	.749
K	-	.001	-	.001	-	-	.044	.044	.035	.043
Ni	-	-	-	.021	-	-	-	-	.003	.004
Cr	.001	-	.008	.015	.003	1.202	.005	.007	.006	.010
Cl	-	-	.003	.006	-	-	-	-	-	.001
Total	4.028	4.001	28.266	28.439	28.311	27.609	16.551	16.559	16.563	16.564
Fe/Fe+Mg	.238	.353	.944	.946	.948	.942	.291	.292	.286	.295
Mg*	-	-	-	-	-	-	-	-	-	-
Ca*	41.830	4.839	-	-	-	-	-	-	-	-
An	-	-	-	-	-	-	-	-	-	-

G291-41 Clinopyroxene as outer coronas of olivine
G291-42 Coronas of orthopyroxene surrounding olivine
G291-43 Magnetite microphenocryst in cumulate
G291-44 Magnetite inclusion in cumulate
G291-45 Magnetite inclusion in cumulate
G291-46 Magnetite groundmass
G291-47 Amphibole
G291-48 Amphibole
G291-49 Amphibole
G291-50 Amphibole

	G291-51	G291-52	G291-53	G291-54	G291-55	G291-56	G291-57	G291-58	G291-59	G291-60
	PLG	PLG	PLG	PLG	PLG	PLG	PLG	PLG	PLG	PLG
Oxide										
SiO2	48.561	48.607	50.140	46.032	50.877	52.155	52.363	49.600	50.922	53.940
Al2O3	33.105	31.957	31.259	34.351	30.641	30.098	29.973	31.503	30.528	28.774
TiO2	-	-	.004	.048	.037	.004	-	.015	.021	.070
FeO	.449	.606	.610	.469	.803	.536	.471	.568	.571	.686
MnO	-	.024	-	-	.020	-	-	-	.073	.024
MgO	.050	.061	.083	.049	.101	.029	.061	.058	.042	.100
CaO	15.771	15.256	14.775	18.008	13.775	12.615	12.837	15.109	14.534	12.070
Na2O	2.696	2.982	3.233	1.361	3.790	4.476	4.388	3.168	3.133	4.745
K2O	.053	.053	.048	.033	.086	.058	.088	.064	.090	.121
NiO	.007	.034	.014	-	-	-	.011	-	-	.020
Cr2O3	-	-	.016	-	.032	-	-	-	.005	-
Cl	-	.014	.005	-	-	-	.008	-	.006	.007
Total	100.691	99.594	100.187	100.351	100.162	99.971	100.200	100.091	99.925	100.557
Cation										
Si	8.847	8.958	9.158	8.467	9.285	9.488	9.506	9.081	9.365	9.740
Al	7.108	6.942	6.729	7.447	6.590	6.453	6.413	6.798	6.575	6.122
Ti	-	-	.001	.007	.005	.001	-	.002	.003	.010
Fe	.068	.093	.093	.072	.123	.082	.071	.087	.087	.103
Mn	-	.004	-	-	.003	.008	-	-	.011	.003
Mg	.014	.017	.023	.014	.027	2.459	.017	.016	.011	.027
Ca	3.078	3.013	2.891	3.549	2.694	1.579	2.497	2.964	2.845	2.335
Na	.952	1.066	1.145	.485	1.341	.013	1.545	1.125	1.110	1.661
K	.012	.012	.011	.008	.020	-	.020	.015	.021	.028
Ni	.001	.005	.002	-	-	-	.002	-	-	.003
Cr	-	-	.002	-	.005	-	-	-	.001	-
Cl	-	.004	20.056	-	-		.003	.002	.002	.002
Total	20.081	20.114	20.056	20.049	20.093	20.082	20.073	20.089	19.972	20.034
Fe/Fe+Mg	.833	.848	.805	.842	.817	.911	.812	.845	.884	.774
Mg*	-	-	-	-	-	-	-	-	-	-
Ca*	-	-	-	-	-	-	-	-	-	-
An	76.150	73.650	71.440	87.800	66.440	60.700	61.470	72.220	71.550	58.027

G291-51 Plagioclase phenocryst core
G291-52 Plagioclase phenocryst core
G291-53 Plagioclase phenocryst rim
G291-54 A wide unzoned core of plagioclase phenocryst
G291-55 Rim of a wide unzoned core of plagioclase phenocryst
G291-56 Core of plagioclase phenocryst in cumulate
G291-57 Core of plagioclase phenocryst in cumulate
G291-58 Core of plagioclase phenocryst core in cumulate
G291-59 Plagioclase phenocryst core
G291-60 Plagioclase phenocryst rim

	G291-61	G291-62	G291-63	G291-64	G291-65	G291-66	G291-67	G290-01	G290-02	G290-03
	PLG	PLG	PLG	PLG	PLG	PLG	PLG	OLV	OLV	OLV
Oxide										
SiO2	45.104	52.449	58.202	51.985	52.155	52.034	46.547	40.353	40.203	40.999
Al2O3	35.023	30.222	20.105	30.449	30.098	30.221	33.994	.014	.001	-
TiO2	-	.109	.347	.031	.004	.058	.035	.029	-	.011
FeO	.502	.893	5.058	.543	.536	.663	.690	9.656	10.452	10.407
MnO	.041	-	.168	.015	-	.017	-	.221	-	.162
MgO	.037	.058	3.297	.069	.029	.113	.034	48.900	48.969	48.276
CaO	18.752	15.109	7.797	13.080	12.615	13.410	17.345	.181	.208	.134
Na2O	1.064	3.168	4.223	4.069	4.476	3.945	1.779	.013	-	-
K2O	.004	.064	.828	.082	.058	.083	.016	.028	-	.019
NiO	-	-	-	.043	-	.002	-	.304	.181	.146
Cr2O3	-	-	-	.026	-	-	-	.504	.097	.034
Cl	.025	-	-	-	-	-	-	.021	-	-
Total	100.551	100.002	100.025	100.391	99.971	100.548	100.440	99.775	100.111	100.188
Cation										
Si	8.307	9.518	10.659	9.426	9.488	9.430	8.551	.993	.989	1.005
Al	7.602	6.464	4.339	6.507	6.453	6.455	7.360	-	-	-
Ti	-	.015	.048	.004	.001	.008	.005	-	-	-
Fe	.077	.135	.775	.082	.082	.101	.106	.199	.215	.213
Mn	.006	-	.026	.002	-	.003	-	.005	-	.003
Mg	.010	.019	.900	.019	.008	.031	.009	1.795	1.795	1.765
Ca	3.700	2.413	1.530	2.541	2.459	2.604	3.414	.005	.005	.004
Na	.380	1.316	1.500	1.431	1.579	1.386	.634	.001	-	-
K	.001	.012	.193	.019	.013	.019	.004	.001	-	.001
Ni	-	.008	-	.006	-	-	-	.006	.004	.003
Cr	-	-	-	.004	-	-	-	.001	.002	.001
Cl	.008	-	-	-	-	-	-	.001	-	-
Total	20.091	19.900	19.970	20.040	20.082	20.037	20.083	3.007	3.010	2.995
Fe/Fe+Mg	.885	.879	.463	.815	.911	.767	.920	.100	.107	.108
Mg*	-	-	-	-	-	-	-	90.000	89.300	89.200
Ca*	-	-	-	-	-	-	-	-	-	-
An	90.660	64.500	47.470	63.670	60.700	64.930	84.250	-	-	-

G291-61 Plagioclase phenocryst core
G291-62 Plagioclase groundmass
G291-63 Plagioclase groundmass
G291-64 Plagioclase groundmass
G291-65 Plagioclase groundmass
G291-66 Plagioclase groundmass
G291-67 Plagioclase inclusion
G290-01 Olivine phenocryst core
G290-02 Olivine phenocryst core
G290-03 Olivine phenocryst core

	G290-04	G290-05	G290-06	G290-07	G290-08	G290-09	G290-10	G290-11	G290-12	G290-13
	OLV	OLV	OLV	OLV	OLV	OLV	OLV	OLV	OLV	OLV
Oxide										
SiO2	40.203	37.412	40.301	39.097	39.765	39.603	39.317	40.337	39.246	38.323
Al2O3	.001	.018	-	.039	.070	-	.109	-	.013	.024
TiO2	-	.011	.022	-	.067	.022	.016	.025	.050	.018
FeO	10.452	24.568	10.767	18.158	11.037	14.305	14.338	11.181	18.621	19.263
MnO	-	.532	.191	.380	.133	.186	.176	.176	.430	.406
MgO	48.969	36.636	48.457	41.585	47.835	45.329	45.575	48.087	40.821	42.310
CaO	.208	.153	.215	.184	.225	.202	.301	.139	.182	.163
Na2O	-	-	.033	.003	-	-	.009	.003	-	.115
K2O	-	.017	.011	-	.016	.007	.006	.031	.011	-
NiO	.181	.031	.177	.078	.309	.144	.126	.242	.109	.065
Cr2O3	.097	-	.006	.021	.014	.061	.064	.097	-	.007
Cl	-	.150	.013	.003	-	.001	.019	-	-	-
Total	100.111	99.393	100.192	99.549	99.471	99.862	100.054	100.317	99.484	100.694
Cation										
Si	.989	.993	.992	1.002	.988	.994	.986	.994	1.008	.979
Al	-	.001	-	.001	.002	-	.003	-	-	.001
Ti	-	-	-	-	.001	-	-	-	.001	-
Fe	.215	.545	.222	.389	.229	.300	.301	.230	.400	.412
Mn	-	.012	.004	.008	.003	.004	.004	.004	.009	.009
Mg	1.795	1.450	1.779	1.589	1.773	1.696	1.704	1.766	1.564	1.611
Ca	.005	.004	.006	.005	.006	.005	.008	.004	.005	.004
Na	-	-	.002	-	-	-	-	-	-	.006
K	-	.001	-	-	.001	-	-	.001	-	-
Ni	.004	.001	.004	.002	.006	.003	.003	.005	.002	.001
Cr	.002	-	-	-	-	.001	.001	.002	-	-
Cl	-	.001	.001	-	-	-	.001	-	-	-
Total	3.010	3.007	3.009	2.997	3.009	3.005	3.012	3.005	2.991	3.023
Fe/Fe+Mg	.107	.273	.111	.197	.115	.150	.150	.115	.204	.203
Mg*	89.300	72.700	88.900	80.300	88.500	85.000	85.000	88.500	79.600	79.700
Ca*	-	-	-	-	-	-	-	-	-	-
An	-	-	-	-	-	-	-	-	-	-

G290-04 Olivine phenocryst core
G290-05 Olivine phenocryst rim
G290-06 Olivine phenocryst core
G290-07 Olivine phenocryst rim
G290-08 Core of olivine phenocryst having coronas of pyroxene
G290-09 Olivine microphenocryst core
G290-10 Olivine microphenocryst core
G290-11 Olivine phenocryst mantle
G290-12 Inner rim of olivine phenocryst
G290-13 Inner rim of olivine phenocryst

	G290-14	G290-15	G290-16	G290-17	G290-18	G290-19	G290-20	G290-21	G290-22	G290-23
	OLV	OLV	PIG	PIG	OPX	OPX	OPX	OPX	OPX	CPX
Oxide										
SiO2	37.412	38.205	53.101	53.170	52.745	53.292	52.665	52.693	53.633	52.951
Al2O3	.018	-	.874	.862	1.409	1.413	1.262	1.777	1.715	2.805
TiO2	.011	-	.326	.360	.226	.224	.170	.396	.391	.415
FeO	24.568	26.770	19.031	19.235	20.106	20.104	20.124	19.812	18.388	5.279
MnO	.532	.703	.881	.726	.675	.783	.694	.537	.519	.120
MgO	36.636	33.430	22.592	22.446	22.706	23.156	24.017	22.553	23.210	16.114
CaO	.153	.147	3.007	2.983	1.603	1.614	1.551	1.939	1.329	22.615
Na2O	-	.128	-	.044	.023	.023	.025	.025	.049	.177
K2O	.017	-	-	.004	.005	-	-	.005	-	-
NiO	.031	.017	.073	-	-	.003	.097	.042	.037	.055
Cr2O3	-	-	-	-	-	-	.072	-	-	.317
Cl	.015	.038	-	.007	-	.010	.029	-	.010	.003
Total	99.393	99.438	99.886	99.836	99.499	100.622	100.706	99.779	100.282	100.852
Cation										
Si	.993	1.022	1.968	1.971	1.962	1.960	1.940	1.953	1.964	1.927
Al	.001	-	.038	.038	.062	.061	.055	.078	.074	.120
Ti	-	-	.009	.011	.006	.006	.005	.010	.011	.011
Fe	.545	.599	.590	.597	.625	.618	.620	.613	.563	.161
Mn	.012	.016	.027	.023	.021	.024	.022	.016	.016	.004
Mg	1.450	1.333	1.248	1.241	1.259	1.269	1.319	1.246	1.267	.874
Ca	.004	.004	.120	.119	.064	.064	.061	.076	.091	.882
Na	-	.007	-	.003	.002	.002	.002	.001	.003	.012
K	.001	-	-	-	-	-	-	-	-	-
Ni	.001	-	.002	-	-	-	.003	.001	.001	.002
Cr	-	-	-	-	-	-	.002	-	-	.009
Cl	.001	.002	-	-	-	.001	.002	-	.001	-
Total	3.007	2.983	4.002	4.003	4.002	4.005	4.030	3.994	3.991	4.003
Fe/Fe+Mg	.273	.310	.321	.325	.332	.328	.320	.330	.308	.155
Mg*	72.700	69.000	-	-	-	-	-	-	-	-
Ca*	-	-	6.000	6.000	3.000	3.000	3.000	3.895	4.700	45.900
An	-	-	-	-	-	-	-	-	-	-

G290-14 Outer rim of olivine phenocryst
G290-15 Outer rim of olivine phenocryst
G290-16 Coronas of pigeonite surrounding olivine
G290-17 Coronas of pigeonite surrounding olivine
G290-18 Orthopyroxene phenocryst in cumulate
G290-19 Orthopyroxene phenocryst in clot
G290-20 Orthopyroxene as core of clinopyroxene phenocryst
G290-21 Orthophyroxene as coronas of olivine microcryst
G290-22 Orthophyroxene as inner coronas of anhedral olivine phenocryst
G290-23 Clinopyroxene as outer coronas of anhedral olivine phenocryst

	G290-24	G290-25	G290-26	G290-27	G290-28	G290-29	G290-30	G290-31	G290-32	G290-33
	CPX	CPX	CPX	CPX	CPX	CPX	MAG	CHR	MAG	MAG
Oxide										
SiO2	52.104	52.314	52.042	51.121	51.788	51.910	.205	1.718	.141	.086
Al2O3	1.986	1.965	2.126	4.261	1.794	2.870	3.216	14.377	3.146	2.966
TiO2	.378	.462	.344	.610	.432	.522	10.712	.417	9.563	10.991
FeO	9.593	10.536	10.379	7.004	10.631	10.487	78.309	23.801	78.408	77.790
MnO	.395	.447	.465	.137	.406	.374	.400	.062	.574	.414
MgO	14.581	14.274	14.616	14.181	14.431	14.459	2.268	13.795	1.915	2.552
CaO	21.072	19.970	19.970	22.682	19.889	19.300	.035	.017	.106	.210
Na2O	.275	-	.298	.264	.329	.294	-	.020	-	.030
K2O	-	-	.002	.015	.018	.031	-	-	.022	-
NiO	-	.049	-	-	-	.009	-	.094	.073	.056
Cr2O3	.015	-	.014	.084	-	.056	.007	43.571	.097	.061
Cl	-	-	.030	-	.003	.005	.013	.009	-	.011
Total	100.400	100.170	100.286	100.360	99.718	100.320	95.207	97.881	94.044	95.168
Cation										
Si	1.939	1.953	1.940	1.888	1.945	1.931	.053	.417	.037	.030
Al	.087	.086	.093	.185	.079	.126	.976	4.116	.971	1.222
Ti	.011	.013	.010	.017	.012	.015	2.075	.076	1.883	2.890
Fe	.299	.329	.324	.216	.334	.326	16.867	4.351	15.448	22.745
Mn	.012	.014	.015	.004	.013	.012	.096	.013	.127	.123
Mg	.809	.795	.812	.781	.808	.801	.871	4.995	.747	1.330
Ca	.840	.799	.798	.897	.800	.770	.010	.004	.030	.079
Na	.020	-	.022	.019	.024	.021	-	.009	-	.020
K	-	-	-	.001	.001	.002	-	-	.007	-
Ni	-	.001	-	-	-	-	-	.018	.015	.016
Cr	-	-	-	.002	-	.002	.002	8.368	.020	.017
Cl	-	-	.002	-	-	-	.006	.004	-	.007
Total	4.017	3.991	4.016	4.011	4.016	4.006	20.955	22.371	19.285	28.478
Fe/Fe+Mg	.270	.293	.285	.217	.292	.289	.951	.466	.954	.945
Mg*	-	-	-	-	-	-	-	-	-	-
Ca*	43.000	41.000	41.000	47.000	40.900	40.335	-	-	-	-
An	-	-	-	-	-	-	-	-	-	-

G290-24 Subhedral clinopyroxene phenocryst
G290-25 Clinopyroxene phenocryst in clot
G296-26 Clinopyroxene phenocryst in cumulate
G290-27 Euhedral clinopyroxene phenocryst core
G290-28 Euhedral clinopyroxene phenocryst rim
G290-29 Clinopyroxene groundmass
G290-30 Magnetite inclusion in orthopyroxene
G290-31 Cr-spinel inclusion
G290-32 Magnetite microcryst in clot
G290-33 Magnetite inclusion in clinopyroxene

	G290-34	G290-35	G290-36	G290-37	G290-38	G290-39	G290-40	G290-41	G290-42	G290-43
	MAG	MAG	MAG	MAG	CHR	HBD	HBD	HBD	HBD	PLG
Oxide										
SiO2	.142	.158	.205	.159	.091	42.682	41.778	41.491	40.331	46.072
Al2O3	3.395	3.426	3.216	2.827	16.699	13.675	14.061	13.261	13.267	34.843
TiO2	9.122	8.985	10.712	11.636	.620	2.215	2.131	2.230	2.294	.041
FeO	79.251	79.701	78.309	78.307	34.992	9.754	10.298	13.773	13.127	-
MnO	.450	.388	.440	.468	.278	.134	.277	.261	.113	-
MgO	2.090	2.072	2.268	1.851	3.820	14.993	14.894	15.254	14.634	.110
CaO	.089	.081	.035	.123	.007	12.268	12.467	12.591	12.507	17.992
Na2O	-	-	-	.006	-	2.624	2.514	1.297	1.305	1.295
K2O	.008	-	-	.013	.008	.254	.197	.075	.100	-
NiO	.051	.059	-	.010	.078	.041	.043	.054	.010	-
Cr2O3	-	.055	.007	.137	43.129	.038	.002	.041	.020	-
Cl	-	-	.013	.002	.010	.054	.020	.012	.064	-
Total	94.598	94.925	95.207	95.539	99.732	98.732	98.682	100.340	97.771	100.354
Cation										
Si	.037	.041	.053	.041	.025	6.424	6.320	6.256	6.236	8.449
Al	1.041	1.046	.976	.856	5.380	2.428	2.507	2.356	2.418	7.531
Ti	1.784	1.751	2.075	2.249	.127	.251	.244	.251	.267	.006
Fe	15.507	15.542	15.177	15.143	8.000	1.228	1.304	1.736	1.698	-
Mn	.099	.085	.096	.102	.064	.017	.035	.032	.015	-
Mg	.810	.801	.871	.709	1.557	3.364	3.360	3.428	3.374	.030
Ca	.025	.023	.010	.340	.002	1.979	2.200	2.036	2.072	3.535
Na	-	-	-	.003	-	.764	.736	.380	.391	.461
K	.003	-	-	.004	.003	.048	.040	.016	.020	-
Ni	.011	.012	-	.002	.017	.004	.004	.008	.001	-
Cr	-	.011	.002	.028	9.322	.004	-	.004	.002	-
Cl	-	-	.006	.001	.005	.011	.004	.004	.017	-
Total	19.316	19.312	19.265	19.172	24.502	16.522	16.574	16.597	16.511	20.011
Fe/Fe+Mg	.950	.951	.946	.955	.837	.267	.279	.336	.335	-
Mg*	-	-	-	-	-	-	-	-	-	-
Ca*	-	-	-	-	-	-	-	-	-	-
An	-	-	-	-	-	-	-	-	-	88.460

G290-34 Magnetite inclusion in clinopyroxene
G290-35 Magnetite inclusion in clinopyroxene
G290-36 Magnetite inclusion in orthopyroxene
G290-37 Magnetite inclusion in orthopyroxene
G290-38 Cr-spinel groundmass
G290-39 Core of amphibole
G290-40 Core of amphibole
G290-41 Rim of amphibole
G290-42 Rim of amphibole
G290-43 Plagioclase phenocryst core

	G290-44	G290-45	G290-46	G290-47	G294-01	G294-02	G294-03	G294-04	G294-05	G294-06
	PLG	PLG	PLG	PLG	OLV	OLV	OLV	OLV	OLV	OLV
Oxide										
SiO2	51.075	45.289	48.930	50.936	38.622	38.409	38.883	38.931	38.876	37.974
Al2O3	30.942	34.275	31.833	30.206	.037	.022	.015	.033	.020	.041
TiO2	.024	.034	.051	.017	.028	-	-	-	-	.031
FeO	.522	.345	.544	.596	12.871	11.626	13.390	11.546	13.402	20.183
MnO	-	.004	.042	-	.235	.184	.195	.319	.150	.389
MgO	.054	.065	.108	.086	47.352	48.777	47.672	48.799	47.119	41.479
CaO	13.935	18.903	15.460	14.255	.166	.165	.196	.209	.225	.206
Na2O	3.624	.909	3.024	3.728	-	.026	-	.011	-	-
K2O	.116	.014	.094	.032	-	-	-	.004	-	-
NiO	-	.052	.061	-	.203	.201	.171	.242	.186	.184
Cr2O3	.059	.032	-	.085	.074	.048	.049	.006	-	-
Cl	.033	-	-	.030	-	-	-	.014	-	.006
Total	100.382	99.922	100.147	99.971	99.589	99.459	100.570	100.115	99.979	100.494
Cation										
Si	9.287	8.385	8.974	9.318	.970	.961	.968	.967	.973	.977
Al	6.631	7.479	6.881	6.512	.001	.001	-	.001	.001	.001
Ti	.003	.005	.007	.002	.001	-	-	-	-	.001
Fe	.079	.053	.083	.091	.270	.243	.279	.240	.281	.434
Mn	-	.001	.006	-	.005	.004	.004	.007	.003	.008
Mg	.015	.018	.029	.023	1.772	1.819	1.770	1.807	1.759	1.591
Ca	2.715	3.750	3.038	2.794	.004	.004	.005	.006	.006	.006
Na	1.278	.326	1.076	1.322	-	.001	-	.001	-	-
K	.027	.003	.022	.007	-	-	-	-	-	-
Ni	-	.008	.009	-	.004	.004	.003	.005	.004	.004
Cr	.008	.005	-	.012	.001	.001	.001	-	-	-
Cl	.010	-	-	.009	-	-	-	.001	-	-
Total	20.053	20.033	20.127	20.092	3.029	3.039	3.031	3.033	3.026	3.022
Fe/Fe+Mg	.845	.748	.739	.795	.132	.118	.136	.117	.138	.214
Mg*	-	-	-	-	86.800	88.200	86.400	88.300	86.200	78.600
Ca*	-	-	-	-	-	-	-	-	-	-
An	67.540	91.930	73.450	67.770	-	-	-	-	-	-

G290-44 Plagioclase phenocryst rim
G290-45 Plagioclase phenocryst core
G290-46 Plagioclase phenocryst mantle
G290-47 Plagioclase phenocryst rim
G294-01 Olivine phenocryst core
G294-02 Olivine phenocryst core
G290-03 Olivine phenocryst core
G294-04 Olivine phenocryst core
G294-05 Olivine phenocryst core
G294-06 Olivine phenocryst rim

	G290-07	G290-08	G294-09	G294-10	G294-11	G294-12	G294-13	G294-14	G294-15	G294-16
	OLV	OLV	OLV	OPX	OPX	OPX	OPX	OPX	OPX	OPX
Oxide										
SiO2	39.616	37.874	37.675	51.675	51.994	52.531	52.189	52.018	52.023	51.105
Al2O3	.040	.032	.018	1.188	1.118	.606	.946	.709	1.224	1.774
TiO2	.001	-	.012	.203	.221	.167	.186	.152	.282	.315
FeO	10.942	19.923	22.706	20.261	21.282	20.195	20.426	20.526	19.729	20.661
MnO	.171	.326	.359	.783	.850	.797	.755	.862	.746	.721
MgO	49.119	41.073	39.170	23.685	23.577	23.509	23.252	23.659	23.875	23.020
CaO	.184	.232	.139	1.465	1.393	1.662	1.464	1.531	1.491	1.518
Na2O	.032	-	-	-	-	.002	.031	.022	.044	.009
K2O	.005	-	.007	-	-	.008	.018	-	-	-
NiO	.268	.046	-	-	-	.048	.056	-	-	.020
Cr2O3	.092	-	.009	-	-	.024	-	-	.027	.054
Cl	.001	-	.003	.007	-	-	-	-	-	-
Total	100.471	99.506	100.098	99.267	100.436	99.548	99.325	99.480	99.440	99.197
Cation										
Si	.976	.982	.983	1.935	1.897	1.960	1.953	1.946	1.938	1.920
Al	.001	.001	-	.052	.048	.027	.042	.031	.054	.079
Ti	-	-	-	.006	.006	.005	.005	.004	.008	.009
Fe	.225	.432	.495	.634	.649	.630	.639	.642	.615	.649
Mn	.004	.007	.008	.025	.026	.025	.024	.027	.024	.023
Mg	1.804	1.588	1.525	1.322	1.282	1.307	1.297	1.320	1.326	1.289
Ca	.005	.006	.004	.059	.054	.066	.059	.061	.060	.061
Na	.002	-	-	-	-	-	.002	.002	.003	.001
K	-	-	-	-	-	-	.001	-	-	-
Ni	.005	.001	-	-	-	.001	.002	-	-	.001
Cr	.002	-	-	-	-	.001	-	-	.001	.002
Cl	-	-	-	-	-	-	-	-	-	-
Total	3.024	3.017	3.015	4.034	3.962	4.022	4.023	4.034	4.028	4.032
Fe/Fe+Mg	.111	.214	.245	.324	.336	.325	.330	.327	.317	.335
Mg*	88.900	78.600	75.500	-	-	-	-	-	-	-
Ca*	-	-	-	3.000	2.848	3.000	3.000	3.000	3.000	3.000
An	-	-	-	-	-	-	-	-	-	-

G290-07 Anhedral olivine phenocryst core
G294-08 Anhedral olivine phenocryst rim
G294-09 Anhedral olivine phenocryst rim
G294-10 Orthopyroxene phenocryst core
G294-11 Orthopyroxene phenocryst core
G294-12 Orthopyroxene phenocryst in cumulate
G294-13 Orthopyroxene phenocryst in cumulate
G294-14 Orthopyroxene groundmass
G294-15 Orthopyroxene in clinopyroxene core
G294-16 Orthopyroxene in clinopyroxene core

	G294-17	G294-18	G294-19	G294-20	G294-21	G294-22	G294-23	G294-24	G294-25	G294-26
	CPX	CPX	CPX	CPX	CPX	MAG	MAG	MAG	MAG	MAG
Oxide										
SiO2	51.307	51.230	51.941	50.347	50.826	.073	.124	.133	.173	.124
Al2O3	1.782	2.652	1.966	2.045	2.988	1.746	3.355	3.291	3.245	3.355
TiO2	.395	.586	.368	.449	.602	9.247	11.052	11.568	11.792	11.052
FeO	10.840	9.392	10.299	10.071	7.592	82.410	77.656	77.008	76.478	77.656
MnO	.373	.313	.502	.452	.245	.746	.398	.514	.487	.398
MgO	14.491	14.673	14.774	14.764	16.420	1.470	2.126	1.975	2.447	2.126
CaO	20.316	21.367	20.448	20.902	20.246	.007	.082	.021	.008	.082
Na2O	.260	.289	.282	.269	.161	-	-	.050	-	-
K2O	.022	-	.004	.013	.016	.011	-	.004	.011	-
NiO	.002	-	.015	.011	-	-	.053	.019	.040	.053
Cr2O3	-	-	-	.032	.150	.030	.071	.081	.016	.071
Cl	.004	.001	-	.009	.002	.005	-	.082	-	-
Total	99.793	100.502	100.597	99.366	99.247	95.744	94.918	94.644	94.697	94.918
Cation										
Si	1.878	1.907	1.934	1.906	1.859	.019	.032	.034	.045	.032
Al	.077	.116	.086	.091	.129	.534	1.021	1.004	.988	1.021
Ti	.011	.016	.010	.013	.017	1.803	2.146	2.251	2.291	2.146
Fe	.299	.292	.321	.319	.209	16.082	15.088	14.997	14.865	15.088
Mn	.012	.010	.016	.014	.008	.164	.087	.113	.107	.087
Mg	.791	.814	.820	.833	.895	.568	.818	.762	.942	.818
Ca	.797	.852	.816	.848	.793	.002	.023	.006	.002	.023
Na	.018	.021	.020	.020	.011	-	-	.025	-	-
K	.001	-	-	.001	.001	.004	-	.001	.004	-
Ni	-	-	-	-	-	-	.011	.004	.008	.011
Cr	-	-	-	.001	.004	.006	.014	.017	.003	.014
Cl	-	-	-	.001	-	.002	-	.036	-	-
Total	3.884	4.029	4.023	4.046	3.925	19.184	19.240	19.250	19.254	19.240
Fe/Fe+Mg	.274	.264	.281	.277	.189	.966	.949	.952	.940	.950
Mg*	-	-	-	-	-	-	-	-	-	-
Ca*	41.969	43.000	42.000	42.000	41.000	-	-	-	-	-
An	-	-	-	-	-	-	-	-	-	-

G294-17 Clinopyroxene phenocryst
G294-18 Clinopyroxene phenocryst
G294-19 Clinopyroxene phenocryst in cumulate
G294-20 Clinopyroxene jacketing orthopyroxene
G294-21 Clinopyroxene groundmass
G294-22 Magnetite microphenocryst
G294-23 Magnetite inclusion in clinopyroxene
G294-24 Magnetite microphenocryst
G294-25 Magnetite inclusion in clinopyroxene
G294-26 Magnetite microphenocryst

	G294-27	G294-28	G294-29	G294-30	G294-31	G294-32	G294-33	G294-34	G294-35	G294-36
	MAG	CHR	CHR	HBD	HBD	PLG	PLG	PLG	PLG	PLG
Oxide										
SiO2	.098	.079	.095	41.088	40.236	46.530	46.148	51.828	43.407	44.322
Al2O3	3.323	14.655	14.130	13.064	12.841	33.354	34.071	29.690	34.876	34.874
TiO2	11.476	.658	.750	2.275	2.181	.005	.011	.017	.005	.003
FeO	78.170	24.993	28.786	11.383	11.164	.483	.457	.508	.569	.617
MnO	.497	.147	.094	.109	.112	.010	-	.069	-	.003
MgO	2.332	11.599	10.150	14.601	14.338	.047	.027	.063	.039	.071
CaO	.031	.008	.004	11.954	11.888	17.275	17.191	13.038	19.342	18.441
Na2O	-	-	-	2.504	2.477	1.870	2.012	4.230	.712	.982
K2O	.013	.015	-	.208	.186	.031	.027	.094	.013	.003
NiO	.016	.133	.058	.012	.087	.051	-	.043	-	-
Cr2O3	-	46.175	44.146	.009	-	-	-	-	.041	-
Cl	.011	.012	-	.006	-	-	-	.004	.013	-
Total	95.967	98.475	98.057	97.213	95.510	99.658	99.945	99.584	99.017	99.315
Cation										
Si	.025	.019	.024	6.343	6.329	8.612	8.519	9.482	8.148	8.263
Al	1.000	4.228	4.096	2.377	2.380	7.276	7.412	6.402	7.715	7.663
Ti	2.203	.121	.136	.264	.258	.001	.001	.002	.001	-
Fe	15.018	4.604	5.334	1.469	1.468	.075	.071	.078	.089	.096
Mn	.108	.031	.016	.015	.015	.002	-	.011	-	-
Mg	.887	4.233	3.720	3.360	3.362	.013	.008	.017	.011	.020
Ca	.008	.002	-	1.977	2.003	3.426	3.400	2.556	3.890	3.684
Na	-	-	-	.749	.755	.671	.720	1.500	.259	.355
K	.004	.005	-	.041	.038	.007	.006	.022	.003	.001
Ni	.003	.026	.008	.001	.011	.008	-	.066	-	-
Cr	-	8.938	8.592	.001	-	-	-	-	.006	-
Cl	.005	.005	-	.002	-	-	-	.001	.004	-
Total	19.262	22.212	21.926	16.599	16.619	20.089	20.137	20.077	20.126	20.083
Fe/Fe+Mg	.944	.521	.589	.304	.304	.851	.904	.819	.891	.830
Mg*	-	-	-	-	-	-	-	-	-	-
Ca*	-	-	-	-	-	-	-	-	-	-
An	-	-	-	-	-	83.490	82.400	62.680	93.690	91.190

G294-27 Magnetite inclusion in orthopyroxene
G294-28 Cr-spinel inclusion in olivine phenocryst
G294-29 Cr-spinel inclusion in olivine phenocryst
G294-30 Amphibole
G294-31 Amphibole
G294-32 Core of plagioclase phenocryst in cumulate
G294-33 Plagioclase phenocryst mantle
G294-34 Rim of plagioclase phenocryst in cumulate
G294-35 Anhedral plagioclase microphenocryst
G294-36 Anhedral plagioclase microphenocryst

	G294-37	G294-38	G294-39	G294-40	G294-41	G294-42	G294-43	G294-44	G294-45	G294-46
	PLG	PLG	PLG	PLG	PLG	PLG	PLG	CPX	CPX	CPX
Oxide										
SiO2	50.661	51.495	48.885	49.746	49.930	51.347	53.902	50.817	51.485	49.363
Al2O3	30.965	29.856	31.698	31.615	31.094	30.230	28.611	2.164	2.182	4.200
TiO2	.061	.047	-	-	.018	.051	.034	.542	.286	.481
FeO	.678	.471	.593	.588	.355	.514	.539	8.389	4.524	4.694
MnO	.035	-	.009	.046	-	.008	-	.347	.158	.136
MgO	.049	.029	.056	.040	.058	.063	.089	15.428	16.958	15.271
CaO	13.939	13.133	15.624	14.525	14.680	13.687	11.857	21.091	22.567	23.412
Na2O	3.723	4.069	2.861	3.302	3.351	3.949	4.897	.317	.178	.178
K2O	.085	.081	.040	.046	.068	.051	.092	-	.005	-
NiO	-	.076	-	.040	.025	.035	.005	-	-	-
Cr2O3	-	.046	.006	.022	.026	.014	-	-	.475	1.135
Cl	.002	-	.010	-	-	.008	.012	.012	.013	.005
Total	100.197	99.302	99.783	99.971	99.605	99.957	100.037	99.107	98.830	98.876
Cation										
Si	9.241	9.445	8.993	9.106	9.166	9.372	9.771	1.912	1.914	1.848
Al	6.657	6.454	6.873	6.820	6.728	6.503	6.112	.096	.096	.185
Ti	.008	.006	-	-	.002	.007	.005	.019	.007	.014
Fe	.103	.072	.091	.090	.055	.078	.082	.264	.141	.147
Mn	.005	-	.001	.007	-	.001	-	.011	.004	.004
Mg	.013	.008	.015	.011	.016	.017	.024	.845	.940	.852
Ca	2.724	2.581	3.080	2.849	2.888	2.677	2.303	.850	.898	.939
Na	1.317	1.447	1.021	1.172	1.193	1.397	1.721	.012	.013	.013
K	.020	.019	.009	.011	.016	.012	.021	-	-	-
Ni	-	.011	-	.006	.004	.005	.001	-	-	-
Cr	-	.007	.001	.003	.004	.002	-	-	.013	.034
Cl	.001	-	.003	-	-	.002	.004	.001	.001	-
Total	20.091	20.051	20.088	20.074	20.070	20.075	20.043	3.950	4.027	4.036
Fe/Fe+Mg	.886	.900	.855	.897	.774	.821	.772	.238	.130	.147
Mg*	-	-	-	-	-	-	-	-	-	-
Ca*	-	-	-	-	-	-	-	43.000	45.000	48.000
An	67.080	63.780	74.940	70.660	70.490	65.520	56.930	-	-	-

G294-37 Plagioclase groundmass
G294-38 Plagioclase groundmass
G294-39 Plagioclase inclusion in clinopyroxene phenocryst
G294-40 Plagioclase inclusion in clinopyroxene phenocryst
G294-41 Plagioclase microphenocryst core
G294-42 Plagioclase microphenocryst mantle
G294-43 Plagioclase microphenocryst rim
G294-44 Clinopyroxene phenocryst core
G294-45 Clinopyroxene phenocryst core
G294-46 Clinopyroxene phenocryst core

	G294-47 CPX	G294-48 CPX	G294-49 CPX	G294-50 CPX
Oxide				
SiO2	50.186	50.696	51.502	50.393
Al2O3	2.530	1.824	1.450	2.415
TiO2	.511	.471	.357	.498
FeO	8.325	9.940	9.561	10.432
MnO	.246	.394	.402	.409
MgO	15.313	14.826	14.537	13.964
CaO	21.234	20.445	20.714	20.643
Na2O	.281	.328	.305	.343
K2O	.006	-	-	.007
NiO	-	-	-	.030
Cr2O3	.022	.011	-	-
Cl	-	-	.001	-
Total	98.654	98.935	98.830	99.134
Cation				
Si	1.898	1.921	1.948	1.912
Al	.113	.081	.065	.108
Ti	.015	.013	.041	.014
Fe	.263	.315	.303	.331
Mn	.008	.013	.013	.013
Mg	.863	.838	.819	.790
Ca	.860	.830	.840	.839
Na	.021	.024	.011	.013
K	-	-	-	-
Ni	-	-	-	.001
Cr	.001	-	-	-
Cl	-	-	-	-
Total	4.041	4.036	4.040	4.020
Fe/Fe+Mg	.234	.273	.270	.295
Mg*	-	-	-	-
Ca*	43.000	42.000	43.000	43.000
An	-	-	-	-

G294-47 Clinopyroxene phenocryst core
G294-48 Clinopyroxene as orthopyroxene mantle
G294-49 Clinopyroxene inclusion in plagioclase
G294-50 Clinopyroxene inclusion in plagioclase

*) Mineral chemistry of olivine (1126C - 1139C) and Cr-spinel (5121 - 5128) in rock sample JPL 10 (High-Mg basalt) given by Nye (1988, pers. comm.).

Sample	1126C	1127R	1128C	1129	1130C	1131C	1132C	1133C	1134R	1135C
SiO2	40.63	39.78	38.70	38.68	38.66	39.75	40.01	39.15	38.84	40.28
TiO2	.03	.01	.04	.03	-	-	-	.02	-	-
Al2O3	.03	.06	.06	.08	.04	.05	.02	.03	.05	.06
FeO	10.46	15.41	18.52	20.91	18.47	12.52	12.10	18.07	19.32	10.63
MnO	.18	.33	.28	.32	.25	.23	.20	.20	.35	.16
MgO	48.09	42.38	42.19	38.67	41.94	49.45	50.26	42.77	40.67	48.47
CaO	.21	.23	.08	.23	.06	.06	.23	.17	.19	.19
NiO	.18	.18	.07	.08	.02	.02	.17	.04	.07	.25
Cr2O3	.09	.01	-	.02	-	-	.03	.02	.01	.02
Total	99.90	98.39	99.94	99.02	99.44	102.08	103.02	100.47	99.50	100.06
Si	1.0007	1.0173	.9903	1.0095	.9936	.9693	.9660	.9934	1.0016	.9924
Ti	.0006	.0002	.0008	.0006	-	-	-	.0004	-	-
Al	.0009	.0018	.0018	.0025	.0012	.0014	.0006	.0009	.0015	.0017
Fe2+	.2155	.3296	.3964	.4564	.3970	.2553	.2443	.3835	.4167	.2190
Mn	.0038	.0071	.0061	.0071	.0054	.0048	.0041	.0043	.0076	.0033
Mg	1.7652	1.6152	1.6090	1.5040	1.6064	1.7971	1.8085	1.6173	1.5631	1.7797
Ca	.0055	.0063	.0022	.0064	.0017	.0016	.0060	.0046	.0053	.0050
Ni	.0036	.0037	.0014	.0017	.0004	.0004	.0033	.0008	.0015	.0050
Cr	.0018	.0002	-	.0004	-	-	.0006	.0004	.0002	.0004
Total	2.9974	2.9815	3.0080	2.9885	3.0058	3.0300	3.0334	3.0056	2.9975	3.0065
Fo	89.12	83.05	80.24	76.72	80.18	87.56	88.10	80.83	78.95	89.04

Sample	1136R	1137C	1138C	1044C	1045	1139C
SiO2	39.16	40.01	39.31	39.94	36.78	40.20
TiO2	.02	.04	-	.01	.02	-
Al2O3	.04	.08	-	.02	.02	.03
FeO	16.07	11.15	11.36	12.46	30.01	9.01
MnO	.27	.25	.20	.20	.60	.17
MgO	41.76	47.49	47.20	47.08	32.89	49.45
CaO	.23	.22	.18	.19	.14	.19
NiO	.16	.26	.35	.20	.02	.33
Cr2O3	.06	.04	.09	.06	.04	.07
Total	97.77	99.54	98.69	100.16	100.52	99.45
Si	1.0121	.9939	.9876	.9916	.9910	.9903
Ti	.0004	.0007	-	.0002	.0004	-
Al	.0012	.0023	-	.0006	.0006	.0009
Fe2+	.3473	.2316	.2387	.2587	.6762	.1856
Mn	.0059	.0053	.0043	.0042	.0137	.0035
Mg	1.6085	1.7581	1.7673	1.7419	1.3207	1.8154
Ca	.0064	.0059	.0048	.0051	.0040	.0050
Ni	.0033	.0052	.0071	.0040	.0004	.0065
Cr	.0012	.0008	.0018	.0012	.0009	.0014
Total	2.9863	3.0038	3.0115	3.0074	3.0079	3.0086
Fo	82.24	88.36	88.10	87.07	66.14	90.72

Sample	5121	5122	5123	5124	5125	5126	5127	5128
SiO2	.75	1.43	.14	.09	.10	.03	.21	.12
TiO2	.57	.51	.50	.53	.61	.57	.51	1.27
Al2O3	15.62	15.56	14.11	15.07	15.58	10.43	15.68	10.16
Fe2O3	16.05	15.46	16.62	16.21	17.41	17.47	16.60	22.89
FeO	7.38	11.52	9.94	9.74	10.24	9.89	8.86	17.84
MnO	.12	.15	.17	.20	.28	.20	.15	.34
MgO	13.54	11.62	11.07	11.44	11.38	10.42	12.26	6.30
CaO	.18	.17	.03	-	.02	.02	.02	.04
Cr2O3	45.70	43.74	47.45	47.57	45.16	52.35	46.28	39.90
NiO	.12	.04	.12	.08	.12	.11	.12	.03
Total	100.03	100.20	100.15	100.92	100.91	101.49	100.68	98.89
FeO meas	21.82	25.43	24.89	24.32	25.91	25.61	23.79	38.44
Si	.0294	.0562	.0057	.0036	.0040	.0013	.0083	.0051
Ti	.0168	.0151	.0154	.0160	.0182	.0182	.0152	.0405
Al	.7226	.7206	.6793	.7139	.7276	.5221	.7320	.5082
Fe3+	.4741	.4569	.5107	.4900	.5191	.5583	.4946	.7308
Fe2+	.2420	.3786	.3394	.3273	.3393	.3512	.2933	.6332
Mn	.0040	.0050	.0059	.0068	.0094	.0072	.0050	.0122
Mg	.7918	.6803	.6737	.6850	.6718	.6594	.7235	.3983
Ca	.0076	.0072	.0013	-	.0008	.0009	.0008	.0018
Cr	.7088	.6792	.7659	.7555	.7071	.8786	.7244	.6691
Ni	.0038	.0013	.0039	.0026	.0038	.0038	.0038	.0010

APPENDIX 4 Geochemistry

A total of 109 samples was analysed for major and trace elements. 41 Samples were analysed in the Analytical Laboratory at Victoria University of Wellington and the rest at the University of Canterbury. As a comparison, three analyses were performed at USGS XRF Laboratory at Denver (Tillings, 1987, pers. comm.; sample number : W223, W224 and W225) and a sample (JPL10) was analysed at University of California, Santa Cruz (Gill, 1987, pers. comm.). Comparisons are given in Table 4.1. There is no apparent interlaboratory variation in XRF results from University of Canterbury and Victoria University of Wellington. Whereas XRF major elements from USGS and University of California have slightly higher in Fe_2O_3, MgO and CaO. Trace element abundances of Ba, Ni and Cr from XRF Lab of University of California are also too high. However, these data can be accepted considering they do not alter the general geochemical trend of Galunggung volcanic rocks.

4.1 Sample preparation and analytical methods at University of Canterbury

Samples were broken into approximately 1 cm rock chips using a steel-jawed hydraulic rock crusher. 200 - 500 Grams of clean chips were crushed and powdered to a 240 B.S. mesh, using a ROCKLABS swing-mill with a tungsten-carbide barrel.

Bulk rock chemical compositions of major elements were determined using the fusion bead technique, as described by Norrish and Hutton (1969) with modifications after Harvey et al. (1973) and Schroeder et al. (1980). The beads were made following sigma chemicals flux " Norish formula" by mixing 0.30 grams of rock sample with 1.61 grams of Lithium Metaborate, Lithium Carbonate and Lanthanum Oxide flux, also ammoniumnitrate was added as an oxidant, then fused for 20 minutes at 1000^{o}C in a platinum-gold crucible. The sample was cooled, reweighed (to obtain Loss of Ignition), reheated and pressed in aluminium moulds, using equipment similar to that described by Harvey et al. (1973). The cooled and annealed glass discs were stored in sealed polypropylene bags, in a desiccator.

Trace element samples were prepared for analysis from 15 grams of rock powder mixed with approximately 33 drops of a 7 % aqueous

Table 4.1 Comparison of Galunggung geochemical data from different laboratories.

A Volcanic bomb erupted on 16 September 1982.
B Lava flow extruded on 1 - 7 January 1983.

XRF Laboratory : na = not analysed.

1) Victoria University of Wellington.
2) University of Canterbury.
3) University of California, Santacruz (Gill, 1987, pers. comm.).
4) USGS, Denver (Tilling, 1987, pers. comm.).

	A			B		
Sample	VB 82[1]	20298[2]	JPL10[3]	1983L[1]	20300[2]	W225[4]
Major elements (wt. %)						
SiO_2	49.14	49.15	49.40	49.33	49.67	49.20
TiO_2	.81	.82	.81	.81	.83	.84
Al_2O_3	16.05	15.85	15.55	16.29	16.36	15.90
Fe_2O_3	9.92	9.90	10.22	9.85	9.96	10.20
MnO	.17	.17	na	.17	.17	.18
MgO	10.59	10.77	11.15	10.02	9.98	10.40
CaO	11.16	11.25	11.44	11.13	11.29	11.50
Na_2O	2.34	2.20	2.20	2.24	2.23	2.20
K_2O	.35	.35	.32	.35	.36	.34
P_2O_5	.10	.10	.11	.10	.10	.11
LOI	-.39	-1.40	-	-.37	-.73	.01
Total	100.24	100.16	101.20	99.92	100.22	100.88
Trace elements (ppm)						
Ba	48	48	88	49	49	na
Rb	7	6	7.9	7	8	na
Sr	205	215	197	213	216	na
Pb	4	5	3	4	6	na
Zr	48	49	49	49	41	na
Nb	4	4	3.9	< 2	6	na
Y	18	18	16	18	17	na
V	264	274	277	272	270	na
Cr	548	558	612	505	516	na
Ni	149	152	189	139	140	na
Ga	18	17	14	14	15	na
Mg#	70.60	70.98	71.04	69.58	69.26	69.63

solution of polyvinyl alcohol ("Mowiol") (to act as a binder). The samples were compressed against the polished steel faces of a die. The resultant 52 mm diameter powder briquettes provided a large analytical surface for irradiation, thus enhancing sensitivity and precision.

Major and trace element analyses were obtaining using a Philips PW 1400 X-ray spectrometer filled with a PW1500 72 position sample changer and coupled to a Hewlett-Packard 9000/300 computer using University of Canterbury software and calibrations set up by S.D. Weaver. Glass beads were irradiated using a 3 kW Cr-tube operating at 40 kV and 50 mA. Full iterative mass absorption corrections were performed by the on-line computer. Pressed-powder pellets were analysed for Zr, Nb, Ba, Ni, Cr, V, Ce, La, Nd, and Zn using a 3 kW Au tube, and for Y, Rb, Sr, Ga, Pb, and Th using a 3 kW Mo tube. Both tubes operated at 40 kV and 50 mA. Mass absorption corrections were made using Compton and Rayleigh tube lines or coefficients calculated from the major element analyses.

A comparison of analyses of international laboratory standards with published results of estimation of the accuracy of major and trace elements is given in Table 4.2.

4.2 Sample preparation and analytical methods at Victoria University of Wellington

Sample Preparation

Large (up to 10 kg) unweathered samples were collected using a sledgehammer and packed in heavy duty plastic bags. The rock samples were processed using a ROCKLABS tungsten carbide hydraulic rock splitter-crusher. Using the splitter bars, weathered surface were first removed, the crusher plates were then used to reduce large pieces to a size (< 1 cm) suitable for placing in the swing mill. Approximately 2 kg of this material was prepared for each sample, however in some cases, e.g. xenoliths, much less material was available.

Powder for analytical purposes was prepared by a two stage milling process. The crushed material was ground to approximately sand size using a TEMA tungsten carbide swing mill. A small amount (100 g) of material was retained for crushing in a chrome-steel mill to enable W and Co determinations to be undertaken at a later date if necessary. The coarsely powdered material (several TEMA loads) was blended by

Table 4.2 International standard rocks.

Det = Determined value, X-ray Laboratory, Geology Department, University of Canterbury, June 1987.
Rec = Recommended value of International Standard.
Values in brackets are not confirmed recommended values.

	AGV-1		G2		GA		MRG-1		NIM-N		WI	
	Det	Rec	Det	Rec	Det	Rec	Det	Rec	Det	Rec	Det	Rec
Major element												
SiO_2	59.74	59.72	68.27	69.19	70.00	69.96	39.23	39.14	52.66	52.56	52.72	52.72
TiO_2	1.05	1.05	.48	.50	.35	.38	3.77	3.75	.19	.20	1.07	1.07
Al_2O_3	17.35	17.22	15.20	15.35	14.76	14.51	8.49	8.56	16.72	16.54	14.87	14.82
Fe_2O_3	6.77	6.88	2.58	2.62	2.71	2.83	17.86	17.79	8.97	8.87	11.10	11.15
MnO	.10	.10	.04	.04	.08	.09	.18	.17	.19	.18	.17	.18
MgO	1.54	1.55	.71	.77	.87	.95	13.53	13.51	7.51	7.48	6.63	6.57
CaO	4.95	5.00	1.91	1.98	2.46	2.45	14.89	14.72	11.56	11.46	10.98	10.94
Na_2O	4.36	4.31	3.99	4.06	3.51	3.55	.75	.71	2.56	2.46	2.15	2.19
K_2O	2.95	2.93	4.44	4.52	4.10	4.03	.19	.18	.24	.25	.64	.63
P_2O_5	.50	.50	.13	.14	.13	.12	.06	.07	< .05	.03	.14	.13
Trace element												
V	123	115	36	33	38	43	520	546	220	229	260	274
Cr	12	11	9	9	12	10	450	556	(30)	33	120	132
Ni	17	21	5	8	7	8	195	194	120	115	75	76
Zn	88	87	85	95	80	74	190	212	68	64	84	88
Zr	225	243	300	329	150	148	105	102	(23)	11	100	97
Nb	15	16	13	12	(10)	13	(20)	18	(2)	< 2	8	6
Ba	1220	1206	1880	1855	850	837	(50)	< 20	100	102	162	146
La	37	46	90	111	38	34	(10)	9	(3)	< 5	11	12
Ce	66	80	160	190	70	70	(25)	17	(6)	< 5	23	27
Nd	34	26	55	73	(25)	19	(19)	< 10	(3)	< 10	15	< 10
Ga	21	18	23	22	16	14	18	20	16	18		
Pb	33	40	30	33	30	30	10	13	7	6	8	11
Rb	67	68	170	170	175	170	8	7	6	4	21	21
Sr	662	663	478	481	310	301	260	275	260	265	190	191
Th	6	6	25	30	17	16	1	1	1	< 1	2	3
Y	19	21	11	14	21	25	16	13	6	7	25	21

rolling on paper. Aliquots (two TEMA loads) of this powder were then milled for a further 40s each. These two loads of fine powder were then blended, stored in plastic zip-top bags and used for the analytical work presented in this report. The coarse powder was retained for future mineral separation procedures should they be undertaken.

Analytical Procedure

The instrumentation used for XRF analysis was a PHILIPS PW1404 automatic sequential X-ray spectrometer fitted with a PW1500 72 position sample changer. The online computer comprised a DEC Professional 350, VR-241 colour monitor and LA210 printer. The operating system was POS-V20A running V20 PHILIPS X-44 software.

1. Major Elements

Fused glass disks were prepared using procedures modified from Norrish & Hutton (1969). SIGMA CHEMICALS Norrish Formula X-ray flux was used with 0.5000 g of rock powder and 0.040 g of AR ammonium nitrate in a covered Pt-5% Au crucible over a muffled gas flame. The nominal amount of flux used was 2.6800 g however this was adjusted according to the moisture content determined by duplicate ignition loss at the start of each weighing session. The exact weight of sample powder was recorded and entered into the computer at run-time. Glass disks were pressed on a graphite die using a polished Al plunger and annealed for several hours before being cooled, labelled and stored in plastic containers in a desiccator. Duplicate disks were prepared for each sample.

All major element determinations were carried out under vacuum using the K-line and Sc/Mo dual anode X-ray tube operated at 45 KV/50 mA. The detection system comprised a flow proportional counter fitted with a 1 μm polypropylene window and using P10 gas (10 % methane in argon). The coarse collimator and large aperture were used in all cases.

The instrument was calibrated using international rock standards chosen to cover a wide range of values for each element and to cover the compositional spectrum of normal silicate rocks.

Regression lines were calculated using the PHILIPS mathematical model, with loss eliminated empirical alphas calculated from factors provided by K. Norrish for the Sc tube.

2. Trace Elements

Trace elements were measured on undiluted, boric acid backed pressed powder pellets (Norrish & Hutton, 1969). The pellets are 40 mm in diameter overall and contain 4.0 g of rock powder. The sensitivities and lower limits of detection are determined for an average rock matrix (AGV-1).

Abbreviations

LOI = loss on ignition
na = not analysed

Sample	VB-17	L 35	20267	L27-3	L27-2	L27-1	L11-C	L 02	VB 10	L 03
Major elements (wt. %)										
SiO_2	52.52	52.05	51.37	53.19	52.33	50.75	51.63	52.55	50.89	53.99
TiO_2	.86	.93	.88	.93	.94	.93	.84	.88	1.04	1.07
Al_2O_3	21.68	19.17	18.90	19.09	19.51	19.70	21.48	20.72	21.12	18.85
Fe_2O_3	7.86	8.93	8.80	9.45	8.79	8.84	8.22	8.70	9.00	9.65
MnO	.15	.16	.14	.17	.17	.16	.15	.16	.16	.19
MgO	2.58	4.42	4.49	4.20	4.82	4.59	3.04	3.35	2.99	2.97
CaO	9.59	9.46	9.54	8.83	9.59	10.33	9.79	9.49	10.10	8.00
Na_2O	3.64	3.27	3.24	3.43	3.29	3.05	3.37	3.57	3.27	4.00
K_2O	.51	.58	.47	.68	.56	.67	.52	.58	.59	.66
P_2O_5	.16	.16	.14	.21	.18	.20	.14	.16	.18	.17
LOI	.17	.64	1.77	-.11	-.25	.02	.74	-.05	.50	-.11
Total	99.72	99.77	99.74	100.07	99.93	99.24	99.16	100.11	99.84	99.44
Trace elements (ppm)										
Ba	77	109	86	146	121	118	98	115	79	130
Rb	9	11	5	16	13	17	10	12	13	13
Sr	297	267	300	297	310	362	288	281	280	258
Pb	5	6	7	5	4	4	6	5	6	5
Zr	74	80	67	87	76	78	68	74	84	84
Nb	5	2	7	3	2	4	2	3	4	3
Y	24	24	20	25	22	22	23	25	22	30
La	na	na	< 5	na	na	na	na	na	na	na
Ce	na	na	14	na	na	na	na	na	na	na
Nd	na	na	19	na	na	na	na	na	na	na
Th	na	na	2	na	na	na	na	na	na	na
Sc	20	27	na	27	30	27	23	24	26	24
V	150	218	221	217	255	249	197	198	203	202
Cr	11	29	24	16	26	72	14	14	47	10
Ni	5	16	15	12	13	24	10	10	20	6
Cu	92	77	na	74	65	87	107	77	71	80
Zn	71	74	77	71	69	71	72	69	70	84
Ga	21	19	18	19	22	21	21	20	18	21

Sample	20346	L11-B	L11-A	L 21	20270	20271	20286	L 31	20347	20280
Major elements (wt. %)										
SiO_2	53.81	50.81	50.67	51.45	49.67	51.76	51.79	51.69	55.93	51.59
TiO_2	1.06	.91	1.03	.78	1.07	1.02	.90	.87	.73	.99
Al_3O_3	18.35	20.30	21.03	19.28	20.74	19.19	20.42	20.38	18.96	20.68
Fe_2O_3	9.41	9.17	8.85	8.58	9.62	9.29	8.96	8.98	8.24	9.19
MnO	.19	.16	.16	.15	.19	.17	.15	.15	.15	.15
MgO	3.05	4.01	3.03	4.63	4.38	4.17	4.47	4.41	3.54	3.55
CaO	8.10	9.53	10.08	9.41	10.85	9.73	10.14	10.05	8.21	9.73
Na_2O	4.05	3.12	3.27	3.10	2.99	3.43	3.41	3.23	3.81	3.34
K_2O	.70	.53	.59	.52	.37	.57	.57	.56	.75	.49
P_2O_5	.15	.14	.18	.14	.13	.18	.17	.16	.16	.13
LOI	-.23	.97	.83	1.35	.52	.37	-.08	-.31	-.16	.51
Total	98.64	99.65	99.72	99.39	100.48	99.88	100.90	100.17	100.32	100.35
Trace elements (ppm)										
Ba	115	77	98	94	92	78	123	131	155	64
Rb	10	11	14	10	12	11	12	13	17	4
Sr	268	268	296	258	268	264	334	322	286	291
Pb	7	5	4	7	4	4	4	5	8	6
Zr	82	69	75	70	75	84	64	73	84	67
Nb	8	4	2	2	6	8	5	3	5	6
Y	30	23	28	19	27	29	18	20	21	22
La	6	na	na	na	< 5	< 5	< 5	na	9	9
Ce	15	na	na	na	10	17	9	na	28	12
Nd	19	na	na	na	18	18	25	na	17	22
Th	< 1	na	na	na	3	< 1	1	na	1	2
Sc	na	28	27	24	na	na	na	25	na	na
V	207	239	230	190	227	232	251	238	159	255
Cr	7	19	16	30	8	10	22	27	11	15
Ni	5	14	9	18	13	12	15	14	9	13
Cu	na	78	64	51	na	na	62	62	na	na
Zn	87	70	71	69	71	75	67	63	74	61
Ga	22	20	20	19	19	22	20	20	19	20

Sample	L 15	L 26	20279	20278	20277	20276	20275	20274	20272	20273
Major elements (wt. %)										
SiO_2	52.27	53.03	51.63	51.61	51.79	51.65	51.46	52.46	52.15	51.67
TiO_2	.98	.80	.99	.97	.99	.99	.96	.97	.90	.91
Al_2O_3	18.49	18.99	20.70	20.86	20.70	20.91	21.26	20.86	20.55	20.85
Fe_2O_3	9.31	8.85	9.21	8.75	8.89	8.99	8.77	8.93	8.62	8.69
MnO	.16	.18	.16	.17	.17	.17	.17	.15	.17	.19
MgO	4.05	3.56	3.54	3.17	3.33	3.37	3.09	3.30	3.27	3.21
CaO	8.96	8.40	9.71	9.90	9.83	9.85	10.12	9.99	9.58	9.59
Na_2O	3.35	3.33	3.23	3.42	3.69	3.31	3.45	3.43	3.43	3.37
K_2O	.62	.65	.48	.44	.46	.45	.40	.47	.52	.44
P_2O_5	.22	.20	.12	.12	.13	.13	.12	.13	.13	.13
LOI	1.05	.58	.77	.12	-.82	.33	1.46	-.47	1.31	1.09
Total	99.46	98.77	100.54	98.87	99.16	100.15	101.26	100.22	100.63	100.14
Trace elements (ppm)										
Ba	73	106	98	60	55	57	65	63	76	68
Rb	13	11	5	7	6	5	5	4	9	5
Sr	237	336	286	278	268	274	279	274	271	276
Pb	3	5	6	7	6	6	7	6	7	8
Zr	113	75	67	54	56	58	63	59	56	56
Nb	6	2	7	5	5	6	6	5	< 2	5
Y	31	19	25	22	24	24	23	24	21	23
La	na	na	< 5	7	< 5	< 5	< 5	5	7	5
Ce	na	na	11	14	< 5	7	15	28	7	10
Nd	na	na	23	13	18	15	15	16	17	22
Th	na	na	< 1	< 1	< 1	1	1	1	1	2
Sc	29	24	na	na	na	na	na	na	na	na
V	205	207	238	234	244	220	244	239	212	199
Cr	34	20	13	10	13	12	10	5	20	10
Ni	15	9	13	11	11	7	10	12	10	11
Cu	62	18	na	na	na	na	na	na	na	na
Zn	79	63	68	67	71	67	80	74	71	74
Ga	18	22	18	19	22	20	18	20	19	20

Sample	20264	20263	20265	20266	20262	20261	20353	20260	L 28	20285
Major elements (wt. %)										
SiO_2	49.93	50.28	52.02	52.10	50.44	53.03	52.73	56.87	51.85	51.98
TiO_2	1.00	1.07	1.03	.97	.95	.75	.81	.85	1.07	.92
Al_2O_3	20.28	20.15	19.32	19.41	21.80	19.72	20.55	18.72	19.10	19.56
Fe_2O_3	9.58	9.42	9.54	9.41	8.77	8.79	8.54	7.79	9.67	9.23
MnO	.21	.22	.16	.17	.15	.15	.15	.14	.18	.14
MgO	4.57	4.62	4.20	4.50	3.42	4.46	3.93	3.41	4.17	4.99
CaO	11.22	10.44	9.56	10.00	10.74	9.25	9.33	7.66	9.19	9.96
Na_2O	2.96	3.00	3.37	3.18	3.18	3.43	3.56	4.26	3.29	3.29
K_2O	.20	.51	.57	.49	.46	.54	.53	.69	.61	.56
P_2O_5	.14	.17	.18	.17	.13	.14	.14	.21	.25	.15
LOI	.42	.48	.24	.10	.36	.07	.02	-.04	.32	-.31
Total	100.51	100.36	100.19	100.50	100.40	100.33	100.29	100.56	99.70	100.47
Trace elements (ppm)										
Ba	53	90	66	78	64	117	94	149	74	83
Rb	5	5	4	9	7	13	11	16	14	9
Sr	290	304	282	269	285	271	281	312	255	301
Pb	6	3	7	6	5	7	8	7	6	4
Zr	61	70	57	77	51	67	66	110	112	60
Nb	7	7	7	7	5	8	5	6	4	5
Y	22	24	22	26	23	20	19	22	34	20
La	6	8	< 5	< 5	8	6	< 5	7	na	< 5
Ce	18	26	15	7	7	27	14	19	na	16
Nd	18	23	20	23	12	19	17	23	na	24
Th	3	3	< 1	< 1	< 1	3	< 1	1	na	1
Sc	na	na	na	na	na	na	na	na	27	na
V	311	278	279	229	242	183	197	183	211	238
Cr	37	38	34	48	5	29	22	17	24	27
Ni	24	26	22	16	9	16	13	12	12	16
Cu	na	na	na	na	na	na	na	na	56	50
Zn	100	86	75	72	70	87	82	78	81	70
Ga	20	17	19	20	21	19	19	21	19	20

Sample	L 34	20348	20349	20350	20288	GG	20287	SKMH	LPdark	LPgrey
Major elements (wt. %)										
SiO_2	51.29	52.89	52.59	52.30	56.88	56.54	51.92	51.76	50.83	51.03
TiO_2	.88	.95	.93	.95	.84	.82	.95	.94	1.01	1.01
Al_2O_3	19.09	19.10	18.96	19.18	18.96	18.76	19.84	19.61	20.86	21.04
Fe_2O_3	9.10	9.60	9.28	9.66	7.66	7.58	9.00	9.02	8.77	8.69
MnO	.16	.15	.16	.16	.12	.13	.14	.15	.16	.16
MgO	4.92	4.55	4.83	4.60	3.21	3.14	4.26	4.26	3.31	3.15
CaO	9.80	9.33	9.39	9.28	7.66	7.53	9.58	9.43	10.10	10.10
Na_2O	3.14	3.52	3.39	3.32	4.29	4.13	3.27	3.29	3.27	3.29
K_2O	.58	.67	.55	.65	.71	.69	.50	.49	.64	.64
P_2O_5	.14	.19	.17	.19	.19	.22	.12	.13	.19	.19
LOI	-.23	-.13	-.30	-.30	-.44	-.04	-.38	.78	.75	.27
Total	98.87	100.82	99.95	99.99	100.08	99.50	99.20	99.86	99.89	99.57
Trace elements (ppm)										
Ba	94	124	94	130	149	150	74	75	73	76
Rb	11	15	11	13	16	9	8	9	12	12
Sr	295	299	273	299	311	294	304	290	289	297
Pb	7	6	7	4	7	5	4	3	3	3
Zr	71	80	80	76	111	117	55	67	73	73
Nb	4	6	5	6	8	3	8	< 2	3	2
Y	20	24	24	25	23	23	20	20	27	28
La	na	8	7	< 5	< 5	na	< 5	na	na	na
Ce	na	15	19	17	19	na	< 5	na	na	na
Nd	na	20	19	19	27	na	15	na	na	na
Th	na	3	2	2	2	na	2	na	na	na
Sc	28	na	na	na	19	19	na	28	28	28
V	238	246	216	228	133	139	246	242	229	229
Cr	30	19	39	18	16	19	29	32	16	16
Ni	15	14	21	13	10	10	16	15	9	9
Cu	50	na	na	na	60	60	34	34	67	76
Zn	65	82	77	79	80	76	68	63	66	69
Ga	20	19	21	21	22	20	19	19	20	19

Sample	X 14	20243	20343	20351	20352	20284	DK-21	20283	DK-26	20281
Major elements (wt. %)										
SiO_2	52.03	51.90	53.83	51.98	51.58	51.59	53.54	50.87	50.60	52.82
TiO_2	.90	.97	.90	.93	.95	.93	.83	.98	.99	1.00
Al_2O_3	19.30	19.44	19.06	21.24	19.14	21.68	20.13	21.06	20.24	18.79
Fe_2O_3	9.20	9.38	8.89	9.03	9.70	8.54	7.60	9.09	8.85	9.34
MnO	.15	.15	.15	.17	.17	.15	.14	.16	.15	.17
MgO	5.29	4.37	4.33	3.09	5.41	2.87	3.31	3.75	2.98	4.07
CaO	9.66	9.51	8.98	9.80	9.96	10.39	8.93	10.03	9.80	9.32
Na_2O	3.01	3.43	3.48	3.48	3.11	3.38	3.50	3.24	3.13	3.41
K_2O	.39	.53	.63	.51	.48	.38	.55	.53	.60	.64
P_2O_5	.17	.18	.16	.14	.15	.13	.14	.15	.22	.21
LOI	-.53	-.36	-.26	-.36	.15	.04	1.70	-.15	1.68	.24
Total	99.57	99.50	100.15	100.01	100.19	100.08	100.37	99.71	99.24	100.01
Trace elements (ppm)										
Ba	55	84	118	76	94	54	116	77	140	75
Rb	8	11	11	8	8	5	14	3	14	12
Sr	264	282	282	298	253	288	279	276	369	248
Pb	5	10	10	8	6	6	6	6	4	6
Zr	84	80	93	60	65	60	91	67	82	109
Nb	3	7	7	7	6	8	4	7	4	7
Y	22	23	25	25	22	21	24	19	23	31
La	na	5	8	6	6	6	na	< 5	na	8
Ce	na	24	10	17	13	10	na	16	na	17
Nd	na	17	18	20	17	20	na	11	na	20
Th	na	2	< 1	< 1	2	2	na	1	na	2
Sc	29	na	na	na	na	na	20	na	23	na
V	238	243	199	202	248	207	181	236	207	208
Cr	67	25	46	8	51	9	15	45	16	36
Ni	28	15	20	7	26	7	9	28	9	16
Cu	69	na	na	na	na	na	65	na	99	na
Zn	83	74	74	79	80	75	77	73	72	84
Ga	19	19	17	22	19	21	22	20	22	19

Sample	20282	20258	VB 6	20289	20345	20344	20254	20253	20252	20256
Major elements (wt. %)										
SiO_2	51.12	47.06	52.49	52.76	52.93	51.25	50.22	55.02	44.52	44.10
TiO_2	.99	.87	.80	.82	.85	.96	1.02	.71	1.01	.95
Al_2O_3	20.51	15.67	19.11	19.12	19.12	18.75	20.66	18.75	16.52	22.22
Fe_2O_3	9.21	9.45	8.87	8.94	8.75	9.58	9.73	7.58	13.61	11.06
MnO	.15	.26	.16	.16	.16	.16	.18	.17	.18	.17
MgO	3.86	10.32	4.58	4.67	4.81	5.80	4.82	4.37	10.42	5.99
CaO	10.09	11.26	9.61	9.77	9.63	10.21	10.74	8.45	13.17	12.71
Na_2O	3.01	1.46	3.04	3.25	3.31	3.18	2.87	3.18	1.31	1.74
K_2O	.27	.56	.59	.61	.57	.52	.46	.68	.10	.16
P_2O_5	.15	.11	.11	.11	.15	.14	.14	.18	.05	.05
LOI	.02	1.54	.37	.41	.36	-.47	-.22	.56	-.90	.41
Total	99.38	98.56	99.73	100.62	100.64	100.35	100.62	99.65	99.99	99.56
Trace elements (ppm)										
Ba	71	44	124	125	72	70	86	129	< 30	< 30
Rb	8	18	15	13	11	10	5	16	< 1	2
Sr	265	188	260	269	326	283	286	329	253	350
Pb	6	8	6	8	6	6	5	8	4	4
Zr	60	43	64	68	69	65	56	86	9	24
Nb	6	6	3	7	7	5	6	7	4	5
Y	22	17	20	19	17	20	21	20	10	18
La	< 5	< 5	na	< 5	< 5	7	6	< 5	< 5	< 5
Ce	9	19	na	24	13	24	20	16	< 5	8
Nd	18	21	na	29	17	21	17	23	10	19
Th	< 1	< 1	na	< 1	< 1	2	2	2	< 1	< 1
Sc	na	na	26	26	na	na	na	na	na	na
V	257	289	216	217	168	261	306	149	448	271
Cr	14	395	41	38	37	82	42	83	119	28
Ni	11	94	16	16	14	29	23	37	11	18
Cu	na	na	49	49	na	na	na	na	na	na
Zn	76	74	70	72	82	88	85	71	40	63
Ga	18	15	18	20	16	18	20	20	16	21

Sample	20257	VB30A	20342	20250	20245	20246	20292	4 AK	20293	4 AH
Major elements (wt. %)										
SiO_2	46.84	55.50	51.08	54.11	54.72	52.61	55.83	55.11	55.68	54.69
TiO_2	1.06	.72	.90	.77	.75	.81	.86	.83	.88	.84
Al_2O_3	21.66	18.07	18.66	19.56	18.75	19.41	19.37	19.15	18.12	17.70
Fe_2O_3	9.73	8.19	9.38	8.74	8.20	8.84	7.99	7.97	7.97	7.69
MnO	.10	.16	.19	.16	.16	.17	.14	.14	.09	.11
MgO	5.73	4.56	5.00	3.95	3.63	4.01	3.56	3.47	3.95	3.93
CaO	12.24	8.47	10.15	8.83	8.45	9.98	8.33	8.17	7.19	6.99
Na_2O	2.52	3.54	2.66	3.38	3.86	3.31	3.98	3.95	3.70	3.61
K_2O	.29	.70	.38	.58	.71	.37	.61	.59	.73	.70
P_2O_5	.06	.16	.16	.17	.16	.15	.17	.17	.22	.24
LOI	.12	-.10	.74	-.29	-.44	.54	-.10	-.04	-.30	3.06
Total	100.35	99.97	99.30	99.96	98.95	100.20	100.74	99.51	98.23	99.56
Trace elements (ppm)										
Ba	< 30	157	77	111	148	89	111	115	131	130
Rb	5	19	7	14	16	11	11	12	12	13
Sr	296	261	293	303	282	278	298	285	259	254
Pb	4	7	6	6	10	6	7	5	6	5
Zr	33	82	69	76	69	70	93	97	117	119
Nb	3	2	6	7	6	5	6	3	7	4
Y	13	20	20	22	20	21	22	22	30	29
La	< 5	na	7	7	8	7	5	na	16	na
Ce	9	na	23	20	< 5	19	22	na	30	na
Nd	14	na	13	20	18	16	17	na	21	na
Th	< 1	na	2	2	2	< 1	2	na	2	na
Sc	na	20	20	na	na	na	na	22	na	21
V	355	164	235	169	174	190	170	174	166	175
Cr	30	91	90	10	13	28	18	22	21	29
Ni	14	28	33	9	10	20	12	12	16	13
Cu	na	72	na	na	na	na	na	43	na	75
Zn	54	70	80	86	83	73	76	73	83	80
Ga	17	19	18	20	18	19	22	20	19	19

Sample	20290	WL	20294	VB13A	20322	20325	20249	20291	VB14A	20295
Major elements (wt. %)										
SiO_2	56.11	55.59	56.82	55.87	57.07	56.03	53.76	54.10	53.66	53.03
TiO_2	.73	.71	.70	.68	.70	.73	.77	.77	.75	.79
Al_2O_3	18.15	18.08	18.34	17.98	18.32	18.05	17.90	17.84	17.88	17.93
Fe_2O_3	8.01	7.97	7.75	7.64	7.83	8.02	8.43	8.43	8.55	8.60
MnO	.14	.16	.15	.16	.15	.16	.15	.14	.16	.15
MgO	4.54	4.45	3.90	3.81	3.60	4.20	5.73	5.77	5.64	6.36
CaO	8.54	8.39	8.13	7.93	7.96	8.31	9.33	9.34	9.23	9.77
Na_2O	3.74	3.53	3.67	3.60	3.65	3.49	3.30	3.28	3.27	3.21
K_2O	.73	.71	.76	.73	.78	.73	.65	.64	.63	.60
P_2O_5	.15	.15	.16	.16	.16	.15	.14	.13	.14	.13
LOI	-.04	.15	0.00	.26	-.93	-.23	-.33	-.37	-.08	-.17
Total	100.80	99.67	100.38	98.82	99.29	99.63	99.83	100.07	99.83	100.40
Trace elements (ppm)										
Ba	168	154	176	162	185	156	128	111	129	116
Rb	17	17	18	18	19	17	15	14	16	14
Sr	271	261	273	263	272	269	261	259	255	260
Pb	9	6	9	5	9	9	11	9	8	8
Zr	78	83	86	87	88	84	71	93	75	62
Nb	6	3	6	3	2	7	6	6	2	4
Y	19	20	18	22	20	20	18	18	20	18
La	5	na	9	na	9	7	< 5	< 5	na	< 5
Ce	18	na	21	na	15	14	11	22	na	11
Nd	< 5	na	20	na	15	19	22	17	na	19
Th	3	na	2	na	3	2	< 1	2	na	< 1
Sc	na	20	na	17	na	na	na	na	25	na
V	174	165	152	149	138	165	196	170	198	210
Cr	78	94	38	46	31	63	146	18	160	175
Ni	28	26	20	17	16	22	45	12	44	53
Cu	na	73	na	15	na	na	na	na	34	na
Zn	73	67	77	73	76	76	75	76	70	74
Ga	18	18	19	18	18	19	19	20	18	17

Sample	VB13B	20326	20328	20336	20340	20341	VB308	20248	20296	VB13C
Major elements (wt. %)										
SiO_2	53.04	53.76	53.77	53.88	53.47	53.38	53.28	52.82	52.52	52.48
TiO_2	.78	.77	.76	.76	.79	.78	.77	.79	.79	.77
Al_2O_3	17.68	17.89	17.93	17.97	17.65	17.68	17.73	17.58	17.94	17.62
Fe_2O_3	8.60	8.48	8.38	8.47	8.70	8.55	8.63	8.83	8.69	8.89
MnO	.16	.16	.14	.15	.15	.16	.16	.15	.16	.16
MgO	6.27	5.80	5.55	5.73	6.41	6.40	6.27	6.85	6.40	6.33
CaO	9.62	9.40	9.28	9.33	9.78	9.67	9.54	9.88	9.81	9.68
Na_2O	3.07	3.43	3.51	3.26	3.16	3.07	3.07	3.06	3.23	3.30
K_2O	.58	.64	.65	.63	.59	.59	.59	.60	.59	.60
P_2O_5	.12	.12	.13	.14	.13	.12	.14	.13	.13	.13
LOI	.11	-.26	.72	-.60	-.91	-.42	-.18	-.19	-.26	-.22
Total	100.03	100.19	100.82	99.72	99.92	99.98	100.00	100.50	100.00	99.74
Trace elements (ppm)										
Ba	113	124	134	132	115	77	117	112	116	115
Rb	14	14	15	15	13	14	15	12	13	14
Sr	248	258	258	263	250	251	249	251	256	247
Pb	5	7	7	9	9	8	7	8	8	5
Zr	70	68	71	78	60	66	70	59	61	70
Nb	3	5	4	10	6	6	2	6	5	3
Y	19	19	18	17	18	18	19	19	18	18
La	na	6	< 5	< 5	< 5	5	na	6	6	na
Ce	na	25	15	18	14	32	na	14	15	na
Nd	na	10	13	19	15	17	na	19	16	na
Th	na	< 1	1	1	< 1	< 1	na	2	2	na
Sc	28	na	na	na	na	na	26	na	na	28
V	207	193	200	189	211	207	203	213	217	210
Cr	187	156	150	146	198	189	179	206	177	192
Ni	54	49	45	44	61	57	53	60	55	55
Cu	61	na	na	na	na	na	23	na	na	25
Zn	71	72	77	71	75	73	71	75	77	71
Ga	19	18	17	17	18	17	18	16	17	18

Sample	V816	V830C	20297	V813D	20323	20324	20329	20330	20331	20332
Major elements (wt. %)										
SiO_2	52.85	52.17	52.66	52.73	52.43	50.75	51.33	50.19	51.26	49.78
TiO_2	.77	.77	.80	.78	.81	.80	.80	.72	.93	.75
Al_2O_3	17.62	17.32	17.83	17.64	17.16	16.21	16.53	16.08	18.47	16.16
Fe_2O_3	8.81	8.86	8.78	8.77	8.90	9.39	9.37	9.33	9.47	9.53
MnO	.16	.16	.16	.16	.14	.15	.15	.15	.14	.16
MgO	6.54	6.93	6.74	6.72	7.14	9.20	8.86	10.68	5.68	10.67
CaO	9.70	9.89	9.96	9.81	10.11	10.79	10.70	11.01	9.98	10.87
Na_2O	3.10	2.96	3.17	2.97	3.02	2.63	2.82	2.41	2.72	2.42
K_2O	.57	.54	.57	.55	.56	.46	.49	.36	.47	.34
P_2O_5	.14	.13	.12	.12	.13	.11	.11	.09	.13	.11
LOI	.15	-.07	-.29	-.22	-.32	-.38	-.67	-.62	-.25	-.41
Total	100.41	99.66	100.50	100.03	100.08	100.11	100.49	100.40	99.00	100.38
Trace elements (ppm)										
Ba	116	113	108	115	104	82	97	63	81	56
Rb	13	14	13	12	12	9	10	7	11	6
Sr	247	241	253	245	244	227	234	222	253	210
Pb	5	7	5	4	8	5	7	5	8	5
Zr	69	65	62	68	63	46	56	45	56	50
Nb	3	2	6	2	6	7	6	6	7	6
Y	19	19	19	20	17	16	17	15	20	16
La	na	na	< 5	na	< 5	< 5	6	< 5	< 5	< 5
Nd	na	na	18	na	13	16	13	13	19	15
Th	na	na	2	na	< 1	2	< 1	3	3	1
Sc	29	30	na	29	na	na	na	na	na	na
V	206	230	218	215	231	251	260	240	275	261
Cr	203	200	212	215	256	384	312	418	196	565
Ni	59	59	60	61	68	110	88	119	50	147
Cu	18	17	na	76	na	na	na	na	na	na
Zn	68	72	72	70	74	74	76	72	83	75
Ga	18	17	18	18	19	16	15	16	18	15

Sample	20244	JPL10	20335	20333	20298	V882	20321	20337	20338	W223
Major elements (wt. %)										
SiO_2	70.49	49.40	49.15	48.96	49.15	49.14	49.05	48.35	48.84	48.80
TiO_2	.24	.81	.81	.81	.82	.81	.81	.81	.79	.82
Al_2O_3	15.17	15.55	15.68	15.78	15.85	16.05	15.59	16.11	15.96	15.80
Fe_2O_3	2.71	10.22	9.91	9.86	9.90	9.92	10.13	10.02	9.71	10.20
MnO	.09	na	.16	.15	.17	.17	.16	.16	.16	.18
MgO	.89	11.15	11.02	10.72	10.77	10.59	10.73	10.45	10.31	10.60
CaO	3.12	11.44	11.35	11.27	11.25	11.16	11.14	10.83	11.57	11.30
Na_2O	4.05	2.20	2.17	2.15	2.20	2.34	2.12	2.22	2.23	2.18
K_2O	2.13	.32	.35	.34	.35	.35	.35	.36	.33	.33
P_2O_5	.09	.11	.08	.09	.10	.10	.09	.10	.09	.11
LOI	.99	0.00	-.83	-.69	-.40	-.39	-1.32	-.43	-.46	.01
Total	99.97	101.20	99.85	99.44	100.16	100.24	98.85	98.98	99.53	100.33
Trace elements (ppm)										
Ba	315	88	< 30	43	48	48	45	47	37	na
Rb	70	7.9	7	7	6	7	7	7	6	na
Sr	226	197	205	204	215	205	209	219	212	na
Pb	8	3	6	4	5	4	7	7	5	na
Zr	106	49	43	46	49	48	44	44	39	na
Nb	8	3.9	5	7	4	4	4	6	5	na
Y	14	16	17	18	18	18	17	17	17	na
La	11	2.4	< 5	< 5	< 5	na	< 5	< 5	6	na
Ce	26	14	10	13	8	na	5	19	< 5	na
Nd	20	6.7	16	11	12	na	< 5	11	13	na
Th	3	0.79	1	< 1	< 1	na	1	3	< 1	na
Sc	na	na	na	na	na	39	na	na	na	na
V	33	277	278	279	274	264	272	281	277	na
Cr	12	612	610	664	558	548	572	515	554	na
Ni	5	189	162	173	152	149	160	151	140	na
Cu	na	na	na	na	na	92	na	na	na	na
Zn	48	na	72	75	75	69	77	78	72	na
Ga	14	na	14	14	17	18	16	17	16	na

Sample	W224	20339	20334A	20334B	20299	L 19	20300	1983L	W225	20327
Major elements (wt. %)										
SiO_2	49.10	49.07	48.81	49.01	49.29	48.98	49.67	49.33	49.20	51.67
TiO_2	.83	.80	.70	.70	.83	.81	.83	.81	.84	.91
Al_2O_3	15.80	15.92	15.04	15.09	16.38	16.20	16.36	16.29	15.90	20.85
Fe_2O_3	10.10	9.97	9.47	9.53	9.84	9.77	9.96	9.85	10.20	8.69
MnO	.17	.15	.16	.16	.16	.17	.17	.17	.18	.19
MgO	10.70	10.85	12.39	12.52	9.95	9.87	9.98	10.02	10.40	3.21
CaO	11.50	11.27	11.56	11.59	11.35	11.16	11.29	11.13	11.50	9.59
Na_2O	2.11	2.20	1.99	1.94	2.34	2.26	2.23	2.24	2.20	3.37
K_2O	.33	.34	.29	.29	.36	.35	.36	.35	.34	.44
P_2O_5	.11	.09	.07	.07	.10	.10	.10	.10	.11	.13
LOI	.01	-1.00	-.35	-.77	-.36	-.38	-.73	-.37	.01	1.09
Total	100.76	99.66	100.13	100.13	100.24	99.29	100.22	99.92	100.88	100.14
Trace elements (ppm)										
Ba	na	49	40	40	53	43	49	49	na	< 30
Rb	na	7	6	6	7	8	8	7	na	< 1
Sr	na	216	197	197	219	214	216	213	na	326
Pb	na	6	5	5	7	4	6	4	na	4
Zr	na	47	39	39	39	50	41	49	na	17
Nb	na	6	5	5	4	4	6	< 2	na	5
Y	na	18	14	14	17	18	17	18	na	9
La	na	< 5	< 5	< 5	5	na	< 5	na	na	< 5
Ce	na	< 5	7	7	< 5	na	6	na	na	< 5
Nd	na	8	13	13	7	na	16	na	na	18
Th	na	< 1	< 1	< 1	< 1	na	< 1	na	na	< 1
Sc	na	na	na	na	na	37	na	38	na	na
V	na	266	264	264	268	265	270	272	na	189
Cr	na	578	711	711	479	486	516	505	na	14
Ni	na	154	193	193	135	133	140	139	na	22
Cu	na	na	na	na	na	92	na	83	na	na
Zn	na	81	71	71	76	70	76	73	na	32
Ga	na	17	14	14	17	16	15	14	na	17

Appendix 5 Geothermometry Calculation

Four methods of geothermometry calculation are used in this thesis following : 1. Roeder & Emslie (1970; for olivine), 2. Glazner (1984; for olivine and plagioclase), 3 Lindsley (1983; for orthopyroxene and clinopyroxene), and 4. Kretz (1982; for coexisting between orthopyroxene and clinopyroxene).

Although there are many other geothermometry calculations, the four methods are chosen because of their close aggreement and applicability for magmatic temperatures.

1. Geothermometry calculation of Roeder & Emslie (1970)

This method is based on an assumption that olivines present in a rock are in equilibrium with their groundmass. Mole per cent values of MgO and Feo in the liquid are plotted to predict the composition of the equilibrium olivine and the temperature at which it will crystallise at 1 atm. This can be obtained by following the steps below :

1. Calculate Fe_2O_3 and FeO from total Fe as Fe_2O_3 (from XRF original data) by using $Fe_2O_3/FeO = 0.15$ (Brooks, 1976).
2. Convert weight per cent analysis to mole per cent by dividing each oxide by its molecular weight.
3. Recalculate to 100 %, the values of FeO and MgO are in mole per cent.
4. Plot MgO vs FeO on Fig. 5.1, and estimate temperature at the point.

An example calculation is given in Table 5.1.

2. Glazner's Geothermometry Calculation

This method is based on the activities of olivine and plagioclase (e.g. forsterite and anorthite, respectively) in silicate melts. Activities can be calculated from the compositions of coexisting melt and crystals, by assuming that : 1. The mineral component is an independently variable component of the crystals, and 2. appropriate thermodynamic data for the activities' are known. Crystallisation temperatures of olivine or plagioclase can be calculated, along with the com-

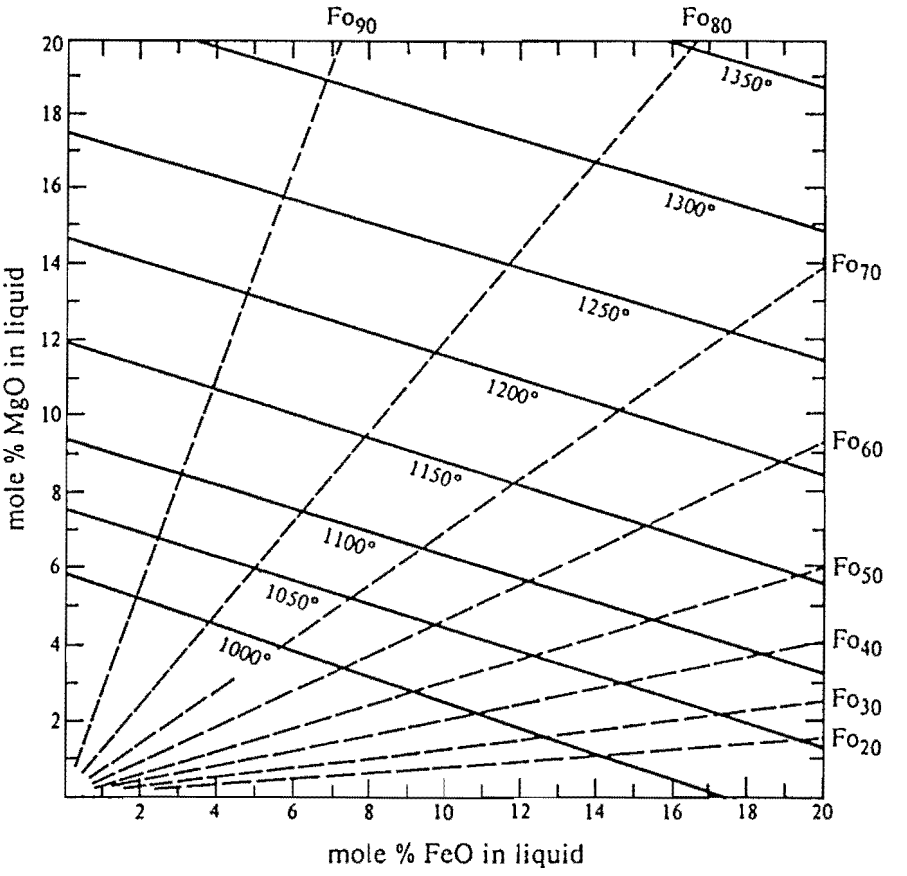

Figure 5.1 Olivine crystallisation temperature as determined by the mole % MgO and FeO in the liquid (Roeder & Emslie, 1970).

Table 5.1 Example of estimation of olivine crystallisation temperature using bulk rock chemical composition of Galunggung high-Mg basalt.

	1	2	3	4
Oxide	Original data	FeO & Fe_2O_3 calculated	Mole prop. of oxides	Recalc. to 100 %
SiO_2	49.01	49.01	.8156	49.76
TiO_2	.70	.70	.0088	.54
Al_2O_3	15.09	15.09	.1480	9.03
Fe_2O_3	9.53	1.13	.0071	.43
FeO	-	7.56	.1052	6.42
MgO	12.52	12.52	.3105	18.94
CaO	11.59	11.59	.2067	12.61
Na_2O	1.94	1.94	.0313	1.91
K_2O	.29	.29	.0031	.19
P_2O_5	.07	.07	.0005	.03
LOI	- .77			
Total	100.13		1.6391	100.00

Mole % FeO = 6.42 and MgO = 18.94. These are plotted on Fig. 5.1 and gives T = 1300°C.

position of the crystals. Standard deviations of approximately 21°C and 55°C are for olivine and plagioclase, respectively (Glazner, 1988, pers. comm.). In mafic to intermediate melts, the forsterite and anorthite models are more satisfactory than the fayalite and albite models.

Crystallisation temperature is calculated for a given mineral by the following steps :

1. Calculate mole fractions of 8 oxide components (SiO_2, TiO_2, Al_2O_3, FeO*, MgO, CaO, Na_2O and K_2O) in the melt and normalise to sum to one.
2. Calculate activities of forsterite and anorthite in the melt by using coefficient variables given in Table 5.2.
   For example : the activity of forsterite in melt =

$$\ln a_{fo}^{m} = -11.415 X_{SiO_2} - 3.3824 + 9.2484 X_{SiO_2}^2 + \ldots \\ -20.410 X_{TiO_2} X_{CaO}.$$

3. The activity of forsterite in olivine :

$$a_{fo}^{ol} = (X_{fo}^{ol} \gamma_{fo}^{ol})^2$$

where

X_{fo}^{ol} = mole fractions of Mg/(Mg + Fe^{2+}) in olivine

$$\gamma_{fo}^{ol} = \exp\{[(6{,}560 \text{ J/mol})(1 - X_{fo}^{ol})^2]/RT\}$$

and

$$\gamma_{fo}^{ol} = \exp\{[(6{,}560 \text{ J/mol})(1 - X_{fo}^{ol})^2]/RT\}$$

R (molar gas constant) = 8.31441
T = temperature (°C)

This temperature must be assumed for the activity calculation, e.g. 1200°C or 1300°C. If the assumed temperature is far from the calculated temperature, then the assumed temperature should be modified .

Table 5.2 Forsterite and anorthite models (Glazner, 1984).

Variable	Coeff	Std error	Mean of var	Coeff × mean
Forsterite				
X_{SiO_2}	−11.415	4.64	0.518	−5.91
constant	−3.3824	1.41	1	−3.38
$X^2_{SiO_2}$	9.2484	4.19	0.270	2.50
X_{MgO}	15.615	4.02	0.128	2.00
$X_{SiO_2} X_{MgO}$	10.608	7.19	0.065	0.69
X^2_{MgO}	−23.121	3.56	0.018	−0.43
X_{K_2O}	133.60	34.31	0.0032	0.42
$X_{CaO} X_{K_2O}$	529.69	133.35	0.00034	0.18
$X_{FeO'} X_{CaO}$	11.407	4.35	0.013	0.15
$X_{FeO'} X_{K_2O}$	−388.37	95.34	0.00034	−0.13
$X_{MgO} X_{K_2O}$	−404.49	126.00	0.00032	−0.13
$X_{Al_2O_3} X_{Na_2O}$	78.438	28.31	0.0015	0.12
$X^2_{K_2O}$	−2,914.6	410.57	0.00003	−0.07
$X_{MgO} X_{Na_2O}$	34.767	16.12	0.002	0.07
$X_{K_2O} X_{Na_2O}$	−946.22	328.04	0.00007	−0.07
$X_{TiO_2} X_{K_2O}$	−1,053.2	258.47	0.00006	−0.06
$X_{FeO'} X_{Na_2O}$	−29.336	15.22	0.002	−0.05
$X_{TiO_2} X_{CaO}$	−20.410	6.11	0.002	−0.05
Anorthite				
constant	−4.1420	0.10	1	−4.14
$X_{Al_2O_3} X_{CaO}$	80.745	12.25	0.010	0.81
$X_{Al_2O_3} X_{FeO'}$	52.309	8.41	0.009	0.47
$X_{CaO} X_{K_2O}$	1,054.1	115.98	0.0004	0.47
$X_{Al_2O_3} X_{MgO}$	49.869	9.84	0.009	0.43
$X_{TiO_2} X_{K_2O}$	−4,710.8	684.49	0.00008	−0.40
$X_{FeO'} X_{K_2O}$	−664.53	113.08	0.0005	−0.33
$X_{CaO} X_{TiO_2}$	−153.16	46.46	0.002	−0.24
$X^2_{TiO_2}$	644.72	205.75	0.0003	0.17
$X^2_{Na_2O}$	−291.00	88.59	0.0006	−0.16
$X_{Na_2O} X_{TiO_2}$	461.28	249.57	0.0004	0.16
$X^2_{K_2O}$	3,979.7	585.02	0.00004	0.16

4. The activity of forsterite in plagioclase :

$$a_{an}^{pl} = X_{an}^{pl}$$

X_{an}^{pl} = mole fractions of Ca/(Ca + Na)

5. Calculate λ_j by equation : $\lambda_j = \ln \frac{a_j^m}{a_j^s}$

where j for fo or an

6. Temperature is obtained from equation :

$$T(^oC) = a + b\lambda_j + c\lambda_j^2$$

where

	a	b	c
Forsterite	1856.1	200.62	6.981
Anorthite	1542.4	190.59	7.706

An example below using the most primitive high-Mg basalt (sample no. 20344) with the highest Fo content in olivine (1139C) and the highest An content in plagioclase (G-298-17).

Oxide	Bulk rock (20344)			Olivine (Fo_{90})			Plagioclase (An_{94})		
	wt.%	Mol. prop.	X	wt.%	Mol. prop.	X	wt.%	Mol. prop.	X
SiO_2	49.01	.8156	.4963	40.20	.6690	.3305	44.34	.7379	.5104
Al_2O_3	15.09	.1480	.0901	.03	.0003	.0001	35.85	.3517	.2433
TiO_2	.70	.0088	.0054	-	-	-	-	-	-
FeO*	8.58	.1194	.0727	9.01	.1254	.0619	.49	.0068	.0047
MgO	12.52	.3105	.1889	49.45	1.2264	.6058	.04	.0010	.0007
CaO	11.59	.2067	.1258	.19	.0034	.0017	18.97	.3383	.2340
Na_2O	1.94	.0313	.0190	-	-	-	.62	.0100	.0069
K_2O	.29	.0031	.0018	-	-	-	.01	.0001	-
Total		1.6434	1.0000		2.0245	1.0000		1.4458	1.0000

I. Olivine crystallisation temperature

$$\ln a_{fo}^m = -11.415\ (.4963) - 3.3824 + 9.2484\ (.4963)^2 + ...$$

$$- 20.410\ (.0054)(.1258)$$

$= - 3.2214$

$a_{fo}^{m} = 0.0399$

Activity of forsterite in olivine :

$a_{fo}^{ol} = (X_{fo}^{ol}\ \gamma_{fo}^{ol})^2$

$X_{fo}^{ol} = .6058/(.0619 + .6058) = .9073$

Assume T = 1300°C

$\ln \gamma_{fo}^{ol} = \quad (6560)(1 - .9073)^2 \quad /(8.31441 \times 1300$

$= - 0.0052$

$\gamma_{fo}^{ol} = 1.0052$

$a_{fo}^{ol} = (.9073 \times 1.0052)^2 = 0.8318$

$\lambda_{fo} = \ln (.0399/.8318) = - 3.0372$

$T\ (^{o}C) = 1856.1 + 200.62\ (- 3.0372) + 6\ 981\ (- 3.0372)^2$

$= 1311^{o}C$ (Olivine begins to crystallise)

II. Plagioclase crystallisation temperature

$\ln a_{an}^{m} = - 4.1420 + 80.745\ X_{Al_2O_3} X_{CaO} \quad + ...$

$+ 3979.7\ X_{K_2O}^2$

$= - 4.1420 + 80.745\ (.0901)(.1258) + ...$

$+ 3.979.7\ (.0081)^2$

$= - 2.0596$

$$= .1275$$

$$a_{an}^{pl} = X_{an}^{pl} = .234/(.234 + .0069) = .9714$$

$$\lambda_{an} = \ln (.1275/.9714) = - 2.0306$$

$$T = 1542.4 + 190.59 (- 2.0306) + 7.706 (- 2.0306)^2$$

$$= 1187^{o}C$$

3. Lindsley's Geothermometry Calculation

This method is based on experimentally determined Ca - Mg - Fe pyroxene phase relations at 800 - 1200°C and less than 1 Atm to 15 Kb. They are combined with calculated phase equilibria for the Di - En and Hd - Fs joins to produce a graphical two - pyroxene thermometer. The effects of pressure are $\leq 8^{o}C/Kb$. This thermometer should be used only for pyroxenes having Wo + En + Fs $\geq$ 90 % and not for those containing large amounts of alumina ($\geq$ 8 wt. %). The primary pyroxene compositions must be reconstructed from textural evidence before correct igneous peak - temperature can be inferred.

In this thesis, the 10 Kb graphical thermometer is chosen because minerals are considered to have begun crystallising in the lower crust.

The first step is to calculate Al(VI) as 2 - Si, with the remaining Al assigned to Al(IV). Fe^{3+} is then calculated from the charge - balance equation (Papike et al., 1974) :

$$Al(VI) + Fe^{3+}(VI) + Cr(VI) + 2\ Ti^{4+}(VI) = Al(IV) + Na(M2)$$

Clinopyroxene Thermometry

This is estimated by following the sequence :

1. Ac = $NaFe^{3+}Si_2O_6$ = Na or Fe^{3+}, whichever is smaller.
2. Jd = Al(VI) or any remaining Na, whichever is smaller.
3. FeCaTs = remaining Fe^{3+}.
4. CrCaTs = Cr.

5. AlCaTs = remaining Al(VI).
6. For augite, "Ca" = Ca;
   for pigeonite, "Ca" = 2 - (Fe^{2+} + Mg).
7. Take Wo = ("Ca" + Ac - AlCaTs - FeCaTs - CrCaTs)/2
   En = (1 - Wo)(1 - X), and
   Fs = (1 - Wo)(X)

   where X = $Fe^{2+}/(Fe^{2+}$ + Mg).

   Plot these Fo, En and Fs values on Figure 5.2.

Orthopyroxene Thermometry

Firstly calculate R^{3+} as (Al(VI) + Cr + Fe^{3+}), and

R^{2+} as (Mg (1 - X) + Fe^{2+}(X)),

where X = $Fe^{2+}/(Fe^{2+}$ + Mg)

Components are then calculated in the sequence :

1. $NaR^{3+}Si_2O_6$ = Na or R^{3+}, whichever is smaller.
2. $NaTiAlSiO_6$ = Ti or Al(IV) or any remaining Na,
   whichever is smaller.
3. $R^{2+}TiAl_2O_6$ = the remaining Ti or (Al(IV))/2,
   whichever is smaller.
4. $R^{2+}R^{3+}AlSiO_6$ = the remaining R^{3+} or Al(IV); in a perfect
   analysis these would be equal.
5. Ca, and the remaining Fe^{2+} and Mg, are then normalised to
   yield Wo + En + Fs = 1.
   Plot these Wo, En and Fs values on Figure 5.2.

Example

Oxide	Clinopyroxene wt.%	Cation	Orthopyroxene wt.%	Cation
SiO_2	51.405	1.892	52.923	1.949
Al_2O_3	3.527	.153	1.414	.061
TiO_2	.433	.012	.276	.008
FeO	5.725	.176	19.981	.615
MnO	.181	.006	.780	.024
MgO	16.091	.883	23.524	1.292
CaO	22.108	.872	1.539	.061
Na_2O	.205	.015	.010	.001
K_2O	-	-	.001	-
NiO	.043	.001	-	-
Cr_2O_3	.372	.011	.036	.001
Cl	-	-	.009	.001

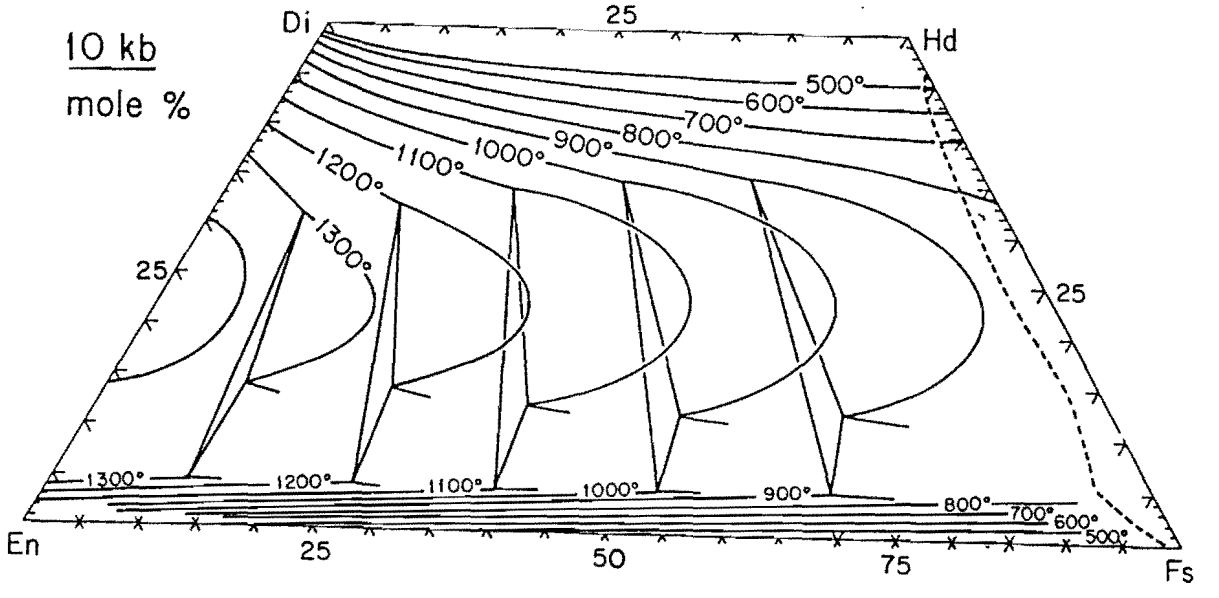

Figure 5.2 Pyroxene thermometry at 10 Kb (Lindsley, 1983). See text for explanation.

Clinopyroxene thermometry

$Al(IV) = 2 - 1.892 = 0.108$ $Al(VI) = 0.153 - 0.108 = 0.045$

$Fe^{3+} = 0.108 + 0.015 - 0.045 - 0.011 - 2\ (0.012) = 0.43$

$Fe^{2+} = 0.176 - 0.043 = 0.133$

$X = 0.133/(0.133 + 0.883) = 0.1309$

1. Ac = Na = 0.015
2. Jd = 0
3. FeCaTs = 0.043 - 0.015 = 0.028
4. CrCaTs = 0.011
5. AlCaTs = Al(VI) = 0.045
6. "Ca" = 0.872
7. Wo = (0.872 + 0.015 - 0.045 - 0.028 - 0.011)/2 = 0.4015
8. En = (1 - 0.4015)(1 - 0.1309) = 0.5202
9. Fs = 0.0783

$T = 1060^{o}C$

Orthopyroxene thermometry

$Al(IV) = 2 - 1.949 = 0.051$ $Al(VI) = 0.061 - 0.051 = 0.010$

$Fe^{3+} = 0.051 + 0.001 - 0.01 - 0.001 - 2(0.008) = 0.025$

$Fe^{2+} = 0.615 - 0.025 = 0.590$

$X = 0.590/(0.590 + 1.292) = 0.3135$

$R^{3+} = 0.01 + 0.001 + 0.025 = 0.036$

$R^{2+} = 1.292\ (1 - 0.3135) + 0.59\ (0.3135) = 1.072$

1. $NaR^{3+}Si_2O_6$ = Na = 0.001
2. $NaTiAlSiO_6$ = 0
3. $R^{2+}TiAl_2O_6$ = Ti = 0.008
4. $R^{2+}R^{3+}AlSiO_6$ = 0.026

5. Ca = 0.061 Wo = 0.0320 T = 1000$^{o}_{C}$
Mg = 1.292 En = 0.6768
Fe = 0.556 Fs = 0.2912
------ +
1.909

4. Kretz's Geothermometry Calculation

This method is based on the study of pyroxenes in igneous and metamorphic rocks. Clinopyroxene thermometer can be calculated by using two equations :

1. For clinopyroxenes crystallising above 1080^{o}C

$$T = 1000/(0.468 + 0.246\ X^{cpx} - 0.123\ \ln\ (1 - 2(Ca))) \quad ....(1)$$

2. For clinopyroxenes crystallising below 1080^{o}C

$$T = 1000/(0.054 + 0.608\ X^{cpx} - 0.304\ \ln\ (1 - 2(Ca))) \quad ....(2)$$

The pyroxene thermometer can also be calculated on the basis of coexisting clinopyroxene and orthopyroxene. This represents a temperature - dependence of the Mg - Fe distribution coefficient, thus

$$T = 1130/(\ln K_D + 0.505) \quad .....(3)$$

where T = absolute temperature
X = $Fe^{2+}/(Mg + Fe^{2+})$
(Ca) = $Ca/(Ca + Mg + Fe^{2+})$ in clinopyroxene

$$K_D = \frac{X^{Opx}}{1 - X^{Opx}} \cdot \frac{1 - X^{Cpx}}{X^{Cpx}}$$

Fe^{2+} is calculated from the charge - balance equation (Papike et al., 1974). The uncertainty in these numbers, due to precision and accuracy, is estimated to be ± 60^{o}. The first two formulae are not significantly different when the temperature is close to 1080^{o}C. For

convenience, these are not used in this thesis. Whereas, the GPP program (Geist et al., 1985) provides the means of computing temperature of pyroxene crystallisation using the third formula.